

Polymer Reaction Engineering

EDITED BY J.M. ASUA



Blackwell
Publishing

Polymer Reaction Engineering

Polymer Reaction Engineering

Edited by

José M. Asua

Professor of Chemical Engineering

Institute for Polymer Materials (POLYMAT)

The University of the Basque Country, Spain



Blackwell
Publishing

©2007 by Blackwell Publishing Ltd

Blackwell Publishing Editorial Offices:

Blackwell Publishing Ltd, 9600 Garsington Road, Oxford OX4 2DQ, UK

Tel: +44 (0)1865 776868

Blackwell Publishing Professional, 2121 State Avenue, Ames, Iowa 50014-8300, USA

Tel: +1 515 292 0140

Blackwell Publishing Asia Pty Ltd, 550 Swanston Street, Carlton, Victoria 3053, Australia

Tel: +61 (0)3 8359 1011

The right of the Author to be identified as the Author of this Work has been asserted in accordance with the Copyright, Designs and Patents Act 1988.

All rights reserved. No part of this publication may be reproduced, stored in a retrieval system, or transmitted, in any form or by any means, electronic, mechanical, photocopying, recording or otherwise, except as permitted by the UK Copyright, Designs and Patents Act 1988, without the prior permission of the publisher.

First published 2007 by Blackwell Publishing Ltd

ISBN: 978-1-4051-4442-1

Library of Congress Cataloging-in-Publication Data

Polymer reaction engineering / edited by José M. Asua.

p. cm.

Includes bibliographical references and index.

ISBN-13: 978-1-4051-4442-1 (alk. paper)

ISBN-10: 1-4051-4442-4 (alk. paper)

1. Polymerization. 2. Polymers. I. Asua, José M.

TP1087.P653 2007

668.9'2-dc22

2007060685

A catalogue record for this title is available from the British Library

Set in 10/12 Minion

by Newgen Imaging Systems (P) Ltd, Chennai, India

Printed and bound in Malaysia

by KHL Printing Co Sdn Bhd

The publisher's policy is to use permanent paper from mills that operate a sustainable forestry policy, and which has been manufactured from pulp processed using acid-free and elementary chlorine-free practices. Furthermore, the publisher ensures that the text paper and cover board used have met acceptable environmental accreditation standards.

For further information on Blackwell Publishing, visit our website:

www.blackwellpublishing.com

Contents

<i>Contributors</i>	xi
<i>Preface</i>	xiii
<i>Notation</i>	xv
<i>Acronyms</i>	xxi
1 Introduction to Polymerization Processes	1
<i>José M. Asua</i>	
1.1 Microstructural features of polymers and their effect on properties	1
1.1.1 Chemical composition and monomer sequence distribution	1
1.1.2 Molecular weight distribution	2
1.1.3 Polymer architecture	4
1.1.4 Chain configuration	7
1.1.5 Morphology	7
1.1.6 Effect of processing and compounding on the microstructure of the polymeric materials	8
1.2 Classes of polymerizations	9
1.2.1 Chain-growth polymerization	9
1.2.2 Step-growth polymerization	14
1.3 Polymerization techniques	16
1.4 Main commercial polymers	18
1.4.1 Polyolefins	18
1.4.2 Styrenic polymers	20
1.4.3 Poly(vinyl chloride)	21
1.4.4 Waterborne dispersed polymers	21
1.4.5 Polyesters and polyamides	22
1.4.6 Thermosets	22
1.5 Polymerization reactors	23
References	27

2	Coordination Polymerization	29
	<i>João B.P. Soares, Timothy McKenna and C.P. Cheng</i>	
2.1	Polyolefin types: microstructural classification and analytical techniques	30
2.1.1	Polyethylene types	31
2.1.2	Polypropylene types	36
2.1.3	Polyolefin microstructural characterization techniques	39
2.2	Catalysts for olefin polymerization	43
2.2.1	Coordination catalyst types	43
2.2.2	Polymerization mechanism	49
2.3	Polymerization kinetics for single- and multiple-site catalysts	54
2.3.1	Homopolymerization	57
2.3.2	Copolymerization	75
2.3.3	Long-chain branch formation	83
2.4	Inter- and intraparticle mass and heat transfer resistances	86
2.4.1	Particle fragmentation and morphology control	87
2.4.2	Single particle models: inter- and intraparticle mass and heat transfer	90
2.5	Industrial olefin polymerization reactors	99
2.5.1	Reactor configurations and designs	100
2.5.2	Polyethylene manufacturing processes	104
2.5.3	Polypropylene manufacturing processes	109
2.5.4	Mathematical models for industrial reactors	112
	Acknowledgments	115
	References	115
3	Free-Radical Polymerization: Homogeneous Systems	118
	<i>Robin A. Hutchinson and Alexander Penlidis</i>	
3.1	Free-radical polymers: properties and applications	118
3.2	FRP mechanisms and kinetics	119
3.2.1	Homopolymerization	119
3.2.2	Copolymerization	137
3.2.3	Diffusion-controlled reactions	144
3.2.4	Kinetic balances for modeling polymer MWs	147
3.3	Controlled radical polymerization	151
3.3.1	Stable free-radical polymerization	153
3.3.2	Atom transfer radical polymerization	154
3.3.3	Reverse addition-fragmentation chain transfer polymerization	155
3.4	Polymer reaction engineering aspects	156
3.4.1	Heat removal and temperature programming	156
3.4.2	Batch reactors	159
3.4.3	Semibatch (semicontinuous) reactors	161
3.4.4	Continuous stirred-tank reactors	163
3.4.5	Tubular reactors	168

3.5	A “roadmap” for mathematical modeling	171
	References	174
4	Free-Radical Polymerization: Heterogeneous Systems	179
	<i>Gregorio R. Meira and Costas Kiparissides</i>	
4.1	Introduction	179
4.2	High-impact polystyrene	179
4.2.1	Interrelationship between microstructure and application properties	182
4.2.2	Modeling HIPS polymerization	187
4.2.3	Optimizing final properties: melt flow index in a continuous HIPS process	194
4.2.4	Final remarks for HIPS	195
4.3	Vinyl chloride monomer bulk polymerization	195
4.3.1	Kinetic mechanism	197
4.3.2	PVC morphology	201
	Acknowledgments	206
	References	206
5	Suspension Polymerization	209
	<i>Costas Kotoulas and Costas Kiparissides</i>	
5.1	Introduction	209
5.2	Surface active agents	212
5.3	Mixing phenomena	214
5.4	The “bead” suspension polymerization process	216
5.5	The “powder” suspension polymerization process	217
5.6	Population balance modeling	220
5.6.1	The drop breakage process	220
5.6.2	The drop coalescence process	223
5.6.3	Numerical solution of the PBE	224
5.7	Physical properties and phase equilibrium calculations	224
5.7.1	Physical and transport properties	224
5.7.2	Phase equilibrium calculations	225
5.8	Effect of operating conditions on PSD	227
5.9	Scale-up of suspension polymerization reactors	227
	References	230
6	Emulsion Polymerization	233
	<i>María J. Barandiaran, José C. de la Cal and José M. Asua</i>	
6.1	Main products and markets	233
6.2	Microstructural features and their effect on properties	234
6.3	Emulsion polymerization fundamentals	236
6.3.1	Description of the process	236
6.3.2	Mechanisms, thermodynamics and kinetics	240

6.4	Reactor engineering	256
6.4.1	Emulsion polymerization reactors	256
6.4.2	Predicting the performance of emulsion polymerization reactors	258
6.4.3	Implementation of emulsion polymerization	261
6.4.4	Residual monomer and VOC removal	265
6.4.5	Scale-up	267
6.5	Related processes	267
6.5.1	Inverse emulsion polymerization	267
6.5.2	Miniemulsion polymerization	268
6.5.3	Microemulsion polymerization	268
6.5.4	Dispersion polymerization	268
	References	269
7	Step-Growth Polymerization	273
	<i>Kyu Yong Choi and Kim B. McAuley</i>	
7.1	Introduction	273
7.1.1	Examples of commercially important polymers produced by step-growth polymerization	273
7.1.2	Basic properties of step-growth polymerization processes	276
7.2	Polymerization kinetics and modeling	278
7.2.1	Reaction kinetics and the most probable distribution	279
7.2.2	Effect of non-stoichiometric composition	282
7.2.3	Molecular weight development in non-linear step-growth polymerization	285
7.3	Industrial step-growth products, processes and modeling	290
7.3.1	Poly(ethylene terephthalate) production and modeling	291
7.3.2	Polyamide production processes and modeling	300
7.4	Summary	312
	References	313
8	Control of Polymerization Reactors	315
	<i>José R. Leiza and José C. Pinto</i>	
8.1	Characterization of the control problem	315
8.2	Classical polymerization reaction control problems	316
8.2.1	Control of reaction rates and of reactor temperature	316
8.2.2	Control of monomer conversion and polymer production	318
8.2.3	Control of molecular weight averages and MWDs	319
8.2.4	Control of copolymer composition	320
8.2.5	Control of particle size and PSDs	320
8.2.6	Control of other reaction parameters	321
8.3	On-line monitoring	322
8.3.1	Introduction	322
8.3.2	On-line sensors for monitoring polymer quality	323
8.3.3	State estimation	330

8.4	Safety	336
8.4.1	Introduction	336
8.4.2	Risk parameter assessment	337
8.5	Optimum operation design and setpoint specification	340
8.5.1	Problem definition and goals	340
8.5.2	Numerical solution of the optimization problem	344
8.5.3	Use of experimental design techniques for optimization	347
8.5.4	Heuristic methods	347
8.6	Calculation of the control action and control schemes	349
8.6.1	Open-loop control	349
8.6.2	Closed-loop control	350
8.6.3	Data handling	355
8.7	Concluding remarks	356
	References	356
	<i>Index</i>	363

Contributors

- Professor José M. Asua** Institute for Polymer Materials (POLYMAT),
The University of the Basque Country, Apdo 1072,
20080 Donostia-San Sebastián, Spain
- Professor María J. Barandiaran** Institute for Polymer Materials (POLYMAT),
The University of the Basque Country, Apdo 1072,
20080 Donostia-San Sebastián, Spain
- Dr C.P. Cheng** Senior Manager, Catalyst Applications,
Process Technologies, Engelhard Corporation,
10001 Chemical Road, Pasadena, TX 77507, USA
- Professor Kyu Yong Choi** Department of Chemical and Biomolecular
Engineering, University of Maryland, College Park,
MD 20742, USA
- Professor José C. de la Cal** Institute for Polymer Materials (POLYMAT),
The University of the Basque Country, Apdo 1072,
20080 Donostia-San Sebastián, Spain
- Professor Robin A. Hutchinson** Department of Chemical Engineering,
Queen's University, Kingston ON K7L 3N6, Canada
- Professor Costas Kiparissides** Department of Chemical Engineering,
Aristotle University of Thessaloniki &
Centre for Research & Technology Hellas
P.O. Box 472, 54124, Thessaloniki, Greece
- Dr Costas Kotoulas** Chemical Process Engineering Research Institute,
Centre for Research and Technology Hellas,
57001 Thessaloniki, Greece
- Professor José R. Leiza** Institute for Polymer Materials (POLYMAT),
The University of the Basque Country, Apdo 1072,
20080 Donostia-San Sebastián, Spain
- Professor Kim B. McAuley** Department of Chemical Engineering,
Queen's University, Kingston, ON K7L 3N6, Canada

- Professor Timothy McKenna** LCPP-CNRS/ESCPE-Lyon, Bat F308, 43 Blvd du
11 Novembre 1918, BP 2077, 69616 Villeurbanne Cedex,
France
- Professor Gregorio R. Meira** Inst. de Desarrollo Tecnol. para la Industria
Química – INTEC, Universidad Nacional del Litoral,
Guemes 3450, S3000GLN – Santa Fe, Argentina
- Professor Alexander Penlidis** Institute for Polymer Research (IPR),
Department of Chemical Engineering,
University of Waterloo, 200 University Avenue West,
Waterloo, Ontario, N2L3G1, Canada
- Professor José C. Pinto** Programa de Engenharia Química, COPPE,
Universidade Federal do Rio de Janeiro, Caixa
Postal 68502, 21945-970 Rio de Janeiro, RJ, Brazil
- Professor João B.P. Soares** Department of Chemical Engineering,
University of Waterloo, 200 University Avenue West,
Waterloo, Ontario, N2L 3G1, Canada

Preface

Synthetic polymers are found in such a large variety of products that they have shaped modern life. The extraordinary versatility of the polymer materials in terms of properties is due to the variety and complexity of the polymer microstructure (chemical composition, chemical composition distribution, molecular weight distribution, polymer architecture, chain configuration and phase morphology).

Polymers are “product-by-process” whose microstructure, and hence their final properties, are mostly determined in the reactor. Therefore, the understanding of the processes occurring in the reactor is crucial to achieve an efficient, consistent, safe and environmentally-friendly production of polymer materials with improved performance.

This book provides the link between fundamentals of polymerization kinetics and the polymer microstructure achieved in the reactor. The aim is to instill a firm understanding of the effect of polymerization kinetics on both reactor performance and polymer quality, learning how to manipulate the process variables to achieve the process goals.

The vast majority of the polymers are produced using a few classes of polymerizations (coordination polymerization, free-radical polymerization and step-growth polymerization). The type of polymerization determines not only the kind of polymer obtained, but also the reactor configuration and the way in which the process is conducted. Therefore, the book is organized according to the type of polymerization.

The production of polyolefins by means of coordination polymerization, which is the highest tonnage polymerization process, is discussed first. The following chapters present the production of polymers by free-radical polymerization in homogeneous, heterogeneous and dispersed (suspension and emulsion) media. Afterwards, the reaction engineering of step-growth polymerization is discussed. The last chapter is devoted to the control of polymerization reactors.

Each chapter starts with a description of the main polymers produced by the particular method, the key microstructural features, the applications and the sought properties. Then the polymerization kinetics and its effect on the configuration of industrial reactors is discussed. Afterwards the mass and energy balances for the reactors are developed. The examples focus on the main polymers produced by the particular class of polymerization, but the general concepts, principles and methodology are emphasized.

The book is addressed to chemists and engineers taking their first steps in the industry, to those beginning an academic research project in the area, as well as to students of both advanced undergraduate and graduate courses in polymer reaction engineering. The book would help them to overcome the gap between a general understanding of

polymer chemistry or engineering and the specifics of working in this field. It is expected that the reader is familiar with the basic notions of polymers, chemical kinetics and mass and heat balances.

The book became a reality through the enthusiastic work of the chapter authors. I am indebted to each of them. I also would like to thank my wife Esmeralda and our daughter Leire for their support and the understanding shown during the preparation of this book.

Notation

a^*	interfacial area per unit volume of the reactor [$\text{m}^2 \text{m}^{-3}$]
a_s	surface area of the polymer particles covered by 1 mol of surfactant under saturation [$\text{m}^2 \text{mol}^{-1}$]
A_i	pre-exponential factor for rate coefficient of mechanism i [same units as rate coefficient]
A_p^*	surface area of the polymer particles [m^2]
A_w	total heat transfer area of the reactor [m^2]
Al	cocatalyst/activator
c	pseudo-first-order rate coefficient for termination (combination + disproportionation) in the polymer particles ($(k_{tc} + k_{td})/2N_A v_p$) [s^{-1}]
c_c	pseudo-first-order rate coefficient for termination by combination in the polymer particles ($k_{tc}/2N_A v_p$) [s^{-1}]
c_d	pseudo-first-order rate coefficient for termination by disproportionation in the polymer particles ($k_{td}/2N_A v_p$) [s^{-1}]
c_p	heat capacity [$\text{kJ kg}^{-1} \text{K}^{-1}$]
c_{pi}	heat capacity of compound i in the reactor [$\text{kJ kg}^{-1} \text{K}^{-1}$]
c_{piin}	heat capacity of compound i in the feed [$\text{kJ kg}^{-1} \text{K}^{-1}$]
c_{pw}	heat capacity of the cooling fluid [$\text{kJ kg}^{-1} \text{K}^{-1}$]
C	catalyst
C^*	active center
C_d	deactivated active center
C_H^*	metal hydride active center
cmc	critical micelle concentration [$\text{mol } \ell^{-1}$]
CTA	chain transfer agent [mol]
C_{tr}^j	ratio of chain transfer rate (k_{tr}^j , $j = \text{mon, pol, sol, CTA, Al, H}$) to propagation rate coefficients
d_p	diameter of polymer particles [m]
d_{32}	Sauter mean diameter [m]
d_{50}	mean particle diameter [m]
D_a	dispersion coefficient [$\text{m}^2 \text{s}^{-1}$]
DB	terminal double bonds [mol]
D_I	impeller diameter [dm]
D_{Mh}	diffusion coefficient of the monomer in phase h [$\text{m}^2 \text{s}^{-1}$]

D_n	dead polymer chains of length n [mol]
$D_{n,b}$	dead polymer chains of length n with b branching points [mol]
$\overline{D_n}$	dead polymer chains of length n with terminal insaturation [mol]
$\overline{\overline{D_n}}$	dead polymer chain with an internal double bond [mol]
DP_n	number-average degree of polymerization
DP_n^{inst}	instantaneous number average degree of polymerization
DP_{nb}	number-average degree of polymerization of branched polymers
DP_w	weight-average degree of polymerization
D_R	reactor diameter [m]
D_{wi}	diffusion coefficient of water in phase i ($i = p$ (polymer); g (gas)) [m^2s^{-1}]
E_i	activation energy of the rate coefficient for mechanism i [kJ mol^{-1}]
$E(t)$	residence time distribution in the reactor
f	initiator efficiency (Equation 3.1)
f_{av}^*	average number of functional groups per monomer molecule (Equation 7.18)
f_i	mol fraction of monomer i in monomer mixture
f_i^j	fugacity of compound i in phase j
$F_{i\text{in}}$	inlet molar flow rate of component i [mol s^{-1}]
$F_{i\text{out}}$	outlet molar flow rate of component i [mol s^{-1}]
F_{pi}	cumulative mol fraction of monomer i in the copolymer
F_{pi}^{inst}	instantaneous mol fraction of monomer i in the copolymer chains being formed
h_p	heat transfer coefficient at the polymer particle surface [$\text{kJ m}^{-2}\text{s}^{-1} \text{K}^{-1}$]
H	total height of the reaction mixture [m]
i_{crit}	critical length of the oligoradicals formed from desorbed radicals
$[i]_j$	concentration of species i in phase j [mol l^{-1}]
I	initiator [mol]
Inh	inhibitor, poison
j_{crit}	critical length of the oligoradicals formed from the initiator
k_a	rate coefficient for radical entry into polymer particles [$\text{l mol}^{-1} \text{s}^{-1}$]
k_{ac}	rate coefficient for catalyst activation [s^{-1}]
k_{am}	rate coefficient for radical entry into micelles [$\text{l mol}^{-1} \text{s}^{-1}$]
k_{bb}	rate coefficient for intramolecular H-abstraction (backbiting) [s^{-1}]
k_d	rate coefficient for radical exit from the polymer particles [s^{-1}]
k_{dac}	rate coefficient for catalyst deactivation [s^{-1}]
k_{dacI}	rate coefficient for catalyst deactivation by impurity [$\text{l mol}^{-1} \text{s}^{-1}$]
k_{dep}	rate coefficient for depropagation [s^{-1}]
k_i	rate coefficient for chain initiation [$\text{l mol}^{-1} \text{s}^{-1}$]
k_t	rate coefficient for thermal initiator decomposition [s^{-1}]
\hat{k}_j	pseudo-kinetic constant for mechanism j (Table 2.12)
k_{t}^{a}	mass transfer coefficient [s^{-1}]
k_p	rate coefficient for propagation and rate constant for forward polyamidation reactions [$\text{l mol}^{-1} \text{s}^{-1}$]
$\overline{k_p}$	average propagation rate coefficient in copolymerization (Equation 3.44) [$\text{l mol}^{-1} \text{s}^{-1}$]
$k_{p\text{ij}}$	rate coefficient for propagation of radicals with terminal unit i with monomer j [$\text{l mol}^{-1} \text{s}^{-1}$]

k_{pLBC}	rate coefficient for macromonomer propagation [$\ell \text{ mol}^{-1} \text{ s}^{-1}$]
k_p^{eff}	effective propagation rate coefficient (Equation 3.23) [$\ell \text{ mol}^{-1} \text{ s}^{-1}$]
k_p^{pol}	rate coefficient for propagation of terminal double bonds [$\ell \text{ mol}^{-1} \text{ s}^{-1}$]
k_r	rate coefficient for reverse hydrolysis reactions of amide links [$\ell \text{ mol}^{-1} \text{ s}^{-1}$]
k_s	mass-transfer coefficient in the boundary layer surrounding the polymer particle [m s^{-1}]
k_t	rate coefficient for termination (combination + disproportionation) [$\ell \text{ mol}^{-1} \text{ s}^{-1}$]
\bar{k}_t	average termination (combination + disproportionation) rate coefficient in copolymerization (Equation 3.48) [$\ell \text{ mol}^{-1} \text{ s}^{-1}$]
k_{tc}	rate coefficient for termination by combination [$\ell \text{ mol}^{-1} \text{ s}^{-1}$]
k_{td}	rate coefficient for termination by disproportionation [$\ell \text{ mol}^{-1} \text{ s}^{-1}$]
k_{therm}	rate coefficient for monomer thermal initiation ($\ell^2 \text{ mol}^{-2} \text{ s}^{-1}$ for styrene, Equation 3.19)
k_{tr}^j	rate coefficient for chain transfer to species j (mon, pol, sol, CTA, Al, H) [$\ell \text{ mol}^{-1} \text{ s}^{-1}$]
k_{tw}	rate coefficient for termination in the aqueous phase [$\ell \text{ mol}^{-1} \text{ s}^{-1}$]
$k_{\text{t}\beta}$	rate coefficient for β -hydride elimination [s^{-1}]
$k(\nu, \nu')$	rate coefficient for coagulation of particles of volumes ν and ν' [$\ell \text{ part}^{-1} \text{ s}^{-1}$]
K_a	apparent equilibrium constant in step-growth polymerization
K_{eq}	equilibrium constant [units depend on stoichiometry]
K_i^j	partition coefficient of monomer i between phase j and aqueous phase
K_D	lumped constant for catalyst deactivation (Equation 2.57) [s^{-1}]
K_{TR}	lumped constant for all transfer reactions (Equations 2.14 and 2.56) [s^{-1}]
$\text{LCB}_{\text{chain}}$	number of long chain branches per polymer chain
\dot{m}_w	mass flow rate of the cooling fluid [kg s^{-1}]
M	monomer [mol]
M_i	amount of monomer i in the reactor [mol]
M_{i0}	initial amount of monomer i in the reactor [mol]
$[M_i]_p$	concentration of monomer i in the polymer particles [$\text{mol } \ell^{-1}$]
$[M_i]_{\text{lw}}$	concentration of monomer i in the aqueous phase [$\text{mol } \ell^{-1}$]
\bar{M}_n	number-average molecular weight [kg kmol^{-1}]
\bar{M}_n^{inst}	instantaneous number-average molecular weight [kg kmol^{-1}]
\bar{M}_w	weight-average molecular weight [kg kmol^{-1}]
\bar{M}_w^{inst}	instantaneous weight-average molecular weight [kg kmol^{-1}]
\bar{n}	average number of radicals per particle
n_m	surfactant aggregation number [molecules micelle $^{-1}$]
$n(\nu)$	number density distribution of particles with volume ν [ℓ^{-1}]
$n_{\text{in}}(\nu)$	number density distribution of particles with volume ν in the reactor feed [ℓ^{-1}]
N	impeller speed [s^{-1}]
N_A	Avogadro's number [mol^{-1}]
N_i	moles of compound i in the reactor [mol]
$N_i(n)$	fraction of all monomer i sequences in the copolymer that are n units long
N_m	number of micelles in the reactor

N_p	number of polymer particles in the reactor
$N_{p(n)}$	number of particles with n radicals in the reactor
p	conversion of the limiting functional group in step growth polymerization
P	impeller power consumption [kJ s^{-1}] and pressure in Equation 3.14 [Pa]
PDI	polydispersity index ($\overline{M}_w/\overline{M}_n$)
P_i	fraction of growing polymer chains with ultimate unit of type i in copolymerization
P_{ij}	probability that monomer i follows monomer j in the copolymer chain (Equation 3.36)
$P_{I\text{crit}}$	radicals of critical length formed from the initiator [mol] (Equation 6.18)
P_{Micrit}	radicals of critical length formed from desorbed radicals [mol] (Equation 6.18)
P_n^i	growing chains of length n terminated in monomer type i
P_n	growing polymer chains of length n [mol]
$P(n)$	probability that a molecule randomly picked from a reaction mixture is of length n
$P_{n,b}$	growing polymer chains of length n with b branch points [mol]
P_n^X	dormant species of length n
P_{tot}	total number of moles of radicals in the system [mol]
$[P_{\text{tot}}]_h$	concentration of radicals in phase h (p: polymer particles; w: aqueous phase) [$\text{mol } \ell^{-1}$]
Q_{in}	volumetric inlet flow rate for continuous reactors [$\ell \text{ s}^{-1}$]
Q_{loss}	heat losses to the reactor surroundings [kJ s^{-1}]
Q_{out}	volumetric outlet flow rate for continuous reactors [$\ell \text{ s}^{-1}$]
Q_r	rate of heat generation by polymerization [kJ s^{-1}]
Q_{removal}	rate of heat removal [kJ s^{-1}]
Q_{stirring}	rate of heat production by stirring [kJ s^{-1}]
r	stoichiometric ratio of mutually reactive groups in step-growth polymerization ($A_0/B_0 \leq 1$)
r_i	reactivity ratio for monomer i (e.g., $r_1 = k_{p11}/k_{p12}$)
r_v	polymer particle volumetric growth rate [$\ell \text{ s}^{-1}$]
R	ideal gas constant [$\text{kJ mol}^{-1} \text{ K}^{-1}$]
R_c	radius of the catalyst fragment
R_{init}	rate of initiation from initiator [$\text{mol } \ell^{-1} \text{ s}^{-1}$]
R_I	rate of initiator decomposition ($\text{mol } \ell^{-1} \text{ s}^{-1}$)
R_{LCB}	rate of formation of long-chain branches [$\text{mol } \ell^{-1} \text{ s}^{-1}$]
R_{mic}	radius of microparticle [m]
R_{mac}	radius of polymer (macro) particle [m]
R_{nuc}	rate of particle nucleation [$\text{particles } \ell^{-1} \text{ s}^{-1}$]
R_p	polymerization rate [$\text{mol } \ell^{-1} \text{ s}^{-1}$]
R_p^{pol}	rate of propagation of terminal double bonds (Equation 3.30) [$\text{mol } \ell^{-1} \text{ s}^{-1}$]
R_{prop}	rate of propagation [$\text{mol } \ell^{-1} \text{ s}^{-1}$]
R_{term}	rate of termination [$\text{mol } \ell^{-1} \text{ s}^{-1}$]
R_{tr}	rate of chain transfer [$\text{mol } \ell^{-1} \text{ s}^{-1}$]
R_{ν_k}	rate of change of moment ν_k [$\ell \text{ mol}^{-1} \text{ s}^{-1}$]
s_i	radical reactivity ratio (Equation 3.47)

S_T	total amount of surfactant in reactor [mol]
S_w	amount of surfactant in aqueous phase [mol]
t	polymerization time [s]
\bar{t}	mean residence time [s]
$t_{1/2}$	initiator half-life time [s]
T	reactor temperature [K]
T_e	temperature of the feed [K]
T_g	glass transition temperature [K]
T_{jin}	inlet temperature of the cooling fluid in the reactor jacket [K]
T_{jout}	outlet temperature of the cooling fluid in the reactor jacket [K]
T_m	melting temperature [K]
T_w	average temperature of the coolant [K]
u	velocity [m s^{-1}]
U	overall heat transfer coefficient [$\text{kJ m}^{-2} \text{s}^{-1} \text{K}^{-1}$]
U_j	free volume [ℓ]
v_p	volume of a monomer swollen polymer particle [ℓ]
V	reactor volume [ℓ]
V_d	volume of monomer droplets in the reactor [ℓ]
V_i	volume of monomer i in the reactor [ℓ]
Vis	viscosity dimensionless number
V_p	volume of monomer swollen polymer particles in the reactor [ℓ]
V_{pol}	volume of polymer in the reactor [ℓ]
V_w	volume of the aqueous phase in the reactor [ℓ]
V_{water}	volume of water in the reactor [ℓ]
W	condensation byproduct
W_i	mass of compound i [kg]
w_i	molecular weight of compound i ($i = m$ for the repeat unit in the polymer chain) [kg mol^{-1}]
$w(n)$	weight distribution of polymer chains of length n
We	Weber dimensionless number
x	conversion
$x(n)$	mol fraction of n -mers
X	mediating species in stable free-radical polymerization (Equation 3.75)
Z	polymer linkages in step growth polymers [mol]

Greek letters

α	parameter defined by Equation 2.119
α^*	branching coefficient (Equation 7.21)
α_c^*	critical value of the branching coefficient
α_{eff}	effective thermal diffusivity [$\text{m}^2 \text{s}^{-1}$]
γ_i	activity coefficient for compound i
δ	fraction of termination events that occur by disproportionation (Equation 3.8)
$\delta(x)$	Kronecker delta function
δ_z	minimum length of the radicals generated from the initiator to enter into the polymer particles

ΔG_p	free energy of propagation [kJ mol ⁻¹]
ΔH_p	enthalpy of propagation ($\Delta H_p \approx \Delta H_r$) [kJ mol ⁻¹]
$(\Delta H_r)_i$	polymerization heat of monomer i under the reactor conditions [kJ mol ⁻¹]
ΔS_p	entropy of propagation [kJ mol ⁻¹]
ΔT_{ml}	logarithmic mean temperature difference [K]
ΔV_i	activation volume (Equation 3.14) [ℓ mol ⁻¹]
ε	volume contraction factor
$\bar{\varepsilon}$	energy dissipation rate [kJ kg ⁻¹ s ⁻¹]
ε_b	porosity of the bed of particles
ε_p	porosity of the polymer (macro) particle
ζ_k	k th moment for bulk (living + dead chains) polymer [mol]
η	viscosity [Pa s ⁻¹]
$[\eta]$	intrinsic viscosity [ℓ mol ⁻¹]
κ	parameter defined in Equation 2.110
λ	kinetic chain length
μ_k	k th moment of growing polymer chain distribution [mol]
ν_k	k th moment of dead polymer chain distribution [mol]
ρ	density [kg ℓ^{-1}]
σ	interfacial tension [N m ⁻¹]
τ	ratio of all transfer reaction rates to propagation rate (Equation 2.84)
τ^*	ratio of all transfer reaction rates plus rate of LCB formation to rate of propagation
τ_s	tortuosity of polymer particle
φ	volume fraction of dispersed phase
ϕ_i^j	volume fraction of compound i in phase j
χ	Flory–Huggins interaction parameter

Acronyms

AA	acrylic acid
ABS	acrylonitrile-butadiene-styrene copolymer
AIBN	2,2'-azobisisobutyronitrile
ATR-FTIR	attenuated total reflection infrared
ATRP	atom transfer radical polymerization
BA	butyl acrylate
BB	dichlorobutyl branch
BHET	bishydroxyethyl terephthalate
BMA	butyl methacrylate
BPO	benzoyl peroxide
CCD	chemical composition distribution
CFD	computational fluid dynamics
CHDF	capillary hydrodynamic fractionation chromatography
CGC	constrained geometry catalyst
CLD	chain length distribution
CRP	controlled radical polymerization
Crystaf	crystallization analysis fractionation
CSTR	continuous stirred-tank reactor
CTA	chain-transfer agent
CTD	crystallization temperature distribution
DA	dodecyl acrylate
DEB	diethyl branch
DMT	dimethyl terephthalate
DSC	differential scanning calorimetry
DSD	droplet size distribution
EAO	ethylaluminumoxane
EG	ethylene glycol
EGDMA	ethylene glycol dimethacrylate
EKF	extended Kalman filter
EPDM	ethylene-propylene-diene monomer
EPS	expandable polystyrene
EVA	ethylene-vinyl acetate copolymer
FFF	field-flow fractionation

FODLS	fiber-optic dynamic light scattering
FRP	free-radical polymerization
FTIR	Fourier-transform infrared spectroscopy
GC	gas chromatography
GPC	gel permeation chromatography
HCPP	high-crystallinity polypropylene
HCSTR	homogeneous continuous stirred-tank reactor
HDPE	high density polyethylene
HIPP	high impact polypropylene
HIPS	high impact polystyrene
HLB	hydrophilic-lipophilic balance
HMD	hexamethylene diamine
HPMC	hydroxypropyl methylcellulose
IDP	iterative dynamic programming
KPS	potassium persulfate
LCB	long-chain branch
LCH	long-chain hypothesis
LDPE	low-density polyethylene
LLDPE	linear low-density polyethylene
LS	light scattering
MA	methyl acrylate
MAO	methylaluminoxane
MFFT	minimum film forming temperature [K]
MFI	melt flow index
MGM	multigrain model
MIR	mid-range infrared
MMA	methyl methacrylate
MPD	most probable distribution
MSD	monomer sequence distribution
MW	molecular weight
MWD	molecular weight distribution
NBR	acrylonitrile-butadiene rubber
NIR	near infrared
NMP	nitroxide mediated polymerization
NMR	nuclear magnetic resonance
ODCB	orthodichlorobenzene
PAN	polyacrylonitrile
PBD	polybutadiene
PBE	population balance equation
PBT	polybutylene terephthalate
PET	polyethylene terephthalate
PFM	polymer flow model
PFR	plug flow reactor
PLP	pulsed-laser-induced polymerization
PMMA	poly(methyl methacrylate)
PS	polystyrene

PSD	particle size distribution
PVA	poly(vinyl alcohol)
PVAc	poly(vinyl acetate)
PVC	poly(vinyl chloride)
QSSA	quasi-steady-state assumption
RAFT	reversible addition-fragmentation chain transfer
RI	refractive index detector
RIM	reaction injection molding
RSA	random search algorithm
RSSA	reactor steady-state approximation
RSSH	reactor steady-state hypothesis
RTD	residence time distribution
S	styrene
SAN	styrene-acrylonitrile copolymer
SBR	styrene-butadiene rubber
SCB	short-chain branch
SCSTR	Segregated continuous stirred tank reactors
SEC	size exclusion chromatography
SFRP	stable free-radical polymerization
SPP	solid-phase polymerization
SQP	sequential quadratic procedures
SSP	solid-state polymerization
TCB	trichlorobenzene
TEA	triethyl aluminium
TEMPO	2,2,6,6-tetramethylpiperidinyloxy
TMA	trimethyl aluminium
TPA	terephthalic acid
TPFB	tris(pentafluorophenyl) borane
TREF	temperature rising elution fractionation
UHMWPE	ultra-high molecular weight polyethylene
ULDPE	ultra low-density polyethylene
VAc	vinyl acetate
VCM	vinyl chloride monomer
VISC	viscometer
VLDPE	very low-density polyethylene
VOC	volatile organic compound
WCLD	weight chain-length distribution

Chapter 1

Introduction to Polymerization Processes

José M. Asua

1.1 Microstructural features of polymers and their effect on properties

Polymers are found in such a large variety of products that they have shaped modern life. The extraordinary versatility of polymers in terms of end-use properties is due to the variety and complexity of the microstructure of the polymeric material. The polymeric material includes both the polymer and the additives with which it is compounded. The microstructure of the polymeric material is determined by the molecular and morphological characteristics of the polymer itself, the way in which the polymer is processed and the additives used for compounding (Figure 1.1). The molecular characteristics of the polymer include chemical composition, monomer sequence distribution (MSD), molecular weight distribution (MWD), polymer architecture, chain configuration and morphology.

Polymers are very high molecular weight materials formed by smaller structural units bound together by covalent bonds. According to this definition, some natural materials such as cellulose and natural rubber are polymers. However, only the synthetic polymers will be considered in this book. These synthetic polymers are made by combination of small molecules, monomers, which form the structural units of the polymer. The reaction of monomers to form a polymer is termed polymerization. The molecular and morphological characteristics of the polymer depend on the formulation (monomers, catalysts, initiators, etc.), the polymerization process (reactor, polymerization technique) and the process conditions (concentrations, temperature, time).

1.1.1 *Chemical composition and monomer sequence distribution*

Homopolymers are polymers formed from a single monomer, namely, containing a single type of structural unit. The properties of the homopolymers are largely determined by the monomer. For example, at room temperature, polystyrene is a rigid material whereas poly(butyl acrylate) is soft and sticky. The range of properties achievable is greatly enlarged by forming polymers (copolymers) derived from more than one monomer. Thus, varying the monomer ratio, styrene–butyl acrylate copolymers ranging from rigid to soft and sticky can be produced.

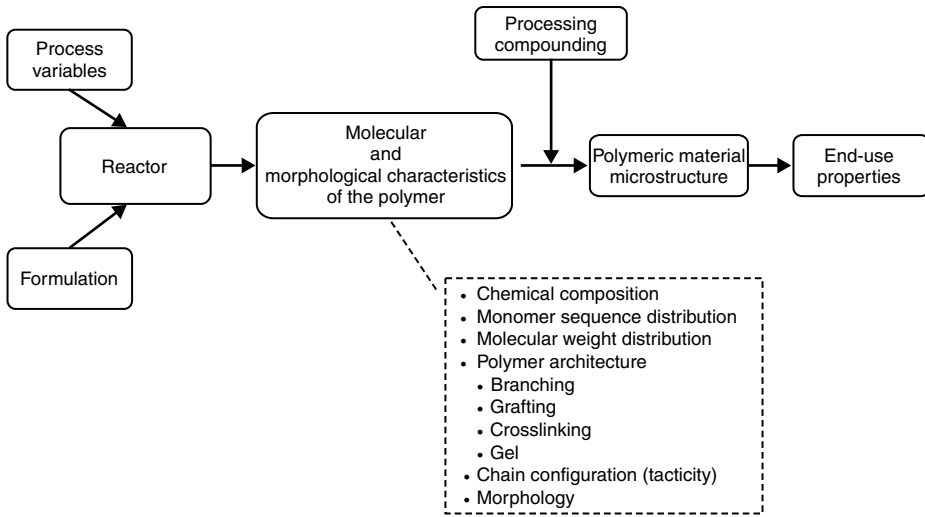


Figure 1.1 Key steps in the production of polymeric materials.

Copolymers differ in the sequence arrangements of the monomer units in the copolymer chain. In terms of MSD, different classes of copolymers can be distinguished (Table 1.1). Statistical copolymers are copolymers in which the sequential distribution of the monomeric units obeys known statistical laws. Strictly speaking, random copolymers are copolymers formed following a Markovian process of zeroth-order because the probability of finding a given monomeric unit at any given site of the chain is independent of the nature of the adjacent units. However, the concept of random copolymer is often used in a broader sense to refer to copolymers in which the comonomer units are rather evenly distributed along the polymer chain. This is the sense in which it is used in this book. An alternating copolymer is a copolymer comprising two species of monomeric units distributed in alternating sequence. Block copolymers are defined as polymers having a linear arrangement of blocks of varying monomer composition. The blocks forming the block copolymer can be different homopolymers, a combination of homopolymers and copolymers or copolymers of different chemical composition. A gradient copolymer is formed by polymer chains whose composition changes gradually along the chain. A graft copolymer is a polymer comprising molecules with one or more blocks connected to the backbone as side chains, having constitutional or configurational features that make them different from the main chain.

1.1.2 Molecular weight distribution

Most polymers contain chains of different lengths and they are characterized by the MWD. MWD strongly affects the properties of polymers. For example, the mechanical strength of polystyrene improves by increasing molecular weight, but the melt viscosity increases making processing more difficult. Although the properties of the polymers are

Table 1.1 Classes of copolymers in terms of MSD

Type of copolymer	Structure	Comonomers/reactants	Polymerization method	Examples
Statistical (random)	ABBABAAAABBABABBBAAABA	Methyl methacrylate, butyl acrylate	Free-radical polymerization	P
Alternating	ABABABABABABABAB	Styrene, maleic anhydride	Free-radical polymerization	P
Block	AAAAAABBBBBBBBBBAAAA	Styrene, butadiene	Ionic polymerization	P
Gradient	AAAABAB/ABBABBBB	Styrene, butyl acrylate	Controlled radical polymerization (CRP)	
Graft	AAAAAAAAAAAAAAAAAAAA B C B C C B	Styrene/acrylonitrile, polybutadiene	Free-radical polymerization	P

^a For unspecified or unknown copolymers the name is poly(monomer 1-co-monomer 2).

determined by the whole MWD, the MWD is often characterized by the average molecular weights.

Number average molecular weight:

$$\overline{M}_n = \frac{\sum n(D_n + P_n)}{\sum (D_n + P_n)} w_m \quad (1.1)$$

where D_n and P_n are the number of moles of dead and growing polymer chains of degree of polymerization n (number of repeated units in the chain, also called length), and w_m is the molecular weight of the repeated unit.

Weight average molecular weight:

$$\overline{M}_w = \frac{\sum n^2 (D_n + P_n)}{\sum n (D_n + P_n)} w_m \quad (1.2)$$

The ratio between these averages is the polydispersity index (PDI) that gives an idea about the broadness of the MWD:

$$\text{PDI} = \frac{\overline{M}_w}{\overline{M}_n} \quad (1.3)$$

PDI affects application properties. Thus, stiffness of polypropylene increases as PDI increases [1]. On the other hand, the mechanical properties of the linear low-density polyethylene (LLDPE) improve when PDI decreases, but it presents a higher melt viscosity and hence a poorer processability [2].

For a homopolymer, w_m is the molecular weight of the monomer, while for a copolymer, w_m is given by

$$w_m = \sum F_{pi} w_i \quad (1.4)$$

where F_{pi} is the molar copolymer composition referred to monomer i and w_i the molecular weight of this monomer.

The number average degree of polymerization (DP_n) and the weight average degree of polymerization (DP_w) are







$$DP_n = \frac{\overline{M}_n}{w_m} \quad (1.5)$$

$$DP_w = \frac{\overline{M}_w}{w_m} \quad (1.6)$$

1.1.3 Polymer architecture

In terms of their architecture, polymers can be classified as linear, branched and cross-linked polymers (Table 1.2). In the linear polymers, the structural units are arranged in a linear sequence. Branched polymers may have short and long branches. Branched polymers include comblike and star polymers. Extensive branching may lead to a dendritic structure.

Table 1.2 Polymer architectures

	Architecture	Examples	
		Comonomers/reactants	Polymerization method
Linear		Ethylene	Coordination
Branched		<i>n</i> -Butyl acrylate	Free-radical polymerization
Comb		Polymethylsiloxane + styrene	Atom transfer radical polymerization (ATRP)
Star		Divinylbenzene + living cationic polyisobutylene	Cationic polymerization
Dendrimer and hyperbranched		Dimethylol propionic acid	Step-growth polymerization
Crosslinked/network		Butadiene	Free-radical polymerization

Crosslinked polymers are formed by polymer chains linked together forming a three-dimensional network. They are characterized by the crosslinking density (number of junction points per 1000 monomeric units). Unlike linear and branched polymers, crosslinked polymers do not melt upon heating and do not dissolve in solvents (although they are swollen by them). Loose networks (low crosslinking density) have an elastic behavior (rubbers). Dense networks are rigid, inflexible and they do not deform unless temperature is high enough to break the covalent bonds.

Gel is often defined as the fraction of the polymer belonging to an infinite three-dimensional network. However, in practice, gel fraction is determined as the fraction of polymer that is not soluble in a given solvent, which may include very large (highly branched) macromolecules. Therefore, the reported gel contents depend on both the solvent and the extraction method used.

The macroscopic behavior of the polymer materials caused by the polymer architecture is the basis of the classification of polymers in thermoplastics, elastomers and thermosets.

Thermoplastics are linear and branched polymers that melt upon heating. They can be molded into any shape and constitute the vast majority of the polymers

including polyethylene, polypropylene, polystyrene, poly(vinyl chloride), poly(ethylene terephthalate) and polyamides (nylons). Melted linear thermoplastics may pack in a regular three-dimensional arrangement forming a crystalline phase upon cooling. The extent of crystallization and the crystal size depend on the type of monomeric unit, chain architecture, the rate of cooling and the use of nucleating agents. Crystallization is never complete and the polymers have crystalline and amorphous regions, namely, they are semi-crystalline. Crystalline regions are characterized by the melting temperature (T_m). Amorphous regions are characterized by the glass transition temperature (T_g), the temperature at which the amorphous polymers change from hard objects to a soft rubbery state. The type of branching has a profound effect on the spatial arrangement of the polymer chains, and hence on properties. The presence of branches disturbs the regular arrangement of the polymer chains, and therefore crystallinity decreases as branching increases. A limited number of long branches still allows the achievement of a relatively high crystallinity [3]. Short branches severely decrease crystallinity. Crystallinity has a strong effect on the end-use properties [4]. Thus, impact strength and tensile strength increase with crystallinity; permeability decreases with crystallinity because permeation takes place only through the amorphous phase; and optical clarity also decreases with crystallinity because the light is dispersed by the crystalline regions.

Elastomers are elastic materials that stretch to high extensions and rapidly recover their original dimensions once the applied stress is released. They are formed by a loose network. Styrene-butadiene rubber (SBR) and ethylene-propylene-diene monomer (EPDM) are examples of important elastomers.

Thermoplastic elastomers are a class of polymers that combine the characteristics of the thermoplastics and those of the elastomers. These materials are A–B–A tri-block copolymers composed by hard and soft segments, which form a processable melt at high temperatures and transform into a solid rubber-like object upon cooling. The transition between the strong elastic solid and the processable melt is reversible. Figure 1.2 illustrates this phase transition for an A–B–A tri-block copolymer, where A is a short hard segment and B a long soft segment. At low temperatures, the hard segments segregate forming a three-dimensional network with physical crosslinks. When temperature is increased above the T_g of the polymer forming the hard segments, the physical crosslinks soften and a polymer melt

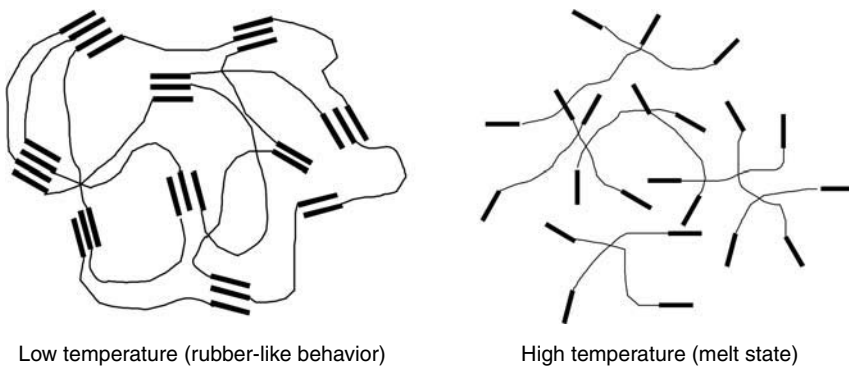


Figure 1.2 Thermoplastic elastomers. — hard segments, — soft segments.

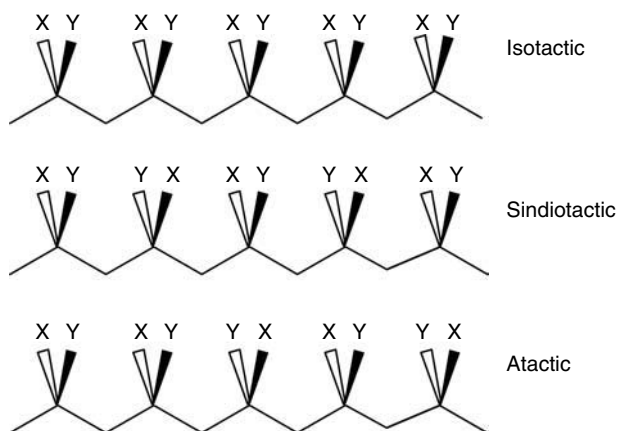


Figure 1.3 Chain configurations (tacticity). — Bonds that are on the paper plane; \triangleleft Bonds that are behind the paper plane; \blacktriangleleft Bonds that are in front of the paper plane.

is formed. Polystyrene-*block*-polybutadiene-*block*-polystyrene is a commercially important thermoplastic elastomer.

Thermosets are rigid polymers that do not melt upon heating. They are densely cross-linked polymers. Polyurethanes, epoxy resins and phenol-formaldehyde resins are some important thermoset polymers.

1.1.4 Chain configuration

In addition to the effects of copolymer composition and chain architecture, the properties of polymers are strongly affected by the chain configuration. Figure 1.3 shows that for a monomer $\text{CH}_2=\text{CXY}$, where X and Y are different substituents, the spatial arrangement of the monomeric unit in the chain leads to different chain configurations. In isotactic polymers all the repeated units have the same spatial configuration, syndiotactic polymers are formed by repeated units with alternate configuration and the configurations are randomly placed in atactic polymers. Tacticity has a profound effect on properties. Commercial polypropylene, which represents about 17% of the total production of synthetic polymer, is essentially isotactic. The regularity of the structure allows the formation of a semi-crystalline structure that yields good mechanical properties. Atactic polypropylene is an amorphous material without commercial value.

1.1.5 Morphology

The commercial value of some polymers depends on their morphology. Thus, high-impact polystyrene (HIPS), which has an impact strength 5–10 times that of the neat polystyrene, is a multiphase material in which polybutadiene rubbery domains are distributed within the polystyrene matrix (Figure 1.4). Each of these domains contains polystyrene

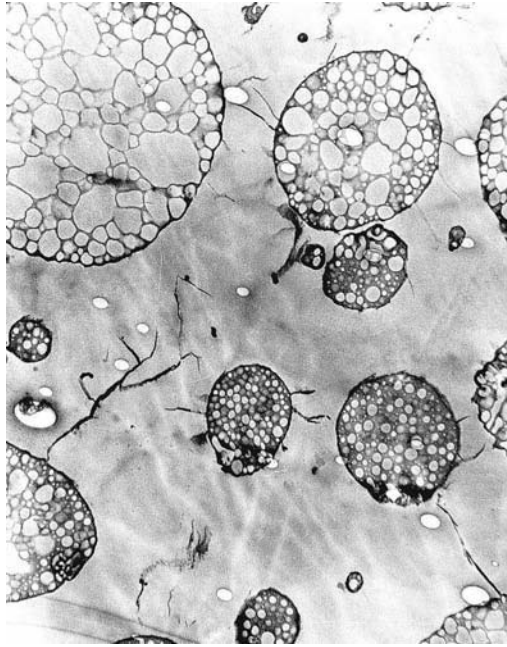


Figure 1.4 High-impact polystyrene.

inclusions. The rubbery domains allow distribution of the stress concentration over a larger volume, toughening the material. The impact resistance strongly depends on the size and morphology of the dispersed composite particles as well as on the grafting. Small particles provide rigidity and gloss, whereas larger particles improve toughness [5]. On the other hand, as the rubber content increases, impact strength increases while rigidity, heat distortion temperature and clarity decrease. Another example of an important commercial polymer with complex morphology is high-impact polypropylene (HIPP) that contains an ethylene–propylene soft copolymer finely dispersed within a semi-crystalline isotactic polypropylene (i-PP).

1.1.6 Effect of processing and compounding on the microstructure of the polymeric materials

Polymer processing refers to different techniques used for converting the polymer and additives (colorants, stabilizers, fillers, etc.) to a final polymeric product. Processing methods include extrusion, injection molding, blow molding, thermoforming and reacting techniques (e.g., reaction injection molding, pultrusion and filament winding) [6]. Processing affects the microstructure of the final products. For example, macromolecules become oriented during injection molding at high shear rates. For amorphous polymers, this leads to improved mechanical properties in the direction in which the polymer chains

are oriented [6]. On the other hand, the thermal characteristics of the mold determine the morphology of crystalline polymers. Additives may also modify the performance of polymeric products. Thus, fiber reinforced plastics approach tensile modulus values typical of metals [7]. Although both polymer processing and compounding are outside the scope of this book, it is important to have in mind that they may strongly affect the properties of the final product.

1.2 Classes of polymerizations

Table 1.3 summarizes the different types of polymerizations [8]. Chain-growth polymerization involves chain growth by reaction of an active polymer chain with single monomer molecules. In step-growth polymerization, polymer growth involves reactions between macromolecules. In addition, non-polymeric byproducts may be formed in both types of polymerization. However, condensative chain polymerization is very rare. Table 1.4 summarizes the differences between chain-growth polymerization and step-growth polymerization.

1.2.1 Chain-growth polymerization

In chain-growth polymerization, monomers can only join active chains. Monomers contain carbon-carbon double bonds (e.g., ethylene, propylene, styrene, vinyl chloride, butadiene, esters of (meth)acrylic acid). The activity of the chain is generated by either a catalyst or an initiator. Several classes of chain-growth polymerizations can be distinguished according to the type of active center:

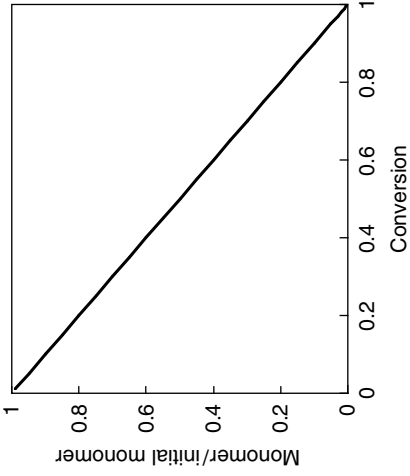
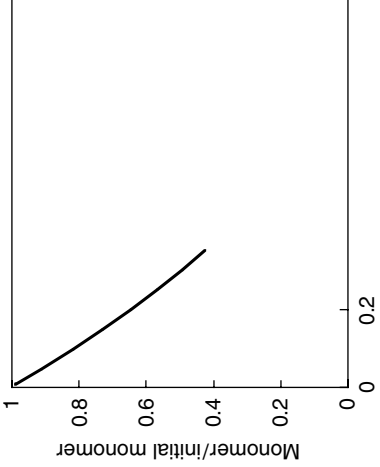
- Coordination polymerization (active center is an active site of a catalyst)
- Free-radical polymerization (active center is a radical)
- Anionic polymerization (active center is an anion)
- Cationic polymerization (active center is a cation)

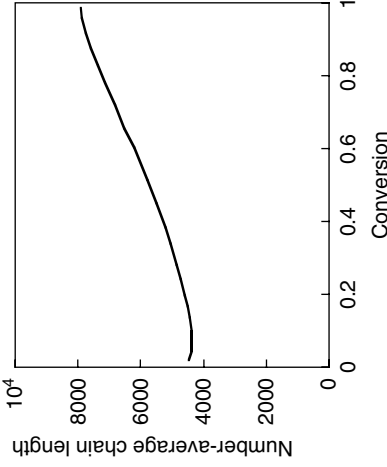
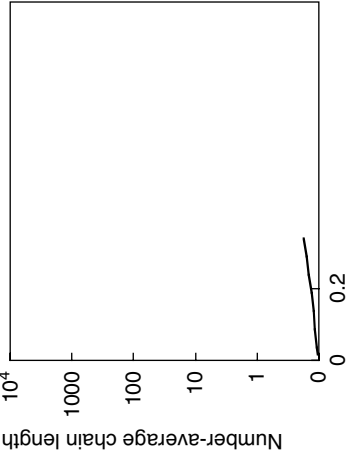
Table 1.3 Types of polymerizations

Chain-growth polymerization	Step-growth polymerization
$P_n + M \rightarrow P_{n+1}$ (chain polymerization) polystyrene	$P_n + P_m \rightarrow P_{n+m}$ (polyaddition) polyurethanes
$P_n + M \rightarrow P_{n+1} + W$ (condensative chain polymerization) amino-acid <i>n</i> -carboxy anhydrides biological polymerizations	$P_n + P_m \rightarrow P_{n+m} + W$ (polycondensation) poly(ethylene terephthalate)

W is byproduct.

Table 1.4 Comparison between chain-growth and step-growth polymerization

Chain-growth	
Monomers	Should contain at least a double bond
Growing principle	Reaction of the monomer with the active center. Chain activity initiated by a catalyst or an initiator
Reacting species	Growing chain and monomer
Number of growing chains	Small (10^{-8} – 10^{-7} mol l^{-1}) ^a
Growing chain life time	Very short (0.5–10 s)
Monomer consumption	Steadily throughout the reaction
	
Monomers	Should contain at least two different functional or monomers) in the reaction
Growing principle	Reactions of the functional the growing chains. No accelerate reactions
Reacting species	Two different functional or monomers) in the reaction
Number of growing chains	All the macromolecules
Growing chain life time	Chains grow during the
Monomer consumption	Faster than in chain-gro
	
Termination	Chain-termination event involved ^b
	No termination involved

Molecular weights	Very high from the beginning of the polymerization ^c No big changes during the polymerization		Smaller than in chain-growth process. Commercial very high monomer conversion
Thermodynamics	Exothermic. Mostly irreversible		Exothermic. Reversible constant decreases with Conversion Critical for achieving high molecular weights
Side reactions	Exothermic. Mostly irreversible		
Stoichiometry	Exothermic. Mostly irreversible		
Viscosity of the reaction media (bulk polymerization)	Severe increase because of the high molecular weights		
Temperature control (bulk polymerization)	Challenging because of the large heat of reaction and the high viscosity		Easier than for chain-growth process when only a limited increase during the process.

^a Only for coordination polymerization and free-radical polymerization.

^b Only for coordination polymerization and free-radical polymerization. Ionic polymerizations do not include a termination reaction.

^c Only for coordination polymerization and free-radical polymerization. In ionic polymerizations and in controlled free-radical polymerization increase during the process.

^d In AA + BB polymerizations.

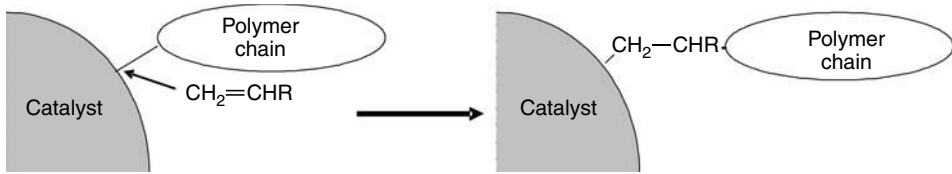


Figure 1.5 Monomer insertion in coordination polymerization.

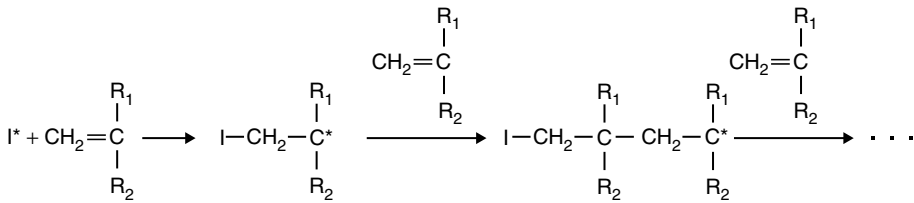


Figure 1.6 Growing of the polymer chain in free-radical polymerization.

1.2.1.1 Coordination polymerization

Coordination polymerizations are carried out on a suitable catalyst and proceed by an insertion mechanism, in which the monomer units are inserted between the catalytic site and the growing polymer chain (Figure 1.5). Catalysts for coordination polymerization include Ziegler–Natta catalysts, transition metal catalysts and metallocenes [9]. The insertion mechanism is tidily controlled by the catalyst, which allows fine-tuning of the polymer microstructure including the production of stereoregular polymers (e.g., i-PP). Catalyst development has been the key technological driving force in the commercial success of coordination polymerization [10]. A consequence of the control exerted by the catalyst on the polymerization is that a different set of kinetic parameters should be estimated for each catalyst.

1.2.1.2 Free-radical polymerization

In free-radical polymerization, the active center is a free-radical (very reactive species that contain an unpaired electron) created from an initiator and polymerization proceeds by addition of monomer units to the active end of the growing polymer chain that in the course of polymerization separates from the bound initiator fragment (Figure 1.6). The growth of the chain is terminated by bimolecular reaction between two radicals or by transfer of the radical to another compound (e.g., monomer, chain transfer agent and polymer). Free-radical copolymerization is attractive because of the huge number of monomers that can be polymerized, the different media that can be used (both organic and aqueous) and the relative robustness of this technique to impurities. In the classical free-radical (co)polymerization, only a few polymer chains are growing at the same time and the time spent in building a chain is very short (typically in 0.5–10 s). This is convenient to produce random, alternating and graft copolymers, but block copolymers and complex polymer

architectures such as star polymers are not accessible by means of classical free-radical polymerization. In addition, no stereoregular polymers can be produced by free-radical polymerization. An exception to this rule is the poly(vinyl chloride), PVC, in which the bulky chlorine group leads to a high syndiotactic index [11] (about 0.5 at the temperature range of the commercial processes, 45–75°C). The statistical termination of the growing chains leads to a relatively broad MWD. Because the species responsible for most of the chain growth and termination (free-radicals and monomers) depend on the monomer system, the kinetic constants are determined by the monomer system, allowing the compilation of tables of rate constants for each monomer [12].

In controlled radical polymerization (CRP), the extent of bimolecular termination is minimized [13–15]. This allows the preparation of almost any kind of copolymer architecture by means of a free-radical mechanism. All CRP methods have in common that a rapid dynamic equilibrium is established between a tiny concentration of growing free-radicals and a large majority of dormant polymer chains. In these processes, each growing chain stays for a long time in the dormant state, then it is activated and adds a few monomer units before becoming dormant again. Because the activation–polymerization–deactivation process is a random process, the MWD of the growing chains becomes narrower as they grow longer. The composition of the polymer chain can be easily modified by controlling the monomer composition in the reactor. Termination between active radicals is minimized by simply maintaining its concentration at a low value. The CRP methods differ in the way in which this dormant species are formed [16]. The most efficient CRP methods are stable free-radical polymerization, best represented by nitroxide mediated polymerization (NMP) [13], atom transfer radical polymerization (ATRP) [14] and reversible addition-fragmentation chain transfer (RAFT) [15].

Free-radical polymerization is a highly exothermic process and reactor temperature control is an important issue for both polymer quality and operation safety. At the temperatures used in commercial practice, most radical polymerizations are irreversible. However, because it is an exothermic reaction, at sufficiently high temperatures the reaction becomes reversible and complete conversion cannot be achieved. Methyl methacrylate is a major monomer that suffers from this problem, with an equilibrium concentration of 0.139 mol L⁻¹ at 110°C [12].

1.2.1.3 Anionic polymerization

Anionic polymerization requires the presence of initiators that provide the initiator anions (Figure 1.7). Anions can only attack those monomers whose electrons can be moved in such a way that a monomer anion results. Therefore, anionically polymerizable monomers should contain electron accepting groups. These include styrene, acrylic monomers, some aldehydes and ketones, and cyclic monomers such as ethylene oxide and other oxiranes, *N*-carboxy anhydrides, glycolide, lactams and lactones that can be polymerized by ring opening polymerization. The kinetic scheme does not include termination because in well purified systems most macroanions grow until all the monomers present in the reactor are polymerized. Such polymerization is called living polymerization, because if additional monomer is added into the reactor the polymer chains undergo further growing. A characteristic of the living polymerization is that, provided that initiation is quick enough, all polymer chains grow to a similar extent yielding very narrow molecular weight distributions.

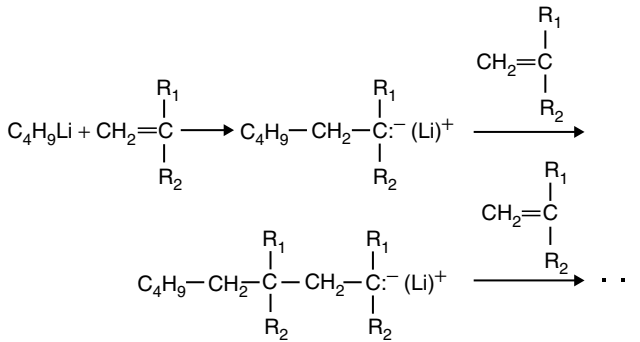


Figure 1.7 Anionic polymerization.

In addition, block copolymers can be produced by adding a second monomer once the first one has completely reacted. Tri- and multi-block copolymers can be prepared by subsequent additions of different monomers. Thus, styrene-butadiene-styrene tri-block copolymers produced by anionic polymerization are used as thermoplastic elastomers. Also, star and hyperbranched polymers can be obtained through this technique by simply using suitable initiation systems [17].

1.2.1.4 Cationic polymerization

In cationic polymerization, cationic initiators formed from carbenium salts, Brønsted acids or Lewis acids, react with monomer to give monomer cations that upon addition of more monomer become macrocations. Monomers suitable for cationic polymerization should have electron donating groups:

- (1) olefins $\text{CH}_2=\text{CHR}$ with electro-rich substituents,
- (2) compounds $\text{R}_2\text{C}=\text{Z}$ with hetero atoms or hetero groups Z and
- (3) cyclic molecules with hetero atoms as part of the ring structure.

Although, there are many more cationically polymerizable monomers than anionically polymerizable ones, relatively few cationic polymerizations (e.g., isobutene polymerization to produce polyisobutene and butyl rubber – copolymer of isobutene with small fractions of isoprene [18]) are performed industrially because macrocations are highly reactive and prone to suffer termination and chain transfer reactions.

1.2.2 Step-growth polymerization

Step-growth polymerization proceeds by reaction of the functional groups of the reactants in a stepwise manner; monomer reacts to form dimmers; monomers and dimmers react to form trimers; and in general

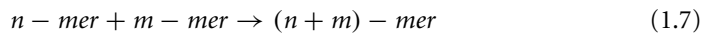
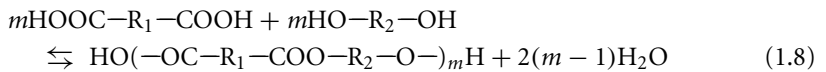


Table 1.5 Examples of chemical reactions in step-growth polymerization

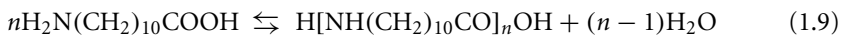
Reaction	Monomers/functional groups	Linking group	Polymer
Esterification	—COOH; —OH	—COO—	Poly(ethylene terephthalate)
Amidation	—COOH; —NH ₂	—CONH—	Nylon 6,6
Transesterification	Φ—O—CO—O—Φ; HO—R—OH	—O—CO—O—	Polycarbonate
Urethane formation	—N=C=O; —OH	—NH—CO—O—	Polyurethane

The chemical reactions that may be used to synthesize materials by step-growth polymerization include esterification, amidation, transesterification and the formation of urethanes among others (Table 1.5).

All step-growth polymerizations fall into two groups depending on the type of monomer(s) employed. The first one implies the use of at least two bifunctional and/or polyfunctional monomers, each one possessing a single type of active group. The monomers involved in this type of reaction are often represented as A—A and B—B, where A and B are the different reactive groups. An example of this reaction is the formation of polyesters from diols and diacids.



The second type of step-growth polymerization involves the use of monomers with different functional groups in the same molecule, A—B type monomers. An example of this reaction is the production of nylon 11 from 11-aminoundecanoic acid.



Bifunctional monomers, such as A—A, B—B and A—B, yield linear polymers. Branched and crosslinked polymers are obtained from polyfunctional monomers. For example, polymerization of formaldehyde with phenol may lead to complex architectures. Formaldehyde is commercialized as an aqueous solution in which it is present as methylene glycol, which may react with the trifunctional phenol (reactive at its two ortho and one para positions). The type of polymer architecture depends on the reaction conditions. Polymerization under basic conditions (pH = 9–11) and with an excess of formaldehyde yields a highly branched polymer (resols, Figure 1.8). In this case, the polymerization is stopped when the polymer is still liquid or soluble. The formation of the final network (curing) is achieved during application (e.g., in foundry as binders to make cores or molds for castings of steel, iron and non-ferrous metals). Under acidic conditions (pH = 2–3) and with an excess of phenol, linear polymers with little branching are produced (novolacs).

In step-growth polymerization, the molecular weight continuously increases with time and the formation of polymer with sufficient high molecular weight for practical applications requires very high conversions of the reactive groups (>98–99%). This requirement imposes stringent conditions on the formation of polymers by step polymerization, such as the necessity for a favorable equilibrium and the absence of side reactions.

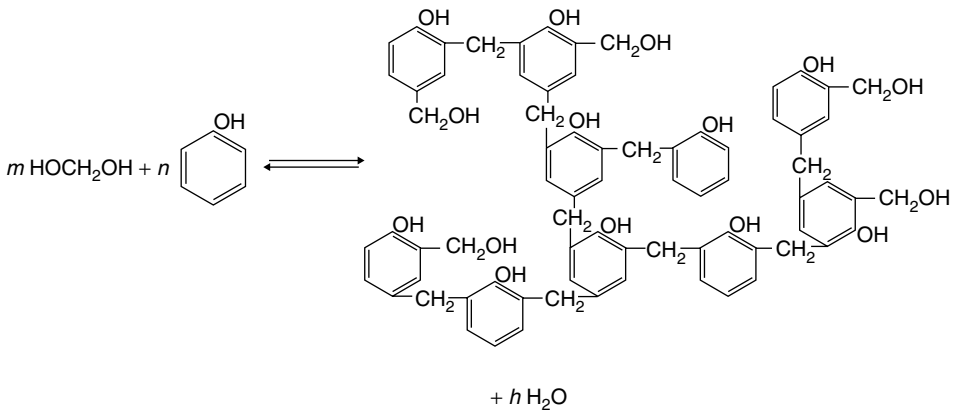


Figure 1.8 Resols.

Some of the most important step-growth polymerizations such as amidation (nylons), esterification (poly(ethylene terephthalate)) and transesterification (polycarbonate) are reversible. In addition, as step-growth polymerization is an exothermic process, the equilibrium constant decreases with temperature. This is a problem because very high conversions are required to achieve high molecular weights (Table 1.4). Actually, in a batch system, the equilibrium conversion is such that only oligomers are formed. In practice, these are reactors from which the byproduct (e.g., water in the esterification process) is continuously removed by using vacuum and/or inner gas. This allows shifting the equilibrium in the forward direction and hence achieving high conversions and high molecular weights. This requires reactors with special geometries. In addition, because the viscosity of the reaction mixture increases continuously, several reactors in series are used, each of them with an agitation system adequate to the viscosity of the polymer melt in that particular reactor. As an example, the reactor system used for the production of polycarbonate by transesterification is presented in Figure 1.9.

1.3 Polymerization techniques

The different polymerization classes discussed above can be implemented in several ways: bulk polymerization, solution polymerization, gas-phase polymerization, slurry polymerization, suspension polymerization and emulsion polymerization.

In bulk polymerization, the only components of the formulation are monomers and the catalyst or initiator. When the polymer is soluble in the monomer, the reaction mixture remains homogeneous for the whole process. Examples of homogeneous bulk polymerization are the production of low-density polyethylene (LDPE), general purpose polystyrene and poly(methyl methacrylate) produced by free-radical polymerization, and the manufacture of many polymers produced by step-growth polymerization including poly(ethylene terephthalate), polycarbonate and nylons. In some cases (e.g., in the production of HIPS and acrylonitrile-butadiene-styrene (ABS) resins), the reaction mixture contains a preformed

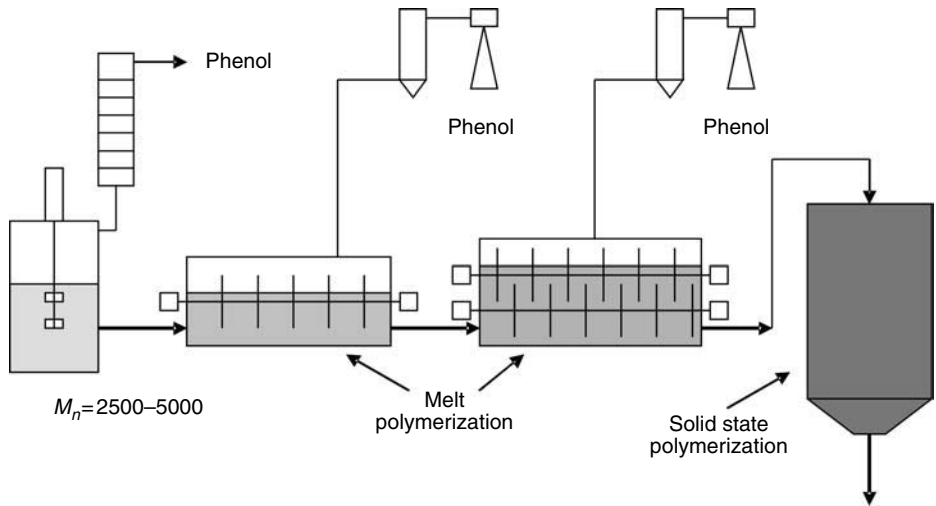


Figure 1.9 Production of polycarbonate by transesterification of phenyl carbonate and bisphenol A.

polymer that is not compatible with the polymer formed by polymerization of the monomer. Therefore, phase separation occurs leading to a multiphase material. Some polymers (e.g., PVC and i-PP) are not soluble in their monomers, and hence they precipitate as they are formed yielding a polymer slurry in their own monomer.

The main advantages of bulk polymerization are that a very pure polymer is produced at a high production rate per unit volume of the reactor. The drawback is that the removal of the polymerization heat is difficult because of the high viscosity of the reaction mixture associated with the high concentration of polymer. The thermal control of the reactor is more difficult in free-radical polymerization than in step-growth polymerization. The reason is that higher molecular weights are achieved in free-radical polymerization, and hence the viscosity is higher and the heat removal rate lower.

The thermal control of the reactor is much easier if the monomer is polymerized in solution. The solvent lowers the monomer concentration, and consequently the heat generation rate per unit volume of the reactor. In addition, the lower viscosity allows a higher heat removal rate and the solvent allows for the use of reflux condensers. Reflux cooling removes the heat of polymerization by evaporation of solvent; the condensed vapor is recycled to the reacting mass. Remixing of the condensed solvent with the viscous reacting mass may be difficult. Solution processes are used for the manufacture of LLDPE [19]. The main drawback is dealing with an environmentally unfriendly solvent, which makes solvent recovery a critical issue.

A way of achieving good thermal control and avoiding the use of solvents is to use suspension polymerization. In this process, drops of monomer containing the initiator are suspended in water. Each of the droplets acts as a small bulk polymerization reactor. Although the internal viscosity of the droplet increases with monomer conversion, the viscosity of the suspension remains low allowing a good heat transfer. Suspension stability and particle size are controlled by the agitation and the type and concentration of the suspension agents used. A particulate product with diameters ranging

from 10 μm to 5 mm is obtained. These particles contain the suspension agents and although some removal is possible, the final product inevitably contains some amount of suspension agent. Only free-radical polymerization is implemented in suspension polymerization. Expandable polystyrene and most of the poly(vinyl chloride) are produced by this process. Suspension polymerization is also used for the manufacture of standard polystyrene for injection molding and poly(methyl methacrylate) (clear transparent polymers require complete removal of the suspension agent). HIPS and ABS are often prepared in a combined bulk-suspension process [20].

Emulsion polymerization is a polymerization technique leading to polymer finely dispersed (particle diameters usually ranging from 80 to 500 nm) in a continuous medium (most often water). This product is frequently called latex. Only free-radical polymerization has been commercially implemented in emulsion polymerization. The basic formulation includes monomers, emulsifiers, water and a water-soluble initiator. The monomer is dispersed in 10–100 μm droplets under agitation. The amount of emulsifier is enough to cover these droplets and to form a large number of micelles. Radicals formed by decomposition of the initiator start polymerization in the aqueous phase. The oligomers formed enter into the micelles or precipitate in the aqueous phase, in both cases forming tiny polymer particles. The growth of these particles by polymerization leads to the final latex. The monomer droplets act as monomer reservoirs and almost no polymerization occurs in them. Consequently, the particle size of the latex is not determined by the size of the monomer droplets but by the number of particles formed. The thermal control of this process is easier than for bulk polymerization. However, it is not trivial as the modest viscosity of the reaction medium and the presence of a high heat capacity continuous medium (water) are counteracted by the fast polymerization rate. A substantial fraction of the SBR used for tires is produced by emulsion polymerization. Emulsion polymers commercialized as dispersed polymers are used for paper coating, paints, adhesives and additives for textiles and construction materials [21].

Polymerization of ethylene is often carried out in gas-phase using a heterogeneous coordination catalyst [22]. Polymer is formed on the active sites of the catalyst forming an expanding catalyst–polymer particle. The gaseous monomer diffuses through the pores of the particle and through the polymer to reach the active sites.

Slurry polymerization is often used in the manufacture of polyolefins. Initially, the reaction system consists of the catalyst dispersed (or dissolved as in the case of soluble metallocene catalysts) in a continuous medium, which may be a diluent in which the monomer is dissolved or pure monomer. The polymer is insoluble in the continuous medium, therefore it precipitates on the catalyst forming a slurry. High-density polyethylene (HDPE) is produced in a slurry of isobutane (Chevron–Phillips process) [22]. Liquid propylene is used in the Spheripol process to produce *i*-PP [22].

1.4 Main commercial polymers

1.4.1 Polyolefins

The yearly world production of synthetic polymers exceeds 200 million metric tons and about half of this amount corresponds to polyolefins [23] (Figure 1.10). Polypropylenes

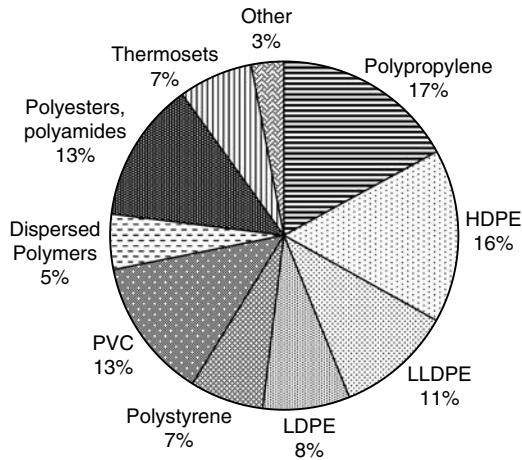


Figure 1.10 World polymer market.

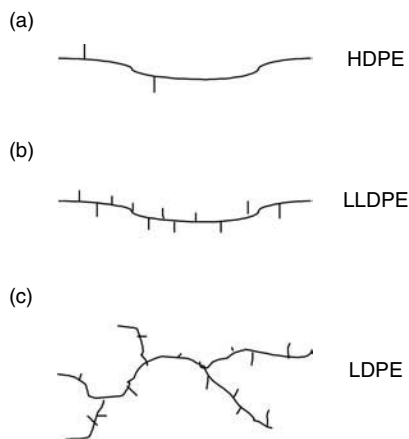


Figure 1.11 Polyethylene chain architectures. (a) Linear, almost no branches, (b) Linear varying amount of short branches and (c) Branched with a large amount of short branches.

include *i*-PP and HIPP. HIPP is a composite polymer composed by a soft ethylene-propylene copolymer dispersed in a matrix of *i*-PP. The main uses of polypropylene are fibers and filaments (carpets, raffia, netting, cordage, clothing, non-woven fabrics), films (food packaging and stationery), automotive parts, appliances, rigid packaging and general consumer products.

Polyethylenes include HDPE, LLDPE and LDPE. The main difference among these polymers is their chain architecture (Figure 1.11). HDPE is a linear polymer with almost no branches, LLDPE is a linear polymer with a varying amount of short branches, and LDPE is a branched polymer (0.5–3 long branches per 1000 carbons in the backbone) with a large amount of short branches (30 short branches per 1000 carbons in the backbone) [24].

Melted linear polyethylene chains crystallize upon cooling yielding a semi-crystalline polymer (about 60% crystallinity). The crystalline fraction decreases as branching increases, and LLDPE and LDPE are amorphous polymers. The names of these polymers come from the effect of crystallization on the density of the polymer, the higher the degree of crystallization the higher the density. The degree of crystallization, which has a strong effect on properties [4], depends on the molecular weight and rate of cooling. The higher the molecular weight, the smaller the crystallinity and hence the smaller the density. Faster cooling rates yield smaller densities.

LDPE and LLDPE are used mainly in film applications. Wire and cable insulation is also an important market. Comparing with the LDPE produced by free-radical polymerization, LLDPE exhibits a higher melting point (objects can be used at higher temperatures), is stiffer (thinner walls can be used) and presents higher tensile and impact strengths (more resistant films). However, the processability of the LLDPE is worse than that of the LDPE. A way of improving processability is to produce bimodal MWD [25]. HDPE is the preferred material for blow-molded containers for liquids, as it combines adequate environmental stress crack resistance with higher rigidity. The major uses are in the domestic market for bleach, detergents and milk. Films and pipes processed by extrusion and injection molded items are other important markets.

1.4.2 Styrenic polymers

Styrenic polymers include general purpose polystyrene, HIPS, expandable polystyrene, and styrene-acrylonitrile (SAN) and ABS copolymers. The mechanical properties of the general purpose polystyrene are mainly determined by its molecular weight ($\overline{M}_w = 150\,000\text{--}400\,000$). The strength and the resistance to heat distortion increase with increasing \overline{M}_w , but the melt viscosity increases making processing more difficult. Lubricants (e.g., butyl stearate) can be added to decrease viscosity, but they also lower the softening point of the polymer. Low viscosity (low \overline{M}_w) grades are used for injection molding whereas high \overline{M}_w grades are used for extrusion of films and sheets. During processing the melt polystyrene is forced through narrow nozzles and, because of the high shear, the polymer chains orientate parallel to the flow. Cooling is usually fast and the orientation is often maintained in the solid polymer leading to anisotropy in the properties [26].

The properties of the HIPS are mainly determined by its complex three-phase “salami” morphology (Figure 1.4) composed by rubbery polybutadiene cellular particles dispersed in a polystyrene matrix. The polybutadiene particles contain inclusions of polystyrene. The rubbery domains allow distribution of the stress concentration in a larger volume, toughening the material. Therefore, the impact resistance of HIPS is much higher than that of the general purpose polystyrene (PS). The properties of HIPS depend on polybutadiene content, particle size distribution and morphology, and degree of grafting of polybutadiene with polystyrene side chains. A drawback of the morphology is that transparency is reduced.

Expandable polystyrene is the raw material used to fabricate expanded polystyrene. It is produced in the form of small polystyrene beads (0.2–3 mm) and it is swollen with 4–7 wt% of blowing agent (e.g., pentane). Molded expanded polystyrene is manufactured

by the expansion and subsequent steam moldings of expandable polystyrene. The main markets are packaging, insulation, flotation and Geofoam (expanded PS used in geotechnical engineering applications such as slope stabilization). Most of the properties of the expanded polystyrene depend on the apparent density. Lower density leads to poorer mechanical properties and higher water absorption and permeation rates, whereas the thermal properties are not affected. Expandable polystyrene foams have applications in thermal insulation, impact soundproofing, formwork elements for concrete in the building industry, insulation of cold-storage depots and storage molded parts for packaging.

Acrylonitrile provides heat and chemical resistance, and barrier properties to SAN copolymers. Most of SAN is used in manufacturing ABS resins. ABS is a two-phase material in which poly(butadiene) is dispersed in a SAN matrix. Mechanical properties depend on the MWD of the matrix (e.g., higher molecular weights increase toughness), the poly(butadiene) content (toughness passes through a maximum), the particle size and particle size distribution, the degree of crosslinking of the rubber and the degree of grafting poly([acrylonitrile-co-styrene]-*graf*-polybutadiene). ABS is used in electrical and electronic equipment, house and office appliances and in the automotive industry.

1.4.3 *Poly(vinyl chloride)*

Poly(vinyl chloride) (PVC), is produced mainly by suspension polymerization. Lower amounts are produced by emulsion and bulk polymerization. The properties of the PVC are largely due to the bulky chloride atom that leads to an almost syndiotactic configuration. Neat PVC is intrinsically unstable because when subjected to heat, the molecular defects in some of the polymer chains initiate a self-accelerating dehydrochlorination reaction. In addition, PVC is a rigid material. Therefore, PVC is heavily compounded with heat stabilizers, lubricants, processing aids, plasticizers, impact modifiers and fillers. Immediately after polymerization, PVC is a particulate polymer. Particle morphology, in particular porosity, is a key characteristic because it determines the easiness of incorporation of the additives. PVC is used in construction (window frames, pipes, roofing, cable insulation), domestic goods (flooring, wallcoverings, shower curtains, leather cloth), packaging and clothing (waterproofs for fishermen and emergency services, life-jackets).

1.4.4 *Waterborne dispersed polymers*

Waterborne dispersed polymers include both synthetic polymer dispersions and natural rubber. Synthetic polymer dispersions are produced by emulsion polymerization. A substantial part of the synthetic polymer dispersions is commercialized as dry products; these include SBR for tires, nitrile rubbers, about 10% of the total PVC production, 75% of the total ABS and redispersable powders for construction materials. Carboxylated styrene-butadiene copolymers, acrylic and styrene-acrylic latexes and vinyl acetate homopolymer and copolymers are the main polymer classes commercialized as dispersions. The main markets for these dispersions are paints and coatings, paper coating, adhesives and carpet backing.

1.4.5 Polyesters and polyamides

Poly(ethylene terephthalate) (PET), and poly(butylene terephthalate) (PBT), are the main polyesters. PET is mainly produced by esterification of terephthalic acid with ethylene glycol. Transesterification of dimethyl terephthalate with butylene glycol is still the main process for the manufacture of PBT. PET and PBT are partially crystalline polymers. They have a high hardness and stiffness, good resistance to weathering and creep strength and high dimensional stability. Most of the PET is processed into fibers. Other applications are gastight bottles for carbonated beverages and highly stressed technical molded parts such as bearings, gear teeth, connectors, bolts, screws and washers. Typical applications of PBT are in automotive industry (headlight frames, wiper arms) as well as domestic appliances and the electrical and electronics industries.

Polyamides are polymers that contain the amide group ($-\text{CONH}-$). Proteins and synthetic nylons are polyamides. Nylon 6 produced by ring-opening polymerization of ϵ -caprolactam and Nylon 6,6 made from a diamine and a diacid each with six carbons are the main synthetic polyamides. Nylons are resistant to oils and solvents, and they present toughness, fatigue and abrasion resistance, low friction, stability at elevated temperatures, fire resistance, good appearance and good processability. These properties allow a wide range of applications, including transportation (main market), electrical and electronic applications (plugs, connectors, antenna mounting devices, wire and cable jacketing), consumer products (ski boots, kitchen utensils, lawn and garden equipment), appliances (laundry equipment and dishwashers) and power tools (handles and parts in contact with hot metal).

1.4.6 Thermosets

Thermosets are densely crosslinked polymers that do not melt upon heating. Polyurethanes, phenol-formaldehyde resins and epoxy resins are the main thermoset polymers.

Polyurethanes are polymers that contain the urethane group ($-\text{NH}-\text{CO}-\text{O}-$). They are produced by polyaddition of a di-isocyanate and a diol. Because of the many different monomers that can be used in their synthesis, widely different products are manufactured [27]. They include highly elastic foams (mattresses, car seats), rigid foams (insulation materials); rigid and flexible moldings with compact skins (window frames, housings, skis, steering wheels, shoe soles), films, hoses, blow-molded parts, roller coatings, sealants, grouting compounds, surfacings for sport and play areas, windsurfer equipment, hydrocyclones, fenders, printing rollers, cable sheathing, catheters, high-quality paints, corrosion protection for steel-reinforced concrete, adhesives, textile coatings, high-gloss paper coatings, leather finishes, poromerics, glass fiber sizes and wool finishing agents.

Phenol-formaldehyde resins include novolacs and resols. Novolacs are mostly linear polymers with little branching produced under acidic conditions with an excess of phenol. They are processed with curing agents (e.g., hexamethylenetetramine) to give crosslinked products. Novolacs find application in textile felts, coatings and grinding wheels. Resols are highly branched polymers produced under basic conditions with an excess of formaldehyde. Resols do not require curing agents to crosslink and are used as binders in applications such as plywood bonding, foundry sand binding and glass fibre insulation.

Epoxy resins are prepolymers that contain epoxide groups. They are mainly produced by reaction of epichlorohydrin and bisphenol A in the presence of a caustic soda solution. A large excess of epichlorohydrin is used and hence epoxide-terminated prepolymers are obtained. The prepolymers are cured using multifunctional curing agents (e.g., polyamines and dicarboxylic acid anhydrides). They are used as coatings (primers – a coating applied to a surface in preparation for a finishing coating, and high-performance, non-decorative, industrial and marine coatings) and for structural applications (fiber-reinforced composites and electrical laminates; casting, encapsulation and tooling; and adhesives).

1.5 Polymerization reactors

Table 1.6 summarizes the reactors used in polymer manufacture. Stirred-tank reactors, tubular reactors, loop reactors and fluidized bed reactors are used commercially. In addition, polymerization in molds allows the production of large polymer structures.

The type of reactor is largely determined by the polymerization technique and by the polymerization class. Thus, batch stirred-tank reactors are used for processes in which mixing/agitation is important, control of the copolymer composition is not an issue and the thermal control of the process is relatively easy. Suspension homopolymerization is a good example of such a process because agitation is critical to control the particle size, which is a key characteristic, and because of the low viscosity and the presence of a high heat capacity continuous medium (water), the thermal control is easy. Expandable polystyrene and PVC are produced by means of batch suspension polymerization [22]. The production of fluorinated latexes by emulsion copolymerization of fluorinated acrylates and long-chain acrylates is also carried out in batch processes because the similarity of the reactivity ratios avoids any substantial composition drift, and the heat of polymerization per unit mass is relatively low due to the high molecular weight of the monomers.

Semibatch stirred-tank reactors are extensively used when fine-tuning of the molecular and morphological characteristics of the polymer is required, when the thermal control of the reactor requires some attention and when a large portfolio of different products should be produced in the same reactor. Most of the emulsion polymers commercialized for paper coating, paints, adhesives, additives for leather, textiles, impact modifiers and additives for construction materials are produced in semibatch stirred-tank reactors [28] with sizes ranging from 10 to 60 m³.

Continuous stirred-tank reactors (CSTRs) are used for large productions of a reduced number of polymer grades. Coordination catalysts are used in the production of LLDPE by solution polymerization (Dowlex, DSM Compact process [29]), of HDPE in slurry (Mitsui CX-process [30]) and of polypropylene in stirred bed gas phase reactors (BP process [22], Novolen process [31]). LDPE and ethylene-vinyl acetate copolymers (EVA) are produced by free-radical polymerization in bulk in a continuous autoclave reactor [30]. A substantial fraction of the SBR used for tires is produced by coagulating the SBR latex produced by emulsion polymerization in a battery of about 10 CSTRs in series [32]. The CSTRs are characterized by a broad residence time distribution, which affects to product properties. For example, latexes with narrow particle size distribution cannot be produced in CSTRs.

Table 1.6 Reactors used for polymer manufacture

Reactor	Operation mode	Polymerization mechanism	Polymerization technique	Examples
Stirred tank reactor	Batch	Free-radical	Suspension	Expanded polystyrene Poly(vinyl chloride) Fluorinated polymers
	Semibatch	Free-radical	Emulsion	Carboxylated styrene-butadiene; Acrylic latexes Vinyl acetate latexes
	Continuous	Coordination polymerization	Solution Slurry Gas phase	LLDPE HDPE Polypropylene
Tubular reactor	Continuous	Free-radical	Bulk Emulsion	LDPE, EVA SBR
	Continuous	Free-radical	Bulk	LDPE
		Step-growth	Bulk	Polystyrene HIPS Nylon 6,6 Nylon 6

Tubular reactor with impeller/agitation and head space	Continuous	Step-growth	Bulk	Poly(ethylene terephthalate)
				Polycarbonate
Loop reactor	Continuous	Coordination	Slurry	HDPE i-PP
		Free-radical	Gas phase Emulsion	Bimodal LLDPE Vinyl acetate-Veova 10 and vinyl acetate-ethylene copolymers
Fluidized bed	Continuous	Coordination	Gas phase	i-PP HIPP
				LLDPE, HDPE
Mold	Batch	Free-radical	Bulk	Poly(methyl methacrylate)
		Step-growth	Reaction injection molding	Polyurethane

Tubular reactors have a large heat removal surface area/volume ratio and therefore they are well suited for conducting bulk polymerizations. LDPE and EVA copolymers are produced by free-radical polymerization in tubular reactors [22]. Because of the narrow residence time distribution of the tubular reactors, the level of branches of the LDPE produced in these reactors is lower than that of the LDPE produced in the continuous autoclave. HIPS is produced by free-radical polymerization in a reactor system including a CSTR prepolymerizer and a tubular polymerization reactor [22]. Tubular reactors are also employed to manufacture Nylon 6 and Nylon 6,6 [33]. The production of these polymers involves polycondensation reactions. Therefore, high conversions are needed in order to obtain high molecular weights, and hence the equilibrium should be shifted forward by removing the byproduct (water in this case). In the production of Nylon 6,6, a two-phase flow coiled tubular reactor of increasing diameter is used. The nylon melt moves along the wall in laminar flow, whereas the water escapes through a fast-moving core. Nylon 6 is produced in a VK-tube that includes two reaction zones. The top reaction zone is a continuously stirred-tank reactor with a built-in evaporator. This is the zone where the reaction is initialized and the water content, which is important for the achievement of a certain degree of polymerization, is adjusted. The middle and the lower part of the VK-tube are built as a tubular reactor.

The production of poly(ethylene terephthalate) [33] and polycarbonate [34] (from diphenylcarbonate and bisphenol A) is carried out in partially filled tubular reactors. Vacuum is applied to remove the byproduct and to achieve high molecular weights. Special agitation devices are needed to move forward the polymer melt and to favor mass transfer from the melt to the headspace. Some common agitation equipments are [33]:

- (1) interfacial surface generators,
- (2) mechanically agitated thin film contactors and
- (3) partially filled screw extruders.

Loop reactors combine the thermal characteristics of the tubular reactors with the residence time distribution of the CSTRs. HDPE and i-PP are produced in loop reactors using coordination catalysts by means of slurry polymerization [22]. HDPE uses isobutane as continuous phase (Chevron–Phillips process) and i-PP uses the monomer as continuous phase (Spheripol process).

Fluidized bed reactors are used for the gas phase polymerization of olefins to produce LLDPE and HDPE (Unipol PE, Innovene and Spherilene processes [22]) as well as for the manufacture of polypropylene (Unipol PP process [22]). The residence time distribution of a fluidized bed reactor is close to that of a well mixed continuous reactor. Therefore, the use of a single fluidized bed reactor leads to a broad particle size distribution and to large variations in the catalyst productivity from particle to particle. The use of two fluidized bed reactors in series narrows the residence time distribution leading to a more uniform product.

A combination of different reactors is frequently used to produce polymers with special molecular and morphological characteristics. For example, polyolefins with a bimodal MWD that combine good mechanical properties (provided by the high molecular weight mode) with a good processing behavior (low melt viscosity provided by the low molecular weight mode) are produced in a combination of a loop reactor and a fluidized

bed reactor [25]. The low molecular weights are produced in the loop reactor in a slurry of propane, and the gas phase fluidized bed reactor produces the high molecular weight polymers. Product properties may also be influenced by modifying the polymer microstructure by incorporating different comonomers in each reactor.

The use of two reactors to produce bimodal MWD inevitably leads to some degree of segregation between the polymers produced in each reactor. A complex gas phase loop reactor has been developed recently for the production of intimate blends of different polymers [35]. This reactor has two distinct reaction zones in which the reaction conditions are different. The polymer particles alternatively circulate through these reaction zones yielding an intimate blend of two different polymers.

HIPP presents a complex morphology consisting of an ethylene-propylene soft copolymer finely dispersed within a semi-crystalline i-PP. In the Spheripol process [22], this material is produced in two steps. In the first one, i-PP is produced in a slurry of propylene in a loop reactor. In the second one, the ethylene-propylene copolymer is produced in a gas phase reactor. The broad residence time distribution of both the loop reactor and the gas phase reactor leads to an uneven distribution of the ethylene-propylene copolymer among the polymer particles, when single reactors are used in each step. A more even distribution is obtained using two loop reactors in the first step [36, 37].

Some special objects are produced by polymerizing the monomers in a mold. Thus, high-quality acrylic glass is produced by cast molding. A pre-polymerized monomer-polymer solution is introduced in the mold avoiding the formation of bubbles. The edges of the mold are made of a flexible material so that the shrinkage occurring during polymerization does not detach the acrylic sheet from the glass plates. Acrylic sheets with thicknesses between a few millimeters and up to about 30 cm are produced [38]. Polyurethane objects are produced by injection reaction molding. In this process, two highly reactive monomers or prepolymers are injected into the mold where they react in batch [33]. Mixing and the adequate dosage of the reactants are critical to achieve high molecular weights.

References

1. Del Duca, D. and Moore, E.P. (1996) In E.P. Moore (ed.), *Polypropylene Handbook*. Hanser Publishers, Munich, p. 243.
2. Van der Ven, S. (1990) *Polypropylene and Other Polyolefins*. Elsevier, Amsterdam, p. 489.
3. Zhang, X.B., Li, Z.S., Lu, Z.Y. and Sun, C.C. (2002) *Macromolecules*, **40**, 1737–1744.
4. Bogdanov, B.G. and Michailov, M. (1993) In C. Vasile and R.B. Seymour (eds), *Handbook of Polyolefins*. Marcel Dekker, New York, pp. 295–469.
5. Okamoto, Y., Miyagi, H., Kakugo, M. and Takahashi, K. (1991) *Macromolecules*, **24**, 5639–5644.
6. Progelhof, R.C. and Throne, J.L. (1993) *Polymer Engineering Principles*. Hanser Publishers, Munich.
7. McCrum, N.G., Buckley, C.P. and Bucknall, C.B. (1988) *Principles of Polymer Engineering*. Oxford Science Publications, Oxford.
8. Elias, H.G. (1997) *An Introduction to Polymer Science*. VCH, Weinheim.
9. Mülhaupt, R. (2003) *Macromol. Chem. Phys.*, **204**, 289–327.
10. Galli, P. and Vecellio, G. (2004) *J. Polym. Sci., Part A: Polym. Chem.*, **42**, 396–415.
11. Langsam, M. (1986) In L.I. Nass and C.A. Heiberger (eds), *Encyclopedia of PVD*, Vol 1, 2nd edn. Marcel Dekker, New York.

12. Brandrup, J., Immergut, E.H. and Grulke, E.A. (eds) (1999) *Polymer Handbook*. Wiley-Interscience, Hoboken, New Jersey.
13. Moad, G., Rizzardo, E. and Salomon, D.H. (1982) *Polym. Bull.*, **6**, 589–593.
14. Gaynor, S., Greszta, D., Shigemoto, T., Mardare, D. and Matyjaszewski, K. (1995) *Macromol. Symp.*, **98**, 73–89.
15. Krstina, J., Moad, G., Rizzardo, E., Winzor, C.L., Berge, C.T. and Fryd, M. (1995) *Macromolecules*, **28**, 5381–5385.
16. Matyjaszewski, K. (2000) In K. Matyjaszewski (ed.), *Controlled/Living Radical Polymerization. Progress in ATRP, NMP, and RAFT*. *ACS Symp. Ser.*, **768**, 2–26.
17. Hadjichristidis, N., Pitsikalis, M., Pispas, S. and Iatrou, H. (2001) *Chem. Rev.*, **101**, 3747–3792.
18. Russell, K.E. and Wilson, G.J. (1977) In C.E. Schildknecht and I. Skeist (eds), *Polymerization Processes*. Wiley-Interscience, Hoboken, New Jersey, pp. 306–336.
19. Debling, J.A., Han, G.C., Kuijpers, F., VerBurg, J., Zacca, J. and Ray, W.H. (1994) *AIChE J.*, **40**, 506–520.
20. Pohlemann, H.G. and Echte, A. (1981) In G.A. Stahl (ed.), *Polymer Science Overview*. *ACS Symp. Ser.*, **175**, 265–287.
21. Urban, D. and Takamura, K. (eds) (2002) *Polymer Dispersions and their Industrial Applications*. Wiley-VCH Verlag GmbH, Weinheim.
22. Petrochemical processes (2003). *Hydrocarbon Processing* 2003, March, 71–134.
23. (2005) Facts and figures for the chemical industry. *Chem. Engng News*, 11 July, 41–76.
24. Kiparissides, C., Verros, G. and MacGregor, J.F. (1993) *J.M.S.-Rev. Macromol. Chem. Phys.*, **C33**(4), 437–527.
25. Avela, A., Karling, R. and Takakarhu, J. (1998) *Dechema Monographs*, **134**, 3–22.
26. Maul, J., Frushour, B.G., Kontoff, J.R., Eichenauer, H. and Ott, K.H. (2002). In H. Pelc (ed.) *Ullmann's Encyclopedia of Industrial Chemistry*, 6th edn. Wiley-VCH Verlag GmbH, Weinheim.
27. Dieterich, D. and Uhling, K. (2002). In *Ullmann's Encyclopedia of Industrial Chemistry*, 6th edn. Wiley-VCH Verlag GmbH, Weinheim.
28. Poehlein, G.W. (1997) In J.M. Asua (ed.) *Polymeric Dispersions. Principles and Applications*. Kluwer Academic Publishers, Dordrecht, pp. 305–331.
29. Petrochemical processes 1999. *Hydrocarbon Processing* 1999, March, 87–158.
30. Petrochemical processes 2001. *Hydrocarbon Processing* 2001, March, 71–146.
31. Schmidt, C.U., Kersting, M., Hungenberg, K.D., Weiss, H., Olbert, G., Böttcher, G., Sollacher, R. and Linzenkirchner, E. (1998) *Dechema Monographs*, **134**, 23–33.
32. Agnely, M. (2006) In J.C. Daniel and C. Pichot (eds), *Les Latex Synthétiques*. Lavoisier, Paris, pp. 417–443.
33. Gupta, S.K. and Kumar, A. (1987) *Reaction Engineering of Step-Growth Polymerization*. Plenum Press, New York.
34. Woo, B.G., Choi, K.Y. and Song, K.H. (2001) *Ind. Engng Chem. Res.*, **40**, 3459–3466.
35. Covezzi, M. and Mei, G. (2001) *Chem. Engng Sci.*, **56**, 4059–4067.
36. Debling, J.A., Zacca, J.J. and Ray, W.H. (1997) *Chem. Engng Sci.*, **52**, 1969–2001.
37. Urdampilleta, I., González, A., Iruin, J.J., de la Cal, J.C. and Asua, J.M. (2006) *Ind. Engng Chem. Res.*, **45**, 4178–4187.
38. Schildknecht, C.E. (1977) In C.E. Schildknecht and I. Skeist (eds), *Polymerization Processes*. Wiley-Interscience, Hoboken, New Jersey, pp. 36–67.

Chapter 2

Coordination Polymerization

João B.P. Soares, Timothy McKenna and C.P. Cheng

Polyethylene and polypropylene are ubiquitous commodity plastics found in applications varying from household items such as grocery bags, containers, toys and appliance housings, to high-tech products such as engineering plastics, automotive parts, medical appliances and even prosthetic implants. They can be either amorphous or highly crystalline, and behave as thermoplastics, thermoplastic elastomers or thermosets.

Despite their versatility, both polyethylene and polypropylene are made only of carbon and hydrogen atoms. We are so used to these remarkable plastics that we do not often stop to ask how materials made out of such simple building blocks can have this extraordinary range of properties and applications. The answer to this question lies on how the carbon and hydrogen atoms are connected to define the molecular architecture or microstructure of polyolefins. Because microstructure plays such a relevant role in polyolefin properties, several characterization techniques have been specifically developed to measure different aspects of their molecular architectures. Section 2.1 classifies the different types of commercial polyolefins according to their microstructures, discusses several microstructural characterization techniques developed for these polymers, and demonstrates how they are essential to understand polyolefins.

At the heart of all polyolefin manufacturing processes is the system used to initiate polymer chain growth. For industrial applications, polyethylene can be made with either free-radical initiators or coordination catalysts, while polypropylene can be produced only with coordination catalysts. When the polymerization of ethylene is initiated with free-radical initiators, low-density polyethylene (LDPE) is obtained. The microstructure and properties of LDPE are different from those of any polyethylene made with coordination catalysts; LDPE is one of the topics of Chapter 3 and will not be described in detail here. Coordination catalysts (Phillips, Ziegler–Natta, metallocene and late-transition metal catalysts) provide a much more versatile way to synthesize polyolefin chains with controlled molecular architectures. It can be said, without fear of exaggeration, that catalyst design is the key to the success of any industrial process for olefin polymerization with coordination catalysts. This is because the catalyst ultimately determines how the monomers will be linked in the polymer chain, effectively defining polymer microstructure and properties. Research, both industrial and academic, on olefin polymerization catalysis has been very dynamic since the 1950s, with many catalyst families being developed and optimized at a rapid pace. Section 2.2 gives a brief overview of this fascinating and very extensive subject and also introduces the mechanism of polymerization with coordination catalysts.

Even though the catalyst is the crucial component determining polyolefin microstructure, we should not prematurely assume that, once the catalyst is selected, all our problems are

solved and we have few degrees of freedom left to control polymer microstructure. Nothing would be farther from reality: it is at this moment that a sound knowledge on polymer reaction engineering comes into play to use the catalyst to its fullest potential. Several phenomena are included under the wide umbrella of polyolefin reaction engineering: polymerization kinetics, inter- and intraparticle mass and heat transfer resistances, and reactor micro- and macromixing are all essential topics for the design, operation, optimization and control of polyolefin reactors.

Section 2.3 describes phenomenological models for polymerization kinetics with coordination catalysts. Molar and population balances will be derived using what we like to call the standard model for olefin polymerization kinetics with coordination catalysts. Also how molecular weight averages can be modeled in batch, semibatch and continuous reactors are shown using the method of moments and the method of instantaneous distributions. Unfortunately, the kinetics of olefin polymerization is complicated by several factors that are not included in the standard model; some of these effects and possible solutions and model extensions are mentioned briefly at the end of Section 2.2.

Even though a few processes for ethylene polymerization use homogeneous catalysts, most olefin polymerization processes operate with heterogeneous catalysts. This creates an additional level of complexity, since there is the possibility of inter- and intraparticle mass and heat transfer resistances during polymerization. If significant, mass and heat transfer limitations create non-uniform polymerization conditions within the catalyst particle and non-uniform polymerization conditions lead to non-uniform polymer microstructures. Many other challenging problems arise when heterogeneous catalysts are used for olefin polymerization, such as catalyst particle break-up, growth and morphological development. The most relevant aspects of the vast and rich literature on this subject are explained in Section 2.4.

Finally, there are several different industrial technologies for olefin polymerization. At the heart of the process is the polymerization reactor, and there are many of them. Olefins are the only monomers that are polymerized in so many types of reactor configurations, including stirred-tank autoclaves, single- and double-loop reactors, tubular reactors, fluidized-bed and conveying-bed reactors. These processes may be run in solution, slurry, bulk or gas phase. Because of such a wide range of polymerization processes and reactor configurations, this field is a polymer reactor engineer's dream come true. Industrial processes for olefin polymerization are the subject of Section 2.5.

In summary, the apparent simplicity of your everyday polyethylene and polypropylene consumer goods is deceptive. Few industrial polymers can claim such richness in catalyst types, reactor configurations and microstructural complexity. In this chapter, we will explain how, from such simple monomers, polyolefins have become the dominant commodity plastic in the 21st century.

2.1 Polyolefin types: microstructural classification and analytical techniques

Polyethylene and polypropylene resins are the only two types of polyolefins produced commercially. Polyethylenes will be discussed first and then polypropylenes.

2.1.1 Polyethylene types

Polyethylene resins are classified in three main types: low-density polyethylene (LDPE), linear low-density polyethylene (LLDPE) and high-density polyethylene (HDPE). The traditional classification distinguishes each polyethylene type according to its density range: approximately $0.915\text{--}0.935\text{ g cm}^{-3}$ for LDPE, $0.915\text{--}0.94\text{ g cm}^{-3}$ for LLDPE and $0.945\text{--}0.97\text{ g cm}^{-3}$ for HDPE. Lower density polyethylene resins ($<0.915\text{ g cm}^{-3}$) are sometimes called very low-density (VLDPE) or ultra low-density polyethylene (ULDPE). HDPE with molecular weight averages of several millions is called ultra-high molecular weight polyethylene (UHMWPE). This classification according to the density and molecular weight of polyethylene, although standard for commercial resins, tells us little about their microstructures. A more comprehensive classification, based on their microstructural characteristics, is presented in Figure 2.1. To reduce the number of acronyms in this chapter, we will group LLDPE, VLDPE and ULDPE under the generic term LLDPE and make no distinction between HDPE and UHMWPE; from a structural point of view, these resins are very similar, as will be seen below.

HDPE and LLDPE are made with coordination polymerization catalysts, while LDPE is made with free-radical initiators. The main difference between LDPE and the other polyethylene types is that LDPE has both long- and short-chain branches (LCB and SCB), while the resins made by coordination polymerization have only SCBs. There is only one exception to this rule: polyolefins made with some metallocene catalysts may also have significant number of LCBs, but their branching structure is completely distinct from that of LDPE resins. Most commercial HDPE and LLDPE resins are made with heterogeneous Ziegler–Natta catalysts. Phillips catalysts are very important for the production of HDPE, but are not used for LLDPE manufacture. Metallocenes can make both HDPE and LLDPE, but metallocene resins are very different from the ones made with either Ziegler–Natta or Phillips catalysts, as will be explained below. The market share of metallocene resins is still small, but has been increasing steadily since the 1990s. Resins made with late transition metal catalysts have had no commercial applications to date and will not be discussed any longer in this section.

The mechanism of branch formation in LDPE, as described in detail in Chapter 3, is different from that in coordination polymerization; in LDPE, LCBs are formed by transfer

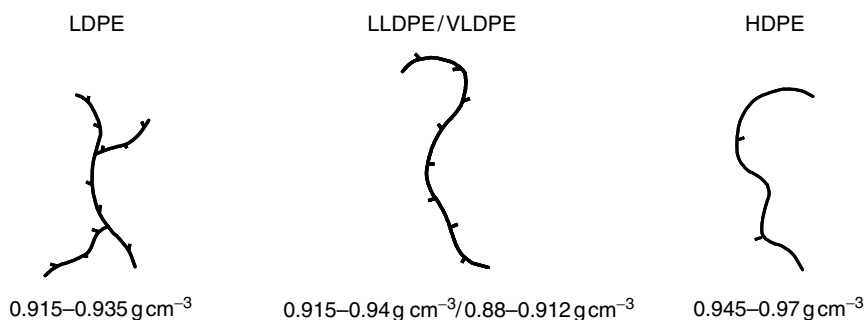


Figure 2.1 Classification of polyethylenes according to branching structure and density.

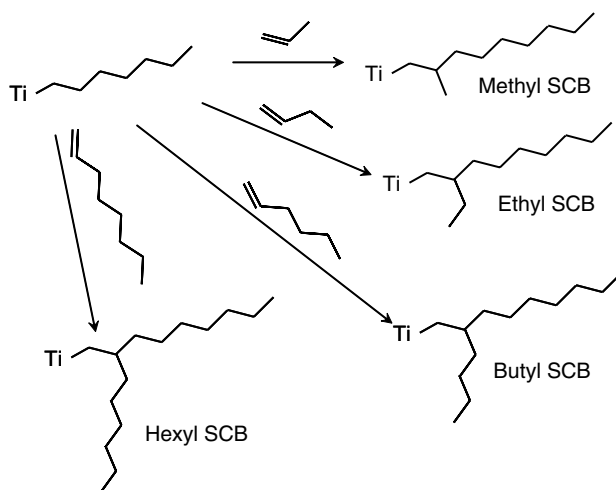


Figure 2.2 Mechanism of short-chain branch (SCB) formation with coordination polymerization. The chains are shown growing on a titanium active site.

to polymer, while SCBs are generated by back-biting reactions. Contrarily, SCBs in HDPE and LLDPE are produced by the copolymerization of α -olefins added to the reactor as comonomers, typically propylene, 1-butene, 1-hexene or 1-octene. LCBs, when present in coordination polymerization resins, are also formed by copolymerization reactions, albeit of a different type. The discussion of LCB formation with coordination catalysts will be postponed to Section 2.2.

A SCB is formed in the polymer backbone when an α -olefin is copolymerized with ethylene, as illustrated in Figure 2.2. From a crystallization point of view, the SCB behaves as a defect on the polymer chain, decreasing polymer density, crystallite size and melting temperature. Therefore, the higher the molar fraction of α -olefin in the polymer chain, the lower its crystallinity. HDPE resins have very low α -olefin comonomer fractions (typically below 1%), while the comonomer content increases from LLDPE to VLDPE and ULDPE. In addition, for the same comonomer molar fraction, the density and melting points of an ethylene/ α -olefin copolymer generally decrease in the order propylene > 1-butene > 1-hexene > 1-octene. Shorter SCBs, such as methyl branches formed when propylene is copolymerized with ethylene, can be partially incorporated into the crystallite and therefore are less effective in decreasing the melting point of the copolymer. This cocrystallization phenomenon is less likely to occur as the size of the SCB increases from methyl to hexyl.

Density is, therefore, a reflection of the α -olefin molar fraction in the polyolefin chain. Is this all there is to say about polyethylene resin classification? Hardly. The microstructure of commercial polyethylenes is much more complex than Figures 2.1 and 2.2 may make us believe. Let us ignore, for now, the molecular weight distribution (MWD) and focus on the chemical composition distribution (CCD) of LLDPEs, that is, the distribution of the α -olefin fraction in the polymer chains. Most commercial LLDPEs are made using heterogeneous Ziegler–Natta catalysts. These catalysts have more than one type of active site, each one producing polymer chains with different average comonomer fractions and molecular weights. As a consequence, when their CCDs are measured, it is found that

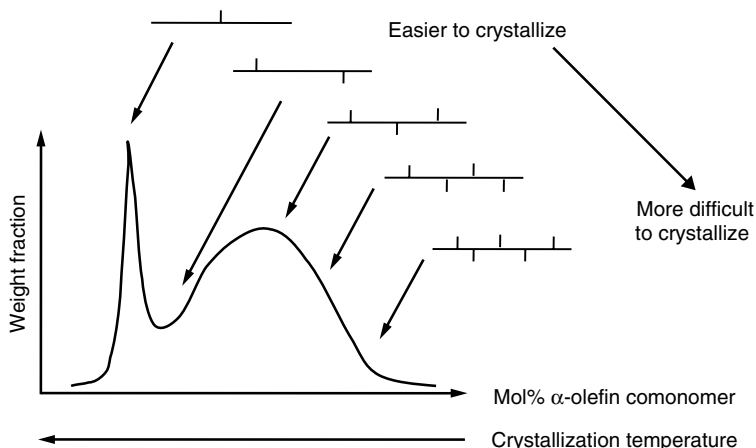


Figure 2.3 Generic CCD of a LLDPE resin made with a heterogeneous Ziegler–Natta catalyst. Chains with more SCBs have lower crystallization temperatures than chains with fewer SCBs.

they are rather broad and bimodal, as illustrated in Figure 2.3. A bimodal CCD is, in fact, the fingerprint of LLDPE resins made with heterogeneous Ziegler–Natta catalysts.

Two distinct regions can be easily identified in Figure 2.3: a sharp high-crystallinity peak (low α -olefin fraction) and a broad low-crystallinity peak (high α -olefin fraction). These two regions are associated with at least two types of active sites, one with a much lower reactivity ratio toward incorporation of α -olefin than the other. As the relative fractions of polymer under these two modes is varied, we go from HDPE – with a unimodal, high-crystallinity peak and sometimes a small, lower crystallinity tail – to LLDPE, VLDPE and ULDPPE resins, having a very pronounced lower crystallinity peak, which may, sometimes, show additional peaks.

From our discussion of Figure 2.3, it is apparent that classifying these non-uniform polymers according to a single density value is a highly inadequate practice. The picture becomes even more complex when we take a simultaneous look at the MWD and CCD of LLDPEs. Figure 2.4 shows how the weight-average molecular weight of a LLDPE resin varies as a function of comonomer content in the chains. The trend illustrated in Figure 2.4 is typical for all conventional polyethylene resins made with heterogeneous Ziegler–Natta catalysts: site types that make chains with lower average comonomer fraction also make them with higher average molecular weights and *vice versa*. This interdependency between average molecular weight and comonomer fraction is another fingerprint of heterogeneous Ziegler–Natta polyolefin resins. It will be shown later how this trend is partially reversed for some polyethylene resins by the ingenious use of polymer reaction engineering principles.

Figure 2.5 depicts the bivariate distribution of molecular weight and chemical composition of another LLDPE resin. This rather appealing tri-dimensional plot summarizes the complexity inherent to most commercial polyolefin resins. It also shows that microstructural characterization techniques, such as the ones used to generate Figures 2.4 and 2.5, are indispensable tools to understand polyolefins. The most important techniques for polyolefin microstructural characterization will be reviewed later in this section.

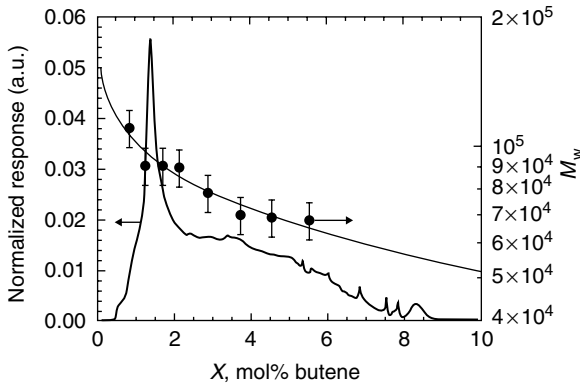


Figure 2.4 Relation between weight-average molecular weight (M_w) and 1-butene molar fraction in a typical ethylene/1-butene LLDPE resin made with a heterogeneous Ziegler–Natta catalyst. The CCD was measured with TREF and the M_w was determined by on-line laser light scattering [1].

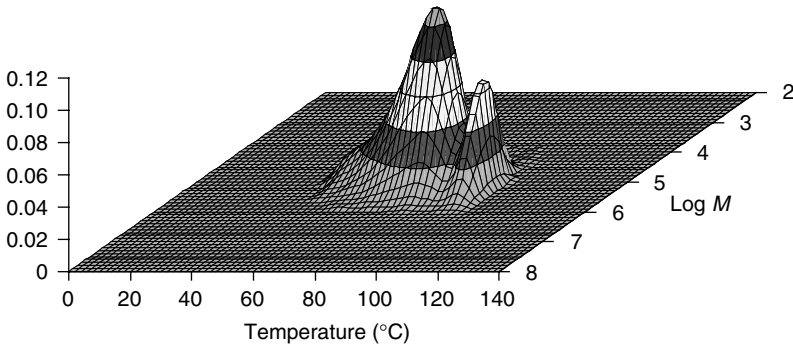


Figure 2.5 MWD and CCD (expressed as a distribution of elution temperatures) of a LLDPE measured by CFC-300. (Courtesy of Polymer Char.)

The $MWD \times CCD$ correlation exemplified in Figures 2.4 and 2.5 is not desirable for certain applications. A notable example is bimodal pipe resins, where much better mechanical and rheological properties are achieved if the higher molecular weight component has a higher α -olefin fraction than the lower molecular weight component. The reasons for this improved performance are related to the presence of tie molecules, a fascinating subject that is, unfortunately, beyond the scope of this chapter. The reader is directed to the references 2 and 3 at the end of this chapter for more information on this subject.

How can we reverse the natural $MWD \times CCD$ correlation observed in all heterogeneous Ziegler–Natta catalysts? This is done industrially by using at least two reactors in series (*tandem reactor process*). The first reactor in the series is used to produce low molecular weight HDPE in the absence of α -olefin or under very low α -olefin concentration. A high concentration of hydrogen (hydrogen is the standard chain transfer agent in olefin polymerization) is used in the first reactor to ensure that the polymer has low molecular weight. This polymer is then transferred continuously to the second reactor. The second reactor

is operated under high α -olefin concentration in the absence (or under a much lower concentration) of hydrogen, thus producing a LLDPE component with higher average molecular weight than the HDPE component made in the first reactor. Many polyethylene manufacturing process configurations include two reactors in series, as described in Section 2.5.

The advent of metallocene catalysts added an entirely new dimension to commercial polyolefin resins. Metallocene catalysts make polyolefins with rather different microstructures from the ones made with Ziegler–Natta and Phillips catalysts, but are still classified loosely as HDPE and LLDPE. Care needs to be taken, however, to distinguish between resins made with Ziegler–Natta and Phillips catalysts on one hand, and metallocenes on the other. Polyethylenes made with metallocene catalysts have a much more uniform microstructure than the ones made with heterogeneous Ziegler–Natta catalysts. Metallocenes are considered single-site catalysts because, under several polymerization conditions, they can make polyolefins with narrow MWD and CCD. Figure 2.6 shows the CCDs of several metallocene polyethylene resins (as measured by crystallization analysis fractionation, Crystaf) with different molar fractions of 1-hexene (more details on Crystaf fractionation will be given later in this section). For now, one can interpret the curves in Figure 2.6 as a reflection of the α -olefin fraction on the polymer chains: chains with higher α -olefin fraction have Crystaf profiles with lower peak temperatures, while chains with lower α -olefin fraction have Crystaf profiles with higher peak temperatures. Notice the uniform incorporation of 1-hexene and the absence of the high crystallinity peak always present in LLDPE resins made with heterogeneous Ziegler–Natta catalysts. In addition, the molecular weight averages of polyolefins made with metallocene catalysts are independent of their CCD.

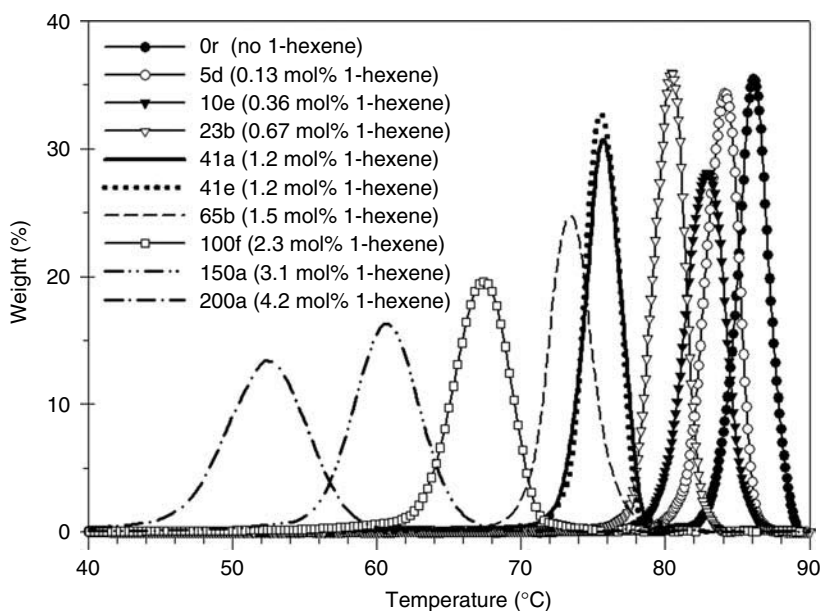


Figure 2.6 CCDs of ethylene/1-hexene copolymers made with a metallocene catalyst [4].

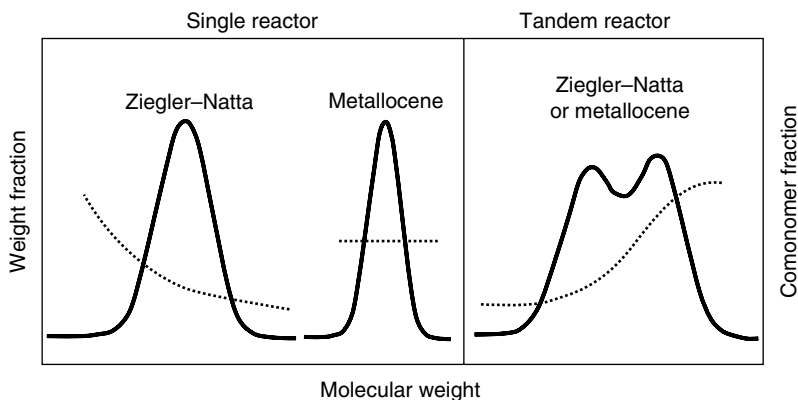


Figure 2.7 A graphical summary of the different types of commercial polyethylene resins made with Ziegler–Natta and metallocene catalysts. MWDs are shown as solid lines and α -olefin comonomer fractions are depicted as dotted lines.

From a polymer reaction engineering point of view, polyolefins made with metallocene catalysts provide an excellent opportunity for model development because they have “well-behaved” microstructures. Later it will be shown that models developed for single-site catalysts can also be extended to describe the more complex microstructures of polyolefins made with multiple-site catalysts such as Ziegler–Natta and Phillips catalysts.

Figure 2.7, showing schematic MWDs of the three main types of commercial polyethylenes, together with their comonomer fractions as a function of molecular weight, illustrates well the diversity of polyethylene resins available today.

2.1.2 Polypropylene types

There are three types of commercial polypropylene resins: isotactic polypropylene, random copolymer and impact copolymer. Both copolymer types use ethylene as comonomer, but otherwise differ significantly.

Because propylene is an asymmetrical monomer, polypropylene can be produced with different stereochemical configurations. The most common types of polypropylene are isotactic, syndiotactic and atactic. In isotactic polypropylene, the methyl groups are placed on the same side of the backbone; in syndiotactic polypropylene they alternate sides; in atactic polypropylene they are arranged randomly along the chain (Figure 2.8). Atactic polypropylene is amorphous and has little commercial value. Both isotactic and syndiotactic polypropylene are semi-crystalline polymers with high melting temperatures. Isotactic polypropylene dominates the market, because it is easily produced with heterogeneous Ziegler–Natta and metallocene catalysts; syndiotactic polypropylene can be produced only with some metallocene catalysts and has not found wide commercial application as yet.

Ziegler–Natta catalysts used for propylene polymerization make mostly isotactic polypropylene with a very small fraction of atactic polypropylene, especially later generation catalysts. Aspecific sites are responsible for the formation of atactic chains in Ziegler–Natta

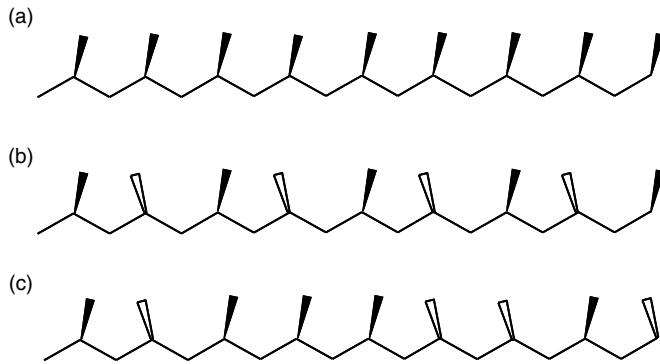


Figure 2.8 Stereo- and regioregularity in polypropylene: (a) isotactic polypropylene; (b) syndiotactic polypropylene and (c) atactic polypropylene.

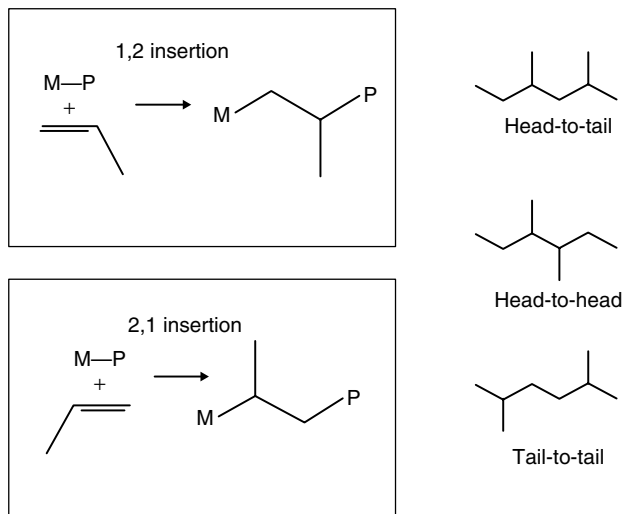


Figure 2.9 Regioregularity in polypropylene polymerization.

catalysts. Many years of catalyst development were required to minimize the fraction of these catalyst sites.

Ziegler–Natta catalysts also make chains with very high regioregularity, favoring 1,2 insertions (Figure 2.9) and head-to-tail enchainment. Regiodefects, such as a 2,1 insertion following a 1,2 insertion, create irregularities along the polymer chain, decreasing its crystallinity and melting temperature. Metallocene catalysts often produce polypropylenes that have very high isotacticity but lower regioregularity and, therefore, have lower melting temperatures than resins made with Ziegler–Natta catalysts. Metallocene catalysts can also make polypropylenes with other unusual stereostructures such as atactic–isotactic block chains, but these products have not found commercial applications yet [5].

Random propylene–ethylene copolymers are produced for applications requiring polymers with lower crystallinity and melting points. Random polypropylene copolymers have,

for instance, higher impact resistance, clarity and flexibility, and decreased haze than homopolymer resins. In these copolymers, propylene is the dominant monomer.

High-impact copolymers (sometimes erroneously called block copolymers) are a more interesting product. They are produced using at least two reactors in series with heterogeneous Ziegler–Natta catalysts or supported metallocenes. The first reactor is used to make isotactic polypropylene; the second reactor produces a fraction of amorphous or very low crystallinity propylene–ethylene copolymer. The amorphous copolymer phase is intimately dispersed in the homopolymer phase, even though the two phases are immiscible. The copolymer phase dissipates energy during impact, greatly increasing the impact resistance of these resins. Several processes have been designed to produce impact polypropylene of high quality, as described in Section 2.5.

The reactor residence time distribution plays an important role in the distribution of the homopolymer and copolymer phases in impact copolymers. It will help the following discussion if each polymer particle (composed of the heterogeneous Ziegler–Natta catalyst surrounded by the polymer produced in the reactor – see Section 2.4 for more details) is visualized as a microreactor itself. The longer each microreactor particle stays in the reactor, the more it grows due to polymer formation over the catalyst sites. Ideally, there should be an optimum ratio of homopolymer to copolymer fractions in each polymer particle exiting the second reactor to guarantee the best impact properties. However, if two continuous stirred-tank reactors (CSTRs) in series are used to produce the impact copolymer, unavoidably there will be a wide distribution for the homopolymer/copolymer ratio in the polymer particles, caused by the exponential residence time distribution of CSTRs, as indicated in Figure 2.10. On the other hand, if two tubular plug flow reactors (PFRs) were used, every polymer particle would have exactly the same homopolymer/copolymer ratio, since the residence times of all polymer particles inside PFRs are the same.

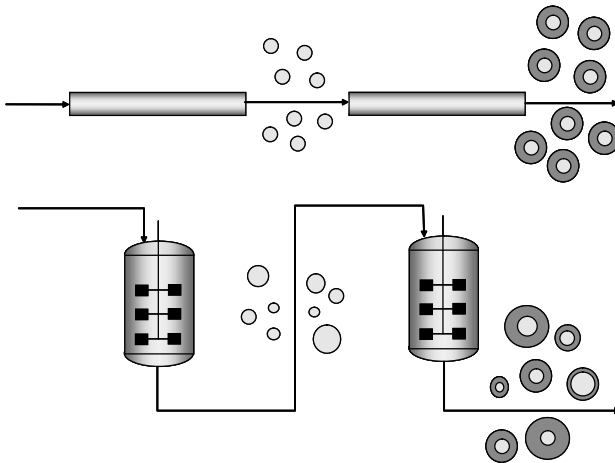


Figure 2.10 Homopolymer/copolymer distribution for impact copolymers made in a series of two tubular reactors or two CSTRs. The wide residence time distribution of the CSTRs is reflected in the non-uniform homopolymer/copolymer distribution in the particles. The distribution of homopolymer (light gray) and copolymer (dark gray) phases is only to illustrate the effect of reactor residence time distribution. In reality, one phase is dispersed into the other.

This broad homopolymer/copolymer distribution is, sometimes, even visible with the naked eye when examining impact copolymer pellets. Pellets where the homopolymer phase is dominant appear opaque due to their higher crystallinity, while those where the amorphous copolymer is the major component are translucent.

Even though tubular reactors are not used industrially for the production of impact copolymers, some reactor technologies (such as gas phase horizontal reactors) were developed to narrow the reactor residence time distribution and, consequently, produce impact copolymer with narrower homopolymer/copolymer distributions.

Evidently, similar considerations for reactor residence time distribution can be made for any polymer made in a series of reactors where the conditions vary from one reactor to the other, such as the polyethylene pipe resins described earlier.

2.1.3 Polyolefin microstructural characterization techniques

The previous discussion demonstrates the relevance of accurate microstructural characterization to understand existing polyolefin resins and to develop new ones. This has been, indeed, a very fertile research area since the very beginning of olefin polymerization technology.

Several analytical techniques are used routinely to analyze polyolefins. The most common are high-temperature gel permeation chromatography (GPC), temperature rising elution fractionation (TREF), crystallization analysis fractionation (Crystaf), differential scanning calorimetry (DSC), Fourier-transform infrared spectroscopy (FTIR) and nuclear magnetic resonance (NMR). Several hyphenated techniques (GPC-FTIR, TREF-GPC, TREF-laser light scattering, for instance) are being applied more and more to describe the interdependency between the MWD and CCD of polyolefins. Due to space limitations, only a brief overview of these techniques is given in this chapter. The reader is referred to a recent review on polyolefin characterization techniques for a more complete coverage of this subject [6].

The MWD is the most fundamental microstructural distribution of any polymer because it has such a large influence on the polymer's mechanical and rheological properties. GPC is the most widely used technique for MWD determination of polymers. Most commercial polyolefins are only soluble at temperatures above 120°C in chlorinated solvents such as trichlorobenzene (TCB) and orthodichlorobenzene (ODCB) and, therefore, require a high-temperature GPC for MWD analysis.

High-temperature GPC is a liquid chromatographic technique that fractionates polymer chains using a series of columns, generally packed with crosslinked poly(styrene-divinylbenzene) gels with varying pore diameters. Polymer chains are separated according to their volumes in solution: chains with higher volumes penetrate only the larger pores and exit the columns faster than chains with lower volumes that can penetrate pores with a wider range of diameters. A refractive index (RI) detector is commonly used to measure the mass concentration of polymers eluting from the columns (GPC/RI). The combination of GPC columns and RI detectors is so common that very rarely the detector is mentioned explicitly – however, the acronym GPC/RI will be used to emphasize that the RI detector is an integral part of most GPC instruments. More recently, single-frequency infrared (IR) detectors have also been used as mass detectors for GPC (GPC/IR). Their main

advantages over the traditional RI detectors are a very stable baseline and lower sensitivity to temperature fluctuations in the IR detector cell.

If the polymer chains are linear, there is a direct relationship between molecular weight, volume in solution and elution time for a given polymer type. This relation is used to create a calibration curve relating elution time to molecular weight. In addition, the universal calibration curve can be used to extend this relation to linear polymers of all types, provided that the relation between intrinsic viscosity and molecular weight of the polymer is known (using, for instance, the Mark–Houwink equation) or measured using an on-line viscometer (GPC/RI-VISC).

Analysis by GPC becomes more involved for polyolefin chains containing LCBs, such as LDPE and resins made with some metallocene catalysts, because for these polymers the volume in solution is a function not only of molecular weight but also of branching density and type. This difficulty can be partially overcome with the use of GPC/RI-VISC or, better still, by adding an on-line laser light-scattering (LS) detector to directly determine the weight-average-molecular weight of the chains exiting the GPC (GPC/RI-VISC-LS). In addition, if the GPC is provided with a LS detector, the measurement of the molecular weight is absolute and a calibration curve is not required. Due to the versatility of triple-detector systems such as GPC/RI-VISC-LS and the microstructural complexity of modern polyolefin resins, the use of triple-detector systems is becoming increasingly more common.

Looking again at Figure 2.7, it will be remembered that resins such as LLDPE made with heterogeneous Ziegler–Natta catalysts and tandem reactors have a rather complex relation between MWD and average comonomer composition. Because this relation has such an important impact on the mechanical properties of polyolefins, an FTIR detector is often added to the GPC (GPC/RI-FTIR) to measure comonomer fraction as a function of molecular weight.

The CCD is the second most important microstructural distribution in polyolefins. Differently from the MWD, the CCD cannot be determined directly; only the distribution of crystallization temperatures (CTD) in solution can be measured and one can try to relate this distribution to the CCD using a calibration curve. Two techniques are commonly used to determine the CTD or CCD of polyolefins: TREF and Crystaf. Both operate based on the same principle: chains with more “defects” (more comonomer molecules or stereo- and/or regioirregularities) have lower crystallization temperatures than chains with fewer “defects.” Figure 2.11 compares the TREF and Crystaf profiles of an ethylene/1-butene copolymer made with a heterogeneous Ziegler–Natta catalyst. Notice that they have very similar shapes; the Crystaf curve is shifted toward lower temperatures because it is measured as the polymer chains crystallize, while the TREF curve is determined as the polymer chains dissolve (melt) and are eluted from the TREF column, as explained in the next few paragraphs.

TREF was developed before Crystaf. In TREF, a very dilute polymer solution (TCB is generally the solvent of choice) is transferred at high temperature to a column packed with an inert support. The polymer solution is then cooled very slowly, typically from 120–140°C to room temperature. As the temperature decreases, chains with higher crystallization temperatures crystallize and precipitate, followed by chains with lower crystallization temperatures. Crystallization is the most important step in TREF. A slow cooling rate (2.0–6.0°C h⁻¹ is a recommended range) allows the polymer chains to crystallize near thermodynamic

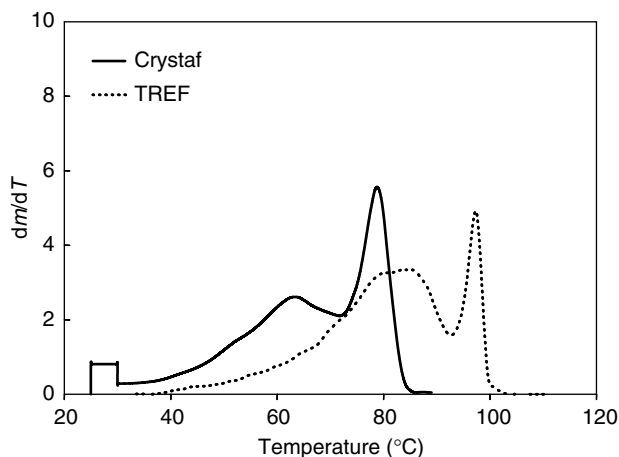


Figure 2.11 Comparison between TREF and Crystaf profiles for an ethylene/1-butene copolymer made with a heterogeneous Ziegler–Natta catalyst. The rectangular region shown in the Crystaf curve is proportional to the fraction of polymer remaining soluble at room temperature. This fraction was not reported for the TREF profile shown here.

equilibrium, minimizing cocrystallization effects and ensuring good resolution of chains with different comonomer fractions. When the cooling step is completed, solvent starts flowing through the column at increasing temperatures, first removing the least crystalline fractions, followed by the more crystalline fractions. A mass detector (generally a temperature-insensitive single-frequency IR detector) placed at the exit of the TREF column measures the concentration of chains being eluted as a function of temperature.

Crystaf is a faster alternative to TREF because it does not require an elution step or inert support. In Crystaf, crystallization takes place inside a vessel equipped with a sampling line capped with a filter. Similarly to TREF, a dilute polymer solution is transferred at high temperature to the Crystaf vessel and the temperature is allowed to decrease very slowly. Differently from TREF, however, where the crystallization process takes place unmonitored, in Crystaf small aliquots of the polymer solution are taken at pre-determined time intervals and sent to an IR mass detector. (The filter in the sampling line eliminates the risk of sampling polymer crystallites that precipitated out of the solution.) The polymer solution concentration versus crystallization temperature curve obtained this way is called the integral Crystaf profile. The differential Crystaf profile, shown in Figure 2.11, is obtained by simply taking the first derivative of the integral Crystaf profile.

Both Crystaf and TREF are calibrated using copolymer standards of narrow CCD and known average comonomer fraction for HDPE and LLDPE resins. A similar procedure may be adopted to determine isotacticity profiles for polypropylene, but is seldom applied since most modern Ziegler–Natta catalysts produce highly isotactic polypropylene (for an interesting case study, using an older Ziegler–Natta catalyst, see Soares and Hamielec [7]). Calibration curves relating comonomer molar fraction to crystallization or elution temperatures are often linear but not universal. Calibration curves for these techniques have to be used with caution because they are affected by many factors [8]. Some TREF and Crystaf setups use on-line FTIR detectors to eliminate the use of calibration curves. For instance,

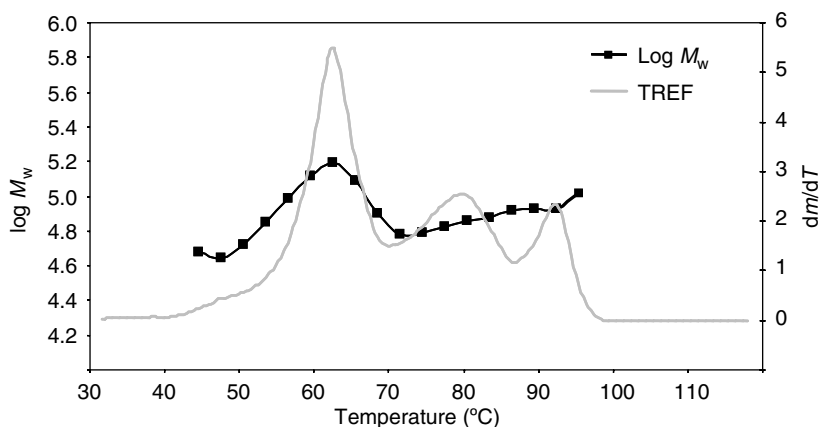


Figure 2.12 TREF profile of a trimodal polyolefin resin showing the correlation between M_w and elution temperature. A laser light-scattering detector was used to measure M_w (TREF/IR-LS). (Courtesy of Polymer Char.)

we can use the ratio of the absorptions coming from the C—H bonds in CH_3 groups to the absorption of the C—H bonds in CH_2 as well as CH_3 . This ratio has a linear relationship with the number of methyl groups in the copolymer chain.

Similarly to GPC, the amount of information obtained with TREF and Crystaf can be increased by adding more detectors to the system. For instance, LS and VISC detectors have been used to determine molecular weight averages as a function of crystallization/elution temperature or comonomer content in the copolymer. The analytical results shown in Figure 2.4, for instance, were measured with a TREF/IR-LS system. Another TREF/IR-LS profile is depicted in Figure 2.12 for a rather complex trimodal polyolefin resin.

The combinations of analytical and fractionation techniques described so far can measure one complete distribution and the averages of another distribution, but not both distributions. For instance, GPC/RI-FTIR determines the MWD and average comonomer content, while TREF/IR-LS the CCD and M_w . If the complete bivariate distribution of molecular weight and chemical composition is required, TREF and GPC fractionation needs to be combined in a single instrument. Figure 2.13 shows the bivariate MWD and CCD for the resin partially described in Figure 2.12. This analysis was done in a cross-fractionation instrument that generates several polymer fractions by TREF and injects them in GPC columns to measure their MWDs. We believe that Figure 2.13 demonstrates, more convincingly than any long argument would, the importance of quantifying the microstructure of polyolefins if we truly want to understand these resins.

High-temperature GPC, TREF and Crystaf are used almost exclusively to analyze polyolefins. Other more general polymer analytical techniques are also commonly used for polyolefin analysis. Because they are less specific to polyolefins, they will be described only very briefly in the remaining part of this section.

When properly used, DSC can generate detailed information that is complementary to Crystaf and TREF. Although very interesting, this subject is beyond the scope of this chapter and the reader is referred to the literature in the field for more details [9–11]. NMR is also very important in polyolefin analysis [12].

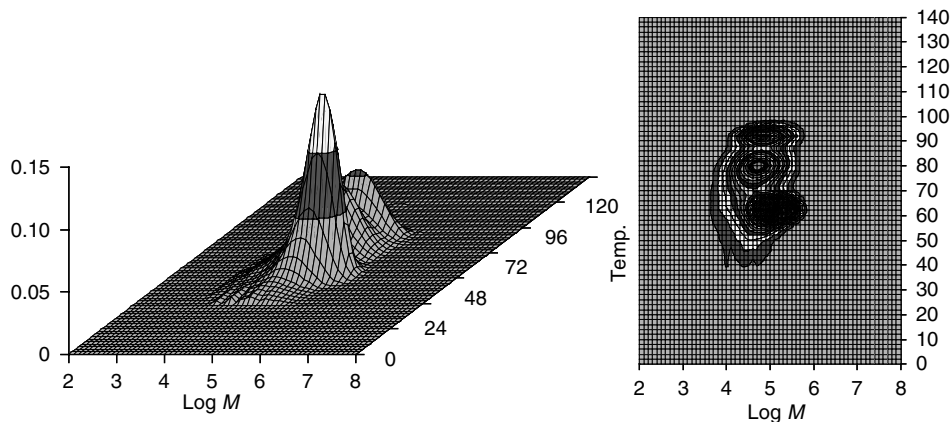


Figure 2.13 TREF-GPC cross-fractionation results for the polyolefin resin shown in Figure 2.12. (Courtesy of Polymer Char.)

Finally, the focus here is only on analytical fractionation techniques for polyolefins. There are, however, several preparative techniques that are used frequently to separate polyolefins into large fractions that can be further analyzed by other analytical techniques. The reader should refer to references 6–13 at the end of the chapter for an overview of this subject.

2.2 Catalysts for olefin polymerization

2.2.1 Coordination catalyst types

There are four major families of catalysts for olefin polymerization: Ziegler–Natta, Phillips, metallocene and late-transition metal catalysts. Their main characteristics are given in Table 2.1, and Figure 2.14 shows some representative chemical structures. Two of these catalysts families, Ziegler–Natta and Phillips, are considered to have multiple-site types, which explains why they make polymer with non-uniform properties: each site type produces polymer populations with different average microstructural properties; the polymer made by these catalysts can be seen as a blend of polymers with different average properties, as discussed in Section 2.1. Ziegler–Natta catalysts can be homogeneous (soluble in the reaction medium) or heterogeneous. Contrarily to their heterogeneous counterparts, soluble vanadium-based Ziegler–Natta catalysts have only one site type and synthesize polyolefins with uniform properties. Phillips catalysts, on the other hand, are always heterogeneous. Two families of single-site catalysts are shown in Table 2.1: metallocene and late-transition metal catalysts. They are usually soluble in the reaction medium, but can be supported onto organic or inorganic carriers. This is commonly done for metallocenes, but not so often for late transition metal catalysts, except in some academic investigations [14]. When metallocene catalysts are supported, their polymerization behavior is affected – notably, there is a reduction on polymerization rate, increase in polymer molecular weight averages, often broadening of the MWD and, in some cases, changes in stereo- and regio-selectivity – but

Table 2.1 Main characteristics of coordination catalysts for olefin polymerization

Type	Physical state	Examples ^a	Polymer type
Ziegler–Natta	Heterogeneous	TiCl ₃ , TiCl ₄ /MgCl ₂	Non-uniform
	Homogeneous	VCl ₄ , VOCl ₃	Uniform
Phillips	Heterogeneous	CrO ₃ /SiO ₂	Non-uniform
Metallocene	Homogeneous	Cp ₂ ZrCl ₂	Uniform
	Heterogeneous	Cp ₂ ZrCl ₂ /SiO ₂	Uniform
Late-transition metal	Homogeneous	Ni, Pd, Co, Fe with diimine and other ligands	Uniform

^a There is a huge variety of coordination catalysts, especially metallocene and late-transition metal catalysts. The examples shown here are just to illustrate some of their very common types.

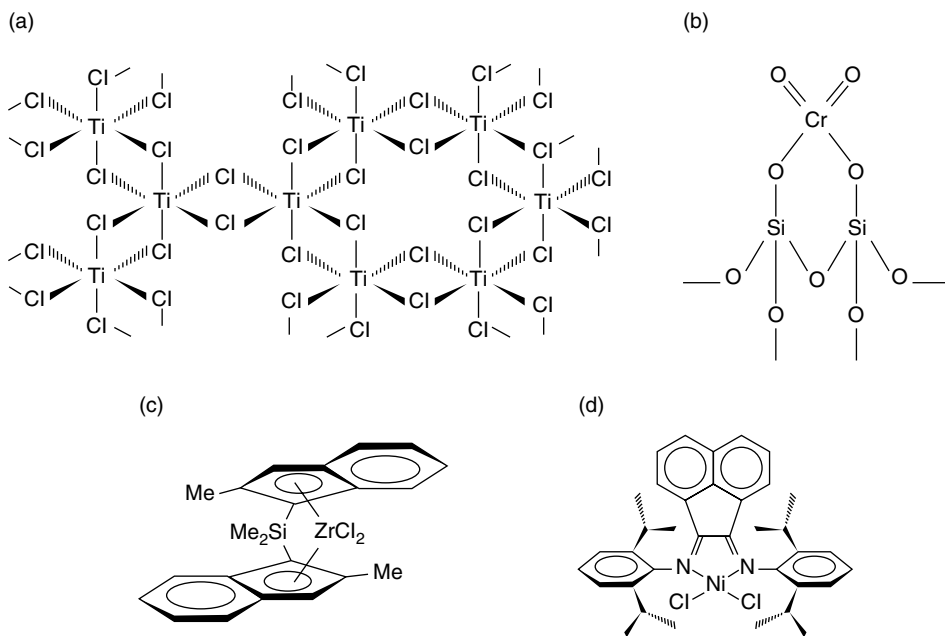


Figure 2.14 Some examples of coordination catalysts for olefin polymerization: (a) Ziegler–Natta; (b) Phillips; (c) metallocene and (d) late-transition metal.

they are still considered single-site catalysts because they produce polymers with much more uniform properties than the ones made with Phillips or heterogeneous Ziegler–Natta catalysts.

Phillips and Ziegler–Natta catalysts were the first used for olefin polymerization. They were discovered in the 1950s and created a revolution in the polyolefin industry; they are,

to this day, the dominant catalysts for polyolefin production. Homogeneous Ziegler–Natta catalysts are generally (but not exclusively) vanadium-based and used to produce ethylene propylene–diene (EPDM) elastomers. They make polymers with uniform microstructures: narrow MWD and CCD, and polydispersity indices (PDI) close to 2.0. These catalysts generally have high deactivation rates and are used in solution processes with low reactor residence times. Homogeneous Ziegler–Natta catalysts are common for EPDM manufacture because they do not make polymer with the high crystallinity peak produced with heterogeneous Ziegler–Natta catalysts. This high crystallinity component has a negative impact on elastomer properties, where the polymer chains must be amorphous to have a good performance as an elastomer.

Ziegler–Natta catalysts are, together with Phillips catalysts, the workhorses of the polyolefin plastic industry. They make heterogeneous polymers, with broad MWD and CCD, as discussed in Section 2.1. The most common type of heterogeneous Ziegler–Natta catalyst today is TiCl_4 supported on MgCl_2 , while one of the first types was crystalline TiCl_3 (Figure 2.14(a)). This description may sound deceptively simple, but there are several different ways to synthesize these catalysts to guarantee high activity, good molecular weight and comonomer incorporation control, stereo- and regio-selectivity, and adequate morphology development during polymerization [15, 16].

Both homogeneous and heterogeneous Ziegler–Natta catalysts must be activated by a cocatalyst. Cocatalysts are alkyl aluminum compounds such as trimethyl aluminum (TMA) and triethyl aluminum (TEA). Cocatalysts are essential for polymerization with Ziegler–Natta, metallocene and late transition metal catalysts, as will be explained below.

The history of the development of Ziegler–Natta catalysts is truly fascinating. Taking catalysts for propylene polymerization as an example (Table 2.2), the original catalysts had relatively lower activity and poor stereo-selectivity, requiring the removal of both atactic polypropylene and catalyst residues (deashing) from the isotactic polypropylene product. Therefore, several post-reactor unit operations were needed to purify the polymer.

Table 2.2 Evolution of heterogeneous Ziegler–Natta catalysts for propylene polymerization

Generation	Catalyst	Yield (kg PP/g Ti)	Isotacticity (% soluble in boiling heptane)	Process steps
1st	$\text{TiCl}_3/\text{AlEt}_2\text{Cl}$	5	90	Removal of catalyst residues (deashing) and atactic PP
2nd	$\text{TiCl}_3/\text{isoamylether}/\text{AlCl}_3/\text{AlEt}_2\text{Cl}$	15	95	Removal of catalyst residues (deashing) and atactic PP
3rd	$\text{MgCl}_2/\text{ester}/\text{TiCl}_4/\text{AlEt}_3/\text{ester}$	300	92	No purification
4th	$\text{MgCl}_2/\text{ester}/\text{TiCl}_4/\text{AlEt}_3/\text{PhSi}(\text{OEt})_3$	600 (in liquid propylene)	98	No purification, no extrusion/pelletization

Polypropylene made with modern catalysts, on the other hand, has an insignificant amount of catalyst residues because of their very high activity and practically no atactic content. For this reason modern processes do not require post-reactor purification. Some catalysts, such as the ones used in the Spheripol process (Section 2.5), will even produce large spherical polypropylene particles that do not necessarily require pelletization. As a consequence of these many advances, modern polypropylene (and polyethylene) manufacturing processes have very few units: basically one or more reactors in series, compressors, recovery systems for diluent (for some processes) and unreacted monomer, and an extruder for making pellets.

These advances were possible because of two main findings: the discovery of MgCl_2 as an ideal support for TiCl_4 (they form a mixed crystal where the TiCl_4 active sites are easily accessible to the monomer) and the use of electron donors such as ethers and esters that selectively poison or modify aspecific sites responsible for the formation of atactic polypropylene.

Phillips catalysts are based on Cr(IV) supported on SiO_2 (Figure 2.14(b)) [17, 18]. They behave differently from Ziegler–Natta catalysts because

- (1) they do not require a cocatalyst;
- (2) the MWD is regulated by the characteristics of the support;
- (3) the catalyst needs to be treated at high temperatures to be active;
- (4) long induction times are very common and
- (5) hydrogen, the usual chain transfer agent for Ziegler–Natta, metallocene, and late-transition metal catalysts, is not effective for Phillips catalysts.

Phillips catalysts also have lower reactivity ratios toward α -olefin incorporation, therefore are not used to produce LLDPE. However, they are excellent catalysts for HDPE and dominate the market for this resin. HDPEs made with Phillips catalysts have a very broad MWD, often with PDIs of 10 or higher.

Metallocene catalysts (Figure 2.14(c)), on the other hand, are single-site catalysts, that is, they produce polyolefins with unimodal and narrow CCD (Figure 2.6) and narrow MWD with PDIs close to 2.0, although, under some conditions, usually when supported, they may make polymer with broader distributions. Metallocenes had a very large impact in the polyolefin industry when they were discovered in the 1980s because, for the first time, polyethylene and polypropylene could be produced under conventional industrial conditions with uniform and well controlled microstructures, without the complex MWD and CCD correlations observed with Ziegler–Natta and Phillips catalysts.

Metallocene catalysts are called sandwich compounds because they are composed of a transition metal atom sandwiched between two rings (indenyl rings in Figure 2.14(c)). The rings may be connected through different bridges (Me_2Si in Figure 2.14(c)) to vary the angle between the two rings. By altering the electronic and steric environment around the active sites, it is possible to modify the accessibility and reactivity of the active sites and produce polyolefins with different microstructures. Figure 2.15 shows how metallocene catalysts can be gradually changed from an initial design to make complexes with different polymerization characteristics. The ability to produce several complexes having different polymerization rates, comonomer reactivity ratios and polymer molecular weight is one of the reasons behind the industrial success of metallocene catalysts [19–22].

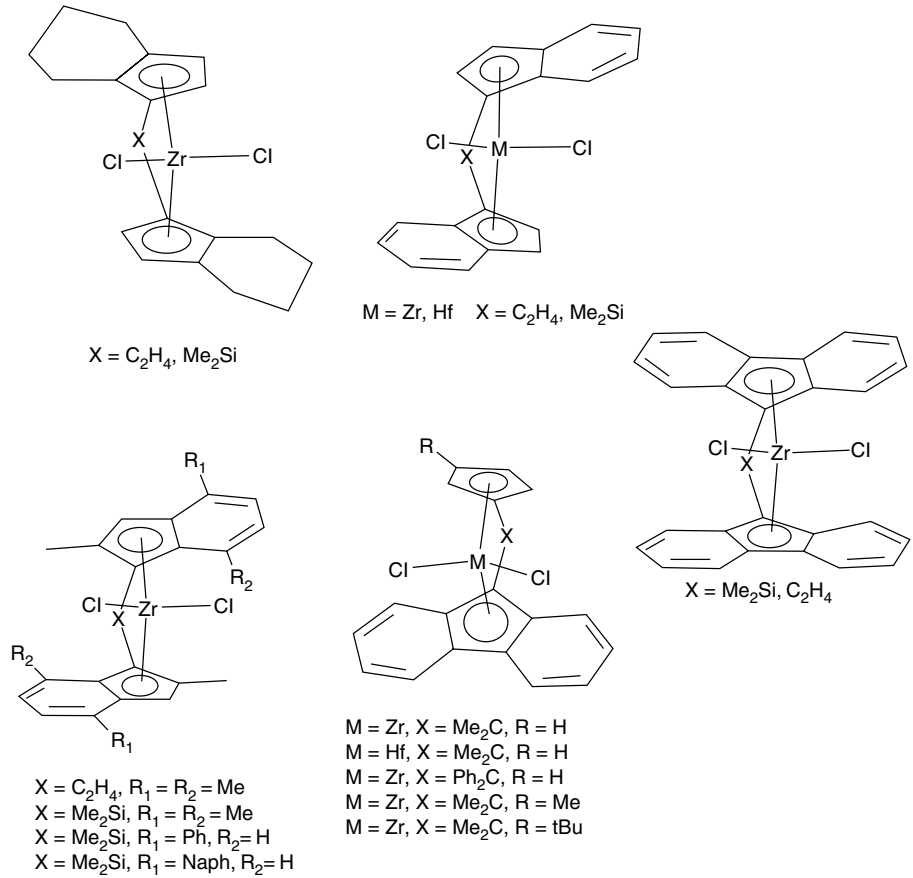


Figure 2.15 Different metallocene catalyst structures.

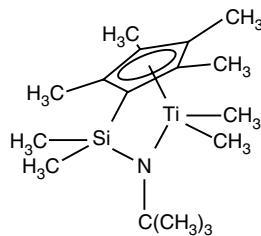


Figure 2.16 Half-sandwich metallocene catalysts.

Figure 2.16 depicts another important type of metallocene catalyst: monocyclopentadienyl complexes, also called constrained geometry catalysts (CGC) or half-sandwich catalysts. Their most important property is a very high reactivity ratio toward α -olefin incorporation, allowing the easy copolymerization of ethylene with long α -olefins and polymer chains having a vinyl terminal group. The latter are called macromonomers, and,

when copolymerized with a growing chain, form a LCB. You can visualize this process in Figure 2.2, by substituting the 1-octene comonomer with a polymer chain with a vinyl termination.

Why is the introduction of LCBs on metallocene polymers important? Metallocene polyolefins have very good mechanical properties because of their narrow MWD but, at the same time, are difficult to process. Broad MWD resins have a low molecular weight component that acts as a lubricant, increasing shear thinning and enhancing processability; this component is absent in metallocene polyolefins. Even in small numbers, LCBs have a large effect on shear thinning and processability, besides improving several other properties such as melt strength and tear resistance, making LCB-polyolefins very attractive materials [23].

Perhaps the most important reason leading to the industrial implementation of metallocene catalysts, in addition to their high activity and excellent microstructural control, is that they can be easily adapted to industrial olefin polymerization processes. The transition from Ziegler–Natta or Phillips catalysts to metallocenes is sometimes called *drop-in technology* exactly to indicate that the new catalysts can simply be “dropped in” the existing reactor. Of course, reality is often not as simple as catchy terms may indicate, but the fact remains that metallocenes can be introduced into existing industrial processes without a prohibitively large number of adjustments.

All olefin polymerization processes described in Section 2.5 have been tested, and some are being operated commercially with metallocene catalysts. Metallocenes can be used directly in solution processes but need to be supported to be used in slurry and gas-phase processes. In the latter case, the support of choice is SiO_2 . There are several supporting techniques for metallocenes, but this subject is beyond the scope of this chapter [24].

One of the surprising facts about metallocenes is that they have been known for a very long time; Natta himself published papers using metallocene catalysts for olefin polymerization. When activated with common alkyl aluminums, however, metallocenes have very poor polymerization rates and rapidly deactivate via bimolecular combination reactions. The important discovery that Sinn *et al.* [25] made in the 1980s was that bulky non-coordinating anions such as methylaluminoxane (MAO) were able to activate and stabilize metallocene catalysts, effectively eliminating bimolecular deactivation reactions and obtaining a highly active, stable catalyst.

MAO is an oligomeric compound with degree of oligomerization varying approximately from 6 to 20. Despite its huge importance, even its structure is not completely established yet; Figure 2.17 shows some proposed structures for MAO. There are several commercial grades of MAO, each with slightly different cocatalyst properties. Other alkyl aluminums can also be reacted with water to produce equivalent aluminoxanes: TEA and water, for instance, produces ethylaluminoxane (EAO); the three-dimensional cage structure in Figure 2.17 is actually for the product of the reaction between *t*-butyl aluminum and water, *t*-BAO.

In general, a large excess of MAO is needed to achieve high activity. Ratios of 1000 aluminum atoms to transition metal atoms are common for solution polymerization; a lower ratio is required when the catalyst is supported on SiO_2 and other carriers, but still in the order of hundreds. It has been claimed that this large excess of the bulky cocatalyst is needed to shield the active sites from one another and prevent bimolecular deactivation reactions.

MAO and other aluminoxanes are the most popular, but not the only, cocatalysts used with metallocene catalysts. Other bulky, non-coordinating anions such as

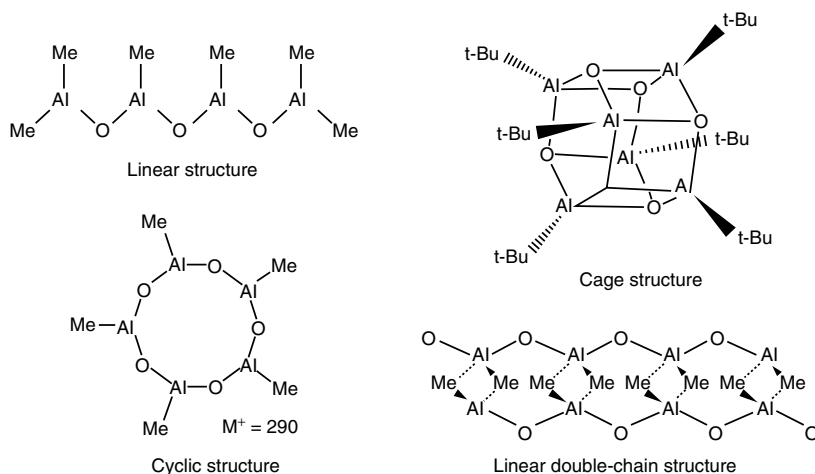


Figure 2.17 Proposed MAO structures.

tris(pentafluorophenyl) borane (TPFB) are also used, especially with half-sandwich catalysts. As compared to MAO, TPFB has the advantage of being required in nearly stoichiometric amounts.

Some late-transition metal catalysts, such as the Ni-diimine catalyst shown in Figure 2.14(d), have an intriguing property called *chain walking*: when polymerizing ethylene, the active center can move away from the chain end and “walk” on the polymer backbone, leading to the formation of SCBs in the absence of α -olefin comonomers. By varying the polymerization temperature and monomer pressure, it is possible to make polymers with densities varying from those of HDPE to LLDPE, VLDPE, ULDPE, and, in fact, to that of a complete amorphous, ethylene–propylene like elastomer [26, 27].

The literature on late-transition metal catalysts is very large and keeps growing as new complexes are developed. Several families have been well studied such as Brookhart (Ni and Pd; see Figure 2.14(d)), Gibson–Brookhart (Co and Fe) and Grubbs (neutral Ni) catalysts. Some of their properties are very enticing: these catalysts are much less sensitive to polar compounds and can be used, although not in industrial-relevant conditions, to copolymerize olefins with polar monomers such as acrylates and methylacrylates [28].

Fascinating as they are, these catalysts have not found commercial applications yet and will not be discussed any further in this chapter. The interested reader is referred to the review by Ittel and Johnson [28] for additional information.

2.2.2 Polymerization mechanism

The polymerization mechanism with coordination catalysts has been studied extensively since the discovery of Ziegler–Natta and Phillips catalysts. Some of the steps in this mechanism are very well known and constitute what we will call the *standard model* for polymerization in this chapter. Some important phenomena are not included in the standard model because, even though they are commonly observed experimentally, there is no

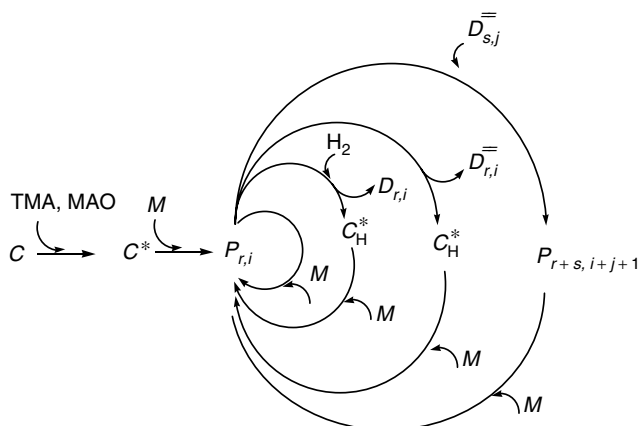


Figure 2.18 Coordination polymerization mechanism (standard model): C – catalyst; TMA and MAO – cocatalysts; C^* – active site; M – monomer; $P_{r,i}$ – living chain with length r and i LCBs; C_H^* – metal hydride site; H_2 – chain transfer agent (hydrogen); $D_{r,i}$ – dead chain with saturated chain end; $D_{r,i}^=$ – dead chain with vinyl chain end (macromonomer).

consensus in how to quantify their polymerization kinetics. A description of some of these phenomena is left to the end of this section.

Figure 2.18 shows some steps in the standard model. An active site (C^*) is formed when a catalyst (C) reacts with a cocatalyst molecule (TMA or MAO, for instance). This is, generally, a very fast reaction. The first monomer insertion produces a living polymer chain of length 1 ($P_{1,i=0}$). The second subscript describes the number of LCBs in the chain; this will be ignored for now and it will be assumed that there are no LCBs in the chain ($i = 0$). The polymer chain then grows through successive monomer insertions (innermost cycle), its chain length increasing to 2, 3, 4, . . . , r until a transfer reaction takes place. Only two types of transfer reaction have been included in Figure 2.18 (more are possible, but were not shown to simplify the catalyst cycle): transfer to hydrogen (second cycle) and β -hydride elimination (third cycle). When a hydrogen molecule reacts with a living chain, one hydrogen atom bonds to the active site, forming a metal hydride site (C_H^*), while the other hydrogen atom is transferred to the end of the living chain, creating a dead polymer chain with chain length r and a saturated chain end ($D_{r,i=0}$). The same metal hydride site is created during β -hydride elimination, but now the hydrogen atom is abstracted from the β -carbon in the living polymer chain, generating a dead chain with a vinyl terminal group ($D_{r,i=0}^=$). As indicated in the diagram, metal hydride sites are also active for polymerization and will initiate another polymer chain through monomer insertion. For linear polymerization, this is all there is to the standard model, plus a few additional transfer steps, such as transfer to monomer and cocatalyst.

However, the vinyl-terminated dead polymer chain opens the door to possible LCB-formation reactions if the correct catalyst is being used. These chains are called macromonomers and they can be considered to be very long α -olefins. If a catalyst that can copolymerize macromonomers is being used, they may be reincorporated in the growing polymer chain, forming LCBs. As seen earlier, catalysts such as CGC are ideally suited for

this type of reaction, as illustrated in the outermost cycle of Figure 2.18: macromonomers with chain length s and j LCBs, when reacting with living chains of length r and i LCBs generate a living polymer chain of length $r + s$ and $i + j + 1$ LCBs. For instance, a linear ($j = 0$) macromonomer of chain length 1000 reacting with a linear ($i = 0$) living polymer of chain length 1500 will create a living polymer with $i + j + 1 = 1$ LCB and length $r + s = 2500$.

So far, it has been mentioned several times that the cocatalyst is required to activate the catalyst, but a mechanism has not been proposed for this reaction. This reaction will now be explored in Scheme 2.1. The cocatalyst (AlR_3) acts as an alkylating and reducing agent, extracting two halogen atoms (X) from, and transferring one alkyl group to, the catalyst. Notice that the active site is cationic and that the cocatalyst product (AlR_2X_2) is a non-coordinating anion required to stabilize the catalyst. The electron-deficient site is now ready to attract the π -electrons in the olefin double bond, leading to polymerization; the alkyl group transferred to the active site becomes, in fact, one of the polymer chain ends, as illustrated in Figure 2.19.

Figure 2.19 illustrates Cossee's mechanism for polymerization with coordination catalysts. The active site is depicted as having a coordination vacancy that attracts the electrons in the olefin π -bond. Coordination is followed by insertion into the polymer chain (R) and the re-establishment of the coordination vacancy for further monomer insertion. This figure also shows an important characteristic of coordination polymerization that makes it very different from free-radical polymerization: the monomer is inserted between the carbon–metal bond. As a consequence, the electronic and steric environment surrounding the transition metal has a huge influence on the kinetics of polymerization. This is why



Scheme 2.1 Catalyst–cocatalyst reaction to form an active site having a coordination vacancy. The transition metal center is represented as A, ligands as L (for instance, cyclopentadienyl rings for metallocenes), X are halogen atoms (usually Cl) and R is an alkyl group.

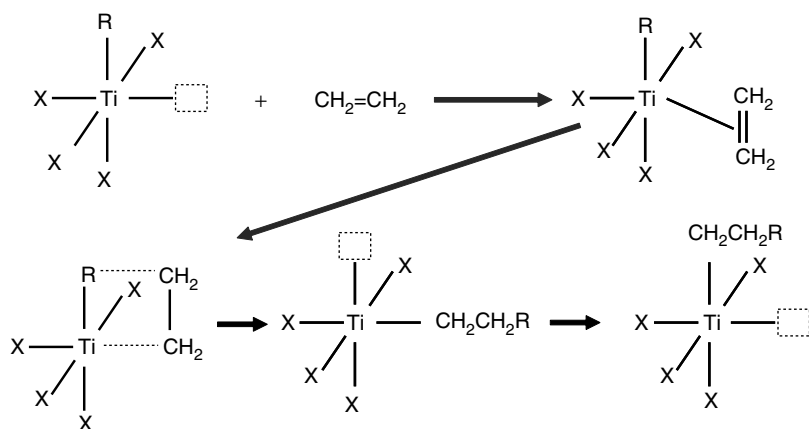


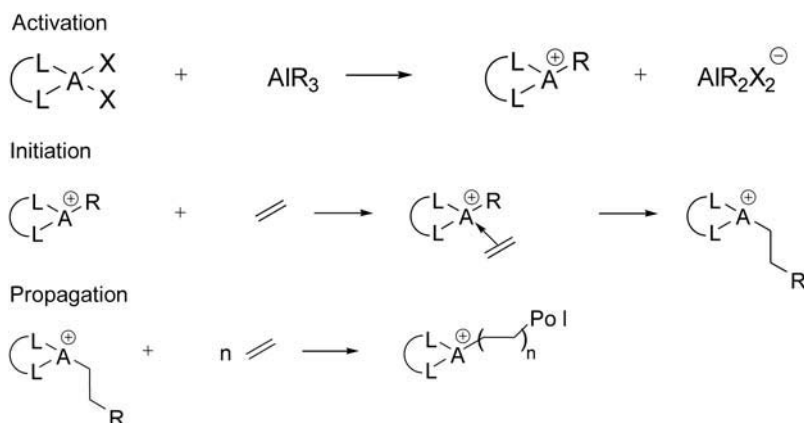
Figure 2.19 Cossee's mechanism: X are ligands, generally Cl atoms and R is the growing polymer chain.

changing the catalyst configuration (see, for instance, the different metallocene structures shown in Figures 2.15 and 2.16) has such an impact on polymerization rates and polymer microstructure. We can say that coordination polymerization is site-based, that is, the nature of the active site regulates the polymerization kinetics. Contrarily, after a few monomer insertions in free-radical polymerization, the polymerization site moves far away from the initiator fragment and is not influenced by its chemical structure. Free-radical polymerization is, therefore, monomer-based: the type of monomer, not the type of free-radical initiator, determines polymerization kinetics. This is why tables for free-radical polymerization rate constants of several monomers can be found and not for coordination polymerization. In coordination polymerization, monomer, catalyst and cocatalyst type must always be mentioned when reporting polymerization rate constants.

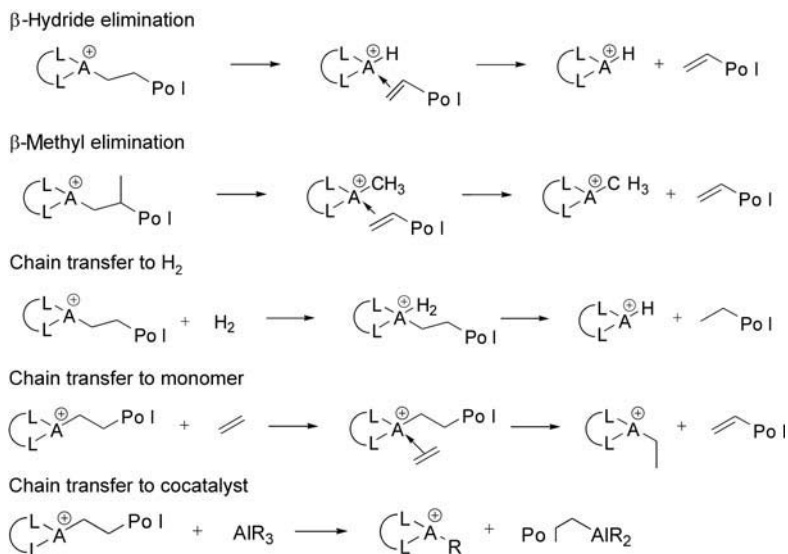
Schemes 2.2 and 2.3 give some more details on the polymerization steps of the standard model.

Even though the discussion has been mainly on homopolymerization, the same polymerization mechanism steps are valid for copolymerization with coordination catalysts. In this case, for a given catalyst/cocatalyst system, propagation and transfer rates depend not only on the type of coordinating monomer, but also on the type of the last monomer attached to the living polymer chain. It is easy to understand why the last monomer in the chain will affect the behavior of the incoming monomer: as the reacting monomer coordinates with the active site, it has to be inserted into the carbon–metal bond and will interact with the last (and, less likely, next-to-last or penultimate) monomer unit inserted into the chain. This is called the terminal model for copolymerization and is also commonly used to describe free-radical copolymerization. In the next section it will be seen that, with a proper transformation, not only the same mechanism, but also the same polymerization kinetic equations for homopolymerization can be used directly to describe copolymerization.

Finally, a few complicating aspects of coordination polymerization should be discussed that were carefully avoided in the standard model. On first inspection, the mechanism described in Figure 2.18 and Schemes 2.1–2.3 does not look very different from the one used for free-radical polymerization, except from the fact that the rate constants, besides



Scheme 2.2 Activation, initiation and propagation steps for coordination polymerization.



Scheme 2.3 Chain transfer steps for coordination polymerization.

depending on monomer type, are also a strong function of catalyst type. This should make us optimistic or suspicious, depending on how we see the problem. It turns out that it should make us very suspicious. Free-radical polymerization, being studied before, lent several ideas to coordination polymerization, but not all of them fit so well. The main difficulties encountered with coordination polymerization are

- (1) the comonomer effect;
- (2) the hydrogen effect and
- (3) the catalyst/cocatalyst ratio effect.

Each one will be discussed briefly in the next paragraphs.

The comonomer effect is one of the best known phenomena in coordination polymerization. In general, the rate of homopolymerization with a given catalyst decreases in the order ethylene > propylene > 1-butene > ... > higher α -olefins. However, when ethylene is copolymerized with small fractions of α -olefins for the production of LLDPE, the rate of copolymerization is higher than the rate of ethylene homopolymerization. This observation cannot be explained with Cossee's mechanism alone. The best mechanism proposed for the comonomer effect is called the trigger mechanism [29]. In simple words, it proposes that the α -olefin comonomer coordinates at the active site and "triggers" the insertion of ethylene at higher rates than would be observed during homopolymerization. There is no consensus that the trigger mechanism is always applicable, but it is the stronger candidate to explain the comonomer effect.

Besides acting as chain transfer agent, hydrogen can also influence the polymerization rate significantly. Hydrogen most often increases the rate of propylene polymerization; this effect is well documented and its explanation is now widely accepted. It has been seen earlier that 1,2 insertions are favored during propylene polymerization but, sometimes,

a 2,1 insertion may happen, generating a regiodeflect on the chain. It is easy to see that the active site after a 2,1 insertion will be sterically hindered because the methyl group is too close to the transition metal (Figure 2.9). It is reasonable to expect that this site will have a lower propagation rate than sites with 1,2 insertions. Hydrogen, being a small molecule, can react more easily with 2,1 terminated sites, freeing up these “dormant” sites for propagation. The effect of hydrogen on ethylene polymerization is less well understood because it may increase, decrease or have no effect on the polymerization rate. Some hypotheses have been suggested to explain this phenomenon, but there is no consensus in the literature regarding a general theory for hydrogen effect on ethylene polymerization [30].

In Scheme 2.1 it was proposed that the cocatalyst alkylates and reduces the catalyst to form the active sites, but these are not the only roles of the cocatalyst. It also acts as a scavenger of polar impurities, helps stabilize the active sites but, if present in too large an excess, will decrease the polymerization rate. In general, if the polymerization rate is plotted as a function of cocatalyst/catalyst ratio, it will initially increase up to a maximum value and then start decreasing. At the same time as the cocatalyst changes the polymerization rate, it also acts as a chain transfer agent, affecting molecular weight averages and MWD width. The effect of cocatalyst is still very difficult to quantify with a theoretical model and most polymerization parameters are determined for a narrow range of catalyst/cocatalyst ratios.

Describing mathematical models to account for all these effects would take too much space in this chapter and would not have the generality of approach that we are aiming for. The comprehensive review by Shaffer and Ray provides a good introduction to this topic [31].

2.3 Polymerization kinetics for single- and multiple-site catalysts

In reference 54, Ray clearly expresses the idea that a chemical process can be represented as a series of interdependent phenomena that occur at different length scales, requiring different types of modeling approaches. Figure 2.20 illustrates this concept for a generic olefin polymerization process for three widely different length scales. A complete process model will, necessarily, involve elements from all three length scales. For instance, the MWD and CCD (microscale) are functions of the local temperature and concentrations of reactive species in the polymer particle (mesoscale). These polymerization conditions are, in turn, determined by the local reaction rate, and possible heat and mass transfer limitations at the level of the single particle (mesoscale). Transport phenomena will be controlled, to a certain extent, by the internal morphology of the particle (mesoscale), which can be influenced by the temperature and pressure inside the reactor, and the effectiveness of heat transfer in the reactor (macroscale). It is instructive to classify these different phenomena according to their length scale, as suggested in Table 2.3.

Olefin polymerization reactors will now be modeled using a bottom-up approach, from microscale to macroscale. In this section polymerization kinetic models will be introduced to describe polymerization rates and polymer microstructures, ignoring any phenomena that may take place in the mesoscale and macroscale. These models depend on the concentration of reagents and temperatures at the active site. As explained in the previous

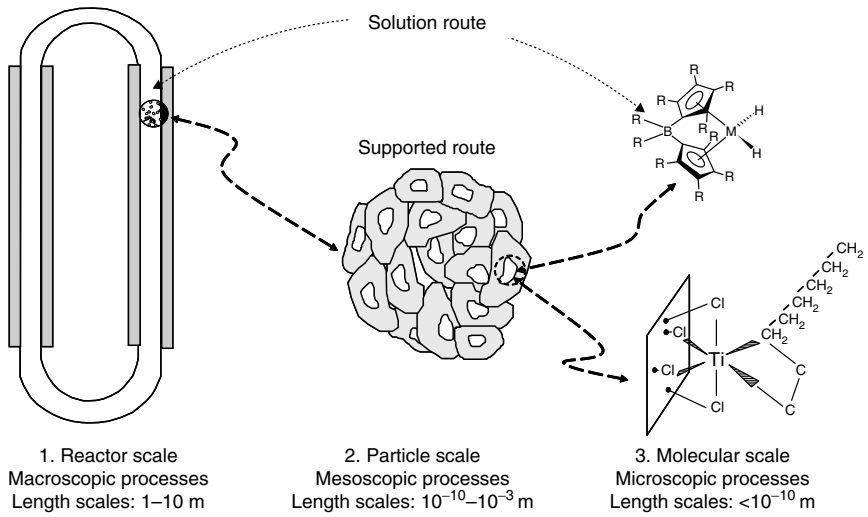


Figure 2.20 Different length scales involved in a polyolefin process. Each length scale needs to be specifically integrated into a well constructed model.

Table 2.3 Description of length scales for olefin polymerization reactors

Length scale	Macroscale (reactor scale)	Mesoscale (particle scale)	Microscale (molecular scale)
Dimensions	10^{-2} –10 m	10^{-10} – 10^{-3} m	10^{-10} m
Phenomena	Macromixing: reactor scale concentration and temperature gradients Residence time distribution and particle size distribution Reactor temperature profiles, hot spots Process safety and reactor stability Fouling and sheeting, static electricity Particle interactions, emulsion phase of a fluidized-bed reactor	Particle morphology: porosity, relative length scale of polymer and pore phases, particle shape, distribution of phases in high-impact polypropylene Interphase heat and mass transfer phenomena Intraphase heat and mass transfer phenomena Observed kinetics, rate limiting steps Phase equilibrium, monomer sorption and desorption in polymer phase, diffusion Particle agglomeration Micromixing	Polymerization kinetics: propagation, transfer, LCB formation, site activation and deactivation Microstructure formation: MWD, CCD, LCB Chain crystallization

paragraph, these concentrations and temperatures can be affected by mass and heat transfer phenomena that take place at meso- and macroscale. For solution processes, these conditions may be the same as the bulk conditions in the reactor, and the modeling problem is greatly simplified. For slurry and gas-phase processes that use supported catalysts, however, there may be significant differences between bulk reactor conditions and conditions at the active site.

It will be assumed that the polymerization conditions at the active site are known in this present section; we will worry about them in a later section. In Section 2.4, mesoscale models will be developed that will tell us how the concentration of reagents, as well as temperature, varies as a function of radial position in the polymer particle. If radial gradients in the polymer particles are significant, the models developed in this section are still valid for the mesoscale, but only locally, at a given radial position in the particle. Finally, at the end of Section 2.5, a simple way to connect micro-, meso- and macroscale in one unified approach for modeling olefin polymerization reactors will be proposed.

The standard model will be used to develop the mathematical models in this section, starting from a very simple subset and gradually modifying the model to include more details.

When modeling the kinetics of a polymerization reaction, two main objectives must be borne in mind. The first is akin to that of any chemical reactor engineering model: to describe how fast reactants are consumed and products are formed and, usually, heat effects associated with these reactions. This piece of information is essential for chemical reactor design, operation, optimization and control. The second objective, however, is unique to polymers and distinguishes a polymer reactor engineer from his colleagues working with small-molecule reactors: the description of the polymer microstructure formed in the polymerization reactor. Most of the modeling effort, in fact, is dedicated to this second objective.

For polyolefins, MWD, CCD and LCB are the most important microstructural distributions. Our discussion will start with methods to model MWD and then progress toward CCD and LCB prediction. Population balances and the method of moments are the traditional ways of modeling MWD, not only for coordination polymerization, but for most polymerization mechanisms. Population balances are simply molar balances for the concentrations of living and dead polymer molecules of several chain lengths present in the reactor. Since one equation is defined for polymer chains of each length, thousands of equations would need to be solved to obtain the solution of the complete population balance for high molecular weight polymers. There are some very elegant numerical methods that can discretize these large sets of equations and solve them efficiently [32, 33], but this topic is beyond the scope of this chapter. A more conventional approach to deal with this problem applies the population balances to define a much smaller set of moment equations that can then be used to calculate molecular weight averages. Generally only the zeroth, first and second moment equations are solved, thus reducing a system of thousands of equations to only three for living polymers and three for dead polymers, as will be explained later.

In the method of moments, only molecular weight averages are calculated and not the complete MWD. For some applications, this simplification is acceptable, but for others it may not be. In this case, the options are solving the discretized population balances or, more elegantly, using the method of instantaneous distributions. Later it will be shown that

Table 2.4 Simplified homopolymerization mechanism for a preliminary model using population balances and the method of moments

Description	Chemical equations	Rate constants
Initiation	$C^* + M \rightarrow P_1$	k_i
Propagation	$P_r + M \rightarrow P_{r+1}$	k_p
β -Hydride elimination	$P_r \rightarrow C^* + D_r$	$k_{t\beta}$
Transfer to H_2	$P_r + H_2 \rightarrow C^* + D_r$	k_{tr}^H
Deactivation	$P_r \rightarrow C_d + D_r$	k_{dac}
	$C^* \rightarrow C_d$	k_{dac}

the method of instantaneous distributions, when applicable, is very powerful because it predicts the complete MWD with little computational effort.

2.3.1 Homopolymerization

Linear chains

We will start with a very simple homopolymerization model that includes only initiation, propagation, transfer to hydrogen, β -hydride elimination and unimolecular catalyst deactivation, as depicted in Table 2.4. From our previous discussion of the standard model for polymerization with coordination catalysts, it is known that several steps are not included in Table 2.4. It will be shown, however, that general expressions for population balances and the methods of moments starting with this simplified mechanism can be developed and later they can be extended, rather easily, to include more polymerization steps.

A few assumptions were made to simplify the algebra of the next derivations:

- (1) site activation (reaction between catalyst and cocatalyst) was assumed instantaneous;
- (2) the only transfer mechanisms are β -hydride elimination and chain transfer to hydrogen and
- (3) transfer reactions were assumed to produce site C^* , formed by activation of catalyst with cocatalyst, and not C_{H}^* as seen in Figure 2.18 and Schemes 2.2 and 2.3.

It will be seen later that, if needed, the mathematical model that will be derived can be changed easily to accommodate a more complex polymerization kinetics mechanism.

Population balance equations for homopolymerization in batch reactors

Population balance equations describe how the concentrations of living and dead chains of different lengths vary in time during the polymerization. The master equation for

deriving population balances in a spatially homogeneous batch reactor for the entire reactor volume, V , is

$$\text{Accumulation rate} = \text{formation rate} - \text{consumption rate} \quad (2.1)$$

The polymerization mechanism described in Table 2.4 can be used to derive the population balance for living polymer chains with $r \geq 2$ as follows:

$$\begin{aligned} \frac{dP_r}{dt} = & (k_p[P_{r-1}][M] - k_p[P_r][M] - k_{t\beta}[P_r] \\ & - k_{tr}^H[P_r][H_2] - k_{dac}[P_r])V, \quad r \geq 2 \end{aligned} \quad (2.2)$$

where P_r is the number of moles of living chains of length r in the reactor and $[P_r] = P_r/V$ is the molar concentration of P_r . Now rearranging Equation 2.2 to a more compact form:

$$\frac{dP_r}{dt} = k_p[M](P_{r-1} - P_r) - (k_{t\beta} + k_{tr}^H[H_2] + k_{dac})P_r, \quad r \geq 2 \quad (2.3)$$

For chains of length 1, a slightly different equation, also obtained with the help of the polymerization mechanism shown in Table 2.4, applies:

$$\frac{dP_1}{dt} = k_i C^*[M] - k_p P_1[M] - k_{t\beta} P_1 - k_{tr}^H P_1[H_2] - k_{dac} P_1 \quad (2.4)$$

Once again, Equation 2.4 can be rearranged to a more compact form:

$$\frac{dP_1}{dt} = k_i C^*[M] - k_p P_1[M] - (k_{t\beta} + k_{tr}^H[H_2] + k_{dac})P_1 \quad (2.5)$$

Equations 2.3 and 2.5 form a set of r_{\max} ordinary differential equations (ODEs) for the concentrations of chains of length 1, 2, 3, ..., r_{\max} . Solving this system cannot be started yet because an additional equation is needed for the molar balance of C^* , given by:

$$\frac{dC^*}{dt} = (k_{t\beta} + k_{tr}^H[H_2]) \sum_{r=1}^{\infty} P_r - k_i C^*[M] - k_{dac} C^* \quad (2.6)$$

The summation term $\sum_{r=1}^{\infty} P_r$ is used in Equation 2.6 because when chains of all lengths undergo a transfer reaction, an active site C^* is formed, according to the mechanism postulated in Table 2.4. The term $\sum_{r=1}^{\infty} P_r$ is, simply, the number of moles of living polymer chains in the reactor, also called the zeroth moment of living chains and defined as

$$\mu_0 = \sum_{r=1}^{\infty} P_r \quad (2.7)$$

Consequently, Equation 2.6 simplifies to:

$$\frac{dC^*}{dt} = (k_{t\beta} + k_{tr}^H[H_2])\mu_0 - (k_i[M] + k_{dac})C^* \quad (2.8)$$

Finally, the concentration of deactivated site types, C_d , can be calculated with the molar balance:

$$C_d = C_0^* - C^* - \mu_0 \quad (2.9)$$

where C_0^* is the initial concentration of active sites in the reactor.

Equations 2.3, 2.5, 2.8 and 2.9 could be solved numerically using an ODE solver to obtain the time evolution profiles of P_r in the reactor. For practical purposes, however, the concentration of dead polymer chains is of concern because there are many more dead chains than living chains in the reactor; the discussion of the solution process will be left until these equations have been derived.

To obtain the population balances for dead polymer chains, Equation 2.1 can be used once again, noticing this time that the rate of consumption is equal to zero. Therefore, for dead chains, with $r \geq 2$:

$$\frac{dD_r}{dt} = k_{tr}^H[H_2]P_r + k_{i\beta}P_r + k_{dac}P_r, \quad r \geq 2 \quad (2.10)$$

Equation 2.10 can be further simplified to:

$$\frac{dD_r}{dt} = (k_{tr}^H[H_2] + k_{i\beta} + k_{dac})P_r, \quad r \geq 2 \quad (2.11)$$

For dead chains $r = 1$ is neglected since this has the length of a monomer unit. Including this additional term in Equation 2.11, however, would not significantly alter the simulation results.

Since these equations are being applied to a batch reactor, both monomer and hydrogen concentration will decrease as a function of polymerization time, according to their molar balances:

$$\frac{dM}{dt} = -k_p[M] \sum_{r=1}^{\infty} P_r = -k_p[M]\mu_0 \quad (2.12)$$

$$\frac{dH_2}{dt} = -k_{tr}^H[H_2] \sum_{r=1}^{\infty} P_r = -k_{tr}^H[H_2]\mu_0 \quad (2.13)$$

A complete set of differential equations has now been derived that describe how the MWD of a polyolefin varies in a batch reactor. For easy reference, these equations are summarized in Table 2.5, where the lumped constant K_{TR} is introduced to account for the frequency of all transfer reactions taking place in the reactor:

$$K_{TR} = k_{tr}^H[H_2] + k_{i\beta} \quad (2.14)$$

Table 2.5 also lists a common set of initial conditions for homopolymerization in a batch reactor. The reactor starts with an initial concentration of monomer, hydrogen and catalyst sites and is free of living and dead polymer chains.

The equations in Table 2.5 could be solved for chain lengths $r = 1, 2, 3, \dots, r_{max}$, to obtain the complete MWD. Evidently, the resulting system of ODEs for polymers with high molecular weights will be too large to be efficiently solved this way. Several numerical discretization methods have been proposed to deal with such large systems in an efficient way [32]. The software package PREDICI is a commercial implementation of such a method [33]. The reader is referred to these references for more details on these solution processes.

On the other hand, if the equations need to be solved only for the chain length averages, the number of equations in Table 2.5 can be significantly reduced using the method of moments described in the next subsection.

Table 2.5 Summary of population and molar balance equations for homopolymerization in a batch reactor

Description	Equations	Initial conditions	(#)
Living polymer, $r = 1$	$\frac{dP_1}{dt} = k_i C^* [M] - k_p P_1 [M] - (K_{TR} + k_{dac}) P_1$	$P_1(0) = 0$	(2.5)
Living polymer, $r \geq 2$	$\frac{dP_r}{dt} = k_p [M] (P_{r-1} - P_r) - (K_{TR} + k_{dac}) P_r$	$P_r(0) = 0$	(2.3)
Dead polymer, $r \geq 2$	$\frac{dD_r}{dt} = (K_{TR} + k_{dac}) P_r$	$D_r(0) = 0$	(2.11)
Active sites	$\frac{dC^*}{dt} = K_{TR} \mu_0 - (k_i [M] + k_{dac}) C^*$	$C^*(0) = C_0^*$	(2.8)
Deactivated sites	$C_d = C_0^* - C^* - \mu_0$		(2.9)
Monomer concentration	$\frac{dM}{dt} = -k_p [M] \mu_0$	$M(0) = M_0$	(2.12)
Hydrogen concentration	$\frac{dH_2}{dt} = -k_{tr}^H [H_2] \mu_0$	$H_2(0) = H_{20}$	(2.13)

The method of moments for homopolymerization in batch reactors

The application of the method of moments to calculate chain length averages from the polymer population balances is rather intuitive. Start by recalling the expressions for number and weight average degree of polymerization, DP_n and DP_w :

$$DP_n = \frac{\sum_{r=1}^{\infty} r P_r + \sum_{r=1}^{\infty} r D_r}{\sum_{r=1}^{\infty} P_r + \sum_{r=1}^{\infty} D_r} = \frac{\text{polymer mass}}{\text{polymer concentration}} \quad (2.15)$$

$$DP_w = \frac{\sum_{r=1}^{\infty} r^2 P_r + \sum_{r=1}^{\infty} r^2 D_r}{\sum_{r=1}^{\infty} r P_r + \sum_{r=1}^{\infty} r D_r} = \frac{\text{polymer mass} \times \text{chain length}}{\text{polymer mass}} \quad (2.16)$$

Since the i th moment of a generic distribution $f(x)$ is defined by:

$$\mu_i = \sum_{x=1}^{\infty} x^i f(x) \quad (2.17)$$

the moments for living and dead polymer chains can be defined as, μ and ν , with the expressions:

$$\mu_i = \sum_{r=1}^{\infty} r^i P_r \quad (2.18)$$

$$\nu_i = \sum_{r=2}^{\infty} r^i D_r \quad (2.19)$$

The summation for the moments of the dead polymer is started at $r = 2$. A dead polymer of length 1 would have the length of a monomer and is, therefore, excluded from

the definition of ν_i . Had the summation started at $r = 1$, the results would be practically indistinguishable from the ones obtained with Equation 2.19.

Now expressing Equations 2.15 and 2.16 in their standard method-of-the-moments formulation:

$$DP_n = \frac{\mu_1 + \nu_1}{\mu_0 + \nu_0} \quad (2.20)$$

$$DP_w = \frac{\mu_2 + \nu_2}{\mu_1 + \nu_1} \quad (2.21)$$

Notice that no new concepts have been introduced here: simply the conventional definitions of DP_n and DP_w have been used and reformulated as a ratio of moments of the chain length distribution (CLD). Now, our task is to find the equation for the zeroth, first and second moments of the CLDs for living and dead polymer chains. Since balances for these polymer populations have been developed already, the final expressions for the method of moments are just a few steps away.

Starting with the zeroth moment for living polymer chains, by definition:

$$\mu_0 = \sum_{r=1}^{\infty} P_r = P_1 + \sum_{r=2}^{\infty} P_r \quad (2.22)$$

Taking the first derivative of Equation 2.22, gives:

$$\frac{d\mu_0}{dt} = \frac{dP_1}{dt} + \sum_{r=2}^{\infty} \frac{dP_r}{dt} \quad (2.23)$$

Now substituting Equations 2.3 and 2.5 into Equation 2.23:

$$\begin{aligned} \frac{d\mu_0}{dt} &= k_i C^*[M] - k_p P_1[M] - (K_{TR} + k_{dac})P_1 \\ &+ \sum_{r=2}^{\infty} \{k_p[M](P_{r-1} - P_r) - (K_{TR} + k_{dac})P_r\} \end{aligned} \quad (2.24)$$

Rearranging Equation 2.24 to a more convenient form, gives:

$$\begin{aligned} \frac{d\mu_0}{dt} &= k_i C^*[M] - k_p[M] \left(P_1 + \sum_{r=2}^{\infty} P_r \right) \\ &- (K_{TR} + k_{dac}) \left(P_1 + \sum_{r=2}^{\infty} P_r \right) + k_p[M] \sum_{r=2}^{\infty} P_{r-1} \end{aligned} \quad (2.25)$$

Since $P_1 + \sum_{r=2}^{\infty} P_r = \sum_{r=1}^{\infty} P_r = \mu_0$ and $\sum_{r=2}^{\infty} P_{r-1} = \sum_{r=1}^{\infty} P_r = \mu_0$, Equation 2.25 can be further simplified to

$$\frac{d\mu_0}{dt} = k_i C^*[M] - k_p[M]\mu_0 - (K_{TR} + k_{dac})\mu_0 + k_p[M]\mu_0 \quad (2.26)$$

and, finally the expression for the zeroth moment of living polymer chains is obtained:

$$\frac{d\mu_0}{dt} = k_i C^*[M] - (K_{TR} + k_{dac})\mu_0 \quad (2.27)$$

Note that Equation 2.27 is simply a molar balance for the number of moles of living chains in the reactor: living chains are formed by initiation of monomer-free active sites (C^*) and consumed by transfer or deactivation reactions; propagation reactions do not change the number of living chains in the reactor.

Similar expressions can be derived for the higher moments of the CLD of living polymer chains. For the first moment:

$$\mu_1 = \sum_{r=1}^{\infty} rP_r = P_1 + \sum_{r=2}^{\infty} rP_r \quad (2.28)$$

$$\frac{d\mu_1}{dt} = \frac{dP_1}{dt} + \sum_{r=2}^{\infty} r \frac{dP_r}{dt} \quad (2.29)$$

Substituting Equations 2.3 and 2.5 into Equation 2.29 gives:

$$\begin{aligned} \frac{d\mu_1}{dt} &= k_i C^* [M] - k_p P_1 [M] - (K_{TR} + k_{dac}) P_1 \\ &+ \sum_{r=2}^{\infty} r \{ k_p [M] (P_{r-1} - P_r) - (K_{TR} + k_{dac}) P_r \} \end{aligned} \quad (2.30)$$

Collecting the common terms:

$$\begin{aligned} \frac{d\mu_1}{dt} &= k_i C^* [M] - k_p [M] \left(P_1 + \sum_{r=2}^{\infty} rP_r \right) \\ &- (K_{TR} + k_{dac}) \left(P_1 + \sum_{r=2}^{\infty} rP_r \right) + k_p [M] \sum_{r=2}^{\infty} rP_{r-1} \end{aligned} \quad (2.31)$$

The term $\sum_{r=2}^{\infty} rP_{r-1}$ in Equation 2.31 must be expressed as a function of moments of the CLD to render this equation useful. Since,

$$\sum_{r=2}^{\infty} rP_{r-1} = 2P_1 + 3P_2 + 4P_3 + \dots \quad (2.32)$$

and

$$\sum_{r=1}^{\infty} P_r = P_1 + P_2 + P_3 + \dots = \mu_0 \quad (2.33)$$

$$\sum_{r=1}^{\infty} rP_r = P_1 + 2P_2 + 3P_3 + \dots = \mu_1 \quad (2.34)$$

then,

$$\sum_{r=2}^{\infty} rP_{r-1} = \sum_{r=1}^{\infty} P_r + \sum_{r=1}^{\infty} rP_r = \mu_0 + \mu_1 \quad (2.35)$$

Therefore, Equation 2.31 simplifies to

$$\frac{d\mu_1}{dt} = k_i C^*[M] - k_p[M]\mu_1 - (K_{TR} + k_{dac})\mu_1 + k_p[M](\mu_0 + \mu_1) \quad (2.36)$$

or, better still:

$$\frac{d\mu_1}{dt} = k_i C^*[M] - (K_{TR} + k_{dac})\mu_1 + k_p[M]\mu_0 \quad (2.37)$$

It should be apparent that the number average chain length for living polymers could be calculated already by solving Equations 2.27 and 2.37. To obtain the weight average chain length, an additional equation is needed for the second moment.

The model development for the second moment is analogous to the ones used for the zeroth and first moments:

$$\mu_2 = \sum_{r=1}^{\infty} r^2 P_r = P_1 + \sum_{r=2}^{\infty} r^2 P_r \quad (2.38)$$

$$\frac{d\mu_2}{dt} = \frac{dP_1}{dt} + \sum_{r=2}^{\infty} r^2 \frac{dP_r}{dt} \quad (2.39)$$

Once again, substituting Equations 2.3 and 2.5 in Equation 2.39 gives:

$$\begin{aligned} \frac{d\mu_2}{dt} &= k_i C^*[M] - k_p P_1[M] - (K_{TR} + k_{dac})P_1 \\ &\quad + \sum_{r=2}^{\infty} r^2 \{k_p[M](P_{r-1} - P_r) - (K_{TR} + k_{dac})P_r\} \end{aligned} \quad (2.40)$$

$$\begin{aligned} \frac{d\mu_2}{dt} &= k_i C^*[M] - k_p[M] \left(P_1 + \sum_{r=2}^{\infty} r^2 P_r \right) \\ &\quad - (K_{TR} + k_{dac}) \left(P_1 + \sum_{r=2}^{\infty} r^2 P_r \right) + k_p[M] \sum_{r=2}^{\infty} r^2 P_{r-1} \end{aligned} \quad (2.41)$$

The term $\sum_{r=2}^{\infty} r^2 P_{r-1}$ needs to be expressed as a function of the moments. Since,

$$\sum_{r=2}^{\infty} r^2 P_{r-1} = 4P_1 + 9P_2 + 16P_3 + \dots \quad (2.42)$$

and

$$\sum_{r=1}^{\infty} (r+1)^2 P_r = \sum_{r=1}^{\infty} (r^2 + 2r + 1)P_r = 4P_1 + 9P_2 + 16P_3 + \dots = \mu_2 + 2\mu_1 + \mu_0 \quad (2.43)$$

then, Equation 2.41 becomes:

$$\frac{d\mu_2}{dt} = k_i C^*[M] - k_p[M]\mu_2 - (K_{TR} + k_{dac})\mu_2 + k_p[M](\mu_2 + 2\mu_1 + \mu_0) \quad (2.44)$$

Collecting similar terms, the final expression for the second moment of the CLD of living chains is obtained:

$$\frac{d\mu_2}{dt} = k_i C^* [M] - (K_{TR} + k_{dac})\mu_2 + k_p [M](2\mu_1 + \mu_0) \quad (2.45)$$

Equations 2.27, 2.37 and 2.45 can be used together with the molar balances for hydrogen and monomer to calculate the number and weight chain length averages for living polymer.

Next, the moment equations for the CLD of dead polymer chains is derived. The zeroth moment of the CLD for dead chain is

$$v_0 = \sum_{r=2}^{\infty} D_r \quad (2.46)$$

$$\frac{dv_0}{dr} = \sum_{r=2}^{\infty} \frac{dD_r}{dr} \quad (2.47)$$

Substituting Equation 2.11 in Equation 2.47, yields:

$$\frac{dv_0}{dr} = (K_{TR} + k_{dac}) \sum_{r=2}^{\infty} P_r \quad (2.48)$$

Remembering the definition of μ_0 , Equation 2.48 becomes,

$$\frac{dv_0}{dt} = (K_{TR} + k_{dac})(\mu_0 - P_1) \cong (K_{TR} + k_{dac})\mu_0 \quad (2.49)$$

where the approximation is generally valid since $\mu_0 \gg P_1$.

Similar expressions are easily derived for the higher moments of the CLD of dead polymer:

$$\frac{dv_1}{dt} = (K_{TR} + k_{dac})(\mu_1 - P_1) \cong (K_{TR} + k_{dac})\mu_1 \quad (2.50)$$

$$\frac{dv_2}{dt} = (K_{TR} + k_{dac})(\mu_2 - P_1) \cong (K_{TR} + k_{dac})\mu_2 \quad (2.51)$$

Table 2.6 summarizes the equations developed for the method of moments. Notice that only nine ODEs need to be solved, instead of the very large system required for the complete solution of the population balance equations. The price paid for this simplification is that the complete CLD can no longer be modeled, only its averages DP_n and DP_w .

The equations in Table 2.6 can be solved using several numerical methods for ODEs. The resulting system is commonly stiff since the moments of the living polymer and active site concentration vary much faster than the other dependent variables in the system. A common way to eliminate this nuisance is to make the steady-state approximation for the moments of living polymer and active site concentration. This possibility will be examined in the following subsection.

Table 2.6 Summary of moment equations for homopolymerization in a batch reactor

Description	Equations	Initial conditions	(#)
0th moment of living chains	$\frac{d\mu_0}{dt} = k_i C^* [M] - (K_{TR} + k_{dac}) \mu_0$	$\mu_0(0) = 0$	(2.27)
1st moment of living chains	$\frac{d\mu_1}{dt} = k_i C^* [M] - (K_{TR} + k_{dac}) \mu_1 + k_p [M] \mu_0$	$\mu_1(0) = 0$	(2.37)
2nd moment of living chains	$\frac{d\mu_2}{dt} = k_i C^* [M] - (K_{TR} + k_{dac}) \mu_2 + k_p [M] (2\mu_1 + \mu_0)$	$\mu_2(0) = 0$	(2.45)
0th moment of dead chains	$\frac{dv_0}{dt} = (K_{TR} + k_{dac}) \mu_0$	$v_0(0) = 0$	(2.49)
1st moment of dead chains	$\frac{dv_1}{dt} = (K_{TR} + k_{dac}) \mu_1$	$v_1(0) = 0$	(2.50)
2nd moment of dead chains	$\frac{dv_2}{dt} = (K_{TR} + k_{dac}) \mu_2$	$v_2(0) = 0$	(2.51)
Active site concentration	$\frac{dC^*}{dt} = K_{TR} \mu_0 - (k_i [M] + k_{dac}) C^*$	$C^*(0) = C_0^*$	(2.8)
Deactivated sites	$C_d(t) = C_0^* - C^* - \mu_0$		(2.9)
Monomer concentration	$\frac{dM}{dt} = -k_p [M] \mu_0$	$M(0) = M_0$	(2.12)
Hydrogen concentration	$\frac{dH_2}{dt} = -k_{tr}^H [H_2] \mu_0$	$H_2(0) = H_{20}$	(2.13)
Number average chain length	$DP_n = \frac{\mu_1 + v_1}{\mu_0 + v_0}$		(2.20)
Weight average chain length	$DP_w = \frac{\mu_2 + v_2}{\mu_1 + v_1}$		(2.21)

The quasi-steady-state approximation for homopolymerization in batch reactors

The quasi-steady-state approximation (QSSA) is commonly made for the moments of living polymer chains since, for most practical situations, an equilibrium is achieved instantaneously between chain initiation and chain transfer, $k_i C^* [M] \cong (K_{TR} + k_{dac}) \mu_0$. This equilibrium results from the fast dynamics of the initiation and transfer reactions compared to that of the overall polymerization rate. In this case, an even simpler system of equations is obtained than the one listed in Table 2.6.

Make the QSSA for Equation 2.27, the zeroth moment of living chains:

$$\frac{d\mu_0}{dt} = k_i C^* [M] - (K_{TR} + k_{dac}) \mu_0 = 0 \quad (2.27.SS)$$

Therefore,

$$\mu_0 = \frac{k_i C^* [M]}{K_{TR} + k_{dac}} \quad (2.52)$$

Also, make the QSSA for the first and second moments of living polymer, $d\mu_1/dt = d\mu_2/dt = 0$, thus simplifying Equations 2.37 and 2.45 to

$$\mu_1 = \frac{k_i C^* + k_p \mu_0}{K_{TR} + k_{dac}} [M] \quad (2.53)$$

$$\mu_2 = \frac{k_i C^* + k_p (2\mu_1 + \mu_0)}{K_{TR} + k_{dac}} [M] \quad (2.54)$$

It is also common to make the QSSA for the active sites, reducing Equation 2.8 to

$$C^* = \frac{K_{TR}}{k_i [M] + k_{dac}} \mu_0 \quad (2.55)$$

A system of algebraic-differential equations has now been obtained that is very easy to solve. This new system of equations is summarized in Table 2.7 for easy reference.

What happens if it is found that other polymerization steps need to be added to our polymerization mechanism of Table 2.4? Would all these equations need to be derived once again to account for these new steps? The answer is an enthusiastic No! It will be shown below that just some of our constants need to be modified, not the equations, to add other mechanism steps to our model.

Addition of other homopolymerization kinetic steps

Additional polymerization steps can be included in the equations described above without significantly altering the population balances and moment equations. For instance, assume that two additional chain transfer steps need to be introduced, chain transfer to monomer and to cocatalyst, and also that a poisoning reaction is to be added to our mechanism, as proposed in Table 2.8. Note that a few simplifying assumptions have been adopted in the mechanism shown in Table 2.8: rigorously speaking, transfer to monomer produces a living polymer chain of length 1 (P_1), not a monomer-free C^* site. In the same way, transfer to cocatalyst produces alkyl-terminated sites, not C^* sites (see Scheme 2.3). These sites could be kept track of separately, but this would require a few additional balances for these new site types. In general, these additional details just make the mathematical treatment more cumbersome and are not very relevant for most simulations, so it was decided that no differentiation would be made between them.

Because adding these new steps to the mechanism does not affect the general structure of the problem, only the lumped constant K_{TR} needs to be redefined to include the new transfer steps and to replace the kinetic constant k_{dac} with the new lumped constant K_D , as follows:

$$K_{TR} = k_{t\beta} + k_{tr}^H H_2 + k_{tr}^{mon} M + k_{tr}^{Al} Al \quad (2.56)$$

$$K_D = k_{dac} + k_{dacI} [I_{nh}] \quad (2.57)$$

Table 2.7 Summary of moment equations for homopolymerization in a batch reactor using the steady-state approximation for the moments of living polymer and active sites

Description	Equations	Initial conditions	(#)
0th moment of living chains	$\mu_0 = \frac{k_i C^*}{K_{TR} + k_{dac}} [M]$		(2.52)
1st moment of living chains	$\mu_1 = \frac{k_i C^* + k_p \mu_0}{K_{TR} + k_{dac}} [M]$		(2.53)
2nd moment of living chains	$\mu_2 = \frac{k_i C^* + k_p (2\mu_1 + \mu_0)}{K_{TR} + k_{dac}} [M]$		(2.54)
0th moment of dead chains	$\frac{dv_0}{dt} = (K_{TR} + k_{dac})\mu_0$	$v_0(0) = 0$	(2.49)
1st moment of dead chains	$\frac{dv_1}{dt} = (K_{TR} + k_{dac})\mu_1$	$v_1(0) = 0$	(2.50)
2nd moment of dead chains	$\frac{dv_2}{dt} = (K_{TR} + k_{dac})\mu_2$	$v_2(0) = 0$	(2.51)
Active site concentration	$C^* = \frac{K_{TR}}{k_i[M] + k_{dac}} \mu_0$		(2.55)
Deactivated sites	$C_d = C_0^* - C^* - \mu_0$		(2.9)
Monomer concentration	$\frac{dM}{dt} = -k_p[M]\mu_0$	$M(0) = M_0$	(2.12)
Hydrogen concentration	$\frac{dH_2}{dt} = -k_{tr}^H[H_2]\mu_0$	$H_2(0) = H_{20}$	(2.13)
Number average chain length	$DP_n = \frac{\mu_1 + v_1}{\mu_0 + v_0}$		(2.20)
Weight average chain length	$DP_w = \frac{\mu_2 + v_2}{\mu_1 + v_1}$		(2.21)

Table 2.8 Additional polymerization mechanism steps

	Chemical equation	Rate constant
Transfer to monomer	$P_r + M \rightarrow C^* + D_r$	k_{tr}^{mon}
Transfer to cocatalyst	$P_r + Al \rightarrow C^* + D_r$	k_{tr}^{Al}
Poisoning	$P_r + I_{nh} \rightarrow C_d + D_r$	k_{daci}
Site activation	$C + Al \rightarrow C^*$	k_{ac}

With these new definitions, the equations shown in Tables 2.5, 2.6 and 2.7 can be applied to obtain the equations for the complete population balance, the method of moments, or the method of moments with the QSSA, respectively. Note that because of chain transfer to monomer, Equation 2.12 should, strictly speaking, include a new monomer consumption term, that is:

$$\frac{dM}{dt} = -(k_p + k_{tr}^{mon})[M]\mu_0 \cong -k_p[M]\mu_0 \quad (2.12a)$$

However, since $k_p \gg k_{tr}^{mon}$ for high polymers, this term is very seldom included when modeling polymerization reactors.

So far, it has been assumed that active site formation was instantaneous. This step could have been taken into consideration by adding the elementary step described in the last row of Table 2.8. In this case, another generation term needs to be added to Equation 2.8,

$$\frac{dC^*}{dt} = k_{ac}[Al]C + K_{TR}\mu_0 - (k_i[M] + K_D)C^*, \quad C^*(0) = 0 \quad (2.58)$$

and a molar balance introduced for the concentration of catalyst in the reactor:

$$\frac{dC}{dt} = -k_{ac}[Al]C, \quad C(0) = C_0 \quad (2.59)$$

It is also usual to make the QSSA for Equation 2.58; in this case, the following equation is obtained:

$$C^* = \frac{k_{ac}[Al]C + K_{TR}\mu_0}{k_i[M] + K_D} \quad (2.60)$$

In general, the concentration of cocatalyst in the reactor is several times higher than that of catalyst; therefore, it is conventional to consider the cocatalyst concentration to be constant throughout the polymerization.

Homopolymerization in semibatch and continuous stirred-tank reactors

Olefin polymerization in batch reactors is not common. Laboratory-scale high-throughput reactors are perhaps one of the few examples of such reactors applied to olefin polymerization. Some olefin polymerization tubular reactors can also be treated as batch reactors, where a polymerization-time to reactor-length transformation can be made and directly applied to the equations derived above if the tubular reactor has plug-flow residence time.

Semibatch and continuous stirred-tank reactors (CSTRs) are much more commonly found in polyolefin production. Semibatch reactors are the standard choice for laboratory-scale polymerizations, while CSTRs dominate industrial production, as will be seen in Section 2.5. The equations derived above are easily translated into semibatch and CSTR operation mode by simply adding terms for the inflow and outflow streams in the reactor. For instance, consider Equation 2.49 for the zeroth moment of dead chains. The molar flow rate [mol s^{-1}] leaving the reactor is given by

$$F_{v_0\text{out}} = \frac{Q}{V}v_0 = \frac{v_0}{\bar{t}} = sv_0 \quad (2.61)$$

where Q [$L s^{-1}$] is the reactor volumetric flow rate, V [L] is the reactor volume, \bar{t} [s] is average reactor residence time, and s is the reciprocal of \bar{t} [s^{-1}]. Therefore, for a single CSTR to which no polymer is fed:

$$\frac{dv_0}{dt} = (K_{TR} + K_D)\mu_0 - sv_0 \quad (2.62)$$

For two or more CSTRs in series, polymer made in a previous reactor is transferred to the next reactor in the series. Therefore, Equation 2.62 becomes

$$\frac{dv_0}{dt} = (K_{TR} + K_D)\mu_0 + F_{v_{0in}} - sv_0 \quad (2.63)$$

where $F_{v_{0in}}$ is the molar flow rate [$mol s^{-1}$] of dead polymer entering the polymerization reactor.

Similar expressions can be obtained for all the species for which equations were derived before for batch operation. Table 2.9 is an extension of Table 2.6; it summarizes a general set of equations for batch, semibatch and continuous reactor operation. The set of initial conditions suggested in Table 2.9 is for polymerization start-up from reactors free of catalyst and polymer, but already containing an initial concentration of monomer and hydrogen. Notice that, as done before for batch reactors, the QSSA can also be made to the equations describing the number of moles of living polymer chains and catalyst sites in the reactor. As mentioned above, this simplification is commonly made to reduce the stiffness of the resulting set of differential equations.

When the CSTR is operated at steady-state, the solution becomes easier. In this case, all the left-hand terms of the differential equations shown in Table 2.9 are simply set to zero and the resulting system of algebraic equations is solved for the moments of living and dead polymer and for the reactant concentrations.

Multiple-site-type catalysts

When catalysts containing more than one type of active sites are used, the conventional approach is simply to repeat the model equations derived for single-site-type catalysts, using distinct kinetic rate constants for each site type. This simply means that the multiple-site catalyst is considered to be a collection of single-site type catalysts. Sometimes, site transformation steps may also be included in the model to permit the conversion of one site type to another, but the polymerization mechanism for each site type remains the one previously described.

Table 2.10 summarizes the model equations for polymerization with multiple-site catalysts in batch, semibatch and continuous reactors. The moment equations are, as expected, the same as the ones developed for single-site types, but applied for each individual site type, as indicated by the subscript j . Notice that the molar balances for monomer and hydrogen use the concentration of all active site types and that the chain length averages are also calculated using polymer made on all active sites. The new variable n appearing in these equations is the number of active site types in the catalyst. Initial conditions were omitted because they are analogous to the ones shown in Table 2.9, now applied for each site type.

Table 2.9 Summary of moment equations for homopolymerization in batch, semi-batch and CSTRs

Description	Equations	Start-up initial conditions	(#)
0th moment of living chains	$\frac{d\mu_0}{dt} = k_i C^* [M] - (K_{TR} + K_D) \mu_0 + F_{\mu_0 in} - s \mu_0 \cong 0$	$\mu_0(0) = 0$	(2.64)
1st moment of living chains	$\frac{d\mu_1}{dt} = k_i C^* [M] - (K_{TR} + K_D) \mu_1 + k_p [M] \mu_0 + F_{\mu_1 in} - s \mu_1 \cong 0$	$\mu_1(0) = 0$	(2.65)
2nd moment of living chains	$\frac{d\mu_2}{dt} = k_i C^* [M] - (K_{TR} + K_D) \mu_2 + k_p [M] (2\mu_1 + \mu_0) + F_{\mu_2 in} - s \mu_2 \cong 0$	$\mu_2(0) = 0$	(2.66)
0th moment of dead chains	$\frac{dv_0}{dt} = (K_{TR} + K_D) \mu_0 + F_{v_0 in} - s v_0$	$v_0(0) = 0$	(2.63)
1st moment of dead chains	$\frac{dv_1}{dt} = (K_{TR} + K_D) \mu_1 + F_{v_1 in} - s v_1$	$v_1(0) = 0$	(2.67)
2nd moment of dead chains	$\frac{dv_2}{dt} = (K_{TR} + K_D) \mu_2 + F_{v_2 in} - s v_2$	$v_2(0) = 0$	(2.68)
Active site concentration	$\frac{dC^*}{dt} = K_{TR} \mu_0 - (k_i [M] + K_D) C^* + F_{C^* in} - s C^* \cong 0$	$C^*(0) = 0$	(2.69)
Deactivated sites	$\frac{dC_d}{dt} = K_D (C^* + \mu_0) - F_{C_d in} + s C_d \cong 0$	$C_d(0) = 0$	(2.9a)
Monomer concentration	$\frac{dM}{dt} = -k_p [M] \mu_0 + F_{M in} - s M$	$M(0) = M_0$	(2.70)
Hydrogen concentration	$\frac{dH_2}{dt} = -k_{tr}^H [H_2] \mu_0 + F_{H_2 in} - s H_2$	$H_2(0) = H_{20}$	(2.71)
Number average chain length	$DP_n = \frac{\mu_1 + v_1}{\mu_0 + v_0}$		(2.20)
Weight average chain length	$DP_w = \frac{\mu_2 + v_2}{\mu_1 + v_1}$		(2.21)

The method of instantaneous distributions – Flory’s most probable distribution for single- and multiple-site catalysts

The method of instantaneous distributions relies on analytical solutions for the microstructural distributions of polymer chains made at a given instant in time during the polymerization. The first instantaneous distribution we will study is Flory’s most probable distribution. According to Flory’s weight distribution of polymer chains of length r , $w(r)$, the CLD of polyolefins made with single-site catalysts is narrow (at least as compared to those made with heterogeneous Ziegler–Natta and Phillips catalysts) and has a PDI = 2.0.

Table 2.10 Summary of moment equations for homopolymerization in batch, semi-batch and CSTRs using a multiple-site-type catalyst

Description	Equations	(#)
0th moment of living chains	$\frac{d\mu_{0,j}}{dt} = k_{i,j}C_j^*[M] - (K_{TR,j} + K_{D,j})\mu_{0,j} + F_{\mu_{0,j}in} - s\mu_{0,j} \cong 0$	(2.72)
1st moment of living chains	$\frac{d\mu_{1,j}}{dt} = k_{i,j}C_j^*[M] - (K_{TR,j} + K_{D,j})\mu_{1,j} + k_{p,j}[M]\mu_{0,j} + F_{\mu_{1,j}in} - s\mu_{1,j} \cong 0$	(2.73)
2nd moment of living chains	$\frac{d\mu_{2,j}}{dt} = k_{i,j}C_j^*[M] - (K_{TR,j} + K_{D,j})\mu_{2,j} + k_{p,j}[M](2\mu_{1,j} + \mu_{0,j}) + F_{\mu_{2,j}in} - s\mu_{2,j} \cong 0$	(2.74)
0th moment of dead chains	$\frac{dv_{0,j}}{dt} = (K_{TR,j} + K_{D,j})\mu_{0,j} + F_{v_{0,j}in} - sv_{0,j}$	(2.75)
1st moment of dead chains	$\frac{dv_{1,j}}{dt} = (K_{TR,j} + K_{D,j})\mu_{1,j} + F_{v_{1,j}in} - sv_{1,j}$	(2.76)
2nd moment of dead chains	$\frac{dv_{2,j}}{dt} = (K_{TR,j} + K_{D,j})\mu_{2,j} + F_{v_{2,j}in} - sv_{2,j}$	(2.77)
Active site concentration	$\frac{dC_j^*}{dt} = K_{TR,j}\mu_{0,j} - (k_{i,j}[M] + K_{D,j})C_j^* + F_{C_j^*in} - sC_j^* \cong 0$	(2.78)
Deactivated sites	$\frac{dC_{d,j}}{dt} = K_{D,j}(C_j^* + \mu_{0,j}) - F_{C_{d,j}in} + sC_{d,j} \cong 0$	(2.79)
Monomer concentration	$\frac{dM}{dt} = - \sum_{j=1}^n k_{p,j}[M]\mu_{0,j} + F_{Min} - sM$	(2.80)
Hydrogen concentration	$\frac{dH_2}{dt} = - \sum_{j=1}^n k_{tr}^H[H_2]\mu_{0,j} + F_{H_2in} - sH_2$	(2.81)
Number average chain length	$DP_n = \frac{\sum_{j=1}^n (\mu_{1,j} + v_{1,j})}{\sum_{j=1}^n (\mu_{0,j} + v_{0,j})}$	(2.82)
Weight average chain length	$DP_w = \frac{\sum_{j=1}^n (\mu_{2,j} + v_{2,j})}{\sum_{j=1}^n (\mu_{1,j} + v_{1,j})}$	(2.83)

It is given by a simple-looking, but powerful, equation:

$$w(r) = \frac{r}{DP_n^2} \exp\left(-\frac{r}{DP_n}\right) = r\tau^2 \exp(-r\tau) \quad (2.84)$$

In Equation 2.84, the parameter $\tau = 1/DP_n$ is the ratio of all transfer reaction rates to the propagation reaction rate. As formulated in Equation 2.84, Flory's distribution describes the CLD (r is the number of monomer molecules in the polymer chain) not the MWD. To obtain the MWD, DP_n is simply replaced by \overline{M}_n and r by the molecular weight of

the polymer, $MW = rw_m$ (where w_m is the average molar mass of the repeating unit in the polymer chain):

$$w(MW) = \frac{MW}{\overline{M}_n^2} \exp\left(-\frac{MW}{\overline{M}_n}\right) = MW\tau_{MW}^2 \exp(-MW\tau_{MW}) \quad (2.84a)$$

We prefer the slightly more generic CLD formulation and will use it in this chapter, but it should be evident that the CLD can be converted into the MWD by simply using the molar mass of the monomer for homopolymers or the average molar mass of the repeating unit for copolymers.

For the standard model for olefin polymerization kinetics, τ is defined as

$$\tau = \frac{k_{t\beta}}{k_p[M]} + \frac{k_{tr}^{mon}}{k_p} + \frac{k_{tr}^{Al}[Al]}{k_p[M]} + \frac{k_{tr}^H[H_2]}{k_p[M]} \quad (2.85)$$

The beauty of Equation 2.84 is that if more transfer reactions are added to the mechanism, we just need to keep including them in the definition of τ ; Flory's distribution remains unaltered.

Even without a formal derivation, the physical meaning of Flory's distribution is very easy to grasp: the CLD predicted by Flory's distribution is just the outcome of any polymerization process where the chains may either grow by monomer addition or stop growing by transfer reactions. Therefore, by accepting the polymerization mechanism shown in Tables 2.4 and 2.8, we are automatically agreeing that the MWD of the polymer made through that mechanism will follow Flory's distribution *instantaneously*. This conclusion should not be lost from sight, because it will help us to understand much about polyolefin microstructure.

In the above paragraph the word "instantaneously" was written in italics for a good reason. An instantaneous distribution predicts the microstructure that is formed at the polymerization conditions existing at a given instant in time in the reactor. To use an analogy, instantaneous distributions are snapshots of the polymer microstructure. Extending this analogy a little more: if the subject in the picture is not moving (steady-state operation), snapshots taken at different times look exactly the same; however, if the subject is in movement, a snapshot taken at a given time will be different from another taken at a later or earlier time (non-steady-state operation) – in fact, seen in sequence, the snapshots will resemble a movie strip. Figure 2.21 illustrates this behavior for a case when the concentration of hydrogen varies as a function of time in the reactor, producing polymer with increasing molecular weight averages. This situation may happen, for instance, during a low-to-high molecular weight grade transition.

Therefore, at steady-state, the complete CLD or MWD of polyolefins can be predicted using Equation 2.84 and the value of τ calculated for the concentrations of monomer, cocatalyst, and chain transfer agent in the reactor, as well as the several required polymerization kinetic constants calculated at a given polymerization temperature. This is a rather straightforward procedure.

Can this approach be extended to non-steady-state reactor operation? The answer is yes, provided that the time-scale for the dynamic phenomena taking place at the reactor scale, such as changes in temperature and reactant concentrations, is much larger than the time-scale for growing a polymer chain. This is a necessary condition for the applicability of the instantaneous distribution method because, if the conditions in the reactor change

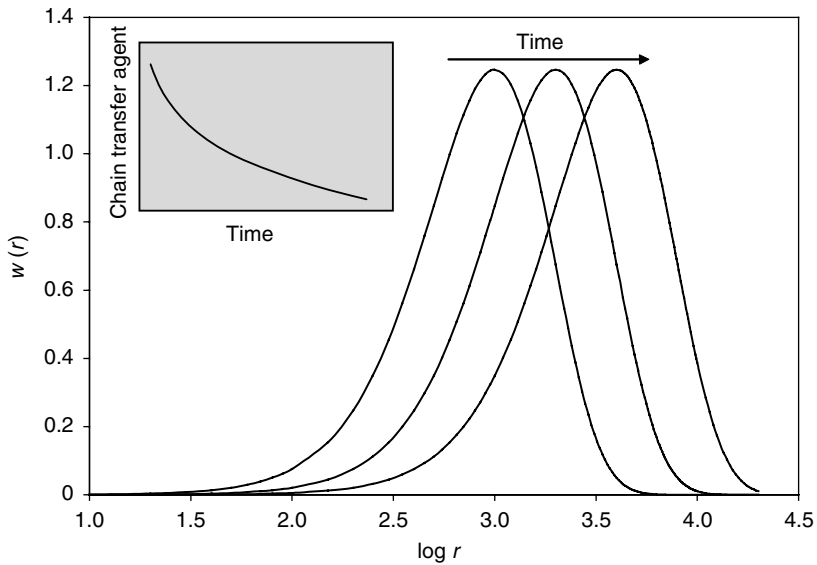


Figure 2.21 Instantaneous CLDs varying as a function of chain transfer agent (H_2) concentration in the reactor.

at rates that are similar to the life-time of a polymer chain, instantaneous distributions are no longer valid. Instantaneous distributions are solved assuming that all conditions are constant during one “snapshot.” Using our analogy again, the subject may move, but not faster than the shutter speed, otherwise the image becomes blurred. Luckily, for olefin polymerization reactors, the reactor residence time is in the order several minutes (for solution processes) to a couple of hours (for most other processes), while the life-time of a polymer chain is in the order of tenths of seconds to a few seconds. Therefore, the method of instantaneous distributions can always confidently be applied to industrial polyolefin reactors.

To calculate the CLD of polymer made during a give time interval at non-steady-state conditions, say one average reactor residence time, simply use the equation:

$$\bar{w}(r) = \frac{\int_0^{\bar{t}} w(r, t) R_p(t) dt}{\int_0^{\bar{t}} R_p(t) dt} \quad (2.86)$$

where $R_p(t)$ is the rate of polymerization at a given time. Notice that the instantaneous distribution is now also a function of time, $w(r, t)$, since τ varies during non-steady-state operation. (In Figure 2.21, the dropping H_2 concentration causes τ to decrease and $w(r, t)$ to shift to the right as time increases.)

It should be apparent that, if the method of instantaneous distributions is used, there is no need to apply the method of moments. Instead, simply solve the molar balances for the concentration of monomer, hydrogen and any other relevant reactants (and energy balances, for non-isothermal polymerization) and follow the value of τ and, consequently, CLD in time. This method is, in fact, very powerful because it predicts the complete CLD instead

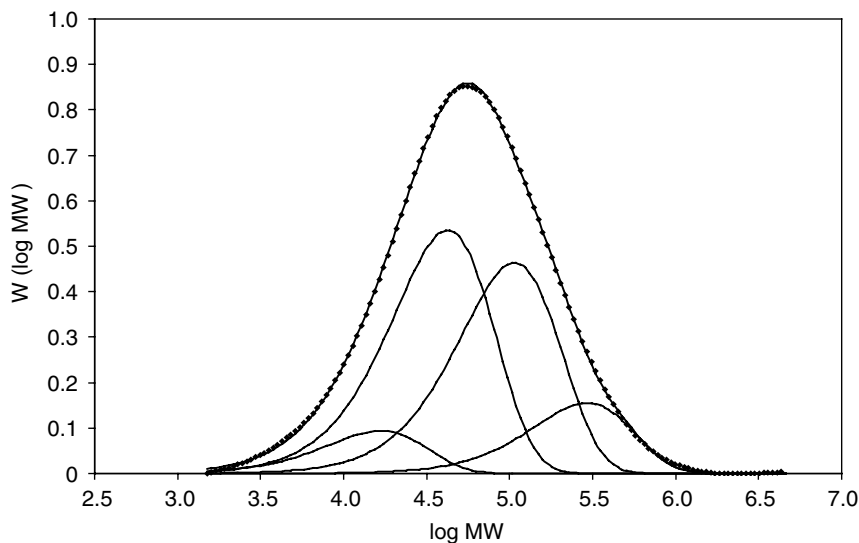


Figure 2.22 MWD of a Ziegler–Natta polyolefin, represented as a superposition of several Flory's distributions. The dotted-line is the GPC-measured MWD of the polyolefin.

of only averages from the method of moments. If the relevant instantaneous distribution is known, and the conditions outlined above for its applicability are met, the method of instantaneous distributions should always be the preferred modeling approach in our opinion.

Figure 2.22 introduces the use of Flory's distributions to model the CLD of polymers made with multiple-site catalysts. The approach described here is straightforward: if one Flory's distribution describes the CLD of polyolefins made with a single-site catalyst, multiple Flory's distributions will be adequate to represent the CLD of polyolefins made with multiple-site catalysts. Mathematically,

$$w(r) = \sum_{i=1}^n m_i \frac{r}{\text{DP}_{n,i}^2} \exp\left(-\frac{r}{\text{DP}_{n,i}}\right) = \sum_{i=1}^n m_i (r\tau_i^2) \exp(-r\tau_i) \quad (2.87)$$

where m_i is the mass fraction of polymer made by each site type and n is the total number of site types on the catalyst.

Equation 2.87 can be used to represent the CLD of polyolefins made with the combination of two or more metallocenes very well [35, 38]. This is a reasonably easy case, since the individual metallocenes can be tested separately to obtain the values of Flory's τ parameter. For multiple-site catalysts, such as heterogeneous Ziegler–Natta and Philips catalysts, the procedure for obtaining τ values for each site type is more elaborate and involves the deconvolution of the MWD into several Flory's distributions. This subject will not be covered in this chapter; the reader is directed to references 39 and 40 at the end of the chapter for more information on this subject. Suffice to say that MWD deconvolution involves the use of a non-linear least-squares optimization routine to

minimize the squares of the error between the measured MWD, $w_{\text{exp}}(M_w)$, and the MWD predicted by Equation 2.87. The objective function used for these optimizations is formulated as

$$F(m_i, \tau_i, n) = \text{Min} \left[w_{\text{exp}}(MW) - \sum_{i=1}^n m_i (MW \tau_{MW_i}^2) \exp(-MW \tau_{MW_i}) \right]^2$$

At the end of the optimization, the “best” values for m_i , τ_i and n should be found. As is usually the case with non-linear optimization problems, there is always a risk of multiple solutions but, because Flory’s distribution has a fixed width (with PDI = 2.0), the MWD deconvolution procedure is generally quite robust.

The results of the MWD deconvolution procedure should be interpreted with care. First, make sure that the polymer was produced under spatially uniform and steady-state conditions. Second, ensure that peak broadening during MWD analysis by GPC is negligible. Third, and more importantly, the MWD deconvolution procedure can only retrieve the minimum number of Flory’s sites required to represent the measured MWD; more sites may be present, but not seen, because of peak superposition. Considerable controversy lingers about the real meaning of the MWD deconvolution procedure. It is, however, important to realize that the use of several Flory’s distributions to describe the MWD of polymer made with multiple-site catalysts is exactly equivalent to using the set of moment equations shown in Table 2.10; they are just different ways of formulating the same problem. One method is not any more valid than the other.

2.3.2 Copolymerization

Linear chains

The models considered earlier were developed for homopolymerization of olefins with single- and multiple-site catalysts. As has already been seen, several industrial polyolefins are, however, copolymers of ethylene, propylene and higher α -olefins. Because, for copolymerization, the kinetic rate constants depend on monomer and chain end type (in the terminal model), modeling these systems may seem daunting at first sight, but it will now be shown that, using the concept of pseudo-kinetic constants, the same equations derived for homopolymerization can be applied for copolymerization as well.

Start by extending the homopolymerization model shown in Table 2.4 to the terminal model for copolymerization in Table 2.11. It is best to keep the polymerization mechanism as simple as possible at this stage; later it will be seen that it is easy to extend this model to include additional polymerization steps.

Now proceed to develop population balances for living chains, similarly to what has already been done for homopolymerization; the only difference is that an equation is needed for chains terminated in monomer type *A* and another for chains terminated in monomer type *B*. For chains with $r \geq 2$ made in a batch reactor,

$$\begin{aligned} \frac{dP_r^A}{dt} = & k_{pAA}(P_{r-1}^A - P_r^A)[A] + k_{pBA}P_{r-1}^B[A] - k_{pAB}P_r^A[B] \\ & - (k_{t\beta A} + k_{trA}^H[H_2] + k_{dacA})P_r^A \end{aligned} \quad (2.88)$$

Table 2.11 Simplified terminal model for binary copolymerization of olefins

Description	Chemical equations	Rate constants
Initiation	$C^* + A \rightarrow P_1^A$	k_{iA}
	$C^* + B \rightarrow P_1^B$	k_{iB}
Propagation	$P_r^A + A \rightarrow P_{r+1}^A$	k_{pAA}
	$P_r^A + B \rightarrow P_{r+1}^B$	k_{pAB}
	$P_r^B + A \rightarrow P_{r+1}^A$	k_{pBA}
	$P_r^B + B \rightarrow P_{r+1}^B$	k_{pBB}
β -Hydride elimination	$P_r^A \rightarrow C_H^* + D_r^{\equiv A}$	$k_{t\beta A}$
	$P_r^B \rightarrow C_H^* + D_r^{\equiv B}$	$k_{t\beta B}$
Transfer to H_2	$P_r^A + H_2 \rightarrow C_H^* + D_r$	k_{trA}^H
	$P_r^B + H_2 \rightarrow C_H^* + D_r$	k_{trB}^H
Monomolecular deactivation	$P_r^A \rightarrow C_d + D_r$	k_{dacA}
	$P_r^B \rightarrow C_d + D_r$	k_{dacB}

and

$$\begin{aligned} \frac{dP_r^B}{dt} = & k_{pBB}(P_{r-1}^B - P_r^B)[B] + k_{pAB}P_{r-1}^A[B] - k_{pBA}P_r^B[A] \\ & - (k_{t\beta B} + k_{trB}^H[H_2] + k_{dacB})P_r^B \end{aligned} \quad (2.89)$$

The change in concentration of chains of length r , terminated on monomer A or B is thus:

$$\frac{dP_r}{dt} = \frac{dP_r^A}{dt} + \frac{dP_r^B}{dt} \quad (2.90)$$

Substituting Equations 2.88 and 2.89 in Equation 2.90 and rearranging the result, the following expression is obtained:

$$\begin{aligned} \frac{dP_r}{dt} = & k_{pAA}P_{r-1}^A[A] + k_{pAB}P_{r-1}^A[B] + k_{pBA}P_{r-1}^B[A] + k_{pBB}P_{r-1}^B[B] \\ & - (k_{pAA}P_r^A[A] + k_{pAB}P_r^A[B] + k_{pBA}P_r^B[A] + k_{pBB}P_r^B[B]) \\ & - k_{t\beta A}P_r^A - k_{t\beta B}P_r^B - (k_{trA}^H P_r^A + k_{trB}^H P_r^B)[H_2] - k_{dacA}P_r^A - k_{dacB}P_r^B \end{aligned} \quad (2.91)$$

It seems clear that, if we were to proceed in this fashion, developing population balances and moment equations for copolymerization would be a procedure even more tedious (as hard as it may be to imagine!) than the one used for homopolymerization. But, do not despair. A few concepts will be introduced that will allow us to translate the homopolymerization equations to copolymerization equations with minimum effort.

First, four new variables will be defined:

$$P_A = \frac{P_r^A}{P_r^A + P_r^B} \quad \text{and} \quad P_B = 1 - P_A \quad (2.92)$$

$$f_A = \frac{A}{A + B} \quad \text{and} \quad f_B = 1 - f_A \quad (2.93)$$

$$P_r = P_r^A + P_r^B \quad (2.94)$$

$$M = A + B \quad (2.95)$$

The variables P_A and f_A are the fraction of chains terminated in monomer A and the fraction of monomer A in the polymerization reactor, respectively. It will be assumed that P_A does not depend on chain length. This hypothesis is intuitive and has been shown to be valid [41, 42]. The variable P_r had already been introduced in Equation 2.90 and M is the total number of moles of monomer in the reactor.

Now divide and multiply the right-hand side of Equation 2.91 by the product $M \times P_r$ to obtain:

$$\begin{aligned} \frac{dP_r}{dt} = & P_{r-1}[M](k_{pAA}P_Af_A + k_{pAB}P_Af_B + k_{pBA}P_Bf_A + k_{pBB}P_Bf_B) \\ & - P_r[M](k_{pAA}P_Af_A + k_{pAB}P_Af_B + k_{pBA}P_Bf_A + k_{pBB}P_Bf_B) - P_r(k_{t\beta A}P_A + k_{t\beta B}P_B) \\ & - P_r(k_{trA}^H P_A + k_{trB}^H P_B)[H_2] - P_r(k_{dacA}P_A + k_{dacB}P_B) \end{aligned} \quad (2.96)$$

Since the polymerization kinetic constants appear as weighted sums in Equation 2.96, this equation can be rewritten using pseudo-kinetic rate constants:

$$\begin{aligned} \frac{dP_r}{dt} = & \hat{k}_p[M](P_{r-1} - P_r) - (\hat{k}_{t\beta} + \hat{k}_{tr}^H[H_2] + \hat{k}_{dac})P_r \\ = & \hat{k}_p[M](P_{r-1} - P_r) - (\hat{K}_T + \hat{k}_{dac})P_r \end{aligned} \quad (2.97)$$

The important property of Equation 2.97 is that it is analogous to Equation 2.3 with the pseudo-kinetic constants replacing the actual polymerization kinetic constants. The same result would be obtained if it were decided to develop equations for any other species in the reactor. As a consequence, all the equations derived above for the homopolymerization model are applicable to copolymerization as well, provided that the polymerization kinetic constants are replaced with pseudo-kinetic constants. Equations in Table 2.10 can be used either for homo- and copolymerization! This elegant approach can considerably reduce the time and effort spent on developing models for copolymerization. Even though it was demonstrated for binary copolymers, this approach is equally valid for higher copolymers. Table 2.12 summarizes the pseudo-kinetic constants associated with the equations shown in Table 2.10.

To calculate the pseudo-kinetic constants, the values of P_A and f_A at each polymerization time need to be known. If the reactor is being operated at steady-state, P_A and f_A do not change and neither do the pseudo-kinetic constants. The value of P_A is calculated by realizing that, for high polymers, the rate of AB insertions must be equal to the rate of BA insertions, that is:

$$k_{pAB}P_r^A B = k_{pBA}P_r^B A \quad (2.98)$$

Table 2.12 Pseudo-kinetic constants for binary copolymerization

Pseudo-constant	Definition
\hat{k}_p	$k_{pAA}P_A f_A + k_{pAB}P_A f_B + k_{pBA}P_B f_A + k_{pBB}P_B f_B$
$\hat{k}_{t\beta}$	$k_{t\beta A}P_A + k_{t\beta B}P_B$
\hat{k}_{tr}^H	$k_{trA}^H P_A + k_{trB}^H P_B$
\hat{k}_{tr}^A	$k_{trA}^A P_A + k_{trB}^A P_B$
$\hat{k}_{tr}^{\text{mon}}$	$k_{trAA}^{\text{mon}} P_A f_A + k_{trAB}^{\text{mon}} P_A f_B + k_{trBA}^{\text{mon}} P_B f_A + k_{trBB}^{\text{mon}} P_B f_B$
\hat{k}_{daci}	$k_{\text{daciA}} P_A + k_{\text{daciB}} P_B$
\hat{k}_{dac}	$k_{\text{dacA}} P_A + k_{\text{dacB}} P_B$

Equation 2.98 is very easy to justify. Consider the following binary copolymer chain:



The number of times that monomer *A* is followed by monomer *B* is $n_{AB} = 11$ and the number of times the monomer *B* is followed by monomer *A* is $n_{BA} = 10$. Had one more unit of monomer *A* been added at the right end of the chain,



the number of *AB* and *BA* sequences would be exactly the same, that is, $n_{AB} = n_{BA} = 11$, which is an equivalent way to postulate Equation 2.98. It is easy to conclude that, for any polymer chain, $n_{AB} = n_{BA} \pm 1$. For long chains, this ± 1 difference is negligible and Equation 2.98 can always be applied.

Dividing Equation 2.98 by the product $M \times P_r$ gives:

$$k_{pAB}P_A f_B = k_{pBA}P_B f_A \quad (2.99)$$

or, equivalently,

$$k_{pAB}P_A(1 - f_A) = k_{pBA}(1 - P_A)f_A \quad (2.100)$$

Finally, solving for P_A :

$$P_A = \frac{k_{pBA}f_A}{k_{pAB}(1 - f_A) + k_{pBA}f_A} \quad (2.101)$$

The fraction of monomers *A* and *B* in the reactor, f_A and f_B , can be obtained from a simple molar balance. For a CSTR:

$$\frac{dA}{dt} = F_{\text{Ain}} - (k_{pAA}P_A + k_{pBA}P_B)[A]\mu_0 - sA \quad (2.102)$$

$$\frac{dB}{dt} = F_{\text{Bin}} - (k_{pBB}P_B + k_{pAB}P_A)[B]\mu_0 - sB \quad (2.103)$$

where F_{Ain} and F_{Bin} are the molar flow rates of monomers A and B to the reactor. Notice that transfer to monomer reactions were neglected in Equations 2.102 and 2.103 since they are negligible compared to the propagation reactions. (Equations for a semibatch reactor are obtained by setting $s = 0$; for a batch reactor $F_{Ain} = F_{Bin} = s = 0$.)

The instantaneous molar fraction of monomer A in the copolymer is given by:

$$F_{pA}^{inst} = \frac{R_{pA}}{R_{pA} + R_{pB}} \quad (2.104)$$

Equation 2.104 is only valid instantaneously. The accumulated average molar fraction of monomer A incorporated in the copolymer, F_{pA} , is calculated from a molar balance of the monomer incorporated in the polymer,

$$\frac{dA_p}{dt} = (k_{pAA}P_A + k_{pBA}P_B)[A]\mu_0 + F_{Apin} - sA_p \quad (2.105)$$

$$\frac{dB_p}{dt} = (k_{pBB}P_B + k_{pAB}P_A)[B]\mu_0 + F_{Bpin} - sB_p \quad (2.106)$$

and

$$F_{pA} = \frac{A_p}{A_p + B_p} \quad (2.107)$$

Multiple-site catalysts

Copolymers made with multiple-site catalysts can be modeled with the same equations derived for homopolymers produced with multiple-site catalysts in Table 2.10. The only modification required is the use of the pseudo-kinetic constants shown in Table 2.12 instead of the actual kinetic constants in the equations presented in Table 2.10.

Remember, however, that for non-steady-state operation, the pseudo-kinetic constants will vary as a function of f_A and P_A and must, therefore, be updated throughout the polymerization until a steady-state is reached.

The method of instantaneous distributions – Stockmayer's distribution for single- and multiple-site catalysts

Stockmayer's bivariate distribution [43] describes, instantaneously, the joint distributions of chain length and chemical composition of linear polymers made with coordination catalysts:

$$\begin{aligned} w(r, y) &= \frac{r}{DP_n^2} \exp\left(-\frac{r}{DP_n}\right) \sqrt{\frac{r}{2\pi\kappa}} \exp\left(-\frac{ry^2}{2\kappa}\right) \\ &= r\tau^2 \exp(-r\tau) \sqrt{\frac{r}{2\pi\kappa}} \exp\left(-\frac{ry^2}{2\kappa}\right) \end{aligned} \quad (2.108)$$

$$y = F'_{pA} - F_{pA}^{inst} \quad (2.109)$$

$$\kappa = F_{pA}^{inst} (1 - F_{pA}^{inst}) \sqrt{1 - 4F_{pA}^{inst} (1 - F_{pA}^{inst}) (1 - r_A r_B)} \quad (2.110)$$

$$r_A = \frac{k_{pAA}}{k_{pAB}} \quad (2.111)$$

$$r_B = \frac{k_{pBB}}{k_{pBA}} \quad (2.112)$$

where F_{pA}^{inst} is the instantaneous copolymer composition given by Equation 2.104, which corresponds to the average composition of all chains produced in a given moment; F'_{pA} is the composition of a given polymer chain, and r_A and r_B are the reactivity ratios. Flory's distribution should be immediately recognizable as one component of Equation 2.108. In fact, if Stockmayer's distribution is integrated over the complete copolymer composition range ($-\infty \leq y \leq \infty$), Flory's distribution will be obtained. This proof will be left as an exercise to the reader.

It is important to point out that the broadening of the CCD described by Stockmayer's distribution is not caused by multiplicity of active site types or non-homogeneous polymerization conditions. This broadening is merely statistical and will happen even when a single-site catalyst is used in a reactor kept at uniform conditions throughout the polymerization. Some conditions that influence the statistical broadening of the CCD will be discussed in more detail in the next paragraphs.

In Equation 2.108, the copolymer composition distribution is quantified by the variable y , defined in Equation 2.109. The variable y measures the difference between the molar fraction of monomer A in a given polymer chain to the average molar fraction of monomer A in all the chains, F_{pA}^{inst} , already defined in Equation 2.104. The classical Mayo–Lewis equation can also be used to calculate F_{pA}^{inst} :

$$F_{pA}^{\text{inst}} = \frac{(r_A - 1)f_A^2 + f_A}{(r_A + r_B - 2)f_A^2 + 2(1 - r_B)f_A + r_B} \quad (2.113)$$

Let us start to explore some implications of Stockmayer's distribution; it is another fundamental equation in polymer science and can be derived from the analytical solution of the copolymerization mechanism described in Table 2.11. Its derivation is long and tedious and not really required here; it is enough to realize that it reflects the MWD and CCD of polymer made according to the copolymerization mechanism shown in Table 2.11 at a given time instant. The same considerations made for Flory's distribution apply to Stockmayer's distribution; they will not be repeated here.

Figure 2.23 shows that the CCD of longer chains is narrower than those of shorter chains. This broadening effect is not associated to any non-uniformity in polymerization conditions. It is only a consequence of the statistical nature of polymerization. Small statistical fluctuations on comonomer incorporation are magnified for smaller chains and tend to disappear as the chains get longer. Taking this behavior to the limit, chains of infinite length would all have the same comonomer fraction, $F'_{pA} = 0.5$ for this particular simulation.

Copolymers can be classified into three main categories: random, block and alternating. In random copolymers, monomer units alternate in a random way, such as indicated below:

ABBABABAABAABBBABBABAABABABABABAABBABAAABBAB

The product of the reactivity ratios in random copolymers is equal to 1 ($r_A r_B = 1.0$).

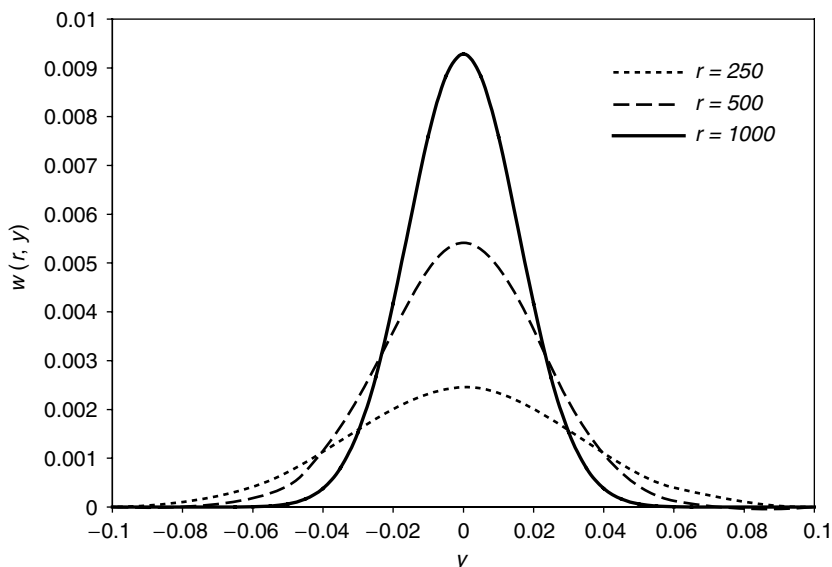


Figure 2.23 Effect of chain length on CCD according to Stockmayer's distribution ($\bar{x}_n = 1000$, $F_{pA}^{inst} = 0.5$, $r_A r_B = 1$).

In alternating copolymers, on the other hand, monomer *A* is always followed by monomer *B* and monomer *B* is always followed by monomer *A*, that is:



For a perfect alternating copolymer, $r_A r_B = 0$, since $k_{pAA} = k_{pBB} = 0$. In general, when $r_A r_B < 1.0$, we say that the copolymer has a tendency toward alternation.

As the name indicates, monomers form long blocks in block copolymers and, consequently, $r_A r_B \gg 1.0$, since $k_{pAA} > k_{pAB}$ and/or $k_{pBB} > k_{pBA}$. A perfect diblock copolymer has the structure:



The comonomer sequence length distribution of the copolymer chain also influences the CCD, as shown in Figure 2.24. Everything being equal, the width of the CCD of a random copolymer ($r_A r_B = 1.0$) falls in between that of a blockier ($r_A r_B = 5.0$) and a more alternating ($r_A r_B = 0.01$) copolymer. Blockier copolymers have wider CCDs, while a tendency toward alternation will necessarily narrow the CCD. This is very neatly captured by Stockmayer's distribution.

The chain length dimension can be eliminated out of Equation 2.108 by integrating over all chain lengths, thus recovering the CCD for chains of all lengths:

$$\begin{aligned}
 w(y) &= \int_0^\infty \frac{r}{DP_n^2} \exp\left(-\frac{r}{DP_n}\right) \sqrt{\frac{r}{2\pi\kappa}} \exp\left(-\frac{ry^2}{2\kappa}\right) dr \\
 &= \frac{3}{4\sqrt{2\kappa/DP_n}(1 + (y^2 DP_n/2\kappa))^{5/2}} = \frac{3}{4\sqrt{2\kappa\tau}(1 + (y^2/2\kappa\tau))^{5/2}} \quad (2.114)
 \end{aligned}$$

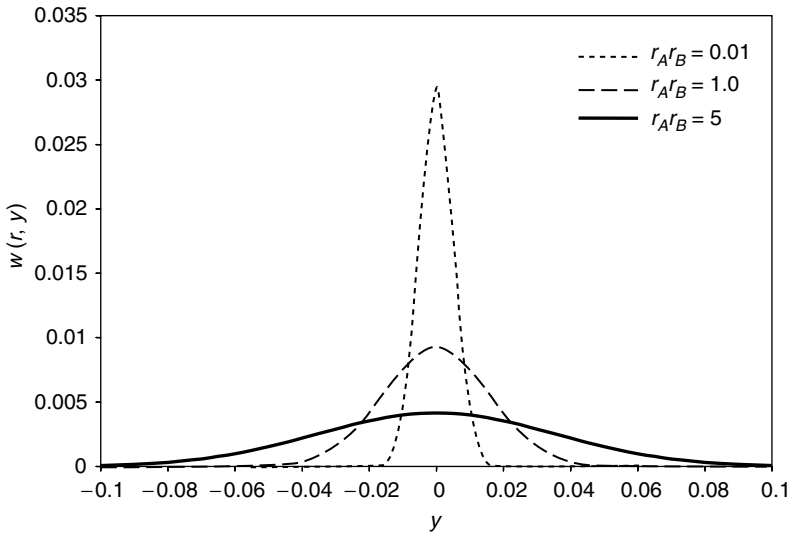


Figure 2.24 Effect of copolymer comonomer sequence length on CCD according to Stockmayer's distribution ($\bar{x}_n = 1000$, $F_{pA}^{\text{inst}} = 0.5$, $r = 1000$).

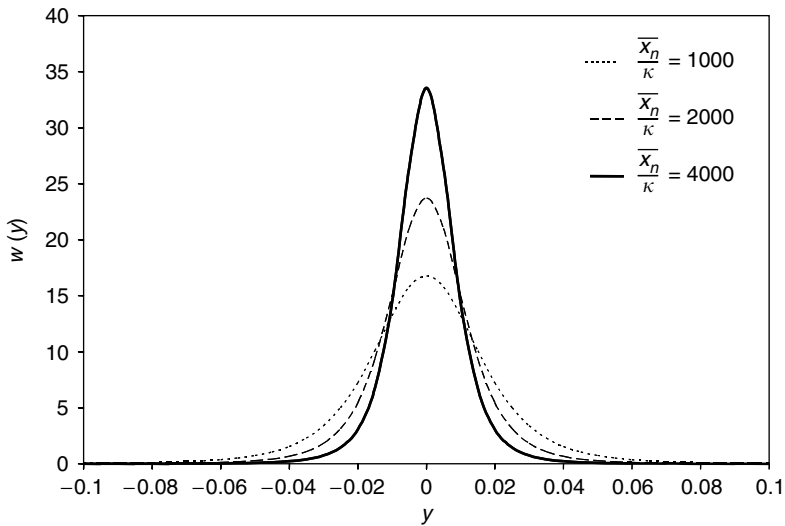


Figure 2.25 CCD for chains of all lengths according to Stockmayer's distribution.

Upon inspection of Equation 2.114, it will be noticed that now the CCD can be described with a single lumped parameter (DP_n/κ or $\kappa\tau$), tidily combining chain length and comonomer sequence length effects. Figure 2.25 aids visualization of the elegant solution captured in Equation 2.114. Notice that the CCD gets narrower as the lumped parameter DP_n/κ increases, that is, as average chain length increases (large DP_n) or the copolymer becomes more alternating (small κ , see Equation 2.110).

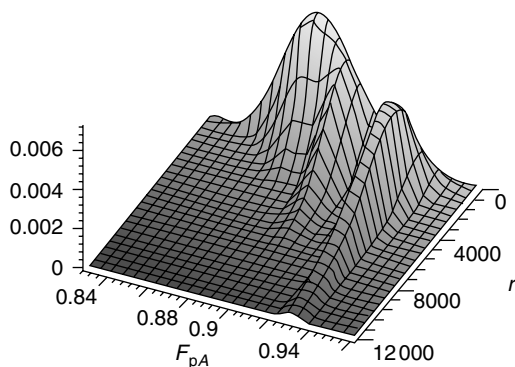


Figure 2.26 Bivariate distribution of chain length and chemical composition of a polymer made with a coordination catalyst containing three different active site types. ($DP_{n,1} = 500$, $DP_{n,2} = 1000$, $DP_{n,3} = 2000$, $F_{pA,1}^{\text{inst}} = 0.88$, $F_{pA,2}^{\text{inst}} = 0.90$, $F_{pA,3}^{\text{inst}} = 0.93$, $m_1 = 0.3$, $m_2 = 0.3$, $m_3 = 0.4$, $(r_A r_B)_1 = (r_A r_B)_2 = (r_A r_B)_3 = 1$.)

Similar to Flory's distribution, Stockmayer's distribution can be applied to non-steady-state solutions and also it can be used to model the CCD of polymer made with multiple-site catalysts [44]. Figure 2.26 shows the $\text{CLD} \times \text{CCD}$ of a model polymer created by superimposing three Stockmayer's distributions. Notice how the trends are similar to the ones measured experimentally using cross-fractionation in Figures 2.5 and 2.12.

2.3.3 Long-chain branch formation

The mechanism on long-chain branch (LCB) formation with coordination catalysts was discussed briefly in Section 2.2 and illustrated in Figure 2.18. LCB formation with coordination catalysts is nothing more than a copolymerization reaction with macromonomers made in the reactor through β -hydride elimination and transfer to monomer reactions for polyethylene, and β -methyl elimination for polypropylene (Scheme 2.2). At this point, the population balances could be re-derived to include LCB-formation reactions and solved by the method of moments. For brevity, however, only the final results of this derivation will be shown, leading to an analytical solution for the instantaneous distribution of MWD for chains containing LCB; derivation details are available in the literature [45–47].

The weight distribution of chain length for polymer populations containing i LCBs per chain, $w(r, i)$ is given by the following equation [45]:

$$w(r, i) = \frac{1}{(2i + 1)!} r^{2i+1} \tau^{*2i+2} \exp(-\tau^* r) \quad (2.115)$$

In Equation 2.115, the parameter τ^* has a slightly different definition from that used before for τ :

$$\tau^* = \frac{\text{rate of chain transfer} + \text{rate of LCB formation}}{\text{rate of propagation}} \quad (2.116)$$

In the absence of LCB formation, $\tau^* = \tau = 1/DP_n$, and Equation 2.115 with $i = 0$ becomes Flory's most probable distribution for linear chains.

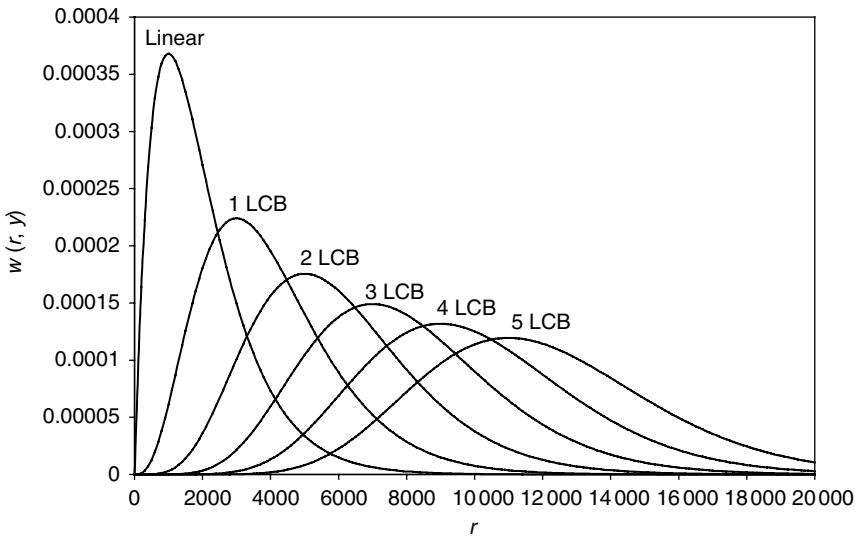


Figure 2.27 CLDs of the several polymer populations of branched polyolefins made with a single-site coordination catalyst ($1/\tau^* = 1000$).

Figure 2.27 shows the CLD for several polymer populations with increasing numbers of LCBs per chain. Notice that the area under each CLD is one; they do not reflect the actual fraction of each population present in the polymer. As expected, the chain length average increases with increasing numbers of LCBs per chain. This powerful solution opens up a window into the molecular structure of the polymer chains by allowing the CLDs of the polymer populations to be visualized with different number of LCBs.

An analytical solution for the instantaneous CLD for the whole polymer produced in a CSTR has also been derived [47]:

$$\bar{w}(r) = \frac{(1 - \alpha)\tau^* \exp(-r\tau^*)}{(1 + \alpha)\sqrt{\alpha}} I_1 \left(2 \frac{r\tau^* \sqrt{\alpha}}{1 + \alpha} \right) \quad (2.117)$$

The function I_1 is the modified Bessel function of the first kind of order 1, defined as:

$$I_1(x) = \sum_{k=0}^{\infty} \frac{(x/2)^{1-2k}}{k! \Gamma(k+2)} \quad (2.118)$$

Bessel functions are easily found in mathematical tables and are readily available in most scientific software applications.

The parameter α is defined by the equation

$$\alpha = \frac{f^{\equiv}}{1 + s/(k_{\text{pLCB}}[\mu_0])} \quad (2.119)$$

where f^{\equiv} is the molar fraction of macromonomer in the reactor, measured with respect to the total concentration of polymer, s is the reciprocal of the average reactor residence time,

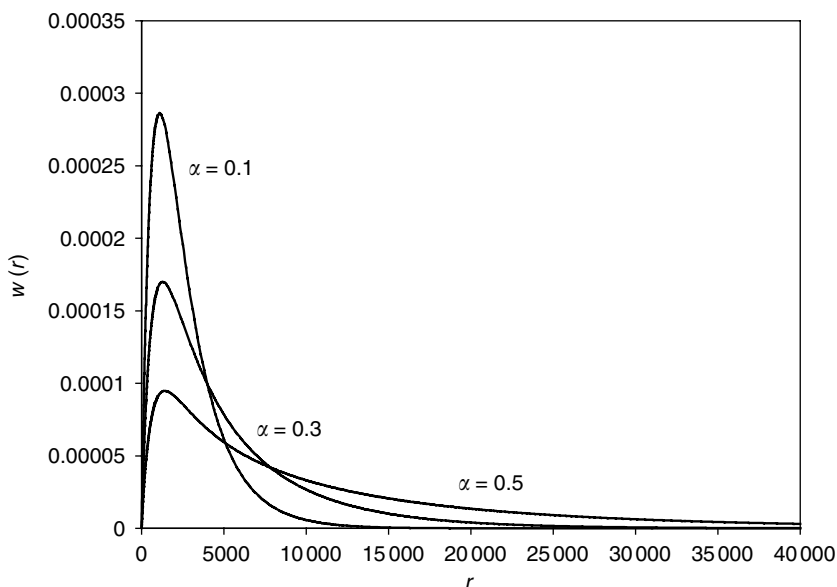


Figure 2.28 Overall CLD for branched polyolefins made with a single-site coordination catalyst ($1/\tau = 1000$).

k_{PLCB} is the rate constant for macromonomer propagation and μ_0 is the concentration of growing polymer chains in the reactor.

Figure 2.28 shows how the CLD of the whole polymer is affected by the value of the parameter α . First, notice that the value of α varies from 0 to 1. All chains are linear when $\alpha = 0$, since this implies that either $f^{\text{---}} = 0$ (without macromonomers, no LCBs can be formed) or $s/(k_{\text{LCB}}[\mu_0]) \rightarrow \infty$. The last condition is obeyed when either $s \rightarrow \infty$ (i.e., the reactor residence time tends to zero) or $k_{\text{LCB}}[\mu_0] = 0$. Both cases imply that no macromonomers are accumulated in the reactor. On the other hand, LCB formation is maximum when $\alpha = 1$, a condition obeyed only when all dead polymer chains in the reactor have terminal unsaturations, $f^{\text{---}} = 1$, and the residence time in the reactor is infinite, $s \rightarrow 0$, or the rate of LCB formation is infinite, $k_{\text{LCB}}[\mu_0] \rightarrow \infty$. Therefore, Equation 2.119 captures all the factors determining LCB formation with a coordination catalyst.

In addition, the parameter α can also be related to the number of LCBs per chain for the whole polymer, $\text{LCB}_{\text{chain}}$, by the equation:

$$\text{LCB}_{\text{chain}} = \frac{\alpha}{1 - \alpha} \quad (2.120)$$

Notice that the average number of LCB per chain can vary from 0 when $\alpha = 0$ to infinity when $\alpha = 1$. Since most long chain-branched polyolefins made with coordination catalysts are only sparsely branched, with values of $\text{LCB}_{\text{chain}}$ rarely exceeding unity, the upper limit should be considered only a theoretical possibility never to be reached in practical situations.

Chain length averages and PDI for the whole polymer can also be related to the parameters α or $\text{LCB}_{\text{chain}}$ with the equations [47]:

$$\text{DP}_n = \frac{1}{\tau^*} (1 + 2\text{LCB}_{\text{chain}}) \quad (2.121)$$

$$\text{DP}_w = \frac{2}{\tau^*} (1 + 2\text{LCB}_{\text{chain}})(1 + \text{LCB}_{\text{chain}}) \quad (2.122)$$

$$\text{PDI} = 2(1 + \text{LCB}_{\text{chain}}) \quad (2.123)$$

These equations demonstrate that the PDI of long chain-branched polyolefins is always greater than 2 and that the chain length averages increase with increasing number of LCBs per chain.

It is also interesting to calculate the mass fraction of polymer populations containing i LCB per chain, m_{LCBi} :

$$m_{\text{LCBi}} = \frac{(2i)!}{i!(i+1)!} \frac{\alpha^i(1-\alpha)(2i+1)}{(1+\alpha)^{2i+2}} \quad (2.124)$$

Notice that, for sparsely branched polymers, most of the chains are linear, but the amount of more highly branched species increases as $\alpha \rightarrow 1$.

Similarly, the following extension of Stockmayer's distribution can be derived for binary copolymers containing LCBs formed by terminal branching [46]:

$$w(r, y, i) = \frac{1}{(2i+1)!} r^{2i+1} \tau^{2i+2} \exp(-r\tau) \sqrt{\frac{r}{2\pi\kappa}} \exp\left(-\frac{ry^2}{2\kappa}\right) \quad (2.125)$$

These equations give a very accurate portrait of the chain microstructure of these polyolefins. They are, in fact, a window into their chain architecture and can be very useful in understanding the constitution of these complex polymers.

The LCB structure of polyolefins obtainable with a single metallocene catalyst can be altered in several ways. For instance, two or more metallocenes can be used to control, simultaneously, the MWD and LCB of polyolefins [48, 49]. If an even more drastic microstructural change is required, one that would make the LCB structure of polyolefins made with coordination catalysts resemble that of LDPE, dienes can be copolymerized with ethylene and α -olefins [50]. The cited references provide some additional information on this subject.

Monte Carlo modeling has also been used extensively to describe LCB formation in coordination polymerization. Monte Carlo methods are very powerful because polymer chains are generated individually and the model keeps track of as many microstructural details as required. Monte Carlo methods will not be discussed here, but some references provided at the end of the chapter illustrate some interesting applications of this technique [51–53].

2.4 Inter- and intraparticle mass and heat transfer resistances

Up to this point, our attention has been focused on models that describe the polymerization kinetics and polymer microstructure, provided that the reaction conditions (reactant

concentration and temperature) were known at the active sites. When dealing with solution polymerization, it is generally acceptable to assume that the conditions at the active sites are approximately the same as the bulk reaction conditions. Even in this case, macro- and micromixing effects can lead to a more complex picture than the one described so far.

The modeling problem becomes more intricate when a heterogeneous catalyst, such as Phillips, Ziegler–Natta and supported metallocenes, is used for polymerization. In this case, temperature and reactant concentrations may vary as a function of radial position in the particle due to mass and heat transfer limitations. The models developed thus far are still valid, but only locally for the conditions existing at each radial position in the catalyst/polymer particle.

As has been mentioned already, most industrial processes employ solid supports to carry the active sites into the reactor. Typical supports for Ziegler–Natta catalysts include SiO_2 and MgCl_2 , whereas Phillips and metallocene catalysts are mostly supported on SiO_2 or $\text{SiO}_2/\text{Al}_2\text{O}_3$.

Regardless of the type of support, modeling particle growth and predicting the microstructure of the polymer chains is a multiphase problem, in many ways typical of well known chemical engineering problems. For instance, classical chemical engineering mass and energy transfer phenomena will be encountered between the particles and the reaction environment (interparticle transfer), as well as inside the particles (intraparticle transfer). Nevertheless, the complexity of the phenomena involved, the distributed nature of the resulting product, the rapidity of the reaction, the highly sensitive and fast evolving nature of the active sites chemistry, and associated changes in length scales all contribute to the unique nature of mesoscale modeling of heterogeneously supported polyolefins. Before discussing how models for particle fragmentation and growth are constructed, what we know about the physical aspects of this phase of the reaction will be reviewed.

2.4.1 Particle fragmentation and morphology control

During polymerization the catalyst particles are rapidly transformed from porous particles into polymer particles that contain fragments of the original catalyst particles, as illustrated in Figure 2.29. When the catalyst particles are injected into the reactor, they enter in contact with the continuous reaction medium containing monomers and, in some reactor types, diluent, inerts and hydrogen. Regardless of the nature of the continuous phase (gas, slurry or supercritical fluid), monomer must diffuse through the boundary layer around the catalyst particles and through its pores to reach the active sites, where polymerization takes place. (Depending on catalyst type, the turnover rate might reach 10^4 – 10^5 monomer insertions per second.) The fast-forming polymer will deposit on the catalyst surface and pores. Monomer must adsorb on the surface of the polymer layer and then diffuse through the polymer phase to reach the active sites. Polymer build-up inside the pores generates stress, or hydraulic pressure, at specific points inside the particle. At this point, one of three things may happen: the catalyst particle resists the building stress, explodes, or fragments in a controlled way, as illustrated in Figure 2.30.

If the particle resists the stresses and does not break up, the pores fill up with polymer and monomer mass transfer limitations become the rate limiting step. This undesirable situation essentially causes the polymerization to shut down.

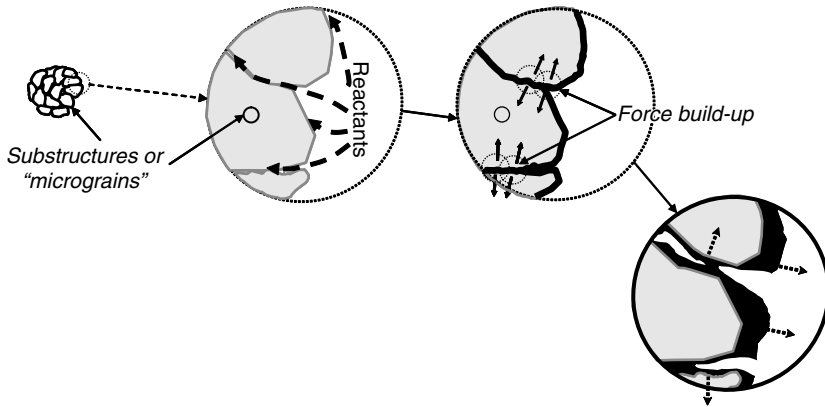


Figure 2.29 Schematic of the steps leading to the fragmentation of a catalyst particle.

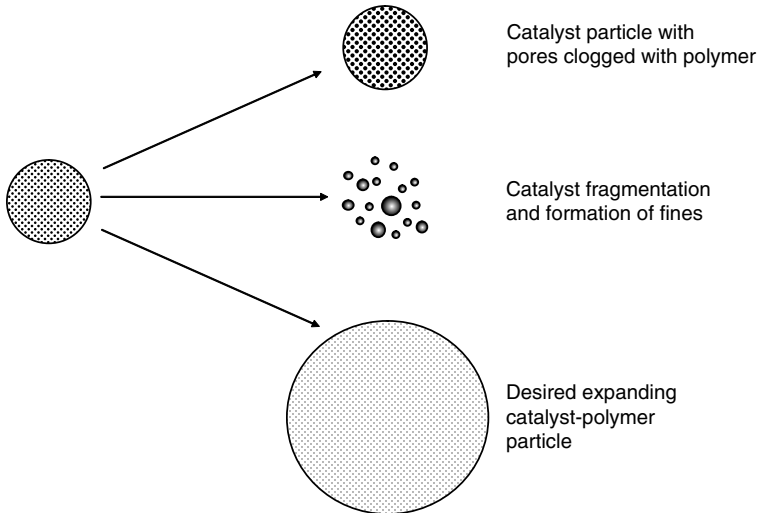


Figure 2.30 Possible scenarios for catalyst particle fragmentation and growth.

If the support is not strong enough, the particle explodes and generates a significant number of finer sub-particles. These *fines* are a considerable nuisance because they hinder smooth reactor operation, may be detrimental to the operation of compressors and fans if they are blown out of the reactor, and may generate significant amounts of static electricity in gas-phase processes.

Finally, in the most desirable situation, the initial internal structure of the support fragments neatly, but the particle retains its integrity. In this case, as the fragmentation proceeds, the catalyst support structure is replaced by a semi-open polymer matrix in which small support fragments (with diameters well below $1.0\ \mu\text{m}$) carrying the active sites are dispersed. Fragmentation is therefore critical to render the active sites accessible throughout the polymerization and to change the internal structure of the particles in such a way that

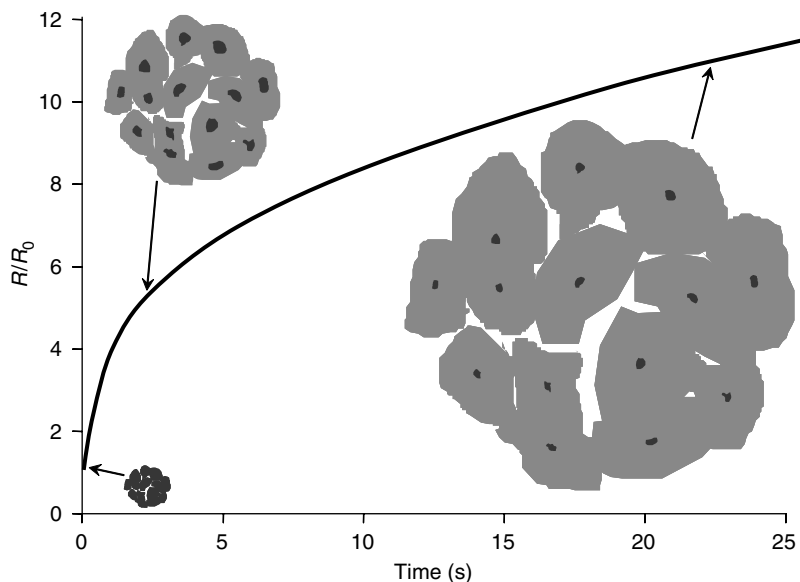


Figure 2.31 Dimensionless particle radius growth rate during the initial instants of polymerization, assuming a rate of polymerization of 50 kg (g/h)^{-1} .

they can expand rapidly. The support should therefore be robust enough not to break under reactor stirring and transport through pumps and injection nozzles, but at the same time allow controlled fragmentation during polymerization.

Traditional commercial catalyst supports are designed to allow fragmentation to take place in this ordered fashion. If the fragmentation step takes place under ideal conditions, one particle of supported catalyst will yield one polymer particle with roughly the same shape. This is referred to as *replication phenomenon* and is one of the most remarkable characteristics of heterogeneous olefin polymerization.

The fragmentation and initial growth phases are typically very fast, as shown in Figure 2.31. In the case of $\text{TiCl}_4/\text{MgCl}_2$ catalysts, particle fragmentation can be complete in times on the order of one-tenth of a second under industrial conditions. In the space of less than one second, the particle diameter is multiplied by roughly a factor of 4, assuming no change in porosity from that of the support. While this is just a rough estimate of the characteristic time scales, it gives us an idea of how quick the changes are that occur during the initial stages of particle growth. Catalysts supported on silica carriers tend to take a bit longer to fragment completely; even so, complete break-up of the internal structure of a SiO_2 support will take on the order of a few seconds to tens of seconds – much less than the typical average residence time of an industrial reactor, which is on the order of hours.

Despite its extremely short duration, the fragmentation step is critical in determining the final morphology of the polymer particles. Carrying out the fragmentation step under mild conditions in a separate reactor – a process called *prepolymerization* – produces particles with better morphology, that is, a relatively compact product (with moderately high bulk powder density), with controlled shape (often, but not always, nearly spherical) and no fines.

Thus, in several processes, catalysts are prepolymerized under milder conditions than in the main reactor. Prepolymerization may also increase catalyst stability and activity, and eliminate the formation of hot spots in the catalyst particles.

Once the fragmentation step is complete, the particle continues to grow as long as monomer arrives at the active sites and the catalyst does not deactivate. The final morphology, size, shape and porosity of the particles will be the result of a complex balance between the conditions during the fragmentation step, the phase in which the reaction takes place, the polymer properties in the particle and, obviously, the polymerization rate.

The influence of the fragmentation step on the final particle morphology and size is difficult to express quantitatively, as is the role that the mechanical properties of the polymer play in determining particle morphology. A detailed treatment of this topic is beyond the scope of the current text. Suffice to say that, as mentioned above, performing the fragmentation step under mild conditions allows better particle replication and morphology to be obtained. It is also likely that the polymer properties will have an influence on particle morphology, especially during the initial fragmentation step. For instance, since fragmentation is a result of the build-up and relaxation of forces in the support matrix, the rate at which the forces generated by polymer accumulation are dissipated in the polymer-support complex will determine particle morphology to a large extent.

Nevertheless, in addition to MWD and CCD, the rate of growth and final size of the polymer particle will obviously depend very strongly on the rate of polymerization inside the particle. Since the process in question is a heterogeneous one, and the characteristic length scales of the particles vary from 10s to 100s of microns, it is necessary to understand the relationship between the observed polymerization rate, intrinsic kinetics, mass and heat transfer mechanisms, and particle size. This can be done on the condition that a workable representation of the morphology of the particle can be constructed, which will be discussed in the following section.

2.4.2 *Single particle models: inter- and intraparticle mass and heat transfer*

The rates of polymerization and particle growth, and the development of the MWD and CCD depend on the temperature and concentration of monomers and chains transfer agent inside the growing polymer particles. In order to do so, the rates of mass transfer from the continuous phase, through the boundary around the particle (interparticle) and then through the particle (intraparticle), and of heat transfer in the other direction need to be predicted simultaneously. Problems combining reaction kinetics, mass and heat transfer phenomena are classical ones in chemical engineering.

Consider the MgCl_2 -supported Ziegler–Natta catalyst particle shown in Figure 2.32. This type of supported catalyst particle is composed of an agglomeration of smaller, identifiable substructures. The particle is often referred to as the *macrograin*, *macroparticle* or *secondary particle*; the substructures are the *micrograins*, *microparticles* or *primary particles*. This type of aggregate structure, combined with the replication phenomenon, is at the origin of the well-known *multigrain model* (MGM) [55–66].

Figure 2.33 shows how the MGM represents particle morphology. The MGM assumes that the original catalyst particle is an aggregate of micrograins, corresponding to individual

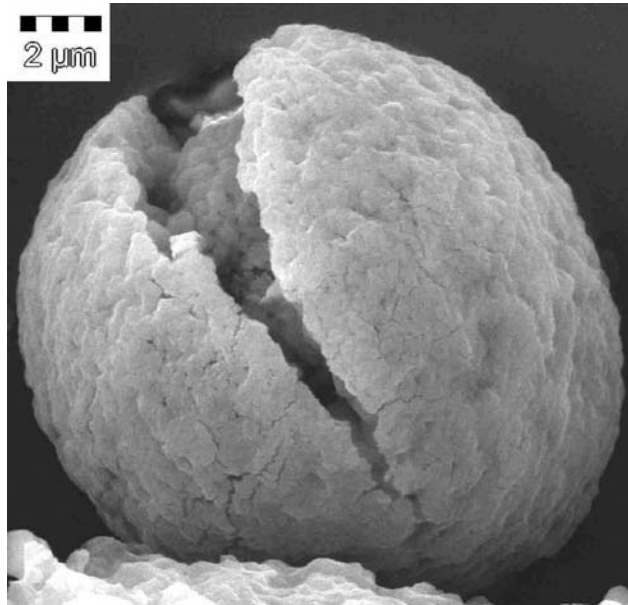


Figure 2.32 An MgCl_2 -supported Ziegler–Natta catalyst. Note the granular structure in the interior of the particle that inspired the development of the MGM.

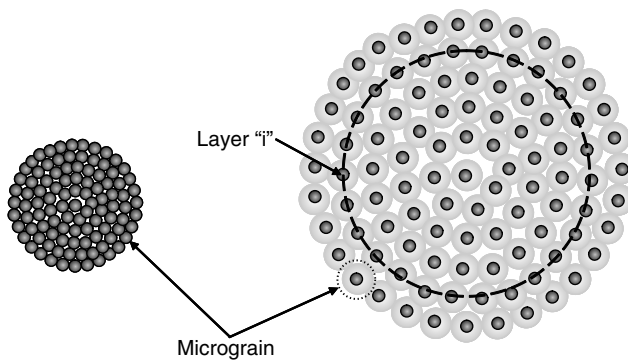


Figure 2.33 Polymer/catalyst particle structure according to the MGM. The catalyst particle (left, also called the secondary particle or macroparticle) is composed of an aggregation of primary particles (micro-particles) arranged in concentric spherical layers. Polymer forms around the microparticles causing the macroparticle to expand.

$\text{TiCl}_4/\text{MgCl}_2$ crystals, which are organized in concentric spherical layers. Each micrograin is likened to a solid spherical structure with active sites on its surface. Once the catalyst particle (the macrograin) is injected into the reactor, monomer is assumed to diffuse through the boundary layer around the particle and through the pores between the micrograins. The polymerization itself begins when monomer coordinates with the active sites on the surface of the micrograins, forming polymer chains that accumulate around the micrograin

surface. This fragments the macrograin, as depicted in Figure 2.29, and makes the particle grow. Based on the replication phenomenon, one micrograin of catalyst produces one micrograin in the polymer particle, where the latter are spheres covered in polymer with the catalyst fragment in its center. Transport of monomer continues from the continuous phase, through the pores of the particle to the micrograins at different radial positions in the macrograin. Monomer is absorbed by the polymer around each micrograin and then diffuses through the polymer layers to the active sites, where it reacts. The heat released at the surface of the micrograins due to the highly exothermic nature of the polymerization will, obviously, follow the reverse path.

The MGM was developed in the early 1980s for the particular case of $\text{TiCl}_4/\text{MgCl}_2$ catalysts, but has been applied to almost all other types of heterogeneous olefin polymerization catalysts.

Assuming that the macroparticles are spherical, and that mass transfer in the particles occurs only by diffusion, then the mass balance for monomer M can be written as

$$\varepsilon_p \frac{\partial [M_s]}{\partial t} = \frac{1}{r_s^2} \frac{\partial}{\partial r_s} \left(D_{M\text{eff}} r_s^2 \frac{\partial [M_s]}{\partial r_s} \right) - R_p^V \quad (2.126)$$

where $[M_s]$ (mol L^{-1}) is the monomer concentration in the pores of the macroparticle as a function of polymerization time, t , and radial position, r_s ; ε_p is the porosity of the macroparticle, $D_{M\text{eff}}$ is the effective diffusivity in the secondary particle and R_p^V is the polymerization rate per unit volume in the secondary particle. Note that Equation 2.126 has been written for the monomer M ; the expressions for hydrogen and comonomers are analogous.

Typically, it is assumed that the average pore radius in the macroparticle is not small with respect to the size of the diffusing species. Thus, $D_{M\text{eff}}$ is estimated using the well-known expression for effective diffusivity in porous heterogeneous catalysts,

$$D_{M\text{eff}} = \frac{\varepsilon_p D_{Mb}}{\tau_s} \quad (2.127)$$

where D_{Mb} is the monomer bulk diffusivity in the reaction medium, and τ_s is the tortuosity of the polymer particle. This treatment implicitly assumes that the particle is spatially homogeneous, that is, it can be characterized with single values for ε_p and τ_s .

Finally, R_p^V is the average volumetric rate of polymerization in the macroparticle at a given radial position and time. Since the polymerization takes place on the surface of the fragments of catalyst inside the micrograins, it is this term that couples the macro- and micrograin balances. In fact, R_p^V is the sum of the rates of polymerization in the microparticles (see Equation 2.137) situated at radial position r_s .

Different initial and boundary conditions can be chosen for Equation 2.126. The most commonly used initial condition is

$$[M_s](r_s, t = 0) = [M_s]_0 \quad (2.128)$$

It is common to make a pseudo-steady-state hypothesis for the initial concentration in the secondary particle at $t = 0$, $[M_s]_0$, to obtain the initial condition for Equation 2.126. This is done by setting the right-hand side of Equation 2.126 to zero and solving the resulting ODE for the radial profile of $[M_s]$. This hypothesis is made because the choice of $[M_s]_0 = 0$ generally leads to stiff differential equations that may be more challenging

to solve. The choice of a value for $[M_s]_0$ will depend on how accurate the predictions for monomer concentration, and therefore MWD and CCD, must be during the initial instants of the polymerization. If high accuracy at very short polymerization times is not an issue, then the pseudo-steady-state approximation is recommended. It is, perhaps, important to realize that the phenomena taking place at very short polymerization times, particularly site activation and particle fragmentation, are far from being well understood; considering all these uncertainties, the pseudo-steady-state approximation becomes even more justified for most practical applications.

A set of common boundary conditions for Equation 2.126 is

$$\frac{\partial[M_s]}{\partial r_s}(r_s = 0, t) = 0 \quad (2.129)$$

$$D_{M\text{eff}} \frac{\partial[M_s]}{\partial r_s}(r_s = R_{\text{mac}}, t) = k_s([M_b] - [M_s]) \quad (2.130)$$

where R_{mac} is the radius of the macroparticle, k_s is the mass transfer coefficient in the external film surrounding the macroparticle and $[M_b]$ is the monomer concentration in the bulk phase. The first boundary condition, Equation 2.129, is simply a symmetry condition (zero flux at the center of the particle). The second boundary condition, Equation 2.130, reflects the classical assumption that the molar flux through the boundary layer is equal to the molar flux inside the surface of the particle. The latter condition is often replaced with Equation 2.131, especially for gas-phase polymerization, where the resistance to mass transfer in the external boundary layer is usually negligible:

$$[M_s](r_s = R_{\text{mac}}, t) = [M_b] \quad (2.131)$$

Mass transfer in the primary particles occurs only by diffusion through the amorphous fraction of the polymer layer to the active sites on the surface of the catalyst fragments. The concentration profile in the micrograins is calculated with the equation:

$$\frac{\partial[M_p]}{\partial t} = \frac{1}{r_p^2} \frac{\partial}{\partial r_p} \left(D_{M_p} r_p^2 \frac{\partial[M_p]}{\partial r_p} \right) \quad (2.132)$$

In Equation 2.132, the subscript p refers to values in the primary particles. The diffusivity in the polymer layer, D_{M_p} , is an important parameter and is usually estimated as a function of polymer crystallinity,

$$D_{M_p} = \frac{D_{M_a}}{\chi^* \iota} \quad (2.133)$$

where D_{M_a} is the diffusivity of monomer in amorphous polymer, and χ^* and ι are correction factors to account for the decrease in diffusivity due to chain crystallinity and immobilization of the polymer amorphous phase due to the crystallites. The correction factors are obviously difficult to obtain *a priori*; either experimental data is needed to estimate D_{M_p} or this value must be treated as an adjustable parameter. In Equation 2.133 it will be noticed that, since the parameters χ^* and ι appear as a product, a single empirical parameter would be enough to correlate D_{M_p} to D_{M_a} . Two parameters are included in Equation 2.133 because in models, such as the one first proposed by Michaels and Bixler [67] about 40 years ago, one factor was used to account for the volume fraction of crystalline

material that the molecules must diffuse around (χ^*) and the other to correct for energetic barriers to diffusion between crystallites that are close together (ι). For practical purposes, D_p is always less than D_{Ma} and the product $\chi^* \iota$ is considered an empirical adjustable parameter.

The initial and boundary conditions for the micrograins are slightly different from those of the macrograin:

$$[M_p](r_p, t = 0) = [M_p]_0 \quad (2.134)$$

$$4\pi R_c^2 D_{M_p} \frac{\partial [M_p]}{\partial r_p} (r_p = R_c, t) = \frac{4}{3} \pi R_c^3 R_p^c \quad (2.135)$$

$$[M_p](r_p = R_{mic}, t) = [M_{eq}] \leq [M_s] \quad (2.136)$$

The inner boundary condition at the surface of the catalyst fragment, Equation 2.135, states that the diffusional flux at the surface of the fragment ($r_p = R_c$) is equal to the rate of reaction R_p^c . The outer boundary condition at the interface of the microparticle ($r_p = R_{mic}$) states that the concentration of monomer in the polymer layer at the interface is in equilibrium with the monomer concentration in the pores of the macroparticle at the position under consideration. If a partition coefficient (K_{eq}^*) is used between the concentrations of monomer in the pores of the macroparticle and absorbed in the polymer layer surrounding the microparticle, then:

$$[M_p](r_p = R_{mic}, t) = [M_{eq}] = K_{eq}^* [M_s] \quad (2.136a)$$

The polymerization rate at the surface of the catalyst fragment is given by:

$$R_p^c = k_p C^* [M_p](r_p = R_c, t) \quad (2.137)$$

where C^* is the concentration of active sites at the surface of the catalyst fragment. Note that the rate of polymerization in this expression has been given with respect to the volume of the fragment. While it might be more rigorous to write this boundary condition in terms of a rate per unit surface area on the fragment, most authors prefer the form given here.

The analogous energy balance equation, and initial and boundary conditions for the macroparticle, are

$$\overline{\rho c_p} \frac{\partial T_s}{\partial t} = \frac{1}{r_s^2} \frac{\partial}{\partial r_s} \left(r_s^2 k_{f,s} \frac{\partial T_s}{\partial r_s} \right) + (-\Delta H_r) R_p^V \quad (2.138)$$

$$T_s(r_s, t = 0) = T_{s,0} \quad (2.139)$$

$$\frac{\partial T_s}{\partial r_s} (r_s = 0, t) = 0 \quad (2.140)$$

$$\frac{\partial T_s}{\partial r_s} (r_s = R_{mac}) = \frac{h_p}{k_{f,s}} (T_s(R_{mac}) - T_b) \quad (2.141)$$

In these equations, T_s is the temperature at coordinates (r, t) in the macrograin, $\overline{\rho c_p}$ is the average value of the heat capacity per unit volume of the macroparticle, $k_{f,s}$ is the effective thermal diffusivity in the macrograin and $(-\Delta H_r)$ the enthalpy of polymerization. In Equation 2.141, the parameter h_p is the average convective heat transfer coefficient, usually calculated from a Nusselt number correlation. Early works tended to use the well-known Ranz–Marshall correlation for evaporation from a droplet; however, it has been

demonstrated that while the Ranz–Marshall correlation is quite accurate for individual particles, it is not a good idea to use it for the prediction of heat transfer coefficients for systems where particle–particle and particle–wall interactions cannot be neglected. It is therefore preferable to use a correlation that takes bed density and, eventually, the particle size distribution into account.

For the micrograins, the model equations, boundary and initial conditions are

$$\rho c_p \frac{\partial T_p}{\partial t} = \frac{1}{r_p^2} \frac{\partial}{\partial r_p} \left(r_p^2 k_{f,p} \frac{\partial T_p}{\partial r_p} \right) \quad (2.142)$$

$$T_p(r_p, t = 0) = T_{p,0} \quad (2.143)$$

$$T_p(r_p = R_p, t) = T_s \quad (2.144)$$

$$4\pi R_c^2 k_{f,p} \frac{\partial T_p}{\partial r_p}(r_p = R_c, t) = \frac{4}{3}\pi R_c^3 R_p^c (-\Delta H_p) \quad (2.145)$$

where the notation is as above, with $k_{f,p}$ being the thermal conductivity of the polymer layer around the fragments.

In boundary condition 2.144, it has been assumed implicitly that the temperature at the surface of micrograins situated at a given point in the macroparticle will be T_s . To a certain extent this is inconsistent with the fact that a single energy balance has been written for the macroparticle (Equations 2.138–2.141). In other words, Equation 2.138 does not allow differentiation between the different phases in the macroparticle. Fortunately, the temperature rise inside a microparticle is negligible for the characteristic dimensions of the micrograins and it may be considered that the temperature at the catalyst surface is T_s .

This set of coupled partial differential equations can be solved in a number of ways. For a discussion of numerical methods for partial differential equations, see the references on the MGM at the end of the chapter [55–66].

At the risk of over-simplifying the findings from a large body of work, the general conclusions of MGM studies are presented in Table 2.13. Mass transfer resistances inside the macroparticle in gas-phase processes are less pronounced than in slurry processes. This is to be expected since the diffusion coefficients in the gas phase are two to three orders of magnitude greater than in slurry. On the other hand, heat transfer resistances in the external film are more significant in gas-phase processes since gases are very poor heat conductors. This conclusion is also based on the assumption that heat transfer from the polymer particle to the surroundings occurs by convection, and therefore depends strongly on the choice of correlation for the heat transfer coefficient. Heat conduction between small hot particles and cooler large particles might also be important [68, 69]. Heat and mass transfer resistances will be greatest in larger virgin particles and will, invariably, decrease as the polymerization continues, and it is easy to see why: the amount of heat released is proportional to the particle volume (R_{mac}^3), whereas energy removal from the particle is proportional to its surface area (R_{mac}^2); thus, the ratio of the rate of energy transfer to the rate of energy release is proportional to R_s^{-1} . In other words, the larger the initial catalyst particle, the higher the risk of overheating. Similarly, the ratio of the potential monomer flux into the particle divided by the rate of consumption of monomer by the reaction also varies as R_{mac}^{-1} . Thus, the larger the initial catalyst particle, the harder it is to supply all of the active sites

Table 2.13 Conclusions on inter- and intraparticle heat and mass transfer resistances according to the MGM

Phase	External film	Macroparticle	Microparticle
Liquid			
Mass transfer	Negligible	Can be important at the beginning of the polymerization for highly active catalysts	Can be important at the beginning of the polymerization, especially for catalysts having large primary particles
Heat transfer	Negligible	Negligible	Negligible
Gas			
Mass transfer	Negligible	Generally negligible except for large, active particles, at the beginning of the polymerization	Can be important at the beginning of the polymerization for catalysts having large primary particles
Heat transfer	Can be important for large, active particles, at the beginning of the polymerization	Generally negligible except for large, active particles at the beginning of the reaction	Negligible

with monomer. However, as the polymer particles grow, the number of active sites either remains constant or (more likely) decreases somewhat. Therefore the heat generation rate in the particle (in terms of watts) or the rate of consumption of monomer either remains constant or decreases. On the other hand, as the particles grow, the surface area available for mass and heat transfer with the bulk phase increases and renders the transport phenomena less difficult.

The sets of equations for micro- and macroparticles can be solved in many different ways, depending on the accuracy required. Typically the particle is divided up into a series of equivolometric shells in which it is assumed that the temperature and concentration in the pores of the macroparticle are identical. The equations can then be solved either by finite differences, collocation methods, or simply by using commercially available ODE solvers such as DASSL.

Since these conclusions indicate that, in most cases, heat and mass transfer resistances at the micrograin level are either very short lived, or not very important, it is possible to reformulate the MGM in a slightly simpler form. If the importance of mass transfer across the layers of polymer in the microparticles is neglected, then it is possible to rewrite Equation 2.137 as

$$R_p^c = k_p C^* M_{eq}(r_p, t) \quad (2.146)$$

This allows an effective volumetric reaction rate at each point in the secondary particle to be calculated without using the micrograin equations. This simplified version of the MGM

is called the polymer flow model (PFM). In the PFM, the macrograin is assumed to be equivalent to a pseudo-homogeneous polymer/pore matrix, in which mass transfer occurs by diffusion, with an effective diffusion coefficient that is, more often than not, treated as an adjustable parameter, just like in the MGM [66].

Generally speaking, the conclusions drawn from the MGM and PFM are valid if the simplifying hypotheses inherent in their development are acceptable:

- (1) the catalyst and polymer particles are spherical;
- (2) the primary particles are identical and are distributed homogeneously throughout the secondary particle (MGM only) at the beginning of the polymerization;
- (3) the structure of the macrograin is isotropic;
- (4) mass is transferred only by diffusion;
- (5) the effective diffusivity in the large particle is described by a single, constant value;
- (6) heat transfer from the particle to the surroundings occurs only by convection and
- (7) particle–particle interaction is not important in determining transport rates.

An in-depth discussion of the validity of these hypotheses has been published [66]; the interested reader is referred to that article for more insight into this problem. Nevertheless, in order to understand the validity of the predictions made with the models presented here, clearly the following questions need to be answered:

- (1) What simplifications and assumptions are justifiable in predictive models in light of the observed results?
- (2) What are reasonable values for model parameters and correlations?
- (3) How is the evolution of the geometry and morphology of the catalyst particle best modeled? How is the transition between virgin catalyst and growing polymer particles best described?
- (4) What happens during the initial instants of the polymerization? Can this be neglected?

Thus far, how to model radial profiles of monomers and chain transfer agents, as well as temperature, has been described but nothing has been said on how these profiles will be reflected on molecular weight averages or chemical compositions. The equations that were derived in Section 2.3, both for the method of moments and instantaneous distributions, can be applied for each radial position in the polymer particle to retrieve this information. Unfortunately these expressions will not be derived here due to space limitations but they can be found in many references in the literature [54–66]. The concept of instantaneous distributions should, however, be easy to visualize, as illustrated in Figure 2.34.

Figure 2.34 simulates the copolymerization of ethylene and propylene in the presence of hydrogen. Ethylene, being the faster comonomer, has a much steeper radial concentration profile than propylene. In the same way, hydrogen reacts much more slowly and also diffuses rather fast and therefore has a flat radial concentration profile. The effect of these profiles on the CLD and CCD is clear: polymer made near the surface of the particle will have higher molecular weight and ethylene fraction than the polymer made near the center of the particle. This modeling approach was first proposed by Soares and Hamielec for a version of the PFM [70].

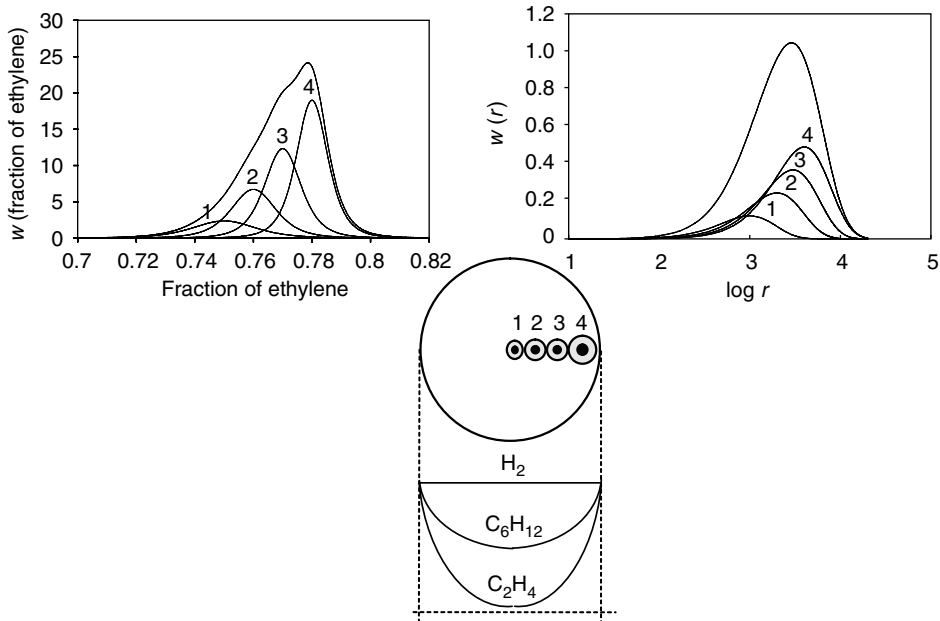


Figure 2.34 CLD and CCD as a function of radial position in a polymer particle subject to mass transfer limitations.

The summation of all these distributions over the polymer particle, weighted by the amount of polymer made at each radial position, gives the distribution for the whole particle at a given instant in time $w_p(r, y)$,

$$w_p(r, y) = \frac{\sum_{i=1}^m R_{p,i} w_i(r, y)}{\sum_{i=1}^m R_{p,i}} \quad (2.147)$$

where $R_{p,i}$ is the rate of polymerization at radial position i and m is the number of radial positions used in the discretization of the macroparticle. Notice that the mathematical treatment used in Equation 2.147 for different radial positions is the same as the one adopted in Equation 2.87 for polymer made in different site types.

These instantaneous distributions can then be integrated in time to obtain the cumulative distribution in the reactor per polymer particle, $\bar{w}_p(r, y)$:

$$\bar{w}_p(r, y) = \frac{\int w_p(r, y) (\sum_{i=1}^m R_{p,i}) dt}{\int (\sum_{i=1}^m R_{p,i}) dt} \quad (2.148)$$

For the case of catalysts containing multiple-site types, such as heterogeneous Ziegler–Natta catalysts, a similar approach applies, by defining one Stockmayer's distribution for each active site type. In this case, the overall distribution of chain length and chemical composition in the particle at a given instant equals the summation of the distributions over

all site types and all radial positions in the particle,

$$\bar{w}_p(r, y) = \frac{\sum_{i=1}^m \sum_{j=1}^n R_{p,i,j} w_{i,j}(r, y)}{\sum_{i=1}^m \sum_{j=1}^n R_{p,i,j}} \quad (2.149)$$

where the subscript j indicates the site type of a catalyst containing n site types.

2.5 Industrial olefin polymerization reactors

It is almost impossible to discuss reactors for polyolefin production without describing the entire polymerization process. There is a strong relationship between the process, the reactor configuration, and the catalyst used for polymerization. Advances in one component often enable or stimulate the development of the other components of the process. The reactor is the heart of the process, and the process is designed to complement the various attributes of a particular reactor setup; while the reactor is the heart of the process, the catalyst is the heart of the reactor.

Modern processes for polyolefin production are extremely efficient in producing large quantities of polymer. World scale plants have grown from 80 kt year⁻¹ in 1980 to more than 300–450 kt year⁻¹ [71] for the newest plants being built now. Despite these changes in production capacity, the basic process for making polyolefins has changed little since it was first commercialized in the 1960s. Figure 2.35 is an illustration of the basic blocks of such a process.

What has changed from the basic 1960s process design is that now each block has much better efficiency and higher throughput, and requires less capital investment. Advances in catalyst technology allowed the design of more efficient reactors and the elimination of some of the intermediate steps, such as catalyst deactivation and deashing.

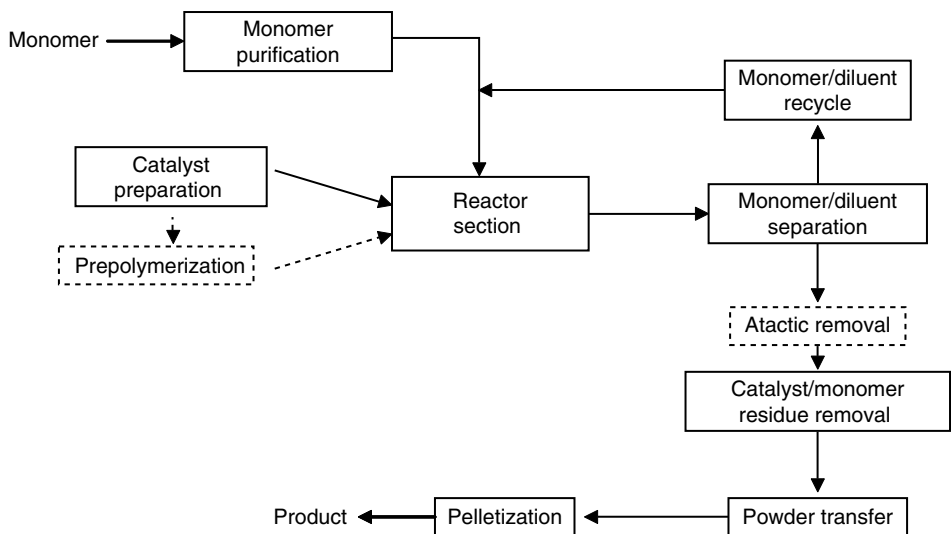


Figure 2.35 Flow diagram of a typical polyolefin manufacturing process.

Processes for polyolefin production can be grouped into the following categories:

- (1) slurry in an inert diluent;
- (2) slurry in monomer or *bulk* polymerization;
- (3) gas phase;
- (4) combination of slurry and gas phase and
- (5) solution.

This variety of reactor configurations is unique for polyolefins among all commodity and specialty polymers.

It is useful to separate the discussion into processes for polyethylene and polypropylene, as the requirements for these two polymers are different and have led to similar, but by no means identical, processes. A short discussion on the various reactor configurations will be presented first, followed by descriptions on how each reactor configuration is used in different polymerization processes throughout the world. Also listed are a few keys references at the end of the chapter for further reading [72–85]. Finally, the chapter will be concluded with a few considerations on the mathematical modeling of industrial olefin polymerization reactors.

2.5.1 Reactor configurations and designs

One of the main concerns during the design and control of polymerization reactors is how to remove the heat of reaction efficiently, since polymerizations are very exothermic reactions. In polymerization reactors, it is also imperative to be able to produce polymer that can be easily separated from unreacted monomer, catalyst residues and other byproducts, while assuring that polymer properties remain on target for a given grade. These stringent requirements led to the design of several reactor types, each with their own advantages and disadvantages. Each of these different reactor configurations will be discussed below.

Slurry-stirred autoclave reactors

The simplest reactor is the stirred autoclave reactor. In polyolefin production, this reactor is operated as a CSTR and is used in slurry, bulk and solution processes. The main advantages of this configuration are that the reactor is easy to build and to run, and provides a relatively uniform reaction medium with proper stirring. Its principal disadvantage is that the heat transfer area-to-volume ratio is relatively low and heat removal is, therefore, limited. This limitation is especially difficult to overcome for new plants with increasing production capacity.

Many modifications to the basic stirred autoclave design have been made to improve its heat transfer characteristics; those commonly used in polyolefin production processes include the use of external coolers, overhead condensers or internal cooling coils.

When external coolers are used, a portion of the polymer slurry in the reactor is circulated through one or more external heat exchanger to remove the heat of polymerization. This is an efficient method of heat removal, but puts stringent requirements on the morphology of the polymer particles being produced. Polymer fines are undesirable as they tend to deposit on the heat exchanger walls and require frequent shutdowns to clean out. An example

of a process that uses stirred autoclaves with external coolers is the Mitsui polyethylene process [72].

A very efficient alternative for heat removal is to use overhead condensers. This modification uses the latent heat of evaporation of the monomer to remove the heat of polymerization. Monomer is evaporated in the reactor, condensed in the overhead condenser, and the cooled liquid monomer is returned to the reactor. This design works well for propylene polymerization, but it is not a good option for ethylene because of its much lower boiling point. Overhead condensers are used in the El Paso bulk polypropylene process [72].

Finally, internal cooling coils are also used to increase the heat transfer area inside the reactor but they are generally less efficient than the other two methods mentioned above, since they are often subject to fouling.

Slurry-loop reactors

Loop reactors are the workhorse of the polyolefin industry. Up to 50% of the world's polyolefin resins are produced in loop reactors. Its success lies in the simplicity of its design since the reactor is, basically, a continuous loop of pipe. Polymer slurry in monomer or a diluent is circulated in the pipe using an axial pump. The residence time distribution of a loop reactor is similar to that of a CSTR, as the polymer slurry is continuously circulated in the pipe loop with a high recirculation ratio, and product is drawn off as a side stream. The main advantage of the loop reactor is the high surface area-to-volume ratio, allowing for very efficient heat removal and achieving very high reactor throughput.

Many different loop reactor configurations are used in industrial processes. The loop can be either in a vertical (Phillips and Spheripol processes [72, 73]) or in a horizontal position (USI process). The pipe can also be bent into multiple legs to increase the reaction volume. Several loops can be arranged in series to produce bimodal polymer, as in the case of Spheripol and Borstar processes [74]. Alternatively, the series of loop reactors can be operated as one single unit to increase average residence time and throughput.

Loop reactors are usually run in a liquid-filled state and the operating temperature is chosen on the basis of optimum catalyst activity and polymer properties. The operating pressure is basically the vapor pressure of the diluent or monomer at the operating temperature. In the Borstar process developed by Borealis, the operating pressure is above the critical pressure of the monomer and, therefore, the reactor is operated in supercritical mode. The higher process pressures allow the reactor to operate at higher temperatures as well, increasing the driving force for heat removal and enhancing the heat transfer capacity for higher reactor throughput.

The overall conversion in the loop polymerization reactor is very high for a polyolefin manufacturing process, and the conversion per pass is limited by the amount of monomer that is needed to carry the polymer out of the reactor. It is desirable to operate the reactor at as high a slurry density as possible to get the highest throughput and the highest conversion. Typically, loop reactors operate at slurry concentrations of about 45–50 wt% polymer.

Gas-phase reactors

Gas-phase processes offer an economical and energy-efficient alternative to liquid phase polymerization. Since the monomer is in the gas phase, separating the polymer from the monomer is relatively easy. There is no need to flash off the liquid monomer, a step with

a high energy requirement. Extended product range is also possible with gas-phase reactors as there is no solubility limit for hydrogen and comonomer in the reaction medium, allowing the production of products with higher melt flow index and increased comonomer content. In solution and slurry reactors, on the other hand, the low solubility of comonomers and hydrogen in the reaction medium puts a limit on the molecular weight and comonomer incorporation that can be achieved in these processes.

Three main types of gas-phase reactors are used in the industry: fluidized-bed, vertical stirred-bed and horizontal stirred-bed reactors.

Fluidized-bed gas-phase reactors

The dynamics and residence time distribution of fluidized-bed reactors are very complex, but have been well studied and approximate to those of a CSTR. Fluidized-bed reactors are very efficient and have high space-time yield. Heat removal is achieved by circulating the monomer gas through an external heat exchanger. In some processes, further heat removal can be achieved by partially condensing the recycled monomer, the so-called *condensed mode operation*, and then letting it vaporize when reintroduced in the reactor. This heat removal through the latent heat of vaporization of the monomer is an extremely efficient heat removal procedure and can significantly increase the throughput of the reactor. A further extension of this concept is the *super-condensed mode* operation where an inert component (such as pentane, for instance) is used as the condensing phase to further enhance heat transfer through evaporation [75–77]. A reactor operating in the super-condensed mode can more than double the throughput of a reactor operating in the normal non-condensed mode.

Another important feature of a modern fluidized-bed reactor for polyolefin production is the *disengaging zone*; the diameter of the reactor is increased at its topmost part to form the disengaging zone. This expanded cross section of the reactor slows down the upward movement of the polymer particles and prevents or minimizes them from being carried out by the fluidizing gas. Using this design procedure, the circulating gas velocity can be increased for better heat transfer.

There are, however, several drawbacks associated with the operation of fluidized-bed reactors. Stable temperature control in the reactor is extremely important; all localized hot spots must be minimized. Hot spots will cause the polymer particles to melt and stick together, forming chunks and lumps. Small chunks and lumps can cause transport and processing problems downstream, while large ones can block the outlet of the reactor. The latter condition creates an extremely dangerous situation, and the reactor has to be shutdown right away; if not shut down properly, the content of the entire reactor may melt together to form a big polymer lump.

Static charges can also be a significant problem in gas-phase reactors in general, and in fluidized-bed reactors in particular. Polymer particles are poor conductors of electricity, and static electricity generated by the intense mixing and high velocity of the circulating monomer may cause fine particles to stick to the reactor walls. In fluidized-bed reactors, the heat transfer coefficient at the wall is small since there is little or no mixing action. The fine particles that are stuck to the wall can continue to polymerize and, because of poor heat transfer, melt to form sheets and chunks. Polymer sheets can block the outlet of the reactor if they fall off the wall, requiring immediate shutdown of the reactor.

Vertical-stirred gas-phase reactor

A vertical-stirred gas-phase reactor for polyolefin production was first developed by BASF [72, 78] in the 1960s. The reactor configuration is basically that of a stirred autoclave, but with a bottom-mounted helical stirrer. Mechanically, this is a fairly complex agitation system. Similar to the fluidized-bed gas-phase reactor, heat is removed by circulating monomer gas through an external heat exchanger. Part of the gas is condensed and returned to the reactor as liquid, and part of the gas is cooled and recycled to the bottom of the reactor. It is important to keep the temperature in the reactor above the dew point of the returning gas to prevent forming a pool of liquid monomer at the bottom of the reactor. Liquid pooling can cause uncontrolled polymerization, forming lumps and chunks, which can block the outlet of the reactor. The dynamics of the reactor approaches that of a CSTR, but some plug flow reactor (PFR) characteristics also exist because of the slow speed of agitation in this reactor configuration.

Horizontal-stirred gas-phase reactor

A horizontal-stirred gas-phase reactor for polypropylene production was first patented by Amoco in the 1970s. This reactor setup has now developed into the Innovene process and the Chisso process [79]. The reactor configuration is that of a horizontal, mechanically-stirred gas-phase reactor. The reactor is separated into different zones by a series of baffles; polymer is moved from one zone to another by an agitator. The residence time distribution of this reactor can be best modeled as a series of CSTRs, making the reactor behavior closer to that of a PFR. This feature is unique among polyolefin reactors. Since the residence time distribution is narrower, the polymers produced have more uniform properties. The narrow residence time distribution also permits faster grade transition times and less off-spec material formation during grade transition.

Heat removal is achieved by feeding liquid monomer as quench liquid along the reactor. This greatly reduces the heat load removed by the recycled monomer gas, and thus the gas velocity can be kept much lower, resulting in lower capital costs as well as lower operating costs.

Gas-phase circulating-bed reactor

This is the latest reactor configuration developed by Basell and first commercialized in the early 2000s as the basis of the Spherizone technology [80, 81]. The configuration of this reactor is an extension of the loop reactor concept. Instead of operating in the liquid phase, like the loop reactor, the circulating-bed reactor operates in the gas phase and with different reaction conditions at different sections of the reactor. This reactor is similar to the riser-tube reactor used in fluidized catalytic cracking. The reactor consists of two interconnecting reaction zones. In the first zone (the riser), the reactor is operated like a (fast fluidization conditions) fluidized-bed reactor, but the fluidization velocity is high enough to entrain the polymer particles in the gas and the entire bed moves to the second zone. The second zone works like a moving-bed reactor, where the polymer particles flow downward and then are recirculated to the first zone. The two zones can be operated at very different polymerization conditions to produce polymers with different compositions in each zone. The growing polymer particles circulate between the two different reaction zones, building up layers of different composition in each successive pass. Heat removal is achieved by operating the reactor in condensed mode, but can also be

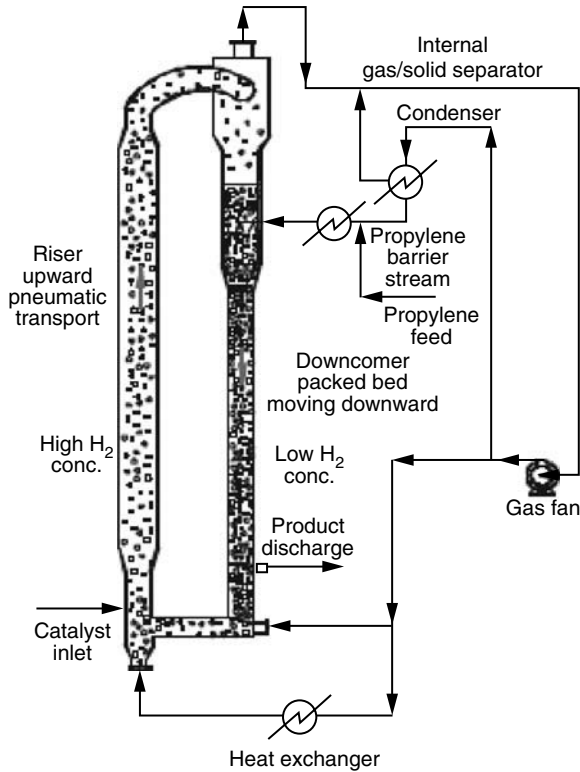


Figure 2.36 Multizone circulating reactor [82].

achieved by jacketing the riser tube. This unique reactor configuration is illustrated in Figure 2.36.

Table 2.14 summarizes the main advantages and disadvantages of each reactor configuration discussed above.

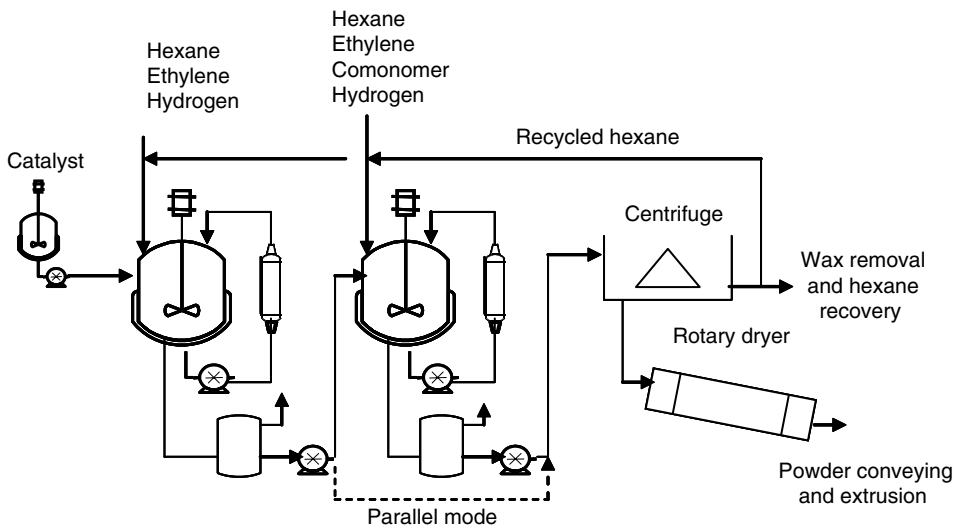
2.5.2 Polyethylene manufacturing processes

Slurry (inert diluent) processes

The slurry process was the first commercial process for the production of polyolefins. The basic process consists of a series of CSTRs with the polymerization taking place in a heterogeneous catalyst suspended on an inert diluent. Many different variations of the slurry process were developed in the early 1970s. The design of the process was dictated by the available catalyst at the time, which typically had low activity. Since catalyst activity was low, a series of CSTRs were needed to push the reaction to completion. Catalyst residue removal, called *deashing*, was also necessary, greatly increasing the capital costs of the process. With the advent of high-activity catalysts, the polymerization can now be completed in one or two reactors without deashing. Despite being the first process for ethylene polymerization, the slurry process is still economically viable and competitive.

Table 2.14 Summary of advantages and disadvantages for several reactor configurations

Reactor configuration	Advantages	Disadvantages
Stirred autoclave	Low capital cost	Low heat transfer area Low space time yield
Loop	Low capital cost High heat removal High space time yield	
Fluidized gas phase	High heat removal High space time yield	Difficult to operate
Stirred gas phase	PFR characteristic allows for fast grade transfer	More complex reactor design, higher capital cost
Circulating bed	Better polymer properties control Different reacting zone allows production of product not possible with traditional reactors	Complex reactor design, high capital cost Still unproven technology

**Figure 2.37** Mitsui CX process for HDPE manufacture.

The Mitsui CX process is typical of a modern slurry process for HDPE production (Figure 2.37). It consists of two CSTRs (hexane is used as diluent), a centrifuge to separate the diluent from the polymer, a dryer to remove the residual diluent, and a diluent recovery system to separate the low molecular weight polymer or wax that is dissolved in the diluent. The two polymerization reactors can be operated in series or in parallel. When run in

parallel, both reactors can operate at the same conditions to increase plant output, or they can be operated at different conditions to produce different polymers, usually with distinct molecular weight averages, that are mixed together downstream to obtain a polymer with bimodal MWD. In the series mode, the reactors are usually operated at very different conditions to produce bimodal polymers. In this case, the two polymers are more intimately mixed and have better properties than the ones produced when the reactors are operated in parallel. This method is important in producing film grade products, where a low molecular weight fraction is desirable for polymer processability, and a high molecular weight fraction is needed for good polymer properties. Pipe resins also may benefit from this mode of operation.

There are several competing hexane slurry processes, but only Basell (Hostalen process) and Equistar–Maruzen still have active licensing activities. Both processes use similar reactor configuration and operating conditions.

The other important slurry process for polyethylene is the Phillips process. The Phillips process is based on the loop reactor, which can operate at higher monomer and slurry concentrations than stirred autoclaves and allows for higher space-time yield. As mentioned above, the residence time distribution in loop reactors is also that of a CSTR, but instead of the usual stirrer, an axial pump is used to circulate the reactants around a pipe loop. It uses isobutane as diluent; isobutane has a lower boiling temperature and can easily be flashed off after the reactor, eliminating the centrifuge and drying steps used in the Mitsui CX process. As seen before, Phillips has developed chromium-based catalysts, which inherently make polymer with very broad MWD thus lessening the need for a second reactor or bimodal operation. This is considered to be one of the most efficient industrial versions of the slurry process. There are over 80 reactors of this type currently operating in the world, producing almost one-third of the world's HDPE. The Phillips process has been refined over the years and the latest plants have impressive capacities of 320 kt year^{-1} using a single loop reactor. Most of the Phillips reactors are for HDPE, although LLDPE can be produced using metallocene catalysts.

The other process that uses a loop reactor is the Borstar process from Borealis [74]. The Borstar process has many unique features such as a loop reactor followed by a fluidized gas-phase reactor; it also uses supercritical propane as a diluent. Polyethylene has lower solubility in supercritical propane than in isobutane and, therefore, causes less fouling in the reactor. The higher operating pressure also allows the reactor to be operated at higher hydrogen concentrations to produce polymers with higher melt indices (lower molecular weight averages). Due to the complexity of the process, however, it requires higher capital investment and only a few plants using this technology have been built to date.

The main characteristics of slurry processes for ethylene polymerization are summarized in Table 2.15.

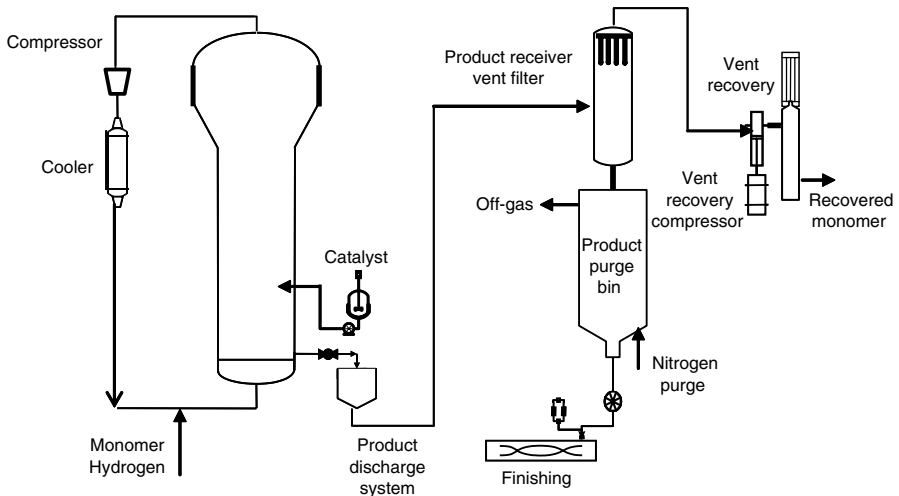
Gas-phase processes

Union Carbide, now part of Dow Chemical, was the first company to commercialize the technology for polyolefin production using fluidized-bed gas-phase reactors. Since polymerization occurs in the gas phase, separation of the unreacted monomer from the polymer product is achieved simply by flashing off the monomer. Any low molecular weight polymer formed remains in the polymer particles and no further separation is necessary. The process only requires a fluidized-bed gas-phase reactor, a product discharge system to get

Table 2.15 Typical reactor conditions for slurry HDPE processes^a

Process	Reactor type	Diluent	Reactor temperature (°C)	Reactor pressure (bar)	Residence time (h)
Mitsui	2 stirred autoclaves in series or parallel	Hexane	80–85	<8	2
Basell (Hostalen Process)	2 stirred autoclaves in series	Hexane	80–85	<8	1–5 (h per reactor)
Equistar–Maruzen–Nissan	2 stirred autoclaves in series	Hexane	80–85	<11	2 × 2
Chevron–Phillips	Single loop (multi-legs)	Isobutane	85–100	30–35	1
Borealis–Borstar	Loop/fluidized gas	Supercritical propane	85–100	60–65	

^a Reactor conditions differ for different product grades; the values shown here are only approximate averages found in these processes.

**Figure 2.38** Unipol process for polyethylene manufacture.

the polymer out of the reactor and flash off the monomer, and a purge column to remove any residual monomer and to deactivate the catalyst. The Unipol plant requires the least capital investment among the major polyolefin production processes (Figure 2.38).

First generation Unipol plants were often plagued by operational problems that caused runaway reactions and formed large lumps of polymer in the reactor. With improvements in catalyst development and in process control, this type of problem has largely been overcome.

Table 2.16 Typical reactor conditions for fluidized-bed processes^a

Process	Reactor type	Mode of operation	Reactor temperature (°C)	Reactor pressure (bar)	Residence time (h)
Unipol (Univation)	Fluidized bed	Condensed/ super condensed	90–110	20–25	~2
Lupotech G (Basell)	Fluidized bed	Condensed	90–110	20–25	~2
Spherilene (Basell)	2 fluidized beds	Non-condensed	70–90	20–25	~3
Innovene (Ineos)	Fluidized bed	Condensed			~2

^a Reactor conditions differ for different product grades; the values shown here are only approximate averages found in these processes.

In addition, modern reactors now operate in condensed mode, which greatly increases their throughput. The Unipol process for LLDPE is now licensed by Univation.

Both HDPE and LLDPE can be made using the Unipol process, although this process has found broader acceptance for the production of LLDPE. Some Unipol plants were designed and operated in the *swing mode* between HDPE and LLDPE, but most plants are designed only for LLPDE production.

Several other companies have developed and are licensing gas-phase polyethylene technologies. They include the Innovene process from BP (now Ineos), and the Lupotech G and Spherilene processes from Basell. All of them are based on the same principle of using a fluidized-bed gas-phase reactor, although the operating mode and conditions differs among these different processes. Table 2.16 details the main characteristics of fluidized-bed processes for olefin polymerization.

Solution processes

Like the slurry polymerization processes, solution polymerization uses one or two stirred autoclaves, but the polymerization takes place at much higher temperatures (up to 250°C) and pressures (up to 100 bar). The average reactor residence times in solution processes are much shorter than in the processes discussed previously, in the order of 5–10 min, and this allows for much faster grade transition. Solution polymerization also allows the use of higher α -olefins comonomers, such as 1-hexene and 1-octene, which produce LLDPE with excellent properties. Solution processes are also most adaptable to metallocene catalyst technology because the catalyst does not need to be supported.

The Dowlex process by Dow Chemicals is the dominant process in solution polymerization, but Dow does not license this technology to other companies (Figure 2.39). The Dowlex process uses two CSTRs in series with a high boiling hydrocarbon solvent. Other competing processes include the DSM process and the Sclairtech process by Nova Chemicals. In some configurations, these processes may also have tubular reactors operated in series with the CSTR to complete monomer conversion.

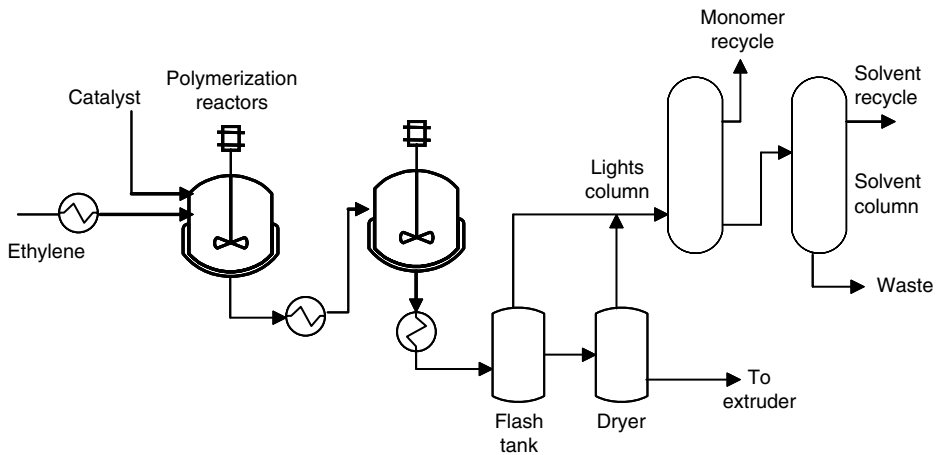


Figure 2.39 Dowlex solution process for polyethylene production.

2.5.3 Polypropylene manufacturing processes

There are many parallels between polypropylene and polyethylene manufacturing processes. The reactor configurations are similar, but, due to the different requirements of the polymer, it will be seen that there are significant differences between the processes as well. While propylene homopolymer can be produced in reactors of various configurations, for impact copolymer production, gas phase is the reactor of choice because of the stickiness of the polymer and the solubility of the copolymer in the monomer and diluent.

Slurry (inert diluent) processes

Like the slurry process for polyethylene manufacture, this is also the first commercial process for the production of polypropylene. The basic process includes a series of CSTRs and polymerization takes place in an inert diluent. Many different variations of the slurry process were developed in the early 1970s. The design of the process was dictated by the available catalyst at the time, which typically had low activity and produced polymer with low isotacticity. Since catalyst activity was low, a series of reactors were needed to push the reaction to completion. It is not unusual to see processes with five reactors in series, and some with even seven reactors in series, designed in those earlier days. Dashing was required to remove the high level of catalyst residue from the product; an atactic polypropylene removal step was also necessary. Different variations of the slurry process included the use of diluents ranging from C_6 to C_{12} hydrocarbons.

Diluent slurry processes for polypropylene are expensive to build and to run because of the number of pieces of equipment involved. They have largely been replaced by the more efficient bulk and gas-phase processes. Most of the remaining diluent slurry plants in the world now focus on producing speciality polymers, as diluent slurry processes do offer some advantages over other bulk and gas-phase processes. An example is the production of high-crystallinity polypropylene (HCPP), where most of the atactic polymer is dissolved in

the diluent and removed from the final product, increasing the crystallinity and stiffness of the resulting polymer.

Slurry (liquid propylene) processes

In this type of process, polymerization takes place in liquid propylene without the use of an inert diluent. This is a significant simplification over the traditional diluent slurry process, as propylene can be separated from the polymer by flashing, and there is no need for the extensive diluent recovery system.

The dominant process in this market segment is the Spheripol process by Basell. Similar to the dominance achieved by the Phillips process in HDPE, roughly one-third of the world's polypropylene is produced using the Spheripol process. The Spheripol process uses loop reactors. A small loop reactor is used to prepolymerize the catalyst; the main polymerization, for homopolymer or random copolymer, takes place in one or two loop reactors. For impact copolymer production, a gas-phase reactor is required after the loop reactor because of the limited solubility of ethylene in liquid propylene. A typical flow diagram of the Spheripol process is shown in Figure 2.40.

Basell has recently developed the Spherizone process using the circulating-bed reactor, already depicted in Figure 2.36. Other than the different reactor configuration, the Spherizone process is essentially the same as the Spheripol process.

The other competing bulk propylene processes include the Mitsui Hypol process and the various offshoots of the El Paso (or Rexene) process. In 2005, ExxonMobil announced that they were licensing a propylene bulk process based on the loop reactor. The front end of the ExxonMobil process is similar to the Spheripol process with a single or double loop, but a fluidized-bed gas-phase reactor is used for impact copolymer instead of the stirred-bed gas-phase reactor in a typical Spheripol process.

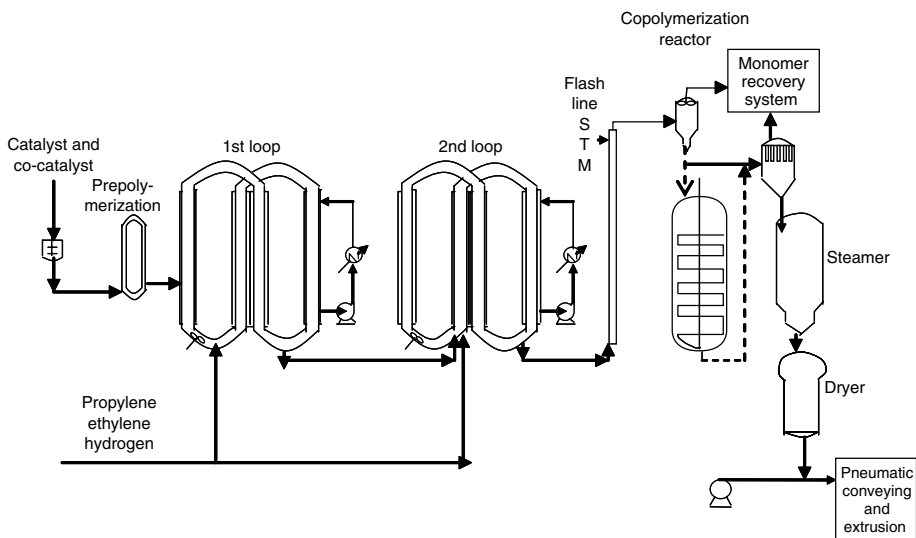


Figure 2.40 Spheripol process for polypropylene manufacture.

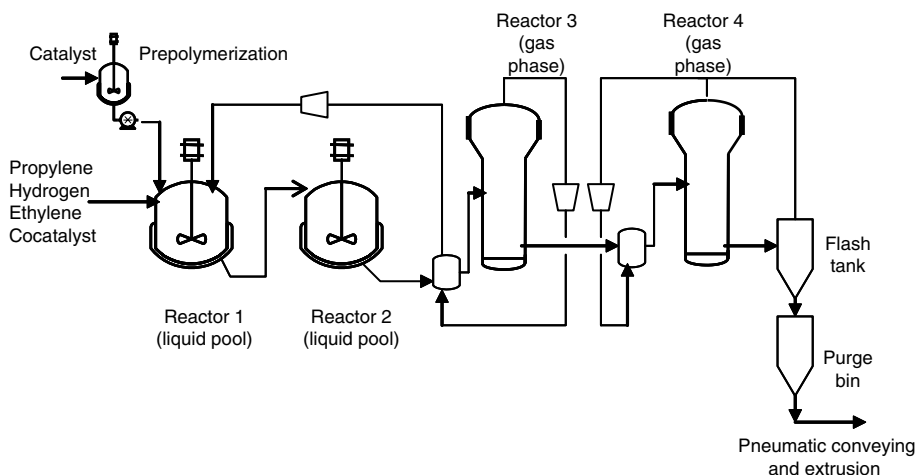


Figure 2.41 Mitsui Hypol process for polypropylene production.

The Mitsui Hypol process is based on two stirred autoclave reactors followed by two fluidized-bed gas-phase reactors (Figure 2.41). The gas-phase reactors are also used in homopolymerization, enabling polymer with better properties to be made. In the more up-to-date Hypol II process, the stirred autoclaves are replaced by loop reactors giving higher throughput and further reducing capital costs.

The El Paso process uses a single, large, stirred autoclave reactor for homopolymer production. For impact copolymer, a second horizontal stirred gas-phase reactor is used.

Gas-phase processes

There are several different gas-phase processes for propylene polymerization, with different reactor configurations; each one having its own unique attributes.

The Unipol process, initially developed for polyethylene production, was later extended to polypropylene manufacture. The process consists of a large fluidized-bed gas-phase reactor for homopolymer and random copolymer production, and a second smaller reactor for impact copolymer production. The second reactor is smaller than the first one because only 20% of the production comes from the second reactor. This reactor typically has a lower pressure rating as copolymerization is usually carried out at lower temperatures and pressures. Condensed mode operation is used in the homopolymer reactor but an inert diluent is not required because propylene is partially fed as a liquid. The copolymerization reactor is operated purely in the gas phase. The Unipol process has a unique and complex product discharge system that allows for very efficient recovery of unreacted monomer, but this does add complexity and capital cost to the process.

The Novolen process [78], now licensed by Novolen Technology Holdings (NTH), uses the vertically stirred reactor for propylene polymerization. The basic process is similar to the Unipol process but with a simpler polymer discharge system. Novolen claims this process requires the lowest capital investment of its class and has low operating costs.

The third reactor configuration is the Innovene [79] process developed by Amoco (which became BP and now Ineos) using the horizontal-stirred reactor. The advantage of this

Table 2.17 Comparison of different polypropylene manufacture processes

Process	Reactor type		Mode of operation	Reactor temperature (°C)	Reactor pressure (bar)	Residence time (h)
	Homopolymer	Impact copolymer				
Slurry	Series of autoclaves	Series of autoclaves	Slurry	65–75	8–12	Up to 5
Spheripol	Loop	Stirred gas	Liquid pool (bulk)/gas	65–75	30–35	~2
Hypol	Stirred autoclave (Hypol I)	Fluidized bed gas	Bulk/gas	65–75	30–35	~2
	Loop (Hypol II)	Fluidized bed gas				
Unipol	Fluidized bed gas	Fluidized bed gas	Condensed gas phase/gas	60–70	25–30	~1
NTH	Vertical stirred gas	Vertical stirred gas	Gas/gas (non-condensed)	80–85	30–35	~1
Innovene	Horizontal stirred gas	Horizontal stirred gas	Gas/gas	60–70	25–30	~1

process is the enhanced polymer properties possible with the plug flow reactor characteristics and fast grade transition, but the complexity of the reactor (particularly its horizontal impeller) increases capital cost.

Both NTH and Innovene technologies require two reactors in series to produce impact polypropylene resins.

Table 2.17 summarizes the most important characteristics of these gas-phase process for the production of polypropylene.

2.5.4 Mathematical models for industrial reactors

Throughout this chapter we have discussed how phenomena taking place in micro-, meso- and macroscale influence olefin polymerization rates and polyolefin microstructure. The catalyst type ultimately determines the polymer microstructure for given a set of polymerization conditions such as temperature and concentration of monomer, comonomer, and chain transfer agent, but also the polymerization conditions themselves are a consequence of the type of support and reactor used to produce the polyolefin.

A complete phenomenological mathematical model for olefin polymerization in industrial reactors should, in principle, include a description of phenomena taking place from microscale to macroscale. It may come as a disappointment to learn that most mathematical models for industrial reactors ignore several of these details. In fact, most models assume

that the conditions in the polymerization reactor are uniform and that the equations derived in Section 2.3 (such as the ones listed in Table 2.10) can be directly applied for bulk values of temperature and concentration of monomer, comonomer and hydrogen. As mentioned before, this may be a good approximation for solution polymerization reactors but will depart from reality (but, not necessarily, by much) for supported catalysts in slurry and gas-phase processes.

If it is known that this hypothesis is an oversimplification, then why is it made so often? Mostly, because the additional effort required to integrate micro-, meso- and macroscale phenomena in a single model does not necessarily lead to better quantitative predictions when it comes to industrial reactors. Uncertainties on model parameter values are, most often, too high to try to decouple “true” polymerization kinetic parameters from mass and heat transfer effects; often apparent kinetic parameters will do an equally good job from an engineering perspective [86].

Therefore, the equations shown in Table 2.10, either in transient or steady-state, are usually applied to industrial reactors as well. To these equations may be added an energy balance to model non-isothermal reaction operation:

$$\sum_i c_{pi} w_{mi} N_i \frac{dT}{dt} = UA_w(T_w - T) + R_p(-\Delta H_r)V - \sum_i F_{in,i} w_{mi} c_{pi}(T - T_{ie}) \quad (2.150)$$

where the subscript i indicates monomer type, hydrogen, nitrogen, diluent, or impurities, N is the number of moles of a given component in the reactor, c_p is its average heat capacity, w_{mi} is the molecular weight of the component, $(-\Delta H_r)$ is the heat of reaction, R_p is the polymerization rate, U is the global heat transfer coefficient, T_w is the coolant temperature, T_{ie} is temperature of feed stream to reactor and A_w is total heat transfer area of the reactor.

For gas-phase or liquid propylene bulk reactors, the bulk monomer concentration in the reactor must be converted to concentration in the polymer phase surrounding the active sites with a thermodynamic relationship. Generally, a simple partition coefficient such as the one used in Equation 2.136a is used. For diluent slurry reactors, where the monomer is introduced in the gas phase, a partition coefficient such as Henry's law constant must also be used to calculate the concentration of monomer in the diluent which, in turn, is used to estimate the concentration of monomer in the polymer phase surrounding the active sites. Evidently, more sophisticated thermodynamic relationships relating the concentration of monomer in the gas phase, diluent and polymer can be used but, from a practical point of view, are only justified when the polymerization kinetic constants are very well known. Similar considerations apply to calculate the concentrations of comonomers, hydrogen and any other reactant in the system.

How can the MGM and effects of reactor residence time be combined to obtain a more complete description of polymerization in industrial reactors? Some of these aspects have been discussed in the literature but would require a lengthier treatment than allowed here [87]. Alternatively, a rather simple, but elegant, treatment will be shown, which combines some of the aspects that have been covered in the discussion on micro-, meso- and macroscale phenomena to model polyolefin reactors under steady-state operation.

Consider the case of a continuous olefin polymerization reactor with residence time distribution $E(t)$ operating with a heterogeneous Ziegler–Natta or supported metallocene catalyst. From classical reactor engineering studies it will be remembered that

the residence time in a CSTR is given by:

$$E(t) = \frac{1}{\bar{t}} \exp(-t/\bar{t}) \quad (2.151)$$

where \bar{t} is the average residence time of the reactor.

Assume that: all catalyst particles have the same size (in fact, they follow a particle size distribution); the reactor is well mixed and its conditions are uniform; and the residence time distribution is independent of catalyst/polymer particle size.

A well-mixed CSTR is a good approximation for most of the continuous reactors used in the production of polyolefins. Therefore, the monomer balance under steady-state conditions is

$$0 = -\bar{R}_p V + F_{M_{in}} - sM \quad (2.152)$$

where \bar{R}_p is the average polymerization rate per unit volume of the reactor, which can be written as

$$\bar{R}_p = \bar{R}'_p N_s \quad (2.153)$$

where N_s is the number of macroparticles per unit volume of the reactor and \bar{R}'_p is the average polymerization rate per particle, given by the expression:

$$\bar{R}'_p = \int_0^{\infty} E(t) R_p(t) dt \quad (2.154)$$

In Equation 2.154, $R_p(t)$ is the polymerization rate in a polymer particle (secondary particle, according to the MGM terminology) with a residence time t in the reactor, which can be calculated by integrating the material balances presented in Section 2.4 for the MGM. For practical purposes, a value of 5–6 average residence times is enough for the upper limit of the integral.

Equations 2.152 and 2.154 can be solved by assuming a value for M , calculating $R_p(t)$ with the MGM, \bar{R}'_p with Equation 2.154 and \bar{R}_p with Equation 2.153, and finally recalculating the value of M with Equation 2.152 until convergence.

Once the concentration of the monomer in the reactor is known, any additive property of the polymer, $X(t)$ (moments of living and dead chains, chain length averages, average comonomer compositions), produced in particles with a given residence time t can be calculated by combining the balances in the particles and the equations in Section 2.3. If the polymer particles are treated as a macrofluid, the average value of any property \bar{X} is given by:

$$\bar{X} = \int_0^{\infty} E(t) X(t) dt \quad (2.155)$$

For the non-additive properties, such as the CLD, $w(r)$, the average value can be obtained by the equation:

$$\overline{w(r)} = \frac{\int_0^{\infty} E(t) v_1(t) w(r, t) dt}{\int_0^{\infty} E(t) v_1(t) dt} \quad (2.156)$$

Among the assumptions made above, the weakest was to consider that all catalyst particles had the same size, since it is now known that industrial catalysts have a distribution of particle sizes. Defining the catalyst particle size distribution (in volume) as $n_c(v)$ such that

$$\int_0^{\infty} n_c(v)dv = 0 \quad (2.157)$$

the treatment proposed above can be extended for catalysts that have a distribution of particle sizes:

$$\bar{X} = \int_0^{\infty} n(v) \left(\int_0^{\infty} E(t)X(t)dt \right) dv \quad (2.158)$$

$$\bar{R}'_p = \int_0^{\infty} n(v) \left(\int_0^{\infty} E(t)R_p(t)dt \right) dv \quad (2.159)$$

$$\overline{w(r)} = \frac{\int_0^{\infty} n(v) \left(\int_0^{\infty} E(t)v_1(t)w(r,t)dt \right) dv}{\int_0^{\infty} n(v) \left(\int_0^{\infty} E(t)v_1(t)dt \right) dv} \quad (2.160)$$

Finally, it should be emphasized that, even though the mathematical treatment described above combines the MGM (or any other single particle model, such as the PFM), the polymerization kinetic models described in Section 2.3, and the different reactor configurations treated in this section (through their respective residence time distributions, $E(t)$) in a relatively simple way, it is not considered the standard treatment for industrial olefin polymerization reactors. A simple cost-benefit argument explains why this is the case: until a more quantitative understanding of polymerization kinetics steps, particle fragmentation and growth, and inter- and intraparticle mass and heat transfer resistances is achieved, the integration of all these phenomena in a single model may be viewed as a stimulating academic exercise but will hardly lead to mathematical models with improved predictive capabilities.

Acknowledgments

We would like to thank our colleague Professor Leonardo Simon, from the University of Waterloo, for kindly allowing us to use some of his excellent illustrations in this chapter. We are also indebted to the editor of this book, Professor José M. Asua, for his insightful comments and discussions during the development of this chapter.

References

1. Faldi, A. and Soares, J.B.P. (2001) *Polymer*, **42**, 3057–3066.
2. Lustiger, A. and Markham, R.L. (1983) *Polymer*, **24**, 1647–1654.
3. Soares, J.B.P., Abbott, R.F. and Kim, J.D. (2000) *J. Polym. Sci.: Part B: Polym. Phys.*, **38**, 1267–1275.
4. Sarzotti, D.M., Soares, J.B.P. and Penlidis, A. (2002) *J. Polym. Sci.: Part B: Polym. Phys.*, **40**, 2595–2611.
5. Soares, J.B.P. and Simon, L.C. (2005) In T. Meyer and J. Keurentjes (eds), *Handbook of Polymer Reaction Engineering*. Wiley-VCH, Weinheim, pp. 365–430.

6. Soares, J.B.P. (2004) In J.I. Kroschwitz (ed.), *Encyclopedia of Polymer Science and Technology*, 3rd edn. Wiley-VCH, Weinheim, pp. 75–131.
7. Soares, J.B.P. and Hamielec, A.E. (1996) *Polymer*, **37**, 4606–4616.
8. Anantawaraskul, S., Soares, J.B.P. and Wood-Adams, P.M. (2005) *Adv. Polym. Sci.*, **182**, 1–54.
9. Sarzotti, D.M., Soares, J.B.P., Simon, L.C. and Britto, J.D. (2004) *Polymer*, **45**, 4787–4799.
10. Starck, P., Rajanen, K. and Löfgren, B. (2003) *Thermochim. Acta*, **395**, 169–181.
11. Adisson, E., Ribeiro, M., Deffieux, A. and Fontanille, M. (1992) *Polymer*, **33**, 4337–4342.
12. Bovey, F.A. and Mirau, P.A. (1996) *NMR of Polymers*. Academic Press, New York.
13. Francuskiewicz, F. (1994) *Polymer Fractionation*. Springer-Verlag, Berlin.
14. Simon, L.C., Patel, H., Soares, J.B.P. and de Souza, R.F. (2001) *Macromol. Chem. Phys.*, **202**, 3237–3247.
15. Soga, K. and Shiono, T. (1997) *Prog. Polym. Sci.*, **22**, 1503–1546.
16. Mulhaupt, R. (2003) *Macromol. Chem. Phys.*, **204**, 289–327.
17. Krauss, H.L. (1998) In W. Kaminsky and H. Sinn (eds), *Transition Metals and Organometallics as Catalysts for Olefin Polymerization*. Springer-Verlag, Berlin, pp. 163–168.
18. Thune, P.C., Loos, J., de Jonga, A.M., Lemstrab, P.J. and Niemantsverdriet, J.W. (2000) *Topics in Catalysis*, **13**, 67–74.
19. Coates, G.W. (2000) *Chem. Rev.*, **100**, 1223–1252.
20. Resconi, L., Cavallo, L., Fait, A. and Piemontesi, F. (2000) *Chem. Rev.*, **100**, 1253–1346.
21. Butenschön, H. (2000) *Chem. Rev.*, **100**, 1527–1564.
22. Alt, H.G. and Köppl, A. (2000) *Chem. Rev.*, **100**, 1205–1222.
23. Chum, S., Kruper, W.J. and Guest, M. (2000) *Adv. Mater.*, **12**, 1759–1767.
24. Hlatky, G.G. (2000) *Chem. Rev.*, **100**, 1347–1376.
25. Sinn, H., Kaminsky, W. and Vollmer, H.J. (1980) *Angew Chem. Int. Engl.*, **19**, 390–392.
26. Simon, L.C., Williams, C.P., Soares, J.B.P. and de Souza, R.F. (2001) *Chem. Engng Sci.*, **56**, 4181–4190.
27. Simon, L.C., de Souza, R.F., Soares, J.B.P. and Mauler, R.S. (2001) *Polymer*, **42**, 4885–4892.
28. Ittel, S.D. and Johnson, L.K. (2000) *Chem. Rev.*, **100**, 1169–1203.
29. Ystenes, M.J. (1991) *J. Catal.*, **129**, 383–401.
30. Kissin, Y.V., Mink, R.I., Nowlin, T.E. and Brandolini, A.J. (1999) *Topics in Catalysis*, **7**, 69–88.
31. Shaffer, W.K.A. and Ray, W.H.J. (1997) *Appl. Polym. Sci.*, **65**, 1053–1080.
32. Canu, P. and Ray, W.H. (1991) *Comp. Chem. Engng*, **15**, 549–564.
33. Wulfov, M. (1996) *Macromol. Theory Simul.*, **5**, 393–416.
34. Flory, P.J. (1953) *Principles of Polymer Chemistry*. Cornell University Press, Ithaca.
35. Soares, J.B.P. and Penlidis, A. (2000) In J. Scheirs and W. Kaminsky (eds), *Preparation, Properties and Technology of Metallocene-Based Polyolefins*. John Wiley & Sons, Chichester, UK, pp. 237–267.
36. Kim, J.D., Soares, J.B.P. and Rempel, G.L. (1998) *Macromol. Rapid Commun.*, **19**, 197–200.
37. Soares, J.B.P. and Kim, J.D. (2000) *J. Polym. Sci.: Part A: Polym. Chem.*, **38**, 1408–1416.
38. Kim, J.D. and Soares, J.B.P. (2000) *J. Polym. Sci.: Part A: Polym. Chem.*, **38**, 1417–1426.
39. Soares, J.B.P. and Hamielec, A.E. (1995) *Polymer*, **36**, 2257–2263.
40. Soares, J.B.P., Abbott, R.F., Willis, J.N. and Liu, X. (1996) *Macromol. Chem. Phys.*, **197**, 3383–3396.
41. Xie, T. and Hamielec, A.E. (1993) *Makromol. Chem., Theory Simul.*, **2**, 421–454.
42. Xie, T. and Hamielec, A.E. (1993) *Makromol. Chem., Theory Simul.*, **2**, 455–483.
43. Stockmayer, W.H.J. (1945) *Chem. Phys.*, **13**, 199–207.
44. da Silva Filho, A.A., de Galland, G.B. and Soares, J.B.P. (2000) *Macromol. Chem. Phys.*, **201**, 1226–1234.
45. Soares, J.B.P. and Hamielec, A.E. (1996) *Macromol. Theory Simul.*, **5**, 547–572.
46. Soares, J.B.P. and Hamielec, A.E. (1997) *Macromol. Theory Simul.*, **6**, 591–596.
47. Soares, J.B.P. (2004) *Macromol. Mater. Engng*, **289**, 70–87.
48. Beigzadeh, D., Soares, J.B.P. and Duever, T.A. (1999) *Macromol. Rapid Commun.*, **20**, 541–545.

49. Soares, J.B.P. (2002) *Macromol. Theory Simul.*, **11**, 184–198.
50. Nele, M., Soares, J.B.P. and Pinto, J.C. (2003) *Macromol. Theory Simul.*, **12**, 582–592.
51. Beigzadeh, D., Soares, J.B.P., Duever, T.A. and Hamielec, A.E. (1999) *Polym. React. Engng*, **7**, 195–205.
52. Simon, L.C. and Soares, J.B.P. (2002) *Macromol. Theory Simul.*, **11**, 222–232.
53. Simon, L.C. and Soares, J.B.P. (2005) *Ind. Engng Chem. Res.*, **44**, 2461–2468.
54. Ray, W.H. (1986) *Ber. Bunsenges. Phys. Chem.*, **90**, 947–955.
55. Nagel, E.J., Kirilov, V.A. and Ray, W.H. (1980) *Ind. Engng Chem., Prod. Res. Dev.*, **19**, 372–379.
56. Debling, J.A. and Ray, W.H. (1995) *Ind. Engng Chem. Res.*, **34**, 3466–3480.
57. Floyd, S., Choi, K.Y., Taylor, T.W. and Ray, W.H. (1986) *J. Appl. Polym. Sci.*, **32**, 2935–2960.
58. Floyd, S., Choi, K.Y., Taylor, T.W. and Ray, W.H. (1986) *J. Appl. Polym. Sci.*, **31**, 2231–2265.
59. Floyd, S., Hutchinson, R.A. and Ray, W.H. (1986) *J. Appl. Polym. Sci.*, **32**, 5451–5479.
60. Floyd, S., Heiskanen, T., Taylor, T.W., Mann, G.E. and Ray, W.H. (1987) *J. Appl. Polym. Sci.*, **33**, 1021–1065.
61. Hutchinson, R.A., Chen, C.M. and Ray, W.H. (1992) *J. Appl. Polym. Sci.*, **44**, 1389–1414.
62. Hutchinson, R.A. and Ray, W.H. (1990) *J. Appl. Polym. Sci.*, **41**, 51–81.
63. Hutchinson, R.A. and Ray, W.H. (1991) *J. Appl. Polym. Sci.*, **43**, 1271–1285.
64. Hutchinson, R.A. and Ray, W.H. (1991) *J. Appl. Polym. Sci.*, **43**, 1387–1390.
65. Hutchinson, R.A. and Ray, W.H. (1987) *J. Appl. Polym. Sci.*, **34**, 657–676.
66. McKenna, T.F. and Soares, J.B.P. (2001) *Chem. Engng Sci.*, **56**, 3931–3949.
67. Michaels, A.S. and Bixler, H.J. (1961) *J. Pol. Sci.*, **50**, 413–439.
68. McKenna, T.F., Cokljat, D. and Spitz, R. (1999) *AIChE J.*, **45**, 2392–2410.
69. Eriksson, E. and McKenna, T.F. (2004) *Ind. Engng Chem. Res.*, **43**, 7251–7260.
70. Soares, J.B.P. and Hamielec, A.E. (1995) *Pol. React. Engng*, **3**, 261–324.
71. Sinclair, K. (1995) *Third-Generation Polyolefin Technologies and their Capabilities*. SPE Polyolefins IX, Houston, USA.
72. Moore, E.P. (1996) *Polypropylene Handbook*. Hanser Publishers, New York.
73. Kirk-Othmer (1996) *Encyclopedia of Chemical Technology*, 4th edn, Vol. 17. Olefin Polymers.
74. Herrgard, G. (2001) *Advantages of Borstar PP Technology, Polypropylene*. Zurich, 11–13 September.
75. Lai, *et al.*, *US Patent* 5,272,236.
76. Jenkins, *et al.*, *US Patent* 4,543,399.
77. DeChellis, M. and Griffin, J., *US Patent* 5,352,749.
78. Kersting, M. (2001) *Novolen Technology, Polypropylene*. Zurich, 11–13 September.
79. Corbin, G. and Lee, K.F. (1993) *Simplified Gas Phase Polypropylene Process Technology*. DeWitt Petrochemical Review, Houston, Texas, USA, 23–25 March.
80. Galli, P. (1999) *MultiZone Circulating Reactor: The Novel Frontier of the Polyolefins Technology*. SPO 99, Houston, Texas, USA.
81. Galli, P. (2001) *Contribution of the Reactor Granule Technology (RGT) to the Expansion of the Polyolefin Product Property Envelope*. FlexPo 2001, Galveston, USA, 22–24 August.
82. Coleman-Kammula, S. (2001) *Expanding Polyolefins Technologies and Applications*. FlexPo 2001, Galveston, USA.
83. (1999) Does Borstar Shine? *ECN Chemscope*, May.
84. Moore, E.P. (1998) *The Rebirth of Polypropylene: Supported Catalysts*. Hanser Publishers, New York.
85. Kissel, W., Han, J. and Meyer, J. (1999) In H. Karian (ed.), *The Handbook of Polypropylene and Polypropylene Composites*. Marcel Dekker, New York.
86. Soares, J.B.P. and Hamielec, A.E. (1995) *Pol. React. Engng*, **4**, 153–191.
87. Soares, J.B.P. and Hamielec, A.E. (1995) *Macromol. Theory Simul.*, **4**, 1085–1104.

Chapter 3

Free-Radical Polymerization: Homogeneous Systems

Robin A. Hutchinson and Alexander Penlidis

3.1 Free-radical polymers: properties and applications

There are numerous molecular features that can have an impact on the final application properties of polymers. Usually, it is necessary to reach some type of compromise in the design and synthesis of a polymer for a given end-use, as varying the molecular structure/composition in order to achieve one desirable property target often causes a loss in some other property. For instance, physical properties of polymers usually improve with an increase in molecular weight (MW), whereas “processing ease” decreases. Hence, there is an optimum molecular weight that maximizes a property without heavily penalizing the processing operations. It is not always easy to decouple all the different factors that define the properties of a polymer chain in order to assess the quantitative impact on observed properties (and the relationships are not necessarily linear). In addition, the statistical nature of polymerization processes is such that it is not possible to synthesize homopolymers or copolymers/terpolymers with precisely equal chain lengths or chains that contain precisely the same number of different repeat units in each chain. Hence, several distributional molecular properties arise involving not only molar mass (molecular weight) but also composition, sequence length and branching.

Some high-tonnage polymers produced by free-radical polymerization (FRP) methods include: low-density polyethylene (LDPE), with applications in household goods, packaging, cable insulation, bottles, etc.; poly(vinyl chloride) (PVC), with applications in wire coating, building/construction products, films, etc.; styrene-butadiene rubber (SBR) and acrylonitrile-butadiene rubber (NBR), with applications in tires, shoe soles, elastomeric applications, etc.; acrylonitrile-butadiene-styrene (ABS), with applications in household appliances, machines, engineering plastics, etc.; poly(methyl methacrylate) (PMMA), with applications in glazing, automobile fittings, medical applications, etc.; polyacrylonitrile (PAN), with applications in fibers, food packaging, etc.; polyacrylamide, with applications in flocculating agents, thickeners, etc.; poly(vinyl acetate) (PVAc), with applications in paints, coatings, adhesives, etc.; polyfluoroethylenes, with electrical applications, “no-stick” kitchen items, etc.; polystyrenics, with a wide variety of applications in styrofoam items, egg cartons, coffee cups, cassette tape holders, appliance cases, foam packing materials,

toys, etc. Of course, the above applications (both for commodity and specialty products) expand considerably with copolymers/terpolymers of the above high-tonnage polymers.

Engineering methodology is directed toward defining appropriate reactor configurations to deal with the issues of manipulating highly exothermic processes and mixing of viscous fluids. This affects the way of changing reagent concentrations and operating condition profiles (with time) in order to adjust/control the different important molecular/structural distributions (molecular weight, copolymer composition, sequence length, branching, crosslink density, etc.). These quality considerations, coupled with productivity considerations, eventually dictate whether a production process will be carried out in bulk, solution, suspension, emulsion or dispersion. These various processes share common FRP mechanisms and kinetics, a major focus of this chapter. In addition, the reaction engineering aspects and modeling methodology pertinent to homogeneous FRP will be summarized.

3.2 FRP mechanisms and kinetics

Free-radical polymerization, like coordination polymerization discussed in Chapter 2, involves the sequential addition of vinyl monomer(s) to an active center. For FRP the active centers are free radicals. The increase in chain length is very rapid; an individual chain is initiated, grows to high MW and is terminated in a few seconds or less. After termination, the high-MW polymer chain does not react further (barring side reactions such as chain transfer to polymer or terminal/internal double bond polymerization) and is considered “dead”. Dead chains have a residence time of minutes or hours in the reactor, such that the final polymer product is an intimate mixture of chains formed under time and/or spatially varying conditions.

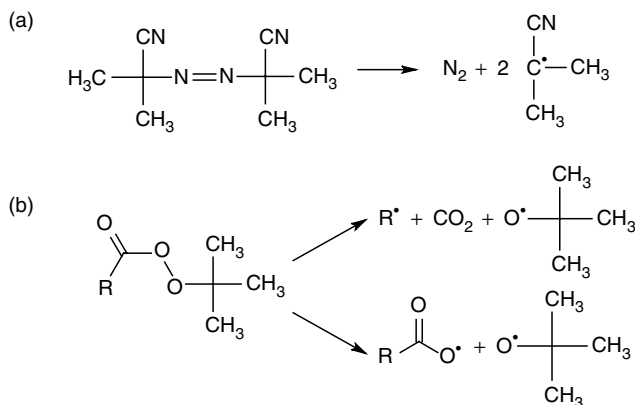
Polymerization rate and average polymer chain length are controlled by the relative rates of initiation, propagation, termination and chain transfer events in the system. Starting from these basic mechanisms, this section derives simple kinetic expressions for a single monomer system. Complicating (but industrially important) secondary reactions are then discussed, followed by extension of the kinetics to multi-monomer systems. Dispersed throughout are values for important FRP rate coefficients, and descriptions of how they are experimentally obtained. More extensive overviews of FRP kinetics and mechanisms are presented in references 1–3.

3.2.1 Homopolymerization

Many commercial polymers, including polystyrene, PMMA and LDPE, are synthesized via homogeneous FRP of a single monomer. Homopolymer properties are controlled by average chain length and chain-length distribution as well as, in some cases, structural characteristics such as branching level.

3.2.1.1 Basic mechanisms

The free radicals that initiate polymerization are usually generated by thermal or photochemical homolytic cleavage of covalent bonds. (A redox (reduction oxidation) process



Scheme 3.1 Decomposition of (a) AIBN and (b) *tert*-butyl peroxyester initiators. In (b), the decomposition pathway is influenced by the nature of the R substituent of the carbonyl group.

is often used to initiate chains in emulsion polymerization, as discussed in Chapter 6.) Commercial thermal initiators include azo and peroxy compounds. The driving force for the dissociation of azo initiators is the release of nitrogen and the formation of resonance stabilized tertiary radicals, as shown for 2,2'-azobisisobutyronitrile (AIBN) in Scheme 3.1. Many types of peroxides ($\text{R}-\text{O}-\text{O}-\text{R}'$) are also utilized as initiators, including diacyl peroxides, peroxydicarbonates, peroxyesters and dialkyl peroxides. Peroxide decomposition can yield both carbon- and oxygen-centered primary radicals that either add to monomer to form a new propagating chain, abstract hydrogen atoms from other molecules (including polymer) in the system, or recombine to form inactive compounds. The relative rates of these processes depend on the nature of the primary radicals formed upon initiator decomposition, as shown in Scheme 3.1 for *tert*-butyl peroxyester. The mechanistic pathway also influences the end-group structures found in the polymeric products, affecting final properties such as thermal stability. Further details on initiator decomposition kinetics and mechanistic pathways can be found in the excellent monograph by Moad and Solomon [1].

The exact nature of the decomposition pathway controls the efficiency of the primary radicals in initiating new polymer chains. When an initiator decomposes, the primary radicals are nearest neighbors surrounded by a "cage" of other molecules through which they must diffuse in order to escape each other before they recombine. Once one radical leaves the cage it is extremely unlikely that the pair will encounter each other again. In-cage reactions can lead to the reformation of the original initiator molecule, or to other species not capable of forming free radicals by dissociation. Thus, the fraction of primary radicals that initiate a new polymer chain is a complex function of the reaction system. The kinetic treatment is usually simplified by the introduction of fractional initiator efficiency (f), defined as

$$f = \frac{\text{initiation rate of propagating chains}}{n(\text{rate of initiator disappearance})} \quad (3.1)$$

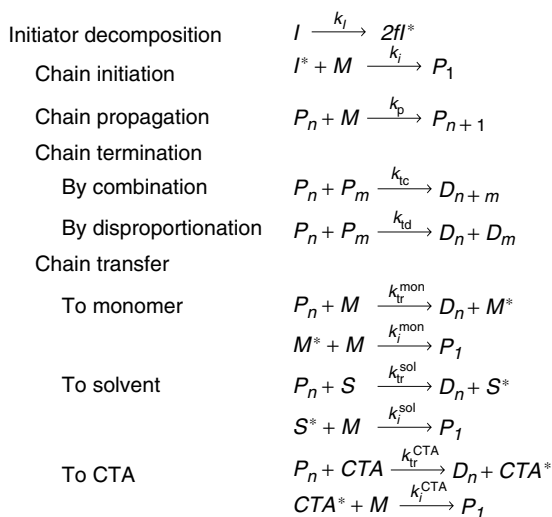
where n is the number of moles of primary radicals generated per mole of initiator (two for most common initiators). The initiator efficiency is normally in the range of 0.4–0.9,

with a low value indicating inefficient usage of the initiator and potentially a high formation rate of undesired byproducts.

The kinetic descriptions in this chapter are developed for unimolecular scission of an initiator to yield two radicals (Scheme 3.1), the most common means of generating radicals in industrial systems. Thermal initiation of monomers is an additional mechanism capable of forming primary radicals at higher temperatures, as discussed for styrene in Section 3.2.1.3. Photoinitiators that produce radicals by ultraviolet irradiation are often used to initiate crosslinking and curing reactions; these polymer modification techniques are not discussed in this chapter.

In addition to initiation, the basic set of FRP mechanisms includes propagation, termination, and transfer to monomer, solvent and/or transfer agent, as shown in Scheme 3.2. Subscript n denotes the number of monomeric repeat units in a growing polymer radical (P_n) or dead polymer chain (D_n). Each mechanism has an associated rate coefficient and kinetic rate law expression. The free-radical initiator (I) unimolecularly decomposes (with rate coefficient k_I) to form two primary radicals (I^*) with efficiency f . Chain initiation occurs when the primary radical adds to monomer M , and chain propagation continues via successive addition of monomer units to the radical center, with rate coefficient k_p . Bimolecular coupling of two growing chains results in the loss of two radicals from the system and the formation of either one (termination by combination, k_{tc}) or two (termination by disproportionation, k_{td}) dead polymer chains. Chain stoppage may also occur via a transfer mechanism, where the growing radical abstracts a weakly bonded atom (usually hydrogen) from monomer or other molecules (solvent S or chain-transfer agent CTA) in the system to generate a dead polymer chain as well as a new radical that initiates another polymer chain.

A key assumption implicit in the formulation of Scheme 3.2 is that the rates of propagation, transfer and termination reactions are independent of n , the length(s) of the radical(s)



Scheme 3.2 Basic free-radical homopolymerization mechanism.

involved. It is known that propagation and likely transfer reactions involving very short chains ($n = 1, 2, 3$) are faster by a factor of 10 than addition to long-chain radicals [4], but this effect diminishes rapidly with chain length and has a negligible effect on the overall kinetics of the system. Chain termination, the coupling of two polymeric radicals, is a very fast chemical reaction that is controlled by the rate at which the two radicals encounter each other in the system. The nature of this diffusion control makes termination the most complex reaction in the polymerization process since, as discussed in Section 3.2.3, the apparent rate coefficient can vary greatly with system conditions such as monomer conversion and solution viscosity. Although termination may also exhibit some chain-length dependence, most engineering treatments of FRP neglect this complex dependence. Further discussion of the individual mechanisms of Scheme 3.2 and their rate coefficients is deferred to later in this chapter.

For most FRP systems, the small radical species I^* , M^* , S^* and CTA^* are not consumed by side reactions and do not accumulate in the system, but are converted to polymeric radicals with close to 100% efficiency. Under this assumption, the set of rate laws formulated from Scheme 3.2 is given below:

$$\text{Initiator decomposition:} \quad R_I = k_I[I] \quad (3.2)$$

$$\text{Chain initiation:} \quad R_{\text{init}} = 2fk_I[I] \quad (3.3)$$

$$\text{Chain propagation:} \quad R_{\text{prop}} = k_p[M][P_{\text{tot}}] \quad (3.4)$$

$$\text{Chain termination:} \quad R_{\text{term}} = (k_{tc} + k_{td})[P_{\text{tot}}]^2 = k_t[P_{\text{tot}}]^2 \quad (3.5)$$

$$\text{Chain transfer:} \quad R_{\text{tr}} = (k_{\text{tr}}^{\text{mon}}[M] + k_{\text{tr}}^{\text{sol}}[S] + k_{\text{tr}}^{\text{CTA}}[\text{CTA}])[P_{\text{tot}}] \quad (3.6)$$

where $[P_{\text{tot}}]$ represents the concentration of all polymer radicals in the system:

$$[P_{\text{tot}}] = \sum_{n=1}^{\infty} [P_n] \quad (3.7)$$

The mode of termination – combination or disproportionation – affects polymer MW but not rate; thus termination is often expressed by the total rate coefficient k_t and δ , the fraction of the termination events that occur by disproportionation:

$$k_t = k_{tc} + k_{td}, \quad \delta = \frac{k_{td}}{k_{tc} + k_{td}} \quad (3.8)$$

It is also important to note that in some literature the right-hand side of the termination rate expression is written as $2k_t[P_{\text{tot}}]^2$; the convention shown in Equation 3.5 is the same as used in reference 5.

The total rate of polymer radical formation is given by $(R_{\text{init}} + R_{\text{tr}})$. However, the net formation of polymeric radicals is R_{init} , since transfer events both consume and create a polymeric radical species. With a continuous source of new radicals in the system, an equilibrium is achieved instantaneously between radical generation and consumption, such that $R_{\text{init}} = R_{\text{term}}$. This equilibrium, shown to be true for almost all FRP conditions [6], results from the fast dynamics of radical reactions compared to that of the overall polymerization system. Often referred to as *radical stationarity* or the *quasi-steady-state assumption* (QSSA), it leads to the well-known analytical expression

for total radical concentration:

$$[P_{\text{tot}}] = \left(\frac{R_{\text{init}}}{k_t} \right)^{0.5} = \left(\frac{2fk_I[I]}{k_t} \right)^{0.5} \quad (3.9)$$

It is also valid to assume that the consumption of monomer by chain-initiation or transfer events is negligible compared to that consumed by propagation. This long-chain hypothesis (LCH) is valid for any system in which high molecular weight polymer is being produced. Thus the rate of polymerization (disappearance of monomer) is equal to the rate of propagation ($R_p = R_{\text{prop}}$), with the rate of heat generation in the system proportional to the rate of this exothermic reaction.

Under these assumptions, the expressions for rate of polymerization (R_p), kinetic chain length (λ , the average number of monomer units on a living chain) and instantaneous number average degree of polymerization (DP_n^{inst} , the average number of monomer units on a dead polymer chain formed at an instant in time) are written as

$$R_p = k_p[M][P_{\text{tot}}] = k_p[M] \left(\frac{2fk_I[I]}{k_t} \right)^{0.5} \quad (3.10)$$

$$\lambda = \frac{R_p}{R_{\text{term}} + R_{\text{tr}}} = \frac{k_p[M]}{k_t[P_{\text{tot}}] + k_{\text{tr}}^{\text{mon}}[M] + k_{\text{tr}}^{\text{sol}}[S] + k_{\text{tr}}^{\text{CTA}}[\text{CTA}]} \quad (3.11)$$

$$DP_n^{\text{inst}} = \frac{k_p[M]}{(k_{\text{td}} + 0.5k_{\text{tc}})[P_{\text{tot}}] + k_{\text{tr}}^{\text{mon}}[M] + k_{\text{tr}}^{\text{sol}}[S] + k_{\text{tr}}^{\text{CTA}}[\text{CTA}]} \quad (3.12)$$

The difference between Equations 3.11 and 3.12 arises because termination by combination yields a single polymer chain such that the chain length of dead polymer formed (DP_n^{inst}) is greater than the chain length of polymer radicals (λ) in the system at the same instant. The instantaneous number-average molecular weight is calculated simply as $\bar{M}_n^{\text{inst}} = w_m DP_n^{\text{inst}}$, where w_m is the molecular weight of the monomeric repeat unit in the polymer chain.

Table 3.1 lists typical values of concentrations and rate coefficients for homogeneous FRP systems at low conversion. The tradeoff between achieving high polymerization rate (R_p) and producing high MW (high DP_n) polymer is understood by substituting these values into Equations 3.9–3.12. The maximum DP_n that can be achieved is calculated by setting $[P_{\text{tot}}]$ in Equation 3.12 to zero so that no chain termination occurs. The resulting value for DP_n is in the range of 10^4 – 10^6 , as calculated from $1/C_{\text{tr}}^{\text{mon}}$ for bulk FRP with no solvent or CTA present. Unfortunately, this theoretical limit is achieved at the expense of polymerization rate, since R_p goes to zero as $[P_{\text{tot}}]$ is decreased. Increased polymerization rate (increased $[P_{\text{tot}}]$) is achieved only by decreasing DP_n . To produce polymer with DP_n in the range of 10^2 – 10^4 (values typical for many commercial products) it is necessary to keep $[P_{\text{tot}}]$ in the range of 10^{-8} – 10^{-6} mol ℓ^{-1} , as typical k_t values are 10^6 – 10^8 ℓ mol $^{-1}$ s $^{-1}$. This requirement dictates the choice of initiator so that R_{init} (the product of k_I and $[I]$) is also in the range of 10^{-8} – 10^{-6} mol ℓ^{-1} s $^{-1}$, as shown in Table 3.1.

To achieve this balance between rate and MW, rates of polymerization (monomer consumption rates) at low conversion are of order 10^{-4} – 10^{-2} mol ℓ^{-1} s $^{-1}$ such that approximately 10^3 – 10^5 s is required to take a batch system to complete conversion. Faster rates can be achieved by increasing R_{init} , but at the expense of decreased polymer MW.

Table 3.1 Typical values of coefficients and concentrations in low conversion homogeneous FRP systems

Coefficient/concentration	Typical range
k_I (s^{-1})	10^{-6} – 10^{-4}
f	0.4–0.9
k_p ($\ell \text{ mol}^{-1} s^{-1}$)	10^2 – 10^4
k_t ($\ell \text{ mol}^{-1} s^{-1}$) ^a	10^6 – 10^8
$C_{tr}^{mon} = k_{tr}^{mon}/k_p$	10^{-6} – 10^{-4}
$C_{tr}^{sol} = k_{tr}^{sol}/k_p$	10^{-6} – 10^{-3}
$C_{tr}^{CTA} = k_{tr}^{CTA}/k_p$	10^{-3} – 10^0
$[I]$ (mol L^{-1})	10^{-4} – 10^{-2}
$[M]$ (mol L^{-1})	1–10
$[S]$ (mol L^{-1})	1–10
$[CTA]$ (mol L^{-1})	0–1
$[P_{tot}]$ (mol L^{-1})	10^{-8} – 10^{-6}

^a At low conversion.

Achievable values of R_p are also often limited by the heat removal capabilities of the reactor system, as the heat released by monomer addition is of the order 50–100 kJ mol⁻¹. While batch times are on the order of minutes or hours, individual polymer radicals live on average only a fraction of a second, as calculated by the expression $\lambda/(k_p[M])$. Thus, after the first few seconds of polymerization, the concentration of dead polymer chains is higher than that of polymeric radicals, and by the end of a typical polymerization the concentration of dead chains is orders of magnitude higher than $[P_{tot}]$. Final polymer MW and MWD (molecular weight distribution) are controlled by how the concentrations and kinetic coefficients in Equation 3.12 vary with polymer conversion.

The coupling of polymer MW and polymerization rate is further illustrated by rearranging Equation 3.12 to

$$\begin{aligned} \frac{1}{DP_n^{inst}} &= \frac{0.5k_{tc}[P_{tot}]}{k_p[M]} + \frac{k_{td}[P_{tot}]}{k_p[M]} + \frac{k_{tr}^{mon}}{k_p} + \frac{k_{tr}^{sol}[S]}{k_p[M]} + \frac{k_{tr}^{CTA}[CTA]}{k_p[M]} \\ &= \frac{0.5k_{tc}R_p}{k_p^2[M]^2} + \frac{k_{td}R_p}{k_p^2[M]^2} + \frac{k_{tr}^{mon}}{k_p} + \frac{k_{tr}^{sol}[S]}{k_p[M]} + \frac{k_{tr}^{CTA}[CTA]}{k_p[M]} \end{aligned} \quad (3.13)$$

R_p (Equation 3.10) and DP_n are both dependent on k_p^2/k_t , with DP_n also a function of mode of termination (disproportionation versus combination) and chain transfer. Transfer can occur to monomer, solvent or any other species in the system. In some cases, chain transfer agents are added deliberately to limit and control polymer DP_n . These agents are

generally chosen such that the rate of abstraction ($C_{tr}^{CTA} = k_{tr}^{CTA}/k_p = 10^{-3}-10^0$) is much higher than that which occurs with monomer or solvent and thus they can be added in trace quantities ($<1 \text{ mol } \ell^{-1}$). The use of transfer agents allows for independent manipulation and control of R_p and DP_n , but is only possible if the desired MW is less than that achieved for the corresponding CTA-free system.

One note of caution: the statements in this section are generalities for a typical FRP system. Rate coefficients vary with monomer, initiator and solvent choice (Section 3.2.1.2) as well as polymerization conditions, and the kinetic treatment is complicated by the occurrence of side reactions (Section 3.2.1.3) and the variation of k_t with conversion and other system conditions (Section 3.2.3). These factors necessitate the use of more powerful modeling techniques to quantitatively describe FRP systems (Sections 3.2.4 and 3.5). Nonetheless, Equations 3.9–3.13 are useful for qualitatively examining rate and MW trends for FRP systems.

3.2.1.2 Kinetic coefficients

Although R_p and DP_n can be measured experimentally, it is not possible to resolve the quantities into estimates of individual rate coefficients. Even the estimation of the ratio k_p^2/k_t from R_p requires independent knowledge of initiator characteristics f and k_I , and is based on the assumption that radicals are not being consumed or retarded by adventitious impurities in the system. These factors have led to considerable scatter in rate coefficients reported in the literature [5]. Yet individual values and how they vary with temperature are required for model development and an accurate representation of multi-monomer systems. The emergence of specialized experimental techniques has greatly improved this situation and is leading to an improved understanding of FRP kinetics. This section highlights some of these advances, as well as summarizes key FRP rate coefficients as expressed by the Arrhenius law:

$$k_i = A_i \exp(-(E_i + 1 \times 10^{-6} \Delta V_i P)/RT) \quad (3.14)$$

Activation energies (E_i) and volumes (ΔV_i) are reported with units of kJ mol^{-1} and $\ell \text{ mol}^{-1}$ respectively, with T in K and P in Pa ($R = 0.008314 \text{ kJ mol}^{-1} \text{ K}^{-1}$). All second-order rate coefficients are reported with units of $\ell \text{ mol}^{-1} \text{ s}^{-1}$.

Initiation. Decomposition of an initiator is characterized by a first-order rate coefficient ($k_I, \text{ s}^{-1}$) such that, for a constant volume isothermal batch system, Equation 3.2 may be integrated to yield:

$$[I] = [I]_0 \exp(-k_I t) \quad (3.15)$$

with $[I]_0$ the initial concentration at $t = 0$. The decomposition rate is often expressed in terms of the half-life of the initiator, defined as the time needed for the concentration to decrease to half of its initial value:

$$t_{1/2} = (\ln 2)/k_I \quad (3.16)$$

The requirements for an initiator depend on the system: a 10-h half-life might be selected for an academic study so that $[I]$ does not change significantly during the experiment,

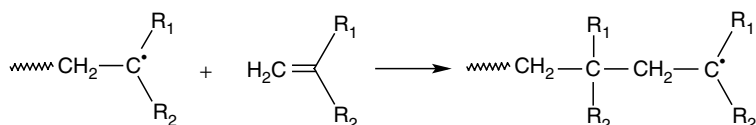
while an initiator used for high-pressure ethylene polymerization typically has a half-life on the order of a few seconds. Activation energies for thermal homolysis of peroxide and azo compounds are in the range of 100–150 kJ mol⁻¹, and thus decomposition rates are very temperature sensitive: the $t_{1/2}$ of benzoyl peroxide decreases from 13 h at 70°C to 0.4 h at 100°C. The dependence on pressure is much less, with ΔV_i in the range of 0 to -15×10^{-3} l mol⁻¹, but must still be considered for high-pressure LDPE systems. Special care must be taken in the handling and transport of thermal initiators, especially those with faster decomposition rates.

Values of k_t at a particular temperature and pressure are determined by measuring how $[I]$ changes with time using infrared spectroscopy or other techniques. The experimental difficulty increases as half-life shortens, as special care must be taken to eliminate transient non-isothermal effects. Decomposition kinetics are summarized for a wide range of initiators in reference 5 and in trade literature available from commercial suppliers. Of special note is the work of Buback *et al.* [7, 8] that systematically examines how E_i and ΔV_i vary with alkyl substituent for the peroxyester family, and how the substituent choice affects the decomposition pathway and initiator efficiency.

Propagation. Chain growth or propagation proceeds in a highly selective manner to yield a polymer chain consisting predominantly of head-to-tail linkages (Scheme 3.3). Addition must occur at a sufficiently high rate in comparison with competing transfer and termination events in order to form high MW polymer. A number of non-steady polymerization rate techniques have been introduced to measure k_p , many prone to significant error [5, and references therein]. The development of a method that couples pulsed-laser-induced polymerization (PLP) with size exclusion chromatographic (SEC) analysis of the resulting polymer [9] has greatly improved the reliability of k_p data. In this technique, a mixture of monomer and photoinitiator is illuminated by short laser pulses separated by a time of t_0 , typically 0.01–0.2 s. Each laser flash generates a burst of radicals in the reaction mixture, with a sufficient fraction of these radicals propagating up to a length DP_0 corresponding to a chain life-time equal to the time between pulses, t_0 . There is a high probability that the new radicals from the next flash will terminate these chains, such that a distinctive peak is formed in the polymer molecular weight distribution (MWD) corresponding to the chain length DP_0 , and directly proportional to the propagation rate coefficient according to the relation:

$$DP_0 = k_p[M]t_0 \quad (3.17)$$

Since radicals have a certain probability to survive the laser flash and to terminate at a later pulse, the relative concentration of polymer with chain lengths $2DP_0, 3DP_0, \dots$, is also increased. As a result, PLP produces a well-structured MWD with peaks at chain length of DP_0 and its multiples. PLP-SEC has proven to be a robust technique for determining k_p and



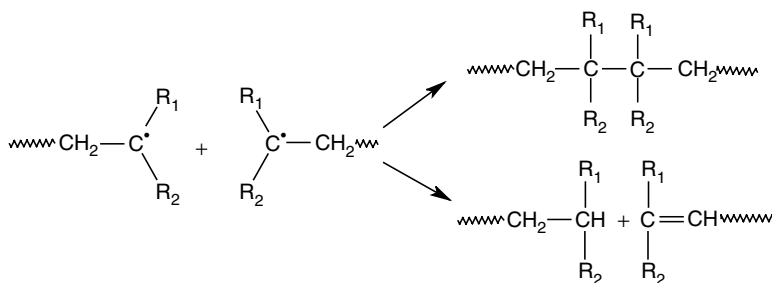
Scheme 3.3 Free-radical chain propagation.

its temperature and pressure dependencies, provided that adequate care is taken with SEC analysis. The technique has been applied to many monomers of industrial significance over a range of temperatures, with good agreement (generally within 15%) achieved between facilities around the world [10].

Termination. With independent measures of k_p available, k_t can be estimated from the lumped ratio of k_p^2/k_t . Specialized techniques involving PLP have also been developed to yield accurate estimates of the ratio k_p/k_t [10]. Termination rates in FRP are always diffusion controlled such that the apparent value of k_t depends on the conditions under which it has been measured, including the lengths of the radicals involved in the reaction (see Section 3.2.3). Nonetheless, the assumption of chain-length independence is usually made for modeling of commercial FRP systems, as the errors introduced are not large. The mode of termination affects the molecular architecture of the polymer formed and thus some of its properties. The instantaneous polymer polydispersity ($PDI = \overline{M}_w^{inst}/\overline{M}_n^{inst}$) is 1.5 if all chains are terminated by combination of two radicals, and 2 if chains are terminated by disproportionation or chain transfer. As shown in Scheme 3.4, termination by combination results in head-to-head linkages in the polymer chain, whereas disproportionation results in the formation of an unsaturated end group that may undergo further reaction. The relative importance of termination by disproportionation versus combination expressed by δ (Equation 3.8) is difficult to measure. The value depends largely on the structure of the monomer: δ is in the range of 0.5–0.8 for α -methylvinyl monomers such as methacrylates and 0.05–0.2 for styrene and acrylates [1].

Table 3.2 summarizes Arrhenius parameters of free-radical propagation and termination rate coefficients for ethylene, styrene (St), and vinyl acetate (VAc), as well as alkyl esters (methyl, butyl and dodecyl) of methacrylic and acrylic acids. An extensive review by Beuermann and Buback [10] contains data for additional monomers. The following observations are noted:

- There is a large variation in k_p values and activation energies between monomer families, but the values within a monomer family are very similar. All methacrylates exhibit a similar temperature (E_p of 21–23 kJ mol⁻¹) and pressure ($\Delta V_p \approx -16 \times 10^{-3}$ l mol⁻¹) dependence, and the k_p values for alkyl methacrylates at 50°C increase with increasing size of the alkyl ester group (methyl to dodecyl) by less than a factor of two. The alkyl acrylate family exhibits the same trends, although the activation energies (17–18 kJ mol⁻¹) and



Scheme 3.4 Free-radical chain termination by combination and disproportionation.

Table 3.2 Arrhenius k_p and k_t parameters for various monomers^a

Propagation	E_p (kJ mol ⁻¹)	ΔV_p (ℓ mol ⁻¹)	A_p (ℓ mol ⁻¹ s ⁻¹)	k_p at 50°C, 1 atm (ℓ mol ⁻¹ s ⁻¹)
Ethylene	34.3	-27.0×10^{-3}	1.88×10^7	54
Styrene	32.5	-12.1×10^{-3}	4.27×10^7	238
Methacrylate				
Methyl	22.4	-16.7×10^{-3}	2.67×10^6	648
Butyl	22.9	-16.5×10^{-3}	3.78×10^6	757
Dodecyl	21.0	-16.0×10^{-3}	2.50×10^6	995
Vinyl acetate	20.7	-10.7×10^{-3}	1.47×10^7	6625
Acrylate				
Methyl	17.7	-11.7×10^{-3}	1.66×10^7	22900
Butyl	17.4	<i>n.d.</i>	1.81×10^7	27900
Dodecyl	17.0	-11.7×10^{-3}	1.79×10^7	32000
Termination	E_t (kJ mol ⁻¹)	ΔV_t (ℓ mol ⁻¹)	A_t (ℓ mol ⁻¹ s ⁻¹)	k_t at 50°C, 1 atm (ℓ mol ⁻¹ s ⁻¹)
Ethylene	4.6	15.6×10^{-3}	1.6×10^9	2.9×10^8
Styrene	6.5	14×10^{-3}	2.2×10^9	2.0×10^8
Methacrylate				
Methyl	4.1	15×10^{-3}	4.3×10^8	9.4×10^7
Butyl	4.1 ^b	15×10^{-3b}	8.5×10^7	1.9×10^7
Dodecyl	4.1 ^b	15×10^{-3b}	2.8×10^7	6.2×10^6
Vinyl acetate	<i>n.d.</i>	<i>n.d.</i>	<i>n.d.</i>	$5\text{--}50 \times 10^{7c}$
Acrylate				
Methyl	6.7	20×10^{-3}	6.0×10^9	5.1×10^8
Butyl	4.0	16×10^{-3}	5.1×10^8	1.2×10^8
Dodecyl	1.7	21×10^{-3}	2.1×10^7	1.1×10^7

n.d. = not determined.

^a All values taken from reference 10 unless otherwise noted.

^b Assumed equal to MMA value.

^c From reference 5.

volumes ($\Delta V_p \approx -12 \times 10^{-3} \ell \text{ mol}^{-1}$) are lower than for methacrylates, and the values of k_p at 50°C are 30–40 times greater.

- The k_t data are for systems at low monomer conversion, the conditions at which most measurements are conducted. Significant scatter, as much as an order of magnitude, is found in the data contained in reference 5, as reflected in the vinyl acetate k_t data. The uncertainty arises from a number of measurement and interpretation factors [11]. The rest of the data are based on PLP studies, and have a higher level of

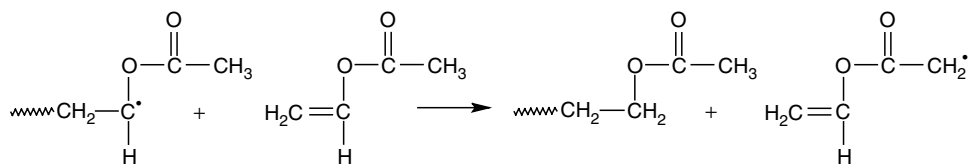
accuracy (within a factor of two); these are taken from the recent review by Beuermann and Buback [10], adjusted to conform to the convention for termination rate used in Equation 3.5.

- As termination is diffusion controlled, the magnitude of k_t is not a function of monomer family, but is related to chain mobility and flexibility. There is a large difference in magnitude between values for styrene, methyl methacrylate (MMA) and methyl acrylate (k_t of $1\text{--}5 \times 10^8 \text{ l mol}^{-1} \text{ s}^{-1}$) and values for dodecyl acrylate and dodecyl methacrylate ($\sim 0.5\text{--}1 \times 10^7 \text{ l mol}^{-1} \text{ s}^{-1}$). This has been attributed to differences in segmental diffusion rates and/or steric hindrance of the large ester side groups. The reported activation energies and volumes are consistent with the diffusion-controlled nature of the reaction.

The PLP–SEC method has been utilized to show that there is little to no solvent influence on propagation kinetics of most monomers; as a diffusion-controlled reaction, the same cannot be said for termination [10]. However, the propagation kinetics of water-soluble monomers such as methacrylic and acrylic acid are a strong function of concentration and degree of ionization in the aqueous phase [12].

Chain transfer. FRP chain transfer involves the transfer of the radical center from a polymeric radical to another molecule. Scheme 3.2 includes transfer to monomer, solvent and CTA; transfer can occur to any substance (initiator, dead polymer chains) present in the polymerization system, and always causes a reduction in λ and DP_n^{inst} . As well as reducing chain length, the fragments from transfer reactions (S^* , CTA^* and M^* in Scheme 3.2) are incorporated as end groups in the final polymer product. The rate and MW equations in Section 3.2.1.1 are derived assuming that these fragments quickly reinitiate new polymeric chains, taking about the same time as that required for a propagation step ($k_i^{\text{CTA}} \approx k_i^{\text{mon}} \approx k_i^{\text{sol}} \approx k_p$). This assumption is valid for transfer to most species, and is verified by examining whether addition of the transfer agent has an observable effect on polymerization rate. The species is classified as a retarding agent or inhibitor if low-conversion polymerization rate is significantly decreased, and Equations 3.9–3.13 no longer describe the kinetics of the system (see Section 3.2.1.3).

Transfer to monomer cannot be avoided, and the maximum upper limit of chain length that can be achieved in a polymerization is $1/C_{\text{tr}}^{\text{mon}}$ ($= k_p/k_{\text{tr}}^{\text{mon}}$), assuming the absence of all other transfer and termination events. For monomers that contain aliphatic hydrogens, such as vinyl acetate and (meth)acrylates, the transfer process involves H-atom abstraction to form an unsaturated new radical, as shown for vinyl acetate in Scheme 3.5. The polymer chain that grows from this radical contains an unsaturated end group that may undergo further reaction. Transfer to monomer rates are generally very low and are difficult to



Scheme 3.5 Free-radical chain transfer to monomer (vinyl acetate).

measure experimentally since the ratio with propagation rate (R_{tr}^{mon}/R_p) is independent of $[M]$. Typical C_{tr}^{mon} values are of the order of $1-50 \times 10^{-5}$ and generally increase with temperature, with $(E_{tr}^{mon} - E_p)$ in the range of $10-40 \text{ kJ mol}^{-1}$ [5].

The chain transfer ability of CTA (or solvent) can be studied by varying its concentration while holding all other conditions fixed. By stopping the reaction at very low conversion such that concentrations and diffusion-controlled k_t values (and thus R_p) are kept constant, Equation 3.13 can be rearranged as

$$\frac{1}{DP_n} = \frac{1}{(DP_n)_0} + \frac{k_{tr}^{CTA}[CTA]}{k_p[M]} \quad (3.18)$$

A plot of $1/DP_n$ against $[CTA]/[M]$ should yield a straight line with slope C_{tr}^{CTA} ($=k_{tr}^{CTA}/k_p$) and intercept $1/(DP_n)_0$, where $(DP_n)_0$ is the average chain length measured in the absence of transfer agent.

Most organic compounds have low transfer rates so that transfer becomes important only when the species are present in high concentration (i.e., when present as a solvent/diluent added to control viscosity and/or heat transfer). In other cases, a small amount of chain transfer agent (CTA) is added specifically to control and reduce the MW of the polymer. Thus values for C_{tr}^{sol} are generally $10^{-6}-10^{-4}$ while values for C_{tr}^{CTA} can be as high as $10^{-1}-10^1$, depending on the number and ease of abstraction of weakly bonded atoms (generally hydrogen or halogen) on the compound. Table 3.3 summarizes values at 50°C for a few typical solvents and CTA compounds with common monomers. For very active compounds it is necessary to account for the consumption of CTA during the course of the polymerization, since a changing ratio of $[CTA]/[M]$ will cause a corresponding drift in polymer MW. In such cases careful control of CTA addition to the system is required. If added at higher concentrations, telomerization (formation of low-MW species) will occur rather than polymerization. Abstraction reactions from organic solvents generally have higher activation energies than propagation, with $(E_{tr} - E_p)$ in the range of $20-50 \text{ kJ mol}^{-1}$ [13, 14]. References 5 and 1 provide a summary of available data for a wider range of monomer-CTA (solvent) pairings.

Table 3.3 Transfer constants (C_{tr}^{CTA} or C_{tr}^{sol}) for various solvent/transfer agent monomer pairings^a

	Styrene	Methyl methacrylate	Methyl acrylate	Vinyl acetate	Ethylene ^b
Benzene	2×10^{-6}	4×10^{-6}	2×10^{-5}	1×10^{-4}	9×10^{-4}
Toluene	1×10^{-5}	2×10^{-5}	1×10^{-4}	2×10^{-3}	1.3×10^{-2}
Ethyl acetate	5×10^{-4}	1×10^{-5}	6×10^{-5}	2×10^{-4}	5×10^{-3}
Triethylamine	5×10^{-4}	8×10^{-4}	4×10^{-2}	4×10^{-2}	1.8×10^{-2}
CCl_4	1×10^{-2}	2×10^{-4}	2×10^{-4}	0.8	1.0
1-Butanethiol	20	0.6	1.5	50	6.0

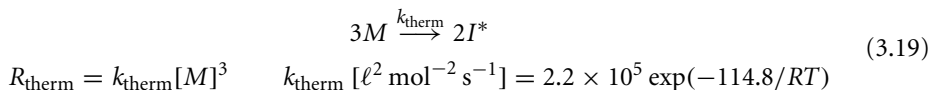
^a Representative values at 50°C [5]; there can be an order of magnitude range in literature data.

^b Ethylene values at 130°C and 1360 atm [14].

3.2.1.3 Additional mechanisms

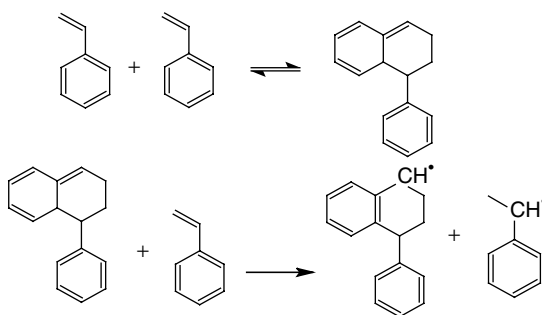
The basic polymerization mechanisms shown in Scheme 3.2 are common to every FRP system. Other mechanisms may also occur, depending on the choice of monomer and the process operating conditions. These additional mechanisms may play an important role in controlling polymerization rate and polymer structure under typical industrial operating conditions, and complicate the kinetic analysis of the system. They can be grouped into two general categories: mechanisms that primarily influence polymerization rate (thermal initiation, inhibition/retardation and depropagation) and those that mainly influence polymer structure and MW (long-chain branching (LCB), short-chain branching (SCB) and chain scission).

Thermal initiation. FRPs can be initiated by the monomer itself, or by reactions involving trace impurities in the system. Generally the rate of radical generation by these processes is negligible compared with R_{init} from an added initiator. Styrene, however, exhibits significant thermal polymerization at temperatures of 120°C or more; at even higher temperatures the rate of thermal initiation is sufficient to make an industrially viable process without added initiator [15]. Acrylates and methacrylates have also been reported to undergo thermal polymerization, but at a significantly slower rate than styrene. The thermal initiation of styrene involves the reversible formation of a dimeric species by a Diels–Alder reaction, followed by the subsequent hydrogen transfer to a third styrene molecule to form two radicals that can initiate polymerization (Scheme 3.6). This complex mechanism is well approximated by a third-order dependency on styrene concentration [16]:



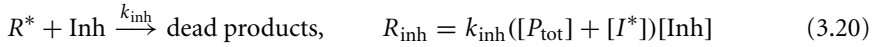
The pre-exponential factor in Equation 3.19 has been increased by a factor of 2–3 to fit 260–340°C data obtained in a more recent study [15].

Retardation and inhibition. As radical concentrations in FPR systems are usually 10^{-8} – 10^{-6} mol ℓ^{-1} , any compound present that consumes radicals may have a significant effect on rate. By decreasing the concentration of reactive radicals in the system,



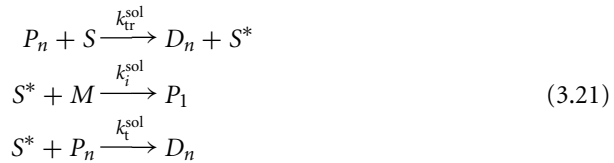
Scheme 3.6 Thermal initiation of styrene.

polymerization rate is completely stopped (*inhibition*) or slowed (*retardation*). Equation 3.20 represents the case in which radicals (R^* represents I^* or P_n) react with the inhibitor to form non-reactive products.



Phenolic inhibitors such as hydroquinone are added to monomers at ppm levels to rapidly and effectively scavenge any radicals that may form during monomer transport and storage so that polymerization does not occur ($R_{\text{inh}} \gg R_p$). Polymerization will still proceed if R_{inh} is of similar magnitude to R_p , but at a lower rate until all of the retarding species is consumed. The kinetic expressions presented in Section 3.2.1.1 cannot be applied to this situation, since termination is no longer the sole mechanism of radical consumption; application of radical stationarity yields $R_{\text{init}} = R_{\text{term}} + R_{\text{inh}}$. In many academic studies, monomer is distilled or passed over a column to remove inhibitor before polymerization. This purification is not done in industry if the concentration of inhibitor is much lower than the concentration of initiator added to the system, since the excess of initiator-generated radicals quickly consumes the inhibitor and the polymerization proceeds at normal rate after a small induction period.

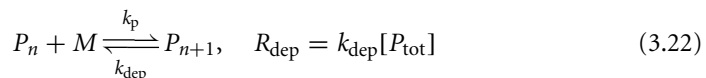
Another form of retardation occurs when a radical species formed from transfer (e.g., S^* in Scheme 3.2) reinitiates at a slow rate. The termination of S^* with other radicals in the system needs to be considered, as well as the slower reaction rate of S^* with monomer to form a polymer radical, as shown by the network of reactions.



Explicit balances must be written for S^* and the extra mechanisms must be included when deriving expressions for $[P_{\text{tot}}]$, R_p and DP_n . As solvent/transfer agent is generally not completely consumed, the retardation effect will last the duration of the polymerization. The degree of retardation depends on the value of k_i^{sol} , which can vary with monomer type; many carbon-centered radicals show lower reactivity toward vinyl esters (e.g., vinyl acetate) than (meth)acrylates [1].

Certain inhibitors (e.g., hydroquinone) require the presence of dissolved oxygen to be effective. In addition, oxygen can inhibit or retard vinyl polymerizations by the formation of less reactive peroxy radicals. Polymeric peroxides will be formed if subsequent monomer addition occurs; these chains will affect the thermal stability of the final polymer product. Good practice requires the removal of air by sparging with nitrogen or freeze–thaw cycles before a reaction is started and exclusion of air during polymerization by operating under an inert atmosphere or refluxing solvent.

Depropagation. Like any reaction, the addition of a radical to a double bond is reversible:



The relative importance of the reverse reaction is governed by the free energy change, $\Delta G_p = \Delta H_p - T\Delta S_p$, where ΔH_p is the enthalpy change and ΔS_p is

the entropy change upon propagation; polymerization can only occur spontaneously when ΔG_p is negative. Depropagation is negligible for many FRP systems at typical reaction temperatures, but increases in importance with increasing temperature and decreasing monomer concentration. The net polymerization rate is written as

$$R_p = R_{\text{prop}} - R_{\text{dep}} = (k_p[M] - k_{\text{dep}})[P_{\text{tot}}] = k_p^{\text{eff}}[M][P_{\text{tot}}] \quad (3.23)$$

$$k_p^{\text{eff}} = k_p - \frac{k_{\text{dep}}}{[M]}$$

$[M]_{\text{eq}}$ is defined as the monomer concentration for a particular temperature at which the effective propagation rate coefficient (k_p^{eff}) and polymerization rate become zero:

$$K_{\text{eq}} = \frac{k_p}{k_{\text{dep}}} = \exp\left(-\frac{\Delta G_p}{RT}\right) = \exp\left(-\frac{\Delta H_p}{RT} + \frac{\Delta S_p}{R}\right) = \frac{1}{[M]_{\text{eq}}} \quad (3.24)$$

This equation can also be rearranged to define the ceiling temperature T_c at which the polymerization rate becomes zero for a given monomer concentration:

$$T_c = \frac{\Delta H_p}{\Delta S_p + R \ln[M]} \quad (3.25)$$

The links between the thermodynamic and kinetic coefficients are

$$\Delta H_p = E_p - E_{\text{dep}} \quad \Delta S_p = R \ln\left(\frac{A_p}{A_{\text{dep}}}\right) + R \ln([M]) \quad (3.26)$$

Values of ΔH_p for common monomers are summarized in Table 3.4. ΔS_p , difficult to measure experimentally, is typically in the range of -100 to $-140 \text{ J mol}^{-1} \text{ K}^{-1}$. Table 3.4 also contains estimates of T_c calculated for $[M] = 1 \text{ mol } \ell^{-1}$. Depropagation of ethylene, vinyl acetate and acrylates does not occur under typical polymerization conditions. Styrene has a slightly lower ceiling temperature than acrylates and depropagation must be considered at the upper range of temperatures used commercially [15]. The addition of a methyl

Table 3.4 Depropagation behavior of common monomers

	$-\Delta H_p$ (kJ mol^{-1}) ^a	T_c ($^{\circ}\text{C}$) ^b
α -Methyl styrene	35	19
Styrene	73	335
Methyl methacrylate	56	194
Methyl acrylate	80	394
Vinyl acetate	88	460
Ethylene	102	577

^a From reference 5.

^b Calculated for $[M] = 1 \text{ mol } \ell^{-1}$, assuming ΔS_p of $-120 \text{ J mol}^{-1} \text{ K}^{-1}$.

group to a monomer greatly reduces T_c , as seen by comparing values for α -methyl styrene to styrene and methacrylates to acrylates. The depropagation behavior of many methacrylate monomers is similar [17], and must be considered above temperatures of 120°C, especially for systems with low monomer concentration [18].

Long-chain branching. None of the mechanisms presented so far change the basic linear architecture of the polymer chains. *Branched polymers*, those in which the repeat units are not necessarily linked in a linear array, can have significantly different physical properties than their linear counterparts, depending on the number and distribution of the branches along the polymer backbone as well as their length. Understanding the mechanisms by which these branches are formed is key to the manipulation and control of polymer structure. The common feature of LCB is the reactivation of a dead polymer chain via reaction with a polymeric radical. Scheme 3.7 illustrates two common mechanisms by which this reactivation occurs.

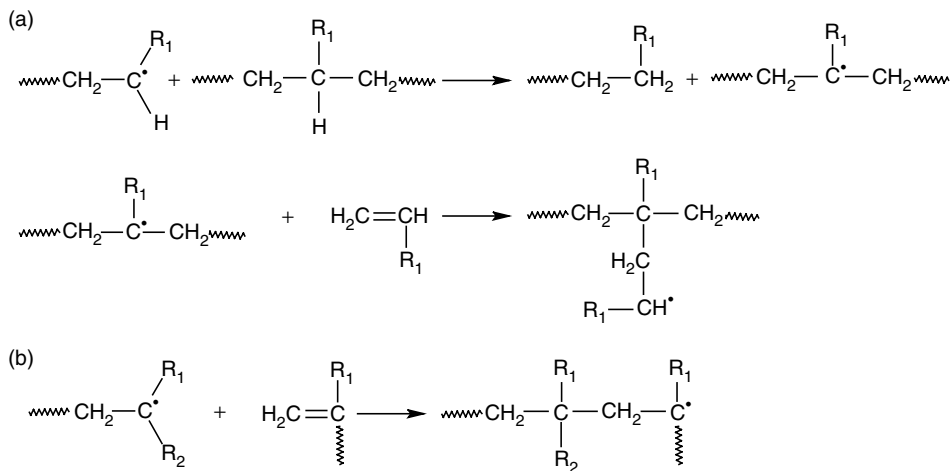
In Scheme 3.7(a), the transfer of a radical center from a polymeric radical to another polymer chain occurs via H-atom abstraction. Addition of monomer to the resulting mid-chain radical produces a polymer with a branch point, with the final length of the newly formed branch controlled by the kinetic chain length of the system. An additional subscript is added to track the number of LCBs formed.



where $[v_1]$ is the total concentration of polymerized monomer units in the system:

$$[v_1] = \sum_{n=1}^{\infty} \sum_{b=0}^{\infty} n [D_{n,b}] \quad (3.28)$$

The rate expression in Equation 3.27 is written assuming that all repeat units on all dead polymer chains have an equal probability of reaction; the reaction is proportional not with



Scheme 3.7 LCB formation by (a) intermolecular chain transfer to polymer and (b) addition to a terminally unsaturated polymer chain.

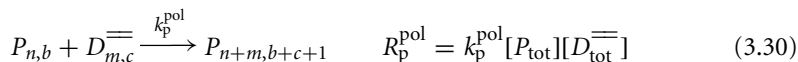
the number of *chains* in the system, but with the number of *repeat units* contained in the chains. This has two important consequences. First, the importance of transfer to polymer increases with monomer conversion (x), as can be seen by looking at the ratio of branching to monomer consumption:

$$\frac{R_{tr}^{pol}}{R_{pol}} = \frac{k_{tr}^{pol}[P_{tot}][v_1]}{k_p[P_{tot}][M]} = \frac{k_{tr}^{pol} x}{k_p(1-x)} \quad (3.29)$$

Thus polymerizations operating at high monomer conversion have significantly higher branching than low-conversion systems. Second, longer polymer chains – those with more repeat units – are more likely to participate in a branching reaction than short chains. Since the re-activated chains increase in length through subsequent propagation, this leads to a broadening of the molecular weight distribution reflected by an increase in the weight-average molecular weight (\overline{M}_w); even low levels of branching can increase polydispersity values to 5–15 compared to 2–3 for linear polymers. The mechanism does not change the number of monomer units that have been polymerized or the number of polymer chains in the system and thus has no effect on \overline{M}_n .

In addition to the dependence on conversion, the importance of the LCB mechanism is a function of the monomer system. Transfer to polymer usually occurs via abstraction of a methine hydrogen, but may also involve other easily abstracted H-atoms, such as the acetate methyl hydrogens on PVAc. The reaction can be important in systems with very reactive radicals such as ethylene, vinyl acetate and acrylate polymerizations, but seldom occurs in styrene and methacrylate systems. Transfer constants to polymer ($C_{tr}^{pol} = k_{tr}^{pol}/k_p$) are not as readily determined as other transfer constants because the process does not decrease DP_n . LCB levels are usually quite low, <2 per 1000 repeat units, making it difficult to employ nuclear magnetic resonance (NMR). Indirect methods are often used, leading to a significant scatter in reported C_{tr}^{pol} values [5]. Like other transfer events, the relative importance increases with temperature.

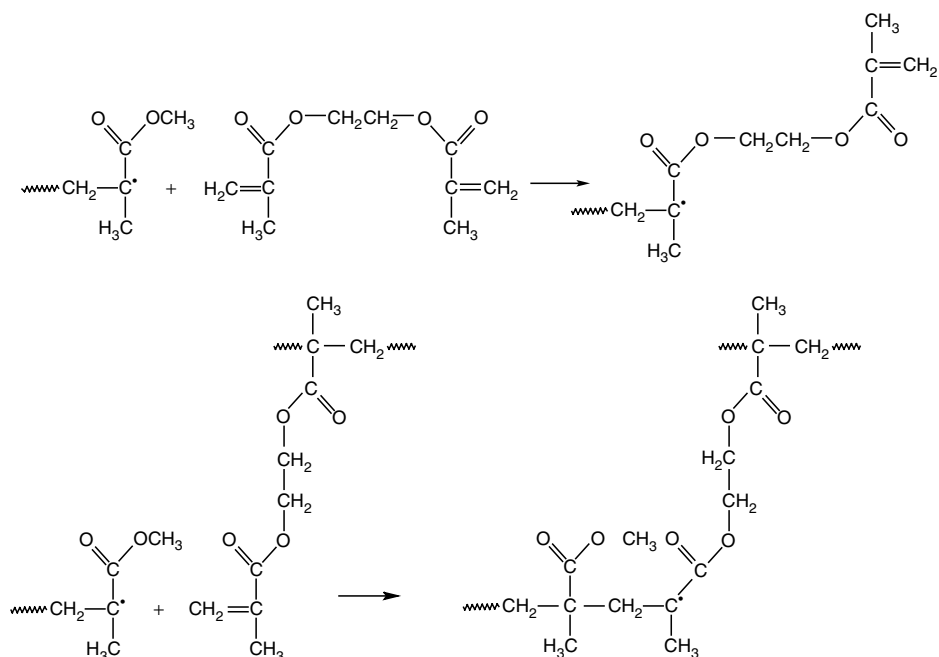
Termination by disproportionation, transfer to monomer and chain scission (discussed later in this section) create polymer chains with terminal unsaturation. These reactive chains, denoted by D^{\equiv} in Equation 3.30 and sometimes called macromonomers, can add to a growing radical to form a LCB as shown in Scheme 3.7(b) and captured by the mechanism:



This reaction is fundamentally different than Equation 3.27 in several aspects. It is an addition rather than a transfer reaction, so that the rate is dependent on the number of unsaturated chain-ends rather than the number of repeat units in the chains, with importance relative to propagation controlled by the ratio $[D_{tot}^{\equiv}]/[M]$:

$$\frac{R_p^{pol}}{R_p} = \frac{k_p^{pol}[P_{tot}][D_{tot}^{\equiv}]}{k_p[P_{tot}][M]} \quad (3.31)$$

Unlike transfer to polymer, the mechanism combines two polymer chains (and all of their repeat units) into one chain, affecting both DP_n and DP_w . Reaction with terminally unsaturated chains can be important in vinyl acetate [19] and higher temperature methacrylate [1]

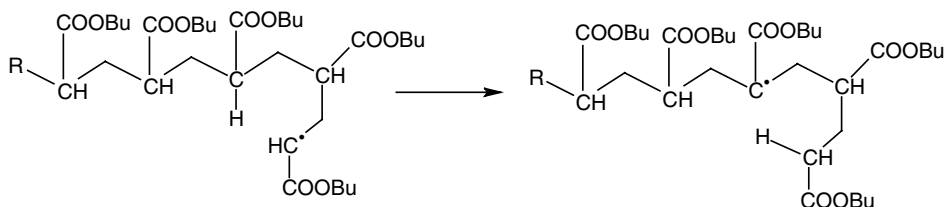


Scheme 3.8 Addition of EGDMA to a MMA radical. The pendant double bond is attacked by another polymer radical to form a crosslink branchpoint.

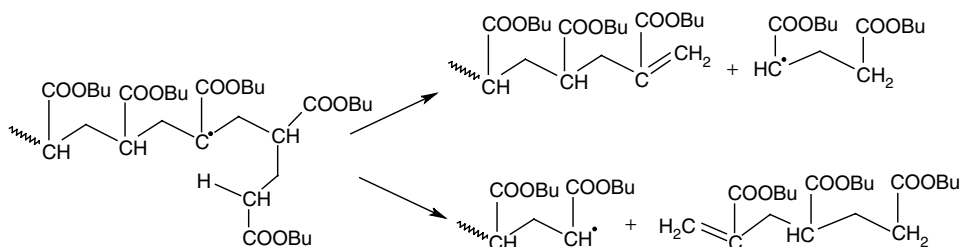
polymerizations. As well as creating branched structures, the reaction significantly broadens the polymer chain-length distribution.

A third way to introduce branching is through addition of a multifunctional monomer such as ethylene glycol dimethacrylate (EGDMA) or divinylbenzene to a polymerization system. Scheme 3.8 shows the reaction of EGDMA with a growing MMA chain. Reaction of the first EGDMA double bond incorporates the monomer in a polymer chain, with the second reactive site remaining as a pendant double bond. This double bond can subsequently react with another polymer radical to create a crosslink structure, called such since the branch point is tetrafunctional rather than trifunctional in nature. The addition of a small amount of difunctional monomer is a means to increase polymer MW without decreasing radical concentration. Addition of higher levels leads to an interconnected branched, or network, polymer.

Short-chain branching (SCB). Intramolecular H-atom abstraction, often called backbiting or, occurs via the formation of a six-membered ring, as shown in Scheme 3.9 for *n*-butyl acrylate (BA). Monomer addition to the resulting interior radical leaves a SCB consisting of two repeat units. This mechanism has long been known important for high-pressure LDPE production at 150–300°C, for which the number of SCBs is in the range of 20–50 per 1000 ethylene repeat units [14]. This level of SCB significantly decreases the polyethylene crystallinity and gives LDPE some of its unique properties; LDPE density is 0.92 g cm⁻³ compared to 0.98 g cm⁻³ for linear polyethylene. Multiple backbiting events lead to other SCB structures; in addition to the common butyl branch in LDPE, ethyl and 2-ethylhexyl



Scheme 3.9 Formation of a midchain radical by intramolecular chain transfer to polymer. Monomer addition to the new radical structure creates a SCB in the polymer.



Scheme 3.10 β -Scission of butyl acrylate midchain radical.

branches have been identified using ^{13}C NMR [14, 20]. The mechanism is also important in acrylate polymerizations, affecting rate as well as polymer structure due to the lower reactivity of the resulting midchain radical [21, 22]. The same type of backbiting reaction has also been shown to occur during styrene polymerization at high temperatures (260–340°C) [15].

Chain scission. The midchain radical structure formed by intra- or intermolecular transfer to polymer is less reactive than a chain-end radical. Under higher temperature conditions, the radical may undergo β -fragmentation (chain scission) as shown in Scheme 3.10 for BA. As well as lowering polymer MW, scission produces an unsaturated chain end that can react further (Scheme 3.7b). Scission is important for acrylate polymerizations at temperatures $>140^\circ\text{C}$ [18, 21], is a dominant mechanism in styrene polymerizations at 260–340°C [15], and also occurs during LDPE production [14]. Kinetic treatment is difficult, as scission is coupled with LCB and/or SCB formation.

3.2.2 Copolymerization

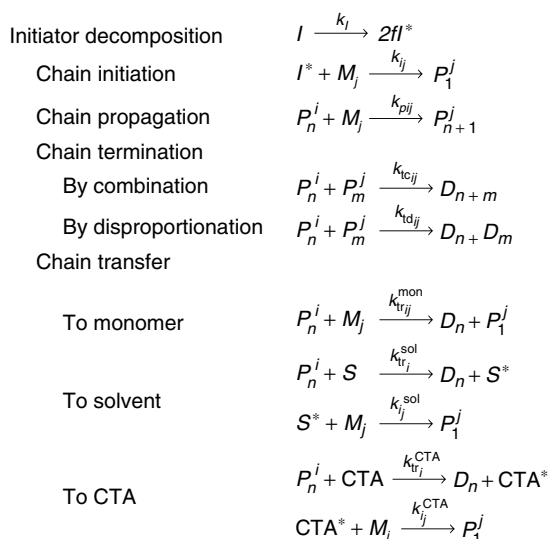
The presence of more than one type of monomer adds extra complexity to FRP kinetics. The monomers in the system form different radical structures, with the relative rates of chain growth dependent on the structure of both monomer and radical. It is these propagation mechanisms that control polymer *composition* (the relative amounts of each monomer unit incorporated into the copolymer) and *sequence distribution* (the way in which these monomer units are arranged along the chain backbone), while the effect of radical structure on termination and transfer rates controls copolymer molecular weight. Reactivity of

a monomer in copolymerization cannot necessarily be predicted from its behavior in homopolymerization. Vinyl acetate polymerizes ten times more quickly than MMA (Table 3.2), yet the product is almost pure PMMA if the two monomers are copolymerized together in a 50/50 mixture. α -Methyl styrene cannot be homopolymerized to form high-MW polymer due to its low ceiling temperature (Table 3.4), yet is readily incorporated into copolymer at elevated temperatures. These, and other similar observations, can be understood by considering copolymerization mechanisms and kinetics.

3.2.2.1 Basic mechanisms

FRP leads to the formation of statistical copolymers, where the arrangement of monomers within the chains is dictated purely by kinetic factors. The most common treatment of free-radical copolymerization kinetics assumes that radical reactivity depends only on the identity of the terminal unit on the growing chain. The assumption provides a good representation of polymer composition and sequence distribution, but not necessarily polymerization rate, as discussed later. This *terminal model* is widely used to model free-radical copolymerization according to the set of mechanisms in Scheme 3.11.

Dead polymer (D_n) and radical- i copolymer chains (P_n^i) are formed from the mixture of monomers (M_j) in the system; the superscript i indicates that monomer- i is the terminal unit controlling the reactivity of the growing chain. Chain growth occurs by addition of M_j to radical- i , with the propagation rate coefficient $k_{p_{ij}}$ dependent on both radical and monomer type. The rate coefficients for transfer and termination reactions are also dependent on the nature of the radical center, as indicated by subscripts. However, since radical-radical termination is a diffusion-controlled reaction, the rate coefficient can usually be assumed to be independent of radical type, such that $\bar{k}_t = k_{t_{ij}}$ for all i and j . Most of the kinetic coefficients in Scheme 3.11 are binary parameters so that the polymerization behavior of



Scheme 3.11 Basic free-radical copolymerization mechanism, assuming terminal radical kinetics.

three or more monomers can be predicted from knowledge of the corresponding binary copolymerizations.

For a two-monomer system, the polymerization rates of the two monomers, assuming long-chain hypothesis, are written as

$$\begin{aligned} R_{p1} &= k_{p11}[P_{\text{tot}}^1][M_1] + k_{p21}[P_{\text{tot}}^2][M_1] \\ R_{p2} &= k_{p12}[P_{\text{tot}}^1][M_2] + k_{p22}[P_{\text{tot}}^2][M_2] \end{aligned} \quad (3.32)$$

where $[P_{\text{tot}}^i]$ ($= \sum_{n=1}^{\infty} [P_n^i]$) represents the concentration of all polymer radicals of type- i in the system. The instantaneous composition ($F_{p_i}^{\text{inst}}$) of the polymer being formed is controlled by the relative polymerization rates:

$$\frac{F_{p1}^{\text{inst}}}{(1 - F_{p1}^{\text{inst}})} = \frac{R_{p1}}{R_{p2}} = \frac{k_{p11}[P_{\text{tot}}^1][M_1] + k_{p21}[P_{\text{tot}}^2][M_1]}{k_{p12}[P_{\text{tot}}^1][M_2] + k_{p22}[P_{\text{tot}}^2][M_2]} \quad F_{p2}^{\text{inst}} = 1 - F_{p1}^{\text{inst}} \quad (3.33)$$

Application of the QSSA yields the ratio of the radical types:

$$\frac{[P_{\text{tot}}^1]}{[P_{\text{tot}}^2]} = \frac{k_{p21}[M_1]}{k_{p12}[M_2]} \quad (3.34)$$

and substitution and rearrangement leads to the well-known Mayo–Lewis equation that describes copolymer composition:

$$F_{p1}^{\text{inst}} = \frac{r_1 f_1^2 + f_1 f_2}{r_1 f_1^2 + 2f_1 f_2 + r_2 f_2^2} \quad (3.35)$$

where f_i is the mole fraction of monomer- i (e.g., $f_1 = [M_1]/([M_1] + [M_2])$), and monomer reactivity ratios r_1 and r_2 are defined as k_{p11}/k_{p12} and k_{p22}/k_{p21} .

Reactivity ratios also control copolymer sequence distribution along the chain. The probability P_{11} that an M_1 unit follows another M_1 unit in the copolymer chain is given by:

$$P_{11} = \frac{k_{p11}[P_{\text{tot}}^1][M_1]}{k_{p11}[P_{\text{tot}}^1][M_1] + k_{p12}[P_{\text{tot}}^1][M_2]} = \frac{r_1 f_1}{r_1 f_1 + f_2} \quad (3.36)$$

and the probability P_{12} that an M_2 unit follows an M_1 is

$$P_{12} = 1 - P_{11} = \frac{f_2}{r_1 f_1 + f_2} \quad (3.37)$$

Similar expressions can be derived for addition to radical-2:

$$P_{22} = \frac{k_{p22}[P_{\text{tot}}^2][M_2]}{k_{p22}[P_{\text{tot}}^2][M_2] + k_{p21}[P_{\text{tot}}^2][M_1]} = \frac{r_2 f_2}{r_2 f_2 + f_1} \quad (3.38)$$

$$P_{21} = 1 - P_{22} = \frac{f_1}{r_2 f_2 + f_1} \quad (3.39)$$

These probabilities are used to calculate $N_1(n)$, the fraction of all M_1 sequences that are exactly n units long, calculated as the probability of having $(n - 1)$ $M_1 M_1$ linkages followed by an $M_1 M_2$ linkage:

$$N_1(n) = P_{11}^{n-1} P_{12} \quad (3.40)$$

Thus the fraction of M_1 sequences that consists of an isolated M_1 unit is P_{12} , the fraction that consists of isolated M_1M_1 diads is $P_{11}P_{12}$, the fraction of triads is $P_{11}^2P_{12}$, etc. The number-average length of M_1 sequences (\bar{N}_1) is given by:

$$\bar{N}_1 = \frac{1}{1 - P_{11}} = \frac{1}{P_{12}}, \quad \bar{N}_2 = \frac{1}{1 - P_{22}} = \frac{1}{P_{21}} \quad (3.41)$$

For long-chain polymers, the ratio of M_1 to M_2 units in the chain must equal the ratio of the respective average sequence lengths:

$$\frac{F_{p1}^{\text{inst}}}{F_{p2}^{\text{inst}}} = \frac{\bar{N}_1}{\bar{N}_2} \quad (3.42)$$

Substitution and rearrangement of this equation yields the polymer composition equation 3.35. Thus it is possible to estimate reactivity ratios for binary copolymers from sequence distributions measured by NMR.

While copolymer composition and sequence distribution are functions only of the reactivity ratios, the same is not true for polymerization rate. The overall rate of monomer consumption is given by:

$$\begin{aligned} R_p &= k_{p11}[P_{\text{tot}}^1][M_1] + k_{p21}[P_{\text{tot}}^2][M_1] + k_{p12}[P_{\text{tot}}^1][M_2] + k_{p22}[P_{\text{tot}}^2][M_2] \\ &= \left(\sum_{i=1}^2 \sum_{j=1}^2 k_{p_{ij}} P_{ifj} \right) [P_{\text{tot}}][M_{\text{tot}}] \end{aligned} \quad (3.43)$$

where $[M_{\text{tot}}]$ indicates the total monomer concentration ($[M_1] + [M_2]$) and the fraction of radical- i in the system, $P_i = [P_{\text{tot}}^i]/([P_{\text{tot}}^1] + [P_{\text{tot}}^2])$, can be calculated from Equation 3.34. The form of Equation 3.43 is analogous to the homopolymerization rate expression Equation 3.10, with a copolymer-averaged rate coefficient for propagation (generalized for a system with N_{mon} monomers) defined as

$$\bar{k}_p = \sum_{i=1}^{N_{\text{mon}}} \sum_{j=1}^{N_{\text{mon}}} k_{p_{ij}} P_{ifj} \quad (3.44)$$

For a two-monomer system, application of the QSSA and simplification leads to

$$\bar{k}_p = \frac{r_1 f_1^2 + 2f_1 f_2 + r_2 f_2^2}{(r_1 f_1 / k_{p11}) + (r_2 f_2 / k_{p22})} \quad (3.45)$$

Thus polymerization rate in the copolymer system can be analyzed as was done for homopolymerization (Section 3.2.1.1), with \bar{k}_p a function of monomer composition.

3.2.2.2 Kinetic coefficients

There is a large body of published monomer reactivity ratios summarized in reference 5. Values are typically determined from a series of low conversion experiments in which copolymer composition F_{p1} is measured (e.g., by NMR) as a function of monomer composition, and r_1 and r_2 estimated from fitting the data set according to Equation 3.35. The estimation is best accomplished by non-linear techniques, and a statistical analysis

can also provide a guide to the optimal monomer compositions at which experimentation should be performed to improve the estimates [23, 24]. The scatter in r values is much less than found in k_p and k_t data, but care must be exercised still when extracting values from reference 5 and similar compilations. Error can occur from the fitting methodology, if the system does not remain homogeneous, or if polymer conversion is high enough such that f_1 deviates significantly from the zero-conversion value (in which case an integrated form of Equation 3.35 must be used [25]). There are also a few systems for which Equation 3.35 does not provide a good description of copolymer composition; these usually include a polar monomer with strong electron-withdrawing or electron-donating properties [1, 26]. The majority of systems, however, are well-behaved and well-represented by the terminal model.

Table 3.5 summarizes typical reactivity ratio values for binary systems including styrene, alkyl methacrylate, alkyl acrylate and vinyl acetate. Values for the (meth)acrylates have negligible differences within the series of alkyl esters (e.g., methyl, butyl, dodecyl) [27]. Figure 3.1

Table 3.5 Representative values for monomer reactivity ratios at 50°C, taken from reference 5

Radical	Monomer			
	Styrene	Alkyl methacrylate	Alkyl acrylate	Vinyl acetate
Styrene	1	0.6	0.8	40
Alkyl methacrylate	0.4	1	2.2	20
Alkyl acrylate	0.2	0.4	1	6
Vinyl acetate	0.02	0.03	0.03	1

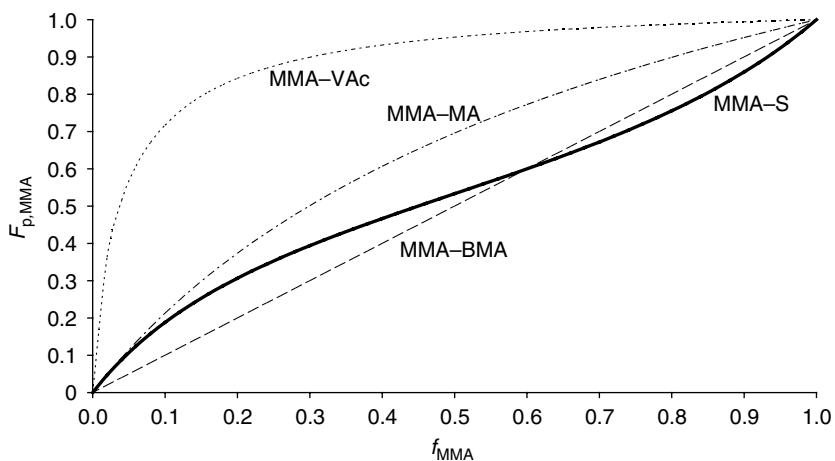


Figure 3.1 Relationship between monomer composition f_{MMA} and corresponding instantaneous polymer composition $F_{\text{p,MMA}}^{\text{inst}}$ for various monomers copolymerized with MMA. (S_s = styrene, MA = methyl acrylate, VAc = vinyl acetate, BMA = butyl methacrylate.)

plots the relationship between polymer and monomer composition for copolymerization with MMA (monomer-1), calculated according to Equation 3.35. For the case where $r_1 = r_2 = 1.0$ (MMA with BMA), the monomers have equal reactivity when adding to either radical, and thus are incorporated into polymer at the same ratio as they are in the monomer phase ($F_{p1} = f_1$). With $r_1 > 1$ and $r_2 < 1$, the copolymer is always richer in monomer-1 (MMA) than found in the monomer phase, so that monomer-1 will become depleted in a batch polymerization. The more the reactivity ratios deviate from unity, the greater the deviation between polymer and monomer composition, as seen by comparing the curves for MMA–MA and MMA–VAc. Common systems that exhibit this behavior include methacrylate-acrylate polymerizations, and styrene, methacrylates or acrylates polymerized with vinyl acetate or ethylene. If both r_1 and r_2 are less than unity (MMA–St in Figure 3.1; also styrene-acrylate systems), cross-propagation is favored over homopropagation and the copolymer tends toward an alternating structure. The system has an azeotropic composition at which copolymer composition is exactly equal to monomer composition.

Reactivity ratios exhibit a weak temperature dependence that is often difficult to measure. With increasing temperature, the ratios tend to approach unity as demonstrated for styrene-butyl acrylate [28], butyl acrylate-methyl methacrylate [29], and ethylene copolymer systems [30, 31]. The temperature dependencies of the latter values agree well with activation energies reported for addition of monomers to small radicals [32].

While copolymer composition is well-described by the terminal model, the copolymer-averaged propagation rate coefficient (\bar{k}_p , Equation 3.45) for many common systems [10, 26, 27] is not. The measured \bar{k}_p values can be higher or lower than the terminal model predictions, with the deviation substantial in some cases. The “implicit penultimate unit effect” model, which accounts for the influence of the penultimate monomer-unit of the growing polymer radical on the propagation kinetics [26, 27], provides a good representation of this behavior:

$$\begin{aligned}\bar{k}_p &= \frac{r_1 f_1^2 + 2f_1 f_2 + r_2 f_2^2}{(r_1 f_1 / \bar{k}_{p11}) + (r_2 f_2 / \bar{k}_{p22})} \\ \bar{k}_{p11} &= \frac{k_{p111} [r_1 f_1 + f_2]}{r_1 f_1 + [f_2 / s_1]} \\ \bar{k}_{p22} &= \frac{k_{p222} [r_2 f_2 + f_1]}{r_2 f_2 + [f_1 / s_2]}\end{aligned}\quad (3.46)$$

The extra parameters s_1 and s_2 , called radical reactivity ratios, capture the effect of the penultimate unit on the addition rate of monomer:

$$s_1 = \frac{k_{p211}}{k_{p111}}, \quad s_2 = \frac{k_{p122}}{k_{p222}} \quad (3.47)$$

A value of s_i greater than unity indicates that a comonomer unit in the penultimate position increases the addition rate of monomer- i to radical- i compared to the homopolymerization case.

The kinetics of diffusion-controlled termination in copolymerization is difficult to study. The original interpretation of low-conversion rate data was based on a chemically controlled model utilizing a cross-termination factor:

$$\bar{k}_t = \sum_{i=1}^{N_{\text{mon}}} \sum_{j=1}^{N_{\text{mon}}} k_{t_{ij}} P_i P_j, \quad \Phi = \frac{k_{t_{12}}}{k_{t_{11}} k_{t_{22}}} \quad (3.48)$$

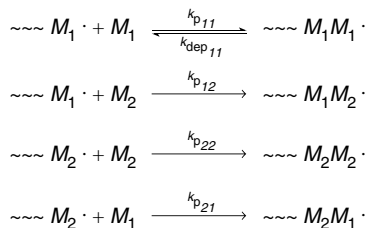
Assuming terminal propagation kinetics, the best fit for Φ was found to be much greater than unity such that \bar{k}_t was greater than either homo-termination value, a non-sensical result as \bar{k}_t is diffusion-controlled. When the deviation of propagation kinetics from the terminal model is taken into account, however, the estimates for \bar{k}_t become well-behaved and bounded by the homo-termination values [26]. Various penultimate models that account for the influence of polymer composition on segmental diffusion have been proposed to fit low-conversion \bar{k}_t data. Equation 3.49 emphasizes the role of the whole chain composition [26], while other formulations use both the terminal and penultimate units to represent the conformational characteristics of the last portion of the polymer chain [33, 34].

$$\bar{k}_t^{-1} = \sum_{i=1}^{N_{\text{mon}}} F_{p_i}^{\text{inst}} k_{t_{ii}}^{-1} \quad (3.49)$$

While the terminal model and reactivity ratios provide a good description of copolymer composition, additional parameters are required to represent \bar{k}_t and \bar{k}_p . These mechanistic complexities are often not considered when developing FRP models for polymer reaction engineering applications. It is expected that this situation will change as more data become available.

3.2.2.3 Additional mechanisms

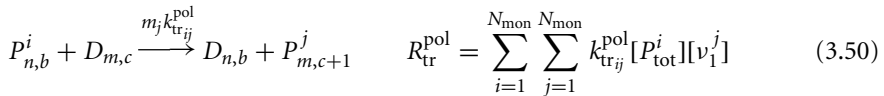
The secondary mechanisms discussed in Section 3.2.1.3 also occur in systems with multiple monomers. The complexity increases, as depropagation, chain transfer to polymer and chain scission are influenced by the penultimate unit on the polymer radical, as well as the identity of the monomer and terminal radical involved in the reaction. As an example, consider a copolymerization in which one of the two monomers undergoes depropagation, shown in Scheme 3.12. Depropagation of radical-1 is a competitive process with addition of



Scheme 3.12 Depropagation in copolymerization for the case where M_2 does not depropagate and M_1 depropagates only when an M_1 -unit is in the penultimate position.

monomer-2, such that monomer-1 units at the radical end become irreversibly trapped in the growing chain as soon as monomer-2 adds. Furthermore, depropagation of monomer-1 will only occur if an M_1 -unit is also in the penultimate position; depropagation to the less stable M_2 -radical can be assumed to be unlikely ($k_{\text{dep}21} \approx 0$). Thus MMA can be successfully copolymerized with ethylene at 290°C [32], and α -methyl styrene with various comonomers at temperatures well above its ceiling temperature [35, 36]. Lowry [37] first derived the composition expressions for the situation where only one monomer depropagates, and general expressions have been developed for the situation where all four of the propagation reactions are reversible [35, 38]. The complexity further increases when depropagation is combined with penultimate propagation kinetics [39]. Understanding these complexities is a focus of current research, as commercial copolymers are produced at conditions at which these mechanisms are of importance [18, 40].

Complexities also emerge when chain transfer to polymer mechanisms are examined. The rate of chain transfer to polymer is dependent on both the reactivity of the radical and the abstractability of the hydrogen atom on the repeat unit in the polymer chain. For the case of intermolecular chain transfer (LCB), this is represented by:



where $[v_1^j]$ represents the total concentration of polymerized monomer- j units in the system and m_j represents the number of monomer- j units on a particular chain of length m .

$$[v_1^j] = \sum_{m=1}^{\infty} \sum_{b=0}^{\infty} m_j [D_{m,b}] \quad m = \sum_{j=1}^{N_{\text{mon}}} m_j \quad (3.51)$$

Active radicals (ethylene, acrylate, vinyl acetate) are more likely to abstract from a polymer chain than styrenic or methacrylate radicals, and acrylate and vinyl acetate monomer units on a chain are more likely to have an H-atom abstracted. Thus it is not uncommon for the overall transfer rate $R_{\text{tr}}^{\text{pol}}$ to decrease rapidly with increasing content of the less-reactive monomer. Similar issues must be examined when looking at cross transfer rates for chain transfer to monomer reactions [41].

The complexity of intramolecular transfer (SCB) mechanisms in ethylene/acrylate [42], styrene/acrylate [43] and methacrylate/acrylate [40] copolymer systems has also been studied, as has the combination of scission and copolymerization [40, 44]. All possible reaction pathways must be carefully considered, building from an understanding of the secondary mechanisms gained from homopolymerization studies.

3.2.3 Diffusion-controlled reactions

Termination is a fast chemical reaction controlled by the rates at which the two radical ends encounter each other. The apparent rate coefficient is affected not only by pressure and temperature, but also by system viscosity (a function of solvent choice, polymer concentration and MW) and the lengths of the two terminating radicals. This complex behavior,

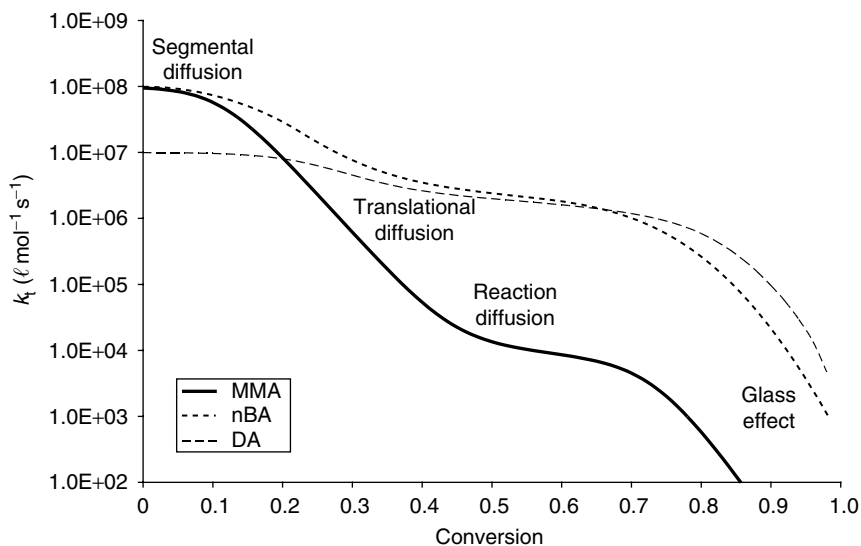


Figure 3.2 Typical variation of k_t with conversion for bulk polymerization of MMA, butyl acrylate (BA) and dodecyl acrylate (DA). The different regions of diffusion control are discussed in the text. (Based upon data from reference 10.)

as well as experimental difficulties in measuring k_t , has led to a large scatter in reported values [5]. Through the application of pulsed-laser experimental techniques [10] and a critical examination of available data [11], the situation is starting to improve.

For most commercial FRPs, the errors involved by neglecting the dependence of k_t on radical chain-length are not large. The change of k_t with conversion (increasing viscosity), however, cannot be neglected. Figure 3.2 shows the 3–4 orders of magnitude decrease typically observed. The shape of the curve reflects the interplay of diffusional mechanisms involved in the reaction process. At low conversion, the system viscosity is low, and the two chains diffuse together quickly. The rate of reaction is controlled by *segmental diffusion*: the internal reorganization of the chain that is required to bring the reactive ends together. The value of k_t in this region is of the order of $10^8 \ell \text{ mol}^{-1} \text{ s}^{-1}$ for many common monomers (Table 3.2), with the value remaining relatively constant up to 10–20% conversion. Solvent choice can have a significant effect on the value [10]. Lower values of $10^7 \ell \text{ mol}^{-1} \text{ s}^{-1}$ for dodecyl (meth)acrylate have been attributed to shielding of the radicals by the long-chain dodecyl ester groups; for these monomers k_t remains relatively constant up to 60% conversion [10, 34]. Even lower k_t values are measured for termination during polymerization of sterically hindered monomers such as the itaconates [45] and acrylate trimer species [46]. As mentioned previously, copolymerization \bar{k}_t values depend on how the chain flexibility varies with copolymer composition in this conversion regime.

As polymer concentration in the system increases with conversion, the viscosity of the system rapidly increases such that the rate at which two polymer chains encounter each other is slower than the rate of segmental reorientation, and the rate of reaction becomes controlled by how quickly the two chains find each other among the tangle of

dead polymer chains in the system. This *center-of-mass* or *translational diffusion* mechanism is complex, affected by the lengths of the reacting chains as well as the system viscosity. The value of k_t can decrease by several orders of magnitude in this regime, as shown for MMA in Figure 3.2.

At even higher conversions, the system may become so viscous that the polymer radicals move more quickly through propagation (addition of new monomer units to the radical) than by translation. This phenomenon, called *reaction diffusion*, leads to a second plateau region in the k_t versus conversion plot, with k_t proportional to $k_p(1 - x)$. It becomes a dominant mechanism for monomers with high k_p values, such as the acrylates (see Figure 3.2). If the glass transition temperature of the reaction mixture exceeds the reaction temperature, the propagation reaction and apparent initiator efficiency [47] also become diffusion-controlled, a phenomenon often termed as the *glass effect*. The decrease in k_p causes a corresponding decrease in k_t at high conversions, as seen in Figure 3.2.

The overall behavior of k_t with conversion is often modeled as a composite of the various diffusional processes:

$$k_t = \frac{1}{(1/k_{t,SD}) + (1/k_{t,TD})} + k_{t,RD} \quad (3.52)$$

The subscripts SD, TD and RD refer to segmental diffusion, translational diffusion and reaction diffusion, with $k_{t,SD}$ set to the low conversion values summarized in Table 3.2. The reaction diffusion term $k_{t,RD}$ is proportional to propagation, with proportionality coefficient C_{RD} estimated from experimental data [10]:

$$k_{t,RD} = C_{RD}k_p(1 - x) \quad (3.53)$$

Under the glass effect, k_p may itself become diffusion controlled at very high conversions [10, 47].

Semi-empirical approaches are often used to model $k_{t,TD}$ as a function of system viscosity (Equation 3.54), conversion (Equation 3.55) or system free-volume (Equation 3.56):

$$k_{t,TD} = \frac{\eta_0}{\eta} k_{t,TD}^0 \quad (3.54)$$

$$k_{t,TD} = k_{t,TD}^0 \exp(C_\alpha x + C_\beta x^2 + C_\gamma x^3) \quad (3.55)$$

$$k_{t,TD} \propto C_1 \exp(C_2 v_f) \quad (3.56)$$

In Equation 3.54, η is the viscosity of the polymerizing medium, η_0 the viscosity of the pure monomer, and $k_{t,TD}^0$ represents the rate coefficient of translational diffusion at zero conversion fit to experimental data [10]. Equation 3.55 has been used to fit, for example, styrene polymerization rate data to high conversion over a range of temperatures [16]. In the free-volume (v_f) approach [48, 49], parameters are fitted to experimental data, with the effect of polymer MW on system viscosity being captured by expressing C_1 as a function of M_w . Further details and variations of these modeling approaches can be found in the literature [10, 50–53].

A good model for k_t is necessary to capture the time-conversion behavior in homogeneous batch FRP systems. The large decrease in k_t at intermediate conversion results in an increase in radical concentration (Equation 3.9) and a corresponding increase in R_p (Equation 3.10), which causes an upward curvature in the time–conversion plot (Figure 3.3).

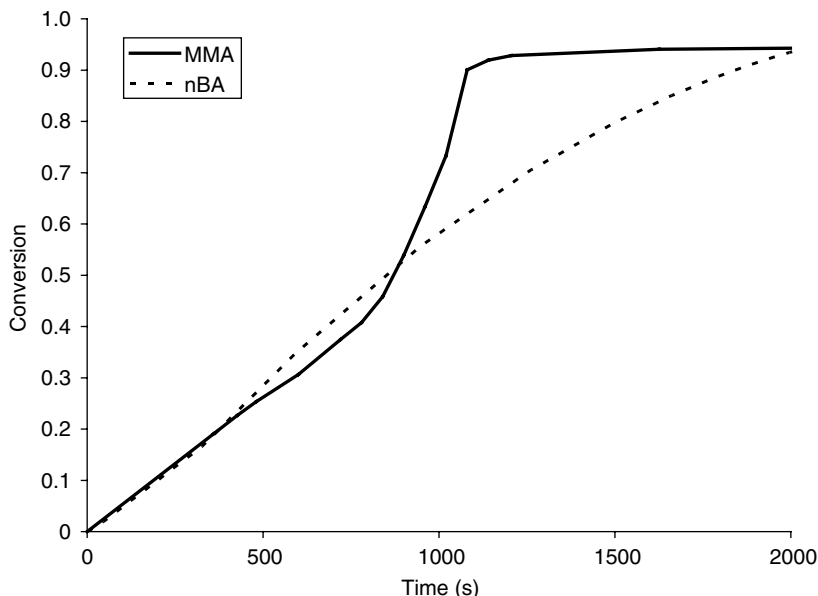


Figure 3.3 Typical time–conversion plots for MMA and butyl acrylate batch polymerizations. The sharp increase in rate seen for MMA, known as the gel effect, is due to the large decrease in k_t with conversion.

This accelerated rate is accompanied by a large heat release that can be difficult to remove from the viscous reaction system. The severity of the gel effect is directly related to the magnitude of the decrease in k_t , as seen by comparing the BA and MMA rate profiles in the figure. The decrease also leads to an increase in DP_n^{inst} (Equation 3.13) for systems where MW is controlled by termination.

3.2.4 Kinetic balances for modeling polymer MWs

The equations in Section 3.2.1 are appropriate for calculating rate of polymerization and instantaneous chain-length, but not for substitution into a generalized reactor model. In addition, they do not track the change in \overline{M}_n with conversion, or higher MW averages that are strongly affected by LCB reactions. A principal challenge in modeling of polymerization kinetics is how to reduce a very large number of individual species (living and dead chains with lengths from 1 to $>10^5$, often with other distributed attributes such as the number of branch points) to a tractable solution. The predominant approach is to reduce the system of equations through definition of the principal moments of the various distributions to track *average* polymer properties [54] such as \overline{M}_n and \overline{M}_w (and possibly \overline{M}_z), and for branched systems the number-average (\overline{B}_n) and weight-average (\overline{B}_w) number of branches per chain. Only the basic mathematical treatment for a homopolymerization system will be given here; more details can be found in recent comprehensive reviews [55, 56].

Consider the basic set of mechanisms shown in Scheme 3.2 combined with LCB (Equation 3.27). The moment concentrations ($\text{mol } \ell^{-1}$) for the radical ($[\mu_k]$), and dead ($[\nu_k]$) polymer distributions are defined as:

$$[\mu_k] = \sum_{n=1}^{\infty} n^k [P_n] \quad (3.57)$$

$$[\nu_k] = \sum_{n=1}^{\infty} n^k [D_n] \quad (3.58)$$

It is also helpful to define moments for the *bulk* (ζ_k) polymer, the total polymer in the system including live radicals:

$$[\zeta_k] = \sum_{n=1}^{\infty} n^k ([D_n] + [P_n]) \quad (3.59)$$

With $[D_n] \gg [P_n]$ there is little difference in magnitude between ν_k and ζ_k but, as described below, the introduction of ζ_k eliminates the moment closure problem created by the LCB mechanism. These moment definitions collapse the infinite set of equations for polymeric species into a manageable subset, and many of the moments have precise physical meanings. The zeroth live moment, $[\mu_0]$, is the concentration of polymer radicals in the system (denoted by $[P_{\text{tot}}]$ in Section 3.2.1), and the first live moment, $[\mu_1]$, is the concentration of monomer units contained in all growing radicals. Similarly, $[\zeta_0]$ is the concentration of all polymer chains in the system, and $[\zeta_1]$ is the concentration of monomer units bound in all polymer chains. These values are used to calculate MW averages, where w_m is the molecular weight of the monomeric repeat unit:

$$\overline{M}_n = w_m \frac{\zeta_1}{\zeta_0}, \quad \overline{M}_w = w_m \frac{\zeta_2}{\zeta_1}, \quad \overline{M}_z = w_m \frac{\zeta_3}{\zeta_2} \quad (3.60)$$

Equations for $[\zeta_0]$, $[\zeta_1]$ and $[\zeta_2]$ will be developed for the calculation of \overline{M}_n and \overline{M}_w .

The first step is to formulate balances (in terms of the net generation rates per unit volume, $\text{mol } \ell^{-1} \text{ s}^{-1}$) for live radicals, dead chains and total chains of length n , accounting for all of the consumption and generation terms from the kinetic mechanisms:

$$\begin{aligned} R_{P_n} = & \left\{ 2fk_I[I] + (k_{\text{tr}}^{\text{mon}}[M] + k_{\text{tr}}^{\text{sol}}[S] + k_{\text{tr}}^{\text{CTA}}[CTA]) \sum_{j=1}^{\infty} [P_j] \right\} \delta(n-1) \\ & + k_p[M]([P_{n-1}] - [P_n]) \\ & - \left\{ k_{\text{tr}}^{\text{mon}}[M] + k_{\text{tr}}^{\text{sol}}[S] + k_{\text{tr}}^{\text{CTA}}[CTA] + (k_{\text{td}} + k_{\text{tc}}) \sum_{j=1}^{\infty} [P_j] \right\} [P_n] \\ & + k_{\text{tr}}^{\text{pol}} n [D_n] \sum_{j=1}^{\infty} [P_j] - k_{\text{tr}}^{\text{pol}} [P_n] \sum_{j=1}^{\infty} j [D_j] \end{aligned} \quad (3.61)$$

$$R_{D_n} = \left\{ k_{\text{tr}}^{\text{mon}}[M] + k_{\text{tr}}^{\text{sol}}[S] + k_{\text{tr}}^{\text{CTA}}[\text{CTA}] + k_{\text{td}} \sum_{j=1}^{\infty} [P_j] \right\} [P_n] \\ + \frac{1}{2} k_{\text{tc}} \sum_{j=1}^{n-1} [P_j][P_{n-j}] + k_{\text{tr}}^{\text{pol}} [P_n] \sum_{j=1}^{\infty} j[D_j] - k_{\text{tr}}^{\text{pol}} n[D_n] \sum_{j=1}^{\infty} [P_j] \quad (3.62)$$

$$R_{P_n+D_n} = \left\{ 2fk_I[I] + (k_{\text{tr}}^{\text{mon}}[M] + k_{\text{tr}}^{\text{sol}}[S] + k_{\text{tr}}^{\text{CTA}}[\text{CTA}]) \sum_{j=1}^{\infty} [P_j] \right\} \delta(n-1) \\ + k_p[M]([P_{n-1}] - [P_n]) - k_{\text{tc}} \left(\sum_{j=1}^{\infty} [P_j] \right) [P_n] + \frac{1}{2} k_{\text{tc}} \sum_{j=1}^{n-1} [P_j][P_{n-j}] \quad (3.63)$$

The origin of each term in these balances is evident by looking at the mechanisms of Scheme 3.2 and Equation 3.27. The Kronecker delta function ($\delta(x) = 1$ if $x = 0$ and $\delta(x) = 0$ if $x \neq 0$) captures the generation of new polymeric radicals (P_1), and the expression for termination by combination accounts for the possibility of creating D_n from any combination of two smaller radical fragments whose lengths sum to n . Transfer to polymer terms account for the probability that transfer to a certain chain D_n is proportional to chain length n .

These species' balances are next substituted into the moment definitions (Equations 3.57–3.59). The use of generating functions [54, 57, 58] eliminates the tedium (and possible errors) of performing the required series summations; both treatments lead to the following equations describing the rates of change of the moments:

Live moments:

$$R_{\mu_0} = 2fk_I[I] - (k_{\text{td}} + k_{\text{tc}})[\mu_0]^2 \quad (3.64)$$

$$R_{\mu_1} = 2fk_I[I] + k_{\text{tr}}^{\text{mon}}[M][\mu_0] + k_{\text{tr}}^{\text{sol}}[S][\mu_0] + k_{\text{tr}}^{\text{CTA}}[\text{CTA}][\mu_0] + k_p[M][\mu_0] \\ - \{k_{\text{tr}}^{\text{mon}}[M] + k_{\text{tr}}^{\text{sol}}[S] + k_{\text{tr}}^{\text{CTA}}[\text{CTA}] + (k_{\text{td}} + k_{\text{tc}})[\mu_0]\}[\mu_1] \\ + k_{\text{tr}}^{\text{pol}}([\mu_0][v_2] - [\mu_1][v_1]) \quad (3.65)$$

$$R_{\mu_2} = 2fk_I[I] + k_{\text{tr}}^{\text{mon}}[M][\mu_0] + k_{\text{tr}}^{\text{sol}}[S][\mu_0] + k_{\text{tr}}^{\text{CTA}}[\text{CTA}][\mu_0] \\ + k_p[M]([\mu_0] + 2[\mu_1]) \\ - \{k_{\text{tr}}^{\text{mon}}[M] + k_{\text{tr}}^{\text{sol}}[S] + k_{\text{tr}}^{\text{CTA}}[\text{CTA}] + (k_{\text{td}} + k_{\text{tc}})[\mu_0]\}[\mu_2] \\ + k_{\text{tr}}^{\text{pol}}([\mu_0][v_3] - [\mu_2][v_1]) \quad (3.66)$$

Dead moments:

$$R_{v_0} = k_{\text{tr}}^{\text{mon}}[M][\mu_0] + k_{\text{tr}}^{\text{sol}}[S][\mu_0] + k_{\text{tr}}^{\text{CTA}}[\text{CTA}][\mu_0] + k_{\text{td}}[\mu_0]^2 + \frac{1}{2} k_{\text{tc}}[\mu_0]^2 \quad (3.67)$$

$$R_{v_1} = \{k_{\text{tr}}^{\text{mon}}[M] + k_{\text{tr}}^{\text{sol}}[S] + k_{\text{tr}}^{\text{CTA}}[\text{CTA}] + (k_{\text{td}} + k_{\text{tc}})[\mu_0]\}[\mu_1] \\ + k_{\text{tr}}^{\text{pol}}([\mu_1][v_1] - [\mu_0][v_2]) \quad (3.68)$$

$$R_{v_2} = \{k_{tr}^{mon}[M] + k_{tr}^{sol}[S] + k_{tr}^{CTA}[CTA] + (k_{td} + k_{tc})[\mu_0][\mu_2] + k_{tc}[\mu_1]^2 + k_{tr}^{pol}([\mu_2][v_1] - [\mu_0][v_3])\} \quad (3.69)$$

Bulk moments:

$$R_{\zeta_0} = 2fk_I[I] + k_{tr}^{mon}[M][\mu_0] + k_{tr}^{sol}[S][\mu_0] + k_{tr}^{CTA}[CTA][\mu_0] - \frac{1}{2}k_{tc}[\mu_0]^2 \quad (3.70)$$

$$R_{\zeta_1} = 2fk_I[I] + k_{tr}^{mon}[M][\mu_0] + k_{tr}^{sol}[S][\mu_0] + k_{tr}^{CTA}[CTA][\mu_0] + k_p[M][\mu_0] \quad (3.71)$$

$$R_{\zeta_2} = 2fk_I[I] + k_{tr}^{mon}[M][\mu_0] + k_{tr}^{sol}[S][\mu_0] + k_{tr}^{CTA}[CTA][\mu_0] + k_p[M]([\mu_0] + 2[\mu_1]) + k_{tc}[\mu_1]^2 \quad (3.72)$$

The set of moment expressions to be substituted into reactor balances consists of *either* the live and dead moments (Equations 3.64–3.69) *or* the live and bulk moments (Equations 3.64, 3.65 and 3.70–3.72, substituting $[\zeta_1]$ and $[\zeta_2]$ for $[v_1]$ and $[v_2]$ in Equation 3.65). Choosing the former, while common practice in the literature, suffers from a moment closure problem, as $[\mu_2]$ and $[v_2]$ depend on $[v_3]$. The Hulburt and Katz [59] method assumes that the molecular weight distribution can be represented by a truncated series of Laguerre polynomials, approximating $[v_3]$ as

$$[v_3] = \frac{[v_2]}{[v_0][v_1]}(2[v_0][v_2] - [v_1]^2) \quad (3.73)$$

Use of the bulk moments eliminates this moment closure problem. It also reduces the number of equations, as Equation 3.66 is not required for solution of Equation 3.72. An additional balance is needed to track the concentration of LCB formed by the transfer to polymer mechanism:

$$R_{LCB} = k_{tr}^{pol}\mu_0[v_1] \quad (3.74)$$

These equations collapse the molecular weight distribution into its principal averages for the calculation of \overline{M}_n , \overline{M}_w and LCB density.

This set of moment equations can be extended to include other mechanisms, such as reaction of terminal double bonds (Equation 3.30, Scheme 3.7(b)) [60], crosslinking (Scheme 3.8) [61], and chain β -scission following intermolecular H-abstraction [62]. The methodology is also extendable to copolymerization systems, either by defining additional moment quantities [60, 61] or by defining copolymer-averaged rate coefficients such as Equations 3.44 and 3.48 [6, 63]. The latter strategy, termed the pseudo-kinetic rate coefficient method, reduces the moment balances for a multicomponent polymerization to that of a homopolymerization. The method is applicable to both terminal and penultimate kinetic models even when the effect of chain-length dependent termination is significant [57] and has also been extended to branched copolymer systems [58]. Furthermore, the method of moments is easy to implement as part of larger-scale reactor modeling and is the standard methodology used in process simulation packages [64–68]. Discussion regarding substitution of the moment expressions into general reactor balances is deferred to Section 3.5.

The major limitation of kinetic models using the method of moments is that they only track average quantities. More detail is sometimes required (e.g., to examine the combined effect of chain-scission and LCB on polymer architecture). In such cases, mechanistic

assumptions can be tested more rigorously through a detailed comparison with full molecular weight distributions (MWDs) measured experimentally. Recent advances in modeling tools make it possible to simulate the complete MWD, as well as how a second distributed quantity (e.g., LCB) varies with chain-length. Approaches that have been taken include Monte-Carlo techniques [69, 70] and a modified moment approach that classifies chains into “generations” based upon the degree of architectural complexity arising from branching reactions [71, 72]. The commercial software package Predici® calculates full MWDs using a discrete Galerkin technique with variable grid and order [73] and has been used to model a number of complex kinetic schemes [21, 40, 74].

3.3 Controlled radical polymerization

The widespread use of FRP to produce commercial polymer grades is due to its versatility; a broad range of vinyl monomers, including functional monomers, can be readily polymerized under relatively mild reaction conditions. However, the technique does not allow for careful control of the polymer microstructure. As the life-time of an individual chain is short compared to the process time, changes in the operating conditions (e.g., temperature, viscosity, monomer concentration and composition) lead to increased heterogeneity in polymer composition, MW, and branching levels. Even if these changes in conditions can be avoided, the minimum PDI remains 1.5 for systems dominated by termination by combination and 2.0 for other systems, and copolymer sequences along the polymer chain are randomly distributed, as controlled by the monomer reactivity ratios. It is not possible to add a sequence of another monomer to form block copolymer, or add a special terminating agent to produce end-functional polymers when the typical life-time of a chain is on the order of a second.

There are some specialized applications where precise control of the polymer microstructure is required. For example, block copolymers find use as compatibilizers and stabilizers in polymer blends, coatings and ink-jet formulations. Polymers with controlled topology such as star, comb and hyperbranched structures may be used as lubricant additives or in applications to modify and control surface properties of materials. Growth of polymer at interfaces holds promise in lithography, corrosion prevention, materials reinforcement or preparation of materials for separation processes. Figure 3.4 is a schematic of some polymer microstructures that are, other than random copolymer, impossible to synthesize by FRP techniques. Some of these architectures may be prepared by ionic living polymerizations; however these systems require stringent conditions and are limited to a relatively small number of monomers. Thus, the emergence of controlled radical polymerization (CRP) techniques offers a route to synthesize new high-value products for specialty applications.

CRP (also referred to as “living radical polymerization”) is a family of promising techniques for the synthesis of macromolecules with well-defined molecular weight, low polydispersities (often close to unity) and various architectures under mild conditions at 20–120°C, with minimal requirements for purification of monomers and solvents. A common feature of the variants is the existence of an equilibrium between active free radicals and dormant species. The exchange between active radicals and dormant species allows slow but simultaneous growth of all chains while keeping the concentration of radicals low enough to minimize termination. The ideal CRP is achieved if all chains are initiated

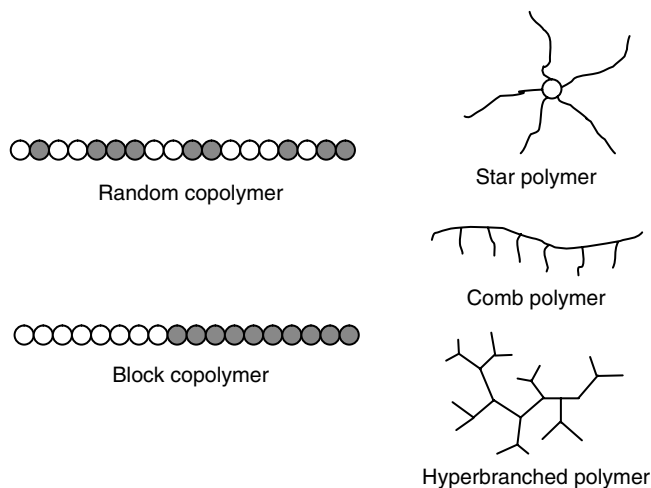


Figure 3.4 Schematic representations of polymer microstructures accessible through controlled radical polymerization techniques.

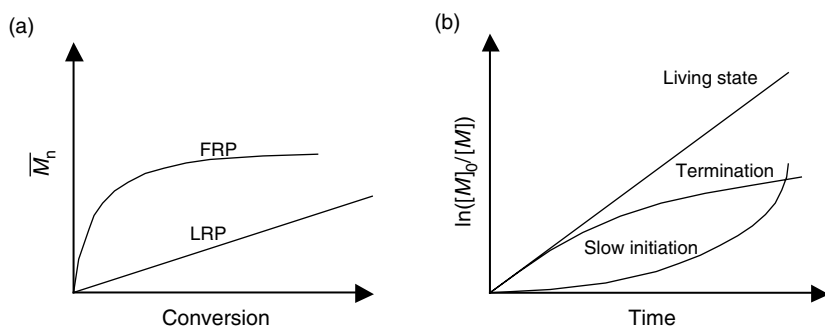


Figure 3.5 (a) The evolution of number-average MW versus conversion for controlled radical polymerization (CRP) and FRP systems. (b) $\ln([M]_0/[M])$ versus time for an ideal controlled radical polymerization system. Deviations from linearity can result from slow initiation or loss of radicals by termination.

immediately at the start of polymerization and if termination and other side reactions are completely suppressed. This ideal system has the following features:

- The average molecular weight increases with conversion linearly, as all chains remain living and grow throughout the entire course of the reaction. In contrast, conventional FRP is characterized by the formation of high molecular weight dead polymer chains at low conversion and continued production of new polymer chains throughout the polymerization (Figure 3.5(a)).
- With instantaneous initiation and no termination, $[P_{\text{tot}}]$ remains constant such that a plot of $\ln([M]_0/[M])$ has a linear relationship with time for an isothermal batch reactor ($[M]_0$: concentration of monomer at time 0; $[M]$: concentration of monomer at time t),

as shown in Figure 3.5(b). Curvature indicates deviation from the ideal situation caused by slow initiation, loss of radicals by termination, or other side reactions.

- The number of polymer chains in the ideal CRP system remains constant at the value formed by initiation at time 0, $[P-X]_0$. The theoretical degree of polymerization is determined by the molar ratio of concentration of reacted monomer to the concentration of chains, $DP_n = ([M]_0 - [M])/[P-X]_0$. Quantitative initiation allows the synthesis of polymer with special architectures and end-functionalities.
- Polymerization proceeds until the monomer has been consumed. Further addition of monomer results in continued polymerization. Thus, block copolymers can be formed by sequential monomer addition.
- The MWD for an ideal CRP system follows the Poisson distribution, such that $PDI = DP_w/DP_n = (1 + 1/DP_n)$. For real CRP systems discussed below, PDIs of 1.1–1.3 are routinely achieved, much lower than can be achieved by FRP.

Since the active species are free radicals, it is impossible to entirely suppress bimolecular termination or other mechanisms such as chain transfer. Nonetheless, CRP chemistries allow unprecedented control of polymer microstructure not achievable by conventional FRP.

Three variants of CRP have emerged as the most promising:

- (1) Stable free-radical polymerization (SFRP),
- (2) Atom transfer radical polymerization (ATRP),
- (3) Reversible addition-fragmentation chain transfer (RAFT) polymerization.

The features of each are outlined briefly below; interested readers can find extensive discussions of the features and kinetics of each system in reference 2.

3.3.1 Stable free-radical polymerization

Solomon *et al.* [75] first used nitroxyl radicals and alkoxyamines in a radical polymerization, but their work was limited to production of low-molecular weight polymers. In 1993, Georges *et al.* [76] used a mixture of benzoyl peroxide (BPO) initiator and 2,2,6,6-tetramethylpiperidinyloxy (TEMPO) to produce low-polydispersity and high molecular weight polystyrene. Since then many papers about SFRP (also known as nitroxide mediated polymerization or NMP), mainly focused on styrene polymerization in the presence of TEMPO, have been published. Other nitroxide mediators are being developed that are better suited to polymerization of more polar monomers such as meth(acrylates) [77].

The basic mechanism of SFRP is the alternating activation–deactivation process between large amounts of dormant species and small amounts of propagating radicals:



Dormant species P_n-X form propagating radicals P_n through the carbon-oxygen bond cleavage; typical values for activation rate coefficient k_{act} are 10^{-2} – 10^{-3} s⁻¹. In the active

state, radicals undergo propagation, transfer or termination events (Scheme 3.2). Only a few monomer addition steps occur, as stable nitroxide radicals X quickly recombine with propagating radicals to form dormant species with (capture) rate coefficient k_{deact} , generally of magnitude 10^7 – $10^8 \text{ l mol}^{-1} \text{ s}^{-1}$. The initial radicals (living chains) are usually generated in the system in one of two ways. The first, addition of a capped radical species to the system, $[R-X]_0$, ensures that there is an initial 1:1 ratio of radicals (R becomes P_n after addition of monomer) and mediating species X . For the second, formation of radicals during the first few minutes of polymerization via fast decomposition of an initiator with a short half-life (Equations 3.3 and 3.16), the ratio of radicals to mediating species is more difficult to control.

The equilibrium of Equation 3.75 dictates that the concentration of active free radicals in the system, $[P_{\text{tot}}]$, remains low. For the system to remain living, the reversible deactivation reaction with nitroxide must be dominant compared to irreversible radical–radical termination (Equation 3.5). However, as it is impossible to totally eliminate the loss of radicals through termination, an imbalance between $[X]$ and $[P_{\text{tot}}]$ arises:

$$\frac{d[X]}{dt} = k_{\text{act}}[P-X] - k_{\text{deact}}[P_{\text{tot}}][X] \quad (3.76)$$

$$\frac{d[P_{\text{tot}}]}{dt} = k_{\text{act}}[P-X] - k_{\text{deact}}[P_{\text{tot}}][X] + R_{\text{init}} - k_t[P_{\text{tot}}]^2 \quad (3.77)$$

For the case where $R_{\text{init}} = 0$ (the number of total chains in the system remains constant), Fischer [78] derived the following expressions for species concentrations and polymerization rate ($K = k_{\text{act}}/k_{\text{deact}}$):

$$[P_{\text{tot}}] = (k_{\text{act}}[P-X]_0/3k_{\text{deact}}k_t)^{1/3}t^{-1/3} \quad (3.78)$$

$$[X] = (3k_tK^2[P-X]_0^2)^{1/3}t^{1/3} \quad (3.79)$$

$$R_{\text{pol}} = k_p[M](K[P-X]_0/3k_t)^{1/3}t^{-1/3} \quad (3.80)$$

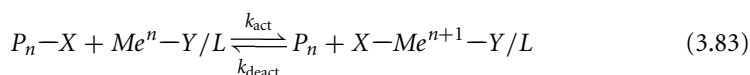
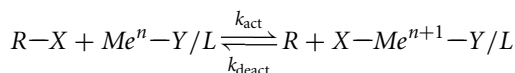
$$\ln\left(\frac{[M]_0}{[M]}\right) = (3k_p/2)(K[P-X]_0/3k_t)^{1/3}t^{2/3} \quad (3.81)$$

The concentration of free nitroxide (Equation 3.79) builds with time while radical concentration (Equation 3.78) and thus reaction rate (Equation 3.80) decreases. This behavior, called the “persistent radical effect” [78], forces the equilibrium in Equation 3.75 toward the dormant species. While promoting the living nature of the system, it is necessary to compensate for the loss of radicals in the system by adding conventional initiator or using a monomer with self-initiation (e.g., styrene) in order to maintain a reasonable polymerization rate, a strategy that broadens polymer MWD from the ideal case. The longer polymerization time is a major economic disadvantage, and thus current research is focused on methods to increase rate while maintaining control.

3.3.2 Atom transfer radical polymerization

The name of ATRP originates from atom transfer radical addition (ATRA), the formation of an adduct ($R-\text{CH}_2-\text{CHR}'-X$) with a halogen in the presence of a metal catalyst.

The polymerization proceeds following the same mechanism, with metal complex activating the carbon-halogen bond and proceeding via the metal-assisted repetitive activation and deactivation.



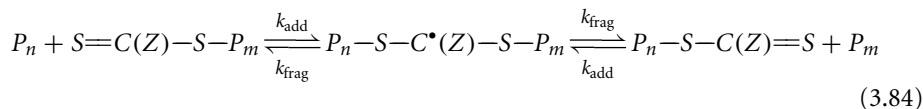
$R-X$ is an alkyl halide initiator (e.g., methyl 2-bromopropionate) and P_n-X is the dormant species while Me^n-Y/L is the complex of catalyst and ligand. Copper(I) bromide (CuBr) or copper(I) chloride (CuCl) are generally chosen as low-cost catalysts (Me^n-Y). The main role of the ligand (L) is to solubilize the catalyst in the organic media and to adjust the redox potential of the metal center for appropriate reactivity and dynamics for the atom transfer. For copper-mediated ATRP, nitrogen-based simple amine ligands are often used, added at a 1:1 molar ratio with the catalyst. The radicals are generated through a reversible redox process catalyzed by a transition metal complex Me^n-Y/L , which undergoes one-electron oxidation of the metal center. During this process $X-Me^{n+1}-Y/L$ acts as a persistent radical to reduce the concentration of growing radicals. Primary radicals R or growing polymer radicals P_n can propagate with monomer or react with the halogen on the $X-Me^{n+1}-Y/L$ to regenerate $R-X$. Other reactions, including termination and chain transfer, occur as in conventional FRP.

In 1994, the first ATRP experiment, polymerization of methyl methacrylate, catalyzed by a $RuCl_2(PPh_3)_3$ complex initiated by CCl_4 , was reported by Sawamoto *et al.* [79]. Shortly after, bulk polymerization of styrene with a copper catalyst was published by Wang and Matyjaszewski [80] in the presence of 1-phenylethyl chloride/CuCl₂/2,2'-dipyridyl. These polymerizations successfully produced polymers with narrow polydispersity (close to one), with molecular weight increasing linearly with conversion, both important attributes of a living mechanism. The kinetic development of Fischer [78] also applies to ATRP systems, as the concentration of Me^n-Y/L remains roughly constant during polymerization. ATRP is robust to a wider range of monomers than SFRP, and is usually conducted at a lower temperature (<90°C). However, the presence of metal catalyst residue causes color and raises toxicity concerns.

3.3.3 Reverse addition-fragmentation chain transfer polymerization

The technique of RAFT, first published in 1998 [81], differs significantly from ATRP and SFRP in the manner by which it controls polymerization. Rather than proceeding through a reversible termination mechanism that affects radical concentration, the exchange between an active and dormant chain occurs via a chain transfer process. Dithioesters $R-S-C(Z)=S$ are effective RAFT agents with Z , typically a methyl or phenyl group, activating and stabilizing the carbon-sulfide thiocarbonyl bond. The R radical leaving group is

generally chosen to be similar to the radical of the propagating monomer. Reaction proceeds by the reaction of an active with a dormant chain to form an intermediate involving both chains.



The intermediate species either decomposes back to the initial reactants or fragments to release the previously dormant radical, which can then propagate, transfer or terminate according to typical free-radical mechanisms. As the concentration of dormant chains is much greater than active radicals, the rate of Equation 3.84 is significantly greater than that of radical–radical termination. Although a conventional initiator is used to start and sustain the reaction, the amount is significantly less than the initial concentration of RAFT agent such that the system MW is controlled by the latter value. The effect of the RAFT agent on polymerization rate depends on the stability of the intermediate complex in Equation 3.84 [2]. Higher reaction rate provides an advantage compared to SFRP and ATRP, although the need to remove the sulfur atoms which cause color remains a significant drawback.

3.4 Polymer reaction engineering aspects

3.4.1 Heat removal and temperature programming

Free-radical polymerizations are highly exothermic. A typical adiabatic temperature rise for bulk (mass) polymerization of $\sim 200\text{--}500^\circ\text{C}$ may not be uncommon. The overall activation energy for polymerization is in the order of $80 \pm 15 \text{ kJ mol}^{-1}$. The dramatic increase in the heat load during the gel-effect period can result in loss of temperature control, non-isothermal reactor operation and potential runaways. Non-isothermal operation, aside from safety concerns, can also adversely affect product quality.

Clearly related to the issue of heat removal is temperature programming policies (and via these policies, there is a direct link to polymer reactor optimization strategies), since in the polymerization industry there is considerable economic incentive to develop real-time optimal operating policies that will increase production rate (and hence reduce production time) and yield polymer with desired molecular weight and branching characteristics. Usually, optimal temperature (and initiator) policies are derived to minimize the time to reach a desired final conversion and some average molecular weight (and/or polydispersity and/or other branching characteristics). Time savings of 15–30% have often been realized when compared to some reference isothermal operation. Starting from the premise that in many industrial applications the reactor cooling system is underutilized, these policies can offer considerable economic advantages and improve both reactor operation and product characteristics. To run a batch reactor at its optimum (minimum) batch time, the heat generation rate at any point in the polymerization should be equal to the heat removal capacity of the system with some allowance for a safety factor. The monomer conversion should vary (almost) linearly with time at a rate consistent with the heat removal capacity

of the system. Another practical solution is to polymerize isothermally and use mixed initiator systems (“cocktails of initiators”) to give a constant rate of heat generation which is somewhat less than the cooling capacity. A mixed (multiple) initiator system includes a range of initiators with different half-lives and concentrations. Checking the feasibility of these optimal policies is an important issue; many times a sub-optimal policy has to be implemented due to process constraints. Product constraints are more important (i.e., one should carefully consider both rate and molecular weight). Early applications for batch reactors included the derivation of policies for PVC reactors (including non-isothermal start-up and adiabatic operation of the reactor at the final stages) [82] and polystyrene reactors [83].

General-purpose polystyrene can be produced in a CSTR reactor. However, due to limitations with respect to mixing and heat removal capacity of a CSTR, polystyrene can only be produced at relatively low temperatures and conversion levels. Efforts have been made for many years to increase the heat removal capacity (e.g., use of additional cooling coils), however such apparatus together with a predetermined temperature profile may lead to undesired product properties. The high viscosity of polystyrene also presents a processing problem for a CSTR reactor. Even though it is of common industrial practice to add a small percentage of solvent like toluene or ethyl benzene into the reaction mixture, polystyrene still cannot be produced in a CSTR up to high conversion. In order to increase productivity and reduce residual monomer, it is highly desired to achieve high conversion. An alternative is to combine the CSTR with a plug flow or tower reactor. A CSTR is suitable for polymerization at low conversion levels where the viscosity is relatively low. The reaction mixture is subsequently transferred to a plug flow reactor. The unagitated plug flow reactor can have several temperature zones and additional reactant can be fed into each zone, providing greater flexibility in comparison to a CSTR. It is also common to use a loop reactor with a static mixer instead of a CSTR reactor. Such a loop reactor has better mixing for more viscous reaction mixtures. Some of these and other related issues have been reviewed by Tieu *et al.* [84] and more recently by Gao *et al.* [85]. The book *Modern Styrenic Polymers* [86] also covers related topics for polystyrenes and styrenic copolymers (including multifunctional initiators).

Several important general features relating to heat transfer in stirred-tank vessels are summarized below:

- (1) High heats of reaction and large activation energies. Therefore, small increases in temperature give rise to large increases in heat generation.
- (2) Large increases in viscosity with monomer conversion. In bulk/solution polymerizations the viscosity at intermediate conversion may approach the limit of what most conventional reactors can handle (20 000–25 000 cP). A very good overview of viscosity increase and its influence on polymerization processes can be found in Moritz [87]. Viscosity significantly affects the polymerization kinetics as well as heat, mass and momentum balances of the polymerization reactor.
- (3) Polymers have a tendency to adhere to the surface of the reactor and often form a hard, growing layer of very high molecular weight material. This polymer build-up, often referred to as scale, increases as the temperature difference between reactor wall and polymerizing mixture increases. Larger reactors would tend to have cooler walls and consequently more scale formation (bulk/solution).

- (4) The autoacceleration in the rate of polymerization with conversion leads to situations where the rate of heat generation is very sensitive to small perturbations in reactor temperature. This also leads to higher heat generation rates where heat is most difficult to remove because of high viscosity and, in addition, scale formation. The situation where the rate of heat generation increases by a factor of 5–10 between 10% and 70% conversion is not unusual. Thus, peak heat generation is frequently several times larger than an average estimate.
- (5) Besides heat of reaction, there might be an additional heat input from the impeller. In many cases this source of heat is negligible compared to heat of polymerization but may be significant with highly viscous mixtures (bulk polymerization at high conversions).
- (6) Heat removal is most commonly achieved through jacket cooling. With large reactors, jacket cooling is not always sufficient to obtain reasonably short batch times, so supplemental heat removal through reflux condensers, external heat exchangers, internal cooling coils and baffles must be used.
- (7) When heat is removed through heat transfer surfaces such as reactor walls and cooling coils, one must keep in mind that the overall heat transfer coefficient can fall dramatically during polymerization (viscosity increase/scale formation).
- (8) As reactors are scaled up in size, it is frequently necessary to add supplemental heat removal capacity since the heat transfer area (of reactor walls) only increases with reactor volume to the 0.67 power, while heat generation rate is proportional to volume. Internal cooling coils and baffles may increase the heat transfer area by 30–50%, however, these can only be used efficiently when scale formation is at a minimum and viscosities relatively low. Poor mixing in dead spots around coils/baffles may actually increase scale formation and thus contribute to poor product quality and operational difficulties.
- (9) Reflux cooling is beneficial in increasing the heat removal capacity when monomer or solvent is volatile at the reaction conditions, provided that excessive foaming does not occur.
- (10) The choice of an operating average ΔT (temperature difference between the temperature of the polymerizing mixture and an average jacket (coolant) temperature) depends on the particular system and often large values of ΔT cannot be used because of scale formation on cold surfaces. Polymerization close to cold surfaces also leads to high molecular weight polymer (and the possible formation of “fish eyes”, which are hard, difficult to dissolve polymer particles).
- (11) Polymerizations are always carried out at an “unstable operating point” (solution of the energy balance equation), because the overall heat transfer coefficient is too small to permit a reasonable production rate at low temperatures. Therefore, careful control of the reaction temperature is necessary and the coolant system must have a fast response. When heat removal is merely through the reactor walls, it is unsafe to polymerize at temperatures where the derivative of the heat generation rate is large (because a very small increment in temperature requires a large drop in coolant temperature to avoid a runaway, and there is a limit in the response rate of the cooling system). As reactors are scaled up, the specific polymerization rate must be decreased if the reactor is to be operated at the same temperature, or additional heat removal capacity must be added.

- (12) Sample calculations indicate that for volumes greater than 20 000 ℓ additional cooling capacity is needed for commercial production rates (depending of course on the choice of ΔT). As reactor volume increases by a factor of 100, the available heat transfer area (walls) increases only by a factor of 20. As volume increases by a factor of 10, the wall thickness usually increases by a factor of 2. For typical commercial rates, the range of the overall heat transfer coefficient (U) (for stainless steel) should be 300–600 $\text{W m}^{-2} \text{K}^{-1}$, whereas reductions as high as 50–80% have been reported due to viscosity increases. For a glass-lined reactor, the overall U may be 2–3 times less than for stainless steel. Refrigerated water may result in a 30–40% increase in heat transfer. Larger reactors require a larger ΔT for the same U . A film on the wall as thin as 0.4 mm may reduce the overall U by about 40%.
- (13) In many polymerizations, polymer quality is largely independent of polymerization rate because transfer reactions control molecular weights. Therefore, production rates may not be limited by requirements of product quality, but rather heat transfer is the factor limiting production rate (so long as spatial and time variations in temperature are not appreciable). If temperature gradients exist, these could lead to a deterioration in polymer quality, in particular, significant broadening of the molecular weight distribution.
- (14) When the heat generation rate decreases with polymerization time, addition of extra initiator or a temperature rise may be used to give a more uniform heat generation rate for the consequent reduction in batch time. This of course requires good mixing in the reactor such that the extra initiator is distributed uniformly in the polymerizing mixture, otherwise “hot spots” will result.

3.4.2 Batch reactors

Despite the fact that many polymers today are produced in very large quantities and thus from this point of view make continuous production feasible, batch operation still finds very wide use in industrial polymerizations (e.g., PVC, poly(styrene), PMMA, PVAc, etc.). The major disadvantage of batch operation is the need for periodic shut-down and start-up with the associated loss of polymerization time. It is obviously desirable to reduce batch time to a minimum by increasing reaction rates. All heat generated must either pass through heat transfer surfaces or be removed by the generation and condensation of vapors in a reflux (condenser) system. With a CSTR, on the other hand, a fraction of the heat generated is removed via the exit stream.

For a batch reactor, a balance on moles of monomer can be written as

$$\frac{dM}{dt} = -R_p V = -k_p [M][P_{\text{tot}}]V \quad (3.85)$$

where M represents the number of moles of (free, unreacted) monomer in the reactor at time t , R_p the rate of polymerization (Equation 3.10) and V the volume of the polymerizing mixture. There are no inflow and outflow terms in a batch reactor. The volume of the polymerizing mixture can be given by:

$$V = V_0 (1 + \varepsilon x) \quad (3.86)$$

where ε is the volume contraction (shrinkage) factor (due to the difference in monomer and polymer densities):

$$\varepsilon = \left(\frac{\rho_0}{\rho_{\text{final}}} - 1 \right) \leq 0 \quad (3.87)$$

The subscript zero denotes initial conditions (at time $t = 0$) and ρ_{final} is the density of the polymerizing mixture at $x = 100\%$ conversion of monomer to polymer.

Combining Equation 3.9 with 3.85, and considering that by definition:

$$x = \frac{M_0 - M}{M_0} \quad (3.88)$$

one can obtain the following ordinary differential equation for the rate of change of monomer conversion, x :

$$\frac{dx}{dt} = \frac{k_p}{k_t^{1/2}} (1-x)(2fk_I[I])^{1/2} \quad (3.89)$$

$[M]$, the monomer concentration in Equation 3.85 is given by (M/V) . Similarly, $[I]$, the concentration of initiator at any time t , in Equation 3.89, is given by (I/V) , where I denotes the number of moles of initiator at time t . Equation 3.89 can be combined with a balance on initiator:

$$\frac{dI}{dt} = -k_I I \quad (3.90)$$

and the set of the two ordinary differential Equations 3.89 and 3.90 can be solved with the appropriate initial conditions, that is, at $t = 0$, $x = 0$ and $I = I_0$.

The material balances for the moments of the *bulk* polymer are

$$\frac{d\zeta_k}{dt} = R_{\zeta_k} V \quad (3.91)$$

where R_{ζ_k} is given by Equations 3.70–3.72. Equations 3.70–3.72 include the zeroth and first live moments that can be calculated from Equations 3.64 and 3.65, by substituting $[\zeta_1]$ and $[\zeta_2]$ for $[v_1]$ and $[v_2]$ in Equation 3.65, and using the QSSA: $R_{\nu_k} = 0$. Eventually, cumulative average molecular weights can be calculated with Equation 3.60.

The balance for LCB is

$$\frac{dLCB}{dt} = R_{LCB} V \quad (3.92)$$

where R_{LCB} is given by Equation 3.74.

The energy balance for a batch reactor is given as

$$\frac{d(V\rho c_p T)}{dt} = V(-\Delta H_r)R_p - UA_w(T - T_w) + Q_E \quad (3.93)$$

In the above equation ρ and c_p are the density and heat capacity of the polymerizing mixture, $(-\Delta H_r)$ is the heat of polymerization, R_p the rate of polymerization (see Equation 3.10), U the overall heat transfer coefficient, A_w the available area for heat transfer (usually reactor walls), T the reactor temperature, T_w the coolant (jacket) temperature; finally, Q_E represents the heat removed by sources other than reactor jacket (condenser and/or other (external) devices).

3.4.3 Semibatch (semicontinuous) reactors

Semibatch polymerization involves the continuous or intermittent addition of monomer (and/or initiator and/or chain transfer agent) to the polymerizing mixture during polymerization. The addition of monomer (and/or other ingredients) has in general the following beneficial effects:

- (1) extra cooling of the polymerizing mixture and hence better temperature control,
- (2) the polymerizing mixture is kept “starved” for monomer and this leads to easier control of the polymerization rate,
- (3) added flexibility for molecular weight control and
- (4) better copolymer composition control.

In ordinary batch copolymerization there is usually a considerable drift in monomer composition because of different reactivities of the two monomers (based on the values of the reactivity ratios). This leads to a copolymer with a broad chemical composition distribution (CCD). In many cases (depending on the specific final product application) a composition drift as low as 3–5% cannot be tolerated, for example, copolymers for optical applications; on the other hand, during production of GRIN (gradient index) lenses, a “controlled” trajectory of copolymer composition is required. This is partly circumvented in semibatch operation where the composition drift can be minimized (i.e., copolymer composition can be kept “constant”) by feeding a mixture of the monomers to the reactor with the same rate by which each of them is consumed in the reactor.

In the absence of an azeotrope, and when one monomer is more reactive than the other in a binary batch copolymerization (e.g., $r_1 > 1$ and $r_2 < 1$), the instantaneous copolymer composition will decrease in monomer A with increase in conversion. The extent of composition drift, which leads to a copolymer heterogeneous in composition, depends on the ratio of reactivity ratios r_1/r_2 (increasing with any increase in r_1/r_2), the initial monomer composition and the monomer conversion. A copolymer which is heterogeneous in composition usually has inferior properties, therefore industrial processes have been developed to reduce composition heterogeneity. These processes are usually semibatch, but sometimes continuous as well.

There are two basic monomer feed policies which may be used in semibatch copolymerization to minimize compositional drift. Effective commercial processes are usually based on one or a combination of these feed policies.

Policy 1: All of the slower monomer, and sufficient of the faster monomer (to give the desired copolymer composition F_{p1}), are added to the reactor at time zero. Thereafter, the faster monomer is fed to the reactor with a time-varying feed rate to maintain M_1/M_2 (the ratio of the number of moles of monomers 1 and 2 in the reactor) and F_{p1} constant with time.

Policy 2: A charge of monomers 1 and 2 at the desired monomer concentration levels (to give the desired F_{p1}) is added to the reactor at time zero. Thereafter, monomers 1 and 2 are fed to the reactor with time-varying feed rates to maintain $[M_1]$, $[M_2]$ and F_{p1} constant with time.

With policy 1, the monomer concentrations are continuously falling, as with a batch copolymerization, and as a consequence, lower levels of LCB and crosslinking are obtained than with policy 2, if reactions which produce long branches are significant. A limiting form of policy 2 ($[M_1]$ and $[M_2] \sim 0$, or monomer-starved feed) can be convenient, as the composition of the copolymer is the same as the composition of monomers in the feed stream. Knowledge of reactivity ratios is thus not required. In addition, the low monomer levels preclude a runaway polymerization. A possible major disadvantage is excessive levels of LCB and crosslinking.

More details are given in Hamielec *et al.* [88], where most of these policies (or modifications of policies) were originally discussed. According to these policies, the monomer inflow rate is, in general, a function of propagation rate constants (i.e., reactivity ratios), monomer concentrations and the total radical concentration. Hence, in order to calculate the optimal monomer feed policy in order to control the polymerization rate that will yield constant copolymer composition, the total radical concentration must be specified in advance and kept at a specific constant value. This may be accomplished through either an initiator feed policy or a heat production policy, in order to keep the total radical concentration constant through the polymerization. Even further, the practical implementation of monomer feed policies requires the use of on-line (or possibly off-line) measurements to permit one to adjust for uncontrolled variations in recipe impurities (such as oxygen and other radical scavengers), which can affect radical concentration. One can thus implement a practical calorimetric control of monomer feed, and obtain eventually, for any monomer feed policy, a relationship between the instantaneous heat generation rate (related to the rate of polymerization, i.e., rate of incorporation of monomers in the copolymer) and the monomer molar feed (inflow) rate. The final relationship dictates that in order to maintain (M_1/M_2) constant for a single feed stream containing the monomers (practical implementation), one should keep the ratio of the instantaneous heat generation rate over monomer molar feed rate constant.

One should note that this ratio should be controlled at the desired level regardless of the magnitude of the total radical concentration, and hence impurities which affect the radical concentration will have no effect on copolymer composition control. The on-line measurement of heat generation rate can thus be used to set the appropriate monomer feed rate. If polymerization is too slow because of radical scavengers, one can increase the radical generation rate to compensate, and, in parallel, increase the monomer inflow rate to maintain the ratio constant (or, *vice versa* to compensate for a possible auto-acceleration operating point). Additional discussion is provided in Dubé *et al.* [56].

For a semibatch reactor, a balance on moles of monomer 1 can be written as

$$\frac{dM_1}{dt} = -R_{p1}V + F_{1in} \quad (3.94)$$

where M_1 denotes the moles of (free, unreacted, unbound) monomer 1 at any time t in the reactor, and R_{p1} is given by Equation 3.32. F_{1in} is the molar flow rate of monomer 1 into the reactor (inflow of monomer 1 for the semicontinuous operation). Similar equations can be written for monomer 2, initiator, CTA and solvent. By manipulating Equation 3.94 (and a similar one for monomer 2) one can derive the copolymer composition control policies described earlier in this section (see also references 56 and 88).

The average molecular weights and LCB are calculated using the same equations as for the batch reactor (Equations 3.91 and 3.92), because no polymer is fed in during the semibatch operation.

The heat balance is as follows:

$$\frac{d(V\rho c_p T)}{dt} = V(-\Delta H_r)R_p - Q_{in}(\rho c_p)_{in}(T - T_{in}) - UA_W(T - T_w) + Q_E \quad (3.95)$$

where the second term of the right-hand side of the equation accounts for the energy required to heat up the feed (inlet stream(s)).

3.4.4 Continuous stirred-tank reactors

For a well-mixed homogeneous CSTR, a material balance on any species h can be written as:

$$\frac{dh}{dt} = Q_{in}[h_{in}] - Q_{out}[h] - VR_h \quad (3.96)$$

V is the volume of the polymerizing mixture (reactor volume for an overflow CSTR), Q_{in} and Q_{out} are the inlet and outlet volumetric flow rates, $[h]$ denotes the concentration of species h , h denotes the number of moles of the species in question and R_h is the rate of reaction of species h . For instance, if Equation 3.96 is applied on monomer, then $[h] = [M]$, and $R_h = \text{rate of polymerization} = k_p [M][P_{tot}]$. Species h can be monomer, initiator, solvent, CTA, and any other possible ingredient in the recipe.

Similar equations can be written for the molecular weight part, for the calculation of moments. For instance, Equation 3.96 becomes as follows for the live and *bulk* moments:

$$\frac{d\mu_k}{dt} = Q_{in}[\mu_{k,in}] - Q_{out}[\mu_k] + VR_{\mu_k} \quad (3.97)$$

$$\frac{d\zeta_k}{dt} = Q_{in}[\zeta_{k,in}] - Q_{out}[\zeta_k] + VR_{\zeta_k} \quad (3.98)$$

Section 3.2.4 gives the equations for the terms R_{μ_k} and R_{ζ_k} . Cumulative molecular-weight averages are calculated by means of Equation 3.60. Equations 3.96–3.98 can readily be reduced to a batch reactor operation by setting the inflow and outflow terms equal to zero.

With reactive species (radicals) the concentration levels are very low and often inflow and outflow terms can be neglected. This approximation is referred to as the reactor steady-state approximation or hypothesis (RSSA or RSSH; see also the discussion around Equation 3.9). In the calculation of rates of polymerization the RSSA gives only a minor simplification. However, in the calculation of polymer quality the reduction in complexity is significant. When the RSSA is made, the MWD in a CSTR is the same as the instantaneous MWD in a batch reactor at comparable conditions of temperature, monomer concentration(s) and initiation rate. The RSSA, valid in most cases, may not hold for very small initiation rates and residence times, and also when branching reactions are excessive. In the latter case, if the outflow of radicals is neglected, the calculations of molecular weights will be erroneous (leading to an overestimation of molecular-weight averages or infinite molecular weights), although the calculation of polymerization rate may be correct.

An energy balance for a CSTR becomes

$$\frac{d(V\rho c_p T)}{dt} = Q_{in}(\rho c_p)_{in}(T_{in} - T) + (-\Delta H_r)VR_p - UA_w(T - T_w) + Q_E \quad (3.99)$$

where T_{in} is the inlet stream temperature, subscript “in” denotes inlet conditions, and all the other terms are as explained below Equation 3.93.

As an example, apply Equation 3.96 to a monomer balance for a steady-state overflow CSTR. Equation 3.96 becomes

$$\frac{1}{\bar{t}} ([M_{in}] - [M]) = R_p \quad (3.100)$$

or, in terms of conversion:

$$\frac{x [M_{in}]}{\bar{t}} = R_p \quad (3.101)$$

The term \bar{t} is the mean residence time of the overflow CSTR ($Q_{in} = Q_{out} = Q$), equal to the ratio of reactor volume V and volumetric flow rate Q .

Depending upon the particular polymer system, a CSTR or a series of CSTRs may offer several advantages over batch and tubular flow reactors both with respect to polymer production rate and polymer quality. With a perfectly mixed CSTR it is often possible to achieve a molecular weight distribution considerably narrower than can be obtained with a batch (or tubular) reactor with the same holdup time. This is true with any polymerization where molecular weights are controlled by termination. By running CSTRs in series or in parallel it is possible to produce tailor-made polymers with a broader MWD simply by operating each CSTR at a different temperature and/or with different residence times. Another feature of CSTRs is that the CCD can be very narrow in comparison with batch (or tubular) reactors, where the CCD is broadened due to the drift in monomer composition.

It is also possible to operate a CSTR at a considerably higher production rate than in a comparable batch (or tubular) reactor. The higher rates which can in principle be achieved in a CSTR also make certain copolymerizations commercially feasible (as they would otherwise be too slow for practical use). Due to the beneficial effects of the cold monomer feed, heat removal in CSTRs is not as serious a problem and therefore higher specific polymerization rates can be tolerated. Typical calculations (compare R_p for a CSTR based on a steady-state version of Equation 3.99 with the R_p for a batch reactor based on a steady-state version of Equation 3.93) indicate that for a set of given conditions, heat removal by flow permits a specific polymerization rate in a CSTR which is almost twice that in a batch reactor of the same volume and heat removal capacity via heat transfer surface area. This advantage of the CSTR vanishes when the residence time takes on very large values. The almost instantaneous heat-up of cold monomer feed to the specific polymerization temperature eliminates the production of higher molecular weight polymer during such a heat-up period (which can be a serious drawback for batch reactors). Batch-to-batch variations are virtually eliminated in CSTRs and reactor clean-up may in general be more efficient.

Typical examples of polymer production in CSTRs include styrene-butadiene rubber (SBR), acrylonitrile-butadiene rubber (NBR) and polychloroprene in CSTR trains; polystyrene and its copolymers; PVC and PVAC (and their copolymers); and LDPE.

In the design of polymer reactors, polymerization temperature is most often dictated by the specified polymer quality characteristics (molecular-weight averages and distribution) and not specific polymerization rate. Therefore, once the production rate is specified and the polymerization temperature chosen in the design of a CSTR, mass and energy balances may be uncoupled (under the assumption that agitation is adequate to give an essentially uniform temperature through the polymerizing mixture).

When the rate of polymerization varies linearly (or decreases) with conversion over the entire conversion range, the mass balance equation for monomer will have one solution, giving a single operating point for the CSTR with any given residence time. However, due to diffusional limitations ("gel effect," see Section 3.2.3), the rate of polymerization curve most often exhibits an autoaccelerating behavior (i.e., the polymerization rate increases with increasing conversion over a certain portion of conversion). In such cases, the monomer mass balance equation will, for certain residence times, have more than one solution, leading to the possibility of multiple (stable and unstable) operating points, often referred to as multiple steady-states (this multiplicity depends on the non-linearity of the mass balance; additional multiplicity may arise from the energy balance). Multiple steady-states may not be observed in practice in many systems because the polymerization is usually controlled at relatively low conversions where the viscosity of the polymerizing mixture is not too high. The subject of multiple steady-states has been analyzed in detail both theoretically and experimentally in the work by Ray (see, e.g., the recent articles by Papavasiliou and Teymour [89] and Pinto and Ray [90], and the one by Schmidt *et al.* [91], for an overview of the area).

In a CSTR, one can consider two classes of fluid, microfluid and macrofluid, and these represent the extremes of mixing in a CSTR, perfect micromixing and segregated flow, respectively. In segregated flow the incoming fluid is broken up into elements of undefined size and shape, but which are small compared to the reactor volume. These fluid elements are uniformly distributed in the reactor and have a residence time distribution (RTD) given by the ideal RTD of a CSTR. There is no mass transfer between single fluid elements and the CSTR becomes effectively a collection of minibatch reactors in parallel with different reaction times. There is a spatial distribution of conversion and concentration on a microscopic scale. However, a (macro) sample taken in the exit stream and from the reactor would indicate equal concentration and conversion. A segregated reactor is indicated by SCSTR. With complete micromixing, on the other hand, the incoming fluid elements rapidly lose their identity as a consequence of rapid mass transfer between fluid elements in the reactor. The spatial distribution of species concentrations is uniform on a microscopic scale. This situation is identified by the symbol HCSTR (homogeneous CSTR).

The effective approach of the fluid to the mixing state depends upon the diffusion coefficients of the species, the speed of polymerization rates and the reactor mean residence time. When the diffusion time is long compared to polymerization time or residence time, then the fluid may be treated as if in segregated flow, for all practical purposes. In most homogeneous polymerizations the interplay between monomer diffusion times (relatively short) and polymerization times (relatively long) is such that approximately micromixed behavior is expected, except at very high viscosities (low diffusion coefficients, very high polymerization rates due to diffusion-controlled steps). For homogeneous polymerizations involving linear polymers the rates of polymerization for HCSTR and SCSTR are not very different, and when transfer reactions (to small molecules) govern molecular weight development

the MWDs obtained are also not very different. Calculations based on HCSTR and SCSTR provide upper and lower bounds on the time behavior in the reactor.

Balances for an HCSTR have been discussed above (Equations 3.96–3.99). In a SCSTR, the average value at the exit of the reactor of any additive quantity, \bar{X} (conversion of monomer(s), initiator, moments of living and dead chains) is given by the following equation:

$$\bar{X} = \int_0^{\infty} E(t)X(t) dt \quad (3.102)$$

where $E(t)$ is the RTD and $X(t)$ the value of the quantity in question calculated by integrating the batch balances (Equations 3.85–3.91) up to time t . The average molecular weights are calculated from Equation 3.60 using the average values of $\bar{\zeta}_k$ calculated from Equation 3.102.

Observations for micromixed fluids (HCSTR):

- (1) In designing a polymer reactor one usually specifies the polymerization temperature to give a desired MWD and also specifies the maximum conversion based on mixing, heat transfer and pumping limitations. For many commercial monomer systems (e.g., vinyl chloride, vinyl acetate), transfer to monomer controls molecular weight and/or chain transfer agents are also used. In these instances the rate of initiation would not affect molecular weights and hence, in reactor design, a certain relationship between initiation rate and residence time is established. The normal procedure to use, both in the design of a new reactor and in the increase of the capacity of an existing reactor, is to employ the largest possible value of the initiation rate to give the smallest residence time with the constraint that heat generation cannot exceed the heat removal capability of the system.
- (2) The MWD is the same as the instantaneous MWD in a batch reactor at the same temperature, initiation rate and conversion (for linear chains). In a batch polymerization, since monomer/radical concentrations and rate constants for termination may vary significantly with conversion, the cumulative MWD would be broader than in a comparable HCSTR.
- (3) In practice, a fundamental difference between CSTR and batch reactors is that at comparable conditions of temperature and conversion, the branching frequency is always higher and the MWD is always broader in the former reactor type. This is because branching reactions occur more frequently at a higher polymer concentration. In a CSTR operating at some conversion level, the concentration of polymer is always higher than the average concentration of polymer in a batch reactor with the same final conversion. Consequently, the polydispersity ratio increases faster in a CSTR than in a batch reactor in the presence of branching reactions.

Observations for segregated fluids (SCSTR):

- (1) Real flow/mixing regimes in polymer reactors will always lie somewhere in between the extremes of HCSTR and SCSTR. The best one can do is calculate upper and lower bounds. The usefulness of these calculations will depend on two factors, the difference between the upper and lower bound and how close the real fluid behaves to one of

- the limiting fluids. The HCSTR approach is certainly valid for systems where the polymer concentration (and, hence, the viscosity) is not excessively high. However, when the RTD is non-ideal, it may be worthwhile to approach the situation as an SCSTR.
- (2) In practice, if transfer reactions (to small molecules) govern molecular weight development, molecular-weight averages for HCSTR, SCSTR and batch reactors are almost identical.
 - (3) If the viscosity of a polymerizing mixture is relatively independent of residence time, then the polymerizing mixture should be closer to complete micromixing (HCSTR) the longer the residence time. However, in polymer reactors operating at relatively high conversions, the viscosity increases strongly with increasing residence time. Hence, the effect of a higher viscosity may very well exceed the effect of larger residence times, such that the degree of micromixing decreases with increasing residence time.
 - (4) For most practical purposes, the discrimination between HCSTR and SCSTR may be of minor importance for commercial homopolymerizations in homogeneous systems. However, the effect may be very important for copolymerizations. In an HCSTR there is no composition drift and the copolymer composition in the exit stream is uniform and given by the copolymer composition (Mayo–Lewis) equation (Equation 3.35). A deviation from micromixing would lead to significant broadening of the CCD. Hence, in a SCSTR, the CCD is very broad and product quality is compromised. It is therefore most important to achieve the highest possible degree of micromixing in a CSTR during production of copolymers. Micromixing can be satisfactorily achieved even in bulk copolymerization up to reasonable (medium) conversion levels. However, very high conversions, even if tolerable from the standpoints of heat transfer and pumping, should be avoided because the high viscosities can lead to significant deviations from micromixing.

More details on mixing phenomena in CSTRs can be found in the book by Biesenberger and Sebastian [92], in work emanating from German academic and industrial units (e.g., see DECHEMA course notes [93–95], just to mention a few representative sources), and in Atiqullah and Nauman [96] and Kim and Nauman [97].

It has been pointed out already that MWDs obtained in CSTRs can be broadened by operating a reactor train with temperature or residence time variations from reactor to reactor. Another way of broadening the MWD involves the periodic operation of a CSTR and, in particular, cycling of the initiator feed. Cycling of other reactor variables such as temperature and monomer feed concentration is generally not practical because reactor response times are too slow at high frequencies, whereas low frequencies may result in substantial (undesirable) oscillations in reactor outputs. A key operational variable in this case is the ratio of the period of the forced oscillation of initiator feed over the initiator half-life (and, of course, the ratio of reactor residence time over the period of the forced oscillation). A large change in product polydispersity can be obtained with a large variation in the initiation rate during the period of the forced oscillation. This is best achieved with a residence time long enough to permit the initiator pulse to essentially completely decay in the reactor and with a period of the forced oscillation long enough to permit this decay to occur before a new pulse of initiator is injected into the reactor. Such a technique may or may not be promising for commercial CSTR operation, yet it may be applicable during the continuous reactive modification of polymers in extruders (e.g., see reference 98).

A special type of continuous reactor operation involves loop reactors. These reactors have been used in polyolefin production and also in emulsion and suspension polymerization. A recent overview in homogeneous polymerizations is provided by reference 99 (solution polymerization).

For the economic production of polymers, it is necessary to recover and recycle unreacted monomer (and solvent). Associated with recycle streams (and by no means only limited to CSTR operation) is the recycle of impurities (which are introduced into the system in the fresh monomer (or solvent) feed or other feed streams (initiator, etc.) or via side reactions). If the recycle streams are not properly purged, impurity levels may build up in the reactor to the point where reactor performance is significantly influenced. Two kinds of impurities can be distinguished, those that are inert and those which react with radicals in the system. The build up of inert impurities in the reactor will reduce the rate of polymerization through a simple dilution effect (both monomer and initiator concentrations are lowered). The build up of inert impurities to significant levels can easily be detected with experimental analytical techniques, hence the solution to this problem is relatively straightforward. Reactive impurities, which can significantly lower both the rate of polymerization and molecular weights even when present at very low concentrations, present a far more difficult problem. A discussion of impurity effects in solution polymerization (and emulsion polymerization, where the effects can be largely unexpected and counterintuitive) can be found in references 100–104 (artifacts due to impurities in discriminating between terminal and penultimate models in copolymerizations; see also Section 3.5).

3.4.5 Tubular reactors

In the commercial production of polymers the use of tubular reactors has serious limitations. With bulk/solution polymerization the viscosity of the polymerizing mixture reaches very high values from intermediate conversion levels, thus leading to highly distorted velocity, temperature and concentration profiles. This enhances operational difficulties associated with temperature control. Furthermore, due to uneven polymerization rates, this leads to a broadening of the molecular weight distribution of the final product. Some streamlines may be hot, resulting in hot spots, while others remain relatively cool. Hot spots are of concern as a potential quality and safety hazard. Another serious problem is that the polymer tends to form a thick layer on the tube wall, thereby reducing the capacity of the reactor and also the overall heat transfer coefficient. If the viscosity is relatively independent of monomer conversion, fluid mechanical factors associated with heat transfer and pumping could be handled, permitting high conversions to be reached. Of course, many of these problems may be overcome through the use of a CSTR train where plug flow can be closely approached.

Tubular reactors are used commercially in the production of LDPE at high temperatures (150–250°C) and pressures (1000–3000 atm). Tubular and/or unagitated tower reactor designs have been used with styrene and high-impact polystyrene (HIPS) polymerization processes, principally as finishing reactors when cooling requirements are small. A combination of CSTR/loop reactor followed by a tower (plug flow) reactor has been described in reference 85, whereas safety aspects have been addressed in Hungenberg *et al.* [105].

Large temperature gradients broaden the MWD significantly. Axial and radial gradients in monomer and initiator concentration add further broadening of the MWD and these effects may be appreciable if high conversions are reached. On the other hand, if transfer to monomer/CTA controls molecular weights, then concentration gradients will have no effect on the MWD, and furthermore, temperature gradients will have a milder effect on the breadth of the distribution. Particularly interesting is the effect of tube diameter and reactor wall temperature on reactor performance. Larger tube diameters and higher wall temperatures give higher throughput and hence result in lower reactor cost. However, a larger tube diameter also results in a steeper radial temperature gradient, which in turn may lead to a less homogeneous product (broader MWD). Operating conditions therefore consist of a compromise between production cost and product quality. Since initiator consumption rate increases more rapidly with temperature than monomer consumption rate, at sufficiently high temperatures the initiator is used up already at lower monomer conversions, thus leading to a decrease in conversion with increasing wall temperature. An increase in initiator concentration gives a larger temperature difference between wall and tube centre. Thus, in addition to the direct kinetic effect of initiator concentration on production rate there is an indirect thermal effect. A smaller tube has the tendency to give higher molecular weights because of lower polymerization temperature and smaller polydispersity index because of more uniform temperature distribution. In general, increasing reactor wall temperature, reactor radius and initiator concentration causes

- (1) conversion to increase to a maximum value after which it rapidly falls,
- (2) molecular-weight averages to decrease and
- (3) polydispersity index to increase.

Many papers have been published in the last 20 years or so on modeling and simulation analysis of tubular reactors. It is difficult to make a clear statement on the validity of these analyses usually because of the lack of experimental verifications. When the velocity profile varies along the tube, a prediction of reactor performance is not much more complex theoretically, but its application to real systems is very difficult (if not impossible) because of lack of information on how the velocity profile changes along the tube at high monomer conversions (and viscosities).

Representative recent analyses of homogeneous polymerizations in tubular scenarios with experimental verifications include the following sources: Biesenberger and Sebastian [92]; Baillagou and Soong [106], MMA polymerization; Hamer and Ray [107], vinyl acetate polymerization; Reichert and Moritz [93], RTD of continuous polymerization reactors and polymerization in laminar-stirred tubular reactors including acrylamide and vinyl acetate; Chen and Nauman [108], styrene polymerization with variable viscosity model; Mallikarjun and Nauman [109], crystal polystyrene with near-adiabatic tubular reactor followed by a shell-and-tube devolatilization preheater; Zabisky *et al.* [62], LDPE polymerization; Cunningham *et al.* [110], MMA bulk polymerization, production of low molecular weight material (and subsequent fouling studies); Brandolin *et al.* [111], ethylene polymerization in industrial reactors; Vega *et al.* [112], styrene solution polymerization; Cavin *et al.* [113], bulk styrene polymerization in a loop tubular reactor followed by a tubular reactor filled with static mixers (recycle reactor); Kim and Nauman [114], anionic polymerization of styrene; Murphy *et al.* [115], studies with mixers for fast-living anionic

polymerizations; Kiparissides *et al.* [116], ethylene copolymerization with acrylates and vinyl acetate; Kondratiev and Ivanchev [117], optimizing reactor performance for LDPE cases (tubular and autoclave reactors).

Computational fluid dynamics (CFD) approaches are emerging as alternative detailed tools for examining polymerization systems with complex mixing and reactor components. Recent examples on LDPE cases include: Kolhapure and Fox [118], micromixing effects in tubular reactors; Zhou *et al.* [119], tubular (and autoclave) reactors; Wells and Ray [120], analysis of imperfect mixing effects applicable to many reactive flow systems, including LDPE autoclaves and Buchelli *et al.* [121], fouling effects.

High-pressure autoclaves for LDPE production represent a special class of (usually elongated) reactors, the analysis of which is handled via combinations of well-mixed and plug flow (with recycle) reactor elements. Information and models can be found in references 122–126.

For a practically useful tubular reactor model, the reacting (polymerizing) mixture is considered homogeneous and only axial dispersion is considered. At each specific position along the tube, perfect radial mixing and a uniform velocity profile are assumed. The tube, therefore, can be modeled as a one-dimensional tubular reactor. Also, instantaneous fluid dynamics are assumed because of the incompressibility of the liquid mixture (hence the calculation of the velocity profile is simplified).

A mass (material) balance equation for each chemical species h is given by:

$$\frac{\partial [h]}{\partial t} + \frac{\partial (u_z [h])}{\partial z} - D_a \frac{\partial^2 [h]}{\partial z^2} = R_h \quad (3.103)$$

where $[h]$ is the concentration of species h , u_z the bulk average axial velocity, z the axial direction of the tube, D_a is a dispersion coefficient (usually, an empirical axial dispersion coefficient is used to describe the axial mixing in the tube and to characterize the RTDs) and R_h denotes the reaction rate term for species h (negative for consumption). Species h can represent monomer(s), initiator, solvent, CTA and the moments of the MWD (see Section 3.2.4 for the equations describing the term R_h for the moments of the live and *bulk* polymer). Average molecular weights are calculated by substituting for the values of ζ_k in Equation 3.60.

The energy balance equation can be written as

$$\frac{\partial T}{\partial t} + \frac{\partial (u_z T)}{\partial z} - \alpha_{\text{eff}} \frac{\partial^2 T}{\partial z^2} = \frac{1}{\rho c_p} \left[(-\Delta H_r) R_p - U \frac{2}{r_{\text{tube}}} (T - T_w) \right] \quad (3.104)$$

where α_{eff} is an effective thermal diffusivity, r_{tube} the radius of the tube, and the rest of the terms have been explained in Sections 3.4.2 and 3.4.4. For a steady-state plug-flow model, the first term of the left-hand side of Equations 3.103 and 3.104 is set equal to zero.

Equations 3.103 and 3.104 require one initial condition and two boundary conditions. Usually, a uniform initial condition is imposed for all species. At the reactor (tube) entrance, Danckwert's boundary conditions are used:

$$[h]_{z=0} = [h]_{\text{in}} + D_a \left[\frac{1}{u_z} \frac{d[h]}{dz} \right]_{z=0} \quad (3.105)$$

$$T_{z=0} = T_{\text{in}} + \alpha_{\text{eff}} \left[\frac{1}{u_z} \frac{dT}{dz} \right]_{z=0} \quad (3.106)$$

whereas zero gradients are assumed at the tube exit:

$$\left[\frac{\partial [h]}{\partial z} \right]_{z=1} = 0 \quad (3.107)$$

$$\left[\frac{\partial T}{\partial z} \right]_{z=1} = 0 \quad (3.108)$$

3.5 A “roadmap” for mathematical modeling

Comprehensive polymerization models may be used by scientists and engineers to reduce the time required to develop new polymer products and advanced production processes for their manufacture as well as to optimize existing processes.

Why, then, are models useful?

- (1) Models enhance our process understanding since they direct further experimentation. They act as the reservoir of our knowledge about a process, and hence they may reveal interactions in a process that may be difficult, if not impossible, to visualize/predict solely from memory or experience, especially when many factors vary simultaneously. Since a model is a concise, compact form of process knowledge, models enhance transferability of knowledge; they may act eventually as an “inference engine”, closely resembling the train of thought of an experienced human. In a sense, mathematical modeling is the best way to find out what one does not know about a process!
- (2) Models are useful for process design, parameter estimation, sensitivity analysis and process simulation. The significance of these is quite obvious. A valid model allows one to test deviations from process trajectories using a simulator in lieu of running experiments. Cost effectiveness implications are also obvious.
- (3) Models are useful for process optimization, especially when dealing with highly non-linear problems such as grade changes/switchovers in batch, semibatch and continuous reactors. Extensions to recipe modifications and design are another application.
- (4) Models are useful for safety/venting considerations. It is very useful to be able to extrapolate to different operating conditions and anticipate “worst-case scenarios” or investigate the possible effects of process factors. In this case one may be better prepared to tackle situations that might not always be apparent from the outset.
- (5) Models are useful for optimal sensor selection and testing, sensor location, filtering and inference of unmeasured properties and process control. The trends nowadays in process control are toward “model-based” control, and, as the term signifies, application of advanced control techniques may not be possible without a model.
- (6) Finally, since a model contains process knowledge and is transferable, interactive models are extremely useful for the education and training of new (and old) personnel.

In addition to the material and energy balances presented above, a “roadmap for modeling” will now be provided, describing basic steps in the modeling (computer simulation) exercise and linking them to key references in the literature, followed

by representative examples of polymerization systems. This roadmap can also serve as the basis for undergraduate and graduate courses in polymer reaction engineering aspects.

- Classical sources of modeling information and mathematical models (material/mass balances for species, energy balances and population balances for radicals and (dead) polymer molecules) can be found in texts by Biesenberger and Sebastian [92] and Dotson *et al.* [127], and in the classical paper by Ray [54].
- Bulk and solution (and several suspension and precipitation polymerization systems) can be modeled as homogeneous single-phase systems, or using a monomer-rich and a polymer-rich phase. The level of model sophistication and detail depends upon the intended use of the model. By their nature, these mathematical models are “semi-mechanistic” or “semi-empirical”, indicating that they are based on polymerization mechanisms with the inevitable use of certain (often many) parameters.
- Translated into computer code, these model equations are solved numerically (with the appropriate initial and/or boundary conditions). They are then combined with experimental data for parameter estimation, sensitivity studies and investigation (corroboration) of model trends.
- Validity of the stationary (steady) state hypothesis (SSH) for radicals (see QSSA of Section 3.2.1.1): (1) Determine the maximum rate of change (with time) of the total radical concentration; (2) Divide (1) by the rate of initiation; (3) If the ratio (plotted versus conversion or any other reaction indicator, e.g., crosslinker concentration or mole fraction) is much less than unity, the SSH is valid. Alternatively, one can check the ratio of propagation rate constant over the (number-average) termination rate constant, evaluated at different conversion levels. If the ratio is less than 0.001, the SSH is valid. More details can be found in references 128–131.
- Information and modeling equations for diffusional limitations in polymerizations (termination and propagation rate constants, and initiator efficiency) are summarized in the (nowadays) classical references by O’Driscoll [132], Marten and Hamielec [133], Soh and Sundberg [50], Hamielec [134], Chiu *et al.* [135], Tirrell [136], Stickler *et al.* [137] and Louie *et al.* [51]. These sources cover the basic concepts from free volume, entanglement and reptation theories for segmental and translational diffusion and reaction-diffusion. Excellent extensions can be found in: Li *et al.* [138] and Hutchinson [61], effect of cross-linkers; Russell *et al.* [47], termination at high conversion and initiator efficiencies; Zhu and Hamielec [128], chain-length dependent termination; Anseth and Bowman [139], reaction-diffusion enhanced termination with multifunctional monomers; Buback *et al.* [140, 141], modeling termination kinetics using a reduced number of parameters and under non-stationary conditions, respectively; Achilias and Kiparissides [142], general mathematical framework for diffusion-controlled polymerizations; Vivaldo-Lima *et al.* [143], comparisons of models for diffusion-controlled polymerizations and copolymerization kinetics up to high conversions with divinyl benzene and Tefera *et al.* [144], modeling up to high conversions with case studies of styrene and MMA. A recent balanced evaluation of free volume approaches to describe the gel effect in FRPs is given by O’Neil and Torkelson [48] and O’Neil *et al.* [49]. Further applications and case studies are given in Hamielec *et al.* [88], Dubé *et al.* [56], Gao and Penlidis [66–68] and Dhib *et al.* [145]. See also the discussion in Section 3.2.3.

- Issues in non-linear parameter estimation (both from single response and multi-response data) are closely linked with mathematical models of polymerization reactors. Vivaldo-Lima *et al.* [143] discussed issues in parameter estimation with the “gel-effect” part of polymerization models. Tefera *et al.* [52] described a method for the selection of models (at high conversions under diffusion-controlled conditions) by simultaneous parameter estimation. Goodner *et al.* [146] suggest a methodology for determining kinetic parameters in diffusion-controlled homopolymerizations of methacrylates and dimethacrylates. The kinetic parameters found via their analysis are unique for a given set of rate versus conversion data. Of course, as our understanding of polymerization processes increases, the complexity of the models developed to describe them also increases. In most of the cases, the equations are highly non-linear in inputs and parameters, and parameters must be estimated from multi-response data. There are usually two shortcomings during (multi-response) non-linear parameter estimations. How effective is the present parameter estimation methodology when applied to such complex models? What advantages can be gained from considering the parameter estimation problem as a whole (i.e., parameter sensitivity analysis, statistical design of experiments, estimation of parameters, and calculation of joint confidence regions)? Polic *et al.* [147] suggest a protocol for the estimation of parameters in complex polymerization models, and present guidelines for two case-studies, one for estimating five parameters during homopolymerization of styrene, and another for estimating five parameters during copolymerization of styrene/MMA. The first case-study uses five response variables (conversion and molecular-weight characteristics), while the second uses seven response variables (conversion, composition, molecular weight and sequence length (triad fractions) characteristics). Parameter estimation for reactivity ratios in copolymerizations has recently been reviewed, with case studies, in reference 148. Finally, a practical approach to simulate polymerizations with minimal information is given in Lona and Penlidis [149]. The approach can be applied successfully if a few or even no parameters (kinetic and/or diffusional) are available.
- The first publications on the modeling of controlled-radical (“living radical”) polymerizations appeared in the early 1990s. Recent representative case studies and modeling reviews include: Bonilla *et al.* [150], modeling of nitroxide-mediated polymerization of styrene; Vivaldo-Lima and Mendoza-Fuentes [151], INIFERTER controlled-radical polymerization; Zhang and Ray [152], modeling in batch, semibatch and continuous reactors, and validation with experimental data for nitroxide-mediated styrene homopolymerization and atom transfer radical copolymerization of styrene/butyl acrylate; Zhang and Ray [153], controlled-radical polymerization in tubular reactors and effect of degree of backmixing on copolymer properties; Delgadillo-Velazquez *et al.* [154], effects of diffusion-controlled steps on atom transfer radical polymerization; Saldivar-Guerra *et al.* [155], alkoxyamine-mediated radical polymerization of styrene. See also Section 3.3.
- The development of (semi) mechanistic process models certainly facilitates many engineering activities including process design, optimization and process control. Engineers and scientists spend a great deal of time estimating parameters, validating models and developing process simulations. But before embarking on such work, how does one decide which model is the “best” model for a process? There are often several models which seem reasonable, and the first problem is to efficiently find the “best” model. This is one of the problems that exist in the area of copolymerization modeling. A number

of models have been proposed for copolymerization kinetics, and at the beginning of a study there is often uncertainty with respect to which one of the models is “best.” Despite the large number of papers that have appeared on the modeling of copolymerization kinetics, there is still healthy debate as to which model is “best” for specific systems of interest and which measurement(s) should be used to elucidate the kinetics.

- Statistical model discrimination methods have been designed specifically for this type of problem. They describe how to design experiments which provide the maximum amount of information with respect to discrimination. They also explain how to analyze the resulting data to determine which of the models provides the “best” description of the system. Several methods have been proposed in the statistics and engineering literature.
- Statistical model discrimination methods have also been compared with past practice in the area of copolymerization. The comparison shows that, although a rigorous statistical analysis has been used in many studies, most employ poorly designed experiments. Therefore, the use of model discrimination methods should improve our ability to discriminate between competing copolymerization models by improving the information obtained from experiments.
- Although the application of model discrimination methods should improve our ability to discriminate, there are still many questions to be answered. How much will the application of model discrimination methods improve copolymerization modeling? Which model discrimination method is the most reliable and efficient? Which of the available copolymerization measurements (copolymer composition, triad fraction or rate data) will provide the most information?
- An overview of the answers to the above questions has been given in Burke *et al.* [156], analyzing differences between the terminal model and penultimate model versions in copolymerization scenarios. These are examples of rigorous model discrimination techniques applied for the first time to complex, non-linear mechanistic models with multi-response measurements. Experimental verification of statistical discrimination techniques with the styrene/MMA system can be found in Burke *et al.* [157]. The above studies considered copolymer composition, polymerization rate and triad fraction data (and combinations thereof) as responses, whereas Landry *et al.* [158] extended the ideas by including molecular weight data as well. Can model discrimination, whether based on our understanding of polymerization mechanisms or on statistical model discrimination methodology, be biased depending on the response(s) used? An extremely interesting question rarely considered is whether simple impurity effects (representing also other potentially lurking bias factors) could lead to incorrect choices about the copolymerization mechanism itself. Landry *et al.* [104] addresses the above questions showing in several case-studies that reactive impurities do (adversely) affect the model discrimination process and, what is more, they may mislead researchers as to the choice of the copolymerization mechanism. This (somehow unexpected) result is further illustrated with commonly collected experimental data.

References

1. Moad, G. and Solomon, D.H. (1995) *The Chemistry of Free-Radical Polymerization*. Elsevier Science Inc., Tarrytown, New York.

2. Matyjaszewski, K. and Davis, T.P. (eds) (2002) *Handbook of Radical Polymerization*. John Wiley & Sons, Inc., New York.
3. Hutchinson, R.A. (2005) Free-radical polymerization: homogeneous. In T. Meyer and Keurentjes (eds), *Handbook of Polymer Reaction Engineering*. John Wiley & Sons, Inc., New York, pp. 153–212.
4. Heuts, J.P.A. and Russell, G.T. (2006) *Eur. Polym. J.*, **42**, 3–20.
5. Brandrup, J., Immergut, E.H. and Grulke, E.A. (eds) (1999) *Polymer Handbook*, 4th edn. John Wiley & Sons, Inc., New York.
6. Tobita, H. and Hamielec, A.E. (1991) *Polymer*, **32**, 2641–2647.
7. Buback, M., Klingbeil, S., Sandmann, J., Sderra, M.-B., Vögele, H.P., Wackerbarth, H. and Wittkowski, L.Z. (1999) *Phys. Chem.*, **210**, 199–221.
8. Buback, M. and Sandmann, J.Z. (2000) *Phys. Chem.*, **214**, 583–607.
9. Olaj, O.F., Bitai, I. and Hinkelmann, F. (1987) *Makromol. Chem.*, **188**, 1689–1702.
10. Beuermann, S. and Buback, M. (2002) *Prog. Polym. Sci.*, **27**, 191–254.
11. Barner-Kowollik, C., Buback, M., Egorov, M., Fukuda, T., Goto, A., Olaj, O.F., Russell, G.T., Vana, P., Yamada, B. and Zetterlund, P.B. (2005) *Prog. Polym. Sci.*, **30**, 605–643.
12. Lacić, I., Beuermann, S. and Buback, M. (2004) *Macromol. Chem. Phys.*, **205**, 1080–1087.
13. Raghuram, P.V.T. and Nandi, U.S. (1969) *J. Polym. Sci.: Part A-1*, **7**, 2379–2385.
14. Ehrlich, P. and Mortimer, G.A. (1970) *Adv. Polym. Sci.*, **7**, 386–448.
15. Campbell, J.D., Teymour, F. and Morbidelli, M. (2003) *Macromolecules*, **36**, 5491–5501.
16. Hui, A.W. and Hamielec, A.E. (1972) *J. Appl. Polym. Sci.*, **16**, 749–769.
17. Hutchinson, R.A., Paquet, D.A. Jr, Beuermann, S. and McMinn, J.H. (1998) *Ind. Engng Chem. Res.*, **37**, 3567–3574.
18. Grady, M.C., Simonsick, W.J. Jr and Hutchinson, R.A. (2002) *Macromol. Symp.*, **182**, 149–168.
19. Graessley, W.W., Hartung, R.D. and Uy, W.C. (1969) *J. Polym. Sci.: Part A-2*, **7**, 1919–1935.
20. Randall, J.C. (1989) *J.M.S.-Rev. Macromol. Chem. Phys.*, **C29**, 201–317.
21. Peck, A.F.N. and Hutchinson, R.A. (2004) *Macromolecules*, **37**, 5944–5951.
22. Plessis, C., Arzamendi, G., Leiza, J.R., Schoonbrood, H.A.S., Charlot, D. and Asua, J.M. (2000) *Macromolecules*, **33**, 4–7.
23. Tidwell, P.W. and Mortimer, G.A. (1965) *J. Polym. Sci.: Part A*, **3**, 369–387.
24. van Herk, A.M. and Dröge, T. (1997) *Macromol. Theory Simul.*, **6**, 1263–1276.
25. Meyer, V.E. and Lowry, G.G. (1965) *J. Polym. Sci.: Part A*, **3**, 2843–2851.
26. Fukuda, T., Kubo, K. and Ma, Y.-D. (1992) *Prog. Polym. Sci.*, **17**, 875–916.
27. Buback, M., Feldermann, A., Barner-Kowollik, C. and Lacić, I. (2001) *Macromolecules*, **34**, 5439–5448.
28. Kostanski, L.K. and Hamielec, A.E. (1992) *Polymer*, **33**, 3706–3710.
29. Hakim, M., Verhoeven, V., McManus, N.T., Dubé, M.A. and Penlidis, A. (2000) *J. Appl. Polym. Sci.*, **77**, 602–609.
30. Buback, M. and Wittkowski, L. (2000) *Macromol. Chem. Phys.*, **201**, 419–426.
31. Buback, M., Wittkowski, L., Lehmann, S.A. and Mähling, F.-O. (1999) *Macromol. Chem. Phys.*, **200**, 1935–1941.
32. Buback, M. and Dietzsch, H. (2001) *Macromol. Chem. Phys.*, **202**, 1173–1181.
33. Buback, M. and Kowollik, C. (1999) *Macromolecules*, **32**, 1445–1452.
34. Buback, M. and Feldermann, A. (2002) *Aust. J. Chem.*, **55**, 475–481.
35. Wittmer, P. (1971) *Adv. Chem. Ser.*, **99**, 140–174.
36. McManus, N.T., Penlidis, A. and Dubé, M.A. (2002) *Polymer*, **43**, 1607–1614.
37. Lowry, G.G. (1960) *J. Polym. Sci.*, **42**, 463–477.
38. Badeen, C. and Dubé, M.A. (2003) *Polym. React. Engng*, **11**, 53–77.
39. Li, D., Leiza, J.R. and Hutchinson, R.A. (2005) *Macromol. Theory Simul.*, **14**, 554–559.
40. Li, D., Grady, M.C. and Hutchinson, R.A. (2005) *Ind. Engng Chem. Res.*, **44**, 2506–2517.

41. Schoonbrood, H.A.S., Pierik, S.C.J., van den Reijen, B., Heuts, J.P.A. and German, A.L. (1996) *Macromolecules*, **29**, 6717–6723.
42. McCord, E.F., Shaw, W.H. Jr and Hutchinson, R.A. (1997) *Macromolecules*, **30**, 246–256.
43. Plessis, C., Arzamendi, G., Leiza, J.R., Schoonbrood, H.A.S., Charriot, D. and Asua, J.M. (2001) *Macromolecules*, **34**, 5147–5157.
44. Yamada, B., Oku, F. and Harada, T. (2003) *J. Polym. Sci.: Part A: Polym. Chem.*, **41**, 645–654.
45. Vana, P., Yee, L.H., Barner-Kowollik, C., Heuts, J.P.A. and Davis, T.P. (2002) *Macromolecules*, **35**, 1651–1657.
46. Hirano, T. and Yamada, B. (2003) *Polymer*, **44**, 347–354.
47. Russell, G.T., Napper, D.H. and Gilbert, R.G. (1988) *Macromolecules*, **21**, 2133–2148.
48. O’Neil, G.A. and Torkelson, J.M. (1997) *Trends Polym. Sci.*, **5**, 349–355.
49. O’Neil, G.A., Wisnudel, M.B. and Torkelson, J.M. (1998) *Macromolecules*, **31**, 4537–4545.
50. Soh, S.K. and Sundberg, D.C. (1982) *J. Polym. Sci.: Polym. Chem. Ed.*, **20**, 1299–1313, 1315–1329, 1331–1344, 1345–1371.
51. Louie, B.M., Carratt, G.M. and Soong, D.S. (1985) *J. Appl. Polym. Sci.*, **30**, 3985–4012.
52. Tefera, N., Weickert, G. and Westerterp, K.R. (1997) *J. Appl. Polym. Sci.*, **63**, 1649–1661.
53. Verros, G.D., Latsos, T. and Achilias, D.S. (2005) *Polymer*, **46**, 539–552.
54. Ray, W.H. (1972) *J. Macromol. Sci. – Revs. Macromol. Chem.*, **C8**, 1–56.
55. Achilias, D.S. and Kiparissides, C. (1992) *J. Macromol. Sci. – Rev. Macromol. Chem. Phys.*, **C32**, 183–234.
56. Dubé, M.A., Soares, J.B.P., Penlidis, A. and Hamielec, A.E. (1997) *Ind. Engng Chem. Res.*, **36**, 966–1015.
57. Xie, T. and Hamielec, A.E. (1993) *Macromol. Chem. Theory Simul.*, **2**, 421–454.
58. Xie, T. and Hamielec, A.E. (1993) *Macromol. Chem. Theory Simul.*, **2**, 455–484.
59. Hulburt, H.M. and Katz, S. (1964) *Chem. Engng Sci.*, **19**, 555–574.
60. Baltsas, A., Achilias, D.S. and Kiparissides, C. (1996) *Macromol. Theory Simul.*, **5**, 477–497.
61. Hutchinson, R.A. (1993) *Polym. React. Engng J.*, **1**, 521–577.
62. Zabisky, R.C.M., Chan, W.M., Gloor, P.E. and Hamielec, A.E. (1992) *Polymer*, **33**, 2243–2262.
63. Arriola, D.J. (1989) *Modeling of Addition Polymerization Systems*. PhD Thesis, University of Wisconsin-Madison, USA.
64. Ochs, S., Rosendorf, P., Hyaneek, I., Zhang, X. and Ray, W.H. (1996) *Comp. Chem. Engng*, **20**, 657–663.
65. Pertsinidis, A., Papadopoulos, E. and Kiparissides, C. (1996) *Comp. Chem. Engng*, **20**, S449–S454.
66. Gao, J. and Penlidis, A. (1996) *J. Macromol. Sci. – Rev. Macromol. Chem. Phys.*, **C36**, 199–404.
67. Gao, J. and Penlidis, A. (1998) *J. Macromol. Sci. – Rev. Macromol. Chem. Phys.*, **C38**, 651–780.
68. Gao, J. and Penlidis, A. (2000) *Macromol. Chem. Phys.*, **201**, 1176–1184.
69. Tobita, H. (1993) *J. Polym. Sci.: Part B: Polym. Phys.*, **31**, 1363–1371.
70. Tobita, H. (1996) *Macromol. Theory Simul.*, **5**, 129–144.
71. Teymour, F. and Campbell, J.D. (1994) *Macromolecules*, **27**, 2460–2469.
72. Butté, A., Ghielmi, A., Storti, G. and Morbidelli, M. (1999) *Macromol. Theory Simul.*, **8**, 498–512.
73. Wulkow, M. (1996) *Macromol. Theory Simul.*, **5**, 393–416.
74. Busch, M. (2001) *Macromol. Theory Simul.*, **10**, 408–429.
75. Solomon, D.H., Rizzardo, E. and Cacioli, P. (1986) *US Patent 4581429*.
76. Georges, M.K., Veregin, R., Kazmaier, P. and Hamer, G. (1993) *Macromolecules*, **26**, 2987–2988.
77. Benoit, D., Chaplinski, V., Braslau, R. and Hawker, C.J. (1999) *J. Am. Chem. Soc.*, **121**, 3904–3920.
78. Fischer, H. (1999) *J. Polym. Sci.: Polym. Chem. Ed.*, **37**, 1885–1901.
79. Sawamoto, M., Kato, M., Kamigaito, M. and Higashimura, T. (1995) *Macromolecules*, **28**, 1721–1723.
80. Wang, J.S. and Matyjaszewski, K. (1995) *Macromolecules*, **28**, 7901–7910.

81. Chiefari, J., Chong, Y.K., Ercole, F., Krstina, J., Jeffery, J., Le, T.P.T., Mayadunne, R.T.A., Meijs, G.F., Moad, C.L., Moad, G., Rizzardo, E. and Thang, S.H. (1998) *Macromolecules*, **31**, 5559–5562.
82. Hamielec, A.E., Gomez-Vaillard, R. and Marten, F.L. (1982) *J. Macromol. Sci. – Chem.*, **A17**, 1005–1020.
83. Wu, G.Z.A., Denton, L.A. and Laurence, R.L. (1982) *Polym. Engng Sci.*, **22**, 1–8.
84. Tieu, D., Cluett, W.R. and Penlidis, A. (1994) *Polym. React. Engng J.*, **2**, 275–313.
85. Gao, J., Hungenberg, K.-D. and Penlidis, A. (2004) *Macromol. Symp.*, **206**, 509–522.
86. Scheirs, J. and Priddy, D. (eds) (2003) *Modern Styrenic Polymers*. Wiley, UK.
87. Moritz, H.U. (1989) *Chem. Engng Technol.*, **12**, 71–87.
88. Hamielec, A.E., MacGregor, J.F. and Penlidis, A. (1987) *Makromol. Chem., Macromol. Symp.*, **10/11**, 521–570.
89. Papavasiliou, G. and Teymour, F. (2005) *Ind. Engng Chem. Res.*, **44**, 2754–2766.
90. Pinto, J.C. and Ray, W.H. (1995) *Chem. Engng Sci.*, **50**, 1041–1056.
91. Schmidt, A.D., Clinch, A.B. and Ray, W.H. (1984) *Chem. Engng Sci.*, **39**, 419–432.
92. Biesenberger, J.A. and Sebastian, D.H. (1983) *Principles of Polymerization Engineering*. Wiley, New York.
93. Reichert, K.H. and Moritz, H.U. (1987) *Makromol. Chem., Macromol. Symp.*, **10/11**, 571–592.
94. Taylor, T.W. and Reichert, K.H. (1985) *J. Appl. Polym. Sci.*, **30**, 227–250.
95. Baade, W., Moritz, H.U. and Reichert, K.H. (1982) *J. Appl. Polym. Sci.*, **27**, 2249–2267.
96. Atiqullah, M. and Nauman, E.B. (1990) *Chem. Engng Sci.*, **45**, 1267–1279.
97. Kim, D.M. and Nauman, E.B. (1997) *Ind. Engng Chem. Res.*, **36**, 1088–1094.
98. Dickson, S.B., Tzoganakis, C. and Budman, H. (1997) *Ind. Engng Chem. Res.*, **36**, 1067–1075.
99. Melo, P.A., Biscaia, E.C. and Pinto, J.C. (2003) *Chem. Engng Sci.*, **58**, 2805–2821.
100. Inglis, M.P., Cluett, W.R. and Penlidis, A. (1991) *Can. J. Chem. Engng*, **69**(1), 120–129.
101. Chien, D.C.H. and Penlidis, A. (1994) *Chem. Engng Sci.*, **49**, 1855–1868.
102. Chien, D.C.H. and Penlidis, A. (1994) *Polym. React. Engng J.*, **2**, 163–213.
103. Dubé, M.A. and Penlidis, A. (1997) *J. Polym. Sci., Polym. Chem.*, **35**, 1659–1672.
104. Landry, R., Penlidis, A. and Duever, T.A. (2000) *J. Polym. Sci., Polym. Chem.*, **38**, 2319–2332.
105. Hungenberg, K.-D., Nieken, U., Zollner, K., Gao, J. and Szekely, A. (2005) *Ind. Engng Chem. Res.*, **44**, 2518–2524.
106. Baillagou, P.E. and Soong, D.S. (1985) *Polym. Engng Sci.*, **25**, 212–231.
107. Hamer, J.W. and Ray, W.H. (1986) *Chem. Engng Sci.*, **41**, 3095–3100.
108. Chen, C.C. and Nauman, E.B. (1989) *Chem. Engng Sci.*, **44**, 179–188.
109. Mallikarjun, R. and Nauman, E.B. (1989) *Polym.-Plast. Techn. Engng*, **28**, 137–149.
110. Cunningham, M.F., O’Driscoll, K.F. and Mahabadi, H.K. (1993) *Polym. React. Engng J.*, **1**, 229–244.
111. Brandolin, A., Lacunza, M.H., Ugrin, P.E. and Capiati, N.J. (1996) *Polym. React. Engng J.*, **4**, 193–241.
112. Vega, M.P., Lima, E.V. and Pinto, J.C. (1997) *Comput. Chem. Engng*, **21** (suppl.), S1049–S1054.
113. Cavin, L., Meyer, Th. and Renken, A. (2000) *Polym. React. Engng J.*, **8**, 201–223.
114. Kim, D.M. and Nauman, E.B. (1999) *Ind. Engng Chem. Res.*, **38**, 1856–1862.
115. Murphy, S.A., Meszena, Z.G. and Johnson, A.F. (2001) *Polym. React. Engng J.*, **9**, 227–247.
116. Kiparissides, C., Baltas, A., Papadopoulos, S., Congalidis, J.P., Richards, J.R., Kelly, M.B. and Ye, Y. (2005) *Ind. Engng Chem. Res.*, **44**, 2592–2605.
117. Kondratiev, J.N. and Ivanchev, S.S. (2005) *Chem. Engng J.*, **107**, 221–226.
118. Kolhapure, N.H. and Fox, R.O. (1999) *Chem. Engng Sci.*, **54**, 3233–3242.
119. Zhou, W., Marshall, E. and Oshinowo, L. (2001) *Ind. Engng Chem. Res.*, **40**, 5533–5542.
120. Wells, G.J. and Ray, W.H. (2005) *AIChE J.*, **51**, 1508–1520.
121. Buchelli, A., Call, M.L., Brown, A.L., Bird, A., Hearn, S. and Hannon, J. (2005) *Ind. Engng Chem. Res.*, **44**, 1493–1501.

122. Chan, W.M., Gloor, P.E. and Hamielec, A.E. (1993) *AIChE J.*, **39**, 111–126.
123. Kwag, B.G. and Choi, K.Y. (1994) *Ind. Engng Chem. Res.*, **33**, 211–217.
124. Zhang, S.X., Read, N.K. and Ray, W.H. (1996) *AIChE J.*, **42**, 2911–2925.
125. Brandolin, A., Sarmoria, C., Lopez-Rodriguez, A., Witeley, K.S. and Del Amo, B.F. (2001) *Polym. Engng Sci.*, **41**, 1413–1426.
126. Ghiass, M. and Hutchinson, R.A. (2003) *Polym. React. Engng J.*, **11**, 989–1015.
127. Dotson, N.A., Galvan, R., Laurence, R.L. and Tirrell, M. (1996) *Polymerization Process Modeling*. VCH Publishers, New York.
128. Zhu, S. and Hamielec, A.E. (1989) *Macromolecules*, **22**, 3093–3098.
129. Zhu, S., Tian, Y., Hamielec, A.E. and Eaton, D.R. (1990) *Macromolecules*, **23**, 1144–1150.
130. Zhu, S., Tian, Y., Hamielec, A.E. and Eaton, D.R. (1990) *Polymer*, **31**, 154–159.
131. Zhu, S. and Hamielec, A.E. (1993) *Macromolecules*, **26**, 3131–3136.
132. O'Driscoll, K.F. (1981) *Pure Appl. Chem.*, **53**, 617–626.
133. Marten, F.L. and Hamielec, A.E. (1982) *J. Appl. Polym. Sci.*, **27**, 489–505.
134. Hamielec, A.E. (1983) *Chem. Engng Commun.*, **24**, 1–19.
135. Chiu, W.Y., Carratt, G.M. and Soong, D.S. (1983) *Macromolecules*, **16**, 348–357.
136. Tirrell, M. (1984) *Rubber Chem. Techn.*, **57**, 523–556.
137. Stickler, M., Panke, D. and Hamielec, A.E. (1984) *J. Polym. Sci., Polym. Chem.*, **22**, 2243–2253.
138. Li, W.H., Hamielec, A.E. and Crowe, C.M. (1989) *Polymer*, **30**, 1518–1523.
139. Anseth, K.S. and Bowman, C.N. (1992–1993) *Polym. React. Engng J.*, **1**, 499–520.
140. Buback, M., Egorov, M. and Kaminsky, V. (1999) *Macromol. Theory Simul.*, **8**, 520–528.
141. Buback, M., Barner-Kowollik, C., Egorov, M. and Kaminsky, V. (2001) *Macromol. Theory Simul.*, **10**, 209–218.
142. Achilias, D.S. and Kiparissides, C. (1992) *Macromolecules*, **25**, 3739–3750.
143. Vivaldo-Lima, E., Hamielec, A.E. and Wood, P.E. (1994) *Polym. React. Engng J.*, **2**, 17–85, 87–162.
144. Tefera, N., Weickert, G. and Westertep, K.R. (1997) *J. Appl. Polym. Sci.*, **63**, 1663–1680.
145. Dhib, R., Gao, J. and Penlidis, A. (2000) *Polym. React. Engng J.*, **8**(4), 299–464.
146. Goodner, M.D., Lee, H.R. and Bowman, C.N. (1997) *Ind. Engng Chem. Res.*, **36**, 1247–1252.
147. Polic, A.L., Lona, L.M.F., Duever, T.A. and Penlidis, A. (2004) *Macromol. Theory Simul.*, **13**, 115–132.
148. Polic, A.L., Duever, T.A. and Penlidis, A. (1998) *J. Polym. Sci., Polym. Chem.*, **36**, 813–822.
149. Lona, L.M.F. and Penlidis, A. (2005) *Ind. Engng Chem. Res.*, **44**, 2634–2648.
150. Bonilla, J., Saldivar, E., Flores-Tlacuahuac, A., Vivaldo-Lima, E., Phaenduer, R. and Tiscareno-Lechuga, F. (2002) *Polym. React. Engng J.*, **10**, 227–263.
151. Vivaldo-Lima, E. and Mendoza-Fuentes, A. (2002) *Polym. React. Engng J.*, **10**, 193–226.
152. Zhang, M. and Ray, W.H. (2002) *J. Appl. Polym. Sci.*, **86**, 1630–1662.
153. Zhang, M. and Ray, W.H. (2002) *J. Appl. Polym. Sci.*, **86**, 1047–1056.
154. Delgadillo-Velazquez, O., Vivaldo-Lima, E., Quintero-Ortega, I.A. and Zhu, S. (2002) *AIChE J.*, **48**, 2597–2608.
155. Saldivar-Guerra, E., Bonilla, J., Becerril, F., Zacahua, G., Albores-Velasco, M., Alexander-Katz, R., Flores-Santos, L. and Alexandrova, L. (2006) *Macromol. Theory Simul.*, **15**, 163–175.
156. Burke, A.L., Duever, T.A. and Penlidis, A. (1997) *Ind. Engng Chem. Res.*, **36**, 1016–1035.
157. Burke, A.L., Duever, T.A. and Penlidis, A. (1996) *J. Polym. Sci., Polym. Chem.*, **34**, 2665–2678.
158. Landry, R., Duever, T.A. and Penlidis, A. (1999) *Polym. React. Engng J.*, **7**, 401–427.

Chapter 4

Free-Radical Polymerization: Heterogeneous Systems

Gregorio R. Meira and Costas Kiparissides

4.1 Introduction

Bulk free-radical polymerizations are carried out in the absence of a dispersion medium, and without (or with a very little) solvent. Many technical polymers such as LDPE, LLDPE, PVC, PS, high-impact polystyrene (HIPS), PMMA, nylon and polyester are manufactured in bulk processes. Compared with suspension, emulsion or solution processes, bulk polymerizations exhibit a higher reactor performance, higher product purity and reduced transfer reactions to solvents or additives. The disadvantages are related with the high process viscosity, which in turn generates problems of heat removal, mixing, pumping and reactor wall fouling by film formation.

Some bulk polymerizations (e.g., the production of crystal or general-purpose PS) are homogeneous because the produced polymer is amorphous and completely soluble in the monomer. In contrast, PVC soon precipitates from its monomer. In the HIPS process, the heterogeneity results from the incompatibility between the initial polybutadiene (PBD) prepolymer and the generated polystyrene (PS) chains.

Many thermoplastics are heterogeneous (or heterophase) because they contain liquid or rubber dispersions that improve their physical properties with respect to those of the continuous brittle phase. Examples of this are the softening of PVC by the presence of phthalate droplets and the improved toughness of HIPS or the polymer of acrylonitrile-butadiene-styrene (ABS) by addition of PBD-based rubber particles. This chapter will focus on the (heterogeneous, bulk and free-radical) polymerizations leading to the production of HIPS and PVC.

4.2 High-impact polystyrene

The three basic polystyrene (PS) plastics are: crystal (or general-purpose), high-impact (HIPS) and expandable beads. In 2004, the annual world consumption was 15.2 million tonnes, with the following approximate breakdown: 45% crystal, 42% HIPS and 13% expandable beads. At present, the largest end use for crystal PS and HIPS is in the packaging industry, which accounts for about 30% of the world consumption. PS polymers and other styrene (S) copolymers such as acrylonitrile-butadiene-styrene (ABS) are

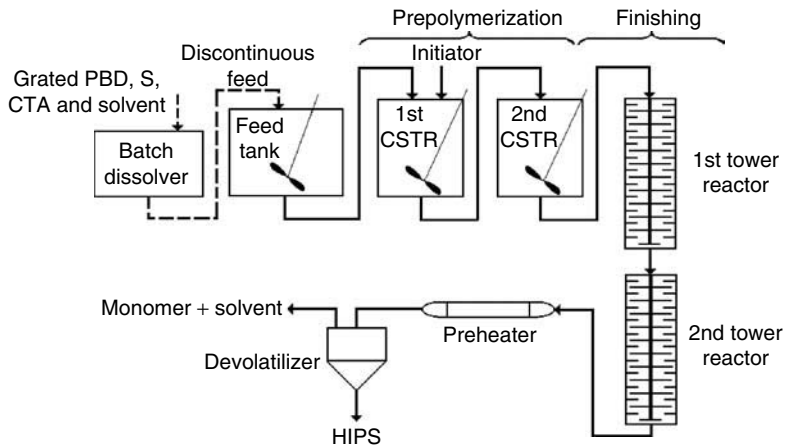


Figure 4.1 Typical continuous bulk process for the production of HIPS.

important thermoplastics of easy processability. The top five PS producers (Dow, BASF, NOVA Chemicals, Total Petrochemicals and Innovene) totalize 40% of the world capacity. A recent book [1] is an excellent review on styrenic polymers that includes a special chapter on preparation, properties and applications of HIPS [2]. Also, two relatively recent encyclopedia articles on PS and styrene copolymers have been published [3, 4].

In the bulk (or quasi-bulk) HIPS process, S is polymerized in the presence of 5–10% in weight of dissolved PBD, a chemical initiator, an antioxidant for preventing rubber degradation and a chain transfer agent (CTA) for controlling the chain lengths of the free PS. In addition, a mineral oil and/or a solvent are incorporated to reduce the viscosity of the reaction mixture. The mineral oil remains in the final product. The HIPS process involves the following stages: dissolution, prepolymerization, finishing and devolatilization (Figure 4.1). In the batch dissolution stage, the rubber is dissolved in the monomer at a relatively low temperature ($\sim 70^\circ\text{C}$), to minimize thermal polymerization. The prepolymerization stage is carried out between 90°C and 120°C under well-stirred conditions, and it ends at around 30% conversion. The half-lives of the chemical initiators (either mono- or bifunctional) are such that they are mainly consumed during the prepolymerization.

The processes occurring during the HIPS production are better understood by considering a bulk polymerization in a batch reactor. These processes can be analyzed with the help of a PS/PBD/S ternary equilibrium diagram (Figure 4.2). This approach neglects the fact that most of the initial PBD is transformed into graft copolymer (a fourth chemical species), the effect of the molar masses, etc. The solid curve represents the binodal line above which the system is homogeneous, and the broken lines denote the “tie-lines.” Point A represents the initial solution of PBD in S. Polymerization starts upon addition of initiator, and the reaction path is represented by a straight line parallel to the PS–S axis. The reaction mixture remains homogeneous until the reaction path reaches point B, where phase separation occurs; leading to the formation of a PS-rich phase dispersed in a PBD-rich continuous phase. From point B onwards the reaction line represents the overall reactor composition, but actually two phases of compositions given by the tie-lines in Figure 4.2 are present. Graft copolymer is produced by attack of primary initiator radicals onto the allylic

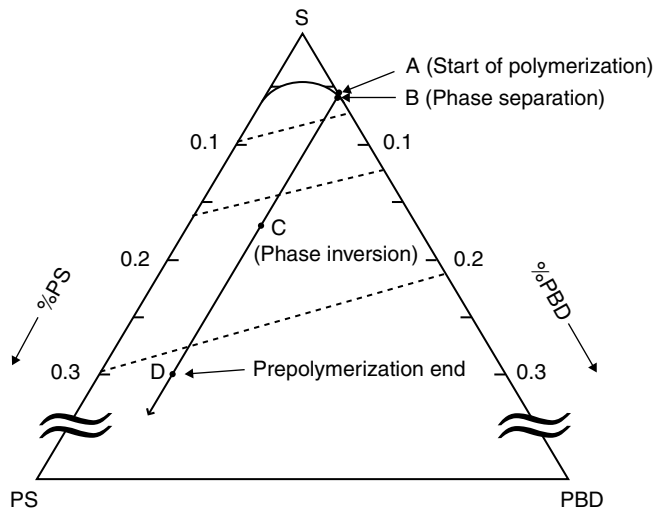


Figure 4.2 Batch polymerization of S in the presence of PB: representation of the reaction path in a S-PBD-PS ternary system. (Adapted from Casis, N. *et al.* (2006) *J. Appl. Polym. Sci.*, **99**, 3023–3039.)

hydrogen of PBD repeating units, with subsequent polymerization of S on the resulting midchain radicals. Graft copolymer molecules stabilize the dispersed PS-rich phase. As polymerization proceeds, the PS-rich phase volume increases, whereas the PBD-rich phase volume decreases. For a conversion between 5% and 25%, and close to the point when the PS-rich phase volume reaches the volume of the PBD-rich phase, phase inversion occurs. Point C in Figure 4.2 represents the overall reactor composition at which inversion occurs. During phase inversion, a co-contiguous morphology is formed, and after phase inversion, the PS-rich phase becomes the continuous phase (Figure 4.3(b),(d)). The dispersed rubber particles present a complex morphology with PS occlusions. This morphology is often referred to as salami morphology. The poly(BD-graft-S) generated at early stages of the prepolymerization reduces the interfacial tension, facilitating the phase inversion and controlling the particle size and morphology (Figure 4.3(c),(d)). It has been suggested [5] that graft copolymers with two or more PS branches place themselves at the external interface of the rubber particles, while graft copolymer molecules with a single PS branch place themselves at the occlusions interface (Figure 4.3(d)). Furthermore, it is claimed that the particle occlusions are a mixture of low-molecular-weight PS homopolymer and PS branches of single-branched copolymer molecules [5]. Both the phase inversion and the particle morphology are governed by stirring and the grafting efficiency (i.e., the fraction of grafted S with respect to the total polymerized S).

In the finishing stage (after point D in Figure 4.2), the temperature is increased to around 150°C, and the system is gently stirred to avoid destroying the developed morphology. In this stage, most of the primary free-radicals are generated thermally from the monomer, and there is a large increase in the system viscosity. In a continuous plant (Figure 4.1), the processes described above do not occur in a sequential manner. The solution of PBD in S enters into a stirred tank in which phase inversion may have taken place. The reaction mixture leaving the prepolymerization stage is completely inverted and, because of

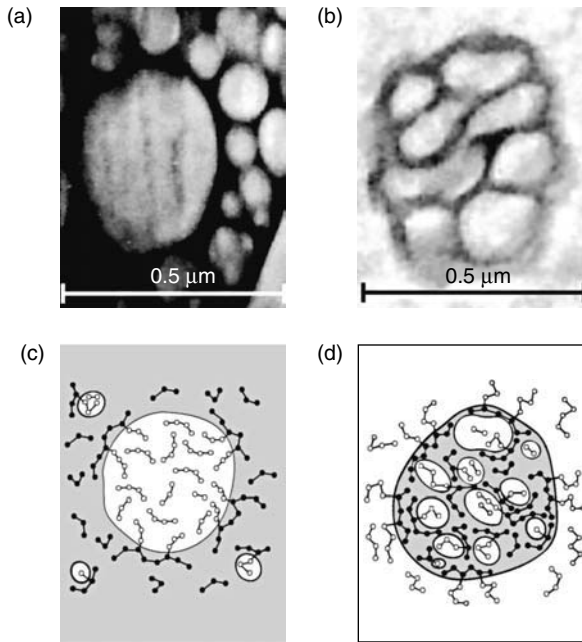


Figure 4.3 Evolution of particle morphology along a batch prepolymerization. (a), (b) TEM micrographs taken shortly before and after the phase inversion; where the PB-rich phase is in black, and the PS-rich phase is in gray. (c), (d) Molecular interpretations by Fischer and Hellmann [5].

the tubular-like design of the finishing reactor, this stage proceeds in a way similar to that in a batch reactor. In the final preheater–devolatilization stage, the temperature reaches around 250°C and vacuum is applied to eliminate the solvent and residual monomer. This high temperature promotes the rubber crosslinking and some polymer degradation. Also, low molecular weight PS chains (both free and grafted) are generated, due to the higher activation energy of the chain transfer to monomer with respect to those of the propagation and the termination by combination (Tables 3.2 and 3.3). The rubber crosslinking is beneficial, since it helps preserve the particle morphology during the material processing. The final S conversion is around 75%.

The ABS bulk process is similar to that of HIPS, except for the fact that S is copolymerized with acrylonitrile in the presence of a PBD rubber.

4.2.1 *Interrelationship between microstructure and application properties*

HIPS and ABS are heterogeneous materials containing dispersed rubber particles in continuous vitreous matrixes. Figure 4.4(a) and (b) exhibit the typical “salami” morphologies of HIPS and ABS when produced in bulk processes with PBD rubber. These products are non-transparent, due to their relatively large particle sizes. Figure 4.5 compares the stress–strain curves of PS, poly(styrene-co-acrylonitrile) (SAN), HIPS and ABS. The area under

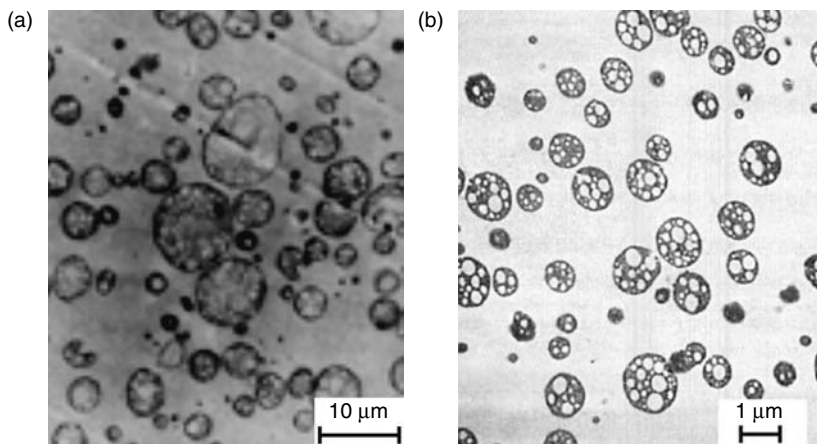


Figure 4.4 Transmission electron micrographs of two typical impact thermoplastic morphologies. (a) HIPS moulding material, with large rubber particles containing lighter PS inclusions. (b) ABS produced by a bulk process. (Adapted from Maul, J. *et al.* (2002) *Ullmann's Encyclopedia of Industrial Chemistry*. Wiley-VCH Verlag GmbH & Co., Germany and Priddy, D.B. (1998) *Kirk-Othmer Encyclopedia of Chemical Technology*, 4th edn. John Wiley & Sons Inc., New York, Vol 42. pp. 1–40.)

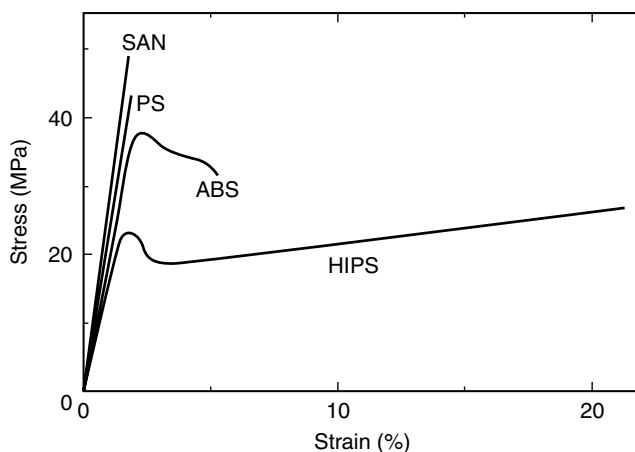


Figure 4.5 Stress–strain curves for styrene-based polymers. (Adapted from *Kirk-Othmer Encyclopedia of Chemical Technology*, 4th edn, 22, 3.)

the curves is an indication of the material toughness. Therefore, ABS is tougher than SAN, and HIPS is tougher than PS. The inclusion of (the highly polar) acrylonitrile in ABS increases not only its tensile strength and modulus with respect to HIPS, but it also increases its resistance to non-polar solvents. While tensile strengths are generally lowered by increasing temperatures, tensile moduli are little affected in the range -40°C to 50°C . In the fabricated specimen, the molecular orientation can significantly alter the stress–strain curve when compared with an isotropic specimen (typically obtained by compression molding).

The performance of HIPS is mainly determined by its microstructure, which is achieved during its synthesis. However, the final article properties are also strongly affected by compounding and processing. The overall quality control problem aims at improving the qualities of HIPS in the intermediate base material and in the final article. Figure 4.6 illustrates the highly multivariable nature of this problem. For the base HIPS material, the mid-column of Figure 4.6 lists the main microstructural characteristics and macroscopic application properties. This base material is then compounded with additives and processed to obtain the final article. The base HIPS characteristics are achieved during polymerization, and the left column of Figure 4.6 lists the process variables of a bulk process. Even without considering the complexities added by compounding and processing, Figure 4.6 illustrates the challenges involved in the production of a HIPS for a given application, determined by the set of macroscopic properties of the material. The first problem is to determine the microstructure of HIPS for a given macroscopic performance. Unfortunately, quantitative structure–property relationships are scarce. Table 4.1 illustrates in a qualitative way the effect of the HIPS microstructure on the macroscopic properties [6]. It shows that almost any variation of a microstructural characteristic yields conflicting macroscopic properties. For example, a high molar mass in the PS continuous phase improves the material modulus and the tensile strength, but it makes processing more difficult. According to the PBD content, the HIPS grades are classified into semi-impact resistant (about 3% PBD) impact-resistant (6% PBD) and highly-impact resistant (8–10% PBD). In addition to the PBD content, the volume fraction of the rubber particles (which includes the grafted PS and the free PS contained in the particle occlusions), plays a crucial role in impact resistance. Toughness first increases with particle size reaching a maximum value for particles in the range of 1–5 μm . For significantly larger particles, impact resistance decreases as crazing occurs at the particles surface. HIPS grades with rubber particles smaller than 1 μm are also produced for their improved surface gloss and transparency, but at the cost of reducing mechanical strength.

HIPS microstructure depends on the process variables used in the polymerization. There are many publications reporting experimental evidence of the effect of the process variables on polymer microstructure [7–16]. For example, Soto *et al.* [15] analyzed the effects of the initiator type, temperature and stirring rate on the particle morphology and molecular weights of the free PS. Heuristic knowledge available indicates that the particle size depends on the ratio between the solution viscosities of the PBD- and PS-rich phases; the agitation rate; and the interface tension between the two phases. The interface tension in turn depends on the grafting efficiency.

The complex nature of the bulk HIPS process requires detailed mathematical models for systematizing and quantifying the interrelationships between the reaction inputs and the polymer quality. Detailed mathematical models are vital for developing alternative reactor control strategies, with the ultimate aim of producing HIPS with *a priori* specified characteristics. An important limitation for understanding the physical chemistry of the bulk HIPS process is the lack of accurate measurements of important variables, such as the partitions of reagents and products among phases and interfaces, the degrees of branching of the graft copolymer, the swollen particle sizes, etc. Even relatively simpler scalar variables such as the grafting efficiency are difficult to quantify [7]. In industrial processes, on-line quality measurements are practically non-existent.

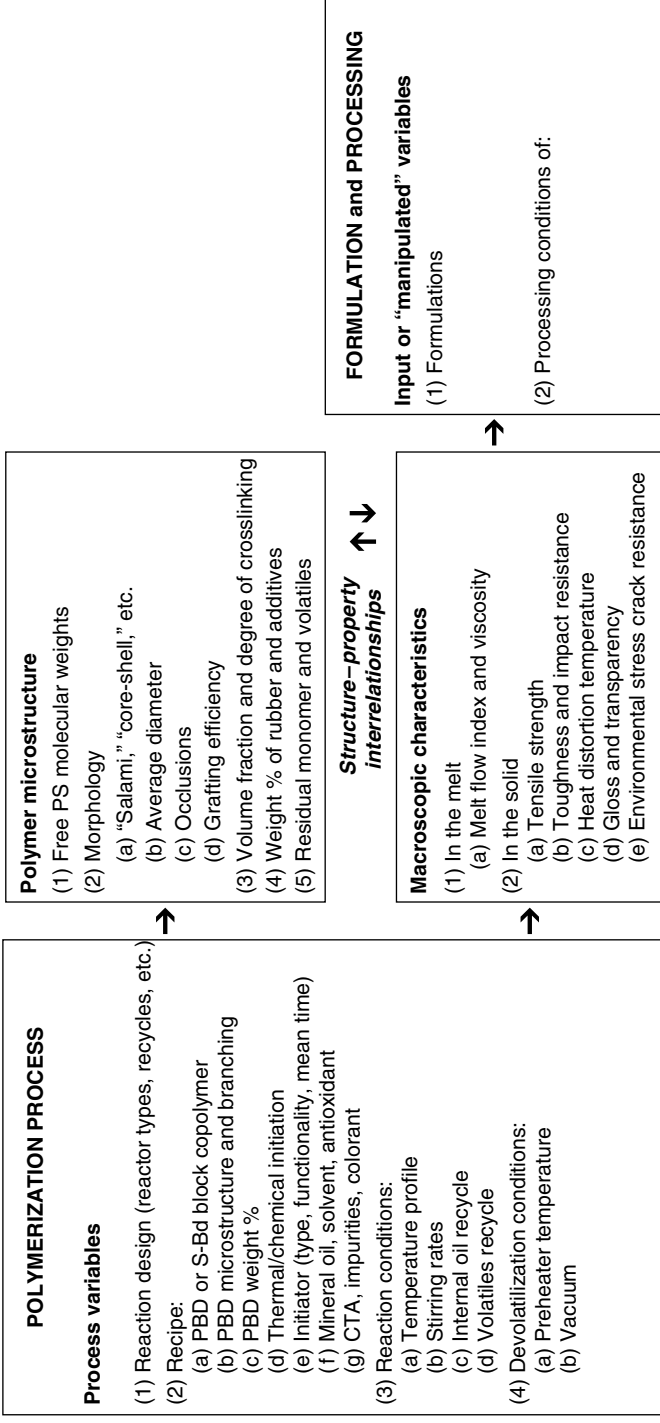


Figure 4.6 A complex quality control problem. The specifications of the base HIPS material (mid-column) are acquired final article, the material quality is also affected by the formulation and processing operations.

Table 4.1 Effects of increasing microstructural characteristics on the macroscopic properties (Adapted from Moore, 16, 68.)

Increase of microstructural characteristic	Macroscopic property			
	Toughness	Heat distortion temperature	Environmental stress crack resistance	Gloss
[PBD]	Increase	Decrease	Increase	Slight decrease
Particle size	First increase, then decrease	No effect	Slight increase	Decrease
\bar{M}_w of free PS	First rapid increase, then no effect	Slight increase	Slight increase	Decrease
Crosslinking density	First increase, then decrease	No effect	Increase	Increase
Mineral oil	Increase	Decrease	Decrease	No effect
Degree of grafting	Increase	No effect	Increase	Decrease

4.2.2 Modeling HIPS polymerization

Most of the existing mathematical models on the synthesis of HIPS via the bulk process cannot predict morphology and are therefore strictly applicable to solution processes [5, 12, 18–26]. However, many of such models [5, 12, 22–26] have been conveniently employed for estimating important global variables of equivalent bulk processes, such as conversion, grafting efficiency, the MWDs of the three HIPS components (i.e., the free PS, the unreacted PBD and the graft copolymer) and the branching distribution of the graft copolymer. During prepolymerization, the rubber crosslinking is negligible, and for this reason size exclusion chromatography can be used to verify many (but not all) of the model predictions on the global evolving molecular structure [25, 27, 28]. Homogeneous models are adequate for predicting the global molecular structure of bulk prepolymerizations because both the monomer and the chemical initiator are almost evenly distributed between the phases. However, homogeneous models are known to somewhat underestimate the molecular weight polydispersity of the global free PS obtained in quasi-bulk prepolymerizations [12, 24].

Models accounting for the heterogeneous nature of the bulk HIPS process are available [29, 30]. In these models, it is considered that polymerization occurs at different rates in each phase (a PS- and PBD-rich phase) due to differences in the reagent concentrations and that the mass transfer between phases is much faster than polymerization rate. Therefore, the concentrations of the monomer and initiator(s) are given by the thermodynamic equilibrium between phases. The monomer and initiator partitioning can be determined experimentally [29, 30]. The polymerization model by Ludwico and Rosen [29] neglected the generation of graft copolymer and therefore the model by Casis *et al.* [30] is considered in this section. None of these models is able to predict particle morphology.

Table 4.2 presents the kinetic mechanism that is assumed to rule polymerization in both phases. This mechanism does not account for the length of the dead graft copolymer and therefore its (bivariate) chain length distribution cannot be calculated (a more detailed kinetic mechanism can be found in reference 30). In Table 4.2, I_2 represents the chemical initiator; I is a primary initiator radical; M is the monomer; D_n is a dead PS chain of length n ; P_n is a growing PS chain of length n ; D_{BD} is a dead chain containing a PBD chain (it may be either a single PBD chain or a graft copolymer); P_{BD0} is a rubber radical generated by abstraction of a hydrogen from a PBD chain (either grafted or unreacted); and P_{BDn} is a rubber radical with a growing branch containing n repetitive units of S. In the transfer reactions to the PBD chains, note that the rate constant k_{tr}^r was defined on a mole-to-mole basis.

In what follows, a batch process is considered assuming that:

- (1) in each phase, the reaction mixture is perfectly stirred;
- (2) the initiator is distributed between the phases according with a partition coefficient that depends on conversion [29], but is unaffected by temperature or molar mass;
- (3) the S monomer, the PS chains and the PBD chains are partitioned among the phases according to the ternary diagram of Figure 4.2, which was adapted from ref. [31];
- (4) the equilibria of Figure 4.2 are unaffected by temperature, molar mass or the presence of graft copolymer or solvent;
- (5) the volumes are additive;

Table 4.2 Heterogeneous polymerization of styrene in the presence of PBD for the production of HIPS. Reaction kinetics applied onto both phases (the PS- and the PB-rich phase) [30] ($s = 0, 1, 2, \dots$); ($b, n, m = 1, 2, 3, \dots$)

Chemical initiation	Transfer to the monomer
$I_2 \xrightarrow{k_1} 2I^\bullet$	$P_n + M \xrightarrow{k_{tr}^{mon}} D_n + P_1$
$I^\bullet + M \xrightarrow{k_{i1}} P_1$	$P_{DBn} + M \xrightarrow{k_{tr}^{mon}} D_{BD} + P_1$
$I^\bullet + D_{BD} \xrightarrow{k_{i2}} D_{BD0}^\bullet$	$P_{DB0} + M \xrightarrow{k_{tr}^{mon}} D_{BD} + P_1$
Thermal initiation	Transfer to the PB or the copolymer
$3M \xrightarrow{k_{therm}} 2P_1$	$P_n + D_{BD} \xrightarrow{k_{tr}^r} D_n + P_{BD0}$
Propagation	$P_{BPn} + D_{BD} \xrightarrow{k_{tr}^r} D_{BD} + P_{BD0}$
$P_n + M \xrightarrow{k_p} P_{n+1}$	Termination by recombination
$P_{BD0} + M \xrightarrow{k_{i3}} P_{BD1}$	$P_n + P_m \xrightarrow{k_{tc}} D_{n+m}$
$P_{BDn} + M \xrightarrow{k_p} P_{BDn+1}$	$P_{BDM-n} + P_n \xrightarrow{k_{tc}} D_{BD}$
	$P_{BDM-n} + P_{BDn} \xrightarrow{k_{tc}} D_{BD}$
	$P_{BD0} + P_{BDn} \xrightarrow{k_{tc}''} D_{BD}$
	$P_{BD0} + P_n \xrightarrow{k_{tc}''} D_{BD}$
	$P_{BD0} + P_{BD0} \xrightarrow{k_{tc}'} D_{BD}$

- (6) in each phase, the “gel effect” is a function of the polymer volume fraction;
- (7) the phase inversion occurs when the PS-rich phase volume equals the PBD-rich phase volume and
- (8) after the phase inversion, the increased viscosity prevents the mass transfer of polymer between the phases, and all of the free PS that is produced in the rubber particles accumulates in the particle occlusions.

In the equations given below, the PS- and PBD-rich phases are denoted with the subscripts I and II, respectively. For any generic species j , $[j]$ represents its molar concentration (mol L^{-1}) and N_j is the total number of moles.

- *Initiator:*

$$\frac{d}{dt} N_{I_2} = -k_1([I_2]_I V_I + [I_2]_{II} V_{II}) \quad (4.1)$$

where V is the reaction volume.

- *Monomer:*

$$\begin{aligned} \frac{d}{dt} N_M &= -k_p[M]_{\text{I}}(P_{\text{StotI}} + P_{\text{BDtotI}}) - k_p[M]_{\text{II}}(P_{\text{StotII}} + P_{\text{BDtotII}}) \\ &= -\sum_i R_{p_i} V_i, \quad i = \text{I, II} \end{aligned} \quad (4.2)$$

- *Ungrafted BD units (B^*):*

$$\begin{aligned} \frac{d}{dt} N_{B^*} &= -\{k_{i2}[I^*]_{\text{I}} V_{\text{I}} + k_{\text{tr}}^r(P_{\text{BDtotI}} + P_{\text{StotI}})\}[B^*]_{\text{I}} + k_{\text{tr}}^{\text{mon}}[M]_{\text{I}} P_{\text{BD0I}} \\ &\quad - \{k_{i2}[I^*]_{\text{II}} V_{\text{II}} + k_{\text{tr}}^r(P_{\text{BDtotII}} + P_{\text{StotII}})\}[B^*]_{\text{II}} + k_{\text{tr}}^{\text{mon}}[M]_{\text{II}} P_{\text{BD0II}} \end{aligned} \quad (4.3)$$

- *Total mass of grafted PS:*

$$\begin{aligned} \frac{d}{dt} G_{\text{GS}} &= \sum_i \frac{d}{dt} G_{\text{GS}_i} = \sum_i \left\{ \frac{P_{\text{BDtot}_i}}{P_{\text{Stot}_i} + P_{\text{BDtot}_i}} R_{p_i} V_i + \frac{P_{\text{Stot}_i}}{P_{\text{Stot}_i} + P_{\text{BDtot}_i}} \right. \\ &\quad \left. \times R_{p_i} \frac{(k_{\text{tc}} P_{\text{BDtot}_i} + k_{\text{tc}}'' P_{\text{BD0}_i})}{(k_{\text{tr}}^{\text{mon}}[M]_i + k_{\text{tr}}^r[B^*]_i + (k_{\text{tc}}/V_i)(P_{\text{Stot}_i} + P_{\text{BDtot}_i}) + (k_{\text{tc}}''/V_i)P_{\text{BD0}_i})} \right\} w_m, \quad i = \text{I, II} \end{aligned} \quad (4.4)$$

with

$$R_{p_i} = \frac{k_p}{V_i} [M]_i (P_{\text{BDtot}_i} + P_{\text{Stot}_i})$$

where $w_m (=104 \text{ g mol}^{-1})$ is the monomer molecular weight and R_{p_i} is the polymerization rate in each phase ($\text{mol L}^{-1} \text{ s}^{-1}$).

- *Total mass of free PS:*

$$\begin{aligned} \frac{d}{dt} G_{\text{PS}} &= \sum_i \frac{d}{dt} G_{\text{PS}_i} = \sum_i \left\{ \frac{P_{\text{Stot}_i}}{P_{\text{Stot}_i} + P_{\text{BDtot}_i}} R_{p_i} V_i \right. \\ &\quad \left. \times \frac{(k_{\text{tr}}^{\text{mon}}[M]_i V_i + k_{\text{tr}}^r[B^*]_i V_i + k_{\text{tc}} P_{\text{Stot}_i})}{(k_{\text{tr}}^{\text{mon}}[M]_i + k_{\text{tr}}^r[B^*]_i + (k_{\text{tc}}/V_i)(P_{\text{Stot}_i} + P_{\text{BDtot}_i}) + (k_{\text{tc}}''/V_i)P_{\text{BD0}_i})} \right\} w_m, \quad i = \text{I, II} \end{aligned} \quad (4.5)$$

- *Global amount of free radicals:*

$$\frac{d}{dt} I_i^* = (2f k_1[I_2]_i - k_{i1}[M]_i[I^*]_i - k_{i2}[I^*]_i[B^*]_i) V_i \cong 0, \quad i = \text{I, II} \quad (4.6)$$

$$\begin{aligned} \frac{d}{dt}P_{1i} &= k_{i1}[I^*]_i[M]_iV_i + 2k_{\text{therm}}[M]_i^3V_i + k_{\text{tr}}^{\text{mon}}[M]_i(P_{\text{Stot}_i} + P_{\text{BDtot}_i}) \\ &\quad + k_{\text{tr}}^{\prime\text{mon}}[M]_iP_{\text{BD0}_i} - \{k_p[M]_i + k_{\text{tr}}^r[B^*]_i + k_{\text{tr}}^{\text{mon}}[M]_i\}P_{1i} \\ &\quad - \left\{ \frac{k_{\text{tc}}''}{V_i}P_{\text{BD0}_i} + \frac{k_{\text{tc}}}{V_i}(P_{\text{Stot}_i} + P_{\text{BDtot}_i}) \right\}P_{1i} \cong 0 \quad i = \text{I, II} \end{aligned} \quad (4.7)$$

$$\begin{aligned} \frac{d}{dt}P_{ni} &= k_p[M]_iP_{n-1i} - \{k_p[M]_i + k_{\text{tr}}^{\text{mon}}[M]_i\}P_{ni} - \left\{ k_{\text{tr}}^r[B^*]_i + \frac{k_{\text{tc}}''}{V_i}P_{\text{BD0}_i} \right. \\ &\quad \left. + \frac{k_{\text{tc}}}{V_i}(P_{\text{Stot}_i} + P_{\text{BDtot}_i}) \right\}P_{ni} \cong 0 \quad n = 2, 3, \dots \quad i = \text{I, II} \end{aligned} \quad (4.8)$$

$$\begin{aligned} \frac{d}{dt}P_{\text{Stot}_i} &= \frac{d}{dt} \sum_n P_{ni} = k_{i1}[M]_i[I^*]_i + 2k_{\text{therm}}[M]_i^3 + k_{\text{tr}}^{\prime\text{mon}}[M]_iP_{\text{BD0}_i} \\ &\quad + k_{\text{tr}}^{\text{mon}}[M]_iP_{\text{BDtot}_i} - k_{\text{tr}}^r[B^*]_iP_{\text{Stot}_i} - \frac{k_{\text{tc}}''}{V_i}P_{\text{BD0}_i}P_{\text{Stot}_i} \\ &\quad - \frac{k_{\text{tc}}}{V_i}(P_{\text{Stot}_i} + P_{\text{BDtot}_i})P_{\text{Stot}_i} \cong 0, \quad i = \text{I, II} \end{aligned} \quad (4.9)$$

$$\begin{aligned} \frac{d}{dt}P_{\text{BD0}_i} &= \{k_{i2}[I^*]_iV_i + k_{\text{tr}}^r(P_{\text{Stot}_i} + P_{\text{BDtot}_i})\}[B^*]_i - \left\{ k_{i3}[M]_i + k_{\text{tr}}^{\prime\text{mon}}[M]_i \right. \\ &\quad \left. + \frac{k_{\text{tc}}'}{V_i}P_{\text{BD0}_i} + \frac{k_{\text{tc}}''}{V_i}(P_{\text{Stot}_i} + P_{\text{BDtot}_i}) \right\}P_{\text{BD0}_i} \cong 0 \quad i = \text{I, II} \end{aligned} \quad (4.10)$$

$$\begin{aligned} \frac{d}{dt}P_{\text{BD1}_i} &= k_{i3}[M]_iP_{\text{BD0}_i} - (k_p + k_{\text{tr}}^{\text{mon}})[M]_iP_{\text{BD1}_i} - \left\{ k_{\text{tr}}^r[B^*]_i + \frac{k_{\text{tc}}''}{V_i}P_{\text{BD0}_i} \right. \\ &\quad \left. + \frac{k_{\text{tc}}}{V_i}(P_{\text{Stot}_i} + P_{\text{BDtot}_i}) \right\}P_{\text{BD1}_i} \cong 0 \quad i = \text{I, II} \end{aligned} \quad (4.11)$$

$$\begin{aligned} \frac{d}{dt}P_{\text{BD}n_i} &= k_p[M]_iP_{\text{BD}n-1_i} - (k_p + k_{\text{tr}}^{\text{mon}})[M]_iP_{\text{BD}n_i} - \left\{ k_{\text{tr}}^r[B^*]_i + \frac{k_{\text{tc}}''}{V_i}P_{\text{BD0}_i} \right. \\ &\quad \left. + \frac{k_{\text{tc}}}{V_i}(P_{\text{Stot}_i} + P_{\text{BDtot}_i}) \right\}P_{\text{BD}n_i} \cong 0 \quad n = 2, 3, \dots \quad i = \text{I, II} \end{aligned} \quad (4.12)$$

$$\begin{aligned} \frac{d}{dt}P_{\text{BDtot}_i} &= \frac{d}{dt} \sum_n P_{\text{BD}n_i} = k_{i3}[M]_iP_{\text{BD0}_i} - \left\{ k_{\text{tr}}^{\text{mon}}[M]_i + k_{\text{tr}}^r[B^*]_i \right. \\ &\quad \left. + \frac{k_{\text{tc}}}{V_i}(P_{\text{Stot}_i} + P_{\text{BDtot}_i}) + \frac{k_{\text{tc}}''}{V_i}P_{\text{BD0}_i} \right\}P_{\text{BDtot}_i} \cong 0 \quad i = \text{I, II} \end{aligned} \quad (4.13)$$

The distribution of reagents and products between the phases was obtained from the corresponding partition coefficients, K_j . These are defined on the basis of the molar concentrations.

- *Initiator partition:*

$$K_{I_2}(x) = \frac{[I_2]_I}{[I_2]_{II}} \quad (4.14)$$

- *Monomer partitioning:*

$$K_M = \frac{[M]_I}{[M]_{II}} \quad (4.15)$$

- *PS partitioning:*

$$K_{PS} = \frac{(G_{PS_I} + G_{GS_I})/V_I}{(G_{PS_{II}} + G_{GS_{II}})/V_{II}} \quad (4.16)$$

- *PBD partitioning:*

$$K_{PB} = \frac{[B^*]_I}{[B^*]_{II}} \quad (4.17)$$

The total reaction volume V is

$$V = V_I + V_{II} \quad (4.18)$$

- *Volume of phase I:*

$$V_I = [M]_I V_I w_m / \rho_m + [B^*]_I V_I w_{BD} / \rho_{PB} + (G_{PS_I} + G_{GS_I}) / \rho_{PS} + \left[G_T \frac{G_I}{(G_I + G_{II})} \right] / \rho_T \quad (4.19)$$

- *Volume of phase II:*

$$V_{II} = [M]_{II} V_{II} w_m / \rho_m + [B^*]_{II} V_{II} w_{BD} / \rho_{PB} + (G_{PS_{II}} + G_{GS_{II}}) / \rho_{PS} + \left[G_T \frac{G_{II}}{(G_I + G_{II})} \right] / \rho_T \quad (4.20)$$

where ρ_k is the density of chemical species k .

Neglecting the initiator contribution, and considering the solvent mass (G_T), the reaction masses of each phase and the total reaction mass are given by:

- *Mass of phase I (the PS-rich phase):*

$$G_I = [M]_I V_I w_m + G_{PS_I} + [B^*]_I V_I w_{BD} + G_{GS_I} + G_T \frac{G_I}{(G_I + G_{II})} \quad (4.21)$$

- *Mass of phase II (the PBD-rich phase):*

$$G_{II} = [M]_{II} V_{II} w_m + G_{PS_{II}} + [B^*]_{II} V_{II} w_{BD} + G_{GS_{II}} + G_T \frac{G_{II}}{(G_I + G_{II})} \quad (4.22)$$

- Total mass:

$$G_I + G_{II} = G_{PS} + G_{PB}^0 + G_{GS} + N_m w_m + G_T \quad (4.23)$$

- Volume of particle occlusions:

$$V_{I,o} = \frac{G_{PS,o}}{\rho_{PS}(1 - [M]_I w_m / \rho_m)} \quad (4.24)$$

- Rubber particles volume:

$$V_p = V_{II} + V_{I,o} \quad (4.25)$$

- Monomer conversion:

$$x = \frac{N_m^0 - N_m}{N_m^0} \quad (4.26)$$

- Styrene grafting efficiency:

$$E_S = \frac{G_{GS}}{G_{GS} + G_{PS}} \quad (4.27)$$

The weight chain-length distribution (WCLD) of the total free PS is obtained through multiplying each molecular species of the number chain-length distribution (in turn derived from the mass balance of Table 4.1) by its molar mass (nw_m), yielding [30]:

$$\begin{aligned} \frac{d}{dt} G_{PS}(n) &= \frac{d}{dt} [G_{PS_I}(n) + G_{PS_{II}}(n)] \\ &= \left\{ (k_{tr}^{mon}[M]_I + k_{tr}^r[B^*]_I) P_{n_I} + \frac{k_{tc}}{2V_I} \sum_{m=1}^{n-1} P_{m_I} P_{n-m_I} \right. \\ &\quad \left. + (k_{tr}^{mon}[M]_{II} + k_{tr}^r[B^*]_{II}) P_{n_{II}} + \frac{k_{tc}}{2V_{II}} \sum_{m=1}^{n-1} P_{m_{II}} P_{n-m_{II}} \right\} nw_m \\ &= \sum_i \left\{ \left[R_{p_i} V_i \varphi_i \frac{(\tau_i - \gamma_i \tau_{1_i})}{\alpha_i} + \frac{R_{p_i} V_i \varphi_i^2 \beta_i}{2} n \right] \alpha_i^2 w_m n e^{-\alpha_i n} \right\} \\ &\quad n = 1, 2, 3, \dots, \quad i = I, II \end{aligned} \quad (4.28)$$

where φ_i , β_i , τ_i , τ_{1_i} , γ_i and α_i , with ($i = I, II$), are dimensionless parameters, defined as follows:

$$\varphi_i = \frac{P_{Stot_i}}{P_{Stot_i} + P_{BDtot_i}}, \quad i = I, II \quad (4.29)$$

$$\beta_i = \frac{k_{tc} R_{p_i}}{(k_p [M]_i)^2}, \quad i = I, II \quad (4.30)$$

$$\tau_i = \frac{k_{tr}^{mon}}{k_p} + \frac{k_{tr}^r[B^*]_i}{(k_p[M]_i)} + \gamma_i \tau_{1i} \quad i = I, II \quad (4.31)$$

$$\tau_{1i} = \frac{k_{tc}'' R_{pi}}{(k_p[M]_i)^2} \quad i = I, II \quad (4.32)$$

$$\gamma_i = \frac{P_{BDtoti}}{P_{Stoti} + P_{BDtoti}} \quad i = I, II \quad (4.33)$$

$$\alpha_i = \tau_i + \beta_i, \quad i = I, II \quad (4.34)$$

In Equation 4.28, it has been assumed that the free PS accumulates in both phases during the very short period following the phase separation (when some of the PS chains are dissolved in the PBD-rich phase, and *vice versa*). But shortly after, the PS and PBD chains become incompatible (point B in Figure 4.2), and until the phase inversion, PS accumulates only in phase I, and its WCLD is given by:

$$\frac{d}{dt} G_{PS_i}(n) = \sum_i \left\{ \left[R_{pi} V_i \varphi_i \frac{(\tau_i - \gamma_i \tau_{1i})}{\alpha_i} + \frac{R_{pi} V_i \varphi_i^2 \beta_i}{2} n \right] \alpha_i^2 w_m n e^{-\alpha_i n} \right\} \\ n = 1, 2, 3, \dots \quad i = I, II \quad (4.35)$$

After the phase inversion, the free PS accumulates in both the continuous phase, indicated by the subscript “c,” and the particle occlusions, indicated by the subscript “o.” Their corresponding WCLDs are

- *Continuous region:*

$$\frac{d}{dt} G_{PS_{I,c}}(n) = \left[\frac{\tau_I}{\alpha_I} + \frac{\beta_I}{2} n \right] R_{pI} V_{I,c} \alpha_I^2 w_m n e^{-\alpha_I n} \quad n = 1, 2, 3, \dots \quad (4.36)$$

- *Particle occlusions region:*

$$\frac{d}{dt} G_{PS_{I,o}}(n) = \left[\frac{\tau_I}{\alpha_I} + \frac{\beta_I}{2} n \right] R_{pI} V_{I,o} \alpha_I^2 w_m n e^{-\alpha_I n} + \left[\frac{(\tau_{II} - \gamma_{II} \tau_{1II})}{\alpha_{II}} + \frac{\varphi_{II} \beta_{II}}{2} n \right] \\ \times \varphi_{II} R_{pII} V_{II} \alpha_{II}^2 w_m n e^{-\alpha_{II} n} \quad n = 1, 2, 3, \dots \quad (4.37)$$

A batch polymerization of S in the presence of PBD (S: 85.67%; toluene: 9.12%; benzoyl peroxide initiator: 0.065% and medium-*cis* PBD: 5.14%) is considered. Figure 4.7 compares some of the model predictions with experimental results. Most of the reaction was carried out at 120°C, except for an initial heating period at 1°C min⁻¹ (Figure 4.7(a)). The prepolymerization was stirred at 125 rpm; and it was ended at 30% conversion. The finishing was completed in unstirred glass ampoules. According to the model, phase separation occurred at a conversion of about 2% and phase inversion at 13% conversion. The monomer partitions preferentially in the rubber phase, while the opposite occurs with the initiator.

Figure 4.7(a) shows the time evolution of the monomer conversion. After the phase separation, the initiator is partitioned between the two phases; and it is almost totally consumed within the prepolymerization (not shown here). For the free PS molecular weights,

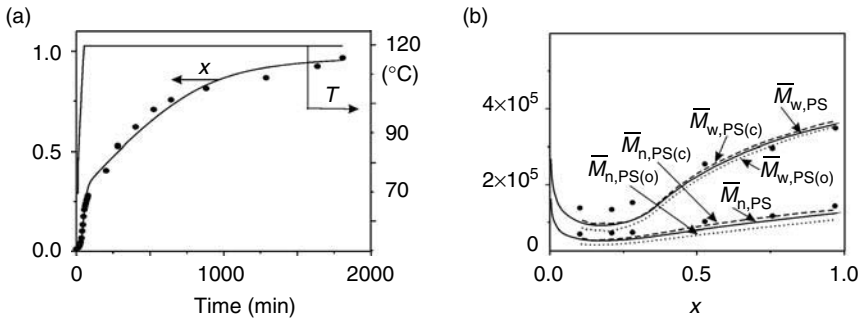


Figure 4.7 Batch polymerization of S in the presence of PBD at 120°C. (a) Time evolution of temperature and S conversion. (b) Molecular weights of the free PS. *Continuous trace*: global free PS. *Dashed trace*: PS in the continuous phase. *Dotted trace*: PS in the occlusions region. (Adapted from Casís, *et al.* (2006) *J. Appl. Polym. Sci.*, **99**, 3023–3039.)

the predictions of Figure 4.7(b) shows an initial drop that was not observed in the measurements. The high initial PS molecular weights are due to the relatively lower temperatures generated in the initial heating ramp period; since at lower temperatures termination by combination prevails over termination by chain transfer to the monomer. Between phase separation and phase inversion, free PS is produced in both phases, but it only accumulates in the PS-rich phase. After phase inversion, the free PS accumulates in two regions: the continuous phase (indicated by the subscript “c”), and the particle occlusions (indicated by the subscript “o”). According to the model, the molecular weights of the free PS contained in the particle occlusions are lower than those of the continuous region; and this result is in agreement with previous reports [5]. Experimentally, only the average molecular weights of the global free PS could be measured, and their values are compared with the theoretical predictions (see $\overline{M}_{n,PS}$ and $\overline{M}_{w,PS}$ in Figure 4.7(b)).

A more complete mathematical model capable of predicting the average molar masses of the unreacted PBD and graft copolymer can be found elsewhere [30]. In this model, the longer PBD chains (contained either in the unreacted PBD or in the graft copolymer) exhibit a higher probability of grafting than the shorter PBD chains. For this reason, there is a steady drop in the average molar masses of the unreacted PBD; and there is an initial drop in the average molar masses of the graft copolymer. However, with increasing conversion, the grafting-over-grafting process then determines a rapid increase in the average molar masses of the graft copolymer, for which reason the averages exhibit a minima.

4.2.3 Optimizing final properties: melt flow index in a continuous HIPS process

As has been seen in Table 4.1, the polymer microstructure influences the application properties of the polymer, such as melt flow index (MFI). The MFI is the mass flow rate [in $\text{g} (10 \text{ min})^{-1}$] of a HIPS melt that flows through a capillary, when forced by a piston loaded by a constant weight. It indicates the processability of the polymer and it is an important quality control variable in the polymerization process. MFI mainly depends

on \overline{M}_w of the free PS and on the mineral oil content; it is little dependent on the particle morphology. Quantitative relationships linking MFI to \overline{M}_w are available [32]. Combination of polymerization models with such a quantitative MFI versus \overline{M}_w relationships were used to design a process strategy aiming at minimizing the off-specs that were generated during grade transitions in a continuous HIPS plant, similar to that presented in Figure 4.1 [26]. An important reduction of the off-specs product was achieved by simply readjusting the intermediate loads of CTA into the batch dissolver [26].

4.2.4 Final remarks for HIPS

The availability of representative mathematical models is crucial for producing “tailor-made” polymers from the point of view of their molecular structures, morphologies and physical properties. In spite of the industrial importance of HIPS and ABS, it is somewhat surprising that so far none of the published mathematical models are capable of predicting the evolution of the rubber particle morphology along the prepolymerization. At present, a heterogeneous model is being developed that predicts the number and average diameter of the rubber particles, and the number and average diameter of occlusions per particle [33]. Mathematical models describing the actual morphology of the reaction system still remain to be developed.

Even if representative batch models for the average particle morphology were developed, the continuous HIPS process would still exhibit many unsolved modeling problems. For example, no publications have as yet appeared on how to transform a batch model into a continuous model, when the first CSTR in the train operates before the phase inversion and the second CSTR after the phase inversion. However, some incipient developments are to be found in reference 34.

4.3 Vinyl chloride monomer bulk polymerization

Poly(vinyl chloride) (PVC) is by volume the second largest thermoplastic manufactured in the world [35]. The world PVC demand in 2003 was about 28 million tonnes and the predicted annual growth rate of world PVC demand is close to 4% [36]. The sustainable expansion of the PVC industry is due to the high versatility of PVC as a plastic raw material together with its low price. A review of the qualitative and quantitative aspects of PVC polymerization can be found in Smallwood [35], Burgess [37], Langsam [38], Tornell and Uustalu [39], Xie *et al.* [40, 41] and Yuan *et al.* [42]. Four polymerization processes (i.e., suspension, bulk, emulsion and solution) are commercially employed in PVC manufacturing.

Bulk polymerization is the simplest process for producing PVC, since there are no difficulties on the separation and recovery of the residual monomer, or on the finishing of the produced polymer. The most well-known bulk vinyl chloride monomer (VCM) polymerization process these days is the Rhone–Poulenc two-stage process. According to this process, only VCM and oil-soluble initiators are introduced into the reactor, since there is no need for water and suspending agents. Due to the absence of water, productivity is very high, with respect to the other VCM polymerization processes (i.e., suspension, emulsion, solution).

However, problems relevant to the heat removal and temperature control, as well as to the extremely high viscosity of the polymerization system, established the suspension polymerization process much more attractive for PVC production. It is indicative that only 8% of the total PVC production is obtained by the bulk polymerization process.

The role of the first-stage polymerization, in the VCM bulk polymerization process, is the preparation of the stable seed PVC particles and to control grain morphology, which is derived from the seed. First, a half amount of VCM is introduced in the first prepolymerization reactor, with initiator. In this stage, the critical operating condition that controls the primary particle distribution and the aggregate cohesion is the temperature. As higher reaction temperatures are used the degree of cohesion between primary particles increases and the final grain porosity decreases. Therefore, to ensure aggregate cohesion, the first stage is always polymerized above 62°C. This has little effect on the molecular weight of the final polymer, since, on average, only 5% of the total polymer is formed in the prepolymerizer. The rate and uniformity of the primary coagulation step alone defines the total morphology of the grains at this stage. In order to achieve a uniform grain, this step is completed as rapidly and as uniformly as possible by the use of very vigorous agitation till 10% monomer conversion by turbine agitator [36]. Polymerization system at this stage is still liquid. Generated polymerization heat is removed by jacket cooling and reflux condenser.

From the first-stage reactor the seed PVC dispersed in VCM is consecutively delivered to the second post-polymerization reactor, where the second half VCM and additional initiator are charged. The temperature of the second-stage polymerization is defined at a certain point to control the molecular weight. The reaction medium has become powdery beyond 20–25% monomer conversion. In the second stage, the grain becomes stronger due to fusion of the primary particle agglomerates, which grow in size with subsequent infilling of the pores between them. Experiments have shown that the porosity is dependent on the temperature of polymerization and on the degree of monomer conversion in the second stage [43]. An increase of monomer conversion lowers porosity and increases bulk density. Under controlled conditions of temperature, pressure and agitation, polymerization is carried out till 80–85% monomer conversion. The reactor has two independent systems of agitation, one is a single-screw agitator introduced from the top and the other is a scraper agitator introduced from the bottom. Heat removal is done by jacket cooling, cooling by screw and reflux condenser.

The polymerization of VCM is highly exothermic (i.e., 100 kJ mol⁻¹). Thus, the efficient removal of the reaction heat is very critical for the operation of large-scale reactors [44]. When all of the free liquid monomer has been consumed, the pressure in the reactor starts to fall as a result of the monomer mass transfer from the vapor phase to the polymer phase due to subsaturation conditions. In industrial PVC production, the reaction is usually stopped when a certain pressure drop has been recorded. Because the polymer is effectively insoluble in its own monomer, once the polymer chains are first generated, they precipitate immediately to form a separate phase in the polymerizing mixture. Thus, from a kinetic point of view, the polymerization of VCM is considered to take place in three stages [45].

During the first stage, primary radicals formed by the thermal fragmentation of the initiator molecules rapidly react with monomer to produce the first polymer chains. During this early polymerization period, the polymer concentration is below its solubility limit in

the monomer (i.e., the VCM conversion is less than 0.01%); therefore, the polymerization occurs in a single homogeneous phase.

The second-stage polymerization extends from the time of the appearance of a separate polymer phase, in addition to the monomer phase, up to a fractional monomer conversion, x_f , at which the separate monomer phase disappears. During this stage, the reaction mixture consists of three phases, namely, the monomer-, the polymer-rich phase and the gaseous phases. The reaction takes place in the monomer and polymer phases at different rates and is accompanied by the transfer of monomer from the monomer phase to the polymer phase so that the latter is kept saturated with monomer. The disappearance of the monomer phase is associated with a characteristic drop in the reactor pressure.

In the third stage, at higher monomer conversions ($x_f < x < 1.0$), the polymerization proceeds exclusively in the polymer-rich phase that is swollen with the residual monomer. Thus, the monomer mass fraction in the polymer phase continuously decreases as the total monomer conversion approaches its final limiting value.

4.3.1 Kinetic mechanism

In general, the free-radical polymerization of vinyl monomers includes chain initiation, propagation, chain transfer to monomer and bimolecular termination reactions. However, there is strong evidence that, in the free-radical polymerization of VCM, some reactions (e.g., chain transfer to monomer, formation of short- and long-chain branches, etc.) involve complex kinetic mechanisms [44]. In fact, the presence of chloromethyl and ethyl short-chain branches in PVC validates the conclusion that the propagation reactions involve several types of radicals [46]. Figures 4.8–4.10 show in detail the mechanisms leading

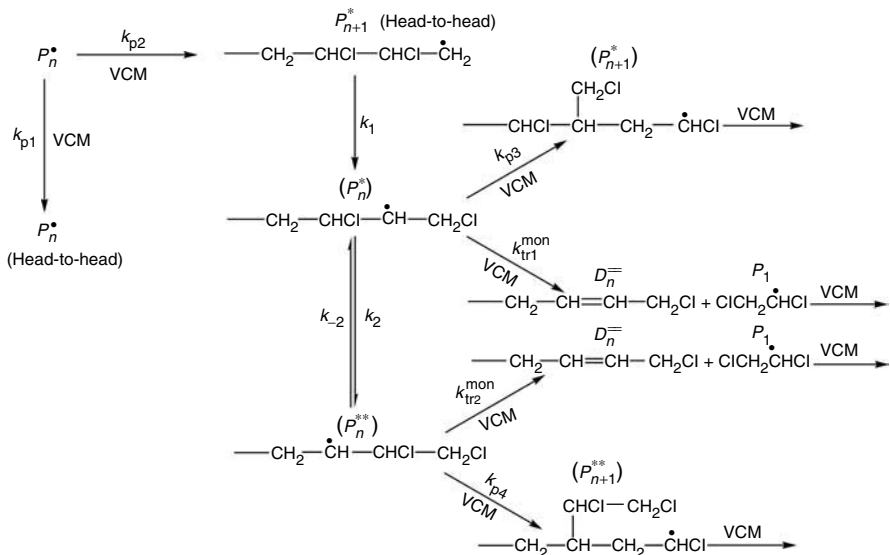


Figure 4.8 Formation of chloromethyl and ethyl branches and terminal double bonds [52].

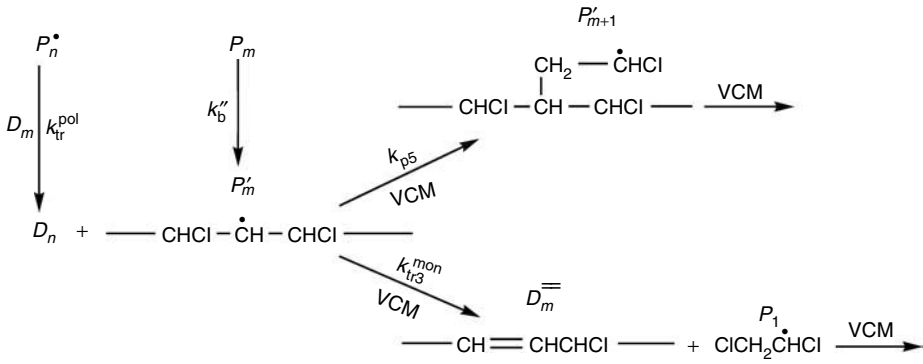


Figure 4.9 Formation of long-chain branches and internal double bonds [49].

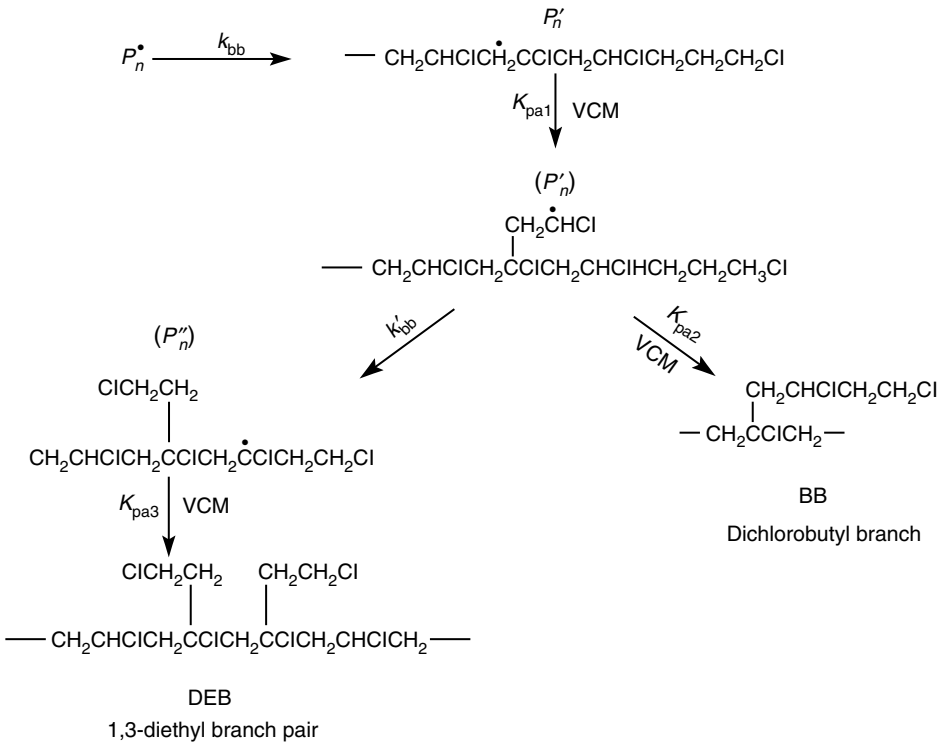


Figure 4.10 Formation of short-chain branches [49].

to the formation of chloromethyl and ethyl branches and terminal double bonds, the formation of long-chain branches and internal double bonds and the formation of short-chain branches via a backbiting reaction mechanism, respectively [47]. According to Xie *et al.* [40], Starnes *et al.* [46] and Starnes [47], a comprehensive kinetic mechanism for the free-radical polymerization of VCM is given in Table 4.3. The symbols *I* and *M* denote the initiator and

Table 4.3 Kinetic mechanism for free-radical VCM polymerization

Decomposition of initiator: $I \xrightarrow{k_I} 2I^*$
Formation of primary radicals: $I^* + M \xrightarrow{k_i} P_1$
Head-to-tail propagation: $P_n + M \xrightarrow{k_{p1}} P_{n+1}$
Head-to-head propagation: $P_n + M \xrightarrow{k_{p2}} P_{n+1}^*$
Chlorine shift reactions: $P_n^* \xrightarrow{k_1} (P_n^*), (P_n^*) \xrightleftharpoons[k_{-2}]{k_2} (P_n^{**})$
Formation chloromethyl branches: $(P_n^*) + M \xrightarrow{k_{p3}} (P_{n+1}^*)$
Formation of ethyl branches: $(P_n^{**}) + M \xrightarrow{k_{p4}} (P_{n+1}^{**})$
1,5 Shift backbiting reaction: $P_n \xrightarrow{k_{bb}} P'_n$
Head-to-tail addition: $P'_n + M \xrightarrow{k_{pa1}} (P'_{n+1})$
Formation of dichlorobutyl branches: $(P'_n) + M \xrightarrow{k_{pa2}} BB$
Six-center backbiting reaction: $(P'_n) \xrightarrow{k'_{bb}} (P''_n)$
Formation of 1,3-diethyl branch pair: $(P''_n) + M \xrightarrow{k_{pa3}} DEB$
Chain transfer to monomer reactions: $(P_n^*) + M \xrightarrow{k_{tr1}^{mon}} D_n^{\overline{\overline{}}} + P_1$
Formation of terminal double bonds: $(P_n^{**}) + M \xrightarrow{k_{tr2}^{mon}} D_n^{\overline{\overline{}}} + P_1$
Formation of internal double bonds: $P_m + M \xrightarrow{k_{tr3}^{mon}} \overline{\overline{D}}_m + P_1$
Hydrogen abstraction: $P_n + D_m \xrightarrow{k_{tr}^{pol}} D_n + P'_m$
1,6 Shift backbiting reaction: $P_m \xrightarrow{k''_{bb}} P'_m$
Formation of long-chain branches: $P'_m + M \xrightarrow{k_{p5}} P'_{m+1}$
Termination by combination: $P_n + P_m \xrightarrow{k_{tc}} D_{n+m}$
Termination by disproportionation: $P_n + P_m \xrightarrow{k_{td}} D_n + D_m$

monomer molecules, respectively. The symbols P_n and D_n are used to identify “live” and “dead” polymer chains, respectively, containing n monomer units. The symbols P_n^* , (P_n^*) and (P_n^{**}) denote the “live” polymer chains formed via a head-to-head emplacement of monomer. The symbol P'_m denotes the intermediate macroradical species produced via the hydrogen abstraction reaction. The symbols $D_n^{\overline{\overline{}}}$ and $\overline{\overline{D}}_n$ denote the “dead” polymer chains with terminal and internal double bond, respectively. Finally, the symbols P'_n , (P'_n) and (P''_n)

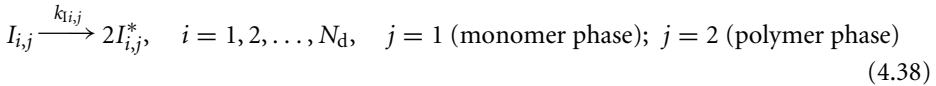
denote the intermediate “live” polymer chains that lead to the formation of DEB (1,3-diethyl branch pair) and BB (dichlorobutyl branch) short-chain branches. All the above reactions can occur in both monomer and polymer phases.

The kinetic mechanism illustrated in Table 4.3 shows that different types of live polymer chains (e.g., P_n , P_n^* , (P_n^*) , (P_n^{**}) , P'_m , etc.) are produced during the vinyl chloride polymerization. However, most of the relevant kinetic rate constants (i.e., k_{p2} , k_{p3} , k_{p4} , k_{p5} , k_{pa1} , k_{pa2} , k_{pa3}) are not known and the concentration of all intermediate species cannot be measured. Taking into account the facts that most of the live polymer chains undergo head-to-tail addition to monomer [46] and that limited information is available on the numerical values of the kinetic rate constants, all of the propagation reactions can be lumped into a single propagation reaction. For the same reason, the three chain transfer to monomer reactions can be lumped into one chain transfer to monomer reaction [48].

According to the work of Starnes *et al.* [46], different types of short-chain branches can be produced via the backbiting reactions. The DEB structure is always produced in low concentrations, thus, it can be ignored [46]. Furthermore, the 1,6 shift backbiting reaction is ordinarily slower than the analogous 1,5 shift backbiting reaction. Thus, a single backbiting reaction can be employed to account for the formation of BB branches.

Taking into account all the above remarks, the detailed kinetic mechanism can be recast into a more realistic and simpler kinetic scheme that can predict the VCM consumption rate and the main molecular features of the PVC chains (e.g., number- and weight-average molecular weights, short- and long-chain branches, double bonds, etc.) [40, 49]:

Initiation:



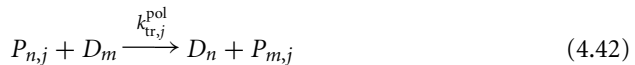
Propagation:



Chain transfer to monomer:



Chain transfer to polymer:



Intramolecular transfer (backbiting):



Termination by combination:



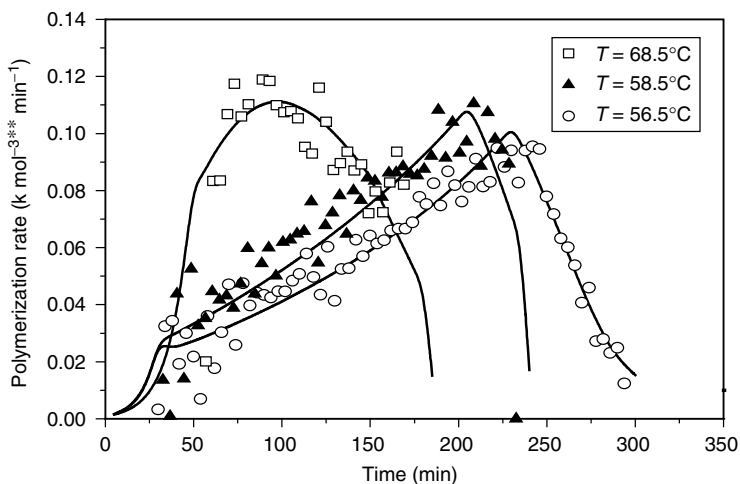
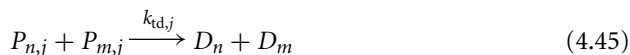


Figure 4.11 Predicted and experimental polymerization rate with respect to polymerization time (polymerization temperatures: 68.5°C, 58.5°C and 56.5°C, $I_{0,PDEH} = 0.606 \text{ g kg}^{-1} \text{ VCM}$). (Courtesy of ATOFINA.)

Termination by disproportionation:



The symbols I^* and N_d represent the primary initiator radicals and the number of initiators in the polymerization system, respectively. It should be noted that all the above reactions apart from the chain transfer to polymer can take place either in the monomer phase ($j = 1$) and/or in the polymer phase ($j = 2$).

The kinetics of VCM polymerization have been the subject of numerous publications over the last 25 years. The mathematical models proposed to describe the evolution of the polymerization rate have been recently reviewed by Sidiropoulou and Kiparissides [45] and Xie *et al.* [40, 41]. The reader is referred to these publications for further details. The derivation of the “live” and “dead” molar balance and moment rate equations for a vinyl chloride bulk polymerization system follow the developments presented in Section 3.2.4. Models developed in such a way show good predictive capabilities. Figure 4.11 shows an example for a series of experimental measurements, kindly provided by ATOFINA. An excellent agreement exists between model predictions and experimental results. It is evident that the polymerization rate increases with temperature, leading to a corresponding decrease of the batch polymerization time (i.e., increase of the reactor productivity). Figure 4.12 presents another example for the evolution of the average molecular weights reported in the open literature [50].

4.3.2 PVC morphology

PVC is insoluble in its own monomer; thus, vinyl chloride polymerization is a heterogeneous process that involves several physical transitions during the polymerization. As a result,

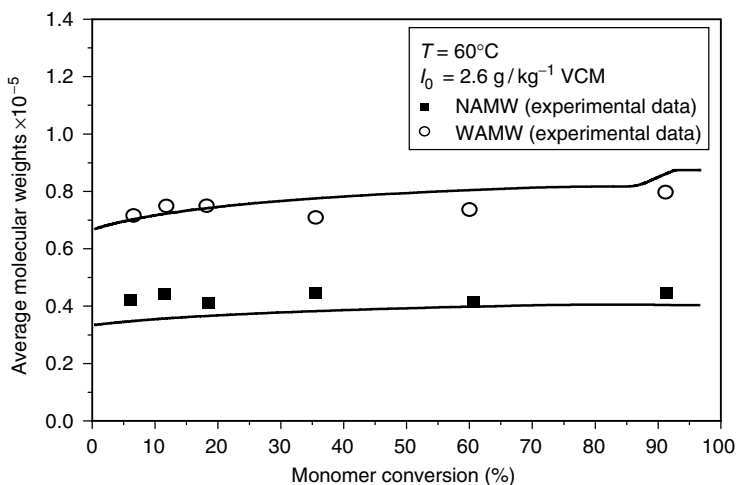


Figure 4.12 Predicted and experimental number- and weight-average molecular weights with respect to monomer conversion (polymerization temperature: 60°C, $l_{0,LP40} = 2.6 \text{ g kg}^{-1} \text{ VCM}$).

the final product of bulk or suspension polymerization is made up of primary particles and its agglomerates. The nucleation, growth and aggregation of these particles are responsible for the formation of particle internal morphology and associated properties, such as porosity, pore size distribution and specific surface area.

Rance [51, 52] reviewed the previously published work on the formation of PVC grains and proposed the following mechanism to describe the nucleation, stabilization, growth and aggregation of PVC primary particles (see Figure 4.13). Primary radicals, formed by initiator decomposition, rapidly react with the monomer to produce PVC macromolecules that are insoluble in the monomer phase. These polymer chains combine together to form unstable polymer microdomains, which have a radius of about 10–20 nm. However, the microdomains (or basic particles) have a limited stability and agglomerate rapidly to generate the primary particle nuclei, also called domains. The initial size of these domains has been found to lie in the range of 80–100 nm (i.e., 0.08–0.1 μm). Contrary to the basic particles, the primary particles carry sufficient negative electrostatic charges [53–55] and, thus, initially form stable colloidal suspensions in the monomer phase. Primary particles can be produced up to about 5–10% monomer conversion and they grow in size by capturing newly formed basic particles and, to a lesser degree, by polymerization of absorbed monomer. The size and number of primary particles depend on the particle stability, which decreases as the monomer conversion increases. At conversions of 10–30%, aggregation of primary particles results in the formation of a continuous network of primary particles. The structure of the flocculated network, its porosity and its strength will depend on the electrostatic and steric interactions between the primary particles, their size and their number density. Primary particles grow and aggregate until the free monomer phase disappears. Finally, at higher monomer conversions, primary particles fuse together to form agglomerates 2–10 μm in size.

The development of structure within grains of PVC was experimentally investigated by Tornell and Uustalu [39, 56] for different temperatures, agitation rates, stabilizers and

- Nucleation and microdomain formation (<0.01%)
- Aggregation and domain formation (0.01–1%)
- Growth and secondary aggregation (1–20%)
- Growth and fusion of primary particles (<70%)
- Pressure drop and decrease in reaction rate (>70%)

Particle unit	Constituents	Approximate size	Origin or description
Micro-domains	~50 radical chains	10–20 nm	Small nucleated entity. Aggregate of polymer chains.
Domain	1000 micro-domains	80–200 nm	Primary particle nucleus. Formed by merger of micro-domains.
Primary particle	One domain	0.6–1.4 μm	Formed by growth from a domain. Can be identified in final grain.
Agglomerate	~10 primary particles	1–10 μm	Formed by aggregation of primary particles. Grows with conversion.
Sub-grain	All primary particles	10–150 μm	Polymerized monomer droplet.
Grain	~1–15 droplets	20–250 μm	Free flowing at room temperature. Contains one or more sub-grains.

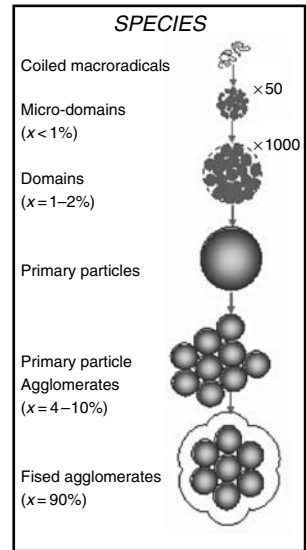


Figure 4.13 The evolution of internal particle morphology.

initiators. The experimental results show that the product's final porosity is strongly related to the conversion at which the primary particle network is formed. At the critical conversion, the structure and strength of the network will be affected by the size, number and interaction forces between primary particles, which are in turn influenced by the polymerization conditions (i.e., polymerization temperature, stirrer speed, type and concentration of stabilizers, etc.).

Despite the commercial importance of PVC particle morphology to its end-use applications, there has been little work done on the development of quantitative models relating the size evolution of primary particles in terms of process conditions. Kiparissides [57] developed a population balance model to describe the time evolution of the primary particle size distribution as a function of the process variables, such as temperature and ionic strength of the medium. However, for the solution of the population balance model, the coalescence rate constant between the primary particles needs to be known. This, in turn, requires the calculation of electrostatic and steric stabilization forces acting on these particles.

Ray *et al.* [58] presented a model for the prediction of the PVC primary particle-size distribution using a semi-empirical form for the calculation of the particle coalescence rate constant. Later on, Kiparissides *et al.* [59] derived detailed expressions for the calculation of the coalescence rate constant of two colloidal particles by taking into account both electrostatic and steric-stabilization forces. It was shown that, in the former case, the particle coalescence rate constant could be expressed as a function of temperature, reciprocal Debye length and the total particle charge, in accordance with the Muller–Smoluchowski coagulation theory [60–62]. In the presence of steric stabilization forces, the variables affecting the particle coagulation kinetics are the molar weight and the total mass of the adsorbed polymer and the Flory–Huggins interaction parameter of the monomer-stabilizing polymer system. In the latter case, the Hesselink, Vrij and Overbeek [63, 64] model was invoked for

the calculation of the interaction potential between two particles covered by an adsorbed layer of neutral polymer.

Kiparissides *et al.* [65] developed a comprehensive mathematical model for the quantitative prediction of the evolution of primary particle-size distribution during the free-radical polymerization of VCM. The population balance equation, describing the evolution of the primary particles in bulk or suspension polymerization, has the following general form:

$$\begin{aligned} \frac{\partial n(v, t)}{\partial t} + \frac{\partial(I(v, t)n(v, t))}{\partial v} \\ = \delta(v - v_0) r(v_0, t) + \frac{1}{2} \int_{v_0}^{v-v_0} \beta(v - u, u) n(v - u, t) n(u, t) du \\ - \int_{v_0}^{v_\infty} \beta(v, u) n(v, t) n(u, t) du \end{aligned} \quad (4.46)$$

where $n(v, t)dv$ denotes the number of particles of volume, v to $(v + dv)$, at time t per unit volume of the reaction medium. Equation 4.46 expresses the change of the density function $n(v, t)$, with respect to time and volume, due to polymerization in the polymer phase (second term). The second and third term on the right-hand side of Equation 4.46 represent the rates at which particles enter and leave the size range v to $(v + dv)$, due to particle–particle coalescence. Finally, the first term represents the rate at which basic particles of volume v_0 are generated in the monomer phase.

The term $\beta(u, v)$ represents the coalescence rate constant of two colloidal particles of volume u and v . Note that the initial particle growth occurs mainly by particle aggregation and, to a smaller extent, by polymerization of the adsorbed monomer in the polymer-rich phase [58]. Thus, knowledge of analytical expressions for the coalescence rate constant is of profound importance to the solution of the population balance model (Equation 4.46), describing the time evolution of the primary particle size distribution. Such expressions have been derived by Kiparissides *et al.* [57, 59].

4.3.2.1 Rate of formation of microdomains

The rate of generation of microdomains, $r(v_0, t)$, in Equation 4.46, will depend on the rate of polymerization in the monomer-rich phase R_{pm} , and will be given by:

$$r(v_0, t) = \frac{R_{pm} w_m}{\rho_p (1 - \varphi_m) v_0^2} \quad (4.47)$$

where w_m , ρ_p and φ_m denote the monomer molecular weight, the density of PVC $\{\rho_p = 10^3 \exp[0.4296 - 3.274 \times 10^{-4} T \text{ (K)}], \text{ g L}^{-1}\}$ and the equilibrium monomer volume fraction in the polymer-rich phase, respectively. The latter can be expressed as

$$\varphi_m = \frac{1 - x_f}{1 - x_f (1 - \rho_m / \rho_p)} \quad (4.48)$$

where x_f is the critical conversion at which the separate monomer phase disappears [$0.8 - 1.9 \times 10^{-3} T$ ($^{\circ}\text{C}$)]. ρ_m and v_0 denote the density of the monomer [$947.1 - 1.746 T$ ($^{\circ}\text{C}$) $- 3.24 \times 10^{-3} T^2$ ($^{\circ}\text{C}$)] and the initial volume of the microdomains, respectively.

4.3.2.2 Calculation of the primary particle growth rate

The rate of growth of the primary particles due to polymerization of the absorbed monomer in the polymer-rich phase, I_V , can be expressed in terms of the overall rates of polymer-rich phase, R_{pp} , using the following equation:

$$I_V = \frac{R_{pp}}{[M_0]x} \nu \quad (4.49)$$

where $[M_0]$ and x are the initial monomer concentration and the fractional conversion, respectively. The growth rate of primary particles in terms of particle diameter can be obtained from Equation 4.49 by substituting ν by $\pi d_p^2/6$.

4.3.2.3 Simulation results

Simulation results were obtained from the numerical solution of the population balance model, Equations 4.46–4.49. The effects of ionic strength, total particle charge, temperature, degree of agitation, initial concentration type of initiator and steric stabilization on the total particle number as well as the average particle size were examined. In Figures 4.14 and 4.15 the average particle size and total particle number determined from the solution of the model are compared to the experimental data of Willmouth *et al.* [55]. It can be seen that during the initial stages of polymerization the primary particle population is controlled by

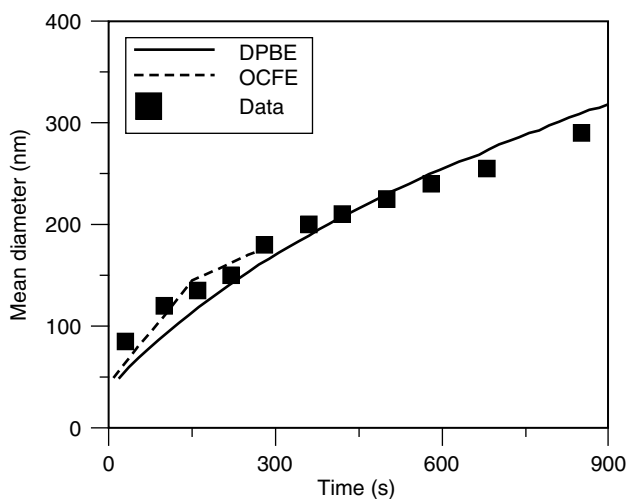


Figure 4.14 Mean diameters of PVC primary particles. Comparison to data of Willmouth *et al.* [55]. $T = 50^{\circ}\text{C}$, initiator LP 1 g kg^{-1} VCM. Particle stability model $E_i = 1$, $\kappa^{-1} = 150 \text{ nm}$, $p = 1.5$. PBE solver DPBE ($n_e = 20$, $q = 1$).

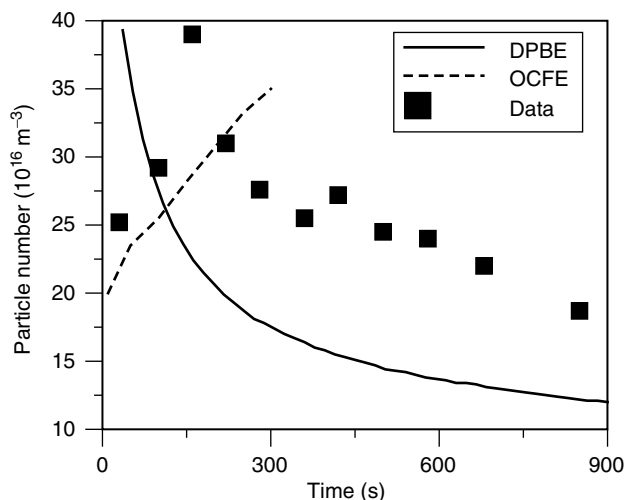


Figure 4.15 Total number of PVC primary particles. Comparison to data of Willmouth *et al.* [55]. $T = 50^{\circ}\text{C}$, initiator LP 1 g kg^{-1} VCM. Particle stability model $E_f = 1$, $\kappa^{-1} = 150 \text{ nm}$, $\rho = 1.5$. PBE solver DPBE ($n_e = 20$, $q = 1$).

particle nucleation. Later, particle aggregation becomes dominant, resulting in a decrease in the number of primary particles. The size and number of primary particles are strongly controlled by the concentrations of electrolyte and secondary stabilizer which influence the electrostatic and steric stabilization mechanisms, respectively.

Acknowledgments

Gregorio Meira thanks the following colleagues and students with whom he had the pleasure of investigating the HIPS process: Diana Estenoz, Haydée Oliva, Natalia Casis and Carla Luciani. Also acknowledged is the financial support by the following Argentine institutions: Conicet, Universidad Nacional del Litoral and ANPCyT.

References

1. Scheirs, J. and Priddy, D. (eds.) (2003) *Modern Styrenic Polymers: Polystyrenes and Styrenic Copolymers*. Wiley Series in Polymer Science. John Wiley & Sons Ltd, Chichester, England.
2. Martin, M.F., Viola, J.P. and Wuensch, J.R. (2003) In J. Scheirs and D. Priddy (eds.) *Modern Styrenic Polymers: Polystyrenes and Styrenic Copolymers*. Wiley Series in Polymer Science. John Wiley & Sons Ltd, Chichester, England, pp. 247–280.
3. Maul, J., Frushour, B.G., Kontoff, J.R., Eichenauer, H. and Ott, K.H. (2002) In *Ullmann's Encyclopedia of Industrial Chemistry*. Wiley-VCH Verlag GmbH & Co., Germany.
4. Priddy, D.B. (1998) In *Kirk-Othmer Encyclopedia of Chemical Technology*, 4th edn. John Wiley & Sons Inc., New York, Vol. 42, pp. 1–40.
5. Fischer, M. and Hellmann, G.P. (1996) *Macromolecules*, **29**, 2498–2509.

6. Moore, E.R. *et al.* (1989) In *Encycl. Polym. Sci. Eng.*, **16**, 68.
7. Brydon, A., Burnett, G.M. and Cameron, G.G. (1973) *J. Polym. Sci., Polym. Chem. Ed.*, **11**, 3255–3269.
8. Huang, N.J. and Sundberg, D.C. (1995) *J. Polym. Sci., Polym. Chem. Ed.*, **33**, 2533–2549.
9. Huang, N.J. and Sundberg, D.C. (1995) *J. Polym. Sci., Polym. Chem. Ed.*, **33**, 2587–2603.
10. Ludwico, W.A. and Rosen, S.L. (1976) *J. Polym. Sci., Polym. Chem. Ed.*, **14**, 2121–2134.
11. Kekhahiov, D. and Mikhnev, B. (1985) *Int. Polym. Sci. Technol.*, **12**, T/70–72.
12. Riess, G. and Gaillard, P. (1983) *Macromol Symp.*, 221–236.
13. Estenoz, D.A., Leal, G.P., López, Y.R., Oliva, H.M. and Meira, G.R. (1996) *J. Appl. Polym. Sci.*, **62**, 917–939.
14. Peng, F. (1986) *J. Appl. Polym. Sci.*, **31**, 1827–1842.
15. Demirrors, M., Veraert, R. and Hermans, C. (1999) *Polym. Preprints*, **40**, 71–72.
16. Soto, G., Nava, E., Rosas, M., Fuenmayor, M., González, I.M., Meira, G.R. and Oliva, H.M. (2004) *J. Appl. Polym. Sci.*, **92**, 1397–1412.
17. Estenoz, D.A., Vega, J.R., Oliva, H.M. and Meira, G.R. (2002) *J. Liq. Chrom. Rel. Technol.*, **25**, 2781–2793.
18. Manaresi, V., Passalacqua, V. and Pilati, F. (1975) *Polymer*, **16**, 520–526.
19. Sundberg, D.C., Arndt, J. and Tang, M.Y. (1984) *J. Dispersion Sci. Technol.*, **5**, 433–445.
20. Chern, Ch.Sh. and Poehlein, G.W. (1987) *Chem. Engng Commun.*, **60**, 101–117.
21. Huang, N.J. and Sundberg, D.C. (1995) *J. Appl. Polym. Sci.*, **33**, 2533–2549.
22. Estenoz, D.A. and Meira, G.R. (1993) *J. Appl. Polym. Sci.*, **50**, 1081–1098.
23. Estenoz, D.A., Valdez, E., Oliva, H.M. and Meira, G.R. (1996) *J. Appl. Polym. Sci.*, **59**, 861–885.
24. Estenoz, D.A., Meira, G.R., Gómez, N. and Oliva, H.M. (1998) *AIChE J.*, **44**, 427–441.
25. Estenoz, D.A., Gonzalez, I.M., Oliva, H.M. and Meira, G.R. (1999) *J. Appl. Polym. Sci.*, **74**, 1950–1961.
26. Luciani, C.V., Estenoz, D.A., Meira, G.R. and Oliva, H.M. (2005) *Ind. Engng Chem. Res.*, **44**, 8354–8367.
27. Estenoz, D.A., Vega, J.R., Oliva, H.M. and Meira, G.R. (2001) *Int. J. Polymer Anal. Charact.*, **6**, 315–337.
28. Vega, J.R., Estenoz, D.A., Oliva, H.M. and Meira, G.R. (2001) *Int. J. Polym. Anal. Charact.*, **6**, 339–348.
29. Ludwico, W.A. and Rosen, S.L. (1975) *J. Appl. Polym. Sci.*, **19**, 757–768.
30. Casís, N., Estenoz, D., Gugliotta, L., Oliva, H. and Meira, G. (2006) *J. Appl. Polym. Sci.*, **99**, 3023–3039.
31. Kruse, R.L. (1974) *Copolymers, Polyblends, and Composites*. A.C.S., Washington D.C., USA, p. 141.
32. Seavey, K.C., Liu, Y.A., Khare, N.P., Bremner, T. and Chen, C.C. (2003) *Ind. Engng Chem. Res.*, **42**, 5354–5362.
33. Luciani, C.V., Estenoz, D.A. and Meira, G.R. (2005) In *Proceedings of 2nd Mercosur Congress on Chemical Engineering (Macro 2006)*. Rio de Janeiro, Brasil, August, pp. 371–381.
34. Luciani, C., Estenoz, D. and Meira, G. (2006) In *Proceedings of IUPAC World Polymer Congress (Macro 2006)*, Rio de Janeiro, Brasil, July.
35. Smallwood, P.V. (1990) In *Encyclopedia of Polymer Science and Technology*, H. Mark (ed.). Wiley, New York, **27**, p. 295.
36. Saeki, Y. and Emura, T. (2000) *Prog. Polym. Sci.*, **27**, 2055–2131.
37. Burgess, R.H. (1982) *Manufacturing and Processing of PVC*. Applied Science Publishers, London.
38. Langsam, M. (1986) In L.I. Nass and C.A. Heiberger (eds), *Encyclopedia of PVC*, 2nd edn. Marcel Dekker Inc., New York, pp. 1–48.
39. Tornell, B. and Uustalu, J.M. (1988) *J. Appl. Polym. Sci.*, **35**, 63–74.
40. Xie, T.Y., Hamielec, A.E., Wood, P.E. and Woods, D.R. (1991) *Polymer*, **32**, 537–557.

41. Xie, T.Y., Hamielec, A.E., Wood, P.E. and Woods, D.R. (1991) *J. Vinyl Techn.*, **13**, 2–25.
42. Yuan, H.G., Kalfas, G. and Ray, W.H. (1991) *J. Macromol. Sci., Rev. Macromol. Chem. Phys.*, **C(31)(2&3)**, 215–232.
43. Allsop, M.W. (1982) In R.H. Burgess (ed.), *Manufacture and Processing of PVC*. Applied Science Publishers, London.
44. Mejdell, T., Pettersen, T., Naustdal, C. and Svendsen, H.F. (1999) *Chem. Engng Sci.*, **54**, 2459–2466.
45. Sidiropoulou, E. and Kiparissides, C. (1991) *J. Macromol. Sci., Chem.*, **A27(3)**, 257–288.
46. Starnes, W.H. Jr., Zaikov, V.C., Chung, H.T., Wojciechowski, B.J., Tran, H.V. and Saylor, K. (1998) *Macromolecules*, **31**, 1508–1517.
47. Starnes, W.H. Jr. (2002) *Prog. Polym. Sci.*, **27**, 2133–2170.
48. Krallis, A., Kotoulas, C., Papadopoulos, S., Kiparissides, C., Bousquet, J. and Bonardi, C. (2004) *Ind. Engng Chem. Res.*, **43**, 6382–6399.
49. Kiparissides, C., Daskalakis, G., Achilias, D.S. and Sidiropoulou, E. (1997) *Ind. Engng Chem. Res.*, **36**, 1253–1267.
50. Cebollada, A.F., Schmidt, M.J., Farber, J.N., Capiati, N.J. and Valles, E.M. (1989) *J. Appl. Polym. Sci.*, **37**, 145–162.
51. Rance, D.G. (1985) In R. Buscall, T. Corner and J.F. Stageman (eds), *Polymer Colloids*. Elsevier, Amsterdam, p. 289.
52. Rance, D.G. and Zichy, E.L. (1981) *Pure Appl. Chem.*, **53**, 377–385.
53. Wilson, J.C. and Zichy, E.L. (1979) *Polymer*, **20**, 264–265.
54. Davidson, J.A. and Witenhafer, D.E. (1980) *J. Polym. Sci. Polym., Phys. Ed.*, **18**, 51–69.
55. Willmouth, F.M., Rance, D.G. and Henman, K.M. (1984) *Polymer*, **25**, 1185–1192.
56. Tornell, B. and Uustalu, J.M. (1986) *Polymer*, **27**, 250–252.
57. Kiparissides, C. (1990) *Makromol. Chem. Macromol. Symp.*, **35/36**, 171–192.
58. Ray, W.H., Jain, S.K. and Salovey, R. (1975) *J. Appl. Polym. Sci.*, **19**, 1297–1315.
59. Kiparissides, C., Moustakis, I. and Hamielec, A.E. (1993) *J. Appl. Polym. Sci.*, **49**, 445–455.
60. Muller, H. (1928) *Kolloid-Reih*, **26**, 257.
61. Fuchs, N.Z. (1934) *Physik*, **89**, 736.
62. Tornell, B.E., Uustalu, J.M. and Jonsson, B. (1986) *Colloid Polym. Sci.*, **264**, 439–444.
63. Hesselink, F., Vrij, A. and Overbeek, J.G. (1971) *J. Phys. Chem.*, **75**, 2094.
64. Sonntag, H. and Strenge, K. (1987) *Coagulation Kinetics and Structure Formation*. Plenum Press, New York.
65. Kiparissides, C., Achilias, D.S. and Chatzi, E. (1994) *J. Appl. Polym. Sci.*, **54**, 1423–1438.

Chapter 5

Suspension Polymerization

Costas Kotoulas and Costas Kiparissides

5.1 Introduction

Free-radical suspension polymerization, originally developed by Hoffman and Delbruch in 1909 [1] is commonly employed for producing a wide variety of commercially important polymers such as poly(vinyl chloride) (PVC), polystyrene (PS), expandable polystyrene (EPS), high-impact polystyrene (HIPS) and various styrene copolymers with acrylonitrile (SAN) and acrylonitrile-polybutadiene (ABS), poly(methyl methacrylate) (PMMA), poly(vinyl acetate) (PVAc), etc. [2].

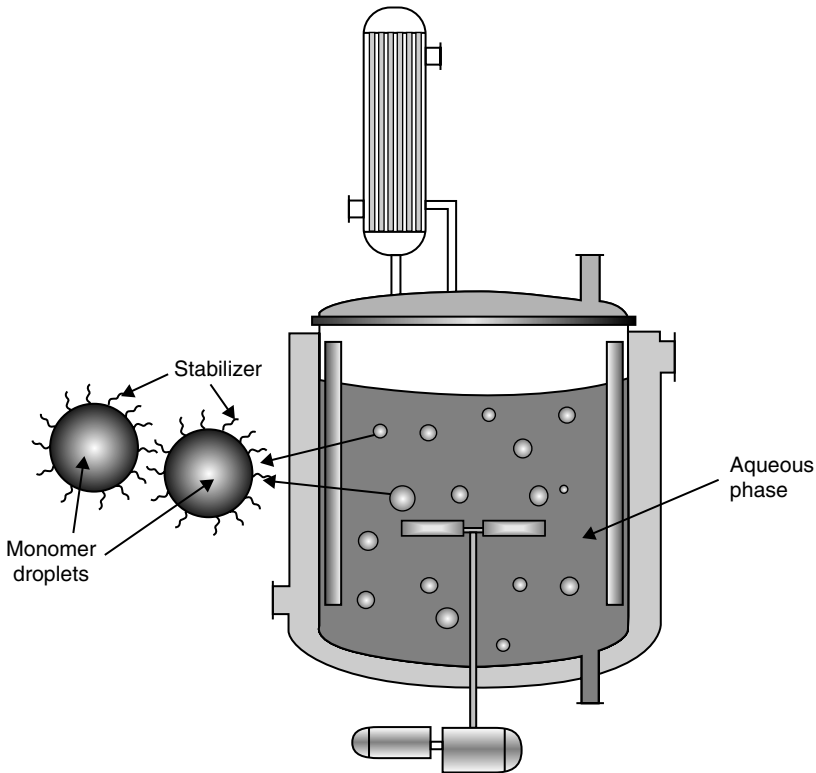
The suspension polymerization process is typically carried out in well-stirred batch reactors. A typical suspension polymerization recipe for PS is shown in Table 5.1. The volume of the reaction vessel can be up to 150 m³ (see Figure 5.1). The monomer(s) is (are) initially dispersed in the continuous phase (commonly water) by the combined action of surface active agents (inorganic or/and water-soluble polymers) and agitation. All the reactants (monomer(s), initiator(s), etc.) reside in the organic or “oil” phase. The polymerization occurs in the monomer droplets that are progressively transformed into sticky, viscoelastic monomer–polymer droplets and finally into rigid, spherical polymer particles in the size range of 50–500 μm [3]. The polymer solids’ content in the fully converted suspension is typically 30–50% w/w. On the other hand, in the inverse suspension polymerization, the hydrophilic monomer(s) (e.g., acrylamide, acrylic acid) and initiator are dispersed in the hydrophobic continuous organic phase (e.g., hexane, paraffin oil).

In general, the suspension polymerization can be distinguished into two types, namely, the “bead” and “powder” suspension polymerization [4]. In the former process, the polymer is soluble in its monomer and smooth spherical particles are produced. In the later process, the polymer is insoluble in its monomer and, thus, precipitates out leading to the formation of irregular grains or particles. The most important thermoplastic produced by the “bead” suspension polymerization process is PS. In the presence of volatile hydrocarbons (C₄–C₆), foamable beads, the so-called EPS, are produced. On the other hand, PVC, which is the second largest thermoplastic manufactured in the world, is an example of the “powder” type suspension polymerization.

The main advantages of suspension polymerization compared to the bulk process are the easier control of the reaction temperature due to the presence of the dispersion medium (e.g., water), the milder reaction conditions and the product homogeneity, especially for

Table 5.1 Typical suspension polymerization recipe for PS production

Styrene	100 parts (by mass)
Water	100–150 parts (by mass)
<i>n</i> -Pentane (only for EPS)	5–10 parts (by mass)
Initiator (BPO, DCP, etc.)	0.2–0.5 parts (by mass)
Pickering dispersant (tricalcium phosphate, barium sulfate, MgCO ₃ , etc.)	1 part (by mass)

**Figure 5.1** Schematic representation of a suspension polymerization reactor.

monomers having a very low solubility in the continuous phase [4]. Polymers produced by suspension polymerization have in general a higher purity than those produced by emulsion polymerization. On the other hand, the main disadvantages of the suspension polymerization process are the low reactor productivity due to the presence of the dispersion medium (e.g., 50% v/v), the required post-treatment of the dispersion medium for removing all the undesired impurities (e.g., suspending agents, etc.), before its recycling, and the difficulty in the production of homogeneous copolymers, especially when the monomers have different reactivities and solubilities in the continuous phase.

One of the most important issues in the suspension polymerization process is the control of the particle size distribution (PSD) [5]. In general, the initial monomer droplet size distribution (DSD) as well as the polymer PSD depends on the type and concentration of the surface active agent, the quality of agitation (e.g., reactor geometry, impeller type, power input, etc.) and the physical properties (e.g., densities, viscosities, interfacial tension) of the continuous and dispersed phases. The dynamic evolution of the droplet/PSD is controlled by the rates of two physical processes, namely, the drop/particle breakage and coalescence. The former mainly occurs in regions of high shear stress (i.e., near the agitator blades) or as a result of turbulent velocity and pressure fluctuations along the drop's surface. Drop/particle coalescence can be either increased or decreased by the turbulent flow field. At sufficiently high concentrations of surface active agents, it can be assumed to be negligible for very dilute dispersions [6].

In regard to the droplet/particle breakage and coalescence phenomena, the suspension polymerization process can be divided into three stages [7, 8]. At low monomer conversions (i.e., low viscosity of the monomer–polymer phase, stage one), drop breakage is the dominant mechanism. As a result, the initial DSD shifts to smaller sizes. During the second sticky-stage of polymerization, the drop breakage rate progressively decreases while drop/particle coalescence becomes the dominant mechanism. Thus, the average particle size starts increasing and the PSD becomes broader. At higher monomer conversions, the particles are sufficiently hard so the collisions between them are elastic and, thus, the particle coalescence ceases. This point is called identification point. After this point, the PSD has been established except for some minor particle shrinkage taking place as monomer conversion increases due to density differences between monomer and polymer.

Specifically for the PS “bead” suspension process, Villalobos *et al.* [9] reported that the end of the first stage occurred at approximately 30% monomer conversion, corresponding to a critical viscosity of about 0.1 Pa s. They also found that the second stage extended up to about a 70% monomer conversion. In the vinyl chloride monomer (VCM) “powder” polymerization, it has been shown that, at monomer conversions around 10–30%, a continuous polymer network is commonly formed inside the polymerizing monomer droplets that significantly reduces the drop/particle coalescence rate [10]. Cebollada *et al.* [11] reported that the PSD was essentially established at monomer conversions of about 35–40% (i.e., end of the second stage).

From a kinetic point of view, the free-radical suspension polymerization follows the same kinetic mechanism as the respective “bulk” polymerization, described in Chapters 3 and 4. In fact, each polymerizing monomer droplet can be viewed as a micron-size “bulk” polymerization reactor. It should be noted that when the monomers are significantly soluble in the continuous phase, the numerical values of the kinetic rate constants commonly applied to “bulk” polymerization, need to be properly modified (i.e., by defining some apparent kinetic rate constants) to take into account the monomer partitioning between the continuous and dispersed phases and the fact that polymerization takes place in two phases (i.e., in the “oil” and in the “aqueous” phase) [12]. For example, the numerical value of the apparent propagation rate constant, k_p , for the suspension polymerization of vinyl acetate significantly varies from that applied to the “bulk” process [13]. Kalfas *et al.* [14] presented experimental evidence showing that the dissolved vinyl acetate in the continuous aqueous phase did not diffuse into the polymerizing monomer droplets, which affects both the overall polymerization rate and the molecular weight

developments. Thus, the monomer(s) solubility(ies) in the aqueous phase can affect the overall polymerization rate, the molecular weight distribution (MWD) and the copolymer composition distribution (CCD) of the polymer. In the suspension copolymerization of styrene-acrylonitrile, the apparent reactivity ratios differ from those reported for the “bulk” or solution process [15], and beads of different sizes have been found to exhibit different MWDs [16].

5.2 Surface active agents

Surface active agents play a very important role in the stabilization of liquid–liquid dispersions. They can be water-soluble copolymers (e.g., poly(vinyl alcohol) (PVA) and cellulose ethers) or colloidal inorganic powders (Pickering dispersants, e.g., tricalcium phosphate, barium sulfate, calcium carbonate, etc.). The former mainly consist of hydrophilic and hydrophobic (lipophilic) monomer units. The lipophilic segments of the polymeric stabilizers are soluble in the organic monomer phase, while the hydrophilic units tend to remain in the continuous aqueous phase. These stabilizers reduce the drop/particle coalescence rate because of steric repulsive forces [17]. Actually, the presence of a protective colloidal film around the droplet prolongs the contact time for drop coalescence, thus, increasing the probability of drop separation by agitation. Hartland [18] argued that stabilizers increase the interfacial viscosity and lower the interfacial tension. The most important factor in determining the effectiveness of a polymeric stabilizer is its hydrophilic–lipophilic balance (HLB), while the molecular mass of the stabilizer is less significant [7].

One of the most commonly used stabilizers in suspension polymerization is PVAc that has been partially hydrolyzed to PVA. By varying the acetate content (i.e., degree of hydrolysis), one can alter the hydrophobicity of PVA and, thus, the conformation and surface activity of the polymer chains at the monomer/water interface [19]. The solubility of PVA in water depends on the overall degree of polymerization (i.e., molecular weight), the sequence chain length distribution of the vinyl alcohol and vinyl acetate units in the copolymer, the degree of hydrolysis and temperature. Depending on the agitation rate, the concentration and type of surface active agent, the average droplet size can exhibit a U-shape variation with respect to the agitation speed (see Figure 5.2(a) and (b)). This U-type behavior has been confirmed both experimentally and theoretically and has been attributed to the balance of breakage and coalescence rates of monomer drops. The initial decrease of the drop size with increasing impeller speed can be explained by the higher drop breakage frequency due to the higher shear stresses. However, as the interfacial area increases due to the formation of a larger number of small-size drops in the system, the effectiveness of the stabilizer molecules to fully cover the generated drops’ surface diminishes. As a result, the drop coalescence increases, leading to an increase in the drop/particle size.

Water-soluble substituted celluloses are another class of stabilizers used in the suspension polymerization, mainly in the manufacture of PVC. These stabilizers are soluble in both the vinyl chloride and the aqueous phase [20]. Consequently, the stabilizer can also affect the stability of the primary particles inside the polymerizing monomer droplets and, thus, the final porosity of the PVC particles. Hydroxypropyl methylcellulose (HPMC) is a cellulose ether, produced by reacting cellulose with propylene oxide and methyl chlorine in an alkaline medium. As a result, a fraction of the hydroxyl groups (hydrophilic groups) of the cellulose

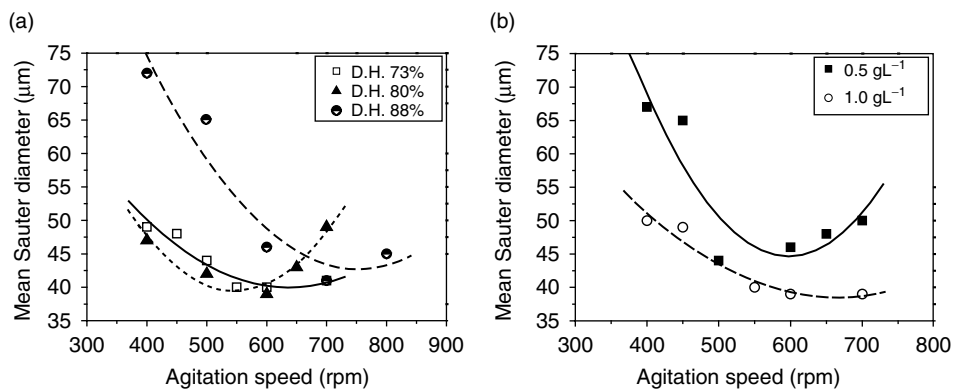


Figure 5.2 Dependence of the steady-state Sauter mean diameter on the agitation speed for (a) various PVA grades and (b) concentrations.

are substituted by hydroxypropyl and methyl groups (lipophilic groups). Cellulose ethers are generally characterized by their solution viscosity, the chemical nature of the substituents, the degree of substitution, their purity, rheological properties, solubility in the aqueous phase and compatibility with the polymer. It has been observed that the HPMC–VCM compatibility is a function of the molecular weight and the degree of substitution of the cellulose derivative. Thus, HPMC of low molecular weight has a higher compatibility with VCM and results in a higher porosity of the final PVC resin [11].

Pickering stabilizers, commonly used in styrene suspension polymerization, are inorganic solids, insoluble in the aqueous phase. Their main advantage is that they can be removed easily from the final particulate product (e.g., by dilute acid), which improves the clarity and transparency of the polymer. Also, the amount of polymer deposited on the wall and on other parts of the reactor decreases, which considerably improves the heat transfer rate from the reaction medium to the coolant. Finally, it should be mentioned that inorganic powders are usually cheaper [5].

The sorption kinetics of the stabilizer molecules from the continuous phase to the organic–water interface changes with time. The time required for the sorption process to reach its steady-state is controlled by the transfer of the stabilizer molecules from the continuous phase to the droplet surface and their subsequent reformation and rearrangement at the organic–water interface. As the stabilizer concentration increases, the time required for the system to reach equilibrium is reduced, indicating an increased polymer diffusion rate [21]. Nilsson *et al.* [22] argued that the stabilizer molecules diffuse very quickly to the liquid–liquid interface, but not in the more thermodynamically stable conformation and, thus, a rearrangement takes place until the system reaches its equilibrium.

Chatzi and Kiparissides [19] studied the aqueous dispersion of *n*-butylchloride in the presence of various PVA stabilizers and they observed two critical concentrations of PVA at which the interfacial tension changed (see Figure 5.3). At low PVA concentrations (e.g., less than 0.001 g L⁻¹), the interfacial tension was relatively independent of the PVA concentration for all types of PVA studied. At higher concentrations, the interfacial tension decreased almost linearly with the PVA concentration on a semi-log scale. This convex behavior was

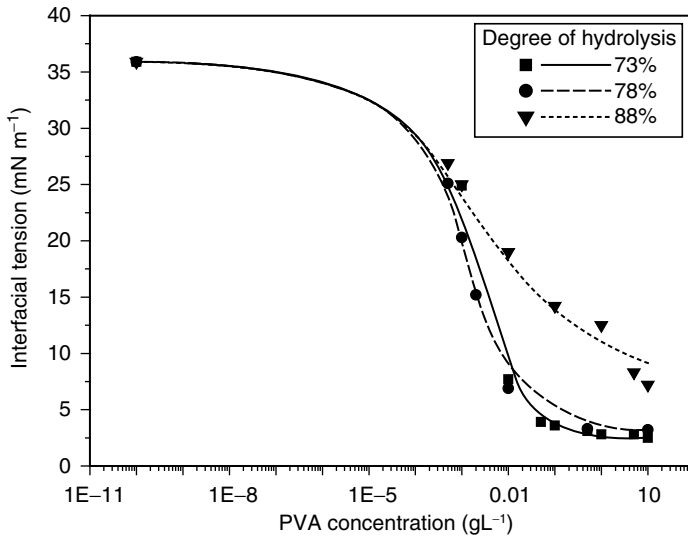


Figure 5.3 Variation of the equilibrium interfacial tension of *n*-butyl chloride/water with respect to the PVA concentration at 20°C for three different PVA grades.

also observed by Lankveld and Lyklema [23] for a paraffin-oil in water system in the presence of a PVA stabilizer with 88% degree of hydrolysis. The results of Figure 5.3 can be fitted to an ideal Langmuir-like adsorption isotherm in terms of the surface coverage, θ , and the PVA concentration ($[PVA]$, g L^{-1}) and assuming a linear dependence of the interfacial tension, σ , with respect to the surface coverage:

$$\sigma = 35 - 32\theta \quad (5.1)$$

where

$$\theta = [PVA]/(0.001 + [PVA]) \quad (5.2)$$

5.3 Mixing phenomena

It has long been recognized that some of the main factors that influence the PSD in a suspension polymerization reactor are the reactor geometry, the type, size and bottom clearance of the impeller, the presence of baffles, and the amount of energy provided to the reaction mixture through the impeller rotation [2]. All these factors determine the flow and energy fields in the vessel. If one were to characterize the quality of mixing in a suspension polymerization reactor using a single “parameter”, the average rate of energy dissipation, $\bar{\epsilon}$ (W kg^{-1} or $\text{m}^2 \text{s}^{-3}$), should be the preferable one.

In a turbulent flow field, a random flow of eddies is commonly superimposed on the overall average fluid flow. In mixing equipment, the motor provides the power, which turns the impeller. This energy is transferred from the agitator into the largest scales of motion (eddies) of the fluid in the tank. This energy is then transferred (cascaded) from the largest

eddies down to the smallest scales of turbulent motion. At this level, the energy is dissipated to heat. Macromixing is accomplished by the largest scales of motion (i.e., those scales responsible for bulk flow in the tank). On the other hand, the micromixing takes place at the smallest scales of motion where the turbulence tends to be uniform. In suspension polymerization, both scales of motion are important. The final particle size obtained is a direct consequence of the turbulent motion in the dissipative range of eddy sizes, while the circulation of particles through the tank, both during the initial drop-sizing operation and subsequent polymerization, is controlled by the bulk flow.

For a turbulent flow field in an agitated vessel, the average energy dissipation rate per unit mass will be equal to the power input into the system, P , per unit mass, and is given by

$$\bar{\varepsilon} = \frac{P}{\rho V} \quad (5.3)$$

where ρ is the density of the fluid ($\text{kg } \ell^{-1}$) and V is the liquid volume (ℓ).

In the presence of a dispersed phase (e.g., the monomer drops in the suspension polymerization), the turbulent intensity decreases due to the decrease of the velocity fluctuations of the continuous phase [24]. Doulah [25] proposed the following relation to account for the reduction of the energy dissipation rate in the presence of a second dispersed phase:

$$\frac{\bar{\varepsilon}_s}{\bar{\varepsilon}_c} = \left(\frac{\nu_c}{\nu_s} \right)^3 \quad (5.4)$$

where ν is the kinematic viscosity and the subscripts c and s denote the continuous phase and the suspension system, respectively. Actually, the decrease in the energy dissipation rate per unit mass is due to the fact that a fraction of the energy content of the eddies is consumed through their interactions with the monomer droplets. In this case, the energy dissipated to heat is lower.

Most mathematical studies on the dynamic evolution of the DSD/PSD in liquid–liquid and solid–liquid systems assume that the Kolmogorov theory of local isotropy holds true [26, 27]. Although the theory of local isotropy does not necessarily imply that a single value for the rate of energy dissipation should be used, in most modeling studies on the prediction of PSD in suspension polymerization reactors do use a single value for $\bar{\varepsilon}_s$ [28]. This simplification implies that the various interactions of eddies with droplets/particles are independent of the position within the vessel. However, numerous experiments over the past decades [29, 30] have shown that turbulence intensity is extremely high near the impeller, whereas the rest of the vessel is relatively calm. Thus, the dissipation rate can vary by a few orders of magnitude within the vessel. Alexopoulos *et al.* [30] and Coualoglou and Tavlarides [31] proposed a two-compartment model to describe turbulence inhomogeneity of a liquid–liquid dispersion in an agitated vessel of volume V . The total volume was divided into an impeller compartment and a circulation one, of volumes V_i and V_c , respectively. Although the local rate of energy dissipation changes continuously with the distance from the impeller tip, they assumed that the two compartments (i.e., impeller and circulation) were homogeneous, but possessed different values of the average rate of energy dissipation, $\bar{\varepsilon}_i$ and $\bar{\varepsilon}_c$, respectively. This approach has been applied to different suspension polymerization systems [2, 8, 32], showing the differences in the PSDs calculated by using a single-compartment or a two-compartment population balance model.

5.4 The “bead” suspension polymerization process

In the “bead” type of suspension polymerization, the polymer is soluble in its monomer and, thus, the monomer–polymer mixture is homogeneous. In this case, the suspension system can be treated as an aqueous dispersion of a time-varying viscoelastic fluid.

Polystyrene used in injection molding is manufactured by the suspension “bead” process. Poly(methyl methacrylate) and its copolymers containing small amounts of acrylate esters are also produced by the “bead” suspension process. Clear transparent polymers are often required, so formulations involving Pickering dispersants (e.g., MgCO_3) that can be removed from the polymer with dilute acid after polymerization, are particularly advantageous.

In the case of styrene–acrylonitrile copolymers, the method of choice for batch suspension polymerization is normally that involving the azeotropic monomer/comonomer composition to minimize copolymer compositional drift. Nevertheless, complications often arise because considerably more acrylonitrile than styrene dissolves in the continuous aqueous phase. As conversion proceeds, acrylonitrile diffuses into the polymer particles and the monomer ratio in the bead changes, causing the composition of the copolymer to change as well [4].

High-impact polystyrene and acrylonitrile-butadiene-styrene copolymer are often prepared in a combined bulk-suspension process. This begins with a solution of polybutadiene in styrene or styrene/acrylonitrile. Subsequently, the polymerization of styrene or styrene/acrylonitrile is initiated and continues under stirring until phase inversion occurs (i.e., polybutadiene is dispersed in a continuous PS matrix – Chapter 4). In the final stage, water and dispersant are added to the system and the polymerization is completed in suspension.

Expandable polystyrene (EPS) is manufactured by suspension polymerization in the presence of a blowing agent (e.g., pentane). It is also possible to introduce the blowing agent to the polymer after polymerization and allowing it to diffuse into the beads. According to the second production method, the required amount of deionized water is initially loaded into the reactor at ambient temperature and the agitation is started. Subsequently, styrene and the initiator mixture, consisting of the primary initiator (with a low activation energy) and a finishing one (with a high activation energy) as well as the stabilizer are pumped into the reactor. Droplet size developments occur during the heating cycle. When the specified polymerization temperature has been reached (e.g., 75–95°C), polymerization begins. As discussed in Section 5.1, the polymerizing monomer droplets pass through three subsequent stages, during which the drop breakage and coalescence rates change continuously. Finally, clear, spherical particles with a smooth surface and zero porosity are formed (Figure 5.4). Autoacceleration of the polymerization rate due to the gel-effect becomes appreciable at relatively low monomer conversion (e.g., about 30%) and it continues until a monomer conversion of about 95%, where a glassy-state transition occurs and the beads become hard. Once the beads are hard, the reaction mixture is heated to a temperature above the glass transition temperature of the PS ($T_g \sim 100^\circ\text{C}$). During heating, the reactor is pressurized with a blowing agent (usually *n*-pentane) at 5–8% w/w with respect to polymer. Subsequently, the reactor is pressurized with nitrogen at 7–9 bars and the so-called impregnation stage starts. During this stage the *n*-pentane diffuses into the “beads.” At the same time, the free volume increases while the finishing initiator rapidly decomposes to

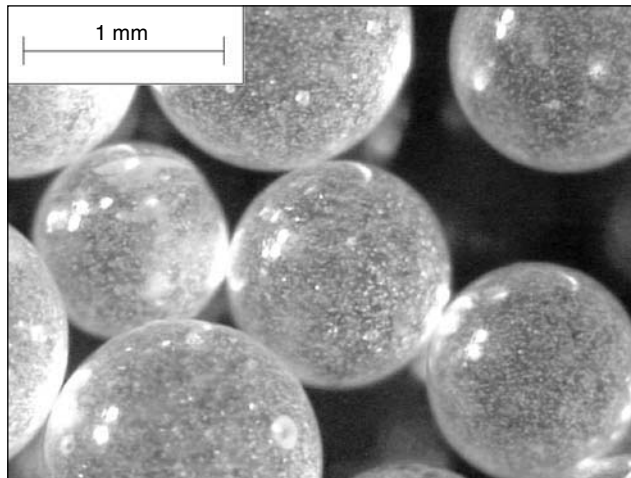


Figure 5.4 EPS polymer particles.

generate free-radicals, resulting in a relatively rapid increase of the monomer conversion to about 99%. It should be noted that the impregnation time should be sufficient to allow the blowing agent to reach the core of the particle. At the end of the impregnation stage, the system is cooled down to 20–30°C, so that no bead expansion can take place during the discharge of the slurry to the downstream equipment. In the next stage, the excess of stabilizer is chemically removed from the particle surface in a washer tank, and the polymer beads are transported in a centrifuge, where they are separated from the water. Finally, the remaining moisture is removed from the particles in a dryer. In the final processing, the EPS beads are warmed up to 80–110°C, generally with steam that causes the beads to expand by foaming and their volume to increase by a factor of 30–50.

Villalobos *et al.* [9] studied the effect of the *n*-pentane on the free-radical suspension polymerization of styrene. They observed that the presence of *n*-pentane reduced the polymerization rate because of the increase of the free-volume of the system that delayed the appearance of the gel-effect. However, the experimentally measured average molecular weights of PS were not affected, despite the delayed appearance of gel-effect and the expected decrease in the average molecular weights. The authors argued that, in the presence of *n*-pentane, the rate of transfer to monomer reaction decreases. In fact, pentane lowers the hydrogen abstraction rate from styrene, a necessary kinetic step for chain transfer to monomer to occur. As a result, the average molecular weights do not significantly change despite the observed delay in the gel-effect. The same authors also studied the effect of *n*-pentane on the PSD and they reported that the final PSD was not significantly affected by the presence of the blowing agent.

5.5 The “powder” suspension polymerization process

The “powder” suspension polymerization is the most important polymerization process for manufacturing PVC. The main advantage of this process is that large (e.g., 300–500 μm),

porous polymer particles can be produced, exhibiting a fast residual monomer removal rate and a large plasticizer uptake capacity. The production of polymer particles with desired PSD and porosity can be achieved by changing the quantities and types of stabilizers as well as the agitator speed, without affecting the molecular properties of the product. The polymerization is commonly carried out isothermally, at temperatures in the range of 45–70°C, depending on the desired molecular weight. VCM is an extremely volatile compound and in the above temperature range its vapor pressure varies approximately from 8 to 12 bars [33].

In the free-radical VCM polymerization, the first polymer chains produced inside the monomer droplets precipitate out to form unstable polymer microdomains with diameters in the range of 10–20 nm (see Figure 4.13). These microdomains exhibit limited stability and, thus, aggregate to form the nuclei of the primary particles, also called domains (at monomer conversions between 0.01% and 10%). The initial size of these domains lies in the range 80–100 nm. The growth of these domains via the polymerization of the absorbed monomer or by aggregation with other domains results in primary particles with diameters in the range of 100–200 nm. At a critical monomer conversion (10–30%), massive aggregation of the primary particles leads to the formation of a three-dimensional polymer skeleton. The primary particles continue to grow until the disappearance of the free monomer phase (i.e., at a fractional monomer conversion, x_f). In the presence of secondary stabilizers at low agitation speeds, the aggregation and subsequent fusion of the primary particles can be limited, while individual primary particles may continue to grow up to 1–1.5 μm in diameter. In the latter case, primary particles can pack closely together without any significant aggregation. This results in a close-packed structure of low porosity. The porosity of PVC grains increases as the agitation rate is increased (see Figure 4.13). Strong agitation can also favor the aggregation of the individual polymerizing particles, leading to the formation of irregular PVC grains with sizes in the range of 50–250 μm in diameter (Figure 5.5). The main difference between the “bulk” and the suspension process is that agitation is used to

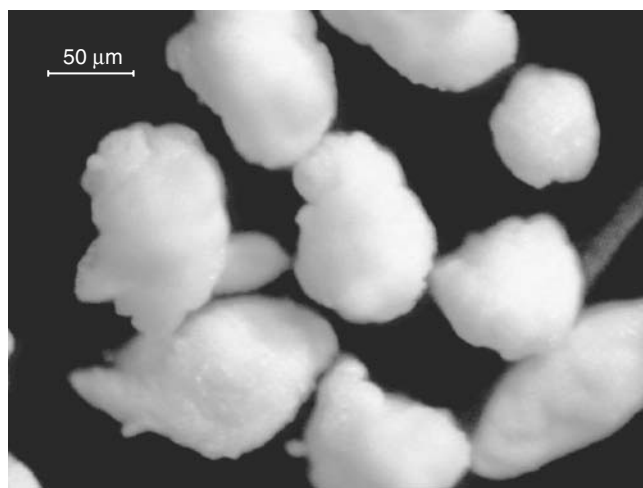


Figure 5.5 PVC polymer grains.

control not only the aggregation of the primary particles but also the size distribution of the final grains [33].

As a result of the above mechanism, the polymerizing VCM droplet loses its viscous characteristics at relatively low monomer conversions, while at larger monomer conversions (i.e., $x > 30\%$) it behaves like a rigid sphere due to the presence of the continuous polymer skeleton. In fact, above a critical monomer conversion (i.e., $x_c \sim 30\%$) the volume contraction of the polymerizing particles stops, which partially explains the appearance of internal particle porosity. Note that the polymer density is approximately 40% higher than the monomer density.

In the VCM suspension polymerization, two types of stabilizers (i.e., the primary and the secondary) are used [34]. The main function of the primary surface active agents is to control the grain size, but they also affect the internal grain porosity. On the other hand, secondary stabilizers are surface active agents with a higher lipophilic content (e.g., PVA stabilizers with low degree of hydrolysis and cellulose ethers with high degree of substitution of the hydroxyl-groups). They are mainly soluble in the VCM droplets wherein they adsorb onto the surface of PVC primary particles. The increased stability of the primary particles, imparted by the adsorbed secondary stabilizers, results in a decrease of the primary particles aggregation rate with a concomitant decrease in PVC grain porosity.

One of the most efficient ways for the removal of the polymerization heat is the use of an overhead reflux condenser. The VCM vapors are condensed and return to the polymerizing suspension, while an equal amount of VCM is being vaporized in order to maintain the thermodynamic equilibrium. However, this process affects the morphological properties of the polymer product (e.g., porosity, PSD, bulk density). Cheng and Langsam [20] reported that the particle size as well as the porosity of the PVC grains increase as the operation time of the condenser or/and the reflux rate increase. This result has also been verified by Zerfa and Brooks [35], who observed a second peak in the PSD at higher sizes as the reflux rate increased while, at the same time, some fine particles were produced. The large peak corresponds to the PVC particles produced either by the polymerization of the larger in size "fresh" monomer droplets returning from the condenser or by the coalescence of "fresh" and "old" droplets. "Fresh" droplets are larger than the "old" ones because the stabilizer concentration in the continuous phase cannot sufficiently cover the newly formed monomer droplets. The operation time of the condenser is another important topic in the suspension polymerization of VCM. Cheng and Langsam [20] reported that the reflux condenser should only be used after a monomer conversion of about 5%, because early utilization of the reflux condenser results in extensive condenser fouling and a coarser resin. On the other hand, if the utilization of the condenser starts at high monomer conversions (20–30%), its effect on the PSD is negligible, while its effect on the grain porosity remains significant.

It should be noted that the utilization of a reflux condenser for heat removal in the VCM suspension polymerization introduces some operational problems. For example, non-condensable gases may be concentrated in the condenser, which can reduce its heat removal capacity. The level of non-condensable gases in the reactor vapor phase will depend on the quality of the monomer, how well the reactor has been evacuated prior to polymerization and whether or not the polymerization process generates inert gases [20]. For example, the use of azo initiators will result in the formation of nitrogen as a byproduct of the initiator

decomposition. In addition, the use of a carbonate buffer can result in the formation of CO_2 if the aqueous phase becomes acidic.

5.6 Population balance modeling

To follow the dynamic evolution of PSD in a particulate process, a population balance approach is commonly employed. The distribution of the droplets/particles is considered to be continuous in the volume domain and is usually described by a number density function, $n(v, t)$. Thus, $n(v, t)dv$ represents the number of particles per unit volume in the differential volume size range $(v, v + dv)$. For a dynamic particulate system, undergoing simultaneous particle breakage and coalescence, the rate of change of the number density function with respect to time and volume is given by the following non-linear integro-differential population balance equation (PBE) [36]:

$$\begin{aligned} \frac{\partial [n(v, t)]}{\partial t} = & \int_v^{v_{\max}} \beta(u, v)u(u)g(u)n(u, t)du + \int_{v_{\min}}^{v/2} k(v - u, u)n(v - u, t)n(u, t)du \\ & - n(v, t)g(v) - n(v, t) \int_{v_{\min}}^{v_{\max}} k(v, u)n(u, t)du \end{aligned} \quad (5.5)$$

The first term on the right-hand side of Equation 5.5 represents the generation of droplets in the size range $(v, v + dv)$ due to drop breakage. $\beta(u, v)$ is a daughter drop breakage function, accounting for the probability that a drop of volume v is formed via the breakage of a drop of volume u . The function $u(u)$ denotes the number of droplets formed by the breakage of a drop of volume u and $g(u)$ is the breakage rate of drops of volume u . The second term on the right-hand side of Equation 5.5 represents the rate of generation of drops in the size range $(v, v + dv)$ due to the coalescence of two smaller drops, $k(v, u)$ is the coalescence rate between two drops of volume v and u . Finally, the third and fourth terms represent the drop disappearance rates due to drop breakage and coalescence, respectively. Equation 5.5 will satisfy the following initial condition at $t = 0$:

$$n(v, 0) = n_0(v) \quad (5.6)$$

where $n_0(v)$ is the initial drop size distribution of the dispersed phase. Commonly, the initial monomer drop size distribution is considered to follow a normal distribution around a mean value V_0 and a standard deviation, σ_0 [36].

5.6.1 The drop breakage process

It has been postulated that drop breakage in turbulent flow fields may be caused by viscous shear forces, by turbulent pressure fluctuations [26, 37] or/and by relative velocity fluctuations [38, 39]. When drop breakage occurs by viscous shear forces, the monomer droplet is first elongated into two fluid lumps separated by a liquid thread (see Figure 5.6(a)). Subsequently, the deformed monomer droplet breaks into two almost equal-size drops, corresponding to the fluid lumps, and a series of smaller droplets corresponding to the liquid thread. This is known as thorough breakage. On the other hand, a droplet suspended

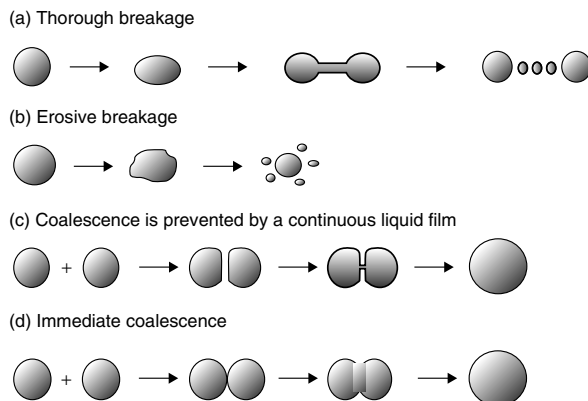


Figure 5.6 Drop breakage and coalescence mechanisms.

in a turbulent flow field is exposed to local pressure and relative velocity fluctuations. For nearly equal densities and viscosities of the two liquid phases, the droplet surface can start oscillating. When the relative velocity is close to that required to make a drop marginally unstable, a number of small droplets are stripped out from the initial one (see Figure 5.6(b)). This situation of drop breakage is referred to as the erosive one. Erosive drop breakage is considered to be the dominant mechanism of low-coalescence systems that exhibit a characteristic bimodality in the PSD [6, 40].

The first approaches to modeling the drop breakage process in liquid–liquid dispersions were based on the Weber number for the calculation of the mean drop diameter (see Table 5.2), as well as a maximum stable drop diameter for breakage to occur and a minimum drop diameter above which coalescence will take place [2, 27, 37]. Both diameters depend on the intensity of agitation and on physical properties of the constituents. However, these calculations were limited to very low dispersed phase viscosities and holdup fractions. Doulah [25] proposed a correction to the derived correlations to account for high holdup dispersed fractions, whereas Arai *et al.* [48] derived an expression for the maximum droplet diameter by incorporating the viscosity of the dispersed phase. Similar expressions were also proposed by Calabrese *et al.* [41].

To calculate the drop breakage rate in liquid–liquid dispersions, several models have been proposed [33, 38, 42, 49–52]. Some of these models have been applied to the suspension polymerization process with great success [8, 36, 49, 53]. In these models, the drop breakage rate is expressed in terms of a breakage frequency, $\omega_b(\nu)$, and a respective Maxwellian efficiency term:

$$g(\nu) = \omega_b(\nu)e^{-\lambda_b(\nu)} \quad (5.7)$$

where $\lambda_b(\nu)$ is the ratio of the required to the available energy for drop breakage to occur.

Assume that a drop of volume u breaks up into N_{da} daughter drops and N_{sa} satellite drops. Furthermore, assume that the daughter and satellite drops are normally distributed about their respective mean values, ν_{da} and ν_{sa} . Then, the following expression can be derived for

Table 5.2 Droplet size correlation for liquid–liquid dispersions in stirred tanks

Researchers	Correlation
Chatzi <i>et al.</i> (1991) [17]	$d_{32}/D_I = 0.045 We^{-0.4}$
Doulah (1975) [25]	$d_{32} = C(1 + 3\phi)We^{-0.6}$
Coulaloglou and Tavlarides (1977) [31]	$d_{32} = 0.081(1 + 4.47\phi)We^{-0.6}$
Calabrese <i>et al.</i> (1986) [41]	$d_{32}/D_I = 0.053(1 + 0.91Vis^{0.84})^{0.6}We^{-0.6}$ $Vis = (\rho_c/\rho_D)^{1/2}(\eta_D\varepsilon^{1/3}/d_{max}^{1/3}/\sigma)$
Wang and Calabrese (1986) [42]	$d_{32}/D_I = 0.053(1 + 0.97Vis^{0.79})^{0.6}We^{-0.6}$
Zerfa and Brooks (1996) [43]	$d_{32}/D_I = 0.027(1 + 3.1\phi)We^{-0.6}$
Chen and Middleman (1967) [44]	$d_{32} = 0.053 We^{-0.6}$
Lagisetty <i>et al.</i> (1986) [45]	$d_{32}/D_I = 0.083(1 + 4.0\phi)^{1.2}We^{-0.6}$
Laso <i>et al.</i> (1987) [46]	$d_{32}/D_I = 0.118\phi^{0.27}(\eta_D/\eta_c)^{-0.056}We^{-0.4}$
Chatzi <i>et al.</i> (1989) [47]	$d_{32}/D_I = 0.0165(1 + 11.94\phi)We^{-0.4}$ (coalescence dominant) $d_{32}/D_I = 0.056(1 + 10.97\phi)We^{-0.4}$ (breakage dominant)

the number of drops of volume v formed by the breakage of a drop of volume u [54]:

$$\beta(u, v)u(u) = N_{\text{da}} \left\{ \frac{1}{\sigma_{\text{da}}\sqrt{2\pi}} \exp\left(-\frac{(v - v_{\text{da}})^2}{2\sigma_{\text{da}}^2}\right) \right\} + N_{\text{sa}} \left\{ \frac{1}{\sigma_{\text{sa}}\sqrt{2\pi}} \exp\left(-\frac{(v - v_{\text{sa}})^2}{2\sigma_{\text{sa}}^2}\right) \right\} \quad (5.8)$$

It should be noted that the daughter drop number density function, $u(u)\beta(u, v)$, should satisfy the following number and volume conservation equations:

$$\int_0^u u(u)\beta(u, v)dv = u(u), \quad \int_0^u vu(u)\beta(u, v)dv = u \quad (5.9)$$

Accordingly, one can calculate the mean volumes of daughter and satellite drops, formed by the breakage of a drop of volume u in terms of N_{da} and N_{sa} and the ratio of their respective volumes, $r_{\text{D}} = v_{\text{da}}/v_{\text{sa}}$ [6]:

$$v_{\text{da}} = \frac{u}{N_{\text{da}} + N_{\text{sa}}/r_{\text{D}}} \quad \text{and} \quad v_{\text{sa}} = \frac{u}{N_{\text{da}}r_{\text{D}} + N_{\text{sa}}} \quad (5.10)$$

where N_{da} , N_{sa} , σ_{da} , σ_{sa} and r_{D} are model parameters.

5.6.2 The drop coalescence process

Two different mechanisms have been postulated in the open literature to describe the coalescence of two drops in a turbulent flow field. The first one [26] assumes that after the initial collision of two drops, a liquid film of the continuous phase is being trapped between the two drops, which prevents their coalescence (see Figure 5.6(c)). However, due to the presence of attractive forces, draining of the liquid film can occur leading to drop coalescence. On the other hand, if the kinetic energy of the induced drop oscillations is larger than the energy of adhesion between the drops, the drop contact is broken before the complete drainage of the liquid film. The second drop coalescence mechanism [55] assumes that immediate coalescence occurs when the relative velocity of the two colliding drops at the collision instant exceeds a critical value. This means that the drops will coalesce (see Figure 5.6(d)) if the energy of collision is greater than the total drop surface energy.

Several mathematical models have also been presented in the open literature to describe the drop coalescence rate [31, 49, 50, 56–62]. As in the case of the drop breakage rate, the drop coalescence rate can be expressed in terms of a collision frequency, $\omega_{\text{b}}(v, u)$, and a Maxwellian efficiency term:

$$k(v, u) = \omega_{\text{c}}(v, u)e^{-\lambda_{\text{c}}(v, u)} \quad (5.11)$$

where $\lambda_{\text{c}}(v, u)$ is the ratio of the required to the available energy for drop coalescence to occur.

Detailed expressions for the calculation of the drop breakage (Equation 5.7) and coalescence (Equation 5.11) rate kernels can be found in the original publication of Kotoulas and Kiparissides [36].

5.6.3 Numerical solution of the PBE

In general, the numerical solution of the dynamic PBEs for a particulate process, especially for a reactive one, is a notably difficult problem due to both numerical complexities and model uncertainties regarding the particle growth, aggregation and breakage mechanisms that are often poorly understood. Usually, the numerical solution of the PBE requires the discretization of the particle volume domain into a number of discrete elements that results in a system of stiff, non-linear differential or algebraic/ differential equations that is solved numerically [54]. In the open literature, several numerical methods have been developed for solving the steady-state or dynamic PBE. These include the full discrete method [63], the method of classes [6, 64], the discretized PBE [65, 66], the fixed and moving pivot techniques [67, 68], the high-order discretized PBE methods [69–71], the orthogonal collocation on finite elements [72], the Galerkin method [73] and the wavelet-Galerkin method [74]. In the reviews of Ramkrishna [75], Dafniotis [76] and Kumar and Ramkrishna [68], the various numerical methods available for solving the PBE are described in detail. Moreover, in three recent publications by Alexopoulos *et al.* [77–79] comparative studies on the different numerical methods are presented. For the suspension polymerization problem the fixed pivot technique was employed for the solution of the resulting PBE [36, 54].

5.7 Physical properties and phase equilibrium calculations

5.7.1 Physical and transport properties

One of the most important issues in modeling the suspension polymerization process is the evaluation of the physical and transport properties of the reacting system as well as the calculation of composition and partitioning of the different species (e.g., monomer(s), polymer, initiator(s), etc.) in the various phases present in the system. In a suspension polymerization process, one can identify, at least, three phases: the dispersed phase (e.g., polymerizing monomer droplets), the continuous aqueous phase and the gas phase. The dispersed phase can be either homogeneous (if the polymer is soluble in its monomer) or heterogeneous (if the polymer is insoluble in its monomer). In the “powder” suspension polymerization, the dispersed phase consists of two different phases: the polymer-rich and the monomer-rich phase. The continuous aqueous phase contains only small amounts of monomer and, finally, the gas phase contains monomer and water vapors.

The density of the suspension system, ρ_s , can be calculated by the weighted sum of the densities of the dispersed (ρ_d) and continuous (ρ_c) phases [80]:

$$\rho_s = \rho_d \varphi + \rho_c (1 - \varphi) \quad (5.12)$$

where φ is the volume fraction of the dispersed phase. The density of the dispersed phase will in turn be a function of the corresponding densities of the polymer (ρ_{pol}) and monomer (ρ_{mon}) and the extent of monomer conversion, x :

$$\rho_d = \left(\frac{x}{\rho_{pol}} + \frac{1-x}{\rho_{mon}} \right)^{-1} \quad (5.13)$$

Accordingly, the viscosity of the dispersion system can be calculated by the following semi-empirical equation [81]:

$$\eta_s = \frac{\eta_c}{1 - \varphi} \left(1 + \frac{1.5\eta_d\varphi}{\eta_d + \eta_c} \right) \quad (5.14)$$

where η_d and η_c are the viscosities of the dispersed and continuous phases, respectively.

For the suspension polymerization of VCM, the viscosity of the polymerizing monomer droplets, η_d , can be calculated from the Eilers equation [82]:

$$\eta_d = \eta_{\text{mon}} \left(1 + \frac{0.5[\eta]_{\text{pol}}}{1 - \varphi_{\text{pol}}/\varphi_{\text{cr}}} \right)^2 \quad (5.15)$$

where η_{mon} is the monomer viscosity, φ_{pol} is the volume fraction of the polymer in the dispersed phase, given by $\varphi_{\text{pol}} = x(\rho_d/\rho_{\text{pol}})$, φ_{cr} is the polymer volume fraction corresponding to the critical monomer conversion x_c , at which a three-dimensional polymer skeleton is formed inside the polymerizing monomer drops. When φ_{pol} approaches the φ_{cr} value, the dispersed-phase viscosity approaches a limiting constant value, corresponding to a rigid structure. The value of φ_{cr} for the VCM suspension polymerization was taken equal to 0.3 [10]. On the other hand, for the suspension polymerization of styrene, the value of φ_{cr} was set equal to the 0.7, which corresponds to the monomer conversion at which particle coalescence stops [36].

The intrinsic viscosity of the polymer solution, $[\eta]_{\text{pol}}$ in Equation 5.15 can be calculated by the well-known Mark–Houwink–Sakurada (MHS) equation as a function of the weight-average molecular weight of the polymer, \overline{M}_w :

$$[\eta]_{\text{pol}} = k\overline{M}_w^a \quad (5.16)$$

Finally, the viscosity of the continuous phase depends on the concentration and type of stabilizer that, in turn, affects the PSD [11]. Okaya [83] employed the following Schulz–Blaschke equation to calculate the viscosity of aqueous PVA solutions:

$$\eta_c = \eta_w \left(1 + \frac{[\eta_{\text{PVA}}][\text{PVA}]}{1 - 0.45[\eta_{\text{PVA}}][\text{PVA}]} \right) \quad (5.17)$$

where η_c , η_w , $[\eta_{\text{PVA}}]$ and $[\text{PVA}]$ are the viscosities of the aqueous PVA solution and pure water, the intrinsic viscosity and the concentration of the stabilizer, respectively.

5.7.2 Phase equilibrium calculations

Phase equilibrium calculations are commonly used for the prediction of monomer distribution in the different phases present in a suspension polymerization reactor. The vapor phase that occupies the free space on top of the liquid mixture in the reactor consists mainly of monomer and water vapors. In the case of the EPS, vapors of *n*-pentane are also present in the gas phase.

In the VCM suspension polymerization, when a separate liquid monomer phase exists (i.e., in the conversion range, $0 < x < x_f$), the reactor pressure will be equal to the sum of the VCM and water vapor partial pressures. It should be noted that a small amount of

residual air might be present in the overhead vapor phase. However, due to the very low vacuum (less than 0.1 bar) typically applied to an industrial reactor before its loading, the amount of air in the overhead vapor phase can be assumed to be negligible in the reactor pressure calculation. In stage II of the VCM polymerization, the polymer-rich phase remains saturated with monomer, reflecting the thermodynamic equilibrium between the two phases (i.e., the monomer- and the polymer-rich phase). However, upon the disappearance of the separate monomer phase (i.e., at the fractional monomer conversion, $x = x_f$), the reactor pressure starts decreasing due to the transfer of monomer from the overhead vapor phase to the dispersed monomer-swollen polymer particles.

During the whole duration of polymerization process, the three phases (four in the case of VCM polymerization) are assumed to be in thermodynamic equilibrium. As a result, the monomer fugacities in the three (four) phases will be equal:

$$f_{\text{mon}}^{\text{g}} = f_{\text{mon}}^{\text{w}} = f_{\text{mon}}^{\text{pol}} (=f_{\text{mon}}^{\text{mon}}) \quad (5.18)$$

The term in the brackets corresponds to the monomer fugacity in the monomer-rich phase in the case of the “powder” suspension polymerization (i.e., VCM polymerization). For the EPS process, the fugacities of the *n*-pentane in the three phases should also be equal:

$$f_{\text{pent}}^{\text{g}} = f_{\text{pent}}^{\text{w}} = f_{\text{pent}}^{\text{pol}} \quad (5.19)$$

To calculate the reactor pressure and the polymerization rates in the monomer- and polymer-rich phases, the monomer distribution in the different phases in the system must be known. Assuming that all the phases in the system (i.e., three for PS and four for VCM) are in thermodynamic equilibrium, the following pseudo-steady-state monomer mass balance can easily be derived:

$$W_{\text{mon}0}(1 - x) = W_{\text{mon}}^{\text{pol}} + W_{\text{mon}}^{\text{w}} + W_{\text{mon}}^{\text{g}} (+W_{\text{mon}}^{\text{mon}}) \quad (5.20)$$

where the symbols $W_{\text{mon}0}$, $W_{\text{mon}}^{\text{pol}}$, $W_{\text{mon}}^{\text{w}}$ and $W_{\text{mon}}^{\text{g}}$ denote the total monomer mass loaded in the reactor, the monomer mass in the polymer (pol), water (w) and gas (g) phases, respectively. $W_{\text{mon}}^{\text{mon}}$ is the monomer mass in the monomer-rich phase in the VCM polymerization case (four phases).

The mass of monomer in the aqueous phase can be considered at any time to be equal to its solubility in water:

$$W_{\text{mon}}^{\text{w}} = K(P/P_{\text{mon}}^{\text{sat}})W_{\text{water}}^{\text{w}} \quad (5.21)$$

where K is the monomer solubility in the aqueous phase and $P_{\text{mon}}^{\text{sat}}$ is the saturated monomer vapor pressure at the polymerization temperature. Accordingly, the mass of water in the continuous phase, $W_{\text{water}}^{\text{w}}$, is given by the following equation:

$$W_{\text{water}}^{\text{w}} = W_{\text{water}0} - (f_{\text{water}}^{\text{g}} w_{\text{water}} V_{\text{g}}/RT) \quad (5.22)$$

where $W_{\text{water}0}$ is the total mass of water loaded in the reactor and V_{g} is the volume of the gas phase. Finally, the monomer mass in the gas phase can be calculated in terms of its fugacity, $f_{\text{mon}}^{\text{g}}$, the volume of the gas phase, V_{g} and temperature, T .

$$W_{\text{mon}}^{\text{g}} = f_{\text{mon}}^{\text{g}} w_{\text{mon}} V_{\text{g}}/RT \quad (5.23)$$

5.8 Effect of operating conditions on PSD

By increasing the input power per unit mass (e.g., increasing the agitation speed or the impeller diameter), the turbulent intensity and the pressure and velocity fluctuations increase. As a result, the drop breakage rate increases, leading to the production of smaller and more uniform polymerizing droplets. At the same time, the increased liquid circulation rate results in more drop collisions, thus, increasing the drop coalescence rate. In general, an increase of the input power to the system results in an increase of the drop breakage and coalescence rates. Depending on which mechanism (i.e., drop breakage or drop coalescence) dominates, an increase of the input power could lead to a shift of the mean drop diameter to lower or higher sizes. Moreover, it has been observed that the mean drop/particle diameter follows a parabolic shape (U-shape) with respect to the impeller speed [19, 84] or impeller diameter [85] (Figure 5.2).

A lot of experimental and theoretical studies have been published on the effect of viscosities of continuous and dispersed phases on the PSD. In general, an increase of the dispersed phase viscosity, η_d , results in a reduction of both breakage and coalescence rates. Cebollada *et al.* [11] reported that in the suspension polymerization of VCM, by increasing the viscosity of the continuous phase, larger and more uniform polymer particles were produced. On the other hand, they found that as the viscosity of the continuous phase decreased, the PVC sub-grains were smaller in size but their agglomeration rate increased. As a result, larger grains with higher porosity were produced.

In general, the increase of holdup fraction of the dispersed phase, φ , decreases the turbulent intensity (i.e., the average energy dissipation rate per unit mass) and, thus, the drop breakage rate. On the other hand, the coalescence frequency increases due to the higher number of droplets, while the coalescence efficiency decreases due to the lower average energy dissipation rate. However, the effect of φ on the coalescence frequency is more important, and, thus, for a constant input power, as the holdup fraction increases the droplet size increases [43].

In Figures 5.7 and 5.8, the dynamic evolution of the PSD and the Sauter mean particle diameter are illustrated, respectively. More specifically, in Figure 5.7 the volume probability density function (defined as $vn(v, t)/v_{tot}$) of PVC particles is plotted with respect to particle diameter. From these figures, the three stages that the suspension polymerization undergoes can easily be distinguished. As can be seen, for the case of VCM suspension polymerization, the PSD is essentially established at monomer conversions of about 35–40%.

5.9 Scale-up of suspension polymerization reactors

The scale-up of suspension polymerization reactors (i.e., from lab to pilot and then to industrial scale) is not straightforward or well established. Probably, the most significant problem in scale-up occurs when different physical processes become limiting at different scales. For example, commercial-scale suspension reactors have to perform several functions simultaneously (dispersion, reaction and heat transfer), which do not scale-up in the same manner. Thus, heat removal can become a limiting factor for reactor performance at large scales while it is rarely a problem for lab-scale reactors [86].

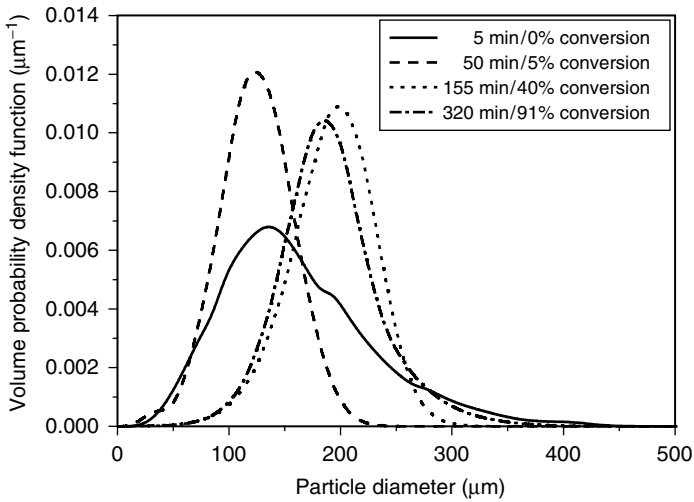


Figure 5.7 Dynamic evolution of the PSD with respect to polymerization time for VCM suspension polymerization (polymerization temperature: 56.5°C; impeller speed: 330 rpm; dispersed phase volume fraction: 40%).

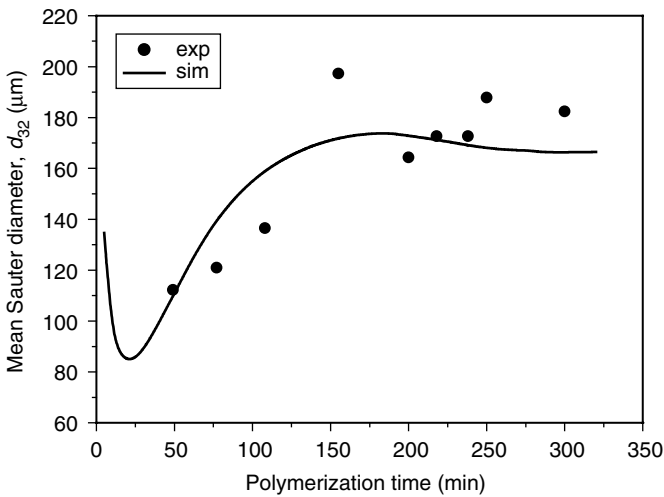


Figure 5.8 Dynamic evolution of the Sauter mean diameter of PVC particles with respect to polymerization time (experimental conditions are the same as Figure 5.7).

In suspension polymerization, scale-up of an agitated tank reactor should keep unchanged the particle morphology (e.g., PSD, porosity, bulk density) of the polymer product, given that the recipe and operating conditions are kept constant, and the reactor design can guarantee the heat removal. Thus, the problem reduces to the scale-up of a liquid–liquid dispersion in an agitated vessel, which can be based on several criteria, including the constant power input per unit volume, the impeller discharge flow rate, the impeller

tip speed, the Weber number, the Reynolds number, etc. [87]. Assuming constant geometry at scale-up, the criterion of constant input power per unit mass yields the following equation:

$$N^3 D_1^2 = \text{constant} \Rightarrow ND_1^{0.66} = \text{constant} \quad (5.24)$$

Equation 5.24 assumes that the power number remains constant. The power number represents the ratio of pressure to inertia forces [88]. Thus, this criterion represents dynamic similarity under conditions of negligible viscous forces (i.e., large Reynolds numbers), and no effect of gravitational forces (e.g., the presence of baffles).

The criterion of equal tip speed, under constant geometry, leads to the following relation:

$$ND_1 = \text{constant} \quad (5.25)$$

Okufi *et al.* [88] studied the scale-up effect on the DSD of *n*-heptane in water, and reported that the rule of equal impeller tip speed provided the best scale-up criterion for equal interfacial areas per unit volume of dispersion, while the criterion of equal input power per unit volume resulted in the production of smaller droplets. Scully [89] used the well-known correlation between the Sauter mean diameter

$$d_{32} = \frac{\int_{V_{\min}}^{V_{\max}} d_p^3 n(v, t) dv}{\int_{V_{\min}}^{V_{\max}} d_p^2 n(v, t) dv}$$

and the Weber number

$$We = N^2 D_1^3 \rho / \sigma$$

(the factor 10^3 was included to account for the units used for density in this book kg L^{-1}) to derive a scale-up criterion for suspension PVC reactors:

$$d_{32}/D_1 = CWe^{-0.6} \quad (5.26)$$

He proposed that in order to keep the Sauter mean diameter of the polymer particles constant in reactor scale-up, the following condition should be satisfied:

$$D_1(N^2 D_1^3)^{-0.6} = \text{constant} \Rightarrow ND_1^{0.66} = \text{constant} \quad (5.27)$$

Equation 5.27 has the disadvantage that it ignores the viscous forces inside the polymerizing droplet. Calabrese *et al.* [41] proposed the following relation for the calculation of the Sauter mean diameter for a viscous dispersion system:

$$d_{32}/D_1 = 0.0053(1 + 0.91 Vis^{0.84})^{0.6} We^{-0.6} \quad (5.28)$$

where

$$Vis = (\rho_c / \rho_d)^{1/2} (10\eta_d ND_1 / \sigma) \quad (5.29)$$

Equation 5.28 can be used as a scale-up criterion in order to produce polymer particles with the same Sauter mean diameter. In this case, the criterion that can be derived is:

$$ND_1^{0.43} = \text{constant} \quad (5.30)$$

Lewis and Johnson [90] studied experimentally the effect of the reactor volume on the mean size and the bulk density of PVC particles. More specifically, they correlated these

properties with the Weber number. First, they observed that We increases substantially with reactor volume, while the mean particle size exhibited a U-shape with the Weber number. The minimum of this parabolic shape was met at different Weber numbers, depending on the reactor size, but the value of this minimum particle size was the same at all scales. However, the authors reported that the mean deviation of the PSD and the bulk density of the product decreased with the We .

Finally, Ozkaya *et al.* [91] studied experimentally the suspension polymerization of VCM at different reactor scales (i.e., from 10 ℓ to 27 m^3). They found that the mean particle size, d_{50} , depended on the Weber number according to the following relation:

$$d_{50}/D_1 = 273\,292.1We^{-0.51} \quad (5.31)$$

while the scale-up criterion that can be derived from Equation 5.31, for geometric similarity of the reactors, is

$$ND_1^{0.52} = \text{constant} \quad (5.32)$$

References

- Hoffman, F. and Delbruch, K. (1909) *Ger. Pat. 250690*. Farbenfabriken Bayer, Germany.
- Vivaldo-Lima, E., Wood, P.E. and Hamielec, A.E. (1997) *Ind. Engng Chem. Res.*, **36**, 939–965.
- Kiparissides, C. (1996) *Chem. Engng Sci.*, **51**, 1637–1659.
- Kalfas, G.A. (1992) *Experimental Studies and Mathematical Modeling of Aqueous Suspension Polymerization Reactors*. PhD Thesis. University of Wisconsin-Madison, USA.
- Yuan, H.G., Kalfas, G. and Ray, W.H. (1991) *J.M.S. – Rev. Macromol. Chem. Phys.*, **C31**, 215–299.
- Chatzi, E.G. and Kiparissides, C. (1992) *Chem. Engng Sci.*, **47**, 445–456.
- Hamielec, A.E. and Tobita, H. (1992) In *Ullmann's Encyclopedia of Industrial Chemistry*, Vol. A21. VCH Publishers, Inc., New York, pp. 305–428.
- Maggiaris, D., Goulas, A., Alexopoulos, A.H., Chatzi, E.G. and Kiparissides, C. (2000) *Chem. Engng Sci.*, **55**, 4611–4627.
- Villalobos, M.A., Hamielec, A.E. and Wood, P.E. (1993) *J. Appl. Polym. Sci.*, **50**, 327–343.
- Kiparissides, C., Achilias, D.S. and Chatzi, E. (1994) *J. Appl. Polym. Sci.*, **54**, 1423–1438.
- Cebollada, A.F., Schmidt, M.J., Farber, J.N., Cariati, N.J. and Valles, E.M. (1989) *J. Appl. Polym. Sci.*, **37**, 145–166.
- Kalfas, G. and Ray, W.H. (1993) *Ind. Engng Chem. Res.*, **32**, 1822–1830.
- Taylor, T.W. and Reichert, K.H. (1985) *J. Appl. Polym. Sci.*, **30**, 227–241.
- Kalfas, G., Yuan, H. and Ray, W.H. (1993) *Ind. Engng Chem. Res.*, **32**, 1831–1838.
- Mino, G. (1956) *J. Polym. Sci.*, **22**, 369–381.
- Bahargava, G.S., Khan, H.U. and Bhattacharyya, K. (1979) *J. Appl. Polym. Sci.*, **23**, 1181–1193.
- Chatzi, E.G., Boutris, C.J. and Kiparissides, C. (1991) *Ind. Engng Chem. Res.*, **29**, 1307–1313.
- Hartland, S. (1968) *Trans Inst. Chem. Engng (London)*, **46**, T275.
- Chatzi, E.G. and Kiparissides, C. (1994) *Chem. Engng Sci.*, **49**, 5039–5052.
- Cheng, J.T. and Langsam, M. (1985) *J. Appl. Polym. Sci.*, **30**, 1365–1378.
- Chatzi, E.G. and Kiparissides, C. (1995) *AIChE J.*, **41**, 1640–1652.
- Nilsson, H., Silvegren, C. and Tornell, B. (1985) *J. Vinyl Techn.*, **7**, 112–122.
- Lankveld, J.M. and Lyklema, J. (1972) *J. Coll. Interface Sci.*, **41**, 454–462.
- Laats, M.K. and Frishman, F.A. (1973) *Fluid Dynam.*, **8**, 153–171.
- Doulah, M.S. (1975) *Ind. Engng Chem. Fundam.*, **14**, 137–138.
- Shinnar, R. and Church, J.M. (1960) *Ind. Engng Chem.*, **35**, 253–256.

27. Shinnar, R. (1961) *J. Fluid Mech.*, **10**, 259–271.
28. Vivaldo-Lima, E., Wood, P.E., Hamielec, A.E. and Penlidis, A. (1998) *Can. J. Chem. Engng*, **76**, 495–505.
29. Cutter, L.A. (1966) *AIChE J.*, **12**, 35–43.
30. Alexopoulos, A.H., Maggioris, D. and Kiparissides, C. (2002) *Chem. Engng Sci.*, **57**, 1735–1752.
31. Coualaloglou, C.A. and Tavlarides, L.L. (1977) *Chem. Engng Sci.*, **32**, 1289–1297.
32. Maggioris, D., Goulas, A., Alexopoulos, A.H., Chatzi, E.G. and Kiparissides, C. (1998) *Comp. Chem. Engng*, **22**, S315–S322.
33. Allsopp, M.W. (1982) In R.H. Burgess (ed.), *Manufacture and Processing of PVC*. Applied Science Publishers Ltd.
34. Allsopp, M.W. and Vianello, G. (1992) In *Ullmann's Encyclopedia of Industrial Chemistry*, Vol. A21. VCH Publishers, Inc., New York, pp. 717–742.
35. Zerfa, M. and Brooks, B.W. (1997) *Chem. Engng Sci.*, **52**(14), 2421–2427.
36. Kotoulas, C. and Kiparissides, C. (2006) *Chem. Engng Sci.*, **61**, 332–346.
37. Hinze, J.O. (1955) *AIChE J.*, **1**, 289–295.
38. Narsimhan, G., Gupta, G. and Ramkrishna, D. (1979) *Chem. Engng Sci.*, **34**, 257–265.
39. Mikos, A.G., Takoudis, C.G. and Peppas, N.A. (1986) *J. Appl. Polym. Sci.*, **31**, 2647–2659.
40. Ward, J.P. and Knudsen, J.G. (1967) *AIChE J.*, **13**, 356–367.
41. Calabrese, R.V., Chang, T.P.K. and Dang, P.T. (1986) *AIChE J.*, **32**, 657–666.
42. Wang, C.Y. and Calabrese, R.V. (1986) *AIChE J.*, **32**(4), 667–676.
43. Zerfa, M. and Brooks, B.W. (1996) *Chem. Engng Sci.*, **51**(14), 3591–3611.
44. Chen, H.T. and Middleman, S. (1967) *AIChE J.*, **13**, 989–996.
45. Lagisetty, J.S., Das, P.K., Kumar, R. and Gandhi, K.S. (1986) *Chem. Engng Sci.*, **41**, 65–71.
46. Laso, M., Steiner, L.I. and Hartland, S. (1987) *Chem. Engng Sci.*, **42**, 2437–2446.
47. Chatzi, E.G., Gavrielides, A.D. and Kiparissides, C. (1989) *Ind. Engng Chem.*, **28**, 1704–1711.
48. Arai, K., Konno, M., Matunaga, Y. and Saito, S. (1977) *J. Chem. Engng Japan*, **10**, 325–239.
49. Alvarez, J., Alvarez, J. and Hernandez, M. (1994) *Chem. Engng Sci.*, **49**, 99–113.
50. Tsouris, C. and Tavlarides, L.L. (1994) *AIChE J.*, **40**(3), 395–406.
51. Sathyagal, A.N., Ramkrishna, D. and Narshimhan, G. (1996) *Chem. Engng Sci.*, **51**(9), 1377–1391.
52. Chen, Z., Pruss, J. and Warnacke, H.-J. (1998) *Chem. Engng Sci.*, **53**(5), 1059–1066.
53. Chen, Z., Pruss, J. and Warnacke, H.-J. (1999) *Chem. Engng Technol.*, **22**, 609–616.
54. Kiparissides, C., Alexopoulos, A., Roussos, A., Dompazis, G. and Kotoulas, C. (2004) *Ind. Engng Chem. Res.*, **43**, 7290–7302.
55. Howarth, W.J. (1964) *Chem. Engng Sci.*, **19**, 33–42.
56. Delichatsios, M.A. and Probstein, R.F. (1976) *Ind. Engng Chem. Fundam.*, **15**, 134–138.
57. Sovova, H. (1981) *Chem. Engng Sci.*, **36**, 1567–1573.
58. Muralidhar, R. and Ramkrishna, D. (1986) *Ind. Engng Chem. Fundam.*, **25**, 554–560.
59. Muralidhar, R., Ramkrishna, D., Das, P.K. and Kumar, R. (1988) *Chem. Engng Sci.*, **43**, 1559–1568.
60. Kumar, S., Kumar, R. and Gandhi, K.S. (1993) *Chem. Engng Sci.*, **48**(11), 2025–2038.
61. Calabrese, R.V., Pacek, A.W. and Nienow, A.W. (1993) *The 1993 ICHIME Research Event*, pp. 642–645.
62. Liu, S. and Li, D. (1999) *Chem. Engng Sci.*, **54**, 5667–5675.
63. Hidy, G.M. (1965) *J. Colloid Sci.*, **20**, 123–144.
64. Marchal, P., David, R., Klein, J.P. and Villermaux, J. (1988) *Chem. Engng Sci.*, **43**(1), 59–67.
65. Batterham, R.J., Hall, J.S. and Barton, G. (1981) In *Proc. 3rd. Int. Symp. on Aggregation*. Nurnberg, W. Germany, p. A136.
66. Hounslow, M.J., Ryall, R.L. and Marshall, V.R. (1988) *AIChE J.*, **34**(11), 1821–1832.
67. Kumar, S. and Ramkrishna, D. (1996) *Chem. Engng Sci.*, **51**(8), 1311–1332.
68. Kumar, S. and Ramkrishna, D. (1996) *Chem. Engng Sci.*, **51**(8), 1333–1342.
69. Bleck, R. (1970) *J. Geophys. Res.*, **75**, 5165–5171.

70. Gelbard, F. and Seinfeld, J.H. (1980) *J. Coll. Interface Sci.*, **78**(2), 485–501.
71. Sastry, K.V.S. and Gaschignard, P. (1981) *Ind. Engng Chem. Fundam.*, **20**, 355–361.
72. Gelbard, F. and Seinfeld, J.H. (1979) *J. Coll. Interface Sci.*, **68**(1), 173–183.
73. Nicmanis, M. and Hounslow, M.J. (1998) *AIChE J.*, **44**, 2258–2272.
74. Chen, M.-Q., Hwang, C. and Shih, Y.-P. (1996) *Comp. Chem. Engng*, **20**(2), 131–145.
75. Ramkrishna, D. (1985) *Rev. Chem. Engng*, **3**, 49–95.
76. Dafniotis, P. (1996) *Modelling of Emulsion Copolymerization Reactors Operating below the Critical Micelle Concentration*. PhD Thesis. University of Wisconsin-Madison, USA.
77. Alexopoulos, A.H., Roussos, A.I. and Kiparissides, C. (2004) *Chem. Engng Sci.*, **59**, 5751–5769.
78. Alexopoulos, A.H. and Kiparissides, C. (2005) *Chem. Engng Sci.*, **60**, 4157–4169.
79. Roussos, A.I., Alexopoulos, A.H. and Kiparissides, C. (2005) *Chem. Engng Sci.*, **60**, 6998–7010.
80. Bouyatiotis, B.A. and Thornton, J.D. (1967) *Institution of Chemical Engineers (London) Symp. Ser.*, **26**, 43–51.
81. Vermeulen, T., Williams, G.M. and Langlois, G.E. (1995) *Chem. Engng Progr.*, **51**, 85F.
82. Krieger, I.M. (1972) *Adv. Coll. Interface Sci.*, **3**, 111–136.
83. Okaya, T. (1992) In C.A. Finch (ed.), *Polyvinyl Alcohol Developments*. John Wiley & Sons Ltd, pp. 1–30.
84. Kelsall, D.G. and Maitland, G.C. (1983) In K.H. Reichert and W. Greiseler (eds), *Polymer Reaction Engineering. Influence of Reaction Engineering on Polymer Properties*. Hansen, Vienna.
85. Johnson, G.R. (1980) *J. Vinyl Technol.*, **2**, 138–140.
86. Alexopoulos, A.H., Maggioris, D. and Kiparissides, C. (2002) *Chem. Engng Sci.*, **57**, 1735–1752.
87. Oldshue, J.Y. (1983) *Fluid Mixing Technology*. McGraw-Hill, New York.
88. Okufi, S., Perez de Ortiz, E.S. and Sawistowski, H. (1990) *Can. J. Chem. Engng*, **68**, 400–406.
89. Scully, D.B. (1976) *J. Appl. Polym. Sci.*, **20**, 2299–2303.
90. Lewis, M.H. and Johnson, G.R. (1981) *J. Vinyl Technol.*, **3**, 102–106.
91. Ozkaya, N., Erbay, E., Bilgic, T. and Savasci, T. (1993) *Angew. Makromol. Chem.*, **211**, 35–51.

Chapter 6

Emulsion Polymerization

María J. Barandiaran, José C. de la Cal and José M. Asua

Emulsion polymerization is a technique leading to colloidal polymer particles dispersed in a continuous medium, most often water. These polymeric dispersions are called latexes. The polymer particles are mostly spherical, but they often have a morphology that strongly affects application properties. The average diameter of the particles ranges from 50 to 1000 nm, more commonly from 80 to 300 nm. This size range is more than one order of magnitude smaller than that of the particles obtained by suspension polymerization, and it is the result of a unique mechanism of particle formation. Emulsion polymers are homopolymers and random and graft copolymers produced by free-radical polymerization. The solids content (weight of solid material/weight of latex) of commercial latexes spans from 40 to 65 wt%, although for some applications higher solids contents are desirable. A 50 wt% solids content latex with a particle diameter of 120 nm contains 5.5×10^{17} particles per liter of latex, which have a surface area of about 25 000 m² (i.e., 2.5 soccer fields). In such a system, the distance among particles is about 10–15 nm, and each particle would contain about 600 macromolecules of 10^6 g mol⁻¹ molecular weight. The dispersed system is thermodynamically unstable, and kinetic stability is provided by emulsifiers (ionic and non-ionic) and by incorporation of hydrophilic groups into the polymer.

6.1 Main products and markets

In a broad sense, polymer dispersions include both synthetic polymer dispersions and natural rubber (Table 6.1). The yearly production of synthetic polymer dispersions is about 10% of the overall polymer consumption [1]. Synthetic polymer dispersions are produced by emulsion polymerization. About half of these polymers are commercialized as waterborne dispersions. Carboxylated styrene-butadiene copolymers, acrylic and styrene-acrylic latexes and vinyl acetate homopolymer and copolymers are the main polymer classes (Table 6.2). The main markets for these dispersions are paints and coatings (26%), paper coating (23%), adhesives (22%) and carpet backing (11%) [2]. Polymer dispersions have also found an interesting market niche in biomedical applications (diagnosis, drug delivery and treatment [3]).

A substantial part of the synthetic polymer dispersions is commercialized as dry products. These include styrene-butadiene rubber (SBR) for tires, nitrile rubbers, about 10% of the total poly(vinyl chloride) production, 75% of the total acrylonitrile-butadiene-styrene

Table 6.1 Emulsion polymers**Natural rubber****Synthetic emulsion polymers***Waterborne dispersions*

Carboxylated styrene-butadiene polymers

Vinyl acetate polymers

Acrylic and styrene acrylic polymers

Commercialized as dry polymer

Styrene-butadiene rubber

Nitrile rubbers (NBR and HNBR)

Poly(vinyl chloride) (10% of the total production)

Redispersable powders (VAc copolymers, SB)

Table 6.2 Polymer dispersions

Polymer classes		
Latex	Share (%)	Applications
Carboxylated styrene-butadiene	34	Paper coating, carpet backing, adhesives, additives for mortar and bitumen
Acrylics and styrene-acrylics	24	Paints, adhesives, textiles (e.g., binders for pigment printing and flocked fabrics), inks, leather treatment, paper coating
Vinyl acetate and copolymers	20	Paints, adhesives for paper and wood and textiles (e.g., non-woven)
Markets		
	Paints and coatings	26%
	Paper coating	23%
	Adhesives	21%
	Carpet backing	11%

(ABS, an elastomer modified thermoplastic used in electrical and electronic equipment, house and office appliances and in the automotive industry) and redispersable powders for construction materials. Natural rubber accounted for 6.5 million tonnes per year, including about 1 million tonnes that is commercialized as a waterborne dispersion.

6.2 Microstructural features and their effect on properties

Figure 6.1 presents some important microstructural features of the emulsion polymers. They include copolymer composition, monomer sequence distribution (MSD),

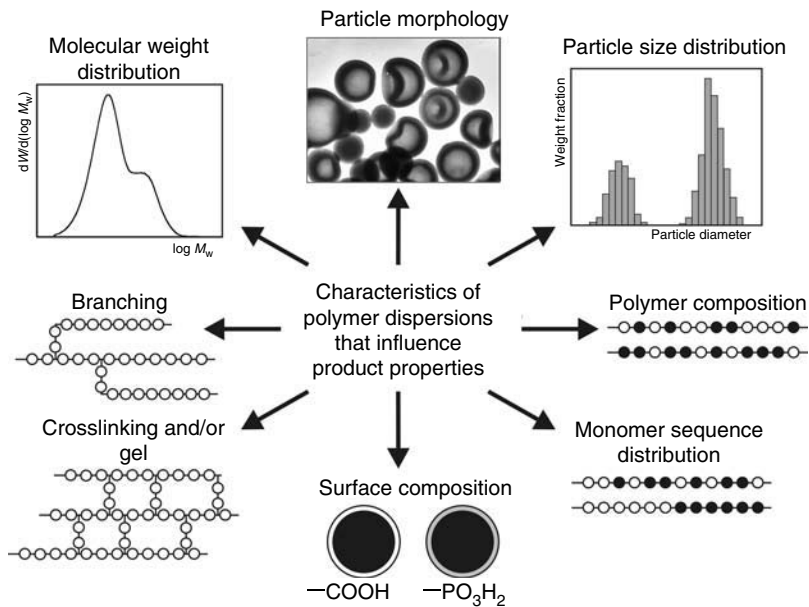


Figure 6.1 Characteristics of polymer dispersions.

molecular weight distribution (MWD), polymer architecture (branching, grafting, crosslinking and gel content), particle surface functionality, particle morphology and particle size distribution (PSD).

Copolymer composition has a direct effect on the T_g of the polymer, which determines the minimum film forming temperature (MFFT) of the latex and the application. Thus, a 95/5 wt/wt butyl acrylate/methyl methacrylate is an adhesive, whereas a 50/50 copolymer of the same monomers is a binder for paints. Copolymer composition affects properties such as resistance to hydrolysis [4] and weatherability. *In situ* formed blends of random copolymers of different compositions may be beneficial for application properties [5]. Conventional free-radical polymerization, which is the process used to manufacture almost all commercial emulsion polymers, does not allow the production of block and gradient copolymers (accessible by means of controlled radical polymerization [6], Section 3.3). Nevertheless, graft copolymers are frequently formed, and the extension of grafting largely determines the application properties. Thus, grafting determines the size of the rubber domains in ABS polymers, and the toughness of these polymers increases with rubber size.

MWD strongly affects application properties. For example, in papers coated with styrene-acrylate copolymers, the dry pick strength (the tensile strength of the coating strip when subjected to splitting during the printing process) increases and the blister resistance decreases as the molecular weight of the polymer increases [2]. In VAc/Veova paints, scrub resistance increases with the molecular weight of the polymer [7]. In adhesives, tack is maximum for low molecular weights, peel resistance is mainly determined by the intermediate molecular weights and shear resistance by the high molecular weights [8].

Polymer architecture plays a crucial role in final properties. Thus, in papers coated with carboxylated styrene-butadiene latexes, blister resistance decreases and dry pick increases

with the gel content, whereas wet pick shows a maximum for relatively low gel contents and binding strength is maximum at relatively high gel contents [9]. For adhesives, an optimal gel content that maximizes the resistance to shear is often found [10].

The application properties of many latexes are strongly affected by the chemistry of the surface of the polymer particles. Relatively small amounts (1–2 wt% based on monomers) of acidic monomers (e.g., acrylic acid, AA) are frequently used in the manufacture of latexes. Because this monomer is water-soluble, upon polymerization, most of the AA-rich polymer chains are located at the surface of the polymer particles. The presence of AA at the surface of the polymer particles is beneficial for both the stability of the latex [11] and the application properties (e.g., both the shear strength of the adhesives [12] and the pick strength of coated paper [9] increase with the AA content). In addition, the type and amount of surfactant affects application properties such as colloidal stability and water sensitivity of the film [13].

Particle morphology expands the properties envelop of the synthetic latexes. Thus, latex particles with a rubbery core and a hard shell are used to toughen plastics such as poly(vinyl chloride), poly(methyl methacrylate), epoxy resins and polycarbonate [14]. Latex particles that become hollow upon drying, and hence refract light, are used to reduce the amount of inorganic pigments in paints and paper coating [15]. Another interesting development is the use of latex particles with special morphologies to avoid the use of coalescent agents, a source of volatile organic compounds (VOCs) emissions, in paint formulation [16]. A promising new field is that of the polymer–polymer and polymer–inorganic hybrid latexes. These are special particle morphologies including polymers produced by processes other than free-radical polymerization and inorganic materials such as silica and clays [17–19].

PSD and the particle surface functionality determine the rheology of the latex [20]. Rheology is critical during emulsion polymerization because it controls mixing and heat transfer. Rheology also determines the maximum solids content achievable. In commercial practice, latexes with high solids content (>55 wt%) are advantageous as they maximize the reactor capacity during production, minimize the transport costs, give more flexibility in product formulation and allow faster drying rates [21]. Rheology also plays a crucial role in the applications (e.g., in paper coating [3]) of the polymeric dispersion. On the other hand, the quality of the film improves when particle size decreases [22].

In most of the applications of the synthetic polymer dispersions (e.g., paints and coatings, adhesives and paper coatings), the commercial product is a complex formulation. Table 6.3 presents an example of a coating formulation. In these formulations, the latex is the key ingredient, but the application properties are also affected by the other components of the formulation. Product formulation is out of the scope of this book.

6.3 Emulsion polymerization fundamentals

6.3.1 Description of the process

Commercial implementation of emulsion polymerization is mostly carried out in stirred-tank reactors operated semicontinuously. Continuous stirred-tank reactors (CSTRs) are used for the production of some high-tonnage emulsion polymers such as SBR. Batch processes are only used to polymerize monomers with similar reactivities and low heat generation rate (e.g., acrylic-fluorinated copolymers for textile applications).

Table 6.3 Paint formulation

Coating	
Component	Function
Polymer dispersion	Binder
Pigments (organic/inorganic – TiO ₂)	Color, opacity
Fillers (calcium carbonate, talc, clays)	Opacity
Thickeners (water-soluble polymers)	Rheology
Wetting agents (surfactants)	Reduce surface tension
Coalescent	Film formation
Defoamer	Reduce foaming
Biocide	Avoid microorganism growth

In the semicontinuous process, the reactor is initially charged with a fraction of the formulation (monomers, emulsifiers, initiator and water). The initial charge is polymerized in batch for some time and then the rest of the formulation is added over a certain period of time (typically 3–4 h). The monomers can be fed either as an aqueous pre-emulsion stabilized with some emulsifier or as neat monomers. Monomers contain inhibitors to allow safe storage and they are used without purification. The initiator is fed in a separate stream. The goal of the batch polymerization of the initial charge is to nucleate the desired number of polymer particles. Because particle nucleation is prone to suffer run-to-run irreproducibility, seeded semicontinuous emulsion polymerization is often used to overcome this problem. In this process, the initial charge contains a previously synthesized latex (seed) and eventually a fraction of the formulation (monomers, emulsifiers, initiator and water). Therefore, nucleation of new particles is minimized leading to better reproducibility.

Although batch emulsion polymerization is not frequently used, it will be discussed first because it is easier to understand as the fundamental processes occur in a sequential way, whereas in the semicontinuous and continuous modes the processes occur simultaneously.

6.3.1.1 Batch emulsion polymerization

Table 6.4 presents a typical formulation for emulsion polymerization. The principal monomers present low water solubility and the ratio between “hard” (leading to high T_g polymers) and “soft” (leading to low T_g polymers) monomers is chosen to achieve the T_g required for the application. Minor functional monomers provide some special characteristics, such as improved latex stability and adhesion. Crosslinking agents and chain transfer agents (CTAs) are used to control the chain architecture and the MWD of the polymer.

The monomers are dispersed in water in the presence of surfactants. The surfactants adsorb on the surface of the monomer droplets, stabilizing them. Ionic surfactant stabilizes the droplets by electrostatic repulsion, whereas non-ionic surfactants provide steric stabilization [23]. In most formulations, the amount of surfactant exceeds that needed

Table 6.4 Typical formulation for emulsion polymerization

Monomers (50–55 wt%)	Chain transfer agent
<i>Principal monomers</i>	Deionized water (45 wt%)
Hard monomers	Surfactants (0.5–3 wt%)
Styrene	<i>Ionic</i>
Methyl methacrylate	Sodium lauryl sulfate (SLS)
Vinyl chloride	<i>Non-ionic</i>
Vinyl acetate	$C_{12}H_{25}-(CH_2-CH_2O)_nH$
Soft monomers	Initiators (0.5 wt%)
Butadiene	<i>Thermal</i>
Butyl acrylate	Potassium persulfate (KPS)
2-Ethyl hexyl acrylate	Ammonium persulfate (APS)
Veova 10	<i>Redox</i>
<i>Minor monomers</i>	APS/Na ₂ S ₂ O ₅
Acrylic acid	
Methacrylic acid	
Itaconic acid	
Acrylamide	
Crosslinking agents	

to completely cover the monomer droplets and saturate the aqueous phase. The excess of surfactant forms micelles that are swollen with monomer.

Thermal initiators are used when the process is carried out at elevated temperatures (75–90°C), and redox systems are used for lower temperatures and when a high rate of initiation is needed. Most initiators are water-soluble, therefore the radicals are formed in the aqueous phase. These radicals are often too hydrophilic to directly enter into the organic phases. Therefore, they react with the monomer dissolved in the aqueous phase, forming oligoradicals that grow slowly because of the low concentration of monomer in the aqueous phase. After adding some monomer units, the oligoradicals become hydrophobic enough to be able to enter into the organic phases of the system. Because the total area of the micelles is about three orders of magnitude greater than that of the droplets, entry of radicals into the micelles is more likely. The entering oligoradicals find a monomer-rich environment within the micelle, and hence they grow fast forming a polymer chain. The new species formed upon entry of a radical into a micelle is considered to be a polymer particle. The process of formation of polymer particles by entry of radicals into micelles is called *heterogeneous nucleation* [24]. Polymer particles can also be formed when the oligoradicals grow in the aqueous phase beyond the length at which they are still soluble in water and precipitate. The precipitated polymer chain is stabilized by the emulsifier present in the aqueous phase, and monomer diffuses into the new organic phase, which allows a fast growth of the polymer chain. The process of formation of polymer particles by precipitation of oligoradicals is called *homogeneous nucleation* [25]. Both homogeneous and heterogeneous nucleation may be operative in a given system. In general, homogeneous nucleation is predominant for monomers of relatively high water-solubility (e.g., methyl methacrylate, 1.5 g/100 g of water; and vinyl acetate, 2.5 g/100 g of water) and heterogeneous nucleation is predominant for water-insoluble monomers (e.g., styrene, 0.045 g/100 g of water).

Irrespective of the mechanism of particle nucleation (heterogeneous or homogeneous), the newly formed particles are very small and suffer a tremendous increase in surface area upon particle growth. It is arguable that the emulsifier molecules may diffuse fast enough to the surface of these fast growing particles to stabilize them. Therefore, the species formed by entry of radicals in micelles and by precipitation of growing radicals in the aqueous phase may be regarded as precursor particles that only become stable particles upon growth by coagulation and polymerization [26–28]. This combined process is sometimes called *coagulative nucleation*.

During nucleation, monomer droplets, monomer swollen micelles and monomer swollen polymer particles coexist in the batch reactor. Polymer particles efficiently compete for radicals and as their number increases, they become the main polymerization loci. The monomer that is consumed by free-radical polymerization in the polymer particles is replaced by monomer that diffuses from the monomer droplets through the aqueous phase. Therefore, the size of the particles increases and that of the monomer droplets decreases. The number of micelles decreases because they become polymer particles upon entry of a radical, and also because they are destroyed to provide surfactant to stabilize both the polymer chains that precipitate in the aqueous phase and the increasing surface area of the growing polymer particles. After some time, all micelles disappear. This is considered to be the end of the nucleation and only limited formation of new particles may occur after this point because heterogeneous nucleation is not possible and there is no free surfactant available in the system to stabilize the particles formed by homogeneous nucleation. The stage of the batch emulsion polymerization in which particle nucleation occurs is called Interval I [24, 29]. At the end of Interval I, which typically occurs at a monomer conversion of about 5–10% (depending on the surfactant/monomer ratio), 10^{17} – 10^{18} particles ℓ^{-1} are formed. Unless coagulation occurs, the number of particles remains constant during the rest of the batch process.

In Interval II, the system is composed of monomer droplets and polymer particles. The monomer consumed by polymerization in the polymer particles is replaced by monomer that diffuses from the monomer droplets through the aqueous phase. The mass transfer rate of monomers with water solubility equal or greater than that of styrene (0.045 g/100 g of water) is in most cases higher than the polymerization rate, and hence monomer partitions between the different phases of the system according to thermodynamic equilibrium. In the presence of monomer droplets, the concentration of the monomer in the polymer particles reaches a maximum value that is roughly constant during Interval II. The transport of reactants (monomers, CTAs) with water solubility lower than that of the styrene from monomer droplets to polymer particles may be diffusionally limited.

Because of the polymerization and monomer transport, the polymer particles grow in size and after some time, the monomer droplets disappear, marking the end of Interval II. The monomer conversion at which Interval II ends depends on the extent in which the polymer particles are swollen by the monomer. The higher the maximum swelling, the earlier the monomer droplets disappear. In general, the more water-soluble the monomer the higher the maximum swelling, and hence the lower the monomer conversion at the end of Interval II. Thus, the transition from Intervals II to III occurs at about 40% conversion for styrene and at about 15% conversion for vinyl acetate. This means that most of the monomer polymerizes during Interval III. In this interval, the monomer concentration in the polymer particles decreases continuously.

6.3.1.2 *Semicontinuous and continuous emulsion polymerization*

In semicontinuous reactors, monomers, surfactant, initiator and water are continuously fed into the reactor. In CSTRs, the whole formulation is continuously fed into the reactor and the product continuously withdrawn. The composition of the outlet is the same as that of the reactor. In these systems, emulsion polymerization does not follow the sequence of events described earlier. Nevertheless the underlying processes are the same. Thus, nucleation occurs whenever there is enough free emulsifier to stabilize the oligoradicals that precipitate in the aqueous phase (homogeneous nucleation) and to saturate the surface of the existing interfaces (particles and monomer droplets if any) and form micelles (heterogeneous nucleation). Nucleation of a new crop of particles can be achieved by adding extra amounts of surfactant at specific moments along the semicontinuous process. Monomer droplets will exist if the rate at which the monomer is fed into the reactor exceeds the polymerization rate. This is a situation that is not desirable because the presence of free monomer in the system lowers the capability for controlling the polymer characteristics. In addition, an excess of free monomer may jeopardize the safety of the operation (see Chapter 8).

6.3.2 *Mechanisms, thermodynamics and kinetics*

In emulsion polymerization most of the polymerization occurs in the polymer particles. Figure 6.2 illustrates the mechanisms involved in emulsion polymerization. Radicals formed in the aqueous phase from water-soluble initiators, react with the monomer dissolved in the aqueous phase forming oligoradicals. These oligoradicals may

- (1) enter into the polymer particles,
- (2) enter into the micelles (heterogeneous nucleation),
- (3) propagate in the aqueous phase until they become insoluble and precipitate forming new polymer particles (homogeneous nucleation) and
- (4) terminate with other radicals in the aqueous phase.

The likelihood of each of these events depends on the particular conditions of the system (e.g., number of polymer particles, emulsifier concentration, initiator concentration, monomer type and concentration, ...). Within the polymer particles, polymerization follows the same mechanisms as in bulk free-radical polymerization. These mechanisms involve chain transfer to small molecules (e.g., monomers and CTAs), that yield small radicals. These small radicals may exit the polymer particles diffusing into the aqueous phase. Figure 6.2 illustrates the case in which monomer radicals are the exiting species.

6.3.2.1 *Radical compartmentalization*

In an emulsion polymerization system, radicals are distributed among the polymer particles. The size of these particles is so small that there are only a small number of radicals per particle, as an average less than one radical per particle in many cases of practical interest. The compartmentalization of radicals among the particles is the most distinctive kinetic

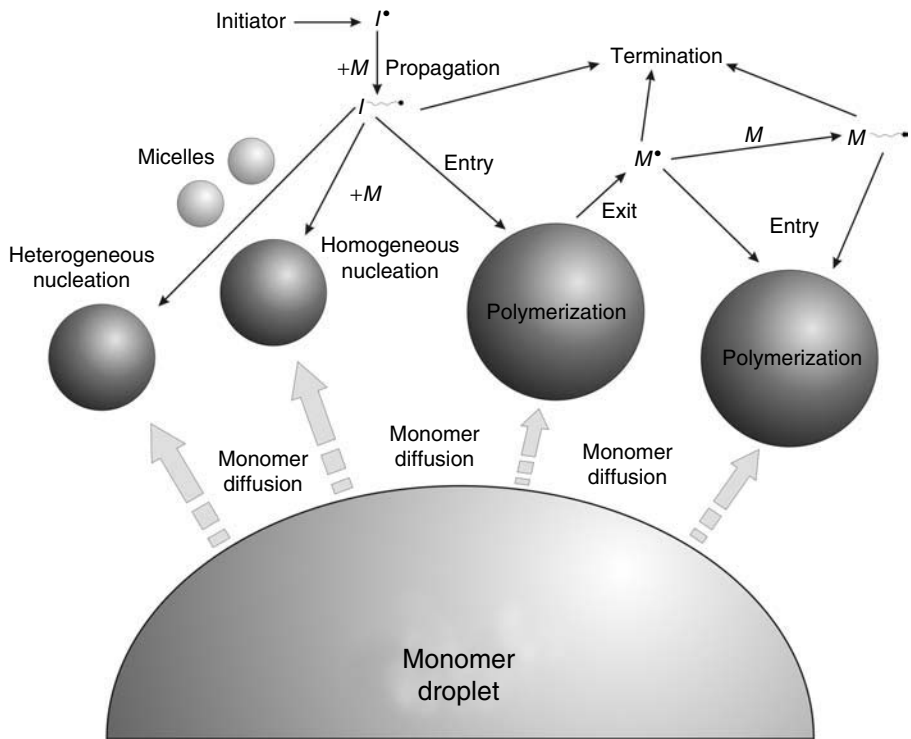


Figure 6.2 Mechanisms involved in emulsion polymerization.

feature of emulsion polymerization and has profound implications in both the polymerization rate and polymer microstructure. Radicals in different particles cannot terminate by bimolecular termination. Consequently; the overall radical concentration in emulsion polymerization is higher than in bulk polymerization. Thus, the radical concentration in a 50 wt% latex with a particle diameter of 120 nm in which half of the particles contain one radical and the rest none is $4.5 \times 10^{-7} \text{ mol } \ell^{-1}$. This is about one order of magnitude higher than the typical radical concentration in bulk ($5 \times 10^{-8} \text{ mol } \ell^{-1}$). This means that the polymerization rate in emulsion polymerization is significantly higher than in bulk polymerization. In a latex, the overall concentration of radicals increases as the number of particles increases (e.g., by decreasing the particle size for a given solids content). This gives a further way of increasing polymerization rate (in addition to increasing temperature and initiator concentration). Radical compartmentalization also results in longer life-time of the radicals, which leads to higher molecular weights. For the system described above, a polymer chain grows until a second radical enters into the polymer particle and terminates with the growing one. Therefore, the chain length is inversely proportional to the entry frequency. For a given concentration of initiator, the frequency of radical entry decreases with the number of particles, therefore the molecular weight increases. Consequently, in emulsion polymerization it is possible to simultaneously increase the polymerization rate and the molecular weight by simply increasing the number of particles.

This is not possible in any other free-radical polymerization technique (bulk, solution, suspension).

6.3.2.2 Polymerization rate

The rate of polymerization of monomer per unit volume of monomer swollen polymer particle, R_p^* , is

$$R_p^* = k_p[M]_p[P_{tot}]_p \quad (\text{mol } \ell^{-1} \text{ s}^{-1}) \quad (6.1)$$

where k_p is the propagation rate constant ($\ell \text{ mol}^{-1} \text{ s}^{-1}$), $[M]_p$ the concentration of monomer in the polymer particles ($\text{mol } \ell^{-1}$) and $[P_{tot}]_p$ the concentration of radicals in the polymer particles ($\text{mol } \ell^{-1}$). In a multimonomer system, the copolymer-averaged rate coefficient for propagation should be used (see Equation 3.44).

An emulsion polymerization system is composed of particles of different sizes. Because of the stochastic entry and exit of radicals, the concentration of radicals in a given particle varies randomly with time, and particles with the same size have a different concentration of radicals. Although there are ways to model such a complex system, for most practical applications the polymerization rate is accurately estimated by considering that the system is represented by a population of particles of an average size. Under these circumstances, $[P_{tot}]_p$ can be expressed in terms of the average number of radicals per particle, \bar{n} , in such a way that the polymerization rate per unit volume of the reactor, R_p , is given by:

$$R_p = k_p[M]_p \frac{\bar{n} N_p}{N_A V} \quad (\text{mol } \ell^{-1} \text{ s}^{-1}) \quad (6.2)$$

where N_A is Avogadro's number, N_p the number of polymer particles in the reactor and V the volume of the reactor.

In order to calculate the polymerization rate, \bar{n} , N_p and $[M]_p$, should be available.

6.3.2.3 Average number of radicals per particle

The average number of radicals per particle is defined as follows:

$$\bar{n} = \frac{\sum_{n=0}^{n=\infty} n N_{p(n)}}{\sum_{n=0}^{n=\infty} N_{p(n)}} \quad (6.3)$$

where $N_{p(n)}$ is the number of particles with n radicals, which depends on the relative rates of radical entry, exit and termination. First principles' equations for the rate of radical entry have been derived [30]. However, these equations contained parameters difficult to estimate and are strongly influenced by the mechanistic assumptions used in their derivation. A pragmatic way of expressing the rate for radical entry is as follows:

$$\text{Rate of entry} = k_a[P_{tot}]_w \quad (\text{radicals particle}^{-1} \text{ s}^{-1}) \quad (6.4)$$

where k_a is the entry rate coefficient ($\ell \text{ mol}^{-1} \text{ s}^{-1}$), which should be estimated for each system and $[P_{tot}]_w$ the concentration of radicals in the aqueous phase ($\text{mol } \ell^{-1}$). It is worth pointing out that $[P_{tot}]_w$ includes radicals of any length.

The rate of radical termination in the polymer particles with n radicals is

$$\text{Rate of termination} = \frac{k_t}{\nu_p N_A} n(n-1) = 2cn(n-1) \quad (\text{radicals particle}^{-1} \text{s}^{-1}) \quad (6.5)$$

where k_t is the termination rate constant ($\ell \text{ mol}^{-1} \text{ s}^{-1}$), ν_p is the volume of a monomer swollen polymer particle, and the pseudo-first order rate coefficient for termination in the polymer particles is

$$c = \frac{k_t}{2\nu_p N_A} \quad (\text{s}^{-1}) \quad (6.6)$$

Radical exit occurs by chain transfer to a small molecule followed by diffusion of the small radical to the aqueous phase. The rate of radical desorption from a particle with n radicals is

$$\text{Rate of exit} = k_{d(n)} n \quad (\text{radicals particle}^{-1} \text{s}^{-1}) \quad (6.7)$$

where $k_{d(n)}$ (s^{-1}) is the desorption rate coefficient from particles containing n radicals. First principles expressions for $k_{d(n)}$ are given elsewhere [31, 32]. The desorption rate coefficient depends on the number of radicals per particle. However, the mathematical treatment simplifies substantially if an average value, k_d , is used.

The population balance of particles with n radicals is

$$\begin{aligned} \frac{dN_{p(n)}}{dt} = & \underbrace{k_a [P_{\text{tot}}]_w N_{p(n-1)}}_{\text{entry in } N_{p(n-1)}} + \underbrace{k_d (n+1) N_{p(n+1)}}_{\text{desorption from } N_{p(n+1)}} + \underbrace{c(n+2)(n+1) N_{p(n+2)}}_{\text{termination in } N_{p(n+2)}} - \underbrace{k_a [P_{\text{tot}}]_w N_{p(n)}}_{\text{entry in } N_{p(n)}} \\ & - \underbrace{k_d n N_{p(n)}}_{\text{exit from } N_{p(n)}} - \underbrace{cn(n-1) N_{p(n)}}_{\text{termination in } N_{p(n)}}, \quad n=0,1,2,3,\dots \quad (\text{particles s}^{-1}) \end{aligned} \quad (6.8)$$

Equation 6.8 includes the concentration of radicals in the aqueous phase. This concentration can be calculated by means of the following material balance:

$$\frac{d[P_{\text{tot}}]_w}{dt} = 2fk_I[I]_w + k_d \bar{n} \frac{N_p}{N_A V_w} - k_{\text{tw}} [P_{\text{tot}}]_w^2 - k_a [P_{\text{tot}}]_w \frac{N_p}{N_A V_w} \quad (\text{mol } \ell^{-1} \text{ s}^{-1}) \quad (6.9)$$

where radical formation from a thermal water-soluble initiator is considered and f is the efficiency factor of the initiator radicals, k_I the rate coefficient for initiator decomposition (s^{-1}), $[I]_w$ the concentration of the thermal initiator in the aqueous phase ($\text{mol } \ell^{-1}$) and k_{tw} the termination rate in the aqueous phase ($\ell \text{ mol}^{-1} \text{ s}^{-1}$).

For most practical cases, the pseudo-steady-state assumption can be applied to the radicals in the polymer particles and in the aqueous phase. Therefore, Equations 6.8 and 6.9 are converted in algebraic equations by making the left-hand side equal to zero. Under pseudo-steady-state conditions the exact solution for \bar{n} is available in terms of Bessel functions [33], but it is not easy to use. A simpler and accurate equation for \bar{n} is as follows [34]:

$$\bar{n} = \frac{2k_a [P_{\text{tot}}]_w}{k_d + (k_d^2 + 4k_a [P_{\text{tot}}]_w c \Psi)^{0.5}} \quad (6.10)$$

$$\Psi = \frac{2(2k_a [P_{\text{tot}}]_w + k_d)}{2k_a [P_{\text{tot}}]_w + k_d + c} \quad (6.11)$$

Table 6.5 Smith–Ewart limiting cases

Smith–Ewart limiting case	Experimental conditions	\bar{n}	Equation to calculate \bar{n}
Case I	(1) Small particles (<100 nm) (2) Relatively water-soluble monomers or relatively water-soluble CTAs (3) Low rate of generation of radicals from the initiator (4) Large number of particles	$\bar{n} \ll 0.5$	$\bar{n} = \frac{k_a[R]_w}{2k_a[R]_w + k_d}$
Case II	(1) No chain transfer to small molecules (i.e., monomers and CTAs) or these small molecules are highly water insoluble (2) Fast bimolecular termination rate (3) The polymer particles are relatively small (typically $dp < 200$ nm)	$\bar{n} = 0.5$	$\bar{n} = 0.5$
Case III	(1) Large particles ($dp > 200$ nm) (2) High initiator concentrations or redox initiators (3) Slow termination rates (gel effect)	$\bar{n} \gg 0.5$	$\bar{n} = \left(\frac{k_a[R]_w}{2c} \right)^{0.5}$

Equations 6.10 and 6.11 should be solved together with Equation 6.9. The solution of this system of algebraic equations includes the three limiting cases of the pioneering work of Smith and Ewart [29] summarized in Table 6.5.

For Case 1, $\bar{n} \ll 0.5$, and it corresponds to a system in which the radical desorption rate is much faster than the rate of radical entry. In Case 2, $\bar{n} = 0.5$ corresponding to a system in which the radical desorption rate is zero, and instantaneous termination occurs when a radical enters a polymer particle already containing one radical. In Case 3, the concentration of radicals in the polymer particle approaches that of bulk polymerization ($\bar{n} \gg 0.5$). For Case 2, the polymerization rate is proportional to the number of particles and the molecular weight also increases with N_p . For Cases 1 and 3 the polymerization rate is independent of the number of polymer particles if radical termination in the aqueous phase is negligible, and increases with N_p when it is significant. In Case 1, the molecular weights are determined by chain transfer, and in Case 3, the molecular weights are similar to those in bulk.

6.3.2.4 Radical concentration profile

The oligoradicals derived from many water-soluble initiators contain an inorganic moiety. When the oligoradical enters into the polymer particle, the inorganic fragment tends to stay in the aqueous phase anchoring the entering radical to the surface of the particle. This leads to a decreasing toward the center radical concentration profile in the particle [35]. Chain transfer to mobile small molecules levels off this profile. This profile is of significance in the development of particle morphology [36], but it is not worth considering it in the calculation of aspects such as the polymerization rate.

6.3.2.5 Particle nucleation

Particle nucleation may occur through both heterogeneous nucleation and homogeneous nucleation (Figure 6.2). The rate of particle formation depends on the nucleation mechanism.

(1) *Heterogeneous nucleation.* The rate of formation of polymer particles by heterogeneous nucleation is

$$R_{\text{nuc}} = k_{\text{am}}[P_{\text{tot}}]_{\text{w}} \frac{N_{\text{m}}}{V} \quad (\text{particles } \ell^{-1} \text{ s}^{-1}) \quad (6.12)$$

where k_{am} is the rate coefficient for radical entry into the micelles and N_{m} is the number of micelles in the reactor given by:

$$N_{\text{m}} = \frac{(S_{\text{w}} - \text{cmc}V_{\text{w}})N_{\text{A}}}{n_{\text{m}}} \quad (\text{micelles}) \quad (6.13)$$

where cmc is the critical micelle concentration ($\text{mol } \ell^{-1}$) and V_{w} the volume of the aqueous phase (ℓ) (therefore, $\text{cmc}V_{\text{w}}$ is the amount of surfactant dissolved in the aqueous phase); n_{m} is the aggregation number (average number of molecules of surfactant per micelle) and S_{w} the amount of surfactant that is dissolved in the aqueous phase and forming micelles, which can be calculated by means of the overall material balance for the surfactant:

$$S_{\text{w}} = S_{\text{T}} - \frac{A_{\text{p}}^*}{a_{\text{s}}} \quad (6.14)$$

where S_{T} is the total amount of emulsifier in the reactor (mol), a_{s} the parking area (the area of the polymer particles covered by one mol of surfactant under saturation conditions) ($\text{m}^2 \text{ mol}^{-1}$) and A_{p}^* , the total surface area of the polymer particles (m^2) given by:

$$A_{\text{p}}^* = 0.048N_{\text{p}}^{0.33} \left(\frac{V_{\text{pol}}}{\phi_{\text{pol}}^{\text{p}}} \right)^{0.66} \quad (6.15)$$

where V_{pol} is the volume of polymer in the reactor (ℓ) and $\phi_{\text{pol}}^{\text{p}}$ the volume fraction of polymer in the polymer particles (see Section 6.3.2.6).

Assuming no termination of radicals in the aqueous phase and that during nucleation $\bar{n} = 0.5$, Equations 6.12–6.15 lead to the following dependence of the number of particles on surfactant and initiator concentrations [29]:

$$\left(\frac{N_{\text{p}}}{V_{\text{w}}} \right) \div \left(\frac{2fk_{\text{I}}[I]_{\text{w}}N_{\text{A}}\phi_{\text{pol}}^{\text{p}}}{r_{\text{v}}} \right)^{0.4} \left(\frac{a_{\text{s}}S_{\text{T}}}{V_{\text{w}}} \right)^{0.6} \quad (6.16)$$

where r_{v} is the volumetric growth rate of one polymer particle ($\ell \text{ s}^{-1}$).

The fulfillment of this equation, in particular the 0.6 power dependence of N_{p} with respect S_{T} is often considered as a proof of the occurrence of micellar nucleation. However, one should be aware of the assumptions used in the derivation of Equation 6.16, in particular that \bar{n} was assumed to be equal to 0.5. Actually, when radical desorption is taken into

account, the solution of Equations 6.12–6.15 leads to [37, 38]:

$$\left(\frac{N_p}{V_w}\right) \div \left(\frac{2fk_I[I]_w N_A \phi_{\text{pol}}^p}{r_v}\right)^{1-z} \left(\frac{a_s S_T}{V_w}\right)^z, \quad 0.6 \leq z \leq 1 \quad (6.17)$$

where z approaches unity as the water solubility of the monomer increases (e.g., $z \approx 0.8$ for MMA).

(2) *Homogeneous nucleation.* The rate formation of particles by homogeneous nucleation is the rate at which the oligoradicals growing in the aqueous phase exceed the maximum soluble length. The critical length depends on the composition of the oligoradical, and hence radicals formed from the initiator (i.e., containing inorganic moieties) and from the desorbed radicals should be distinguished. The oligomers formed from the initiator present a minimum length (δ_z) to be hydrophobic enough to be able to enter into the polymer particles, whereas any oligomer formed from the desorbed radicals may enter into the particles directly.

The rate of formation of particles by homogeneous nucleation is the rate of polymerization of oligoradicals of critical length:

$$R_{\text{nuc}} = k_p[M]_w \frac{(P_{Ij_{\text{crit}}} + P_{\text{Micrit}})}{V} N_A \quad (\text{particles } \ell^{-1} \text{ s}^{-1}) \quad (6.18)$$

where $[M]_w$ is the concentration of monomer in the aqueous phase, and $P_{Ij_{\text{crit}}}$ and P_{Micrit} are the number of oligoradicals of critical length (with $j_{\text{crit}} > i_{\text{crit}}$) formed from the initiator and from desorbed radicals, respectively. $P_{Ij_{\text{crit}}}$ and P_{Micrit} are calculated from the balances of radicals of both types in the aqueous phase assuming that pseudo-steady-state conditions apply

$$P_{Ij_{\text{crit}}} = \alpha_1^{j_{\text{crit}} - \delta_z + 1} \alpha_2^{\delta_z - 1} \frac{2fk_I I}{k_p[M]_w} \quad (\text{mol}) \quad (6.19)$$

$$P_{\text{Micrit}} = \frac{k_d \bar{n} N_p}{k_p[M]_w N_A} \alpha_1^{i_{\text{crit}}} \quad (\text{mol}) \quad (6.20)$$

where α_1 is the probability of propagation of radicals able to enter into the polymer particles (generated from desorbed radicals and from the initiator with lengths equal or greater than δ_z) and α_2 the probability of propagation of radicals generated from the initiator of length shorter than δ_z . It is assumed that the radicals generated from the initiator with a length shorter than δ_z are too hydrophobic to enter into the organic phases. These probabilities are given by:

$$\alpha_1 = \frac{k_p[M]_w}{k_p[M]_w + k_{\text{tw}}[P_{\text{tot}}]_w + k_a(N_p/(N_A V_w)) + \delta_{(\text{mic})} k_{\text{am}}(N_m/(N_A V_w))} \quad (6.21)$$

$$\alpha_2 = \frac{k_p[M]_w}{k_p[M]_w + k_{\text{tw}}[P_{\text{tot}}]_w} \quad (6.22)$$

where $\delta_{(\text{mic})} = 0$ if only homogeneous nucleation is applied. In systems including rather water-soluble monomers and surfactant concentrations high enough so that micelles are present, particle nucleation may be formed by both heterogeneous and homogeneous mechanisms. In this case, the overall nucleation rate includes both Equations 6.12 and 6.18, and $\delta_{(\text{mic})} = 1$ (Equation 6.21). The particles formed by homogeneous nucleation need emulsifier to be stable. In the absence of micelles, this emulsifier is obtained from the existing polymer particles. In this regard, it is worth pointing out that particle stability does not require full surface coverage. Actually, most commercial latexes are only partially covered by emulsifier. When the particles formed by heterogeneous and/or homogeneous nucleation are not well stabilized by the emulsifier, particle coagulation occurs. Both detailed [39, 40] and simplified [41] modeling for this case are given elsewhere.

6.3.2.6 Monomer partitioning

During Intervals I and II of a batch emulsion polymerization, monomers partition among monomer droplets, aqueous phase and polymer particles. The monomer that is consumed by polymerization in the polymer particles is replaced by monomer that diffuses from the monomer droplets through the aqueous phase. In Interval III, there are no droplets and the monomer is mostly located in the polymer particles. In semibatch processes, monomers are continuously fed into the reactor, usually under starved conditions, namely, at high fractional conversions (polymer/monomer ratios close to 90/10 on weight basis). Under these circumstances, only the newly fed monomer droplets are present in the reactor, and the life-time of these droplets is short because the monomers diffuse through the aqueous phase to the polymer particles where they are consumed by polymerization. The concentration of monomer in the polymer particles depends on the relative values of mass transfer and polymerization rates. Except for poorly emulsified highly water-insoluble monomers, the rate of mass transfer is faster than the polymerization rate, and hence the concentrations of the monomers in the different phases are given by the thermodynamic equilibrium.

For a multimonomer system, the calculation of the concentrations of the monomers in the different phases involves the simultaneous solution of the thermodynamic equilibrium equations and the material balances. Equilibrium equations based on partition coefficients [42] and on the Morton–Flory–Huggins equation [43] may be used. For a multimonomer system, the parameters of the Morton–Flory–Huggins equation are not usually available, and for solids contents typical of commercial latexes (>50 wt%) the use of the Morton–Flory–Huggins equation does not provide significant advantages over the use of partition coefficients [44]. In the later case, the system of algebraic equations to be solved is as follows:

Equilibrium equations:

$$K_i^j = \frac{\phi_i^j}{\phi_i^w} \quad j = \text{polymer particles, droplets} \quad (6.23)$$

Material balances:

$$\begin{aligned}
 \phi_{\text{pol}}^p + \sum_i \phi_i^p &= 1 \\
 \phi_{\text{water}}^w + \sum_i \phi_i^w &= 1 \\
 \sum_i \phi_i^d &= 1 \\
 V_p \phi_i^p + V_d \phi_i^d + V_w \phi_i^w &= V_i \\
 V_w \phi_{\text{water}}^w &= V_{\text{water}} \\
 V_p \phi_{\text{pol}}^p &= V_{\text{pol}}
 \end{aligned} \tag{6.24}$$

where K_i^j is the partition coefficient of monomer i between the phase j and the aqueous phase, ϕ_i^j the volume fraction of monomer i in phase j , the superscript w denotes the aqueous phase, V_p , V_d and V_w are the volumes of monomer swollen particles, monomer droplets and aqueous phase, respectively, and V_i , V_{pol} and V_{water} are the volumes of monomer i , polymer and water, respectively. Efficient methods for solving Equations 6.23 and 6.24 are given elsewhere [45].

6.3.2.7 Molecular weights

In free-radical polymerization the polymer chains grow in a very short period of time (0.5–10 s) and the length of the macromolecules depends on the environment in which they grow. Therefore, the molecular weights are largely controlled by the average number of radicals per particle. Mathematical models for the calculation of the MWD of linear [46] and non-linear [47–53] polymers in systems with any value of \bar{n} are available. A detailed discussion of this issue is out of the scope of this chapter. Instead, particular solutions for the limiting cases of Smith and Ewart [29] are presented. In what follows the models will be presented in terms of the rate of generation of the moments of the MWD. These generation rates should be included in the material balances characteristics of each particular reactor (Section 6.4.2.1).

(1) *Linear polymers.* Linear polymers are formed from monofunctional monomers with a polymerization scheme that does not include chain transfer to polymer (e.g., styrene and methyl methacrylate).

(i) Smith–Ewart Cases 1 and 2 (zero–one system). In Smith–Ewart Cases 1 and 2, the probability of having particles with more than one radical is almost negligible, and hence the system may be considered to be formed by particles with no radicals and particles with one radical. This is called a zero–one system. In such a system, the inactive polymer chains are formed in particles containing one radical by chain transfer to monomer and by instantaneous termination upon entry of one radical.

The rate of generation of inactive chains of length m in particles with one radical ($N_{p(1)}$) per unit volume of reactor is

$$R_{D_m} = \left(\underset{\substack{\text{chain transfer} \\ \text{to monomer}}}{k_{\text{tr}}^{\text{mon}}[M]_p P_m} + \underset{\substack{\text{termination with} \\ \text{entering radical}}}{k_a[P_{\text{tot}}]_w P_m} \right) \frac{1}{V}, \quad m = 1, 2, 3, \dots \quad (\text{mol } \ell^{-1} \text{ s}^{-1}) \quad (6.25)$$

where $k_{\text{tr}}^{\text{mon}}$ is the monomer chain transfer rate coefficient ($\ell \text{ mol}^{-1} \text{ s}^{-1}$) and P_m is the total number of growing chains of length m in particles $N_{p(1)}$. If a CTA is used, in what follows $k_{\text{tr}}^{\text{mon}}[M]_p$ should be substituted by $k_{\text{tr}}^{\text{mon}}[M]_p + k_{\text{tr}}^{\text{CTA}}[\text{CTA}]_p$, where $k_{\text{tr}}^{\text{CTA}}$ is the chain transfer rate constant to the CTA ($\ell \text{ mol}^{-1} \text{ s}^{-1}$) and $[\text{CTA}]_p$ the concentration of chain transfer in the polymer particles ($\text{mol } \ell^{-1}$).

Integration of Equation 6.25 allows the calculation of the whole MWD. However, this is computationally demanding and often the MWD is represented in terms of the moments of the distribution, the k th order moment of the distribution being defined as

$$v_k = \sum_{m=1}^{\infty} m^k D_m \quad (6.26)$$

Combination of Equations 6.25 and 6.26 yields R_{v_k} that is the generation rate of the k th order moment of the distribution of inactive chains (see Section 2.3 for details about the calculation of the moments):

$$R_{v_k} = (k_{\text{tr}}^{\text{mon}}[M]_p + k_a[P_{\text{tot}}]_w) \frac{\mu_k}{V} \quad (6.27)$$

where μ_k is the k th-order moment of the distribution of growing chains.

The rate of generation of active chains of length m in particles with one radical ($N_{p(1)}$) is

$$R_{P_m} = \left(\left(k_a[P_{\text{tot}}]_w \frac{N_{p(0)}}{N_A} + k_{\text{tr}}^{\text{mon}}[M]_p \sum P_m - k_d \frac{N_{p(1)}}{N_A} \right) \delta(m-1) + k_p[M]_p (P_{m-1} - P_m) - k_{\text{tr}}^{\text{mon}}[M]_p P_m - k_a[P_{\text{tot}}]_w P_m \right) \frac{1}{V} \quad (6.28)$$

The Kronecker delta function ($\delta(x) = 1$ if $x = 0$ and $\delta(x) = 0$ if $x \neq 0$) accounts for both the generation of radicals of length one by radical entry and chain transfer and the desorption of these radicals. Notice, that the entering radicals are assumed to be of length one. In high molecular weight polymers, this assumption has no effect on the calculated molecular weights. Using the quasi-steady-state assumption (QSSA, see Section 3.2.1.1) the first moments of the active polymer chain distribution can be calculated from Equation 6.28 as follows:

$$\begin{aligned} \mu_0 &= \bar{n} \frac{N_p}{N_A} = \frac{N_{p(1)}}{N_A} \\ \mu_1 &= \frac{k_a[P_{\text{tot}}]_w N_{p(0)} + (k_{\text{tr}}^{\text{mon}}[M]_p + k_p[M]_p - k_d) N_{p(1)}}{(k_a[P_{\text{tot}}]_w + k_{\text{tr}}^{\text{mon}}[M]_p) N_A} \\ \mu_2 &= \mu_1 \left(1 + \frac{2k_p[M]_p}{k_a[P_{\text{tot}}]_w + k_{\text{tr}}^{\text{mon}}[M]_p} \right) \end{aligned} \quad (6.29)$$

Notice that in copolymerizations, $k_p[M]_p$ and $k_{tr}^{mon}[M]_p$ should be substituted by the appropriate expressions (pseudo-kinetic rate coefficients).

The cumulative number (\bar{M}_n) and weight (\bar{M}_w) average molecular weights can be calculated from the moments of the MWD as follows:

$$\bar{M}_n = \frac{\nu_1}{\nu_0} w_m, \quad \bar{M}_w = \frac{\nu_2}{\nu_1} w_m \quad (6.30)$$

where w_m is the molecular weight of the repeated unit in the polymer chain.

On some occasions, it is interesting to know the average molecular weights produced at a given moment in the process. These instantaneous average molecular weights can be calculated by means of the following equation:

$$\bar{M}_n^{inst} = \frac{R_{v1}}{R_{v0}} w_m; \quad \bar{M}_w^{inst} = \frac{R_{v2}}{R_{v1}} w_m \quad (6.31)$$

Combination of Equations 6.27, 6.29 and 6.31 yields

$$\begin{aligned} \bar{M}_n^{inst} &= \frac{\mu_1}{\mu_0} w_m = \frac{k_a[P_{tot}]_w N_{p(0)} + (k_{tr}^{mon}[M]_p + k_p[M]_p - k_d) N_{p(1)}}{(k_a[R]_w + k_{tr}^{mon}[M]_p) N_{p(1)}} w_m \\ &\approx \frac{k_p[M]_p}{k_a[R]_w + k_{tr}^{mon}[M]_p} w_m \end{aligned} \quad (6.32)$$

$$\bar{M}_w^{inst} = \frac{\mu_2}{\mu_1} w_m = 1 + \frac{2k_p[M]_p}{k_a[P_{tot}]_w + k_{tr}^{mon}[M]_p} w_m \approx 2\bar{M}_n^{inst}$$

For the Smith–Ewart Case 2, $k_a[R]_w \gg k_{tr}^{mon}[M]_p$ and then,

$$\bar{M}_n^{inst} \approx \frac{k_p[M]_p}{k_a[P_{tot}]_w} w_m \quad (6.33)$$

If radical termination in aqueous phase is negligible, Equation 6.9 yields

$$k_a[P_{tot}]_w = 2fk_I[I]_w \frac{N_A V_w}{N_p} \quad (6.34)$$

and hence

$$\bar{M}_n^{inst} \approx \frac{k_p[M]_p}{2fk_I[I]_w N_A} \frac{N_p w_m}{V_w} \quad (6.35)$$

Consequently, the molecular weight increases with the number of polymer particles and the concentration of monomer in the polymer particles, and decreases as initiator concentration increases. In addition, because the activation energy of the initiator decomposition rate constant is greater than that of propagation (see Section 3.2.1.2), the molecular weights decrease with temperature.

For the Smith–Ewart Case 1, $k_{tr}^{mon}[M]_p \gg k_a[P_{tot}]_w$ and then

$$\bar{M}_n^{inst} \approx \frac{k_p}{k_{tr}^{mon}} w_m \quad (6.36)$$

therefore, the molecular weights are controlled by chain transfer reactions and are independent of N_p , $[M]_p$ and $[I]_w$. Usually, the activation energy of the chain transfer reaction

is greater than that of propagation, and therefore the molecular weight decreases with increasing temperature.

(ii) Smith–Ewart Case 3 (pseudo-bulk system). For Smith–Ewart Case 3, the number of radicals per particle is large and the kinetics approaches bulk polymerization. In this case, the concentration of radicals in the polymer particles is given by the equation in Table 6.5, and the molecular weight is mainly controlled by chain transfer and bimolecular termination. The rate of generation of polymer of length m in particles with i radicals is

$$R_{D_m^i} = \left(k_{\text{tr}}^{\text{mon}} [M]_{\text{p}} P_m^i + 2c_{\text{d}}(i-1)P_m^i + \frac{c_{\text{c}}N_{\text{A}}}{iN_{\text{p}(i)}}(i-1) \sum_{k=1}^{i-1} P_k^i P_{m-k}^i \right) \frac{1}{V} \quad (\text{mol } \ell^{-1} \text{ s}^{-1}) \quad (6.37)$$

From Equation 6.37 the rate of change of moments of the inactive chains can be calculated as follows:

$$\begin{aligned} R_{v_0} &= (2c_{\text{d}} + c_{\text{c}}) \frac{\mu_0^2 N_{\text{A}}}{N_{\text{p}} V} + k_{\text{tr}}^{\text{mon}} [M]_{\text{p}} \frac{\mu_0}{V} \\ R_{v_1} &= (2c_{\text{d}} + 2c_{\text{c}}) \frac{\mu_0 \mu_1 N_{\text{A}}}{N_{\text{p}} V} + k_{\text{tr}}^{\text{mon}} [M]_{\text{p}} \frac{\mu_1}{V} \\ R_{v_2} &= (2c_{\text{d}} + 2c_{\text{c}}) \frac{\mu_0 \mu_2 N_{\text{A}}}{N_{\text{p}} V} + 2c_{\text{c}} \frac{\mu_1^2 N_{\text{A}}}{N_{\text{p}} V} + k_{\text{tr}}^{\text{mon}} [M]_{\text{p}} \frac{\mu_2}{V} \end{aligned} \quad (6.38)$$

The rate of generation of active chains of length m is:

$$\begin{aligned} R_{P_m} &= \left(\left(k_{\text{a}} [P_{\text{tot}}]_{\text{w}} N_{\text{p}} + k_{\text{tr}}^{\text{mon}} [M]_{\text{p}} \sum P_m \right) \delta(m-1) + k_{\text{p}} [M]_{\text{p}} (P_{m-1} - P_m) \right. \\ &\quad \left. - k_{\text{tr}}^{\text{mon}} [M]_{\text{p}} P_m - 2 \frac{(c_{\text{c}} + c_{\text{d}}) N_{\text{A}}}{N_{\text{p}}} P_m \sum P_m \right) \frac{1}{V} \end{aligned} \quad (6.39)$$

Applying the quasi-steady-state assumption (QSSA), the moments of the active chains are:

$$\begin{aligned} \mu_0 &= \frac{\bar{n} N_{\text{p}}}{N_{\text{A}}} = \left(\frac{k_{\text{a}} [P_{\text{tot}}]_{\text{w}} N_{\text{p}}^2}{(2c_{\text{d}} + 2c_{\text{c}}) N_{\text{A}}^2} \right)^{0.5} \\ \mu_1 &= \frac{k_{\text{a}} [P_{\text{tot}}]_{\text{w}} (N_{\text{p}}/N_{\text{A}}) + k_{\text{p}} [M]_{\text{p}} \mu_0 + k_{\text{tr}}^{\text{mon}} [M]_{\text{p}} \mu_0}{(2c_{\text{d}} + 2c_{\text{c}}) (\mu_0 N_{\text{A}}/N_{\text{p}}) + k_{\text{tr}}^{\text{mon}} [M]_{\text{p}}} \\ &\approx \frac{k_{\text{p}} [M]_{\text{p}} \mu_0}{(2c_{\text{d}} + 2c_{\text{c}}) (\mu_0 N_{\text{A}}/N_{\text{p}}) + k_{\text{tr}}^{\text{mon}} [M]_{\text{p}}} \\ \mu_2 &= \frac{k_{\text{a}} [P_{\text{tot}}]_{\text{w}} (N_{\text{p}}/N_{\text{A}}) + k_{\text{p}} [M]_{\text{p}} (2\mu_1 + \mu_0) + k_{\text{tr}}^{\text{mon}} [M]_{\text{p}} \mu_0}{(2c_{\text{d}} + 2c_{\text{c}}) (\mu_0 N_{\text{A}}/N_{\text{p}}) + k_{\text{tr}}^{\text{mon}} [M]_{\text{p}}} \\ &\approx \frac{2k_{\text{p}} [M]_{\text{p}} \mu_1}{(2c_{\text{d}} + 2c_{\text{c}}) (\mu_0 N_{\text{A}}/N_{\text{p}}) + k_{\text{tr}}^{\text{mon}} [M]_{\text{p}}} \end{aligned} \quad (6.40)$$

The instantaneous number- and weight-average molecular weights are then:

$$\begin{aligned}\bar{M}_n^{\text{inst}} &= \frac{k_p[M]_p}{(2c_d + c_c)(\mu_0 N_A/N_p) + k_{\text{tr}}^{\text{mon}}[M]_p} w_m \\ \bar{M}_w^{\text{inst}} &= \frac{(2c_d + 2c_c)(\mu_0 \mu_2 N_A/N_p) + 2c_c(\mu_1^2 N_A/N_p) + k_{\text{tr}}^{\text{mon}}[M]_p \mu_2}{(2c_d + 2c_c)(\mu_0 \mu_1 N_A/N_p) + k_{\text{tr}}^{\text{mon}}[M]_p \mu_1} w_m\end{aligned}\quad (6.41)$$

If bimolecular termination is predominant, then the instantaneous average molecular weights reduce to:

$$\begin{aligned}\bar{M}_n^{\text{inst}} &= \frac{k_p[M]_p N_p}{(2c_d + c_c)\mu_0 N_A} w_m \\ \bar{M}_w^{\text{inst}} &= \left[\frac{\mu_2}{\mu_1} + \frac{c_c \mu_1}{(c_d + c_c)\mu_0} \right] w_m \approx \bar{M}_n^{\text{inst}} \left(\frac{2c_d + c_c}{c_d + c_c} \right) \left(1 + \frac{c_c}{2(c_d + c_c)} \right) w_m\end{aligned}\quad (6.42)$$

Therefore:

$$\begin{aligned}\bar{M}_w^{\text{inst}} &= 2\bar{M}_n^{\text{inst}}, \quad \text{if bimolecular termination is only by disproportionation and} \\ \bar{M}_w^{\text{inst}} &= \frac{3}{2}\bar{M}_n^{\text{inst}}, \quad \text{if bimolecular termination is only by combination}\end{aligned}$$

Because for a given polymer content both c_c and c_d are proportional to N_p , the molecular weights are independent of the number of particles, and decrease with increasing temperature and initiator concentration.

On the other hand, when a CTA is used, chain transfer is predominant over bimolecular termination and the instantaneous molecular weights are

$$\begin{aligned}\bar{M}_n^{\text{inst}} &= \frac{k_p[M]_p}{k_{\text{tr}}^{\text{CTA}}[CTA]_p} w_m \\ \bar{M}_w^{\text{inst}} &= 2\bar{M}_n^{\text{inst}}\end{aligned}\quad (6.43)$$

For this case, polydispersity is equal to two, the molecular weights depend on the ratio $[M]_p/[CTA]_p$, are independent of N_p and initiator concentration, and decrease with increasing temperature.

(2) *Non-linear polymers.* In free-radical polymerization, non-linear polymers are formed by (see Section 3.2.1.3)

- transfer of a radical center from a polymeric radical to another polymer chain (intermolecular chain transfer to polymer),
- polymerization with terminal double bonds (resulting from disproportionation, transfer to monomer and chain scission) and
- polymerization of multifunctional monomers.

The rate of generation of the first moments of the dead chains is calculated from Equation 6.44 by substituting in that equation the moments of the active chains calculated from Equation 6.45, considering the QSSA:

$$\begin{aligned}
 R_{v_0} &= \left(k_{tr}^{mon}[M]_p + k_a[R]_w - \frac{k_p^{pol}}{V_p} DB \right) \frac{N_{p(1)}}{N_A V} \\
 R_{v_1} &= (k_a[P_{tot}]_w + k_{tr}^{mon}[M]_p + k_p[M]_p) \frac{N_{p(1)}}{N_A V} \approx k_p[M]_p \frac{N_{p(1)}}{N_A V} \\
 R_{v_2} &= (k_a[P_{tot}]_w + k_{tr}^{mon}[M]_p + k_p[M]_p) \frac{N_{p(1)}}{N_A V} + \left(2k_p[M]_p + \frac{2k_p^{pol}}{V_p} DB \frac{v_1}{v_0} \right) \frac{\mu_1}{V} \\
 &\approx \left(2k_p[M]_p + \frac{2k_p^{pol}}{V_p} DB \frac{v_1}{v_0} \right) \frac{\mu_1}{V} \quad (6.46)
 \end{aligned}$$

The first moment of the distribution of the active polymer chain is calculated from Equation 6.45 by considering quasi-steady-state conditions:

$$\begin{aligned}
 \mu_1 &= \frac{(k_a[P_{tot}]_w + k_{tr}^{mon}[M]_p + k_p[M]_p + (k_{tr}^{pol}/V_p)v_2 + (k_p^{pol}/V_p)DB(v_1/v_0))(N_{p(1)}/N_A)}{k_a[P_{tot}]_w + k_{tr}^{mon}[M]_p + (k_{tr}^{pol}/V_p)v_1} \\
 &\approx \frac{(k_p[M]_p + (k_{tr}^{pol}/V_p)v_2 + (k_p^{pol}/V_p)DB(v_1/v_0))(N_{p(1)}/N_A)}{k_a[P_{tot}]_w + k_{tr}^{mon}[M]_p + (k_{tr}^{pol}/V_p)v_1} \quad (6.47)
 \end{aligned}$$

The generation rate for the terminal double bonds and long-chain branching are as follows:

$$\begin{aligned}
 R_{DB} &= \left(\underbrace{k_{tr}^{mon}[M]_p}_{\text{chain transfer to monomer}} - \underbrace{\frac{k_p^{pol}}{V_p} DB}_{\text{propagation of terminal double bounds}} \right) \frac{N_{p(1)}}{N_A V} \\
 R_{LCB} &= \left(\underbrace{\frac{k_{tr}^{pol}}{V_p} v_1}_{\text{chain transfer to polymer}} + \underbrace{\frac{k_p^{pol}}{V_p} DB}_{\text{propagation to terminal double bounds}} \right) \frac{N_{p(1)}}{N_A V} \quad (6.48)
 \end{aligned}$$

The cumulative molecular weights are calculated from the values of v_i using Equation 6.30.

6.3.2.8 Particle morphology

Latexes made out of composite polymer particles (i.e., particles containing different phases) present definitive advantages in many applications. Thus, particles formed by an elastic core and a hard shell are used as impact modifiers for polymer matrices [14]. Hard-core, soft-shell particles are particularly useful for paints because they have a low MFFT and are not sticky at higher temperatures [16]. Hollow particles are efficient opacifiers [15], and

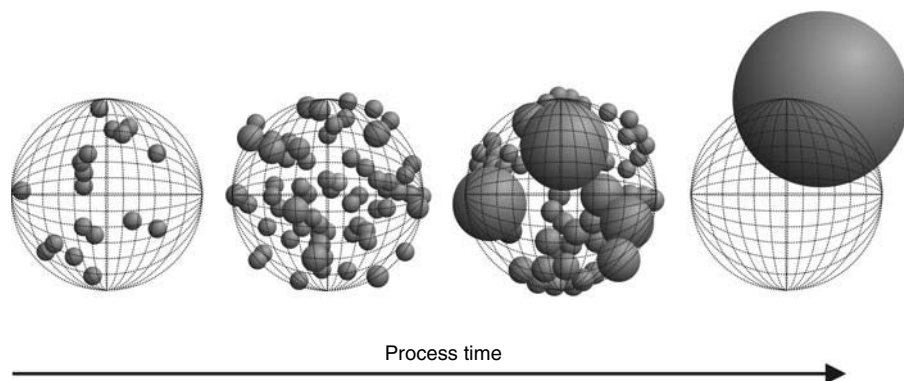


Figure 6.3 Evolution of the particle morphology.

hybrid polymer–polymer particles, for example, alkyd-acrylic polymer particles, combine the properties of the constituent polymers in a synergetic way [17].

Particles with special morphologies are commonly manufactured by seeded semicontinuous polymerization. In this process, the reactor is initially charged with a previously formed latex (seed), monomers, initiator, emulsifier and water. When polymerization of the initial charge starts, the rest of the formulation is added over a certain period of time (3–4 h). The conditions are adjusted so that the polymerization occurs inside the existing polymer particles. Figure 6.3 illustrates the development of the morphology. The position at which each polymer chain is formed depends on the radical concentration profile inside the polymer. If the entering radicals are anchored to the surface of the polymer particles, the new polymer chains will be mainly located in the outer layer of the polymer particle. As the concentration of the newly formed polymer chains increases, phase separation occurs leading to the formation of clusters. Polymerization occurs in the clusters as well as in the polymer matrix, therefore both the size and the number of clusters increase. The resulting system is not thermodynamically stable because of the large surface energy associated to the large polymer–polymer interfacial area. In order to minimize the free energy the clusters migrate toward the equilibrium morphology. During this migration, the size of the cluster increases because of

- polymerization in the cluster,
- diffusion of polymer into the cluster and
- coagulation with other clusters.

The motion of the clusters is ruled by the balance between the van der Waals attraction/repulsion forces and the resistance to flow that arises from the viscous drag. The van der Waals forces between clusters always attract. On the other hand, the van der Waals forces between clusters and aqueous phase may either attract, which brings the clusters toward the surface of the particle, or repel, which brings the clusters toward the center of the polymer particle. Figure 6.3 illustrates a case in which the clusters are attracted by the water. It is worth mentioning that the van der Waals forces are proportional to the interfacial tensions. The final morphology heavily depends on the kinetics of

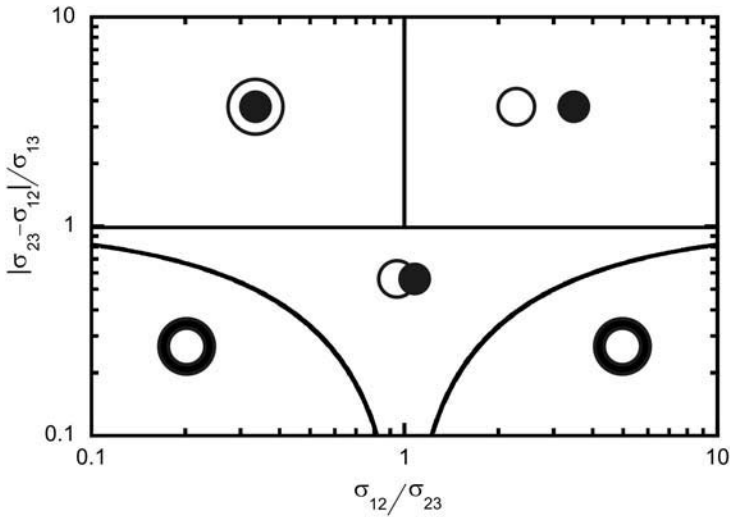


Figure 6.4 Equilibrium particle morphology.

cluster migration [59–61]. Metastable morphologies can be achieved by working under starved conditions (high internal viscosity of the particles) and promoting grafting reactions (low interfacial tensions). Equilibrium morphologies may be attained if the internal viscosity of the particle is low, the polymers are very incompatible (high interfacial tensions resulting in high van der Waals forces) and in long process times. The equilibrium morphology is the one that minimizes the interfacial energy of the system and depends on the polymer–polymer (r_{12}) and polymer–water (r_{13} and r_{23}) interfacial tensions [59] (Figure 6.4).

6.4 Reactor engineering

6.4.1 Emulsion polymerization reactors

Emulsion polymers are used in a wide variety of applications (paints and coatings, paper coating, adhesives, carpet backing, leather treatment, additives for textiles and construction materials, impact modifiers for plastics and in biomedical applications), each of them requiring a particular microstructure and a different production rate. On the other hand, emulsion polymers are products-by-process whose microstructure is determined in the reactor. Therefore, the reactor should

- allow fine-tuning of the polymer microstructure;
- be useful to prepare many different grades in the same reactor and
- be adaptable to a wide range of production rates.

The semicontinuous stirred-tank reactor is the reactor that fulfils the best of these requirements and it is the most widely used. For very large tonnages of a small number of grades,

batteries of CSTRs are used. Batch reactors are rarely used. Among the tubular reactors, only the continuous loop reactor has been used in commercial production.

6.4.1.1 *Semicontinuous stirred-tank reactor*

In the semicontinuous process, a fraction of the formulation (without initiator) is initially charged in the reactor and heated. Then, the initiator is added, and the initial charge is at least partially polymerized in batch. In this process, most of the polymer particles are formed. In some cases, the initial charge of the reactor is a pre-formed latex. In these cases, the initial batch period is not necessary. This process is called seeded semicontinuous emulsion polymerization. The rest of the formulation is continuously fed to the reactor over some period of time (typically 2–4 h). The main characteristic of this process is the great flexibility. Varying the composition and amount of the initial charge, as well as the composition and flow rates of the feeds, both temperature and polymer quality may be controlled. A wide range of products is accessible using this technique, which allows tailoring of any polymer property, including copolymer composition, MWD, polymer architecture, particle morphology and PSD. In addition, a large portfolio of products can be produced with a single reactor. The main drawback of this operation mode is its relatively low productivity, which is compensated by using larger reactors (up to 60 m³).

6.4.1.2 *Continuous stirred-tank reactor*

The main characteristic of a continuous stirred-tank reactor (CSTR) is the broad residence time distribution (RTD). Therefore, it is not possible to obtain narrow PSD using a single CSTR. In addition, CSTRs are prone to suffer intermittent nucleations [62, 63] that lead to multimodal PSDs. This may be alleviated by using a tubular reactor before the CSTR, in which polymer particles are formed in a smooth way [64]. On the other hand, the copolymer composition is quite constant, even though it is different from that of the feed. The broad RTD together with the problem of heat removal in large stirred tanks make it difficult to achieve high conversions in a single tank. An arrangement of multiple stirred tanks in series allows a better heat removal and presents a narrower RTD, which in turn leads to a narrower PSD. Moreover, copolymer composition and molecular weight can be controlled by intermediate feeds of monomer or CTAs.

Trains of up to 12 large CSTRs are used in the production of waterborne polymer commodities such as SBR [65]. Large CSTRs are not well adapted to the production of specialties because of the difficulties associated with grade transitions. Flexibility significantly increases by decreasing the average residence time in the CSTR. Thus, the production of a family of specialty emulsion polymers in a single CSTR has been reported [66].

6.4.1.3 *Tubular reactors*

Tubular reactors are attractive because of their simple mechanical design and their large area/volume ratio that allows an efficient heat removal. The use of single-pass tubes [67], pulsed columns [68], Couette–Taylor flow reactors [69], the Wicker reactor [70] and loop reactors [71] have been proposed. The poor mixing occurring in the single-pass tubes makes these reactors prone to suffer phase segregation [67]. Mixing can be improved by using

pulsed tubular reactors [72] combined with sieved plates or stocked Rasching rings [73]. However, in the case of coagulation, cleaning of the reactor may be difficult.

The Couette–Taylor flow reactor consists of two concentric cylinders in which the outer one is fixed and jacketed, while the inner one rotates. Under some particular conditions, a flow pattern characterized by counter-rotating toroidal vortices is formed. This Couette–Taylor flow makes the RTD in this reactor similar to that of a train of CSTRs [74]. However, because viscosity may change substantially as polymerization proceeds (along the reactor), it is difficult to maintain the required Taylor number in the whole reactor. The use of a conical outer cylinder may counteract the viscosity increase [75]. However, no example of the production of a commercial-like latex (i.e., high solids content) has been reported.

The Wicker reactor consists of a tube, which meanders between solid, fixed and cylindrical supports. The tube has a plurality of curves with an alternative curve direction, maintaining its circle of curvature, and it is coiled from the bottom to the upper part of the supports [70]. It is claimed that this peculiar configuration allows the production of polymeric dispersions with very low coagulum content [76].

The continuous loop reactor is likely to be the only tubular reactor used on commercial production of emulsion polymers [71], although its use is limited to production of vinyl acetate homopolymers and copolymers (with ethylene and Veova10) [77–79]. A continuous-loop reactor consists of a tubular loop that connects the inlet and the outlet of a recycle pump. These reactors combine the heat transfer characteristics of a tubular reactor with the RTD of a CSTR. The main drawback of this reactor is that the requirements for the mechanical stability of the latex are stringent because the recycling pump may induce shear coagulation.

6.4.2 Predicting the performance of emulsion polymerization reactors

The commercially used emulsion polymerization reactors (stirred-tank and continuous-loop) are designed to achieve perfect mixing. As will be discussed in Section 6.4.5, perfect mixing is not always achieved. Nevertheless, this flow model allows a good prediction of the emulsion polymerization reactor performance with a moderate mathematical effort, and it will be used here. Macroscopic balances (i.e., considering the reactor as a whole) are used. For the sake of generality, inlet and outlet streams are included in the balances. Both terms should be removed for batch operation, the outlet term should be eliminated in semibatch; and both maintained in continuous processes.

6.4.2.1 Mass balance

The mass balance for any species is

$$\frac{dN_i}{dt} = F_{i\text{in}} - F_{i\text{out}} + (R_i)V \quad (6.49)$$

where N_i is the amount of compound i in the reactor (mol); $F_{i\text{in}}$ the inlet molar flow rate of component i (mol s^{-1}); $F_{i\text{out}}$ the outlet molar flow rate of i (mol s^{-1}); (R_i) the net generation rate of i in the reactor ($\text{mol } \ell^{-1} \text{s}^{-1}$) and V the reactor volume (ℓ).

Equation 6.49 applies for the monomers, initiator, water, emulsifier and moles of each monomer incorporated into the polymer. Equation 6.49 also applies to the number of polymer particles, precursor particles and the moments of the MWD. The specific forms of the net generation rates were discussed in Section 6.3.2. Usually, the polymerization rate of monomer j is expressed as rate of monomer consumption (R_{pj}), and hence $R_{Mj} = -R_{pj}$.

For the continuous operation F_{iout} can be calculated as follows:

$$F_{iout} = Q_{out} \frac{N_i}{V} \quad (6.50)$$

where the volume of the reactor, V , is constant in a continuous operation and Q_{out} is the volumetric outlet flow rate. In emulsion polymerization, the density of the reaction medium does not change significantly. Therefore, the volumetric inlet and outlet flow rates can be considered to be the same.

6.4.2.2 Heat balance

The energy balance is

$$\sum_i N_i w_i c_{pi} \frac{dT}{dt} = \sum_j R_{pj} (-\Delta H_r)_j V - \sum_i F_{iin} c_{p\ddot{i}in} w_i (T - T_e) + Q_{removal} + Q_{loss} + Q_{stirring} \quad (6.51)$$

where c_{pi} and $c_{p\ddot{i}in}$ ($\text{kJ kg}^{-1} \text{K}^{-1}$) are the heat capacity of compound i in the reactor and at the entry conditions, respectively, R_{pj} is the polymerization rate of monomer j ($\text{mol } \ell^{-1} \text{s}^{-1}$), $(-\Delta H_r)_j$ is the polymerization heat of monomer j at the reactor conditions (kJ mol^{-1}), T is the reactor temperature (K), T_e the temperature of the feeds (K), Q_{loss} are the heat losses to the surroundings (e.g., through the reactor lid, kJ s^{-1}), $Q_{stirring}$ the heat produced by the agitator (kJ s^{-1}) and $Q_{removal}$ the heat removed through the heat removal devices (cooling jacket, cooling baffles, external heat exchanger and reflux condenser, kJ s^{-1}).

For heat removal through the cooling jacket, $Q_{removal}$ is given by:

$$Q_{removal} = -UA_w \Delta T_{ml} \quad (6.52)$$

where U is the overall heat transfer coefficient ($\text{kJ m}^{-2} \text{s}^{-1} \text{K}^{-1}$), A_w the total heat transfer area (m^2) and ΔT_{ml} the logarithmic mean temperature difference between the cooling fluid and the reaction medium given by:

$$\Delta T_{ml} = \frac{(T - T_{jin}) - (T - T_{jout})}{\ln((T - T_{jin})/(T - T_{jout}))} \quad (6.53)$$

where T_{jin} and T_{jout} are the inlet and outlet temperatures of the cooling fluid in the jacket (K).

The overall heat transfer coefficient includes several resistances in series, but the internal resistance usually controls the heat transfer rate. The internal heat transfer coefficient is a function of several factors as the impeller type and dimension, impeller speed, reactor diameter and physical properties of the reaction mixture. It can be calculated by means of empirical correlations based on dimensionless groups [80].

A practical method to determine the heat transfer through any cooling device is to measure the flow rate, and the inlet and outlet temperatures of the cooling fluid:

$$Q_{\text{removal}} = \dot{m}_w c_{pw} (T_{jin} - T_{jout}) \quad (6.54)$$

where \dot{m}_w is the mass flow rate (kg s^{-1}).

Combination of Equations 6.51 and 6.54 allows the estimation of the polymerization rate from temperature measurements. This technique, which is called reaction calorimetry, is a powerful non-invasive on-line monitoring technique, and it has been extensively applied to polymerization reactors. This subject is discussed in detail in Chapter 8.

6.4.2.3 Population balance: PSD

Now the PSD will be defined in terms of the number density of polymer particles of unswollen volume v , $n(v)$. The units of $n(v)$ are number of particles per unit of unswollen volume of particle. From this definition, the number of particles with unswollen volumes between v_1 and v_2 is

$$N_p(v_1 \rightarrow v_2) = \int_{v_1}^{v_2} n(v) dv \quad (6.55)$$

and the total number of particles is

$$N_p = \int_0^{\infty} n(v) dv \quad (6.56)$$

The macroscopic population balance for a CSTR is

$$\begin{aligned} \frac{\partial n(v)}{\partial t} &= \frac{Q_{in}}{V} n_{in}(v) - \frac{Q_{out}}{V} n(v) - \frac{\partial r_v(v) n(v)}{\partial v} \\ &\quad - \frac{n(v)}{V} \int_{v_0}^{\infty} k(v, v') n(v') dv' + \frac{1}{2V} \int_{v_0}^{v-v_0} k(v-v', v') n(v-v') n(v') dv' \end{aligned} \quad (6.57)$$

particle accumulation
entry of particles
exit of particles
formation and loss of particles of size v by particle growth

loss of particles of size v by coagulation
formation of particles of size v by coagulation of other particles

where $n(v)$ and $n_{in}(v)$ are the reactor and inlet number density of polymer particles, $Q_{in} = Q_{out}$ is the volumetric flow rate ($\ell \text{ s}^{-1}$), $r_v(v)$ the volumetric growth rate of a particle of unswollen volume v ($\ell \text{ s}^{-1}$), $k(v, v')$ the coagulation rate constant for particles of volumes v and v' , and v_0 the volume of particles formed by nucleation. This equation is a partial-differential-integral equation, and the nucleation term is best incorporated as a boundary condition at volume v_0 [81].

$$n(v_0) = \frac{R_{nuc}}{r_v(v_0)} V \quad (6.58)$$

where R_{nuc} is the nucleation rate discussed in Section 6.3.2.5.

The coagulation terms may be neglected for stable formulations. Equations 6.57 and 6.58 are conveniently solved by using orthogonal collocation [81, 82].

6.4.3 Implementation of emulsion polymerization

In a scenario of increasing international competition, margin reduction and public sensitivity to environmental issues, emulsion polymer producers are forced to achieve an efficient production of high-quality materials in a consistent, safe and environmentally friendly way [83]. Most emulsion polymers are produced in semicontinuous stirred-tank reactors. Therefore, this discussion is focussed on these reactors.

6.4.3.1 Efficient production

To achieve higher production rates, the size of the semicontinuous stirred-tank reactors has increased over the years, to 50–60 m³ for the new units. The production is limited by the heat removal capacity of the reactor. Namely, from a kinetic point of view, the processes could be carried out at a much faster rate than that at which they are implemented in industrial practice. For some high vapor pressure monomers, such as vinyl acetate, the use of reflux cooling, which substantially increases the heat removal capacity of the reactor, is possible. However, the mixing of the condensed monomer with the viscous reaction medium may be challenging. For lower vapor pressure monomers (e.g., methyl methacrylate and butyl acrylate) reflux cooling is not an option, and recirculation of the reaction medium through external heat exchangers has been used. However, highly mechanically stable latexes are needed. For many processes, heat transfer to a cooling jacket accounts for most of the heat removal. Non-isothermal processes, starting at low temperature and using the polymerization heat to increase reactor temperature allow higher production rates [7].

6.4.3.2 Safety

Polymerization reactors are prone to suffer thermal runaways because the reaction is highly exothermic. The risk is lower in emulsion polymerization because of the relatively low viscosity of the latex and the high heat capacity of the water. Nevertheless, in the case of failure of the cooling system (e.g., interruption of the electricity supply) runaways may take place. Thermal runaways are deleterious for product quality and lead to a pressure build-up in the reactor. Thus, relatively high pressure increases (6×10^5 Pa) have been monitored in thermal runaways in emulsion polymerization reactors [84]. Reactors are equipped with rupture disks and venting lines to protect the reactor from overpressure that can cause catastrophic failure. Nevertheless, to avoid risky situations, the amount of free monomer in the reactor should be limited. The limiting value should be experimentally determined by means of adiabatic calorimetry [84]. Unexpected inhibitions caused by varying levels of inhibitors in the monomers and feeding errors are the main cause for monomer accumulation in the reactor leading to risky situations. Adequate on-line monitoring and control ensure safe operation [85]. This subject is discussed in detail in Chapter 8.

6.4.3.3 Polymer quality

Emulsion polymers are complex materials whose application properties are determined by many microstructural features. In what follows, methods for controlling some important microstructural features are discussed.

(1) *Copolymer composition.* Most emulsion polymerization formulations involve several monomers of different reactivity and different water-solubility. The simplest way of controlling the copolymer composition is to conduct the process under monomer-starved conditions. In practice, this is done by feeding the monomer mixture at a rate smaller than the polymerization rate that could be reached in the system in the presence of monomer droplets, namely, when the concentration of monomer in the polymer particle is at a maximum. Under monomer-starved conditions the polymerization is controlled by the monomer feed rate, and the copolymer composition equals the monomer molar ratio in the feed. Because of different monomer partitioning, the composition of the polymer formed in the aqueous phase is different to that of the polymer formed in the polymer particle. The fraction of polymer formed in the aqueous phase is small but it may have a strong effect on properties. An example is the formation of AA-rich polymer chains that affects the stability of the latex [11], the shear strength of adhesives [12] and the pick strength of coated paper [9]. Blends of copolymers of different composition may be obtained by varying the monomer ratio in the feed. It is worth pointing out that because the polymer chains are formed in a very short period of time, the composition of each chain is constant along the chain. An important exception to this rule are the systems in which intermolecular chain transfer to polymer occur. In this case, each branch has the composition of the monomer fed in the moment in which it was formed. An additional advantage of the monomer-starved process is that it is intrinsically safe (provided no unexpected inhibitions occur) because the concentration of the monomer in the reactor is low. A disadvantage is that sometimes the process is not conducted at the maximum production rate. When adequate on-line monitoring systems are available, maximum production and good copolymer composition can be achieved simultaneously [86]. In this strategy, the total monomer concentration in the reactor is chosen to make the rate of heat generation by polymerization equal to the heat removal rate, and the monomer ratio is adjusted so that the ratio of polymerization rates equals the desired copolymer composition, F_{p1}^* .

$$\frac{R_{p1}}{R_{p1} + R_{p2}} = F_{p1}^* \quad (6.59)$$

where R_{pj} is given by

$$R_{pj} = (k_{p1j}P_1 + k_{p2j}P_2)[M_j]_p \frac{\bar{n}}{N_A} \frac{N_p}{V} \quad (6.60)$$

and P_i is the fraction of the active radicals with ultimate unit of type i [87].

$$P_1 = \frac{k_{p21}[M_1]_p}{k_{p21}[M_1]_p + k_{p12}[M_2]_p}; \quad P_2 = 1 - P_1 \quad (6.61)$$

Substituting Equations 6.60 and 6.61 into Equation 6.59, the monomer ratio needed to obtain the desired copolymer composition F_{p1}^* is obtained:

$$\frac{[M_2]_p}{[M_1]_p} = \frac{(1 - k) + [(k - 1)^2 + 4r_1r_2k]^{0.5}}{2kr_2} \quad (6.62)$$

where $k = F_{p1}^*/(1 + F_{p1}^*)$, and r_1 and r_2 are the reactivity ratios.

(2) *Molecular weight distribution.* The kinetic length of the polymer chains is given by the competition between propagation rate and the chain-termination rate. Therefore, any process variable affecting those rates has an influence on the MWD. As discussed in Section 6.3.2.7, these process variables include initiator type and concentration, number and size of the polymer particles, temperature and monomer concentration. However, these process variables strongly affect other kinetic aspects (e.g., polymerization rate), and hence they are not easily used with the purpose of tailoring the MWD. The MWD is better controlled by means of both CTA and multifunctional monomers.

In the presence of CTAs, chain transfer to CTA is the main chain-termination event and the instantaneous MWD has a number-average chain length given by:

$$DP_n^{\text{inst}} = \frac{k_p[M]_p}{k_{tr}^{\text{CTA}}[\text{CTA}]_p} \quad (6.63)$$

with a polydispersity index (PDI) = 2. Therefore, the instantaneous MWD can be controlled by adjusting the monomer/CTA ratio. Varying this ratio along the process, linear polymers with widely different MWDs can be produced [88]. It is worth pointing out that the maximum molecular weight achievable is that obtained in the absence of CTA.

Non-linear polymers are frequently characterized by their solubility in a given solvent. The insoluble part, which corresponds to high molecular weight heavily branched polymer and polymer networks, is called gel. In the polymerization of monofunctional monomers that form gel by intermolecular chain transfer to polymer followed by termination by combination (e.g., butyl acrylate), the addition of CTA may reduce the gel content to nil, whereas the sol MWD remains essentially unaffected [89].

Multifunctional monomers (crosslinkers) are used to create polymer networks. Relatively modest amounts of bifunctional monomers (0.5 mol%) are enough to obtain very high (90%) gel fractions [90]. However, the sol molecular weight decreases severely. An independent control of the sol MWD and the gel content can be achieved by balancing the concentration of CTA and multifunctional monomer in the formulation [91]. The post-treatment of latexes with initiator systems producing highly reactive tert-butoxyl radicals is a way of modifying the MWD. Thus, it lowers the molecular weight of VAc-rich polymers by hydrogen abstraction followed by β -scission and leads to gel formation in acrylic polymers by hydrogen abstraction followed by termination by combination [92]. This represents a possible way to extend the range of properties achievable with a given base emulsion polymer.

(3) *Particle size distribution.* PSD strongly affects rheology [21, 93], which in turn influences heat removal rate, mixing, mass transfer and stability of the latex. All these aspects determine on many occasions the scale-up and the feasibility of the operation. In addition, PSD affects film formation and some application properties [22, 94, 95].

Equations 6.57 and 6.58 show that PSD is the result of the competition between nucleation, particle growth and coagulation. Particle growth broadens the PSD because of the higher number of radicals in large particles. This is an intrinsic feature of the system and there is little that the operator can do to modify it. Particle nucleation depends mainly on the availability of the emulsifier, but it is also affected by the radical generation rate, the water-solubility of the monomers and the number of particles already

present in the system. The simplest way of nucleating new particles is to add enough emulsifier to form micelles. It is worth pointing out that the larger the surface area of the polymer particles, the more emulsifier is needed to form micelles (see Equations 6.13 and 6.14). Therefore, the formation of a second crop of polymer particles is more difficult in high solids content latexes of small particle size. The number of particles nucleated by heterogeneous nucleation usually increases by increasing the initiator concentration. However, this is not a good process variable to control PSD because it affects many other characteristics (polymerization rate, MWD, polymer architecture). Homogeneous nucleation often yields secondary nucleations in systems in which there are no micelles. Equations 6.18–6.22 show that the homogeneous nucleation rate increases with the concentration of monomer in the aqueous phase and the concentration of the initiator, and it decreases with the number of polymer particles. Therefore, secondary nucleation is very difficult to avoid in large particle size latexes containing water-soluble monomers (e.g., acrylic acid).

Irrespective of the nucleation mechanism, the newly formed particles undergo a substantial increase in size by polymerization. Therefore, they need additional emulsifier. Fast-diffusing anionic emulsifiers are much more efficient at stabilizing the new particle than the slow-diffusing non-ionic emulsifiers. Therefore, a larger number of polymer particles are obtained by using ionic surfactants. Coagulation is a second-order process, therefore its rate increases with the concentration of polymer particles, namely, by increasing the solids content and decreasing the particle size. Particle stability is the key aspect in controlling coagulation [23]. The first condition for stability is a sufficient coverage of the polymer particles. The efficiency of the surfactants may be severely affected by the process conditions. Thus, ionic strength reduces the efficiency of ionic surfactants. Therefore, deionized water is commonly used in emulsion polymerization, and an excess of inorganic initiator may cause coagulation. Strong agitation may cause shear induced coagulation [96].

Narrow PSDs are obtained when all the particles are formed during the polymerization of the initial charge, and neither secondary nucleations nor coagulations occur during the semicontinuous operation. High solids content (>55 wt%) latexes are advantageous because they maximize the reactor production, minimize transport costs and give more flexibility in product formulation. In practice, the maximum solids content is limited by the viscosity of the latex. Bimodal PSDs with the small particles accounting for 20 wt% of the polymer minimize the latex viscosity. Bimodal PSDs are produced by creating a second crop of polymer particles by adding a shot of emulsifier. Alternative methods to produce bimodal PSDs are the growth of bimodal seeds and controlled partial coagulation of monomodal latexes. In all cases, the formation of undesired particles by homogeneous nucleation should be prevented.

(4) *Particle morphology.* Particle morphology is controlled by the interplay between thermodynamics and kinetics. The thermodynamically preferred morphology corresponds to that of minimum surface energy (Figure 6.4). Equilibrium-favored morphologies are relatively easy to obtain because the particle morphology naturally evolves toward them. The only precaution is that the phases should be mobile, which may be achieved by maintaining a certain monomer concentration in the polymer particles. The first obvious choice when

trying to produce a given particle morphology is to make this morphology the one thermodynamically preferred. This implies modifying the interfacial tensions. There are several possible ways. The polymer–water interfacial tension can be lowered by increasing the emulsifier concentration, and by choosing the type and concentration of initiator used in their synthesis. Initiators yielding hydrophilic radicals (e.g., sulfate ion radicals) lower the polymer–water interfacial tensions. The use of a functional comonomer may also substantially modify the polymer–water interface. The use of block and graft copolymers lowers the polymer–polymer interfacial tension.

In the cases in which the desired morphology cannot be made thermodynamically favored, kinetic control may be applied. An example is the formation of a hydrophobic shell over a hydrophilic core. In this process, crosslinked hydrophilic polymer particles are used as seeds in a seeded semicontinuous emulsion polymerization of the hydrophobic monomer. The hydrophobic polymer cannot be accommodated within the polymer network of the seed and it is expelled to the surface where it forms a shell. Another strategy to achieve the same morphology is to carry out the process under very monomer-starved conditions using initiators that form hydrophilic radicals. Under these conditions, surface anchoring of the entering radicals (Section 6.3.2.4) leads to a radical concentration profile with maximum values close to the particle surface. This means that the hydrophobic polymer is produced mainly near the surface of the particle. Under very monomer-starved conditions, the high viscosity of the particle restricts cluster migration.

6.4.4 Residual monomer and VOC removal

Emulsion polymerization never proceeds until complete conversion, and there is inevitably a certain amount of unreacted monomer at the end of the process. In addition, the latex contains non-polymerizable VOCs arising from impurities in the raw materials and from by-side reactions. There are two main ways to reduce the residual monomer content in waterborne polymers: post-polymerization or/and devolatilization [97, 98].

6.4.4.1 Post-polymerization

Post-polymerization consists of adding, after the end of the main polymerization process, fresh radical-generating systems to polymerize the residual monomer. Water-soluble redox systems are preferred because they can be added as aqueous solutions and generate a high flux of radicals at mild conditions, leading to shorter post-polymerization. Water-soluble redox initiators yielding hydrophobic radicals (such as organic hydroperoxides) are advantageous for monomer removal by post-polymerization because the hydrophobic radicals can enter directly into the polymer particles, whereas the hydrophilic radicals must undergo a number of propagation steps before becoming hydrophobic enough to be able to enter into the polymer particle. These growing processes take a relatively long time, because under post-polymerization conditions, monomer concentration in the aqueous phase is very low. Consequently, a significant fraction of the oligoradicals may suffer bimolecular termination leading to low initiator efficiency. The main advantages of post-polymerization

are that it can be carried out either in the polymerization reactor or in the storage tank, and no additional equipment is needed. However, only the polymerizable residual volatiles can be eliminated, and, in some cases, new VOCs are produced from the initiators used in the post-polymerization. Thus, formaldehyde is formed when sodium sulfoxilate formaldehyde is used as reductant [99], and acetone and tert-butanol are formed when tert-butyl hydroperoxide is used as oxidant [100]. In addition, inorganic water-soluble initiators may be deleterious to both stability and water sensitivity of the film formed with the latexes. It is worth mentioning that some initiator systems may modify the polymer microstructure [92, 101], which is both a problem and an opportunity to extend the range of properties achievable with a given aqueous dispersion polymer. Mathematical modeling and optimal strategies for post-polymerization have been reported [102].

6.4.4.2 Devolatilization

Although flash devolatilization has been applied for high volatility monomers removal, such as vinyl chloride from poly(vinyl chloride) [103] and butadiene from polybutadiene [104], devolatilization of aqueous polymer dispersions is usually carried out using a stripping agent (steam and nitrogen are the most commonly used; air can also be used, but explosive vapor mixtures can be produced). Devolatilization of aqueous phase dispersions is a mass-transfer process, which involves the following steps in series:

- (1) diffusion of the VOCs to the particle surface;
- (2) transfer from the polymer surface to the aqueous phase;
- (3) diffusion through the aqueous phase and
- (4) transfer from the aqueous phase to the gas phase.

For emulsion polymers, the monomer devolatilization rate is often limited by the mass transfer through the interface between the aqueous phase and the gas phase [105]. For these systems, diffusion in the polymer particles is fast because the particle size is small, and often the T_g of the polymer is low. In addition, the mass transfer from the particles to the aqueous phase is fast because of the huge interfacial area. For water-soluble VOCs such as acetaldehyde and *t*-butanol, the rate limiting step is also the mass transfer through the liquid–gas interface. Therefore, all the process variables that increased the interfacial area between the aqueous phase and the gas phase, such as agitation, geometry of the sparger or gas flow rate, would improve devolatilization. Several equipment arrangements have been proposed to allow fast devolatilization without affecting the stability of the dispersion and avoiding foaming. Englund [106] reviewed the different latex strippers used in commercial practice. Batch, semibatch and continuous tanks, using countercurrent or cross-flow gas [107], packed or perforated columns in countercurrent flow [108] and tubular devolatilizers [109] have been used. For low T_g polymers, tank reactors are more convenient. The undesirable foaming can be suppressed by lowering the temperature, but this reduces the recovery of the low boiling point substances. Chemical defoaming agents may be used, but they may accelerate thermal degradation of the polymer when the polymer is processed at an elevated temperature (as it occurs with the poly(vinyl chloride)) and it adds contaminants to the latex. A way to control foam formation is by a sudden increase of the pressure. This method has been proven to be very efficient in the stripping of acrylic latexes

in tank reactors. Mathematical models for devolatilization are available [110]. Combination of devolatilization and post-polymerizations has proven to be advantageous on some occasions [105].

6.4.5 Scale-up

The objective of the scale-up is to produce at commercial scale latexes of the same quality as those developed in the laboratory. The production of the industrial reactors is limited by their heat removal capacity, and there is a trend to use large reactors (up to 60 m³) to increase production. Because of geometric considerations, the larger the volume of the reactor, the smaller its heat transfer area/volume ratio. Therefore, large reactors require longer process times to carry out the process under good thermal control. Although agitation may improve heat transfer, the workable range is limited because a vigorous agitation may cause shear induced coagulation. Reduction of the latex viscosity by using a bimodal latex is not always a choice because this may modify the application properties. Obviously, the heat removal capacity, and hence the production rate, increases by increasing the polymerization temperature. In addition, the use of non-isothermal processes, namely, starting the polymerization at low temperature and using the polymerization enthalpy to heat the reactor may be advantageous [7]. The bottom line is that for a given process temperature, the process time, and therefore the production rate of a given reactor is practically fixed. Therefore, the thermal performance of the industrial scale reactor should be scaled-down to the laboratory reactor, and the product must be developed taking into account these thermal limitations. The challenges of the scale-up of latexes developed accounting for these limitations are often related to particle nucleation. Nucleation is a fast, highly non-linear process and hence very sensitive to local variations of the concentrations of the reactants. In large-scale reactors, it is difficult to reproduce the nearly instantaneous mixing typical of small reactors, and this is a common source of variability in particle nucleation and hence in PSD. PSD affects the radical distribution, which in turn influences MWD and polymer architecture, and consequently latex properties. A way of reducing this variability is to avoid the nucleation step by using a seed.

6.5 Related processes

Dispersed polymers are also produced by inverse emulsion polymerization, miniemulsion polymerization, dispersion polymerization and microemulsion polymerization.

6.5.1 Inverse emulsion polymerization

In this process, an aqueous solution of a water-soluble monomer (e.g., acrylamide) is dispersed in an organic continuous phase using an excess of surfactant. Water-in-oil micelles are formed. The polymerization is initiated by oil-soluble initiators, and the mechanisms involved in this process are similar to those occurring in emulsion polymerization. The product is a dispersion of an aqueous solution of water-soluble polymer in an organic

liquid. Polymers and copolymers of acrylamide for tertiary oil recovery and flocculants are produced by this technique.

6.5.2 Miniemulsion polymerization

In miniemulsion polymerization [111–113], the size of the monomer droplets is substantially reduced ($d_d = 50\text{--}1000$ nm) by combining a suitable emulsifier and an efficient emulsification apparatus, and stabilizing the resulting monomer miniemulsion against diffusional degradation by using a costabilizer (hydrophobic low molecular weight compound). The available surfactant adsorbs on the large surface area of the droplets, and hence no micelles are formed. When the initiator is added to the system, the radicals enter into the monomer droplets that become polymer particles. Droplet nucleation minimizes the diffusional limitations encountered in conventional emulsion polymerization and allows the incorporation of water-insoluble compounds (monomers, polymers, catalysts, catalytic CTA, inorganic materials and agents for controlled-radical polymerization) to the reaction loci. In the last few years, plenty of new applications have been discovered. These applications include the production of polymer–polymer and polymer–inorganic material hybrid dispersions, catalytic polymerization, controlled radical polymerization in dispersed media and the production of high-solids low-viscosity latexes.

6.5.3 Microemulsion polymerization

Microemulsion polymerization [114] involves the polymerization of oil-in-water and water-in-oil monomer microemulsions. Microemulsions are thermodynamically stable and isotropic dispersions, whose stability is due to the very low interfacial tension achieved using appropriate emulsifiers. Particle nucleation occurs upon entry of a radical into a microemulsion droplet. Microemulsion polymerization allows the production of particles smaller than those obtained by emulsion polymerization. This leads to a higher number of polymer particles, which results in a more compartmentalized system. Under these conditions, the life-time of the polymer chains increases leading to ultra-high molecular weights. Inverse microemulsion polymerization is used to produce highly efficient flocculants.

6.5.4 Dispersion polymerization

In dispersion polymerization [115], the monomers, the initiator and the stabilizer (or stabilizer precursor) are dissolved in a solvent that is not a solvent for the polymer. Polymerization starts in a homogeneous phase and the polymer precipitates forming unstable nuclei. The nuclei are stabilized by the stabilizer present in the system. This stabilizer may be included in the formulation or formed in the reactor by grafting onto the stabilizer precursor. Nucleation ends when the number of stable polymer particles increases to a point in which all new nuclei are captured by the existing stable particles. Because of the compartmentalization of the radicals among the polymer particles, the polymerization locus changes from

the continuous to the dispersed phase. Dispersion polymerization allows the production of monodispersed micron-size particles, which are too large for emulsion polymerization and too small for suspension polymerization. Dispersion polymerization in supercritical CO₂ are used to produce fluorinated polymers [116].

References

1. Daniel, J.C. (2006) In J.C. Daniel and C. Pichot (eds), *Les Latex Synthétiques. Élaboration, Propriétés, Applications*. Lavoisier, Paris, pp. 319–329.
2. Schmidt-Thümmes, J., Schwarzenbach, E. and Lee, D.I. (2002) In D. Urban and K. Takamura (eds), *Polymer Dispersions and Their Industrial Applications*. Wiley-VCH Verlag GmbH, Weinheim, Germany, pp. 75–101.
3. Delair, T. (2006) In J.C. Daniel and C. Pichot (eds), *Les Latex Synthétiques. Élaboration, Propriétés, Applications*. Lavoisier, Paris, pp. 699–718.
4. Anquetil, J.Y. and Vu, C. (2006) In J.C. Daniel and C. Pichot (eds), *Les Latex Synthétiques. Élaboration, Propriétés, Applications*. Lavoisier, Paris, pp. 365–386.
5. Laureau, C., Vicente, M., Barandiaran, M.J., Leiza, J.R. and Asua, J.M. (2001) *J. Appl. Polym. Sci.*, **81**, 1258–1265.
6. Qiu, J., Charleux, B. and Matyjaszewski, K. (2001) *Progr. Polym. Sci.*, **26**, 2083–2134.
7. Unzue, M.J., Urretabizkaia, A. and Asua, J.M. (2000) *J. Appl. Polym. Sci.*, **78**, 475–485.
8. Satas, D. (1989) *Handbook of Pressure Sensitive Adhesive Technology*, 2nd edn. Van Nostrand Reinhold, New York.
9. Lee, D.I. (1997) In J.M. Asua (ed.), *Polymeric Dispersions: Principles and Applications*. Kluwer Academic Publishers, Dordrecht, pp. 497–513.
10. Plessis, C., Arzamendi, G., Leiza, J.R., Schoonbrood, H.A.S., Charriot, D. and Asua, J.M. (2001) *Macromolecules*, **34**, 5147–5157.
11. Waters, J.A. (1997) In J.M. Asua (ed.), *Polymeric Dispersions: Principles and Applications*. Kluwer Academic Publishers, Dordrecht, pp. 421–433.
12. Urban, D. and Egan, L. (2002) In D. Urban and K. Takamura (eds), *Polymer Dispersions and Their Industrial Applications*. Wiley-VCH Verlag GmbH, Weinheim, Germany, pp. 151–292.
13. Warson, H. and Finch, C.A. (2001) *Applications of Synthetic Resin Latices*. John Wiley & Sons, Chichester, UK.
14. Lovell, P.A. and Pierre, D. (1997) In P.A. Lovell and M.S. El-Aasser (eds), *Emulsion Polymerization and Emulsion Polymers*. John Wiley & Sons, Chichester, UK, pp. 657–695.
15. McDonald, C.J. and Devon, M.J. (2002) *Adv. Colloid Interf. Sci.*, **99**, 181–213.
16. Schuler, B., Baumstark, R., Kirsch, S., Pfau, A., Sandor, M. and Zosel, A. (2000) *Progr. Org. Coat.*, **40**, 139–150.
17. Xu, X.Q., Schork, F.J. and Gooch, J.W. (1999) *J. Polym. Sci. Part A: Polym. Chem.*, **37**, 4159–4168.
18. Bourgeat-Lami, E. (2004) In Fr. Villeurbanne (ed.), *Encyclopedia of Nanoscience and Nanotechnology*. American Scientific Publishers, Stevenson Ranch, California, USA, Vol. 8, pp. 305–332.
19. Castelvetro, V. and de Vita, C. (2004) *Adv. Colloid Interf. Sci.*, **108–109**, 167–185.
20. Arevalillo, A., do Amaral, M. and Asua, J.M. (2006) *Ind. Engng Chem. Res.*, **45**, 3280–3286.
21. Guyot, A., Chu, F., Schneider, M., Graillat, C. and McKenna, T.F. (2002) *Progr. Polym. Sci.*, **27**, 1573–1615.
22. Keddie, J.L. (2006) *Mat. Sci. Engng*, **221**, 101–170.
23. Ottewill, R.H. (1997) In J.M. Asua (ed.), *Polymeric Dispersions: Principles and Applications*. Kluwer Academic Publishers, Dordrecht, pp. 217–228.

24. Harkins, W.D. (1947) *J. Am. Chem. Soc.*, **69**, 1428–1444.
25. Priest, W.J. (1952) *J. Phys. Chem.*, **56**, 1077–1082.
26. Fitch, R.M. and Tsai, C.H. (1971) In R.M. Fitch (ed.), *Polymer Colloids*. Plenum Press, New York, pp. 73–102.
27. Ugelstad, J. and Hansen, F.K. (1976) *Rubber Chem. Technol.*, **49**, 536–609.
28. Feeney, P.J., Napper, D.H. and Gilbert, R.G. (1987) *Macromolecules*, **20**, 2922–2930.
29. Smith, W.V. and Ewart, R.H. (1948) *J. Chem. Phys.*, **16**, 592–599.
30. Hansen, F.K. and Ugelstad, J. (1978) *J. Polym. Sci., Polym. Chem. Edn.*, **16**, 1953–1979.
31. Asua, J.M. (2003) *Macromolecules*, **36**, 6245–6251.
32. Asua, J.M., de la Cal, J.C. and Leiza, J.R. (2006) In J.C. Daniel and C. Pichot (eds), *Les Latex Synthétiques. Élaboration, Propriétés, Applications*. Lavoisier, Paris, pp. 331–361.
33. O'Toole, J.T. (1965) *J. Appl. Polym. Sci.*, **9**, 1291–1297.
34. Li, B.G. and Brooks, B.W. (1993) *J. Polym. Sci., Part A: Polym. Chem.*, **31**, 2397–2402.
35. Chern, C.S. and Poehlein, G.W. (1987) *J. Polym. Sci., Polym. Chem. Edn.*, **25**, 617–635.
36. de la Cal, J.C., Urzay, R., Zamora, A., Forcada, J. and Asua, J.M. (1990) *J. Polym. Sci., Polym. Chem. Edn.*, **28**, 1011–1031.
37. Nomura, M., Harada, M., Eguchi, W. and Nagata, S. (1976) *ACS Symp. Ser.*, **24**, 102–121.
38. Hansen, F.K. and Ugelstad, J. (1979) *Makromol. Chem.*, **180**, 2423–2434.
39. Richards, J.R., Congalidis, J.R. and Gilbert, R.G. (1989) *J. Appl. Polym. Sci.*, **37**, 2727–2756.
40. Araújo, P.H.H., de la Cal, J.C., Asua, J.M. and Pinto, J.C. (2001) *Macromol. Theory Simul.*, **10**, 769–776.
41. Urretabizkaia, A., Arzamendi, G. and Asua, J.M. (1992) *Chem. Engng Sci.*, **47**, 2579–2584.
42. Omi, S., Kushibiki, K., Negishi, M. and Iso, M. (1985) *Zairyo Gijutsu*, **3**, 426–441.
43. Ugelstad, J., Mork, P.C., Mfutakamba, H.R., Soleimany, E., Nordhuus, I., Nustad, K., Schmid, R., Berge, A., Ellingsen, T. and Aune, O. (1983) In G.W. Poehlein, R.H. Otewill and J.W. Goodwin (eds), *NATO ASI Series*, Vol. 1, pp. 51–99.
44. Gugliotta, L.M., Arzamendi, G. and Asua, J.M. (1995) *J. Appl. Polym. Sci.*, **55**, 1017–1039.
45. Armitage, P.D., de la Cal, J.C. and Asua, J.M. (1994) *J. Appl. Polym. Sci.*, **51**, 1985–1990.
46. Lichti, G., Gilbert, R.G. and Napper, D.H. (1982) In I. Piirma (ed.), *Emulsion Polymerization*. Academic Press, New York, pp. 93–144.
47. Tobita, H. and Hamielec, A.E. (1990) *Makromol. Chem., Macromol. Symp.*, **35–36**, 193–212.
48. Charmot, D. and Guillot, J. (1992) *Polymer*, **33**, 352–360.
49. Tobita, H. (1993) *Macromolecules*, **26**, 836–841.
50. Teymour, F. and Campbell, J.D. (1994) *Macromolecules*, **27**, 2460–2469.
51. Arzamendi, G. and Asua, J.M. (1995) *Macromolecules*, **28**, 7479–7490.
52. Butté, A., Storti, G. and Morbidelli, M. (2002) *Macromol. Theory Simul.*, **11**, 37–52.
53. Zubitur, M., Ben Amor, S., Bauer, C., Amram, B., Agnely, M., Leiza, J.R. and Asua, J.M. (2004) *Chem. Engng J.*, **98**, 183–198.
54. Ghielmi, A., Fiorentino, S., Storti, G. and Morbidelli, M. (1998) *J. Polym. Sci., Part A: Polym. Chem.*, **36**, 1127–1156.
55. Tobita, H. and Yamamoto, K. (1994) *Macromolecules*, **27**, 3389–3396.
56. Tobita, H. and Uemura, Y. (1996) *J. Polym. Sci., Part B: Polym. Phys.*, **34**, 1403–1413.
57. Tobita, H. (1997) *J. Polym. Sci., Part B: Polym. Phys.*, **35**, 1515–1532.
58. Jabbari, E. (2001) *Polymer*, **42**, 4873–4884.
59. González-Ortiz, L.J. and Asua, J.M. (1995) *Macromolecules*, **28**, 3135–3145.
60. González-Ortiz, L.J. and Asua, J.M. (1996) *Macromolecules*, **29**, 383–389.
61. González-Ortiz, L.J. and Asua, J.M. (1996) *Macromolecules*, **29**, 4520–4527.
62. Greene, R., González, R.A. and Poehlein, G.W. (1976) *ACS Symp. Ser.*, **24**, 341–358.
63. Kiparissides, C., MacGregor, J.F. and Hamielec, A.E. (1980) *Can. J. Chem. Engng*, **58**, 48–55.
64. Lee, H.C. and Poehlein, G.W. (1986) *Chem. Engng Sci.*, **41**, 1023–1030.

65. Agnely, M. (2006) In J.C. Daniel and C. Pichot (eds), *Les Latex Synthétiques. Élaboration, Propriétés, Applications*. Lavoisier, Paris, pp. 417–441.
66. Alarcia, F., de la Cal, J.C. and Asua, J.M. (2006) *Ind. Engng Chem. Res.*, **45**, 3711–3717.
67. Paquet, D.A. Jr. and Ray, W.H. (1994) *AIChE J.*, **40**, 73–87.
68. Mayer, M.J.J., Meuldijk, J. and Thoenes, D. (1994) *Chem. Engng Sci.*, **49**, 4971–4980.
69. Wei, X., Takahashi, H., Sato, S. and Nomura, M. (2001) *J. Appl. Polym. Sci.*, **80**, 1931–1942.
70. Apostel, M., Pauer, W., Moritz, H.U., Kremeskotter, J. and Hungenberg, K.D. (2001) *Chimia*, **55**, 229–230.
71. Geddes, K.R. (1989) *Brit. Polym. J.*, **21**, 433–441.
72. Sayer, C., Palma, M. and Giudici, R. (2002) *Braz. J. Chem. Engng*, **19**, 425–431.
73. Sayer, C., Palma, M. and Giudici, R. (2002) *Ind. Engng Chem. Res.*, **41**, 1733–1744.
74. Wei, X., Yoshikawa, K., Oshima, A., Sato, S. and Nomura, M. (2002) *J. Appl. Polym. Sci.*, **86**, 2755–2762.
75. Conrad, I., Kossak, S., Moritz, H.U., Jung, W.A. and Rink, H.P. (2001) *DECHEMA Monogram*, **137**, 117–124.
76. Heibel, C., Kremeskotter, J., Kastenhuber, W., Funkhauser, S. and Hiibinger, W. (1998) *PCT*, W099/44737/1998.
77. Abad, C., de la Cal, J.C. and Asua, J.M. (1994) *Chem. Engng Sci.*, **49**, 5025–5037.
78. Abad, C., de la Cal, J.C. and Asua, J.M. (1995) *J. Appl. Polym. Sci.*, **56**, 419–424.
79. Araújo, P.H.H., Abad, C., de la Cal, J.C., Pinto, J.C. and Asua, J.M. (1999) *Polym. React. Engng*, **7**, 303–326.
80. Nagata, S. (1975) *Mixing. Principles and Applications*. John Wiley & Sons, New York.
81. Rawlings, J.B. and Ray, W.H. (1988) *Polym. Engng Sci.*, **28**, 237–256.
82. Araújo, P.H.H., de la Cal, J.C., Asua, J.M. and Pinto, J.C. (2001) *Macromol. Theory Simul.*, **10**, 769–779.
83. Asua, J.M. (2004) *J. Polym. Sci., Part A: Polym. Chem.*, **42**, 1025–1041.
84. Azpeitia, M., Leiza, J.R. and Asua, J.M. (2005) *Macromol. Mater. Engng*, **290**, 242–249.
85. Sáenz de Buruaga, I., Armitage, P.D., Leiza, J.R. and Asua, J.M. (1997) *Ind. Engng Chem. Res.*, **36**, 4243–4254.
86. Sáenz de Buruaga, I., Echevarria, A., Armitage, P.D., de la Cal, J.C., Leiza, J.R. and Asua, J.M. (1997) *AIChE J.*, **43**, 1069–1081.
87. Forcada, J. and Asua, J.M. (1985) *J. Polym. Sci., Polym. Chem. Edn.*, **23**, 1955–1962.
88. Echeverria, A., Leiza, J.R., de la Cal, J.C. and Asua, J.M. (1998) *AIChE J.*, **44**, 1667–1679.
89. Plessis, C., Arzamendi, G., Leiza, J.R., Alberdi, J.M., Schoonbrood, H.A.S., Charmot, P. and Asua, J.M. (2001) *J. Polym. Sci.*, **39**, 1106–1119.
90. Bouvier-Fontes, L., Pirri, R., Arzamendi, G., Asua, J.M. and Leiza, J.R. (2004) *Macromol. Symp.*, **206**, 149–164.
91. Chauvet, J., Asua, J.M. and Leiza, J.R. (2005) *Polymer*, **46**, 9555–9561.
92. Ilundain, P., Alvarez, D., Da Cunha, L., Salazar, R., Barandiaran, M.J. and Asua, J.M. (2003) *J. Polym. Sci., Polym. Chem. Ed.*, **41**, 3744–3749.
93. do Amaral, M., van Es, S. and Asua, J.M. (2004) *J. Polym. Sci., Part A: Polym. Chem.*, **42**, 3936–3946.
94. Peters, A.C.I.A., Overbeck, G.C. and Annable, T. (1996) *Prog. Org. Coatings*, **29**, 183–194.
95. Peters, A.C.I.A., Overbeck, G.C. and Annable, T. (2000) *Prog. Org. Coatings*, **38**, 137–150.
96. Zubitur, M. and Asua, J.M. (2001) *J. Appl. Polym. Sci.*, **80**, 841–851.
97. Araújo, P.H.H., Sayer, C., Poço, J.G.R. and Giudicci, R. (2002) *Polym. Engng Sci.*, **42**, 1442–1468.
98. Barandiaran, M.J. and Asua, J.M. (2005) In T. Meyer and J. Keurentjes (eds), *Handbook of Polymer Reaction Engineering*. Wiley-VCH, Weinheim, pp. 971–994.
99. Becchi, D., Montesoro, E., Saija, L.M. and Sempio, C. (1997) *EP 0767180*.

100. Da Cunha, L., Ilundain, P., Salazar, R., Alvarez, D., Barandiaran, M.J. and Asua, J.M. (2001) *Polymer*, **42**, 391–395.
101. Tangpakdee, J., Mizokoshi, M., Endo, A. and Tanaka, Y. (1998) *Rubber Chem. Technol.*, **71**, 795–802.
102. Ilundain, P., Salazar, R., Alvarez, D., da Cunha, L., Barandiaran, M.J. and Asua, J.M. (2004) *Ind. Engng Chem. Res.*, **43**, 1244–1250.
103. Patel, P.J. and Miringoff, W. (1977) *US 4031056*.
104. Suzuki, T., Nakano, H. and Kobayashi, K. (1992) *JP 4239506*.
105. Salazar, R., Alvarez, D., Ilundain, P., da Cunha, L., Barandiaran, M.J. and Asua, J.M. (2003) *Progr. Colloid Polym. Sci.*, **124**, 116–120.
106. Englund, S.M. (1981) *Chem. Engng Progress*, **77**, 55–59.
107. Chandra, B.P., Greaves, J.C. and Lovelock, V.G. (1981) *US 4283 526*.
108. Kano, T., Okada, H., Masuko, S. and Itagaki, H. (1985) *US 4526656*.
109. Baughman, L.C. (1976) *US 3930931*.
110. Salazar, R. (2002) *Eliminación de monómero residual y compuestos orgánicos volátiles de látex acrílicos y vinílicos mediante desvolatilización*, PhD Thesis, The University of the Basque Country.
111. Ugelstad, J., El-Aasser, M.S. and Vanderhoff, J.W. (1973) *J. Polym. Sci., Polym. Lett.*, **111**, 503–513.
112. El-Aasser, M.S. and Millar, C.M. (1997) In J.M. Asua (ed.), *Polymeric Dispersions: Principles and Applications*. Kluwer Academic Publishers, Dordrecht, pp. 109–126.
113. Asua, J.M. (2002) *Progr. Polym. Sci.*, **27**, 1283–1346.
114. Candau, F. (1997) In J.M. Asua (ed.), *Polymeric Dispersions: Principles and Applications*. Kluwer Academic Publishers, Dordrecht, pp. 127–140.
115. Sudol, E.D. (1997) In J.M. Asua (ed.), *Polymeric Dispersions: Principles and Applications*. Kluwer Academic Publishers, Dordrecht, pp. 141–154.
116. Mueller, P.A., Storti, G., Morbidelli, M., Apostolo, M. and Martin, R. (2005) *Macromolecules*, **38**, 7150–7163.

Chapter 7

Step-Growth Polymerization

Kyu Yong Choi and Kim B. McAuley

7.1 Introduction

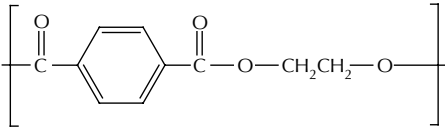
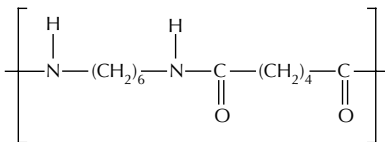
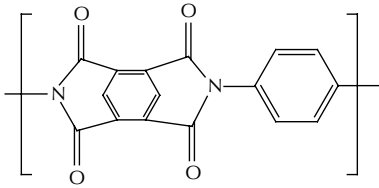
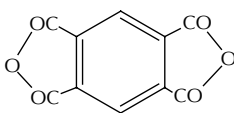
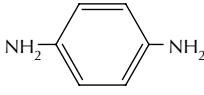
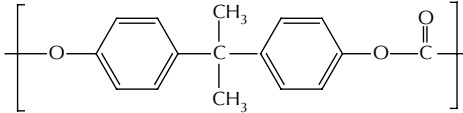
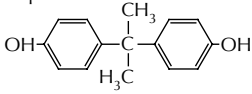
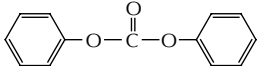
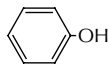
Step-growth polymerization is important for synthesizing various types of commodity, engineering and specialty polymers such as polyesters, polyamides, polyurethanes, polycarbonates, polyarylates and silicon- and sulfur-containing polymers. In step-growth polymerization, polymer linkages occur between macromolecules containing reactive functional groups, most often at the chain ends. The primary characteristics of step-growth polymerization are that any two species containing appropriate functional end-groups can react with each other, and that the polymer molecular weight increases gradually with functional-group conversion (see Tables 1.4 and 1.5). Step-growth polymerization produces linear polymer chains if bifunctional monomers are used. Monomers with three or more functional groups can be added to the reaction medium to produce branched or crosslinked polymers.

7.1.1 Examples of commercially important polymers produced by step-growth polymerization

The repeat groups for several well-known step-growth polymers of industrial importance are shown in Table 7.1. Step-growth polymerizations that produce small byproduct molecules (all examples in Table 7.1, except for polyurethane) are commonly called condensation polymerization.

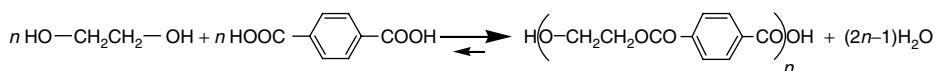
Linear step-growth polymerizations fall into two categories, depending on the type of monomer(s) employed. In one category, *AB*-type polymerization, each monomer molecule has two types of functional groups, *A* and *B*. An example of this type of polymerization is the production of polyester from monomers with structure $\text{HO}-\text{R}-\text{COOH}$. In this polymerization, the hydroxyl end group from one molecule (end group *A*) reacts with the carboxyl group (end group *B*) from a second molecule to produce an ester linkage and water. Polymerization proceeds until very long polymer chains are formed. Since each molecule has both end groups, the number of hydroxyl groups and carboxyl groups in the reaction medium is the same, unless impurities are present. In theory, all of the monomer in the reaction medium could react to form a single long polymer chain. In practice, however, cyclic molecules form along with the linear polymer chains, reducing the average molecular

Table 7.1 Common industrial polymers produced by step-growth polymerization

Repeat unit	Monomers	Byproduct
Poly(ethylene terephthalate) 	Terephthalic acid $\text{HOOC}-\text{C}_6\text{H}_4-\text{COOH}$ or Dimethyl terephthalate $\text{H}_3\text{C}-\text{O}-\text{C}(=\text{O})-\text{C}_6\text{H}_4-\text{C}(=\text{O})-\text{O}-\text{CH}_3$ and Ethylene glycol $\text{HO}-\text{CH}_2\text{CH}_2-\text{OH}$	H_2O or CH_3OH
Nylon - 6,6 	Hexamethylene diamine $\text{H}_2\text{N}(\text{CH}_2)_6\text{NH}_2$ and Adipic acid $\text{HOOC}(\text{CH}_2)_4\text{COOH}$	H_2O
Polyimide 	Pyromellitic dianhydride  and Phenyl amine 	H_2O
Polyurethane $\left(\text{R}-\text{OCONH}-\text{R}'-\text{NHCO}-\text{O} \right)$	Diol $\text{HO}-\text{R}-\text{OH}$ and Diisocyanate $\text{OCN}-\text{R}'-\text{NCO}$	None
Polycarbonate 	Bisphenol A  and Diphenyl carbonate 	

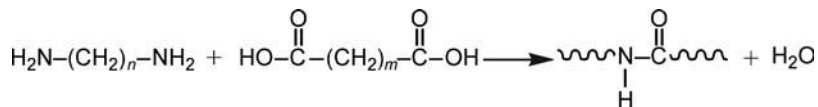
weight of the polymer that can be produced. In the second category, *AA* and *BB* polymerization, each bifunctional monomer has two similar functional groups (e.g., $\text{HO}-\text{R}-\text{OH}$ and $\text{HOOC}-\text{R}'-\text{COOH}$). All of the polymerizations in Table 7.1 are *AA* and *BB* polymerizations. In this type of system, it is important to carefully control the stoichiometry of the reacting mixture so that long polymer molecules can be formed. An excess of *AA* or *BB* will limit the molecular weight of the polymer that is obtained.

Another important difference between polymer molecules produced by the two types of polymerization is the nature of the repeat units. In a step-growth polymer produced from *AB* monomer, each monomer molecule that is consumed corresponds to a repeat unit along the polymer chain. For example, the monomer $\text{HO}-\text{R}-\text{COOH}$ produces the polyester chains $\text{HO}-(\text{R}-\text{C}-\text{OO}-)_n\text{H}$. However, in an *AA* and *BB* polymerization, each repeat unit arises from two monomer molecules. For example, consider the esterification of ethylene glycol and terephthalic acid to produce poly(ethylene terephthalate) (PET):



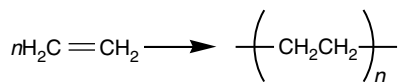
Each repeat unit for this polymer arises from an ethylene glycol unit and a terephthalic acid unit, joined by an ester linkage.

Other commercially important polymers produced by *AA* and *BB* step-growth polymerization include aliphatic polyamides of the form:



Polyamides of this type are called nylon ($n, m + 2$), where n is the number of carbons in the diamine monomer and $m + 2$ is the number of carbons in the diacid. Nylon 6,6, the most commercially important aliphatic polyamide with this structure, is produced from hexamethylene diamine (HMD) ($n = 6$) and adipic acid ($m + 2 = 6$). Nylon 4,6, nylon 6,10 and nylon 6,12 are also produced commercially [1].

To better understand the fundamental and practical differences between *step-growth* polymerization and *chain-growth* polymerization (see Table 1.4), consider the industrial *chain-growth* polymerization of ethylene (by either coordination polymerization or high-pressure free-radical polymerization) to produce polyethylene.



In this chain-growth process, ethylene monomer adds rapidly to the end of the growing chain, one unit at a time, and each coordination site or free radical grows a single long chain until chain transfer or termination occurs. Very long polymer molecules are present almost from the beginning of the polymerization. The double bonds in the ethylene monomer are converted to single bonds as each new monomer unit is added, generating considerable heat, but no side products. Removing the reaction heat is frequently one of the main process design and control challenges. Most commercial chain-growth processes are irreversible at industrial reactor operating conditions, so depolymerization reactions can usually be ignored.

By contrast, consider the *step-growth* polymerization of ethylene glycol and terephthalic acid to produce PET. In this step-growth polymerization, the time required for the formation of individual polymer chains is much longer (i.e., the residence time of the polymerization vessel), and the amount of heat generated by polymerization is very small. In fact, in industrial PET processes, reactors are *heated* to keep the polymerizing melt above its melting point ($\sim 260^\circ\text{C}$). The polycondensation process is reversible, so that high molecular weights cannot be obtained unless nearly all the side product (e.g., water) is removed from the reaction medium. As a result, commercial step-growth polymers tend to have much lower molecular weights than chain-growth polymers. A high-molecular-weight PET will have a number-average molecular weight approaching $20\,000\text{ g mol}^{-1}$ (~ 100 repeat units), whereas commercial high-molecular-weight polyethylene can have $M_n > 100\,000\text{ g mol}^{-1}$ (> 3000 repeat units). Fortunately, the polar repeat units in many step-growth polymers result in strong intermolecular forces (e.g., hydrogen bonding), so that lower-molecular-weight step-growth polymers often produce stronger materials than higher-molecular-weight chain-growth polymers.

Since step-growth polymerization reactions are reversible, it is more straightforward to recycle many step-growth polymers back to monomers or oligomers that can be used to form new polymer products than it is to recycle chain-growth polymers [1, 2]. Furthermore, the functional end-groups on step-growth polymer molecules provide important opportunities for using step-growth polymers in a variety of applications. For example, amine end groups on polyamides interact with acid dyes, making nylon polymers valuable for producing carpeting and textiles in a wide variety of vibrant colors. Also, block copolymers can readily be produced by joining oligomers of different types of step-growth polymers. Elastane (also called spandex or Lycra[®]) is an elastomeric block copolymer produced by reacting polyurethane and polyethylene glycol oligomers. The polyurethane segments are hard and crystalline, whereas the polyethylene glycol segments are soft and flexible [3].

7.1.2 Basic properties of step-growth polymerization processes

In the initial stages of step-growth polymerization processes, the degree of polymerization increases very slowly with the fractional conversion of functional groups, because many end groups must be consumed to produce each high-molecular-weight polymer chain. In the later stages of polymerization, however, small changes in conversion correspond to large increases in molecular weight as very large molecules add together.

In most step-growth processes, the final conversion, and hence the average molecular weight, is limited by the reaction equilibrium. Equilibrium functional-group concentrations are affected by the concentration of the eliminated compound (i.e., the condensation byproducts shown in Table 7.1). Removing the byproduct from the reaction medium reduces its concentration and lowers the rate of the reverse reaction, thereby encouraging net consumption of functional groups and production of higher-molecular-weight polymer. To prepare polymers of high molecular weight, the reaction must be driven to very high conversions, which can lead to the reaction medium becoming very viscous. High viscosity makes it difficult for condensation byproducts to diffuse through the reaction medium so that they can be removed. Since byproduct removal can limit the growth of polymer chains, mass transfer is often the rate-controlling factor in step-growth polymerizations.

Many polycondensation reactor designs provide large surface areas for mass transfer of condensation byproducts out of the polymer phase. In some processes, high vacuum is applied to encourage byproduct removal.

Polycondensation can be carried out by various polymerization techniques including melt polymerization, solution polymerization, interfacial polymerization, emulsion polymerization and solid-state polymerization. These polymerization processes will be summarized briefly in the following paragraphs.

In *melt polycondensation*, step-growth reactions occur in a homogeneous molten polymer phase at a temperature above the polymer's melting temperature. To encourage byproduct removal from the polymer melt, a vacuum can be applied to remove volatile condensation byproducts, or an inert purge gas can be supplied to the reactor to reduce the partial pressure of the side product in contact with the polymer phase. Polymer products obtained by melt polymerization are generally pure (except for perhaps a catalyst or other additives, such as whiteners or pigments added to modify polymer appearance, or stabilizers added to increase polymer longevity), so that no additional solvent removal or product purification steps are required. Since the viscosity of the polymerizing mass increases dramatically as the conversion increases, the removal of small byproduct molecules from the viscous mass becomes the rate-controlling process. The high temperatures employed to ensure that the polymer remains molten can cause unwanted side-product formation [4].

Solution polycondensation is used in industry to produce polyurethanes, polycarbonates and certain types of polyamides and polyesters. Polycondensation in solution is most frequently used when it is difficult or impossible to keep the reactants in the same phase using bulk polymerization, or when the melting point of the resulting polymer is too high. Solution polycondensation takes place at lower temperatures than melt polymerization and enables efficient heat transfer to be maintained due to lower viscosity. However, solution polycondensation requires polymer separation from solution, recovery of solvent, and polymer washing and drying.

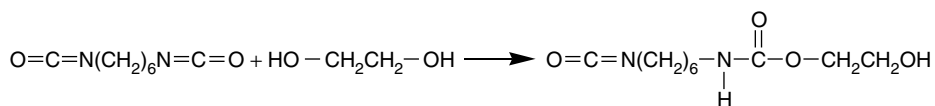
In *interfacial polycondensation*, the formation of polymer takes place at the interface of two immiscible liquids in which the starting reactants are dissolved separately. The interfacial reactions are diffusion-limited, and the system is usually stirred to ensure better contact of the two liquids. The polymers formed at the interface are filtered, washed and dried. Highly reactive monomers, which constitute a large volume of the reaction mixture, are required. Polymers that can be prepared by interfacial polymerization include polyamides, polyureas, polyurethanes, polyesters, polysulfonamides, phenol-formaldehyde polymers and polycarbonates. In interfacial polymerization, the materials employed need not be of the highest degree of purity, and the polycondensation takes place rapidly at low temperature under atmospheric pressure. Polymers obtained by interfacial polycondensation usually have a high melting point, which makes melt-phase polymerization undesirable. Interfacial polymerization techniques are used to make reverse osmosis membranes, and for encapsulation of inks, insecticides and drugs [5–7].

In *emulsion polycondensation*, the polymer formation reaction occurs in the bulk of one of the liquid phases. This method is employed for irreversible, exothermic polycondensations, accompanied by the liberation of a side product. Highly reactive monomers (e.g., dichlorides or dicarboxylic acids, diamines, etc.) are most suitable for emulsion polycondensation. To date, the number of step-growth polymers that are prepared using emulsion or mini-emulsion polymerization methods is small, and the technological aspects of this technique

require further development [8, 9]. Other heterogeneous polycondensation techniques that are used to make specialty products at low volumes include suspension and dispersion polycondensations [10, 11].

Solid-state polymerization, also called solid-phase polymerization, is used in the final stages of some industrial polymer production processes (e.g., nylon, polyester and polycarbonate production) to produce very high molecular weight polymers. Molten low-molecular-weight polymer produced in a melt-phase or solution reactor is cooled and formed into solid particles (by extrusion or by spray drying). In the solid-state reactor, the pellets are held at temperatures above the glass transition temperature (but below the melting point) of the polymer so that functional end-groups are sufficiently mobile to react. The polycondensation byproduct is removed from the pellets by applying high vacuum or by contacting the pellets with an inert gas stream (e.g., nitrogen). The low temperatures employed in solid-state polymerization makes it advantageous for production of polymers that are prone to undesirable thermal degradation reactions. Since the polymerization rate is very low, residence times in solid-state polymerization reactors are long.

Reaction injection molding (RIM) is suitable for some step-growth polymerization processes in which no condensation byproducts are generated, and reactions are very rapid (e.g., polyurethane synthesis from diisocyanates and diols or multifunctional alcohols):



High conversions and molecular weights are obtained because reversible reactions and side-product removal is not an issue. In RIM processes, liquid monomers are mixed using impinging jets and must quickly flow into the mold before the reacting mixture becomes too viscous. The complete cycle time for injection, reaction and unmolding (so that the mold can be used to make the next product) is often only 30–60 s. RIM is used to produce rigid molded polyurethane automobile parts and polyurethane foam seat cushions [3].

7.2 Polymerization kinetics and modeling

The primary objectives in kinetic modeling of step-growth polymerization processes are prediction of polymerization rate and polymer structure properties including molecular weight averages, molecular weight distribution and functional end-group concentrations. These fundamental molecular structure properties, which can be difficult and time-consuming to measure, are often correlated with easier-to-measure properties that are used for industrial monitoring and control of product quality. For example, companies use intrinsic viscosity, IV, and relative viscosity, RV, measurements to obtain information about the average molecular weights of polyesters and nylons. For non-linear step-growth polymers, predicting the degree of branching or crosslinking is also important. In step-growth copolymerizations, prediction of sequence-length distributions can also be of interest. Kuchanov *et al.* [12] provide a comprehensive review of the mathematical models that have been developed to predict molecular architecture in step-growth polymers and copolymers.

Kinetic models are applied to the design and simulation of polycondensation reactors, so that overall reactor performance can be predicted and reactor operation can be optimized.

Since most industrial step-growth polymerizations are not as exothermic as chain-growth polymerization, process modeling is generally focused on accurately describing the kinetics of functional-group conversion and molecular-weight development, rather than predicting reactor temperature. Some readers might have noticed in many textbooks or references that polycondensation kinetics are treated rather lightly with a very simple reaction stoichiometric equation such as



or



where P_n is a polymer chain of length n and W is the condensation byproduct. If W is perfectly removed from the reacting mixture, then the reaction can be assumed to be irreversible as in Equation 7.2. The assumption of complete removal of side product (W), as in Equation 7.2, is usually an oversimplification because, in practice, it is not easy to remove all of the condensation byproduct. If significant condensation byproduct is present, the reverse reaction can occur, and very high-molecular-weight polymer is not obtainable. Therefore, industrial reactor designs focus on ensuring nearly complete removal of the condensation byproduct.

A further complication of many industrial step-growth polymerization processes is that side reactions occur, which affect the quality of the polymer product as well as the concentrations of reactive end groups. For example, during PET production, trace amounts of acetaldehyde are produced by thermal degradation reactions. It is important to model and control the amount of acetaldehyde produced because it can adversely affect the taste of liquids stored in PET beverage bottles. During melt-phase nylon 6,6 polymerization, undesirable reactions at high temperatures lead to the production of cyclopentanone, ammonia and carbon dioxide as gaseous byproducts, to the consumption of carboxyl end groups, and to the formation of branch points on the polymer chains [4]. These branching reactions make the polymer more difficult to spin into fibers. As a result, kinetic models that include key side reactions are important for reactor design and for developing improved reactor operating conditions [13–17].

Some of the equations commonly used to predict molecular weight distributions in batch step-growth polymerizations are introduced below, and then, in subsequent sections, some more specialized equations used to predict reaction rates and molecular weight development in models of continuous reactor systems of industrial interest.

7.2.1 Reaction kinetics and the most probable distribution

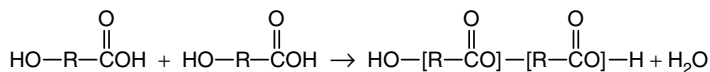
To quantify the kinetics of step-growth polymerization, the reactivities of functional groups on monomers and growing polymer chains need to be considered. First of all, the hypothesis of *equal reactivity of functional groups* [18] applies in most step-growth polymerization systems. The collision frequency of each functional group with neighboring groups, which is a major factor that governs the rate of polymerization, is approximately the same for functional groups on the ends of polymers and on small molecules. Also, in most

cases, the reactivity of a functional group is not altered by the presence of other nearby groups so simple polymerization rate expressions can be written in terms of the total concentrations of the functional end-groups. For example, in melt-phase batch nylon polymerization reactors the polymerization rate, which is the rate of disappearance of amine (and carboxyl) functional groups and the rate of formation of amide links, can be expressed in terms of the overall concentrations of the various types of functional groups in the reactor:

$$R_p = \frac{1}{V} \frac{-dA}{dt} = \frac{1}{V} \frac{-dB}{dt} = \frac{1}{V} \frac{dZ}{dt} = k_p \left([A][B] - \frac{[Z][W]}{K_a} \right) \quad (7.3)$$

$[A]$, $[B]$, $[Z]$ and $[W]$ are the concentrations of amine ends, carboxyl ends, amide linkages (within the polymer chains) and water, respectively, in the polymer melt. k_p is the rate constant for the forward (polyamidation) reaction, and K_a is an apparent equilibrium constant that is equal to k_p divided by the rate constant for the reverse (hydrolysis) reaction. The reaction rate expression on the right-hand side of Equation 7.3 confirms that removal of water from the reactor, to ensure that $[W]$ is small, increases the net polymerization rate. This rate expression is valid for melt-phase nylon polymerization in either a batch or a continuous reactor system. Appropriate inflow and outflow terms would be required to develop dynamic material balances for the concentrations of amine and carboxyl end-groups in a continuous reactor. If the reactor is operated at high temperatures where thermal degradation reactions are significant, then terms accounting for consumption of end-groups by these side reactions would also be required. A dynamic material balance for water would need to account for the rate of mass transfer from the liquid phase into the vapor phase. Development of kinetic models to account for these phenomena is described in Section 7.3 using several examples.

One of the most important properties in condensation polymers is the polymer's molecular weight. Consider a linear step-growth polymerization of AB -type monomers. For illustrative purpose, let A refer to a hydroxyl group and B to a carboxylic acid group, so that a polyester is formed. The polymerization reaction is:



or



As the reaction proceeds to a fractional conversion of p for either functional group A or B , the reaction mixture contains polymer molecules with a variety of chain lengths. Thus, the modeling objective here is to quantify the development of polymer chain length distribution (CLD) at different end-group conversions.

In step-growth polymerization, it is common to use the symbol p (rather than x) to refer to conversion of the limiting functional group, because the conversion is equal to the *probability* that a particular functional group (e.g., an $-\text{OH}$ group) in the original reaction

mixture has reacted with another functional group (e.g., $-\text{COOH}$). Using this type of thinking, Flory [18] showed that if any molecule is picked randomly from the reacting mixture, the probability that it will have chain length n is:

$$P(n) = p^{n-1}(1 - p) \quad (7.4)$$

Consumption of exactly n monomers to form this polymer chain requires $n - 1$ independent chain-linking reactions, each with probability p , and also that one hydroxyl group (i.e., the one at the end of the resulting molecule) has not been consumed, which has probability $1 - p$. The distribution in Equation 7.4 is called the most probable distribution (MPD) or Schulz–Flory distribution. This same distribution also arises in some chain-growth polymerization systems (e.g., Equation 2.84 in Chapter 2 is another form of the MPD).

The probability $P(n)$ corresponds to the mole fraction of n -mer, $x(n)$. At 90% conversion ($p = 0.9$), the mole fraction of monomer ($n = 1$) in the reaction mixture is 0.09, the mole fraction of dimer ($n = 2$) is 0.081, and the mole fraction of trimer ($n = 3$) is 0.0729, with successively larger chains having smaller and smaller mole fractions. As conversion increases ($p \rightarrow 1$), the mole fractions of small molecules decrease, and the mole fractions of larger molecules increase, but the species with the largest concentration is always the monomer, so that the number CLD (Equation 7.4) is a decreasing function of chain length.

Now use Equation 7.4 to develop an expression for the weight CLD for this AB polymer system. Let N be the total number of molecules remaining at conversion p and N_0 be the initial number of monomer molecules. Then, $N = N_0(1 - p)$ and the *mole fraction* of n -mer is

$$x(n) = \frac{N_n}{N_0(1 - p)} \quad (7.5)$$

Since $x(n) = P(n) = p^{n-1}(1 - p)$, the *number of moles* of n -mer is

$$N_n = N_0 p^{n-1}(1 - p)^2 \quad (7.6)$$

and the *weight fraction* of n -mer is

$$w(n) = \frac{N_n(nw_m)}{N_0 w_m} = \frac{N_0(1 - p)^2 p^{n-1} n}{N_0} = (1 - p)^2 p^{n-1} n \quad (7.7)$$

where w_m is the molecular weight of a repeat unit (assuming that the total mass of the repeat units in the polymer chains is large compared to the mass of the end groups). Figure 7.1 shows the polymer weight CLD curves for three different conversions ($p = 0.96, 0.97, 0.98$). As conversion increases, notice that the peak shifts to the right and the CLD broadens.

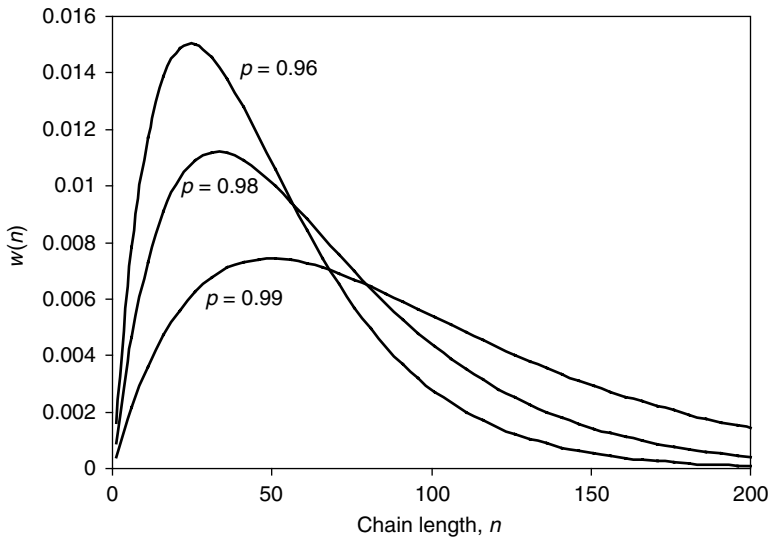


Figure 7.1 Weight chain length distribution at different end group conversions.

The number-average degree of polymerization (DP_n) and the weight-average degree of polymerization (DP_w) can be calculated easily from the number and weight CLD:

$$\begin{aligned}
 DP_n &= \sum_{n=1}^{\infty} nx(n) = \sum_{n=1}^{\infty} (1-p)np^{n-1} = (1-p)(1 + 2p + 3p^2 + \dots) \\
 &= \frac{1-p}{(1-p)^2} = \frac{1}{1-p}
 \end{aligned} \tag{7.8a}$$

$$DP_w = \sum_{n=1}^{\infty} nw(n) = \sum_{n=1}^{\infty} (1-p)^2 n^2 p^{n-1} = (1-p)^2 (1 + 2^2 p + 3^2 p^2 + \dots) = \frac{1+p}{1-p} \tag{7.8b}$$

The polydispersity index (PDI) ($=DP_w/DP_n$) is $1+p$. Since p is very close to 1.0 for linear high-molecular-weight step-growth polymers, the polydispersity is very close to 2.0. Equations 7.8a and b indicate that, for this simple step-growth polymerization, the molecular weight averages can be calculated easily from the conversion, and that the conversion p must be very close to 1.0 to obtain high-molecular-weight polymer. For example, if $p = 0.99$, then the number-average degree of polymerization is 100.

7.2.2 Effect of non-stoichiometric composition

In Section 7.2.1, the polymerization of AB -type monomers was considered. In AB systems, equal numbers of functional end-groups of both types are guaranteed due to structure of the monomer (unless functional impurities or additives are present in the reaction mixture).

However, for *AA* and *BB* systems, like those shown in Table 7.1, stoichiometric imbalance can occur, with serious consequences for the polymerization. The molar ratio of the two types of functional end-groups (*A* and *B*) that are available for polymerization is determined by the initial molar ratio of the two monomers in a batch reactor, and by any monomers or oligomers that might escape from the reacting mixture during the polymerization. Note that escape of volatile monomers with the resulting influence on the ratio of functional groups is a serious practical problem for some industrial polymerizations that use volatile monomers (e.g., HMD in nylon 6,6 production and diphenyl carbonate in polycarbonate production).

Suppose there is a slight excess of *BB* monomers at the beginning of an *AA* and *BB* polymerization (and that no molecules with functional groups leave the reacting mixture). To see how the average molecular weight of the polymer can be calculated, define:

$$N_{A0} = \text{number of } A \text{ groups present at } t = 0$$

$$N_{B0} = \text{number of } B \text{ groups present at } t = 0$$

$$r = N_{A0}/N_{B0} (<1; B \text{ groups in excess})$$

$$p = \text{conversion (based on } A \text{ groups, which are limiting)}$$

Then, the initial number of molecules is

$$n_0 = \frac{N_{A0} + N_{B0}}{2} = \frac{N_{A0}}{2} \left(1 + \frac{1}{r}\right) \quad (7.9)$$

The total number of chain ends after reaction progresses to conversion *p* is

$$\begin{aligned} N_{\text{total}} &= \underbrace{2N_{A0}(1-p)}_{\text{ends eligible for polymer formation}} + \underbrace{(N_{B0} - N_{A0})}_{\text{excess B functions that cannot be consumed}} \\ &= N_{A0} \left\{ 2(1-p) + \frac{1-r}{r} \right\} \end{aligned} \quad (7.10)$$

Since the final number of molecules at conversion *p* is $N_{\text{total}}/2$, the number-average chain length is given as

$$\begin{aligned} DP_n &= \frac{\text{initial number of molecules}}{\text{final number of molecules}} = \frac{(N_{A0}/2)(1 + (1/r))}{(N_{A0}/2)\{2(1-p) + (1-r)/r\}} \\ &= \frac{r+1}{2r(1-p) + 1-r} \end{aligned} \quad (7.11)$$

“Chain length” means the total number of monomer molecules consumed to make a polymer chain (i.e., the number of repeat groups plus one in an *AB* polymerization or (approximately) the number of repeat groups multiplied by *two* in an *AA* + *BB* polymerization). Equation 7.11 shows that if equal numbers of *AA* and *BB* monomers are present initially (so that $r = 1$), then $\bar{X}_n = 1/(1-p)$, the same result as in Equation 7.8a for *AB* polymerization.

Equation 7.11 can also be expressed as

$$DP_n = \frac{r+1}{2r(N_A/N_{A0}) + 1-r} = \frac{N_{A0} + N_{B0}}{2N_A + N_{B0} - N_{A0}} \quad (7.12)$$

If Z is the number of moles of polymer linkages formed, then

$$N_{A0}p = Z = N_{A0} - N_A \quad (7.13)$$

and the following useful equations are obtained relating the number of moles of end-groups to the conversion and the number of linkages:

$$N_{A0} = N_A + Z \quad (7.14)$$

$$N_B = N_{B0} - N_{A0}p \quad (7.15)$$

and

$$\begin{aligned} N_{B0} &= N_B + N_{A0}p \\ &= N_B + N_{A0} - N_A \\ &= N_B + Z \end{aligned} \quad (7.16)$$

Finally, the following equation describing the number-average chain length in an AA and BB polymerization is obtained:

$$DP_n = \frac{N_A + N_B + 2Z}{N_A + N_B} = 1 + \frac{2Z}{N_A + N_B} \quad (7.17)$$

The development of Equations 7.4–7.17 assumed that linear polymer molecules are formed, with one functional group on each end. In step-growth systems that form a substantial number of cyclic oligomers or polymeric molecules, which have no functional end-groups, Equations 7.8a, 7.8b, 7.11, 7.12 and 7.17 will over-predict the true average chain lengths. The propensity to form cyclic oligomers, in either AB or $AA + BB$ systems depends on the size and shape of the monomer molecules and on the thermodynamic stability of the various cyclic molecules that can form.

Example 1 (Effect of non-stoichiometric composition): If $r = 0.99$ (1% excess B groups in an AA and BB polymerization) and $p = 0.99$ (99% conversion), then from Equation 7.12, $DP_n = 1.99 / \{(2)(0.99)(0.01) + 0.01\} = 66.8$. On the other hand, if $r = 1$ (perfect stoichiometric ratio) and $p = 0.99$ then $DP_n = 1 / (1 - 0.99) = 100$. This example illustrates that, if the composition is just 1% different from the ideal stoichiometric ratio, the molecular weight decreases by 33%! A nearly perfect stoichiometric ratio of the functional end-groups must be maintained to obtain high-molecular weight step-growth polymer. This requirement is one of the challenges in operating step-growth polymerization processes. Note, however, that some step-growth products (e.g., nylon 6,6) are made with a deliberate small imbalance in the types of functional groups in the reaction mixture whenever it is preferable to produce polymer grades that have more of one type of end group on the final polymer molecules (e.g., amine end-groups to improve dyeability).

Example 2 (Effect of escaping monomer): Consider an AA and BB polycondensation system that uses a slightly volatile AA monomer (e.g., HMD used in nylon 6,6 polymerization) that escapes from the reaction mixture during the early stages of the polycondensation, when monomer concentrations are high and side-product removal is rapid. To compensate for the loss of volatile AA monomer, assume that the recipe is designed so that 105 moles of AA are

used for every 100 mol of non-volatile BB . If exactly 5 moles of AA evaporate over the course of the reaction, then the resulting polymer will have perfectly balanced end groups, as in Example 1, and at 99% conversion the number-average chain length will be 100. However, if only 4 mol of AA escape (so that there is a 1% excess of AA) or if 6 mol escape (so that there is a 1% excess of BB), the number-average chain length will be only 67. This example shows the importance of careful recipe design and well-controlled process operating conditions to ensure that high quality $AA + BB$ polymers can be produced. Since AB polycondensations do not have the same problems with end-group imbalance, one might ask why commercial $AA + BB$ polymerizations are more widespread than AB . The answer is that AA and BB monomers are usually cheaper and easier to make.

Example 3 (Effect of monofunctional chain stoppers or impurities): Let us suppose we have N_0 moles of AB -type monomers and N_I moles of monofunctional impurity containing an A functional group, but no B group. Whenever this monofunctional impurity adds to the end of a molecule, that end can no longer participate in step-growth polymerization reactions. As in Equation 7.11, the number-average chain length is equal to the initial number of molecules divided by the final number of molecules, so that:

$$DP_n = \frac{N_0 + N_I}{N_0(1 - p) + N_I} = \frac{1 + N_I/N_0}{1 - p + N_I/N_0}$$

If the monofunctional impurity A is 2% and the conversion is 98%, then,

$$DP_n = \frac{1 + 2/98}{1 - 0.98 + 2/98} = 25$$

whereas, if the monofunctional impurity is absent and the conversion is 98%, then $DP_n = N_0/N = 1/(1 - p) = 1/(1 - 0.98) = 50$, which is twice as large. This example illustrates the importance of ensuring good quality monomer feed stocks so that high-molecular-weight step-growth polymers can be produced. Monofunctional impurities are a common problem in step-growth polymerization processes. Note that sometimes monofunctional chain stoppers are added deliberately to limit the average molecular weight in products where it is desired to restrict molecular weight below what could be achieved without the chain stopper.

7.2.3 Molecular weight development in non-linear step-growth polymerization

When monomers with more than two reactive end groups (e.g., trifunctional or tetrafunctional monomers) are used, step-growth polymerizations produce non-linear polymer molecules like the hyperbranched polymer, dendrimer and crosslinked polymer shown in Figure 7.2. Dendrimers, which have highly regular branching with a strict geometric pattern, are generally made using a large number of synthetic steps, requiring purification after each step and resulting in low overall yields. The growth of a dendrimer starts at the core and continues radially outward from the center by a stepwise addition of monomers. For example, the dendrimer shown in Figure 7.2 begins with a tetrafunctional molecule, B_4 ,

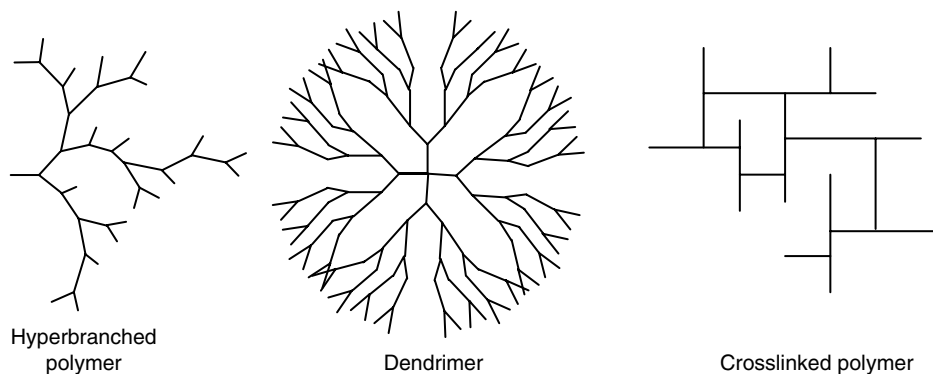


Figure 7.2 Branched polymer structures that can be produced using step-growth polymerizations.

with subsequent additions of AB_2 to produce the trifunctional branch points. The attractive secondary forces in dendrimers are weaker than in linear polymers, because molecules cannot pack compactly to attract each other. Since no chain entanglement occurs, dendrimers do not have sufficient strength for fibers and plastics. Dendrimers have high solubility and miscibility with other materials, making them useful as viscosity modifiers [19].

Synthesis of hyperbranched polymers, which have less regular structures than dendrimers, can be conducted in a single step using multifunctional monomers of type AB_n ($n \geq 2$), or by combining linear and multifunctional monomers (e.g., AA and B_3). The branching in hyperbranched polymers prevents crystallization, so hyperbranched polymers are used as functional modifiers for crosslinked polymers and as components in adhesives and coatings. Examples of hyperbranched polymers include polyphenylenes, polyesters, polycarbonates, polyureas, polyurethanes and polyethers. Excellent reviews on the hyperbranched polymers and dendrimers are available in the literature [20, 21]. When hyperbranched polymers are produced using AB_n monomers, the large majority of functional end-groups is of type B , so it is impossible for large molecules to add together to produce larger crosslinked gel molecules. However, if AA monomer is added to an AB_n reaction mixture (or if AA and B_n are polymerized), then crosslinking and gelation can occur. The crosslinked structure shown in Figure 7.2 could be produced by a number of ways using linear molecules (e.g., AB or a combination of AA and BB) together with trifunctional crosslinking molecules (e.g., AB_2 , A_3 or B_3). Tetrafunctional branches (with an X structure rather than a T at the branch points) can be produced using tetrafunctional molecules (e.g., B_4). The crosslink density can be increased by increasing the mole fraction of multifunctional monomers.

7.2.3.1 Effect of functionality on molecular weight development

In Sections 7.2.1 and 7.2.2, relationships were developed between conversion and molecular weight, assuming that each monomer has two functional groups. In this section, these results are extended to account for branched polymer chains produced using monomers with more than two functional groups. The multifunctional monomer molecules can have a single type of functional group (e.g., A_3), or multiple types of groups (e.g., AB_2). To treat the

polymerization kinetics for such cases, the average functionality f_{av}^* for a stoichiometrically balanced system (with equal numbers of A and B groups) is defined as the average number of functional groups per monomer molecule, that is,

$$f_{av}^* = \frac{\sum n_i f_i^*}{\sum n_i} \quad (7.18)$$

where f_i^* is the functionality of monomeric species i in the reacting mixture. If n_0 is the initial number of molecules and n is the total number of molecules at time t , then the number of initial functions is $n_0 f_{av}^*$. The fractional conversion of functional groups is

$$p = \frac{2(n_0 - n)}{n_0 f_{av}^*} = \frac{2}{f_{av}^*} \left(1 - \frac{n}{n_0}\right) \quad (7.19)$$

Therefore,

$$DP_n = \frac{n_0}{n} = \frac{2}{2 - p f_{av}^*} \quad (7.20)$$

If the average functionality is 2.0 (e.g., a recipe with only AB monomer), Equation 7.20 simplifies to Equation 7.8(a), $DP_n = 1/(1 - p)$.

For non-stoichiometric mixtures with $N_A < N_B$, no reactions can occur after the A groups are completely consumed, and it is more convenient to think about conversion of the limiting functional group, rather than the overall conversion of all groups. In this case, the effective average functionality, f_{av}^* , is the total number of functional groups that could possibly react (two times the number of deficient A functional groups) divided by the number of molecules (containing A or B groups or both) initially in the system. Using this definition for f_{av}^* , the fractional conversion of A is given by Equation 7.19 and the number-average chain length is given by Equation 7.20, which is the Carothers equation (named after W.H. Carothers [22]). Note that DP_n is the number-average chain length for the entire reaction mixture, including any unreacted monomer molecules. Also note that the development of Equation 7.20 assumes that each step-growth reaction converts two molecules into one larger molecule (i.e., that cyclization reactions can be neglected).

Examination of the denominator of Equation 7.20 reveals that $DP_n \rightarrow \infty$ as $p \rightarrow 2/f_{av}^*$. So, if $f_{av}^* \geq 2$, and the conversion of limiting functional groups is sufficiently large, the number-average chain length can become infinite, and gelation of the polymer occurs. By gelation, we mean the formation of very large molecules, which are insoluble in the polymer solution or melt. It is important to predict the onset of gelation because large gel molecules precipitate to cause imperfections in polymer products, and can cause severe fouling in polymerization equipment. Since the presence of a few extremely large molecules is not sufficient to make the number-average chain length infinite, gel molecules begin to form and cause problems at conversions below $2/f_{av}^*$. Probabilistic methods to predict the formation of the first gel molecules are described below.

7.2.3.2 Growth of a non-linear network and prediction of gelation using Flory's approach

To further explore the development of branched polymer networks and the formation of gel molecules, consider a mixture of two bifunctional monomers (AA , BB) and a trifunctional monomer (A_3). Under certain conditions, molecules in this type of system can form

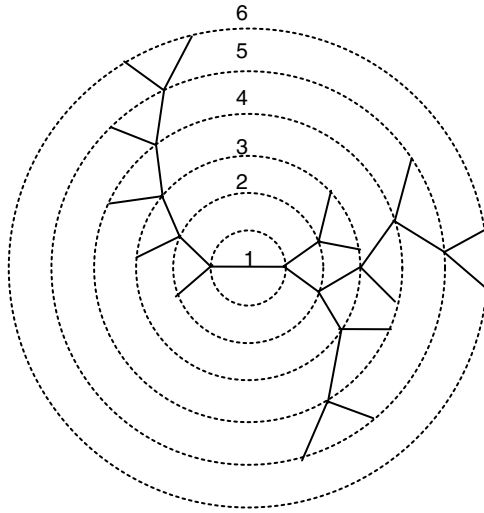
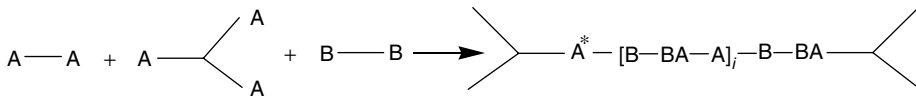


Figure 7.3 Branched polymer molecule formed from a mixture of AA , BB and A_3 monomers.

an infinite polymer network (i.e., the system can undergo gelation). Imagine a network structure formed from these monomers as shown in Figure 7.3; this network can be used to explore the classical theory of non-linear step-growth polymerization first developed by Flory. Flory defined a *chain* (or section of a branched polymer) as a portion of a molecule between two branch units, or between a branch unit and a terminal unreacted functional group. A chain from the molecule in Figure 7.3 (between two branches) would have the structure:



To make predictions about the onset of gelation, Flory considered the conditions under which there will be a finite probability that any chain element, picked at random from the reaction mixture, occurs as part of an infinite network. He also introduced the *branching coefficient*, α^* , defined as the probability that a particular functional group belonging to a branch unit leads (via bifunctional units) to another branch unit.

Assuming equal reactivities of all functional groups, the following variables can be defined:

p_A = the probability that a particular A group along the chain has reacted
(i.e., the conversion of A groups)

p_B = the probability that a particular B group along the chain has reacted
(i.e., the conversion of B groups)

ρ^* = the ratio of A groups (reacted or unreacted) on multifunctional crosslinker units to the total number of A groups in the initial mixture.

Then, the probability that the A group of a branch unit (denoted A^* in the chain above) is connected to the sequence of units shown is $p_A[p_B(1 - \rho^*)p_A]^i p_B \rho^*$. This probability is derived by multiplying the probabilities for the following independent events:

- (1) that the A^* group has reacted with a BB molecule: p_A
- (2) that the resulting B end group has reacted with an AA molecule: $p_B(1 - \rho^*)$
- (3) that the resulting A end group has reacted with a BB molecule: p_A
- (4) that events 2 and 3 occur $(i - 1)$ more times: $[p_B(1 - \rho^*)p_A]^{i-1}$
- (5) that the B group at the end of the chain has reacted with a multifunctional A_3 : $p_B \rho^*$

Therefore, the probability that any randomly selected group on a branch unit (arising from a multifunctional monomer) leads to another branch unit (via a chain of any length) is

$$\begin{aligned} \alpha^* &= \sum_{i=0}^{\infty} p_A p_B (1 - \rho^*) p_A [p_B (1 - \rho^*) p_A]^{i-1} p_B \rho^* \\ &= \sum_{i=0}^{\infty} [p_A p_B (1 - \rho^*) p_A]^i p_A p_B \rho^* \\ &= \frac{p_A p_B \rho^*}{1 - p_A p_B (1 - \rho^*)} \end{aligned} \quad (7.21)$$

Note that the functional-group conversions p_A and p_B are related by:

$$\frac{p_A}{p_B} = \frac{N_{B0}}{N_{A0}} \quad (7.22)$$

where N_{A0} and N_{B0} are the initial moles of functional groups A and B , respectively.

Now conduct a thought experiment, where we begin at A^* , and walk along the chain to the branch point at the other end. When we arrive at the new branch point, several alternatives are possible: we may find two new chains that both lead to additional branch points; we may find one chain that leads to an additional branch point and one that leads to a terminal end; or we may find two chains that lead to terminal ends. If we tend to find branch points that lead to additional branch points, more often than to terminal ends, which happens if $\alpha^* > 0.5$, there is a finite probability that we are walking on an infinite gel molecule, so some very large gel molecules will be present in the reacting mixture.

As shown in Figure 7.3, we can also think about the possibility of gel formation by moving from a particular chain section (in envelope 1) outward to explore the chain sections in envelopes that are further and further away from our initial chain (Figure 7.3 shows six envelopes). If Y_i is the number of chains in the i th envelope, and Y_{i+1} is the number of chains in the next envelope out from the initial chain, then if $Y_{i+1} > Y_i$ for all values of i , the molecule will extend outward to infinity. Since each branch point (using our trifunctional crosslinker) starts two new chains, and the probability that either of these new chains leads to a new branch is α^* , then on the average $Y_{i+1} = 2\alpha^* Y_i$. As a result, $Y_{i+1} > Y_i$ implies that $\alpha^* > 0.5$. This same thinking can be extended to systems with crosslinking monomers that have any arbitrary functionality f^* , so that the critical value of α^* for gelation is $\alpha_c^* = 1/(f^* - 1)$. This critical value can be used to solve Equations 7.21 and 7.22 for the conversion of the limiting functional group when large gel molecules first appear.

Example 4 (Number-average chain length and conversion at the gel point for an imbalanced multifunctional system): Consider a batch reactor that initially contains 10 mol of A_4 , 5 mol of AA and 21 mol of BB . This system has more A end-groups than B end-groups, with $N_{A0} = 50$ mol and $N_{B0} = 42$ mol, so B functional groups are limiting. The effective average functionality for this system, taking into account the stoichiometric imbalance, is

$$f_{av}^* = \frac{\text{functional groups that can possibly react}}{\text{initial number of molecules}} = \frac{2(42)}{10 + 5 + 21} = 2.3333$$

Using Equation 7.20, DP_n can be computed at any conversion of the limiting functional group below the limiting conversion of B groups where $DP_n \rightarrow \infty$, which is $p = 2/f_{av}^* = 0.857$. For example, at 85% conversion, $DP_n = 2/(2 - 0.85(2.3333)) = 120$. Also the conversion can be computed where very large gel molecules first appear using Equation 7.21. From Equation 7.22, $p_A = 42p_B/50 = 0.84p_B$. Since our multifunctional monomer has four A groups, $\alpha_c^* = 1/(4 - 1) = 0.3333$. The ratio of A groups on the multifunctional monomer to total A groups in the mixture is $\rho^* = 40/50 = 0.8$. Therefore, at the point of gelation, Equation 7.21 becomes

$$0.3333 = \frac{0.84p_B^2(0.8)}{1 - 0.84p_B^2(1 - 0.8)}$$

giving $p_B = 0.677$. Very large gel molecules will begin to appear at about 68% conversion of the limiting functional groups. At this conversion, the number-average chain length (including the large number of unreacted monomer molecules) will be only $DP_n = 2/(2 - 0.677(2.3333)) = 4.76$ because the reacting system will also contain a very large number of very small molecules.

7.3 Industrial step-growth products, processes and modeling

Polyesters and nylons (polyamides) are the largest-volume commercial polymers produced by step-growth polymerization. They are used for a wide variety of applications including fibers, molded products, wire coating and engineering composites. Polycarbonate, a step-growth polymer that has high transparency and toughness, is becoming increasingly important for use as a digital-storage-media substrate and for electronic-display materials. Costa and Bachmann [17] describe the commercial processes used for these and many other commercially important step-growth polymers, including phenolic resins, polyurethanes and epoxy resins.

Poly(ethylene terephthalate), the lowest cost and most commonly used polyester, is produced using ethylene glycol (EG) and either dimethyl terephthalate (DMT) or terephthalic acid (TPA) (see Table 7.1). Processes using DMT were commercialized first, but when very pure TPA became available, TPA processes became more economical for large-scale fiber production. Poly(butylene terephthalate) (PBT), produced from 1,4 butanediol and DMT, is another commercially important polyester, which is used for computer housings and many other molded products. Poly(trimethylene terephthalate) (PTT), made from TPA and 1,3 propanediol, is a relatively new commercial polyester, that shows promise for

carpeting and other fiber applications [18]. The propanediol monomer used to make PTT can be produced commercially by a biochemical route, using a renewable feedstock (corn) instead of petroleum.

The two main commercial polyamides are nylon 6,6, produced by condensation polymerization of HMD and adipic acid (see Table 7.1), and nylon 6, an *AB*-type polymer, which is produced from caprolactam. Other commercial polyamides include nylons 4,6, nylon 6,12 (which are *AA*- and *BB*-type polymers) and nylon 11 and nylon 12 (which are *AB* polymers made from linear aliphatic amino acids containing 11 and 12 carbons, respectively) [1]. Polyamides are also produced using monomers with aromatic, rather than aliphatic segments. Polyamides that contain 85% or more of the amide bonds attached to aromatic rings are called aramids. Commercial examples include poly(*p*-phenyleneterephthalamide) or Kevlar™ and poly(*m*-phenyleneisoterephthalamide) or Nomex™ [23].

In the remainder of this chapter, industrial processes for PET and for nylon 6 and nylon 6,6 production will be described. Our aim is to help readers understand the main difficulties encountered during large-scale production of step-growth polymers (i.e., removing condensation side products and oligomers, maintaining end-group balance and avoiding thermal degradation), along with the polymerization processes that have been designed to address these difficulties. Kinetic models are developed for a variety of reactors used at different stages of PET and nylon 6,6 production. We hope that the examples will help readers to understand the mathematical models that appear in the literature [15, 16, 24–33] and in developing the skills required to create new models for step-growth polymerization reactors. A comprehensive review by Costa and Bachmann [17] provides additional information about industrial processes for polyesters, polyamides, polycarbonates, polyurethanes, epoxy resins and phenolic resins, and the models that have been used to describe them.

7.3.1 Poly(ethylene terephthalate) production and modeling

Poly(ethylene terephthalate) is manufactured by a stage-wise melt polymerization process, which consists of (trans)esterification, prepolymerization and finishing polymerization steps. Figure 7.4 is a schematic diagram of a typical continuous melt-polycondensation process for the manufacture of PET. In the esterification stage, either DMT or TPA is reacted with EG to produce bishydroxyethyl terephthalate (BHET) and some linear oligomers in the presence of metal acetate catalyst (e.g., zinc acetate). For example, EG and TPA are fed at a molar rate of approximately 1.4:1 (with DMT, this ratio is 1.8:1), along with some catalyst, to the esterification stage, which is operated at 160–180°C. This stage takes about 3–4 h. The reaction byproduct, water (methanol when DMT is used), is separated from EG vapors in a reflux column. After adding stabilizer and additives, the BHET mixture is forced through a superfine filter (to remove residues associated with some additives) and flows to the second stage (prepolymerization). The prepolymerization is carried out under vacuum (15–25 mmHg) and elevated temperatures (260–280°C). Ethylene glycol is removed by a vacuum pump while the product (with chain length of 15–30) is pumped to the finishing reactor after a reactor residence time of approximately 2 h. The finishing (polycondensation stage) reactor requires large surface areas for the removal of ethylene glycol from the viscous polymer melt. Several different types of reactors are used in the finishing

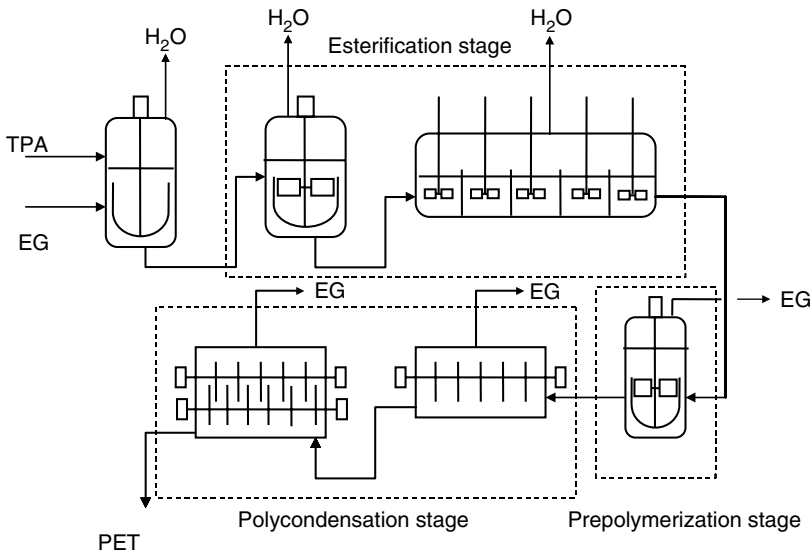


Figure 7.4 Typical process for commercial PET production.

stage including: cage reactors, rotating disk reactors, wiped film reactors and extruder type reactors.

When polyesters are made using melt-phase polymerization, small amounts of cyclic oligomers (1.4–1.8 wt%) are produced, which are in equilibrium with the linear polymer chains [23]. These oligomers, which can migrate to the surface of molded products and interfere with their appearance, can be removed from solid polymer pellets using solvent extraction processes. Unfortunately, the oligomers quickly reappear (due to transesterification reactions) if the polymer is remelted for further processing.

If very high-molecular-weight PET is required, melt polycondensation can be followed by solid-state polymerization (SSP). It is important to ensure that the solid polymer particles (sometimes called chips) formed by cooling and pelletizing the molten polymer, have sufficient time to crystallize via an annealing process, to prevent sintering of the PET particles in the SSP reactor [28, 32, 33]. SSP of the semicrystalline polymer particles is carried out at a temperature above the glass transition temperature (T_g) to provide mobility of reactive end groups in the amorphous phase of the polymer particles, and below the polymer's melting point (T_m) to prevent the sticking of polymer particles. SSP is usually carried out at a temperature close to the melting point of the polyester so that the mobility of reactive end groups is not the rate-controlling factor [32–34]. Therefore, the diffusion rate of condensates (water, methanol, ethylene glycol) from the particle interior to the surrounding gas phase has the strongest effect on the rate of SSP and on polymer molecular weight. The performance of SSP is influenced by temperature, prepolymer molecular weight, reactive end-group ratios, degree of crystallinity, particle size and catalyst concentration. Either vacuum, inert-gas purging or supercritical carbon dioxide can be used to remove the condensation byproduct. A schematic diagram of a typical moving bed SSP reactor is shown in Figure 7.5. SSP can also be done batch-wise in heated rotating vessels.

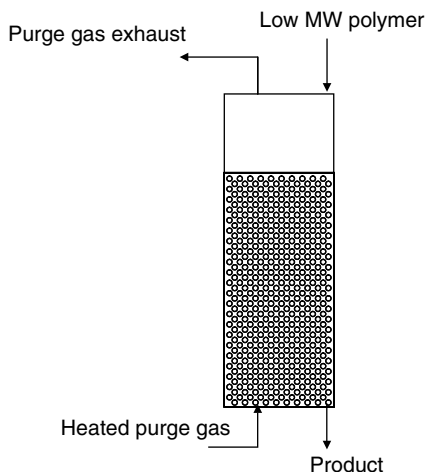
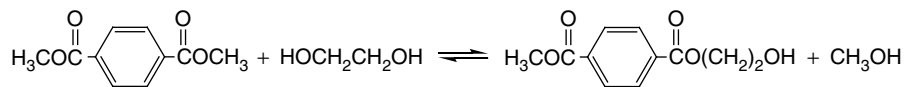


Figure 7.5 A moving-bed reactor for solid-state polymerization of PET and other step-growth polymers.

7.3.1.1 *Developing mathematical model equations for production processes*

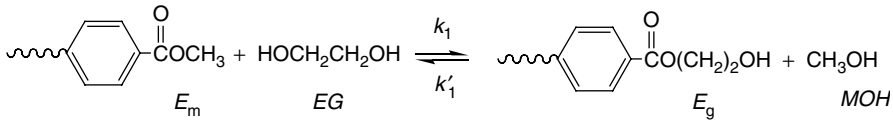
In the discussion in Section 7.2, polymer molecular-weight averages and molecular-weight distributions were calculated using the *conversion* of a limiting end group as a known independent variable. To simulate or design a step-growth polymerization reaction process it is important to be able to calculate the conversion using the polymerization rate, which varies with time. In other words, a kinetic model is needed. There are two different approaches for modeling the kinetics of condensation polymerization: functional-group modeling and molecular-species modeling.

To explore the difference between these two approaches, consider the following esterification reaction (more precisely known as ester interchange reaction) where dimethyl terephthalate (DMT) is reacted with ethylene glycol (EG) in presence of metal acetate catalyst:

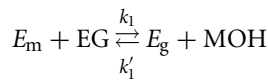


Material balance equations can be used to predict the total concentrations of methyl ester and hydroxyl end groups on the monomer molecules as the polymerization proceeds. Then molecular weight averages (i.e., from Equation 7.11) can be calculated using the conversion of the limiting functional group. This modeling approach is called *functional-group modeling*. However, if we want to predict the concentrations of monomers, dimers, trimers and *n*-mers during the polymerization, it is necessary to keep track of each molecular species with each different chain length and different functional end-groups. This modeling approach is called the *molecular-species modeling* approach and, inevitably, the resulting kinetic model is more complex than functional group modeling [35, 36].

In modeling the polycondensation kinetics, there is also a question of how we define the reaction rate constants. In the above reaction represented by a functional-group modeling framework, the forward rate constant k_1 is the reaction rate constant for reaction of a methyl ester group with a hydroxyl group, not the reaction rate constant for DMT and ethylene glycol *molecules*. For example, the above reaction can be represented as follows:

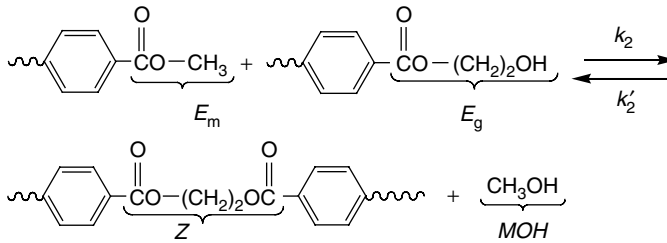


where E_m is the methyl ester group, E_g is the hydroxyethyl group and MOH is methanol. Since the reaction rate constants are defined for these reactive end groups, the above reaction can be expressed more simply in symbols as

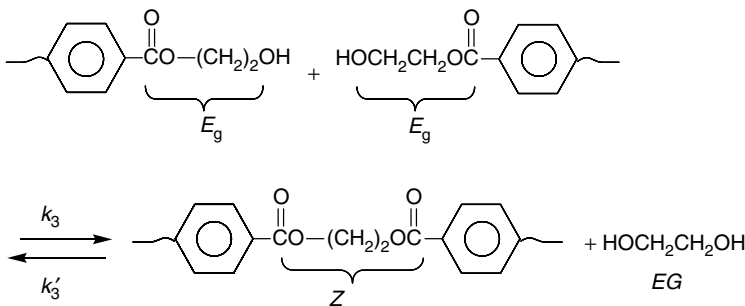


In the process for making PET from DMT and EG, the following two additional main reactions also occur:

Transesterification:



Polycondensation:



The net reaction rates for these three reactions are given by the following expressions:

$$\text{Ester interchange: } R_1 = 2k_1[E_m][EG] - k'_1[E_g][\text{MOH}] \quad (7.23)$$

$$\text{Transesterification: } R_2 = k_2[E_m][E_g] - 2k'_2[Z][\text{MOH}] \quad (7.24)$$

$$\text{Polycondensation: } R_3 = k_3[E_g]^2 - 4k'_3[Z][EG] \quad (7.25)$$

The kinetic rate constants in Equations 7.23–7.25 depend on temperature and catalyst concentration. Since carboxyl groups can catalyze the reactions, the kinetic rate constants can also depend on the concentration of carboxyl groups (when TPA rather than DMT is used as a monomer) [17]. If mathematical models are required to predict the concentrations of cyclic oligomers, or the influence of high-temperature side reactions, then additional reactions and kinetic expressions are required for model development.

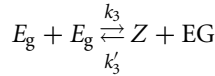
Example 5 (Modeling melt-phase PET production in a batch reactor using the functional-group modeling approach): Using the reaction rates in Equations 7.23–7.25, the following dynamic component material balance equations can be derived:

$$\begin{aligned}\frac{dE_m}{dt} &= -(R_1 + R_2)V \\ \frac{dE_g}{dt} &= (R_1 - R_2 - 2R_3)V \\ \frac{dZ}{dt} &= (R_2 + R_3)V \\ \frac{dMOH}{dt} &= (R_1 + R_2)V - (k_L a)_{MOH} V ([MOH] - [MOH]^*) \\ \frac{dEG}{dt} &= (-R_1 + R_3)V - (k_L a)_{EG} V ([EG] - [EG]^*)\end{aligned}$$

This model assumes that small molecules, methanol and ethylene glycol, are being removed from a well mixed vapor phase in contact with the molten liquid. $[MOH]^*$ and $[EG]^*$, the liquid phase concentrations that would be in phase equilibrium with the gas phase, can be determined using a Flory–Huggins expression (or Henry’s law, if the small molecule concentrations in the melt are sufficiently low). The mass-transfer coefficients, $(k_L a)_{MOH}$ and $(k_L a)_{EG}$, depend on the reactor geometry, the type of agitation, the surface area between the two phases and the viscosity of the liquid phase. These coefficients need to be estimated from experimental data for each particular reactor system. Solving the set of differential equations requires knowledge of the liquid-phase volume, V , which may become significantly smaller with time, due to evaporation of MOH and EG. V can either be determined using a level measurement, or from a total mass balance on the liquid phase in the reactor. After solving the differential equations, the concentrations of all the reactive end groups can be calculated and hence the polymer molecular-weight averages and CLD, which follows the most probable distribution [16, 27].

In practice, the above reactions are carried out in several stages because the physical state of the reaction mixture changes significantly with the progress of reaction. For example, DMT and EG are reacted in the first stage to produce BHET and oligomers, and then these first reaction products are polymerized to low molecular weight prepolymers in the second stage. In industrial processes, a train of reactors is used in each stage to gradually increase the conversion. The low-molecular-weight prepolymers are then transferred to a finishing reactor and polymerized further to obtain high-molecular-weight polymers. Finishing reactors are equipped with specially designed reactor internals or mixing elements that can handle highly viscous polymer melts and facilitate the removal of condensation byproduct effectively from the viscous polymer solution or melt.

Example 6 (Effect of reaction equilibrium): If ethylene glycol is not removed from the reaction mixture, the polycondensation reaction quickly reaches equilibrium and high-molecular-weight polymer is not obtainable. To illustrate this effect, consider a simple experiment where we begin with pure BHET in a batch reactor (no MOH or EG are present and there are no E_m end groups). In this situation, only the main polycondensation reaction occurs:



When the conversion of E_g is p , so that $E_{g0}p$ moles of E_g have been consumed, the number of moles of Z and EG that have formed is $0.5E_{g0}p$. Assuming that no EG has been removed from the liquid phase, then the concentrations of functional end-groups and ethylene glycol are

$$[E_g] = [E_g]_0(1 - p)$$

$$[Z] = [Z]_0 + 0.5[E_g]_0p$$

$$[EG] = [EG]_0 + 0.5[E_g]_0p$$

The net reaction rate for the polycondensation reaction is:

$$R_3 = k_3[E_g]^2 - 4k'_3[Z][EG] \quad (7.26)$$

The value of 4 appears in the expression for the reverse reaction, because each EG molecule has two hydroxyl end-groups, and each diester linking group, Z , has two esters, so the rate of reaction of an EG molecule with Z is four times the rate of reaction for an individual hydroxyl group and an individual ester group.

At equilibrium, the net reaction rate is zero, so the equilibrium constant for the polycondensation is given by:

$$K_a = \frac{k_3}{k'_3} = \frac{4[Z]_e[EG]_e}{[E_g]_e^2} = \frac{4([Z]_0 + 0.5[E_g]_0p_e)([EG]_0 + 0.5[E_g]_0p_e)}{([E_g]_0(1 - p_e))^2} \quad (7.27)$$

where the subscript e denotes the equilibrium value. Since $[Z]_0 = 0$ and $[EG]_0 = 0$ (because we begin with pure BHET), the following is obtained:

$$K_a = \frac{p_e^2}{(1 - p_e)^2}$$

For polyesters, a typical value of the equilibrium constant, K_a , is approximately 0.5 at the conditions used in melt-phase reactors [17]. Fortunately, for other step-growth polymerizations K_a can be much larger (e.g., for polyamides, $K_a \approx 100$). Using $K_a = 0.5$ gives $p_e = 0.414$. As a result, the number-average chain length (using Equation 7.8(a), which is applicable for systems where end-group imbalance is not an issue) is $DP_n = 1/(1 - 0.414) = 1.707$. This example shows that only low-molecular-weight oligomers are produced if the polycondensation reaction reaches equilibrium without removal of EG . Therefore, it is critical to remove the reaction byproduct, EG , from the reactor to promote the forward chain-growth reaction. This is why high vacuum is applied to industrial PET reactors.

Example 7 (Two-phase model for a continuous finishing-stage reactor): In designing a finishing-stage polycondensation reactor, the following important factors need to be

considered:

- (1) maximizing the mass-transfer efficiency for the removal of low-molecular-weight and volatile condensation byproducts,
- (2) ensuring a smooth flow of the viscous polymer melt in the reactor,
- (3) maintaining a plug flow profile of the polymer melt to avoid any stagnant zones in the reactor and to ensure high molecular weight is obtained and
- (4) ensuring a uniform reactor temperature to prevent hot spots and thermal degradation.

Since many industrial finishing polymerization reactors are equipped with devices of complex geometry to provide maximum interfacial area for mass transfer areas, it is practically quite difficult to develop a model that accurately includes the detailed geometric structure of the reactor.

Laubriet *et al.* [16] developed a two-phase approach for modeling continuous finishing-stage melt polycondensation reactors. Figure 7.6 depicts the concept of the two-phase model. Here, it is assumed that the flow pattern of the melt phase is ideal plug flow, and that the vapor phase is well mixed. As far as the polymer melt phase is concerned, no distinction between the film phase (polymer layer on a rotating disk surface) and the bulk phase (liquid pool) is made. In other words, the polymer phase in the reactor is viewed as a mixture of both the film and bulk phases. No reactions are assumed to occur in the vapor phase. As in Example 5, the rate of removal of volatile compounds is described through an effective mass-transfer coefficient, k_L , and the specific interfacial area per unit volume of the melt, a . Note that mass-transfer coefficients in finishing-stage reactors are much lower than in the earlier well mixed reactors in the process, due to the very high viscosity of the melt at high

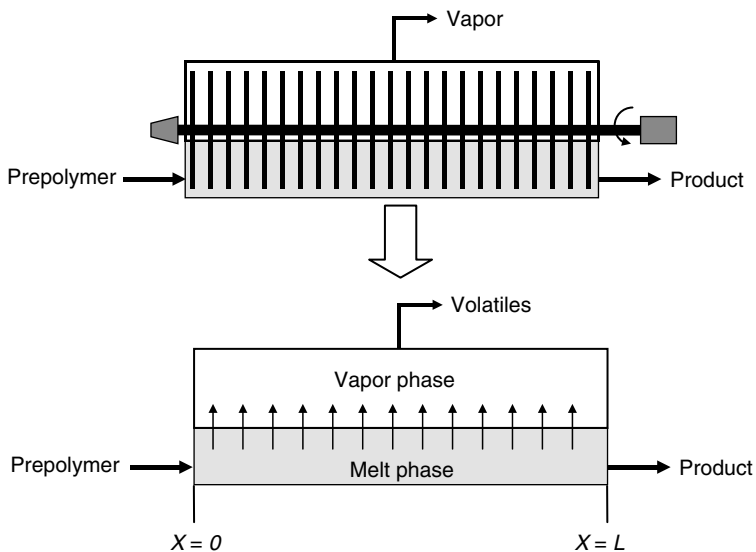
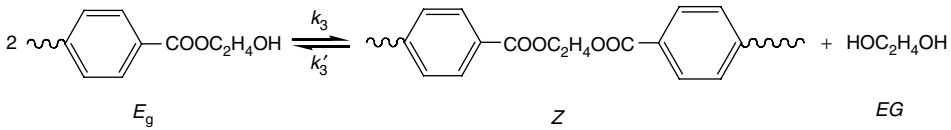


Figure 7.6 Schematic diagram of a continuous two-phase finishing-stage melt polycondensation reactor for PET production.

conversions. Here, the specific interfacial area represents the total contact area. If there is an increase in the vapor–liquid contact area due to the formation of bubbles of the volatiles, this type of effect is reflected in the overall specific interfacial area. The two-phase model can be applied to a finishing reactor of any geometry using the combined mass-transfer parameter ($k_L a$) as a single reactor-specific model parameter.

To illustrate the two-phase modeling technique, consider the following ester interchange reaction:



Here, E_g is the ethylhydroxy end group, Z is the diester linking group and EG is the ethylene glycol. There can be many other side reactions leading to the formation of diethylene glycol, water, acetaldehyde, etc., which are included in comprehensive mathematical models of industrial finishing-stage reactors, but here the main polycondensation reaction only is considered, whose rate expression was given in Equation 7.26.

The following steady-state model equations can be derived for non-volatile polymers and volatile ethylene glycol:

$$\frac{1}{\bar{t}} \frac{d[E_g]}{dz} = -2R_3 \quad (7.28)$$

$$\frac{1}{\bar{t}} \frac{d[Z]}{dz} = R_3 \quad (7.29)$$

$$\frac{1}{\bar{t}} \frac{d[EG]}{dz} = R_3 - (k_L a)_{EG}([EG] - [EG^*]) \quad (7.30)$$

where \bar{t} is the mean residence time, z is the dimensionless distance from the reactor inlet ($z = x/L$), and $[EG^*]$ is the hypothetical liquid-phase concentration of ethylene glycol that would be in phase equilibrium with the well mixed vapor. Assuming that all of the resistance to mass transfer is in the liquid phase, then $[EG^*]$ is the liquid-phase ethylene glycol concentration at the surface of the polymer melt. If the partial pressure of ethylene glycol in the gas phase is P_{EG} , then the following Flory–Huggins expression:

$$P_{EG} = \frac{1}{m_{EG}} \exp \left(1 - \frac{1}{m_{EG}} + \chi_{EG} \right) P_{EG}^0 x_{EG} \quad (7.31)$$

can be used to calculate x_{EG} , the mole fraction of ethylene glycol in the liquid phase that would be in equilibrium with the vapor. m_{EG} is the ratio of molar volumes of polymer and ethylene glycol and χ_{EG} is the Flory–Huggins interaction parameter. The mole fraction x_{EG} can be used to calculate $[EG^*]$ using the molecular weights of EG and the polymer and the density of the polymer phase.

The two-phase model can easily be extended to the system with many side reactions [16] and also to systems with multiple reactors with multiple reaction zones [27].

In the two-phase model, the mass-transfer parameter needs to be determined using actual polymerization reactor data because the specific interfacial area is strongly dependent upon the geometry of the reactor internals. Moreover, the formation of bubbles of volatile species contributes to the total vapor–liquid contact area, and the liquid holdup on a rotating disk can change with the melt viscosity or polymer molecular weight, affecting the mass-transfer coefficient.

The universality of the two-phase model is certainly a great advantage in developing a macroscopic reactor model. However, this advantage of the two-phase model is also a weakness, because the model is not capable of predicting the effects of specific reactor design parameters or operational parameters, such as the rotating speed of the reactor internals and number of disks on EG removal and molecular weight development.

Example 8 (Multi-compartment model for a PET finishing reactor): A multi-compartment model has been proposed to more realistically model the continuous finishing-stage reactor. Figure 7.7 is a schematic of the model structure. Here, the reactor is a rotating-disk-type reactor equipped with N equal-sized disks that divide the whole reactor volume into N equal-sized virtual compartments. Each compartment contains a disk and consists of a vapor phase, a film phase (polymer layer on a rotating disk) and a bulk phase in which a disk is partially immersed. The bulk melt phase is modeled as a continuous stirred-tank reactor (CSTR) whereas the film phase is modeled as a plug flow reactor. In practice, the polymer layers on the disk surfaces may not be perfectly mixed with the bulk phase as the disk rotates, but it is assumed that the polymers on the disk are completely mixed with the bulk phase while the disk is immersed and rotating in the bulk phase. The typical

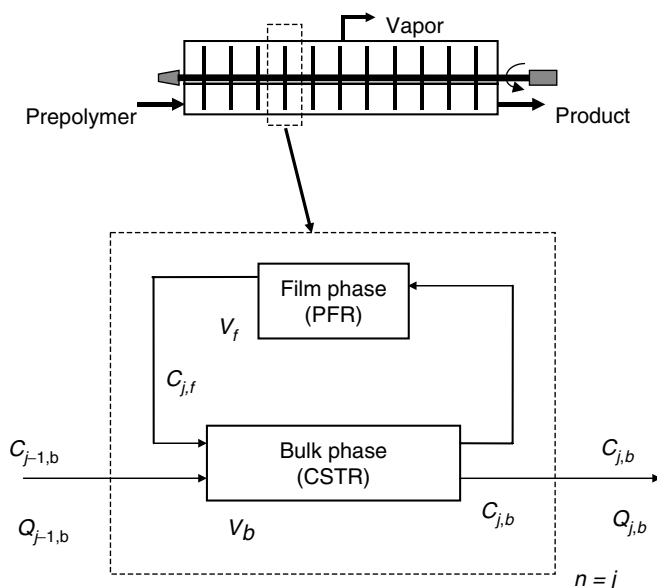


Figure 7.7 Schematic diagram of the compartments in a multi-component finishing reactor model.

reactor model equations take the following form:

Bulk phase:

$$\frac{d[E_g]_{j,b}}{dt} = -2R_{3j,b} + \frac{Q_{j,b}}{V_{j,b}}([E_g]_{j-1,b} - [E_g]_{j,b}) + \frac{V_{j,f}}{V_{j,b}t_f}([E_g]_{j,f} - [E_g]_{j,b}) \quad (7.32)$$

$$\begin{aligned} \frac{d[EG]_{j,b}}{dt} = & R_{3j,b} - (k_L a)_b([EG]_{j,b} - [EG^*]) + \frac{Q_{j,b}}{V_{j,b}}([EG]_{j-1,b} - [EG]_{j,b}) \\ & + \frac{V_{j,f}}{V_{j,b}t_f}([EG]_{j,f} - [EG]_{j,b}) \end{aligned} \quad (7.33)$$

$$\frac{d[Z]_{j,b}}{dt} = R_{3j,b} + \frac{Q_{j,b}}{V_{j,b}}([Z]_{j-1,b} - [Z]_{j,b}) + \frac{V_{j,f}}{V_{j,b}t_f}([Z]_{j,f} - [Z]_{j,b}) \quad (7.34)$$

Film phase:

$$u \frac{d[E_g]_{j,f}}{dx} = -2R_{3j,f} \quad (7.35)$$

$$u \frac{d[EG]_{j,f}}{dx} = R_{3j,f} - (k_L a)_f([EG]_{j,f} - [EG^*]) \quad (7.36)$$

$$u \frac{d[Z]_{j,f}}{dx} = R_{3j,f} \quad (7.37)$$

The subscripts b and f represent the bulk phase and the film phase, respectively, and j refers to the j th compartment. Q is the axial flow rate, V is the volume, x is the distance for the polymer melt film (layer) on the disk to travel at speed u after the leading edge of the disk ($x = 0$) departs from the bulk phase and t_f is the surface-renewal time determined by the disk rotating speed. $R_{j,b}$ and $R_{j,f}$, the net polycondensation rates in the bulk and film phases, respectively, can be obtained by substituting appropriate concentrations into the right-hand-side of Equation 7.26. The polymer holdup on the rotating disk surface is given by the following equation [27, 37]:

$$V_f = \int_{r_i}^{r_0} r \omega h \left(1 - \frac{\rho g h^2}{3\eta r \omega} \right) dr \quad (7.38)$$

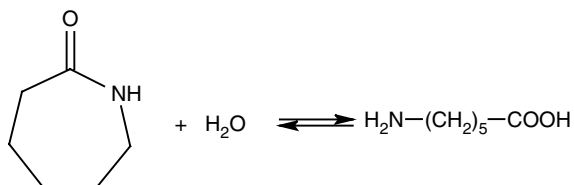
where r_i is the inner radius of the wetted area, r_0 the outer radius of the wetted area, ω the disk rotating speed, ρ the fluid density and η the viscosity.

7.3.2 Polyamide production processes and modeling

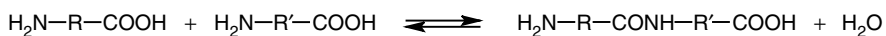
This section describes industrial processes for making nylon 6 and nylon 6,6, the two highest-volume commercial polyamides. Nylon 6 and nylon 6,6 are isomers that have very similar physical properties and commercial uses. However, due to the slightly different placement of amide links along the polymer molecules, nylon 6,6 enjoys stronger attractive forces between adjacent molecules, resulting in stronger fibers and a higher melting point than nylon 6. Further information about the industrial production and application of these and other polyamides is provided in several reviews of the academic and patent literature [1, 17].

7.3.2.1 Nylon 6 production processes

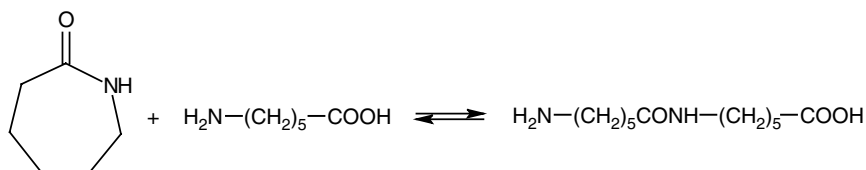
The primary commercial route for nylon 6 production involves the ring-opening polymerization of caprolactam. The first stage of this process involves hydrolysis of the caprolactam monomer:



Only a small amount of water is required, because step-growth polymerization of the resulting linear molecules regenerates water, which can participate in further caprolactam ring opening:



Chain-growth polymerization reactions, where caprolactam adds directly to the ends of linear chains, are also important in nylon 6 production [38], for example:



Substantial amounts of cyclic dimer form, due to condensation reactions between the end-groups on linear dimer molecules. Like caprolactam, cyclic dimer molecules are consumed by hydrolytic ring-opening reactions and chain-growth polymerization reactions.

Although batch processes are used to make specialty grades, most commercial nylon 6 is made using continuous reactor systems, which are more economical for large-scale production [1]. In the early stages of the process, water is added (2–4 wt%) to induce hydrolysis reactions. However, in the later stages, water must be removed to ensure that high molecular weights are obtained. Continuous polymerization can occur in a series of interconnected reactors, or in a single vertical column reactor, called a VK tube [39]. A mixture of caprolactam and water are fed at the top, and polymer is withdrawn at the bottom. One of the unfortunate features of nylon 6 polymerization is the high equilibrium monomer and cyclic oligomer content (10–12 wt%) in the molten polymer product, which adversely affects the quality of the fibers or resin if it remains in the product. To remove these small molecules, the polymer is cooled and cut into pellets, from which the monomer and some of the oligomer molecules are extracted using hot water (105–120°C), which is at a low enough temperature so that the small molecules will not reform, yielding pellets with oligomer levels less than 0.2 wt%. Final melting and processing of the nylon 6 into fibers or molded products is done as quickly as possible to keep the amount of cyclic monomer and oligomers in the final product to approximately 2–3%. An alternative to water extraction of the residual

monomer and cyclic oligomers is vacuum stripping of the nylon 6 melt, which eliminates the need to pelletize, perform water extraction and then dry and remelt the polymer before spinning into fibers [1].

7.3.2.2 Nylon 6,6 production processes

Nylon 6,6 is made from HMD and adipic acid, producing water as a condensation byproduct (see Table 7.1). The first step in commercial nylon 6,6 production involves dissolving nearly equimolar amounts of HMD and adipic acid in a liquid solution typically containing 50 wt% water. Considerable heat is produced during the dissolution process, due to ionization of a portion of the carboxyl and amine end groups. The pH of the resulting “salt” solution is carefully measured, and a final amount of HMD is carefully added, to reach the desired balance of amine and carboxyl end groups and to account for the anticipated amount of volatile HMD that will be lost during the polymerization process. High-purity monomers (without monofunctional impurities) and precise preparation of the salt solution are required to produce high molecular weight nylon 6,6 with the desired final end-group balance.

In the second stage of the process, the salt solution is boiled at atmospheric pressure to remove much of the water from the initial solution and water generated by oligomerization reactions. The evaporation process continues until the combined monomer and oligomer concentration is approximately 65–75 wt%. HMD vapor, which evaporates along with the steam, may be recovered and recycled. The evaporation stage can be carried out using either a batch or a continuous reactor.

In the third stage, polymerization and water removal continue in a pressurized vessel, with conditions that change with time (for batch nylon 6,6 production) or with position (for continuous nylon 6,6 production in tubular reactors [14] or in a series of back-mixed reactors) as shown in Figure 7.8. High pressure is required to maintain a sufficiently high

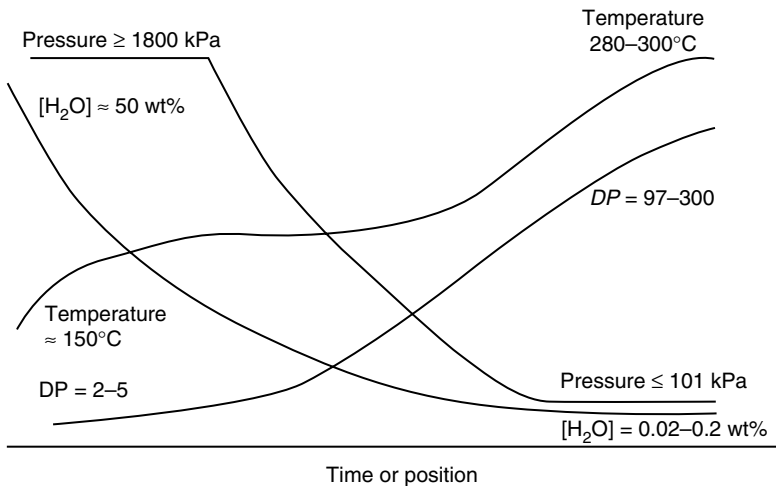


Figure 7.8 Process conditions and reaction mixture properties in the course of a typical batch or continuous melt-phase nylon 6,6 polymerization process [42].

boiling temperature for the liquid solution to prevent the dissolved nylon 6,6 oligomers from precipitating. As the temperature and average chain length increase and the water concentration decreases, the pressure can safely be reduced to improve water removal rates, without causing phase separation. Newer continuous polymerization trains that produce nylon 6,6 at high rates make use of a pressurized column reactor for the high-pressure part of the third stage shown in Figure 7.8. Steam is removed from the top of this column, where HMD is separated from the steam and returned to the reacting mixture. The molten high-pressure nylon (at about 98% conversion), which is removed from the bottom of column reactor is depressurized in a flasher, operated at 275°C, to remove water from the reacting mixture.

If higher-molecular-weight polymer is desired, the molten nylon can be further polymerized in a vacuum finishing step, or the polymer can be cooled, solidified, cut into pellets and sent to a solid-state polymerizer (see Figure 7.5), which has a counter-current nitrogen stream that assists in water removal. The main advantage of using SSP for the final stage of nylon 6,6 polymerization is that SSP operates at low temperatures where undesirable thermal degradation reactions do not occur, so linear polymers with very high molecular weights can be produced. The main disadvantage of SSP is that the nylon must be remelted before it can be spun into fibers, consuming additional energy. When a melt-phase finishing step is used, the molten polymer can flow directly to spinning machines for immediate fiber production.

Thermal degradation is a more serious problem for nylon 6,6 than for most other polyamides, because the adipic acid portions of the polymer molecule can cyclize to form five-membered rings, leading to the production of cyclopentanone, carbon dioxide and ammonia as gaseous byproducts and to trifunctional branch points on the polymer chains, that can lead to gelation [4].

Modeling nylon 6,6 polymerization reactors: In the PET reactor modeling examples earlier in this chapter, a functional-group modeling approach was used to keep track of the concentrations of the various functional groups of different types, and the number-average degree of polymerization was calculated from the conversion. Below a batch nylon 6,6 evaporator example is used to demonstrate the relative merits of the functional-group modeling approach and the more complex molecular-species modeling methodology. We also show how to incorporate effects of cyclic-oligomer formation into step-growth polymerization models.

Example 9 (Models for nylon 6,6 oligomerization in a batch evaporator reactor): When modeling the autoclave stage of a nylon 6,6 polymerization process, we may want to account for the amount of HMD that is lost by evaporation and for the production of cyclic oligomers. We may also want to predict the concentrations of all species (with different chain lengths and end-groups) in the reactor. With these goals in mind, the two alternative reaction schemes are written in Table 7.2. M_{AA} refers to HMD monomer, which has two amine end-groups, M_{BB} is adipic acid monomer, which has two carboxyl end groups, and C_2 is a cyclic oligomer containing one HMD segment and one adipic acid segment. Both schemes assume that larger cyclic molecules can be neglected, because they have very low concentrations in the reacting mixture. Chain-growth reactions, wherein C_2 adds directly to a chain end

Table 7.2 Alternative reaction schemes for nylon 6,6 oligomerization in a batch evaporator

Reaction scheme using molecular-species modeling approach	Scheme using functional-group modeling approach
$M_{AA} + M_{BB} \rightleftharpoons P_{AB1} + W$	$M_{AA} + M_{BB} \rightleftharpoons P_{AB1} + W$
$P_{AB1} \rightleftharpoons C_2 + W$	$P_{AB1} \rightleftharpoons C_2 + W$
$M_{AA} + P_{ABn} \rightleftharpoons P_{AA_{n+1}} + W$	$M_{AA} + P_{AB1} \rightleftharpoons 2Z + 2A + W$
$M_{AA} + P_{BBn} \rightleftharpoons P_{AB_{n+1}} + W$	$M_{BB} + P_{AB1} \rightleftharpoons 2Z + 2B + W$
$M_{BB} + P_{AA_n} \rightleftharpoons P_{AB_{n+1}} + W$	$2P_{AB1} \rightleftharpoons 3Z + A + B + W$
$M_{BB} + P_{AB_n} \rightleftharpoons P_{BB_{n+1}} + W$	$A + M_{BB} \rightleftharpoons Z + B + W$
$P_{AA_n} + P_{BB_i} \rightleftharpoons P_{AB_{n+i+1}} + W$	$B + M_{AA} \rightleftharpoons Z + A + W$
$P_{AB_n} + P_{AB_i} \rightleftharpoons P_{AB_{n+i+1}} + W$	$A + P_{AB1} \rightleftharpoons 2Z + A + W$
$P_{AA_n} + P_{AB_i} \rightleftharpoons P_{AA_{n+i+1}} + W$	$B + P_{AB1} \rightleftharpoons 2Z + B + W$
$P_{BB_n} + P_{AB_i} \rightleftharpoons P_{BB_{n+i+1}} + W$	$A + B \rightleftharpoons Z + W$

via a ring-opening reaction is neglected, as are back-biting reactions, wherein amine end-groups undergo transamidation reactions with a nearby link on the same chain to produce C_2 and a shortened linear chain. P_{ABn} refers to linear oligomeric molecules containing n amide links, as well as one amine end-group and one carboxyl end-group. In Table 7.2, P_{AB1} and its end groups are kept track of separately from the other linear polymer molecules, because P_{AB1} reacts to produce cyclic oligomer. In the more complicated molecular-species-modeling scheme in the left column, P_{ABn} is kept track of individually for all values of n , and also the polymeric molecules of types P_{AA_n} and P_{BB_n} , which have two amine end groups and two carboxyl endgroups, respectively. Note that molecules of type P_{ABn} always have an odd number of amide links, and that molecules of types P_{AA_n} and P_{BB_n} always have an even number of amide links.

Rather than having individual material balances for all of the different types of polymer chains with two or more amide links, the functional-group-based reaction scheme lumps all of these larger molecules together. This simpler scheme keeps track of Z , the amide links in all linear polymer chains that have more than one amide link, and A and B , the amine and carboxyl end-groups, respectively, on these larger linear molecules. If escape of HMD from the solution and the concentration of cyclic oligomer could be neglected, then it would be appropriate to lump all of the amide links (including those in P_{AB1}) into Z , and all of the end-groups (including those on the monomers and on P_{AB1}) into A and B , so that the entire functional-group modeling scheme in the right column of Table 7.2 would reduce to $A + B \rightleftharpoons Z + W$, producing the simple reaction rate expression in Equation 7.3.

While deriving the dynamic batch-reactor models in Tables 7.3 and 7.4, the *equal-reactivity-of-functional-groups* assumption was made, so that k_p is the rate constant for all forward linear polyamidation reactions and k_r is the rate constant for all reverse hydrolysis reactions involving amide links on linear chains. Let the rate constant for the forward cyclization reaction be k_c and the rate constant for hydrolysis of an amide link on cyclic oligomers be k'_c . In practice all of these rate constants depend on the reactor temperature and

Table 7.3 Dynamic model of a batch nylon 6,6 evaporator, accounting for cyclic oligomer and HMD loss using the functional-group modeling approach

$$\begin{aligned} \frac{dM_{AA}}{dt} &= (-2k_p[M_{AA}](2[M_{BB}] + [P_{AB1}] + [B]) + k_r[W]([A] + [P_{AB1}]) \\ &\quad - (k_L a)_{M_{AA}}([M_{AA}] - [M_{AA}]^*))V \\ \frac{dM_{BB}}{dt} &= (-2k_p[M_{BB}](2[M_{AA}] + [P_{AB1}] + [A]) + k_r[W]([B] + [P_{AB1}]))V \\ \frac{dP_{AB1}}{dt} &= \left(-k_p[P_{AB1}](2[M_{AA}] + 2[M_{BB}] + 4[P_{AB1}] + [A] + [B]) - k_c[P_{AB1}] - k_r[P_{AB1}][W] \right) V \\ &\quad + 4k_p[M_{AA}][M_{BB}] + 2k'_c[C_2][W] + k_r[W]([A] + [B]) \\ \frac{dC_2}{dt} &= (k_c[P_{AB1}] - 2k'_c[C_2][W])V \\ \frac{dA}{dt} &= (-k_p[A]([B] + 2[M_{BB}]) - k_r[A][W] + k_p(4[P_{AB1}][M_{AA}] + 2[P_{AB1}]^2) \\ &\quad + k_r[W]([Z] - 2[A] - [B]))V \\ \frac{dB}{dt} &= (-k_p[B]([A] + 2[M_{AA}]) - k_r[B][W] + k_p(4[P_{AB1}][M_{BB}] + 2[P_{AB1}]^2) \\ &\quad + k_r[W]([Z] - 2[B] - [A]))V \\ \frac{dZ}{dt} &= (-k_r[W]([Z] + [A] + [B]) + k_p(2[M_{AA}][B] + 2[P_{AB1}]) + 2[M_{BB}](A + 2[P_{AB1}]) \\ &\quad + [P_{AB1}](2[A] + 2[B] + 6[P_{AB1}]) + [A][B]))V \\ \frac{dW}{dt} &= \left(\begin{array}{l} -k_r[W]([P_{AB1}] + [Z]) - 2k'_c[W][C_2] \\ + k_p(2[M_{AA}](2[M_{BB}] + [P_{AB1}] + [B]) + 2[M_{BB}](P_{AB1} + [A]) + [P_{AB1}]) \\ \times (2[P_{AB1}] + [A] + [B]) + [A][B]) + k_c[P_{AB1}] \\ - (k_L a)_W([W] - [W]^*) \end{array} \right) V \\ [h] &= h/V; \quad h = M_{AA}, M_{BB}, P_{AB1}, C_2, A, B, Z, W \\ \frac{dV}{dt} &= \left(- (k_L a)_{M_{AA}}([M_{AA}] - [M_{AA}]^*) \frac{w_{M_{AA}}}{\rho_{M_{AA}}} - (k_L a)_W([W] - [W]^*) \frac{w_W}{\rho_W} \right) V \end{aligned}$$

catalyst type and concentration. A dynamic model obtained using the functional-group modeling scheme is shown in Table 7.3, and the analogous molecular-species model is shown in Table 7.4.

The functional-group model (in Table 7.3) has nine differential equations, whereas the molecular-species model has an infinite number. The final equation at the bottom of both tables accounts for changes in the volume V of the reacting mixture, due to evaporation of water and HMD. The differential equations in the tables can be solved numerically using standard ordinary differential equation (ODE) solvers.

Note that the models in Tables 7.3 and 7.4 have been developed assuming that reactant concentrations are in standard units of moles per unit volume of reacting mixture. Be careful

Table 7.4 Dynamic model of a batch nylon 6,6 evaporator developed using the molecular-species modeling approach

$$\frac{dM_{AA}}{dt} = \left(\begin{array}{l} -2k_p[M_{AA}](2[M_{BB}] + \sum_{n=1}^{\infty}[P_{ABn}] + 2\sum_{n=1}^{\infty}[P_{BBn}]) \\ + k_r[W](2\sum_{n=1}^{\infty}[P_{AAn}] + \sum_{n=1}^{\infty}[P_{ABn}]) \\ - (k_L a)_{M_{AA}}([M_{AA}] - [M_{AA}]^*) \end{array} \right) V$$

$$\frac{dM_{BB}}{dt} = \left(-2k_p[M_{BB}](2[M_{AA}] + \sum_{n=1}^{\infty}[P_{ABn}] + 2\sum_{n=1}^{\infty}[P_{AAn}]) + k_r[W](2\sum_{n=1}^{\infty}[P_{BBn}] + \sum_{n=1}^{\infty}[P_{ABn}]) \right) V$$

$$\frac{dP_{AB1}}{dt} = \left(\begin{array}{l} -k_r[P_{AB1}][W] - k_c[P_{AB1}] - k_p[P_{AB1}](2[M_{AA}] + 2[M_{BB}] + \sum_{n=1}^{\infty}2[P_{AAn}]) \\ + \sum_{n=1}^{\infty}2[P_{BBn}] + \sum_{n=1}^{\infty}2[P_{ABn}] \\ + 4k_p[M_{AA}][M_{BB}] + 2k'_c[C_2][W] + k_r[W](\sum_{n=1}^{\infty}2[P_{AAn}] \\ + \sum_{n=1}^{\infty}2[P_{BBn}] + \sum_{n=3}^{\infty}2[P_{ABn}]) \end{array} \right) V$$

$$\frac{dC_2}{dt} = (k_c[P_{AB1}] - 2k'_c[C_2][W])V$$

$$\frac{dP_{ABn}}{dt} = \left(\begin{array}{l} -k_p[P_{ABn}](2[M_{AA}] + 2[M_{BB}] + 2\sum_{i=1}^{\infty}[P_{ABi}] \\ + 2\sum_{i=1}^{\infty}[P_{AAi}] + 2\sum_{i=1}^{\infty}[P_{BBi}]) \\ + k_p(4[M_{AA}][P_{BBn-1}] + 4[M_{BB}][P_{AAn-1}] + \sum_{i=1}^{n-2}4[P_{AAi}][P_{BBn-i-1}]) \\ + \sum_{i=1}^{n-2}[P_{ABi}][P_{ABn-i-1}] \\ + k_r[W](2\sum_{i=1}^{\infty}[P_{ABn+2i}] + 2\sum_{i=1}^{\infty}[P_{AAn+i}] + 2\sum_{i=1}^{\infty}[P_{BBn+i}]) \end{array} \right) V \quad \text{for } n > 1$$

$$\frac{dP_{AAn}}{dt} = \left(\begin{array}{l} -2k_p[P_{AAn}](2[M_{BB}] + \sum_{i=1}^{\infty}[P_{ABi}] + 2\sum_{i=1}^{\infty}[P_{BBi}]) \\ + k_p(2[M_{AA}][P_{ABn-1}] + \sum_{i=1}^{n-2}2[P_{AAi}][P_{ABn-i-1}]) \\ + k_r[W](\sum_{i=1}^{\infty}[P_{ABn+i}] + 2\sum_{i=1}^{\infty}[P_{AAn+i+1}]) \end{array} \right) V$$

$$\frac{dP_{BBn}}{dt} = \left(\begin{array}{l} -2k_p[P_{BBn}](2[M_{AA}] + \sum_{n=1}^{\infty}[P_{ABn}] + 2\sum_{x=1}^{\infty}[P_{AAn}]) \\ + k_p(2[M_{BB}][P_{ABn-1}] + \sum_{i=1}^{n-2}2[P_{BBi}][P_{ABn-i-1}]) \\ + k_r[W](\sum_{i=1}^{\infty}[P_{ABn+i}] + 2\sum_{i=1}^{\infty}[P_{BBn+i+1}]) \end{array} \right) V$$

$$\frac{dW}{dt} = \left(\begin{array}{l} k_p(4[M_{AA}][M_{BB}] + k_p\sum_{i=1}^{\infty}[P_{ABi}](2[M_{AA}] + 2[M_{BB}] + \sum_{n=1}^{\infty}2[P_{ABn}] \\ + \sum_{n=1}^{\infty}2[P_{AAn}] + \sum_{n=1}^{\infty}2[P_{BBn}]) \\ + k_p(2[M_{AA}]\sum_{n=1}^{\infty}([P_{ABn}] + 2[P_{BBn}]) + 2[M_{BB}]\sum_{n=1}^{\infty}([P_{ABn}] + 2[P_{AAn}])) \\ + k_p\sum_{i=1}^{\infty}2[P_{AAi}](\sum_{n=1}^{\infty}2[P_{BBn}]) \\ + 2k'_c[C_2] - k_r[W](\sum_{i=1}^{\infty}i[P_{ABi}] + \sum_{i=1}^{\infty}i[P_{AAi}] + \sum_{i=1}^{\infty}i[P_{BBi}]) \\ - (k_L a)_W([W] - [W]^*) \end{array} \right) V$$

$$[h] = h/V; \quad h = M_{AA}, M_{BB}, P_{ABx}, C_2, P_{AAx}, P_{BBx}, W$$

$$\frac{dV}{dt} = \left(- (k_L a)_{M_{AA}}([M_{AA}] - [M_{AA}]^*) \frac{W_{M_{AA}}}{\rho_{M_{AA}}} - (k_L a)_W([W] - [W]^*) \frac{W_W}{\rho_W} \right)$$

$[P_{ABn}] = 0$ for even values of n , and $[P_{AAn}] = [P_{BBn}] = 0$ for odd values of n , so differential equations do not need to be solved for these cases.

because modelers of industrial polycondensation reactors often express concentrations (as well as kinetic rate constants and mass-transfer coefficients) using mass-based units (i.e., moles per unit mass per time) [13, 14, 24, 30–32, 40–44] rather than volume-based units.

The infinite set of coupled ODEs in Table 7.4 could be solved numerically, by selecting a maximum practical chain length (e.g., $x = 100$) that could conceivably be encountered in the evaporator and assuming that the concentrations of molecules longer than this chain length are zero. This modeling approach is very computationally burdensome. An alternative approach would be to use the method of moments [45] to convert the infinite set of differential equations into a finite set, if only molecular weight averages and some higher moments of the CLD are desired, instead of the complete distribution (see Section 2.3 for details about the use of moments to calculate the average molecular weights).

A third approach for computing the entire chain length distribution involves first solving the functional-group model equations in Table 7.3 to determine the time-varying concentrations of the small molecules and functional groups. Next, assume that the hydrolysis reaction for long polymer chains can be neglected (i.e., that the forward reactions in the evaporator are very fast compared to the reverse reactions because the amine and carboxyl end-group concentrations are high), then the right-hand sides of the simplified material balances for P_{ABn} , P_{AAn} and P_{BBn} depend only on the concentrations of species with smaller values of n . As a result, the ODEs for the larger molecules can be solved sequentially, starting at $n = 2$ and then calculating the concentrations for successively longer chains, finally stopping when the concentrations become too small to be of interest.

The easiest method for obtaining the number-average chain length for the evaporator contents, using either of the two models, is to divide the total number of molecules that have been consumed by polymerization or remain unreacted in the vessel by the final number of molecules in the vessel. For example, using the functional-group modeling approach, first solve the differential equations to obtain concentrations for all of the species at the time of interest and then compute:

$$DP_n = \frac{[M_{AA}] + [M_{BB}] + 2[P_{AB1}] + 2[C_2] + [Z] + ([A] + [B])/2}{[M_{AA}] + [M_{BB}] + [P_{AB1}] + [C_2] + ([A] + [B])/2}$$

If an alternative value of DP_n that includes only the linear molecules is desired, then $[C_2]$ can be removed from the expressions in both the numerator and the denominator. Note that, as conversion increases in subsequent reaction vessels, and the concentration of P_{AB1} becomes smaller due to consumption by polycondensation, $[C_2]$ will decrease, so that the amount of cyclic oligomer that remains in the final nylon 6,6 product is small ($\approx 1\%$). As a result, cyclic oligomer extraction is not required in industrial nylon 6,6 processes.

The example above demonstrates that it is often more convenient to use the functional-group modeling approach rather than detailed molecular-species-modeling. The full molecular-species-modeling approach is required in complicated situations that are not well handled by the simpler functional-group modeling approach [12, 17].

Example 10 (Modeling melt-phase nylon polymerization at high temperatures): When modeling the final stages of nylon 6,6 polymerization processes, in which temperatures range

from 270°C to 300°C (see Figure 7.8), it is important to account for thermal degradation reactions [4]. These side reactions cause a decrease in the concentration of carboxyl end-groups, formation of branches and generation of gaseous side products, leading to problems with product quality. In 1991, Steppan *et al.* [13] fit a simplified kinetic model for melt-phase nylon 6,6 polymerization, using the limited amount of high-temperature kinetic data available at that time. Their kinetic scheme (reactions 7.5.1 to 7.5.5 in Table 7.5) and kinetic parameters have been used [14, 24, 43, 46] to model industrial batch and plug flow reactors.

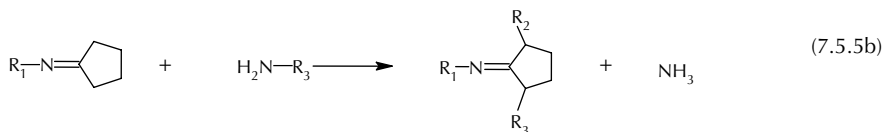
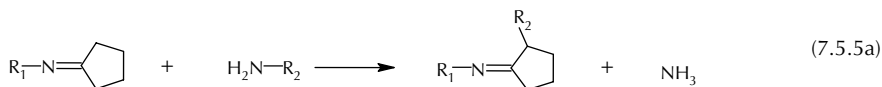
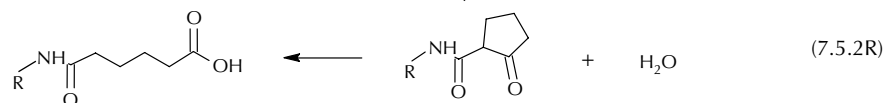
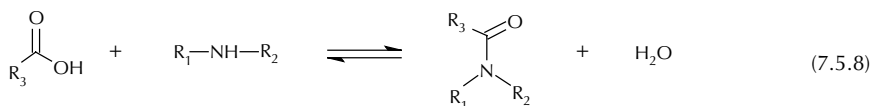
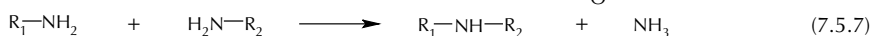
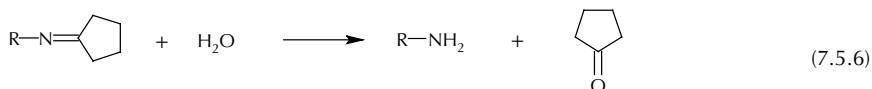
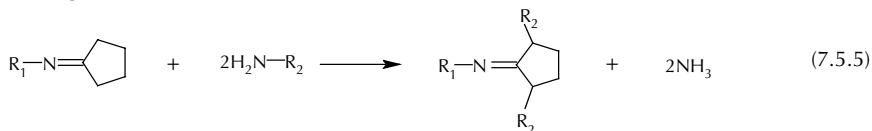
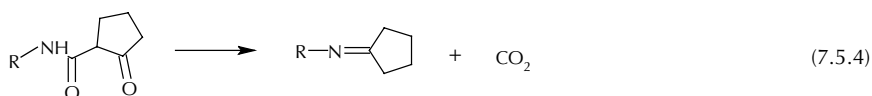
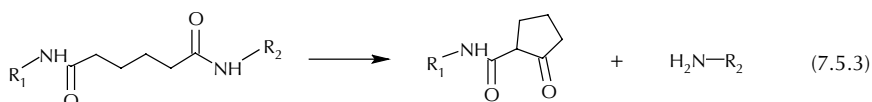
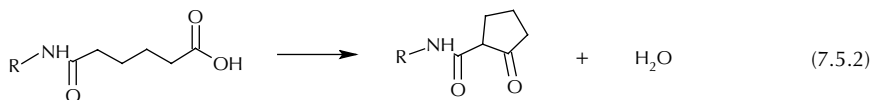
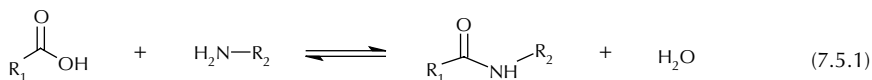
Recently, additional experiments [42] were performed to investigate the effects of temperature and water concentration on polyamidation and thermal degradation rates in nylon 6,6, so that better information is now available for designing and optimizing autoclave and vacuum finishing reactors. Samples of molten polymer and off-gas were collected and analyzed from a series of dynamic experiments. Because of the significant quantities of cyclopentanone found in the off-gas, and tertiary amine branch points observed in the polymer product, three additional reactions 7.5.6–7.5.8 were added to the Steppan kinetic scheme. Also, since experiments with higher water concentrations had reduced levels of thermal degradation, the reverse of reaction 7.5.2 was included in the revised scheme. Reaction 7.5.5 was split into two separate amine-addition steps to make the model more mechanistically realistic.

It is very challenging to estimate kinetic parameters for polyamidation reactions (reaction 7.5.1) using high-temperature nylon 6,6 polymerization experiments, because the amine and carboxyl end-group concentrations used to fit these parameters are influenced by thermal degradation reactions. To obtain kinetic information about high-temperature polyamidation, without the confounding influence of degradation reactions, a series of experiments was performed using nylon 6,12 instead of nylon 6,6 [41, 44]. Nylon 6,12 was selected because reactions 7.5.2–7.5.6 do not occur in polyamides that contain dodecanedioc-acid segments rather than adipic-acid segments. Kinetic parameters obtained from the nylon 6,12 data can be used to predict polycondensation rates in many different aliphatic polyamides, including nylon 6 and nylon 6,6. Note, however, that some care must be taken when applying values of the apparent equilibrium constant, $K_a = k_p/k_r$, obtained from nylon 6,12 experiments to other polyamides. The apparent equilibrium constant, K_a , which is a ratio of products of concentrations, rather than activities, is related to the true thermodynamic equilibrium constant, K_{eq} , by:

$$K_a = \frac{k_p}{k_r} = \frac{[Z][W]}{[A][B]} = K_{eq} \frac{\gamma_A \gamma_B}{\gamma_Z \gamma_W} \quad (7.39)$$

where γ_A , γ_B , γ_Z and γ_W are activity coefficients for amine groups, carboxyl groups, amide groups and water, respectively, in the molten nylon. Polyamidation reactions in nylon polymers with the same functional end-group structures have the same thermodynamic equilibrium constant, K_{eq} , at a given temperature. However, different aliphatic polyamides can have significantly different values of γ_W , because different relative mole ratios, R_{AM} , of amide groups to methylene groups in the repeat unit. For example, nylons 6 and 6,6 have $R_{AM} = 0.2$, but nylon 6,12 has $R_{AM} = 0.125$, which makes nylons 6 and 6,6 more hydrophilic than nylon 6,12. The following Flory–Huggins-based correlation [47] obtained

Table 7.5 Kinetic scheme to account for polyamidation and thermal degradation in melt-phase nylon 6,6. Reactions 7.5.1–7.5.5 are the kinetic scheme of Stepan *et al.* [13]. Reactions 7.5.6–7.5.5b were added by Schaffer [41]



from vapor–liquid equilibrium data, can be used to calculate γ_W for aliphatic polyamide melts in the temperature range from 225°C to 300°C:

$$\gamma_W = 1 + \frac{1}{R_{AM}} \left(1.078 - \frac{451.6}{T} \right) \quad (7.40)$$

where T is the temperature in Kelvin.

Let us calculate K_a for nylon 6,6 at 276°C (and low moisture levels) from $K_a = 53.78$ for nylon 6,12 [38] and Equation 7.39. First, assume that both polymers have the same thermodynamic equilibrium constant K_{eq} and the same ratio of activity coefficients for the functional groups $(\gamma_A\gamma_B)/\gamma_Z$ so that, rearranging Equation 7.39 gives:

$$\gamma_{W66}K_{a66} = \gamma_{W612}K_{a612} \quad (7.41)$$

Next compute the activity coefficients γ_{W66} and γ_{W612} for water in nylons 6,6 and 6,12 at 594.15 K using Equation 7.40:

$$\begin{aligned} \gamma_{W66} &= 1 + \frac{1}{0.2} \left(1.078 - \frac{4521.6}{594.15} \right) = 2.59 \\ \gamma_{W612} &= 1 + \frac{1}{0.125} \left(1.078 - \frac{4521.6}{594.15} \right) = 3.54 \end{aligned} \quad (7.42)$$

so that $K_{a66} = 53.78(3.54/2.59) = 73.51$. Zheng *et al.* [44] provide a correlation for predicting K_{a612} at different temperatures and water concentrations, which can be converted to apparent equilibrium concentrations for nylon 6,6 and other aliphatic polyamides using the method outlined above.

This example shows the kinetic schemes that have been used to account for thermal degradation in high-temperature melt-phase nylon 6,6 polymerization. Reducing the water concentration (and increasing the temperature) in the melt phase increases the net rate of polycondensation, but also increases the rate of degradation reactions. As a result, there is an opportunity to use kinetic models to optimize the trade-off between fast increases in conversion, and fast rates of thermal degradation in melt-phase nylon 6,6 reactors. This example also shows how activity coefficients of water in different polyamides depend on the relative concentrations of methylene groups and amide links in the polymer units. Using this information, apparent reaction-equilibrium constants from nylon 6,12 can be used to predict the apparent equilibrium constants for other similar polyamides.

Example 11 (Dynamic modeling of solid-state polymerization of nylon 6,6): In moving-bed SPP reactors (see Figure 7.5), cold, moist, low-molecular-weight polymer particles are fed to the top of a cylindrical vessel. After contact with counter-current nitrogen gas (at approximately 200°C for 6–24 h) [1], hot, dry, high-molecular-weight particles emerge from the bottom of the bed, in nearly perfect plug flow. As the particles move downward through the bed, polyamidation reactions consume amine and carboxyl end-groups and generate amide links and water. Water diffuses to the outer edge of the particles where it evaporates into the nitrogen gas stream. Nylon 6,6 reactor models in the literature [30, 31, 40] use the kinetic rate constants of Mallon and Ray [32] to predict the net rate of polyamidation (i.e., reaction 7.5.1 in Table 7.5, but at much lower temperatures). The thermal degradation reactions in Table 7.5 do not occur to any appreciable extent at the low temperatures encountered in SPP reactors.

Table 7.6 Dynamic model of a nylon 6,6 solid-state polymerization reactor*Polymer phase*

$$\frac{\partial[W]}{\partial t} = D_{wp} \left(\frac{2}{r_s} \frac{\partial[W]}{\partial r_s} + \frac{\partial^2[W]}{\partial r_s^2} \right) + R_W - u_p \frac{\partial[W]}{\partial z}$$

$$\frac{\partial[h]}{\partial t} = R_h + u_p \frac{\partial[h]}{\partial z} \quad h = A, B, Z$$

Gas phase

$$\frac{\partial[W]_g}{\partial t} = -u_g \frac{\partial[W]_g}{\partial z} + D_{wg} \frac{\partial^2[W]_g}{\partial z^2} + \frac{k_s a^*}{\varepsilon_b} ([W]_{gs} - [W]_g)$$

A simple dynamic model for describing a nylon 6,6 SSP reactor is shown in Table 7.6. This partial differential equation (PDE) model is a set of material balances (on water, amine groups, carboxyl groups and amide links in the particles and on water in the gas phase). Energy balances are also required to predict temperatures within the reactor [30, 31, 40]. Concentrations (and temperature) vary radially within the polymer particles, and with vertical position and time as the particles move downward through the reactor. As a result, the independent variables that appear in the model are the radial direction r_s within the particles, the vertical direction z within the bed, and time, t .

A material balance on water in the polymer particles will now be developed (the first equation in Table 7.6) to illustrate how the PDEs are derived. Make the following assumptions: the polymer particles move downward through the bed in perfect plug flow with velocity u_p (which is a negative number); the moist nitrogen gas flows upward in perfect plug flow with velocity u_g (which is positive); the particles are spheres of radius R_s ; ε_b , the voidage in the bed (the volume fraction occupied by gas) is uniform over the height of the bed; a_c , the cross-sectional area of the bed (perpendicular to z) is also uniform over the height of the bed; the diffusion of amine groups, carboxyl groups and amide links within the polymer is negligible; water has diffusivity D_{wp} in the polymer phase and D_{wg} in the gas phase. Consider a short vertical section of the bed with height Δz . The number of particles in this section is $N_p = (1 - \varepsilon_b) a_c \Delta z / (\frac{4}{3} \pi R_s^3)$. Within each pellet, consider a thin shell of thickness Δr_s at a distance r_s from the center of the pellet. A dynamic material balance on water in these thin shells at radius r_s within the N_p polymer particles is

$$\begin{aligned} & \left(\begin{array}{l} \text{accumulation of} \\ \text{water in the shells} \end{array} \right) \\ &= \left(\begin{array}{l} \text{water diffusing} \\ \text{in at } r_s \end{array} \right) - \left(\begin{array}{l} \text{water diffusing out} \\ \text{at } r_s + \Delta r_s \end{array} \right) + \left(\begin{array}{l} \text{water generated within} \\ \text{the shells by reaction} \end{array} \right) \\ &+ \left(\begin{array}{l} \text{water entering in shells} \\ \text{flowing in at } z + \Delta z \end{array} \right) - \left(\begin{array}{l} \text{water exiting in shells} \\ \text{flowing out at } z \end{array} \right) \end{aligned} \quad (7.43)$$

The number of moles of water that accumulate within the shells during a short period of time Δt is $\Delta(4\pi r_s^2 \Delta r_s N_p [W])$. The number of moles of water that diffuse into the shells, across the spherical surface at r_s is $(-D_{wp}(\partial[W]/\partial r)4\pi r_s^2 N_p)|_{r_s} \Delta t$, and the number of

moles that diffuse out at $(r_s + \Delta r_s)$ is $(-D_{wp}(\partial[W]/\partial r)4\pi r_s^2 N_p)|_{r_s+\Delta r_s} \Delta t$. The number of moles of water generated by reaction in the shells within the N_p particles is $R_w N_p (4\pi r_s^2 \Delta r_s) / (\frac{4}{3}\pi R_s^3) \Delta t$ where $R_w = k_p[A][B] - k_r[Z][W]$ is the local rate of water generation. The number of moles of water in the shells that flow into the section of bed at height $(z + \Delta z)$ is $(-u_p a_c (1 - \varepsilon_b)[W](4\pi r_s^2 \Delta r_s) / (\frac{4}{3}\pi R_s^3))_{z+\Delta z}$, and the moles of water that flow out at bed height z is $(-u_p a_c (1 - \varepsilon_b)[W](4\pi r_s^2 \Delta r_s) / (\frac{4}{3}\pi R_s^3))_z$. The first PDE in Table 7.6 is obtained by substituting all of the terms into Equation 7.43; dividing by $4\pi r_s^2 \Delta r_s N_p \Delta t$; substituting for N_p in terms of Δz ; taking the limit as Δr_s , Δz and Δt approach zero.

The remaining equations in Table 7.6 can be derived in a similar fashion. Note that no partial derivatives with respect to r_s appear in the polymer-phase balances on the functional groups ($[A]$, $[B]$ and $[Z]$) because it was assumed that these groups cannot diffuse. Radial concentration gradients in end-groups are observed when the equations are solved, because the local reaction rates:

$$-R_A = -R_B = R_Z = R_W = k_p[A][B] - k_r[Z][W] \quad (7.44)$$

depend on the water concentration $[W]$. The material balance on water in the gas phase contains a term that accounts for evaporation of water from the surface of the particles. Yao *et al.* [30] provide appropriate values of the gas-side mass transfer coefficient k_g and for the Henry's law coefficients required to obtain $[W_{gs}]$, the water concentration in equilibrium with the particle surface. The surface area of the particles per unit volume of reactor, a^* , is $3(1 - \varepsilon_b)/R_s$. Solving the model equations (which is done numerically) [30] requires initial conditions as well as boundary conditions for all of the concentrations of interest. Because the amount of water leaving the surface of the polymer particles is equal to the amount of water that enters the gas phase, the following boundary condition applies at the particle surface:

$$\left. \frac{\partial[W]}{\partial r_s} \right|_{r_s=R_s} = -\frac{k_s}{D_{wp}} ([W_{gs}] - [W_g]) \quad (7.45)$$

Additional boundary conditions, as well as energy balance equations [30], are required to predict the concentration and temperature distributions within the particles and in the gas phase.

This example describes a mathematical model for predicting dynamic operation of SSP reactors. The model can be used to predict end-group concentrations (and hence DP_n as in Example 9) as they change in response to dynamic changes in reactor operating conditions. Steady-state SSP models (with the time derivatives set to zero) are helpful in determining reactor conditions for producing high-molecular-weight polymer grades as efficiently as possible, particularly since SSP can be slow and energy intensive.

7.4 Summary

This chapter provides an introduction to step-growth polymerization, as it is conducted in a number of industrial polymerization reactors. Although a variety of challenges are associated with producing different step-growth polymers, some common themes emerge.

Because molecular weight builds gradually over time, high conversions are required to produce high-molecular-weight step-growth polymers. When AA- and BB-type monomers are used, a nearly perfect stoichiometric balance of functional groups is also required. Most step-growth polymerizations are reversible, and produce a condensation byproduct that must be removed from the reaction mixture so that high polymerization rates can be achieved. Fortunately, the reversible nature of step-growth polymerization makes step-growth polymers, such as polyesters and polyamides, easier to recycle than chain-growth polymers. Multifunctional monomers can be used to produce speciality products with random branches or with carefully controlled branching structures. Large numbers of branches can lead to the formation of infinite polymer networks or gels. Some step-growth polymerizations are accompanied by undesirable side reactions. Solid-state polymerization, for long times at low temperatures, can provide an effective means to avoid these reactions, especially when very high-molecular-weight polymers are desired. We hope that this chapter has provided a helpful introduction to the various types of reactors that are used to conduct industrial step-growth polymerizations and to the mathematical models that are used to describe these commercially important polymerization systems.

References

1. Weber, J.N. (1996) In *Kirk-Othmer Encyclopedia of Chemical Technology*. Wiley-Interscience, New York, pp. 1–54.
2. Wan, B.Z., Kao, C.Y. and Cheng, W.H. (2001) *Ind. Engng Chem. Res.*, **40**, 509–514.
3. Oertel, G. (1993) *Polyurethane Handbook: Chemistry, Raw Materials, Processing, Application Properties*, 2nd edn. Hanser, New York.
4. Schaffer, M.A., Marchildon, E.K., McAuley, K.B., et al. (2000) *J. Macromol. Sci. Revs Macromol. Chem. Phys.*, **C40**, 233–272.
5. Karode, S.K., Kulkarni, S.S., Suresh, A.K., et al. (1997) *Chem. Engng Sci.*, **52**, 3243–3255.
6. Karode, S.K., Kulkarni, S.S., Suresh, A.K., et al. (1998) *Chem. Engng Sci.*, **53**, 2649–2663.
7. Fialla, P., Hampel, E.F. and Iqbal, M.M. (1993) *European Patent EP0542320*.
8. Barrerre, M. and Landfester, K. (2003) *Macromolecules*, **36**, 5119–5125.
9. Saam, J.C. and Chou, Y.J. (1985) *US Patent US5355154*.
10. Arshady, R. and George, M.H. (1993) *Polym. Engng Sci.*, **33**, 865–876.
11. Mistry, K.K., Preston, J.A. and Symes, K.C. (2004) *European Patent EP1337323*.
12. Kuchanov, S., Slot, H. and Stroeks, A. (2004) *Prog. Polym. Sci.*, **29**, 563–633.
13. Steppan, D.D., Doherty, M.F. and Malone, M.F. (1991) *J. Appl. Polym. Sci.*, **42**, 1009–1021.
14. Pimentel, R.O. and Giudici, R. (2006) *Ind. Engng Chem. Res.*, **45**, 4558–4566.
15. Besnoin, J.M. and Choi, K.Y. (1989) *J. Macromol. Sci. Revs Macromol. Chem. Phys.*, **C29**, 5–81.
16. Laubriet, C., LeCorre, B. and Choi, K.Y. (1991) *Ind. Engng Chem. Res.*, **29**, 2–12.
17. Costa, M.R.P.F.N. and Bachmann, R. (2005) In T. Meyer and J. Keurentjes (eds), *Handbook of Polymer Reaction Engineering*, Vol. 1. Wiley-VCH, Weinheim, pp. 57–151.
18. Flory, P.J. (1953) *Principles of Polymer Chemistry*. Cornell University Press, London.
19. Frauenrath, H. (2005) *Prog. Polym. Sci.*, **30**, 325–384.
20. Gao, C. and Yan, D. (2004) *Prog. Polym. Sci.*, **29**, 183–275.
21. Yates, C.R. and Hayes, W. (2004) *Eur. Polym. J.*, **40**, 1257–1281.
22. Hermes, M.E. (1996) *Enough for One Lifetime: Wallace Carothers, Inventor of Nylon*. Chemical Heritage Foundation, Philadelphia, USA.

23. East, A.J. (1996) In *On-Line Edition of Kirk-Othmer Encyclopedia of Chemical Technology*, Vol. 20. Wiley-Interscience, New York, pp. 31–95.
24. Russell, S.A., Robertson, D.G., Lee, J.H., *et al.* (1998) *Chem. Engng Sci.*, **53**, 3685–3702.
25. Kim, Y.S., Choi, K.Y. and Chamberlin, T.A. (1992) *Ind. Engng Chem. Res.*, **31**, 2118–2127.
26. Kim, Y.S. and Choi, K.Y. (1993) *J. Appl. Polym. Sci.*, **49**, 747–764.
27. Cheong, S.I. and Choi, K.Y. (1995) *J. Appl. Polym. Sci.*, **58**, 1473–1483.
28. Kim, I.S., Woo, B.G., Choi, K.Y., *et al.* (2003) *J. Appl. Polym. Sci.*, **90**, 1088–1095.
29. Ye, Y.S., Machado, B., Choi, K.Y., *et al.* (2005) *Ind. Engng Chem. Res.*, **44**, 2494–2505.
30. Yao, Z.K., McAuley, K.B., Berg, D.A., *et al.* (2001) *Chem. Engng Sci.*, **56**, 4801–4814.
31. Yao, Z.K. and McAuley, K.B. (2001) *Chem. Engng Sci.*, **56**, 5327–5342.
32. Mallon, F.K. and Ray, W.H. (1998) *J. Appl. Polym. Sci.*, **69**, 1233–1250.
33. Gantillon, B., Spitz, R. and McKenna, T.F. (2004) *Macromol. Mater. Engng*, **289**, 88–105.
34. Goodner, M.D., Gross, S.M., DeSimone, J.M., *et al.* (2001) *J. Appl. Polym. Sci.*, **79**, 928–943.
35. Lei, G.D. and Choi, K.Y. (1990) *J. Appl. Polym. Sci.*, **41**, 2987–3024.
36. Lei, G.D. and Choi, K.Y. (1992) *Ind. Engng Chem. Res.*, **31**, 769–777.
37. Cheong, S.I. and Choi, K.Y. (1996) *J. Appl. Polym. Sci.*, **61**, 763–773.
38. Gupta, S.K. and Kumar, A. (1987) *Reaction Engineering of Step Growth Polymerization*. Plenum Press, New York.
39. Xiao, W.H., Huang, N.X., Tang, Z.L., *et al.* (2003) *Macromol. Mat. Engng*, **283**, 235–244.
40. Yao, K.Z., McAuley, K.B. and Marchildon, E.K. (2003) *J. Appl. Polym. Sci.*, **89**, 3701–3712.
41. Schaffer, M.A., McAuley, K.B., Cunningham, M.F., *et al.* (2003) *Ind. Engng Chem. Res.*, **42**, 2946–2959.
42. Schaffer, M.A. (2003) *Chemical Pathways and Kinetics of the Later Stages of Nylon Polymerization Processes*. PhD Thesis, Queen's University, Kingston.
43. Russell, S.A., Robertson, D.G., Lee, J.H., *et al.* (2000) *J. Process Control.*, **10**, 317–332.
44. Zheng, W., McAuley, K.B., Marchildon, E.K., *et al.* (2005) *Ind. Engng Chem. Res.*, **44**, 2675–2686.
45. Jacobsen, L.L. and Ray, W.H. (1992) *J.M.S. Rev.-Macromol. Chem. Phys.*, **C32**, 407–519.
46. Nisoli, A., Doherty, M.F. and Malone, M.F. (2004) *Ind. Engng Chem. Res.*, **43**, 428–440.
47. Schaffer, M.A., Marchildon, E.K., McAuley, K.B., *et al.* (2003) *Polym. Engng Sci.*, **43**, 639–646.

Chapter 8

Control of Polymerization Reactors

José R. Leiza and José C. Pinto

8.1 Characterization of the control problem

The operation of polymerization reactors is very complex for a number of reasons.

- (1) Polymers are performance materials, whose market values usually depend on the balance of a large set of end-use properties, such as transition temperatures, rheological characteristics, mechanical properties, etc. Therefore, the process operation conditions must assure that many distinct end-use properties reach a certain set of target values simultaneously after completion of the polymerization. The market value of the polymer will be lessened if one of the possibly many desired final properties is not satisfactory.
- (2) Improvements of some of the end-use properties are generally obtained with the simultaneous worsening of other end-use properties. For instance, rubber particles (ethylene/propylene copolymers) are usually introduced into homopropylene matrixes in order to increase the impact resistance of polypropylene resins. However, this normally causes the decrease of the flexural modulus of the polymer blend, which is often undesirable [1]. Therefore, optimum operation conditions can only be defined in terms of a tradeoff among the many end-use properties that are required for a specific final application.
- (3) The relationship between the molecular structure and the end-use properties of most polymer materials is poorly understood and relies heavily on empirical observation and testing [1, 2]. This means that control of end-use properties cannot benefit completely from the fast development of phenomenological models of polymerization reactors, which provide detailed information about how operation variables affect the molecular structure of produced polymer materials.
- (4) The relationship among process operation variables and final molecular and/or end-use properties of polymer materials is strongly non-linear, which means that the classical linear control theory is of limited use in the polymerization field. For this reason, advanced non-linear control techniques should be used in many process applications.
- (5) The operation of polymerization reactors is subject to different sorts of instabilities, which may be caused by thermal, viscous, hydrodynamic and kinetic effects, among other reasons. For instance, the increase of the system viscosity (or polymer build-up on heat transfer surfaces) leads to significant reduction of heat transfer coefficients and

consequently to increase of reactor temperatures, leading to very serious safety issues. This implies that control schemes must also include very tight safety procedures, in order to guarantee that process operation will not be driven into regions of unstable operation.

- (6) Most molecular and/or end-use properties of polymer materials cannot be measured on-line, which means that control procedures have to rely frequently on inferred values provided by process models and on measured values provided with long delays by plant laboratories (off-line measurements).
- (7) A typical polymer plant produces tens of different polymer grades, which means that grade transitions are performed very frequently at plant site. This implies that the control procedures should be designed to present adequate performance at different operation conditions and to allow for fast transition between the different operation conditions to reduce off-spec production.

For all the reasons presented above, research and technical activities are very intense and diversified in the field of polymerization reactor control, so that no sort of general control solution can be provided without taking into consideration the particular characteristics of the analyzed polymerization system [3].

The scenario described in the previous paragraphs probably explains the large number of surveys that have been published in the open literature about the control of polymerization reactors. Therefore, the main objective of this chapter is not reviewing the whole field of polymerization reactor control, but presenting the main features and discussing the main trends of the area [3]. Illustrative examples are selected among the many publications in the field. Detailed presentation and analysis of the different proposed control approaches [4–10] and of the distinct used monitoring techniques [11–14] can be found in the available surveys.

8.2 Classical polymerization reaction control problems

8.2.1 Control of reaction rates and of reactor temperature

The control of the reactor temperature and of the reaction rates are perhaps the most common control problems in this field [15]. Polymerization reactions are usually very exothermic (heat of reaction about 100–200 kJ (gmol)⁻¹) and present very high apparent activation energies (around 10–30 kJ (gmol)⁻¹), which means that they are subject to all sorts of thermal instabilities. This is because a small increase of the reactor temperature may lead to a significant increase of the reaction rate (due to the high activation energies) and consequently to a large increase of the rate of heat release (due to the large heat of reaction). This mechanism of positive thermal feedback may lead to development of undesirable complex oscillatory responses (such as self-sustained oscillatory behavior) in continuous polymerization reactors [16–18] and to runaway conditions in batch polymerization reactors [19].

Figure 8.1 illustrates the evolution of reaction rates in batch methyl methacrylate (MMA) bulk reactors under limited heat transfer conditions (large reaction vessels without internal refrigerating coils). Acceleration of reaction rates due to positive thermal feedback is

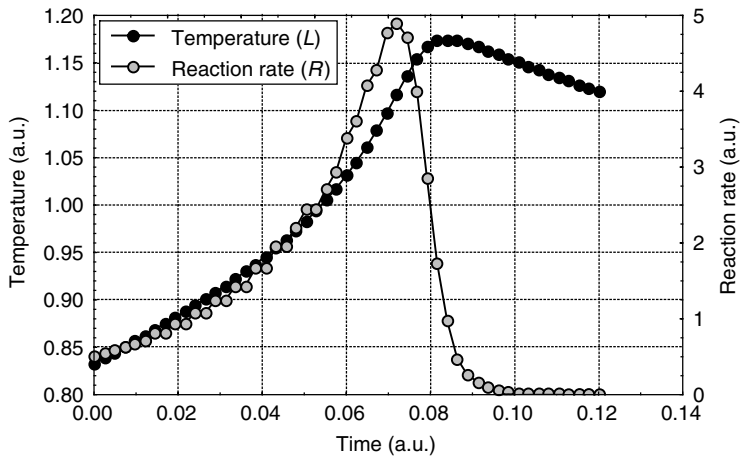


Figure 8.1 Evolution of reaction rates in bulk MMA reactions under limited heat transfer conditions (a.u. stands for arbitrary units).

very clear during the beginning of the batch. Reaction rate decreases sharply at the end of the batch because of monomer depletion, although reactor temperature decreases more slowly because of the heat transfer constraints. Reaction rate also increases because of the strong gel effect of MMA polymerizations, although the initial increase of the reaction rate shown in Figure 8.1 is due mostly to the temperature increase. Figure 8.1 shows that the maximum rate of reaction may be almost one order of magnitude larger than the initial rate of reaction. It is important to notice that non-linear kinetics (e.g., particle nucleation in emulsion polymerizations [20, 21] and reaction inhibition in free-radical polymerizations [17]) and viscous effects (e.g., the gel effect [22, 23]) may cause the continuous increase of reaction rates and reaction runaway even when the reactor temperature is kept constant.

An interesting point regarding Figure 8.1 is that the heat transfer system has to be designed to remove the heat released by reaction at the peak reaction rate values, which means that the heat transfer system remains underused most of the time. For this reason, reaction temperatures are often allowed to vary during batch polymerizations. Starting at low temperature, the heat released by polymerization is used to heat the reactor. This type of operation may allow for more rational design of the heat transfer system and for significant energy savings [24, 25].

Although some dynamic thermal effects can be minimized during continuous operations, unstable thermal conditions can also develop in continuous reactors. Figure 8.2 presents the heat generation and heat removal rates in continuous stirred-tank reactors (CSTRs) and shows that the heat of reaction tends to increase when the reactor temperature increases (due to the increase of reaction rate coefficients). However, a maximum heat of reaction is attained because of the depletion of monomer inside the reactor (the maximum heat of reaction is obtained when monomer conversion becomes equal to one). Figure 8.2 also shows that the heat transferred through the cooling surfaces and process streams increases when the reactor temperature increases, due to the increasing temperature difference between the reactor medium and the surroundings. (The rate of heat removal does not necessarily follow a straight line in some polymerization systems, as suggested in

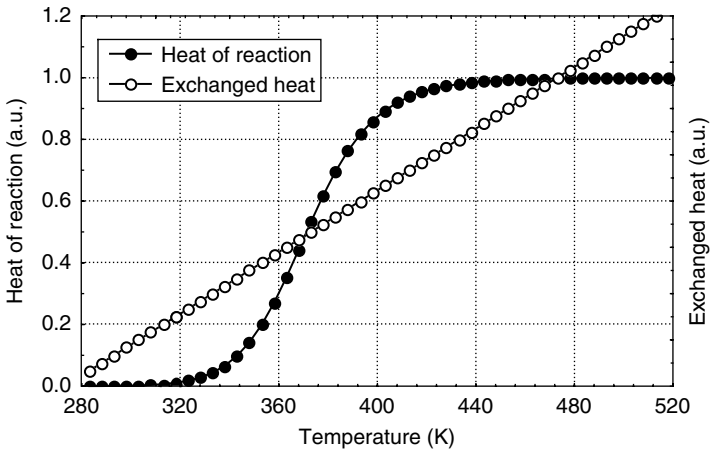


Figure 8.2 Steady-state multiplicity in CSTRs (a.u. stands for arbitrary units).

Figure 8.2, due to the existence of important non-linear effects, such as the dependence of heat transfer coefficients on the system viscosity [26].) Steady-state solutions are obtained when the heat of reaction and the heat transferred to the surroundings become equal. According to Figure 8.2, multiple equilibrium points (steady-state solutions) are possible, which means that attainment of the desired steady-state solution depends on the reactor start-up strategy. (It has been shown that bulk and solution free-radical polymerizations can present up to five distinct steady-state solutions [27].) The lowest steady state is usually uninteresting, because of the low conversions that are obtained. The highest steady state is normally undesirable because of the very high operation temperatures, which pose serious safety problems and contribute with polymer degradation. The problem is that the middle steady state is open-loop unstable, due to the positive thermal feedback mechanism described previously (a small temperature increase leads to additional temperature increase and *vice versa*). This means that the continuous operation becomes possible only if a control scheme is used to stabilize the reactor operation, avoiding temperature perturbations being magnified by the positive thermal feedback mechanism. The analysis of a bulk propylene polymerization plant showed that proportional-integral (PI) controllers can be used effectively to stabilize the desired middle steady state [28]; however, the failure of the controller can lead to potentially serious accidents at plant site, due to thermal runaway conditions.

8.2.2 Control of monomer conversion and polymer production

A second classical control problem is the control of the residual monomer content (monomer conversion) of the polymer material that is withdrawn from the reactor and of the polymer productivity. Maximum monomer conversion and polymer production are limited by short reaction batch times (or residence times in continuous reactors), by the existence of diffusional limitations in the reaction medium (glass effect

in bulk polymerizations) and by fast decay of initiators and catalysts (in free-radical and coordination polymerizations).

Reduction of the final monomer content of the produced polymer is of fundamental importance for many practical reasons. First, increase of monomer conversion usually leads to increase of polymer productivity (unless significant increases of batch times and/or residence times are implemented simultaneously), which may cause a significant impact on the process economics. Besides, monomer (and other volatile organic compounds (VOCs)) content of the final polymer product is limited by law and market preferences. This limiting concentration is usually much lower than the one achieved during polymerization, which means that additional post-polymerization treatments are required. As these are costly operations, it is interesting to minimize the amount of monomer at the end of polymerization (maximize monomer conversion).

Reduction of residual monomer (increase of monomer conversion) and increase of polymer productivity can be obtained through manipulation of reaction times [29], of reactor temperatures (which may be allowed to increase at the end of the polymerization to promote the conversion of the residual monomer) [30], of monomer feed rates [31] and of mixtures of initiators (or of bifunctional initiators) and catalysts with different decay characteristics [32].

8.2.3 Control of molecular weight averages and MWDs

As reaction conditions (reaction temperature, catalyst and monomer concentrations) vary along the reaction time in batch and semibatch processes, and during grade transitions in continuous processes, the reaction rates of all elementary reaction steps that constitute the complex network of the polymerization reaction mechanism also vary along the reaction time. As a consequence, the molecular properties of the produced polymer material usually change continuously along the time during transient operations [33]. Similar drifts of the average molecular weights can be observed along the vessels that constitute the reactor trains of some emulsion [34] and olefin polymerization processes [35].

Control of the molecular weight averages and of the molecular weight distribution (MWD) is usually attained through manipulation of chain transfer agents (CTA) [36, 37] such as hydrogen in coordination polymerizations and mercaptans in free-radical polymerizations. However, reactor temperature [29, 38], initial initiator and catalyst concentrations [29, 39], monomer feed rates and batch times [39, 40] can also be used for controlling the main averages of the MWD. Temperature can be used effectively for control of the molecular weight averages when the ratio between the rate constants for propagation and chain transfer to monomer is sensitive to temperature variations, as in the PVC technology. In general terms, however, manipulation of reactor temperatures for control of the MWD should be avoided because of the sluggishness of temperature responses and because of safety issues. Manipulation of initiator and monomer compositions should also be avoided because of the strong coupling with the production targets and with the energy balance variables (and, therefore, with the control of the reactor temperature). For all these reasons, manipulation of CTA concentrations is usually preferred at plant site. However, mixing of CTAs (or other chemical species) during the reaction course can constitute a very complex task, due to the very small amounts of CTA that are required, to the high system viscosities

and to the heterogeneous nature of the reaction medium. For this reason, CTAs are normally mixed with the monomer feed stream during batch, semibatch and continuous reactions and are rarely fed as a separate feed stream in most technologies. An important exception is the independent feeding of hydrogen in most olefin polymerizations, although mixing of hydrogen and monomer feed is also practiced in some olefin technologies.

The recent development of living and controlled free-radical polymerizations opened new possibilities for design and control of molecular weight distributions, as living products with narrower MWD can be produced at each process stage, allowing for more precise design of the MWD of the final polymer product. Therefore, manipulation of initiator and monomer feed rates provide means for designing the shape of the final MWD of the polymer material [41–43]. It is certain that this technology will gain importance in the upcoming years.

8.2.4 Control of copolymer composition

Most monomers have different reactivity ratios, which lead to production of copolymers that do not have the same composition of the monomer mixture. In batch copolymerization, the copolymer produced at the beginning of the process is richer in the most reactive monomer, while the copolymer becomes richer in the less reactive monomer at the end of the batch. This composition drift causes the production of heterogeneous polymer mixtures, which may be deleterious for the performance of the polymer material. With the exception of the azeotropic reactions, most copolymerization systems experience composition drifts during batch copolymerizations, which must be corrected if homogeneous copolymer materials are to be produced. For this reason, copolymerizations are usually performed in semibatch (with manipulation of monomer feed flow rates) or continuous mode.

The previous discussion leads to the definition of the fourth classical control problem, which is the control of the copolymer composition along the reaction batch (or at the end of the batch). This objective is normally attained through manipulation of monomer feed flow rates [44, 45]. The feed stream usually contains the most reactive monomer species, so that composition control is obtained by keeping the concentration of the most reactive monomer concentration at the desired low levels throughout the batch time. It is important to emphasize that implementation of monomer feed strategies may lead to runaway conditions in the presence of heat transfer limitation [46], which partially explains why control of copolymer composition in emulsion reactors is normally attained by working under starved conditions.

It is very important to notice that the strategy used to control the copolymer composition may exert a significant impact on the MWD of the final polymer material. Therefore, it is advisable to design control strategies for the simultaneous control of copolymer composition and the MWD in copolymerization reactions.

8.2.5 Control of particle size and PSDs

Many polymerizations are performed in heterogeneous media, so that the final polymer product is obtained as a particulate material. The characteristics of the final particle size distribution (PSD) of the product may be of fundamental importance for many applications.

For instance, in order to increase the polymer concentration of polymer latexes, multimodal and/or broad PSDs may be required [47]. It must also be stressed that the PSD and the polymerization rates are coupled in many heterogeneous polymerizations. This leads to the definition of the fifth classical control problem, which is the control of some features of the PSD of the final polymer material.

Manipulation of PSDs is generally attained through modification of surfactant concentrations (mostly in emulsion polymerizations) [48, 49], agitation speeds (mostly in suspension polymerizations) [50], and initial catalyst size distributions and reaction times (residence time distributions in continuous reactors, mostly in coordination polymerizations) [51]. Effects of agitation speeds and surfactant concentrations on the PSD of polymer particles produced in suspension and emulsion polymerizations are discussed in detail in Chapters 5 and 6, respectively. When the catalyst is fed into the reactor as a solid material, as in typical polyolefin reactions, then the residence times and the initial PSD of the catalyst particles are used to manipulate the PSD of the final polymer product. Similar strategies are used in seeded emulsion polymerizations, where an initial load of preformed particles can be used to improve the control over the concentration of polymer particles in the latex and over the PSD of the final polymer product.

8.2.6 Control of other reaction parameters

Although many additional control problems can be defined in a polymerization process, there is no doubt that the five classical control problems defined previously are the most important ones. This is certainly connected to the availability of measuring techniques that can be used for on-line evaluation of the process performance, as it will be discussed in the following sections. In spite of that, some other important control problems can be found in particular polymerization fields. The control of the branching frequency constitutes an important problem in certain olefin polymerization processes because it may exert a profound impact on the final performance of the polymer materials [52, 53]. Control of the branching frequency (gel content) is also very important in certain emulsion polymerizations, especially when acrylic and multifunctional monomers are used [54, 55]. In both cases, molecular weight averages, copolymer compositions and branching frequencies are strongly coupled and cannot be controlled independently. Fundamental process models can be very helpful in these cases for optimization of the process operation and of the final polymer properties. Control of copolymer composition distributions in copolymer materials is also desirable in some applications [56, 67]. It was shown that monomer and catalyst feed rate policies can be manipulated for proper open-loop control of copolymer composition distributions in living radical polymerizations [57–60], although the on-line control of copolymer composition distribution is not possible at the present. Finally, control of particle porosity is very important in the PVC field, although this is normally achieved through manipulation of concentrations of cocktails of stabilizers and is not performed on-line.

Very often, the control problem is posed in terms of performance indices that are not the molecular properties defined previously, but that are directly connected to them. For instance, this is the case of the melt flow index [61], of the Mooney viscosity [62] and of the intrinsic viscosity [63, 64], which may be regarded as indirect evaluations of

the average molecular weights of the polymer materials. Some examples will be discussed in the following sections.

8.3 On-line monitoring

8.3.1 Introduction

Monitoring of polymerization variables is necessary to fully implement advanced closed-loop control strategies and to ensure the consistent, safe and optimal production of polymeric materials with the required quality. Even when advanced control strategies are not implemented, on-line monitoring of polymerization processes is a must, as it generates an enormous amount of useful information that can be used for modeling and optimization purposes in the long term and to modify reaction formulations in the short term. Furthermore, it may allow for significant reduction of time-consuming off-line analyses performed in the lab.

Sensors used for monitoring of polymerization reactors can be classified into two large categories:

- (1) sensors for monitoring of *reactor operation conditions or process variables* and
- (2) sensors for monitoring of the *trajectory of polymer properties* during polymerization.

Temperature, pressure, flow rates and level are measurements in the first group that are routinely performed at plant site. These measurements are well established and will not be addressed in this section, even though tracking the trajectory of these operational variables might be enough to ensure the production of the polymer of interest in some processes. On the other hand, sensors used for monitoring of trajectories of structural polymer properties are very difficult to develop, but provide much more useful information to carry on closed-loop control strategies.

Sensor technology for on-line monitoring of polymerization processes has evolved significantly in the last decades, based on advances coming from other disciplines. The fast advancements in computer, electronic and process control technologies in the mid-1980s allowed for automation of sensors that had been used previously only for off-line analysis of polymer properties (e.g., on-line gas chromatography of reactor content). More recently, in the late 1990s, the development of fiber optic technology has provided an efficient and simple way of performing different spectroscopic techniques (ATR-FTIR, NIR, MIR and Raman) in polymerization processes.

However, there are still a number of important polymer properties that can only be measured by laborious and time-consuming off-line analyses. In this category one can include the MWD (especially in dispersed systems and/or for polyolefins), branching and crosslinking density, the gel content, the PSD, among other properties. (Despite the several examples reported in the scientific literature, at present no commercial equipment can ensure the fast and robust on-line measurement of the entire size distribution of polymer particles in industrial reactors.)

Some of the properties that cannot be measured on-line can be inferred from the measurements of other variables by means of state estimation methods and software sensors

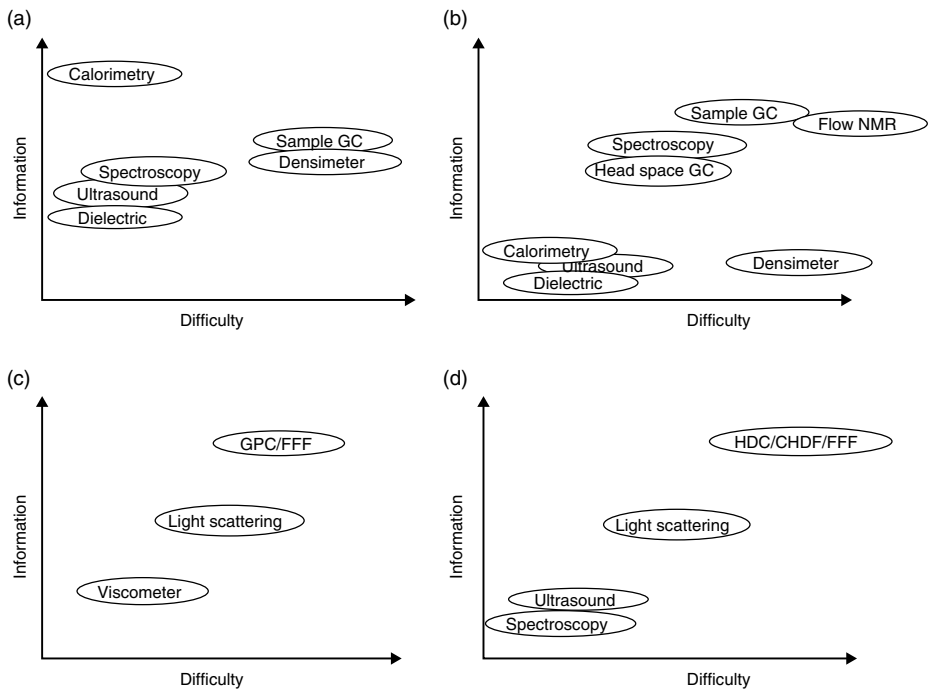


Figure 8.3 Charts for sensor selection: (a) polymerization rate; (b) comonomer concentration; (c) molecular weight distribution; (d) particle size distribution.

that combine mathematical models of the process with the available measurements. In this section a brief summary of on-line monitoring and state estimation techniques is presented, addressing the pros and cons of their implementation in an industrial environment.

8.3.2 On-line sensors for monitoring polymer quality

One of the most important issues for monitoring of polymerization reactors is the selection of the most appropriate technology. Excellent reviews discuss the different available techniques in the literature [11–14]. Figure 8.3 shows some of the available solutions for on-line monitoring, organized in terms of the amount of information provided and the difficulty of implementation (including robustness in a harsh environment, maintenance required and know-how). The ideal technique would be located in the upper left-hand corner of the charts. Unfortunately, one can find monitoring solutions in this part of the figure only for polymerization rate measurements.

8.3.2.1 Polymerization rate

Polymerization rate can be measured by several techniques, although calorimetry (the heat of reaction, Q_r , is monitored by solving the energy balances of the reactor and the cooling jacket) is often the most convenient one for industrial reactors.

This measurement can also be used to evaluate monomer conversion and/or concentration (which is straightforward in homopolymerizations [65], but requires a mathematical model in the case of copolymerizations [66, 67]), as explained in Section 8.3.2.2.

8.3.2.2 Monomer concentration (conversion and copolymer composition)

Table 8.1 presents a summary of the techniques that are currently available to monitor the concentration of monomer in polymerizations reactors. For each technique, advantages and disadvantages of the sensor and the potential usage in distinct polymerization systems are compiled. Attenuated total reflection infrared, ATR-FTIR, near infrared, NIR, mid-range infrared, MIR, and Raman spectroscopies are capable of monitoring different polymerization reactions in a non-invasive manner (without handling the reactor contents outside the reaction vessel). Handling of reactor contents outside the vessel can always constitute a major drawback due to the high viscous and unstable nature of the produced polymer solutions/dispersions.

Monomer concentration can be measured directly in polymerization reactions by gas chromatography (GC). GC measurements are invasive and hence not suited for industrial application in many cases (head space GC would not be as demanding, but it requires equilibrium to be attained and equilibrium parameters for accurate determination of monomer concentration). Therefore, at least in principle, spectroscopic techniques are better suited for real on-line implementations than chromatographic techniques. An example of the application of the Raman technique, possibly the best suited spectroscopic technique for monitoring monomer concentrations in waterborne systems, is provided in Figure 8.4. This figure shows the time evolution of the Raman spectra taken during the semibatch emulsion copolymerization of VAc/BA/AA = 78.5/18.5/3 and the concentration of the free vinyl acetate (VAc), calculate in real time from these spectra using chemometric models and off-line through GC measurements [68].

Other non-invasive (e.g., calorimetry and ultrasounds) and invasive (e.g., densimetry) techniques can also be used for monitoring of monomer concentration in homopolymerization reactions. However, in multimonomer formulations the individual monomer concentrations cannot be obtained with these techniques, meaning that a state estimator is required [66, 67, 69]. The use of reaction calorimetry is appealing because the hardware is very cheap and, when coupled with a state estimator, provides good estimation of the monomer concentration. The performance of calorimetry was compared with that of the Raman spectroscopy in emulsion polymerization to monitor overall and individual monomer conversions [68]. Calorimetry was as good as FT-Raman spectroscopy when monomer concentrations in the reactor were relatively high, but the performance of calorimetry was poorer when monomer concentrations were low.

8.3.2.3 Molecular weight distribution

Measurement of the MWD of a polymer depends on the nature of the analyzed/produced polymer. The following classes can be distinguished:

- (1) *Soluble polymers*. These are polymers that dissolve in a solvent; hence, the molecular weight can be measured on-line by means of gel permeation chromatography/size

Table 8.1 On-line sensors to monitor monomer concentration in polymerization reactors

Technique	Examples	Advantages / disadvantages
ATR-FTIR (attenuated total reflection infrared)	Olefin polymerization (ethene/1-hexene) [70] Polycondensation of diols and carbamic acid, equilibrium of isocyanates with alcohols [71]	Non-invasive, well suited for polycondensation / Poor fiber-optic transmission, not well suited for waterborne polymerization
NIR (near infrared)	Epoxy/amine systems [72] Homogeneous (bulk and solution) and heterogeneous (suspension and emulsion) polymerizations [73–75]	Non-invasive / Broad bands, chemometry required and of limited usefulness for waterborne systems because of the strong absorption of water
MIR (mid-range infrared)	Epoxy/amine systems [76, 77] Acrylate/styrene emulsion copolymerization [78]	Non-invasive, richer in information than NIR and IR / Fiber-optic transmission difficult (expensive), remote monitoring not achieved
Raman	Bulk, solution, suspension and emulsion polymerizations [68, 75, 79–85]	Non-invasive, excellent for waterborne systems, highly sensitive to C=C and polymer structure (crystallinity) / Fluorescence and low signal intensity (almost solved with dispersive equipments with lasers operating at 830 nm)

Table 8.1 (Continued)

Technique	Examples	Advantages / disadvantages
Calorimetry	Semibatch emulsion polymerization of VAc/BA [66, 67] Epoxy-amine curing polymerization [86]	Non-invasive, robust and almost continuous / Requires state estimators and the values of the reactivity ratios for multimonomer systems
Gas chromatography	Solution and emulsion polymerization systems (VAc/BA, all acrylics, BA/St, St/AN, ...) [87-90] Ring-opening polymerization [91] and polyolefin gas-phase polymerization [92]	Direct measurement of concentrations / Invasive, non-robust in industrial environment, requires sampling and dilutions loops or head-space (equilibrium parameters required)
Densimetry	Emulsion homo and copolymerizations [69, 93, 94] Solution homopolymerization of MMA [95, 96]	Continuous measurement / Invasive, requires state estimators and values of the reactivity ratios for multimonomer systems, non-robust for industrial environment
Ultrasound	Emulsion (VAc and MMA) and suspension (VCI) homopolymerizations [97, 98]	Non-invasive and continuous / Requires modeling for copolymerization (complex)
Dielectric	Epoxy, polyester and emulsions [99, 100]	Non-invasive, continuous, it can be used during synthesis and curing / System-specific, few examples in the literature

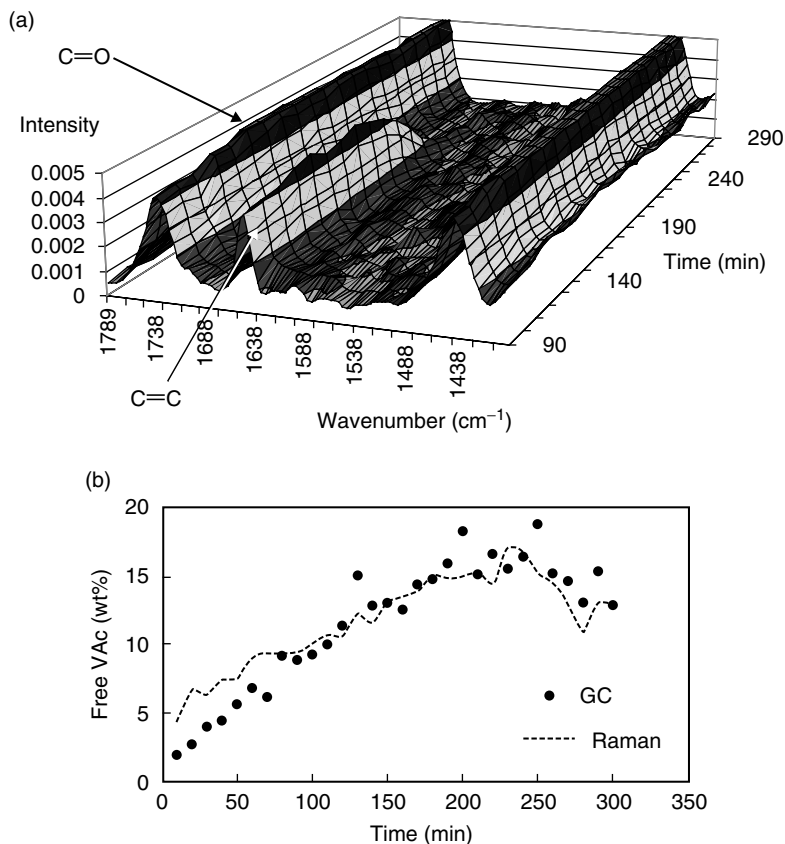


Figure 8.4 (a) Time evolution of the Raman spectral region $1400\text{--}1800\text{ cm}^{-1}$ taken during the emulsion copolymerization of VAc/BA/AA; (b) evolution of the free VAc calculated from the Raman spectra as compared with the GC measurements.

exclusion chromatography (GPC/SEC) and light scattering equipments [101, 102]. Both linear and non-linear (branched) polymers can be found in this category, although the accurate determination of the MWD is more sophisticated for non-linear polymers because combination of refractive index, viscosity and light scattering detectors must be used. Table 8.2 summarizes the available on-line techniques used to measure the MWD and/or the average molecular weights of soluble polymers.

- (2) *Insoluble polymers.* These polymers do not dissolve in a good solvent and usually have extremely high molecular weights and/or are partially or fully crosslinked. The on-line measurement of the MWD is not possible in these cases. The soluble polymer fraction (which is normally non-linear) may be extracted from the sample and analyzed (for instance, in a GPC/SEC equipment). At present, the insoluble part is only characterized by the insoluble amount (the so-called gel fraction). Additional information regarding the crosslinking density can also be obtained off-line using swelling experiments or spectroscopic techniques (e.g., NMR).

Table 8.2 On-line sensors to monitor MWD of soluble polymers in polymerization reactors

Technique	Examples	Advantages/ disadvantages
GPC/SEC (gel permeation chromatography/ size exclusion chromatography)	Solution polymerization [95, 96, 102, 108, 109]	The whole MWD obtained/ Invasive, non-robust, sampling loop required, large delay times (30 min to 1 h)
HT-GPC/SEC (high throughput GPC)	Ring-opening polymerization [91]	The whole MWD, time delay is shorter/ Invasive, minimum and maximum molecular weights limited, non-robust, sampling required
Light scattering	Solution polymerization of acrylamide, vinyl pyrrolidone, inverse microemulsions, polyurethanes, polyelectrolytes [101, 110–112]	Commercial equipment (ACOMP), continuous measurement/ Average molecular weight only, invasive, continuous sampling of the reactor
Viscometer	Solution homopolymerization of MMA, VAc [95, 96, 113]	Some commercial equipments available/ Invasive, only average molecular weight, sampling required, non-robust

- (3) *Polyolefins*. Polyethylene (PE) and polypropylene (PP) homopolymers and copolymers can only be dissolved in chlorinated solvents at high temperatures. High temperature and pressure fractionation equipment is available to measure the MWD of these polymers. The reader is referred to Chapter 2 (Section 2.1.3) for further information. For ultra-high molecular weight PE and PP polymers, the high temperature GPC may be misleading. It has been recently demonstrated that high temperature asymmetrical flow field flow fractionation (HTAF4, PostNova Analytics) provides molecular weights that are in agreement with rheological properties of these polymers [103]. In principle, the on-line measurement of the MWD of polyolefins produced in solution or slurry processes might be possible, although this has not yet been reported in the literature.

When the on-line measurement of the MWD or average molecular weight is not possible or not feasible, state estimation becomes an alternative. The simplest state estimation scheme is the one that can be applied for linear polymers when CTAs are employed to control the MWD of the polymer. In these systems, the ratio of unreacted monomer to CTA provides an estimate of the instantaneous number chain length, $DP_n = R_p/R_t = k_p[M]/k_{tr}^{CTA}[CTA]$. Therefore, if the ratio can be measured on-line by one of the techniques described in the previous section, a good estimate of DP_n can be achieved. This feature has been used to monitor and control the MWD of linear homopolymer and copolymers produced in emulsion polymerization systems [104–107].

For non-linear soluble and insoluble polymers, open-loop state estimators (see Section 8.3.3 for details) can be used. The prediction capabilities of these estimators rely on the mathematical models that describe the development of the molecular weights. These models may include complex mechanisms (chain transfer to polymer, backbiting, propagation to pendant double bonds) that depend on uncertain (or even unknown) rate coefficients. Therefore, we are far from having reliable and robust on-line sensors to estimate the MWD of non-linear and/or insoluble polymers.

8.3.2.4 Particle size distribution

In heterogeneous polymerizations, the final product is obtained in the form of a distribution of polymer particles in the submicron (emulsion and related techniques such as miniemulsion and microemulsion; 0.05–1.0 μm) and micron (suspension, precipitation, liquid slurry and gas–solid polymerization; 10–10⁴ μm) size range. Most of the developments related to the on-line evaluation of the PSD and/or of the average particle sizes in heterogeneous polymerizations have been obtained in the submicron range size, for polymer latexes produced in emulsion polymerization processes. There had also been some attempts to monitor the average particle sizes on-line in suspension polymerizations. These techniques are not well suited for monitoring of particle sizes in polyolefin processes, so that there are no published reports related to the on-line monitoring of particle sizes and/or PSD in polyolefin reactors. Nevertheless, in principle it should be possible to implement some of these techniques in liquid slurry polyolefin reactors.

The techniques that are able to perform the on-line evaluation of PSDs include fiber-optic dynamic light scattering (FODLS), turbidimetry, size fractionation techniques (such as capillary hydrodynamic fractionation chromatography, CHDF and field-flow fractionation,

FFF) and ultrasound spectroscopic techniques. Table 8.3 presents a compilation of these techniques with examples, discussion of advantages and disadvantages and fields of application. Other techniques also give an indirect measurement of particle sizes, such as measurement of surface tension [93] and conductivity [114] of latexes during emulsion polymerization. Surface tension has been used to monitor free emulsifier concentration, while conductivity was used to predict the number of particles and the surfactant concentration with the help of a semi-empirical model [115].

To conclude it can be stated that the on-line monitoring of the PSD is still an unsolved and challenging problem.

8.3.3 State estimation

As shown in the previous section, at present the on-line measurement of polymer quality can only be achieved in a robust, safe and consistent manner for monomer concentration and polymerization rate. For properties like MWD or PSD, the current technology is not yet sufficiently mature to be implemented routinely in industrial environments (and in most of the cases in lab environments either). The lack of easily available frequent on-line measurements for polymer quality has been the driving force for the development of state estimators that are capable of estimating unmeasurable polymer properties from readily available measurements [129].

State variables of a process are the variables that uniquely specify the process at any given time (such as temperature, monomer concentration and molecular weights). Effective monitoring and control of a process requires reliable real-time information of the state variables.

State estimation techniques provide estimates of the states of a dynamic system, which are obtained by balancing the contribution made by a deterministic dynamic process model with that given by the measurement model and the actual measurements. In formal mathematical terms,

$$\hat{\mathbf{x}}(t) = \int_0^t f(\mathbf{x}, \mathbf{u}, \tau) d\tau + K(\mathbf{y}(t) - h(\mathbf{x}, t)) \quad (8.1)$$

where $\hat{\mathbf{x}}(t)$ is the vector of estimated states $\mathbf{x} = [x_1, \dots, x_n]^T$ at time t , $f(\mathbf{x}, \mathbf{u}, \tau)$ is the non-linear process model that is solved from 0 to t , $\mathbf{u}(t)$ is the vector of manipulated input variables $\mathbf{u} = [u_1, \dots, u_m]^T$, $\mathbf{y}(t)$ is the vector of process outputs $\mathbf{y} = [y_1, \dots, y_l]^T$ (note that the process outputs are often equal to state variables; for instance, temperature can be a measurement and a state variable simultaneously), $h(\mathbf{x}, t)$ is the non-linear measurement model (prediction of measurements based on the estimated state variables) and K is the estimator gain. Each state estimation algorithm calculates the estimator gain in different ways. The estimator gain gives more or less weight to the process model with respect to the measurements, depending on its value. If K is small, the contribution of the measurements to the estimation of state variables is small. This is normally performed when precision of the measurements is poor. The opposite is true when a large value of K is used. It is important to say that K may vary along the time and may depend on the measured outputs. A more rigorous definition of the state estimation problem can be found in the literature [130, 131].

Table 8.3 On-line sensors to monitor PSD in polymerization reactors

Technique	Examples	Advantages/ disadvantages
FODLS (fiber-optic dynamic light scattering)	Lab and pilot scale emulsion polymerization reactions [116–118]	Non-invasive, no dilution necessary / Only average particle size, multiple scattering not fully solved [119]
Turbidity	Emulsion polymerization [116, 120–122]	PSD can be obtained/ Invasive, dilution required, mathematical treatment not simple
CHDF (capillary hydrodynamic fractionation)	Semibatch emulsion polymerization of styrene, and VAc/BA [49, 123]	PSD directly measured/ Invasive, dilution or sampling loop required, non-robust for industrial environment, time delay
Ultrasound	Non-reacting latexes (PVC and PTFE) [124] Diluted slurries [125]	PSD, non-invasive/ Inversion of the raw data not straightforward, system specific, not suitable for concentrated systems
NIR and Raman	Suspension and emulsion polymerization [126–128]	Non-invasive/ Average particle size only, calibration required, system specific, chemometric required

8.3.3.1 Observability

An important point regarding state estimation is that the observability/detectability criteria must be met in order for any state variable to be correctly estimated [132]. A linear system is considered observable if there is a finite time t such that the knowledge of the manipulated variables, $\mathbf{u}(t)$, and the measured output, $\mathbf{y}(t)$, is sufficient to determine the initial state, $\mathbf{x}(0)$, of the system. In non-linear systems the observability is classed as global and local observability. Loosely speaking, a system is observable if the measurable outputs contain useful information on all the state variables [129, 130]. In polymerization reactors, the MWD is not observable from available monomer conversion and temperature measurements, and therefore molecular weights can only be inferred by using open-loop observers [132–134]. This means that the states corresponding to the molecular weight are calculated based on the prediction of the model (i.e., with $K = 0$). Similarly, copolymer composition or individual monomer conversions are not strictly observable from calorimetric measurements (reactor and jacket temperatures and cooling fluid flow rates) [135]. However, it has been shown that, due to the robust structure of the mathematical model that describes the copolymerization and the availability of the parameters of this model (reactivity ratios), open-loop observers allow for accurate estimation of the copolymer composition in co- and terpolymerization systems [67, 136] (see the example below). In the same vane, cascade high-gain observers were successfully used to estimate compositions in co- and terpolymerization systems [137, 138].

When the system is completely observable, all process state variables can be estimated from the process model and the measurements. In this case, the rate of convergence of the estimator can be adjusted by the estimator gain.

8.3.3.2 Open-loop observers

Open-loop observers are used when the state variables are not observable from the available measurements. In this case, the estimation is based on the predictions of a process model. In this section, the development and use of open-loop observers is illustrated for estimation of monomer concentrations in an emulsion copolymerization reactor when only the heat of reaction is measured on-line. In this case the observability criterion is not fulfilled, which means that the estimation of the monomer concentrations cannot be carried out with feedback correction [135].

The process model equations (material balances of the species present in the reactor) can be written as follows:

$$\frac{dM_i}{dt} = F_{i\text{in}} + (R_{pi})V, \quad i = 1 \text{ and } 2 \quad (8.2)$$

$$\frac{dI}{dt} = F_{I\text{in}} - fk_I[I]_w V_w \quad (8.3)$$

where the net generation of monomer i in the reactor is given by:

$$R_{pi} = -\left(\sum_j k_{pji}P_j\right)[M_i]_p \frac{\bar{n}}{N_A} \frac{N_p}{V}, \quad j = 1 \text{ and } 2 \quad (8.4)$$

$$P_1 = \frac{k_{p21}[M_1]_p}{k_{p21}[M_1]_p + k_{p12}[M_2]_p}, \quad P_2 = 1 - P_1 \quad (8.5)$$

For simplicity, it is assumed that there are no monomer droplets and that the amount of monomer dissolved in the aqueous phase is negligible (water-insoluble monomers, high solids content latex). Therefore, all the monomer is in the polymer particles. Equations 8.2–8.5 provide the overall mass balances inside the reactor during the whole batch.

The overall heat of polymerization can be related to the individual rates of polymerization by the following equation:

$$Q_r = \sum_i R_{pi}(-\Delta H_{r,i}) \quad (8.6)$$

The ratios of the individual polymerization rates for a copolymerization are:

$$D_{12} = \frac{R_{p1}}{R_{p2}} = \frac{(k_{p11}P_1 + k_{p21}P_2)[M_1]_p(\bar{n}N_p/N_A V)}{(k_{p22}P_2 + k_{p12}P_1)[M_2]_p(\bar{n}N_p/N_A V)} = \frac{r_1 + ([M_2]_p/[M_1]_p)}{r_2([M_2]_p/[M_1]_p)^2 + ([M_2]_p/[M_1]_p)} \quad (8.7)$$

where r_i is the monomer reactivity ratio, defined as $r_i = k_{pii}/k_{pij}$. Combining Equations 8.2–8.5 (for the material balances of the monomers) with Equations 8.6 and 8.7, the material balances for the monomers can be written as a function of the heat released by polymerization and the reactivity ratios as follows:

$$\frac{dM_i}{dt} = F_{iin} - \frac{Q_r}{(-\Delta H_{r,1}) + (-\Delta H_{r,2})(1/D_{12})}, \quad \text{for } i = 1, 2 \quad (8.8)$$

Equations 8.2–8.8 constitute an open-loop observer/estimator that is completely dependent on model responses and whose rate of convergence is not adjustable (no feedback action) [132]. Note that if the observer error at $t = 0$ is equal to zero (the initial conditions are known with very high precision), it will remain equal to zero during the rest of the process, provided that the model is correct. All the model contributions to the estimator are included in D_{12} , where the only parameters are the reactivity ratios and the heat of polymerization. These parameters can be obtained by independent experiments with a good accuracy.

Figure 8.5 shows an example of the performance of this type of estimation scheme for a semibatch emulsion copolymerization of VAc/BA carried out at 70°C with 33 wt% solids content. It can be seen that the estimated overall monomer conversions and copolymer composition calculated from the estimated amounts of unreacted monomer compared well with the off-line measurements.

8.3.3.3 Closed-loop state estimation

In the example of the previous section assume that the available on-line measurements include the unreacted monomer concentrations obtained by means of a spectroscopic technique, such as Raman spectroscopy. Therefore, $y(t)$ in Equation 8.1 is available and the system is fully observable. The model for the process is given by Equations 8.2–8.8. \bar{n} can be

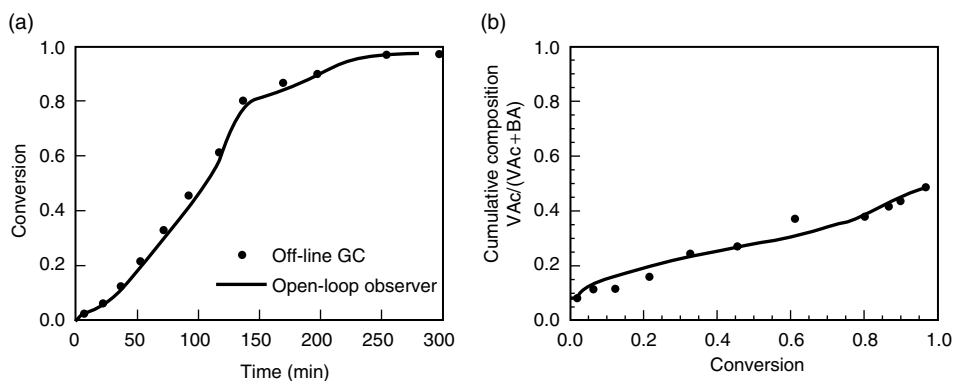


Figure 8.5 Monitoring a semibatch emulsion polymerization reaction of VAc/BA by means of an open-loop observer based on calorimetric measurements. (a) Conversion and (b) copolymer composition.

calculated as described in Chapter 6, which requires a number of parameters (e.g., radical entry and exit coefficients) that are uncertain and might affect the quality of the estimation. However, \bar{n} can also be included in the estimation scheme as an additional “state/parameter” to be estimated together with the concentration of monomer. For this purpose one can use a random walk model for \bar{n} (as performed by several authors [135, 138, 139]) or use a simplified dynamic model for \bar{n} (such as a polynomial function of time) and estimate the parameters of the simpler model within the estimation procedure [104, 135, 140].

For implementation of the state estimation algorithm, it is necessary to define the estimator gain. Several state estimator algorithms have been proposed in the literature to calculate K . Table 8.4 highlights the most common state estimator algorithms with the respective strengths and weaknesses. Table 8.4 also presents some examples of implementations in polymerization reactors. For illustrative purposes the extended Kalman filter (EKF) will be briefly shown below.

The extended Kalman filter in its discrete predictor/corrector form (spectroscopic measurements are not obtained as continuous functions of time) can be written as follows:

Prediction: Based on the estimated values of the state variables at a given time ($\hat{x}_{k-1/k-1}$), the states for the next time ($\hat{x}_{k/k-1}$) are calculated using the mathematical model (Equations 8.2–8.5). This gives the first term of the right-hand side of Equation 8.1. In addition, the covariance matrix of the estimation error ($P_{k/k-1}$), which is needed to determine K , is calculated (for details see Jazwinski [131]):

$$\hat{x}_{k/k-1} = f(\hat{x}_{k-1/k-1}, u_k) \quad (8.9)$$

$$P_{k/k-1} = A_{k/k} P_{k-1/k-1} A_{k/k}^T + Q \quad (8.10)$$

with

$$A_{k/k} = \left. \frac{\partial f}{\partial \hat{x}} \right|_{\hat{x}_{k/k}} \quad (8.11)$$

Table 8.4 State estimation algorithms to monitor polymerization reactions

Algorithm	Examples	Advantages / disadvantages
Extensions of Kalman filters and Luenberger observers [131]	<p>Solution polymerizations (conversion and molecular weight estimation) with and without on-line measurements for M_w [102, 113, 133, 134]</p> <p>Emulsion polymerization (monomer concentration in the particles with parameter estimation or not (n)) [45, 139]</p> <p>Heat of reaction and heat transfer coefficient in polymerization reactors [135, 141, 142]</p>	<p>Computationally fast, reiterative and constrained algorithms are more robust, multi-rate (having fast/frequent and slow measurements can be handled) / Trial and error required for tuning the process and observation model covariance errors, model linearization required</p>
High-gain Luenberger like observers or non-linear state observers [132, 144]	<p>Solution polymerizations (concentration and molecular weight) with M_w measurement [145]</p> <p>Emulsion polymerization (conversion, composition and parameter estimation, n [146 147])</p> <p>Heat of reaction and heat transfer coefficient in polymerization reactors [148–150]</p>	<p>Computationally fast, multi-rate schemes also reported, less tuning parameters / Tuning required</p>
Optimization formulations [151, 152]	<p>Emulsion polymerization processes (for monitoring and control purposes, parameter estimation included) [104, 140, 152, 153]</p>	<p>Constraints can be easily handled, parameter and state estimation / Computationally more demanding, this requirement can be reduced if a moving horizon is used</p>

Correction: The correction calculates the filter gain (K_k), which corrects the prediction made by the model:

$$K_k = P_{k/k-1} H_{k/k-1}^T (H_{k/k-1} P_{k/k-1} H_{k/k-1}^T + R)^{-1} \quad (8.12)$$

$$\hat{x}_{k/k} = \hat{x}_{k/k-1} + K_k (y_k - h(\hat{x}_{k/k-1})) \quad (8.13)$$

$$P_{k/k} = (I - K_k H_{k/k-1}) P_{k/k-1} \quad (8.14)$$

with

$$H_{k/k-1} = \left. \frac{\partial h}{\partial \hat{x}} \right|_{\hat{x}_{k/k-1}} \quad (8.15)$$

where Q and R are the covariance matrices for the model error and the measurement error, respectively, which are usually used as tuning parameters for the optimum convergence of the state estimates.

As discussed in Section 8.3.2, in addition to the fast and frequent on-line measurement, some measurements may be available at infrequent and/or irregular times and with significant delays. For example, there may be a combination of MWDs and PSDs measured off-line by chromatographic methods and monomer concentrations measured in real time by spectroscopic methods. In these cases, the so-called multi-rate state estimators may be applied. In these estimators, the fast measurements are used to estimate the state variables that are observable, while estimation of the non-observable variables is obtained in open-loop mode. When the (infrequent) measurement becomes available, the close-loop estimator is used. Ellis *et al.* [102] and Mutha *et al.* [108] used a multi-rate EKF to estimate monomer conversion and average molecular weights in the solution polymerization of MMA.

A way of improving the performance of state estimators in the presence of modeling errors and unmeasurable disturbances is to use adaptive estimation schemes. This involves the simultaneous estimation of state variables and model parameters. One approach is to assume a model for each parameter (usually random walk type models are used) and then to estimate the parameters together with the state variables by using a state estimator such as an EKF or non-linear high gain observer [139, 154, 155].

8.4 Safety

8.4.1 Introduction

The primary causes of accidents in the chemical industry are technical failures, human failures and the chemical reaction itself (due to lack of knowledge of the thermochemistry and the reaction kinetics) [156]. As discussed previously, polymerization reactions are subject to thermal runaway, so that it is not surprising to learn that polymerization reactions (64 from 134 cases) are more prone than other processes to serious accidents [157]. Among the polymerization processes, the phenol-formaldehyde resin production seems to be the worst case, although incidents have been reported for vinyl chloride, vinyl acetate and polyester resins polymerization processes.

In order to prevent accidents, the main areas of concern should be maintenance of equipment and facilities, qualification and training of the operators, better knowledge of the thermochemistry and reaction kinetics and automation and on-line control, in order to prevent technical and human failure. Advanced control strategies for polymerization reactors should aim at maximizing production, obtaining a product of consistent quality and simultaneously avoiding unsafe situations [158]. Therefore, advanced control schemes should always consider safety as a hard constraint during the process optimization step. This certainly requires the accurate understanding and prediction of the thermochemistry of the polymerization reaction.

8.4.2 Risk parameter assessment

Runaway reactions occur when the rate of heat removal is lower than the rate of heat generation. Therefore, the worst-case scenario is obtained when no heat is removed and all of the energy released by reaction is used for heating the reaction medium (when the polymerization reaction proceeds under adiabatic conditions). For this reason, adiabatic reaction calorimetry is best suited to study the thermochemistry and kinetics of polymerization under runaway conditions. Rates of energy release and dynamic trajectories of reactor temperature and reactor pressure can be measured during the reaction. As a consequence, the onset temperature of the runaway, the rate of reaction, the adiabatic temperature increase, the reaction enthalpy and the maximum reactor temperature and reactor pressure can be readily obtained. Moreover, a wide range of temperatures (up to 500°C) and pressures (upto 170 atm) can be reached using commercial equipments. Previous knowledge of side reactions is not needed because experimental heat of reaction is obtained, and not calculated with the help of a reaction model.

In adiabatic calorimetry, the thermal inertia of the test cell, Φ , is a key factor

$$\Phi = 1 + \left(\frac{m_{\text{reactor}} c_{\text{preactor}}}{m_{\text{medium}} c_{\text{pmedium}}} \right) \quad (8.16)$$

where m_{reactor} and c_{preactor} are the mass and the specific heat of the reactor (test cell), and m_{medium} and c_{pmedium} are the mass and the specific heat of the reaction medium. When the thermal inertia (Φ , phi-factor) is high, an important fraction of the heat of the reaction is used for heating the reactor, and hence reactions are not carried out under adiabatic conditions. Under truly adiabatic conditions, thermal inertia equals 1. In industrial reactors, the phi-factor is usually equal or lower than 1.05, so that less than 5% of the heat released is used for heating the reactor walls. Examples of this type of reactor are the VSP2 (Vent Sizing Package 2, Fauske and Associates, Inc., $\Phi = 1.035\text{--}1.055$) and the PHI-TEC II (HEL Calorimeters, $\Phi = 1.05$). Good equipment should allow for controlled heating of the reactor content until the reaction becomes self-sustained. This means that the reaction self-heating rate (measured as K min^{-1}) is higher than an arbitrary onset criterion, which depends on the sensitivity of the equipment. This occurs at the so-called *onset temperature* of the reaction, T_{onset} . As soon as the onset temperature is detected, the equipment should switch to the adiabatic mode and continuously monitor the evolution of reactor temperature and pressure.

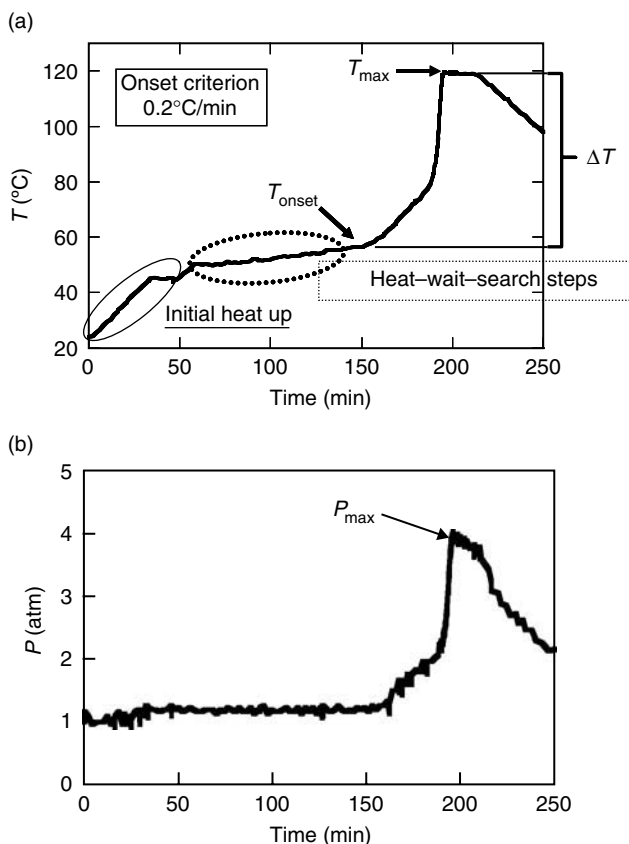


Figure 8.6 Time evolution of (a) temperature and (b) pressure during an adiabatic emulsion polymerization reaction of VAc/BA/AA (78.5/18.5/3) [159].

Figure 8.6 illustrates typical temperature and pressure profiles obtained in an adiabatic calorimeter during a polymerization reaction (VAc/BA/AA emulsion copolymerization of 50 wt% solids content [159]). The onset temperature of the runaway (T_{onset}) is calculated during the heat-wait-search steps. If during the wait step the reaction is self-heated at a rate higher than $(dT/dt)_{\text{onset}}$ (0.2 K min^{-1} in the experiment shown in Figure 8.6), that temperature is considered as T_{onset} . Note that different equipments can give different onset temperatures for the same reaction, and therefore this data must be used with care [160]. T_{onset} is used as reference to calculate the adiabatic temperature increase, ΔT of each experiment. Thus ΔT is readily calculated from the monitored maximum temperature as follows:

$$\Delta T = T_{\text{max}} - T_{\text{onset}} \quad (8.17)$$

T_{max} and P_{max} are the maximum temperature and pressure reached due to the runaway reaction and are obtained from the maximums on the P and T versus time plots (see Figure 8.6).

The dependence of the risk parameters on process variables such as the concentrations of monomer, polymer, initiator or catalyst, solvent, water and particle size (in emulsion) and MWD are of paramount importance to establish the safe operation regions of polymerization reactors, and furthermore to develop optimal control strategies under safe conditions. The maximum pressure, P_{\max} , and maximum temperature, T_{\max} , achieved during the runaway depends on the process conditions (e.g., the higher the amount of monomer in the reactor and the process temperature, the higher P_{\max} and T_{\max}). Also important is the rate at which the runaway reaches the maximum pressures and temperatures. This rate will provide an indication of the time that the operator/control system of the plant has to react in order to keep the polymerization under safe conditions.

In order to run and maintain a process under safe conditions even in the event of a system failure, the pressure build-up during the polymerization process must be lower than the maximum pressure that the reactor can withstand. Therefore, the correlation between reactor pressure, reactor temperature and the other operation conditions of the system is of paramount importance for both the development of control strategies and the design of countermeasures and relief systems in case of a runaway.

An example of the safety limits for the VAc/BA/AA emulsion polymerization system is shown in Figure 8.7. The plot is constructed assuming that the polymerization is carried out at 80°C (T_{work}) and that the maximum temperature allowed to run the process, T_{limit} , is 100°C . This temperature must be calculated according to the following points:

- (1) The maximum pressure that the reactor can withstand must be known; this is usually a design constraint that will depend on the material used to build the reactor and the thickness of the wall, among other technical considerations. If a relief system has been incorporated, the pressure at which the reactor will be vented will determine the maximum pressure.

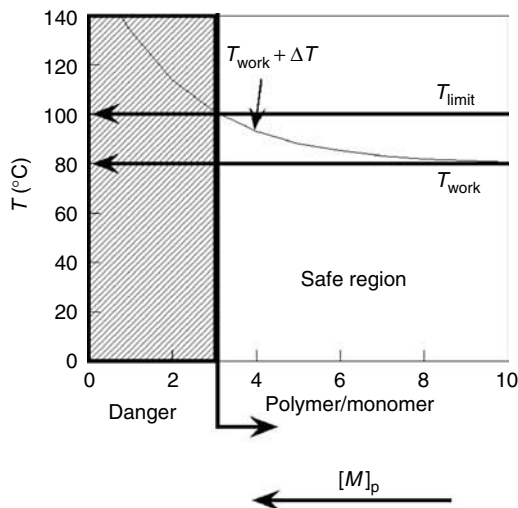


Figure 8.7 Safety regions for a VAc/BA/AA emulsion polymerization. Polymerization temperature is 80°C and the maximum temperature allowed for the process is 100°C .

- (2) The thermochemistry and kinetics of the polymerization will allow the dependence of the pressure of the system as a function of the temperature to be experimentally determined, with the reagents present during the polymerization (these include monomer, polymer, solvent or water if it is an emulsion or suspension polymerization, and also the volatile compounds that can be formed during the process or during the runaway; for instance, *t*-butanol is formed in the polymerization of butyl acrylate and formaldehyde in VAc containing recipes, to name a few).

The graph shows that the region of polymer/monomer ratio smaller than 3 will not be safe. In other words, if higher monomer concentrations are used and the cooling system fails there is a risk of exceeding the T_{lim} temperature ($T_{work} + \Delta T > T_{lim}$). Above the limit $polymer/monomer = 3$, the process can be operated safely because the operating line $[T_{work} + \Delta T]$ does not exceed the limit of the safe operation temperature. These data must be included in the optimization as a constraint to correctly compute safe profiles of the manipulated variables (monomers, CTAs and initiators) that would ensure the production of the polymer with the required quality under safe process conditions.

8.5 Optimum operation design and setpoint specification

8.5.1 Problem definition and goals

Optimization of reactor operation policy is of paramount importance if improvement of product quality and increase of business profits are sought. In very specific terms, optimization of the reactor operation conditions is equivalent to producing the maximum amount of polymer product, presenting the best possible set of end-use properties, with minimum cost under safe and environmentally friendly conditions. This optimum solution is almost always a compromise. Increase of polymer productivity is usually obtained with the increase of the operational costs (increase of reactor volumes, reaction temperatures and reaction times, for instance). Besides, the simultaneous improvement of different end-use properties is often not possible (the improvement of mechanical performance is usually obtained through increase of molecular-weight averages, which causes the simultaneous increase of the melt viscosity and decrease of product processibility). Therefore, the optimization can only be performed in terms of a relative balance among the many objectives that are pursued.

In formal mathematical terms, the design of the optimum operation policy requires the definition and minimization of an objective function, in the form:

$$\text{Min}_u \{F(\mathbf{y}, \mathbf{x}, \mathbf{u}, \boldsymbol{\alpha}; \mathbf{x}^d, \mathbf{y}^d)\} \quad (8.18a)$$

$$\mathbf{x} = g(\mathbf{u}, \boldsymbol{\alpha}, t) \quad (8.18b)$$

$$\mathbf{y} = h(\mathbf{x}, t) \quad (8.18c)$$

$$\mathbf{x}_{min} \leq \mathbf{x} \leq \mathbf{x}_{max} \quad (8.18d)$$

$$\mathbf{y}_{min} \leq \mathbf{y} \leq \mathbf{y}_{max} \quad (8.18e)$$

$$\mathbf{u}_{\min} \leq \mathbf{u} \leq \mathbf{u}_{\max} \quad (8.18f)$$

$$\Delta \mathbf{u}_{\min} \leq \Delta \mathbf{u} \leq \Delta \mathbf{u}_{\max} \quad (8.18g)$$

where F stands for the objective function. The term α represents a set of model parameters (kinetic parameters, physico-chemical properties, etc.) and the remaining variables have been defined before. The superscript d represents sets of desired values, which depend on the particular final applications that are sought. Equations 8.18d and 8.18e indicate that certain hard constraints must be obeyed for actual implementation of the designed operation strategy. For instance, reactor temperatures should not surpass a maximum temperature value for safety reasons (Equation 8.18d, Figure 8.7). Similarly, it may be necessary to specify a minimum melt-flow index if a certain injection-molding machine is to be used to produce the final injected pieces (Equation 8.18e). Besides, the reboiler that is available at the plant site cannot produce more than a certain flow rate of heating steam (Equation 8.18f). Finally, the operation pressure of the reboiler cannot be changed too fast, because its operation depends on the characteristics of the heating device used to heat the water (Equation 8.18g). As shown for batch MMA solution polymerizations [161], inequality constraints may be of paramount importance for definition of the final problem solution, so that the importance of process constraints should not be minimized in real applications. Unrealistic operation policies are generated very frequently when process constraints are neglected.

Based on the previous discussion, the design of the optimum operation policy (computation of \mathbf{u}) requires the minimization of an objective function that is subject to equality and inequality constraints. It is important to emphasize that \mathbf{x} , \mathbf{y} , \mathbf{u} , α , \mathbf{x}^d and \mathbf{y}^d may (or may not) depend on time, depending on the particular analyzed problem. It is also important to observe that initial conditions required to solve dynamic problems (as during the analysis of batch reactions) can be included in the set \mathbf{u} of manipulated variables. Simulation platforms have been proposed and used to solve these complex optimization problems and they are robust enough to cope with unstable dynamic trajectories and large polymerization reactor models [38, 162–164].

The objective function F is usually presented as a weighted sum of deviation values, in the form:

$$F(\mathbf{y}, \mathbf{x}, \mathbf{u}, \alpha; \mathbf{x}^d, \mathbf{y}^d) = \sum_{i=1}^{NX} \lambda_i^x (x_i - x_i^d)^2 + \sum_{i=1}^{NY} \lambda_i^y (y_i - y_i^d)^2 + \sum_{i=1}^{NX} C_i^x x_i + \sum_{i=1}^{NY} C_i^y y_i + \sum_{i=1}^{NU} C_i^u u_i \quad (8.19)$$

where the first two terms of the summation weigh the relative importance of deviations from desired specification values (usually based on technical considerations) and the remaining terms weigh the relative importance of the obtained results (usually based on economical considerations). NX , NY and NU stand for the number of analyzed state variables, end-use properties and manipulated variables, respectively. In dynamic problems, the final batch time (or transition time, during grade transitions) can be explicitly incorporated as an additional state variable into Equation 8.19. In this case, the following equation has to be

added to the set of model equations:

$$\frac{dx_{NX}}{dt} = 1, \quad x_{NX}(0) = 0 \quad (8.20)$$

Equation 8.19 can be used for analysis of both steady-state and dynamic optimization problems. In time-varying processes, actual implementation of optimum operation policies requires discretization of the dynamic trajectories [165]. In these cases, the vectors of state variables, end-use properties and manipulated variables include the set of discretized values along the whole dynamic trajectory. This means, for example, that NX equals the number of state variables multiplied by the number of discretized intervals (or sampling intervals). Finally, it must be clear that some of the weighting values can be equal to zero, which means that some of the available data may not be relevant for operation of the analyzed polymerization problem.

Although Equation 8.19 is frequently used for design of optimum operation policies, it can be criticized for many reasons. For instance, Equation 8.19 puts much emphasis on the desired values. Assuming that the weighting values are constant, operation strategies that are able to reduce differences between desired and obtained values can always be regarded as improved operation strategies. However, in practical terms it may be difficult to discriminate between the performances of different proposed operation strategies when the observed differences are small. This happens because of the unavoidable errors associated with the experimental characterization of the final polymer properties and because of the unavoidable model inaccuracies. Therefore, when the performances of different operation strategies are within the experimental and modeling inaccuracies, then the distinct operation strategies may be regarded as equivalent. In these cases, Equation 8.19 may be modified by defining the weighting factors as functions of the measured values, in the form:

$$F(\mathbf{y}, \mathbf{x}, \mathbf{u}, \boldsymbol{\alpha}; \mathbf{x}^d, \mathbf{y}^d) = \sum_{i=1}^{NX} \lambda_i^x(x_i)(x_i - x_i^d)^2 + \sum_{i=1}^{NY} \lambda_i^y(y_i)(y_i - y_i^d)^2 + \sum_{i=1}^{NX} C_i^x(x_i)x_i + \sum_{i=1}^{NY} C_i^y(y_i)y_i + \sum_{i=1}^{NU} C_i^u(u_i)u_i \quad (8.21)$$

with the weighting values for state variables written as

$$\lambda_i^x(x_i) = \begin{cases} \frac{(x_i - x_i^{\min})^2}{(x_i - x_i^d)^2}, & x \leq x_i^{\min} \\ 0, & x_i^{\min} \leq x_i \leq x_i^{\max} \\ \frac{(x_i - x_i^{\max})^2}{(x_i - x_i^d)^2}, & x \geq x_i^{\max} \end{cases} \quad (8.22)$$

Equation 8.21 allows for definition of target regions, instead of target values. Target regions may be defined as regions where the process performance can be regarded as equivalent. This may be interesting when small deviations from target values cannot be observed at plant site or are unimportant for the particular problem being analyzed. As a result, operation strategies that lead final values to the target regions (instead of target values) are considered to be similar. Equation 8.22 can be easily extended for the remaining weighting factors.

A second important source of criticism is the definition of the weighting values (or functions) in Equations 8.19 and 8.21, as they define the relative importance of the many analyzed process variables. When many distinct objectives are pursued simultaneously, definition of weighting values may be very difficult and sometimes may sound completely arbitrary. As a consequence, one may be tempted to solve the optimization problem for different sets of weighting values and to compare the different sets of calculated optimum operation strategies and obtained solutions (product properties). However, selection of the best operation policy (as a single operation policy must be selected for implementation at plant site!) may be very difficult in this case, as improvement of some objectives is obtained at the expense of others. As a matter of fact, selecting the weighting values and/or objective functions (and, therefore, the relative importance of the distinct pursued objectives) is one of the most important roles of the plant manager.

The multi-objective optimization problem can be put into more formal mathematical grounds if the *multi-objective optimization theory* is used to define the setpoint trajectory [166–169]. In this case, the existence of multiple objective functions is considered explicitly, so that Equation 8.21 can be written as

$$F_k(\mathbf{y}, \mathbf{x}, \mathbf{u}, \boldsymbol{\alpha}; x^d, y^d) = \sum_{i=1}^{NX} \lambda_{k,i}^x(x_i)(x_i - x_i^d)^2 + \sum_{i=1}^{NY} \lambda_{k,i}^y(y_i)(y_i - y_i^d)^2 + \sum_{i=1}^{NX} C_{k,i}^x(x_i)x_i \\ + \sum_{i=1}^{NY} C_{k,i}^y(y_i)y_i + \sum_{i=1}^{NU} C_{k,i}^u(u_i)u_i \quad k = 1, \dots, NF \quad (8.23)$$

where NF stands for the different objective functions that are analyzed simultaneously. Obviously, it is not possible to minimize all distinct objective functions simultaneously. For this reason one has to rely on a different concept to provide a solution for the proposed problem. A possible solution for this problem involves the definition of the Pareto sets. A Pareto set is a set of non-minimal operation points where improvement of each of the objective functions is always obtained at the expense of at least one of the others. Figure 8.8 illustrates this point for a simple optimization problem defined in the one-dimensional space. It can be observed in Figure 8.8 that the distinct minima of the two analyzed objective functions are placed at different values of the decision variable. Simultaneous improvement of the distinct objective functions is not possible in the interval limited by the two distinct minima; however, it is clear that the proposed solution for the decision variable should be placed inside this interval, which constitutes the Pareto set for this problem. It is also clear that the proposed solution does not necessarily minimize any of the analyzed objective functions, so that the final solution can only be obtained through detailed analysis of the proposed multi-objective optimization problem. For multidimensional problems, the Pareto sets may constitute surfaces in subspaces of relative high dimensions and may be difficult to visualize, requiring the use of more involved image analysis techniques.

It is important to observe that Pareto sets usually define a region of operating variables; however, a single operation policy should still be selected for real implementation. Therefore, the user still has to rely on some sort of arbitrary procedure to select the best operation policy among the possibly infinite number of solutions that constitute the Pareto set. Besides, solutions in the Pareto set can indeed lead to very poor reactor operation, as none of the objectives is reached optimally.

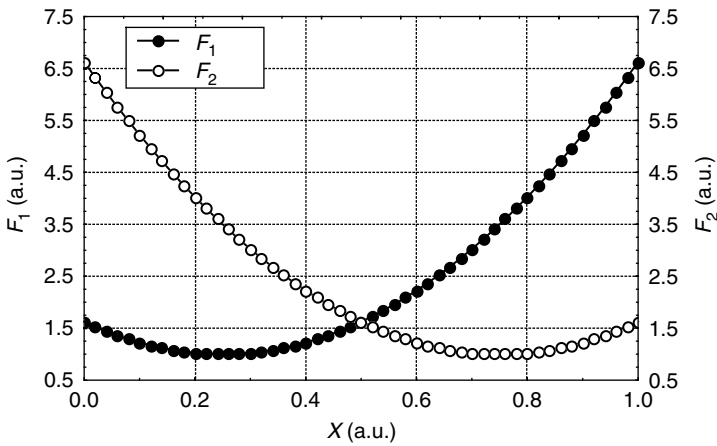


Figure 8.8 Multi-objective optimization problem. The Pareto set is constituted by the interval between the two distinct minima (a.u. stands for arbitrary units).

Multi-objective optimization procedures were used for the simultaneous maximization of monomer conversion and minimization of side products during low-density polyethylene polymerizations performed in tubular reactors under steady-state conditions [170]. Genetic algorithms were used to compute the Pareto sets. Multi-objective optimization procedures were also used for the simultaneous maximization of molecular weight averages and minimization of batch times in epoxy semibatch polymerizations [171]. In this case, monomer feed rates were used as the manipulated variable.

8.5.2 Numerical solution of the optimization problem

In order to obtain the solution of Equation 8.19 (or similar problems defined in Equations 8.21 and 8.23), non-linear minimization numerical techniques are required, as analytical solutions are not available for real polymerization problems. A large number of numerical procedures can be used to solve the proposed problem, although they can be grouped generically into two sets. In the first set one may include SQP (sequential quadratic procedures) and related techniques [165]. According to these numerical procedures, an initial guess for the searched solution has to be initially provided by the user. A quadratic approximation of the objective function is then constructed (which may incorporate the equality and inequality constraints explicitly or implicitly) and the minimum of the quadratic approximation is used as the next guess. The procedure is repeated iteratively in the form:

$$u_{k+1} = u_k - H_k^{-1}(\nabla F)_k \quad (8.24)$$

where the index k stands for the iteration number, H is the Hessian matrix of the objective function, defined as

$$[H_{i,j}]_k = \left[\frac{\partial^2 F}{\partial u_i \partial u_j} \right]_k \quad (8.25)$$

where i and j refer to the i -th and j -th components of the vector of manipulated variables \mathbf{u} at iteration k , and

$$[\nabla F_i]_k = \left[\frac{\partial F}{\partial u_i} \right]_k \quad (8.26)$$

As it may be hard (or even impossible) to compute the derivatives of F with respect to the manipulated variables, approximations are normally provided for both H and ∇F in Equations 8.25 and 8.26. (The use of numerical procedures based on variational principles was very popular in the past [161]. In order to solve variational problems numerically, standard Newton–Raphson procedures are generally used to solve the resulting two-boundary value problem that is associated with the variational formulation. For this reason, optimization of dynamic problems based on variational principles is also included in this set of SQP-related numerical techniques.)

In the second group of numerical techniques used to solve the optimization problem one may include random search algorithms (RSAs). RSA proposes the use of direct search routines, based on the direct evaluation of F in different regions of the space of manipulated variables, in order to provide the searched problem solution. Basically, a heuristic procedure is used to generate test points in a pre-defined search region, where F is evaluated. The best results are used to redefine the search region and the procedure is repeated until convergence. Test points are almost always defined at random (Monte Carlo techniques) or through combination of deterministic and random rules (simulated annealing, genetic algorithms, Swarm optimization, Taboo search, etc.) [164, 166, 167, 169, 172–174]. Although the number of proposed RSA is relatively large, based on available current knowledge it is not possible to unequivocally select any of the available RSA as the best one.

The use of RSA is becoming more popular in the literature for many reasons. First, computer codes are short, simple, and can be debugged and implemented very easily. Second, RSA can handle all sorts of objective functions (discontinuous, discrete, etc.) without using any sort of complex mathematics. Third, equality and inequality constraints can be inserted into the problem through very simple numerical procedures. For instance, if a trial point does not satisfy a certain constraint, it can simply be discarded from the set of trial points. Finally, RSA do not require the definition of an initial guess. The main disadvantage of RSA, when compared to SQP, is the usually much larger number of objective function evaluations (and the longer simulation times) that are necessary to reach the searched solution. For this reason, hybrid methods, which combine the use of RSA and SQP, have also been used to solve optimization problems [30]. In this case, RSA are used to provide a set of initial guesses for SQP, allowing for acceleration of RSA simulations and for reduction of SQP sensitivity to initial guesses. Despite that, the fast development of computer technology encourages the use of RSA techniques in actual production environments, including real time and control applications.

The performances of SQP and RSA were compared during the optimization of grade transitions in solution MMA polymerizations performed in CSTRs [174]. As it was shown that multiple optima were possible, the use of RSA is advantageous because it leads to the global optimum solution more frequently than the SQP and is less sensitive to initialization of the numerical procedure.

A numerical technique that has become very popular in the control field for optimization of dynamic problems is the IDP (iterative dynamic programming) technique. For application of the IDP procedure, the dynamic trajectory is divided first into NS piecewise constant discrete trajectories. Then, the Bellman's theory of dynamic programming [175] is used to divide the optimization problem into NS smaller optimization problems, which are solved iteratively backwards from the desired target values to the initial conditions. Both SQP and RSA can be used for optimization of the NS smaller optimization problems. IDP has been used for computation of optimum solutions in different problems for different purposes. For example, it was used to minimize energy consumption and byproduct formation in poly(ethylene terephthalate) processes [176]. It was also used to develop optimum feed rate policies for the simultaneous control of copolymer composition and MWDs in emulsion reactions [36, 37].

8.5.2.1 Illustrative example

Assume that an optimum feed flow rate trajectory is searched for the emulsion copolymerization problem described in Section 8.3.3. In this case, also assume that the copolymer composition should be constant throughout the batch. Also assume that the final monomer conversion should be as close as possible to 1, to allow for minimization of the residual monomer. In order to achieve the control objectives, one is allowed to manipulate the feed flow rate of monomer 1, which is assumed to be the most reactive monomer, and the initial monomer concentrations. In this particular case, one may write the following objective function:

$$F = \sum_{i=1}^{NU} \lambda_i \left(\frac{R_{p1}(t_i)}{R_{p2}(t_i)} - Y_p^2 \right)^2 + \left(\frac{M_1(t_0) + M_2(t_0) + \sum_{i=1}^{NU} F_{1in}(t_i) - M_1(t_{NU}) - M_2(t_{NU})}{M_1(t_0) + M_2(t_0) + \sum_{i=1}^{NU} F_{1in}(t_i)} - 1 \right)^2 \quad (8.27)$$

Equation 8.27 assumes that the batch time t_F can be discretized into NU time intervals, where the feed flow rate is kept constant; Y_p represents the desired copolymer composition; λ_i are the weighting functions or the relative importance of controlling the instantaneous copolymer composition, when compared to controlling the final residual monomer. (As discussed previously, the proposed control strategy may lead to thermal runaway, if serious heat transfer limitations are present. If this is the case, the energy balance must be included in the model and constraints should be imposed on temperature values and temperature profiles.) The process model can be written as

$$\frac{dM_1}{dt} = F_{1in} - R_{p1}V, \quad M_1(0) = M_{10} \quad (8.28a)$$

$$\frac{dM_2}{dt} = -R_{p2}V, \quad M_2(0) = M_{20} \quad (8.28b)$$

where M_{20} is assumed to be known, in order to guarantee the production of a certain amount of polymer material. The remaining mass balance equations can be written as

presented before. According to Equation 8.18, the set of manipulated control variables is

$$\mathbf{u}^T = [M_{10} \quad F_{\text{lin}}(t_1) \quad F_{\text{lin}}(t_2) \quad \cdots \quad F_{\text{lin}}(t_{NU})] \quad (8.29a)$$

while the set of end-use properties is

$$\mathbf{y}^T = \left[\begin{array}{cccc} \frac{R_{p1}(t_1)}{R_{p2}(t_1)} & \frac{R_{p1}(t_2)}{R_{p2}(t_2)} & \cdots & \frac{R_{p1}(t_{NU})}{R_{p2}(t_{NU})} \\ \frac{M_1(t_0)+M_2(t_0)+\sum_{i=1}^{NU} F_{\text{lin}}(t_i)-M_1(t_{NU})-M_2(t_{NU})}{M_1(t_0)+M_2(t_0)+\sum_{i=1}^{NU} F_{\text{lin}}(t_i)} & & & \end{array} \right] \quad (8.29b)$$

and the set of state variables comprises the masses of all chemical species at the distinct sampling intervals inside the reactor.

The optimum can be obtained with the help of RSAs. In this case, \mathbf{u} is made equal to different N_{GUESS} trial vectors. The mass balance equations can then be solved with the help of numerical integration procedures and the results can be used for evaluation of the N_{GUESS} distinct values of F in Equation 8.27, for each distinct trial vector. The best trial vector is the one that leads to the lowest value of F . After identification of the best control strategy among the N_{GUESS} trials, a new set of trial vectors can be generated in the vicinities of the best control strategy. The procedure can be repeated until convergence is achieved.

After solving the optimization problem, the user obtains the optimum operation policy (\mathbf{u}^{opt}) and the optimum reference values for state variables (\mathbf{x}^{opt}) and end-use properties (\mathbf{y}^{opt}). These values can be used for implementation of open-loop operation of the polymerization reactors and for closed-loop control purposes, as discussed in the following section.

8.5.3 Use of experimental design techniques for optimization

The discussion presented in the previous sections assumes that a process model is available. However, optimization of process operation is also possible when process models are not available. In this case, one must rely on available experimental process data and/or empirical modeling approaches. For instance, the process performance can be mapped within the experimental region of interest with the help of experimental design techniques. Experiments are performed in accordance with the proposed experimental design and empirical cubic models (or other types of empirical models) are fitted to the obtained experimental data. Then, the empirical models can be used to provide the searched optima. This type of experimental design-based optimization procedure was performed to optimize the operation of fermentors used for production of bacterial polyesters [177], as it is very difficult to develop a fundamental model for bacterial polymerizations. In this particular case, the medium composition was manipulated to allow for maximization of polymer production and minimization of the batch time.

8.5.4 Heuristic methods

In order to control a process, it is necessary first to define the desired control reference or setpoint. The setpoint may be computed as the optimum reference trajectories ($\mathbf{u}^{\text{set}} = \mathbf{u}^{\text{opt}}$),

as described in the previous section, or can be defined based solely on heuristic procedures and previous experience (\mathbf{u}^{set} is not the solution of an optimization problem) [142, 178]. In the first case, optimum operation of the polymerization process and attainment of a balanced set of final performance indices can be obtained. In the second case, optimal operation cannot be guaranteed (which is not equivalent to saying that reaction cannot be controlled or that the process performance is not good!). For instance, for the illustrative example in the previous section, one might be tempted to define

$$\mathbf{u}^{\text{set}} = \left[0 \quad \frac{\alpha M_{20}}{t_F} \quad \frac{\alpha M_{20}}{t_F} \quad \cdots \quad \frac{\alpha M_{20}}{t_F} \right] \quad (8.30)$$

which assumes that the most reactive monomer is not present in the initial charge and should be fed into the reactor at constant flow rate.

Very frequently non-optimal setpoint trajectories are used for controlling reactor temperatures in batch reactors [25, 39, 179, 180]. Reactor temperatures may be allowed to increase from ambient temperatures up to a maximum temperature value, in order to use the heat released by reaction to heat the reaction medium and save energy (reduce energy costs). The temperature increase is almost always performed linearly, because of hardware limitations and simplicity of controller programming. After reaching the maximum allowed temperature value, reactor temperature is kept constant for a certain time interval, for production of polymer material at isothermal conditions. At the end of the batch, the reaction temperature is increased in order to reduce the residual monomer content of the final resin, usually with the help of a second catalyst. Heuristic optimum temperature trajectories were also formulated for batch polymerizations of acrylamide and quaternary ammonium cationic monomers, in order to use the available heat of reaction [181]. The batch time was split into two batch periods: an isothermal reaction period and an adiabatic reaction period.

Semibatch reactions are performed very frequently for control of average molecular weights, copolymer compositions and PSDs. In this case, a feed stream containing CTAs, comonomer mixtures and/or emulsifiers is used to provide the control action [36, 55, 142, 182]. Many times, although, the total amount of feed is distributed evenly along the batch, in the form of a constant feed flowrate [36]. However, in most cases this kind of operation does not provide the desired control solution, which normally is the production of polymer material with constant and uniform properties. Even when this operation approach can be justified on sound theoretical grounds, as when it is used for control of copolymer composition in starved seeded emulsion polymerizations, the reference trajectory should not be regarded as optimum, because it generally leads to longer polymerization times (and lower polymer productivities) [36, 142].

Similarly, agitation speeds are normally kept constant throughout the batch during suspension polymerizations. However, it is well-known that polymer characteristics change a lot along the batch, causing the continuous and non-linear drift of average particle sizes and broadening of PSDs. Although manipulation of agitation speeds along the batch leads to much more complex process operation, the variation of agitation speeds along the batch seems to contribute with production of more uniform particle size distributions in suspension polymerizations [50, 126]. Near infrared spectroscopy and electrical resistance tomography measurements can be used for determination of the leading moments of PSDs in suspension polymerization reactions in real time, providing the means for controlling the average particle size and the distribution width through manipulation of the agitation

speed [50, 183]. These techniques allow for production of polymer beads with more uniform sizes.

Heuristic control trajectories are also analyzed during grade transitions in continuous gas-phase propylene polymerizations [184]. It is shown through simulations that production of off-spec polymer material can be reduced and that plant stability can be improved when some process states (solids level, reactor temperature, reactor pressure, etc.) are kept constant during the transient period. Similar grade transition analysis was performed for gas-phase ethylene polymerizations aiming at the reduction of particle melting and agglomeration [185], while keeping reaction temperature at well-defined and narrow operation limits.

A control technique based on high-frequency pressure measurements was developed and implemented to avoid hydrodynamic instabilities in continuous olefin slurry-loop reactors [186]. The obtained high-frequency pressure patterns are compared to typical process responses and then used to classify the status of the plant operation. The idea is that pressure fluctuations that do not follow the standard pattern indicate some sort of process instability. When hydrodynamic instabilities are detected, monomer flow rates and/or reactor temperatures are manipulated to reduce the polymer density and the reaction rates and reduce the risks of plant shutdown. Similar procedures can be used for detection and correction of abnormal plant operation in suspension [187] and emulsion [188] polymerizations with the help of Raman and near infrared spectroscopy techniques.

8.6 Calculation of the control action and control schemes

8.6.1 Open-loop control

After definition of the optimum operation policies, different strategies can be used for actual implementation at the polymerization plant. The simplest strategy is the implementation of \mathbf{u}^{opt} at the plant, without using any sort of feedback signal for \mathbf{x} and/or \mathbf{y} , for evaluation of the operation performance. In mathematical terms, one might define the implementation of open-loop control strategies in the form:

$$u_i(t) = u_i^{\text{set}}(t) = u_i^{\text{opt}}(t) \quad (8.31)$$

However, control variables are usually manipulated indirectly. For instance, one has to change the valve position to increase the flow rate through the reactor jacket. Similarly, one has to reduce the electrical resistance of the heating bath in order to increase the inlet temperature of the cooling fluid. For this reason, one may also define the open-loop control problem as

$$w_i(t) = f[u_i(t), u_i^{\text{set}}(t)] \quad (8.32)$$

where $w_i(t)$ is the actual signal provided by the control instrument, $u_i(t)$ is the current measured value of the manipulated variable and f is a function that describes how the instrument control signal can provide the desired control variable response. For instance, for the illustrative example of Section 8.5.4, a variac may provide the output voltage that feeds the process pump and allows for variation of the flow rates. A mass flowmeter can be

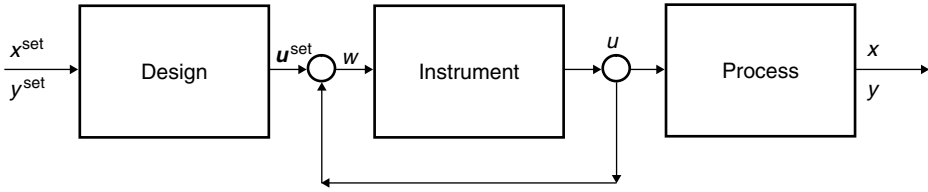


Figure 8.9 Schematic representation of the open-loop control strategy.

installed in-line to provide readings of the real flow rate, which can be compared to the desired setpoint values. When standard PI controllers are used to control the instrument performance, Equation 8.32 can be written as

$$w_i(t) = f[u_i^{\text{set}}(t)] + K_P[u_i(t) - u_i^{\text{set}}(t)] + K_I \int_0^t [u_i(\tau) - u_i^{\text{set}}(\tau)]d\tau \quad (8.33)$$

where f connects the desired variable response with the instrument control signal (usually presented as a linear calibration curve) and K_P and K_I are the proportional and the integral gains of the internal instrument controller, respectively. Figure 8.9 presents the schematic representation of the open-loop control approach.

Although open-loop strategies are very popular in the polymerization field (given the lack of robust and fast measuring techniques for real-time applications), this strategy does not guarantee that good results can indeed be obtained during actual operation. This is because polymerization reactions are subject to many disturbances and are very sensitive to small modifications of the reaction conditions. For instance, the presence of traces of contaminants (such as oxygen, water or carbon dioxide in Ziegler–Natta polymerizations) can cause dramatic effects on catalyst efficiencies. Open-loop strategies cannot eliminate process disturbances like this and often lead to inefficient process operation when unexpected problems occur. In the illustrative example of Section 8.5.2.1, the existence of contaminants in the monomer feed can cause sharp changes of the reaction rates and accumulation of monomer inside the reaction vessel, leading to undesired drift of copolymer composition and thermal runaway.

Open-loop control strategies were developed and implemented to allow for reduction of transition times during grade transitions in continuous high-impact styrene polymerizations [61]. Similar strategies were also used to control the MWDs in emulsion homopolymerizations and to control the copolymer composition and the MWDs simultaneously in non-linear emulsion polymerizations [36, 37, 182].

8.6.2 Closed-loop control

In order to cope with the frequent existence of process disturbances, closed-loop strategies can be implemented. If some of the state variables and/or end-use properties are monitored in real time, then the simplest closed-loop strategies can be implemented in the form:

$$x_i(t) = x_i^{\text{set}}(t) = x_i^{\text{opt}}(t) \quad (8.34a)$$

$$y_i(t) = y_i^{\text{set}}(t) = y_i^{\text{opt}}(t) \quad (8.34b)$$

which indicates that state variables and end-use properties should follow the optimum reference trajectories. As these variables are manipulated indirectly, one may also define the closed-loop control problem as

$$\mathbf{u}^{\text{set}}(t) = f_1[\mathbf{x}(t), \mathbf{x}^{\text{set}}(t), \mathbf{y}(t), \mathbf{y}^{\text{set}}(t)] \quad (8.35a)$$

$$w_i(t) = f_2[u_i(t), u_i^{\text{set}}(t)] \quad (8.35b)$$

where $\mathbf{u}^{\text{set}}(t)$ is updated in real time, to compensate for deviations between the measured and the setpoint values for both \mathbf{x} and \mathbf{y} .

In the illustrative example of Section 8.5.2.1, implementation of a closed-loop strategy requires that the instantaneous copolymer composition be evaluated with the help of some of the techniques described in Section 8.3. For instance, combination of calorimetric and spectroscopic techniques can allow for monitoring of monomer concentrations and reaction rates in real time. If copolymer compositions can be inferred in-line, then these values can be compared to the desired setpoint values for formulation of a closed-loop strategy.

Depending on how $\mathbf{u}^{\text{set}}(t)$ is updated, different control strategies can be formulated. For instance, when standard PI controllers are used to control the process performance [15], Equation 8.35 can be written as

$$\mathbf{u}^{\text{set}}(t) = f_3[\mathbf{x}^{\text{set}}(t)] + K_P^u[\mathbf{x}(t) - \mathbf{x}^{\text{set}}(t)] + K_I^u \int_0^t [\mathbf{x}(\tau) - \mathbf{x}^{\text{set}}(\tau)] d\tau \quad (8.36a)$$

$$w_i(t) = f_4[u_i^{\text{set}}(t)] + K_P^w[u_i(t) - u_i^{\text{set}}(t)] + K_I^w \int_0^t [u_i(\tau) - u_i^{\text{set}}(\tau)] d\tau \quad (8.36b)$$

where it is assumed that \mathbf{x}^{set} and \mathbf{y}^{set} are related through Equation 8.18c. In Equation 8.36, f_3 represents a process model or a calibration model that connects the desired values of \mathbf{x}^{set} and \mathbf{u}^{set} (actually, the results obtained after optimization of the process operation). Figure 8.10 presents the schematic representation of the closed-loop control approach.

If multiple variables are being monitored and controlled, the proportional and integral gains of the controller in Equation 8.36 are matrices. Nevertheless, controller gains are usually presented as diagonal matrices, by assuming that each controlled variable can be controlled independently through manipulation of a single control variable. This control strategy has been used successfully for the temperature control and improved distribution of reaction heat along the polymerization batch in PVC suspension polymerizations [25]. An algorithm based on Equation 8.36 was proposed to control the reactor temperature during batch polymerization reactions using fuzzy logic [189]. According to the proposed scheme, the proportional-integral-differential (PID) controller is activated only when

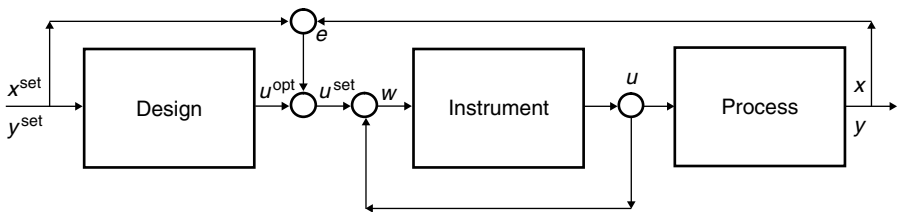


Figure 8.10 Schematic representation of the closed-loop control strategy.

a certain combination of rules is satisfied. As shown through simulation and experiments, the final controller performance can be much better than the one obtained with the use of standard PID control.

Selection and tuning of controller gains are performed most often with the help of process models and/or of heuristic procedures. When there is a strong coupling among many of the controlled and manipulated variables, tuning of controller gains may require the implementation of complex tuning techniques, based on decoupling of process responses. This is the case of most polymerization reactors. For instance, modification of catalyst concentration affects monomer conversion and consequently affects the reaction temperature, MWDs and copolymer compositions. As most polymerization variables are strongly coupled, empirical tuning of controller gains may constitute a cumbersome task. Besides, Equation 8.36a assumes that variables \mathbf{x} and/or \mathbf{y} are monitored, although most of the times monitoring of \mathbf{x} and/or \mathbf{y} can only be carried out with the help of a process model. Therefore, very frequently process models are developed for real-time applications.

8.6.2.1 Model-based closed-loop control

If a reliable process model is available and can provide solutions in real time, the model can be used to provide the corrected setpoint trajectories for \mathbf{u}^{set} without decoupling or empirical tuning of controller gains. If a process performance index is defined, then the controller action can be computed directly by inverting the process model. For instance, if it is assumed that the current process states $[\mathbf{x}(t), \mathbf{y}(t)]$ are known and that it is desired to reach the optimum reference trajectory after t_f time units, then Equations 8.18b and 8.35 can be written as

$$\mathbf{x}^{\text{set}}(t_f) = g[\mathbf{x}(t), \mathbf{u}^{\text{set}}(t), \boldsymbol{\alpha}(t)] \quad (8.37a)$$

$$w_i(t) = f_4[u_i^{\text{set}}(t)] + K_p^w[u_i(t) - u_i^{\text{set}}(t)] + K_I^w \int_0^t [u_i(\tau) - u_i^{\text{set}}(\tau)] d\tau \quad (8.37b)$$

Equation 8.37a can be inverted to provide the corrected trajectory \mathbf{u}^{set} . This can be performed with the help of standard Newton–Raphson routines or of RSA techniques. In the illustrative example, assuming that the initial states are known (evaluated through combination of spectroscopic and calorimetric techniques, for instance), then one may compute the feed flow rate value that allows for attainment of the desired composition after some time, with the help of the process model. In order to do that, as an explicit solution is not available, it would be necessary to calculate the model responses for different flow rate values and select the best result.

Inversion of Equation 8.37a implicitly resolves the strong coupling of the process variables and provides the correct tuning for control actions. The main adjustable tuning parameter of Equation 8.37a is t_f , the moment when reference and actual trajectories are expected to coincide with each other (usually called prediction horizon). If t_f is too short, computed control actions may be too strong; if t_f is too long, process performance may be very poor. Typically, t_f is between 1 and 5 sampling intervals, depending on the sampling frequency. Equations 8.37a and b constitute the core of the most used advanced control technique, which is known as non-linear model predictive control. Figure 8.11 presents the schematic representation of the model-based closed-loop control approach.

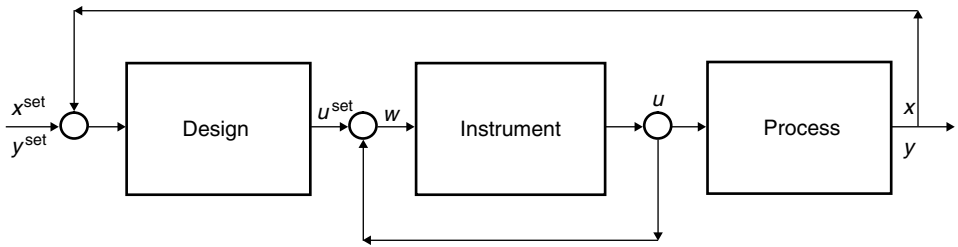


Figure 8.11 Schematic representation of the model-based closed-loop control strategy.

Model-based open-loop and closed-loop control strategies were developed and implemented to allow for control of PSDs in emulsion polymerization reactions [49, 190–192]. PSD was measured in real time using CHDF (capillary hydrodynamic fractionation) and control actions were provided by monomer, initiator and surfactant feed flow rates. An interesting application was developed for optimization of transitions in continuous solution processes [63]. In this case, monomer feed policies were designed to minimize the transition time during reactor load changes, while keeping polymer concentration and viscosity measurements close to target values. Model-based control strategies were also implemented for controlling the copolymer composition and the MWD in emulsion polymerizations [105]. Calorimetric measurements and state observers were used for evaluation of the process states in real time.

Near infrared spectroscopy was used to monitor concentrations and provide estimates of molecular weight averages in solution acrylic acid polymerizations [40, 193]. Then, geometric control (based on a simple model representation of the polymerization reactor) was used to design the monomer feed rates in real time in order to keep the concentrations and molecular weight averages at the desired levels. Near infrared spectroscopy was also combined with torque readings to allow for in-line monitoring of compositions and weight-average molecular weights in solution polyurethane reactors [194]. A process model was then used to indicate feed rate profiles for chain extender, in order to maximize the average molecular weight of the final polymer material and avoid the formation of gel.

A model-based closed-loop controller was designed for maximization of polymer production under safe process condition in emulsion copolymerization processes, while keeping the copolymer composition constant [195]. The interesting feature of the proposed controller was the use of a fuzzy model for design of the optimum reference trajectories.

8.6.2.2 Model-based closed-loop control and real-time optimization

Equations 8.36a–b and 8.37a–b assume implicitly that the optimum reference trajectories remain constant throughout the time. Although this does allow for removal of process disturbances and significant improvement of the process performance, the fact is that optimum reference trajectories depend on the initial states. As process disturbances modify the state variables (this is why $\mathbf{x}(t)$ and $\mathbf{x}^{\text{set}}(t)$ become different), it is certain that the optimum reference trajectory should also respond to unexpected process disturbances. Therefore, if $\mathbf{x}(t)$ and $\mathbf{x}^{\text{set}}(t)$ are not coincident, then $\mathbf{x}^{\text{set}}(t)$ should be recalculated in real time. Then, an improved version of the model predictive control scheme can be formulated

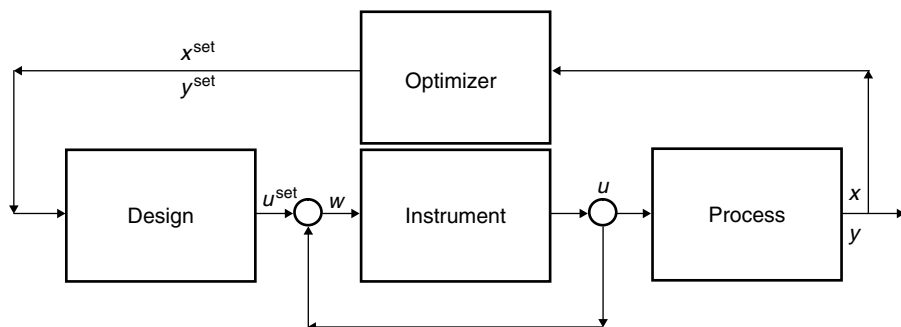


Figure 8.12 Schematic representation of the optimum model-based closed-loop control strategy.

if Equations 8.18, 8.19, 8.21, 8.22 are solved in real time whenever the vector of state variables is updated, after measuring and/or inferring of x and/or y . Figure 8.12 presents the schematic representation of the updated model-based closed-loop control approach.

In the illustrative example of Section 8.5.2.1, this closed-loop strategy is equivalent to reoptimizing the reactor operation after each sampling interval. For instance, after the first sampling interval, the states (masses of individual chemical components) can be estimated with the help of the process model and combination of calorimetric and spectroscopic techniques. Therefore, Equations 8.27–8.29 can be solved again, for a different set of initial conditions and a reduced number of time intervals (given the fact that one cannot modify the past implemented control actions), leading to a new set of optimum state variables, output variables and control variables. The new calculated values become the new setpoints. (In order to increase the speed of the process responses, one may certainly reduce the sampling time and increase the number of time intervals to perform the new optimization problem. It must be clear, although, that hardware and software constraints should be flexible enough to allow for modification of sampling parameters.)

An optimal predictive controller was developed and implemented to allow for maximization of monomer conversion and minimization of batch times in a styrene emulsion polymerization reactor, using calorimetric measurements for observation and manipulation of monomer feed rates for attainment of control objectives [31]. Increase of 13% in monomer conversion and reduction of 28% in batch time were reported. On-line reoptimization of the reference temperature trajectories was performed to allow for removal of heater disturbances in batch bulk MMA polymerizations [64]. Temperature trajectories were manipulated to minimize the batch time, while keeping the final conversion and molecular weight averages at desired levels. A reoptimization procedure was implemented to remove disturbances caused by the presence of unknown amounts of inhibitors in the feed charge [196]. In this case, temperature trajectories were manipulated to allow for attainment of specified monomer conversion and molecular weight averages in minimum time.

Near infrared spectroscopy was used for control of molecular weight averages and monomer conversion in styrene solution polymerizations [29]. Kalman filters were used to provide real-time estimates of the process states and initiator feed rates and reaction temperatures were manipulated to allow for attainment of specified monomer conversion and

molecular weight averages at the end of the batch in minimum time. Near infrared was also used for closed-loop control of molecular weight averages and copolymer composition in non-linear emulsion copolymerization reactions [197]. Monomer and chain transfer feed rates were manipulated in order to control the attainment of desired composition and molecular weight dynamic profiles.

An algorithm based on the real-time optimization of the process operation was proposed and implemented for the simultaneous control of PSD, MWD and copolymer composition in emulsion copolymerizations, through manipulation of feed flow rates (monomers, initiator and surfactant) and of reactor temperature [48]. On-line reoptimization of reference trajectories was also implemented in order to allow for improved operation during grade transitions in other continuous reactions [198].

An optimum model-based predictive controller was developed to allow for control of molecular weight averages (intrinsic viscosities) and reactor temperatures in solid-state PET polymerizations, through manipulation of the inert gas temperatures and flowrates [199]. Simulation studies also showed that predictive controllers might lead to significant improvement of process operation in PVC suspension reactors, when temperatures are allowed to vary along the batch time [200]. Simulation studies performed for continuous styrene solution polymerizations showed that the closed-loop predictive control can also be used to stabilize the reactor operation at unstable open-loop steady-state conditions [201].

8.6.3 Data handling

Many distinct variations of the basic control procedures discussed in the previous sections can be formulated and implemented, depending on how the control procedure handles the available experimental data and model responses.

Regarding handling of experimental measurements, measured data can be used as obtained experimentally or can be filtered before feeding the controller algorithm. Filtering is advisable when measurements are subject to large variations and process noise. Diverse filtering techniques can be used for identification and removal of outliers (wrong measurements) or reduction of process variability. Filtering can be based on heuristic statistical procedures (for instance, by using moving averages, instead of single measurement values) or on more involving estimation of process states (for instance, using Kalman filters [131], on-line estimation of model parameters [190, 202] or standard data reconciliation schemes [197, 202]). The use of distinct filtering techniques leads to implementation of different control procedures and to distinct process performances.

Regarding handling of model responses, process inversion (calculation of \mathbf{u}^{opt} with the help of the model) can be performed implicitly with the help of numerical procedures (the model provides process responses \mathbf{y} as functions of inputs \mathbf{u} and initial states \mathbf{x}), or can be performed explicitly, by developing empirical and/or hybrid neural models off-line (the model provides inputs \mathbf{u} as functions of process responses \mathbf{y} and initial states \mathbf{x}) [196, 203–206]. In the first case, model responses are more robust, although model inversion is much faster in the second case. Besides, if the process model can be fairly described by linear or bilinear models, then analytical results can be provided for the optimization problem [40, 193, 207, 208], which makes the real-time implementation of predictive controllers much easier.

8.7 Concluding remarks

It seems clear that the fast development of computer resources and process instrumentation will make the implementation of on-line closed-loop control of polymerization processes much more frequent in the upcoming years. It also seems clear that the development of robust and sound phenomenological models will play a very important role in this scenario, as process models allow for estimation of several molecular properties that are difficult to measure otherwise. Besides, process models provide adequate decoupling of the very complex and non-linear relationships among the many process variables.

The review of the most recent publications in the field indicates very clearly that the number of communications of successful control implementations in laboratory and small-scale reaction processes has grown exponentially in the last few years. This certainly encourages the implementation of similar closed-loop strategies at plant site. However, measurement of end-use polymer properties in line and in real time remains an unsolved challenge in the field, especially because sound phenomenological models have yet to be developed for these variables.

References

1. Latado, A., Embirucu, M., Neto, A.G.M. and Pinto, J.C. (2001) *Polymer Testing*, **20**, 419–439.
2. Bicerano, J. (2002) *Prediction of Polymer Properties*. Marcel Dekker, New York.
3. Vieira, R.A.M., Embirucu, M., Sayer, C., Pinto, J.C. and Lima, E.L. (2003) *Comp. Chem. Engng*, **27**, 1307–1327.
4. Congalidis, J.P. and Richards, J.R. (1998) *Polym. React. Engng*, **6**, 71–111.
5. Elicabe, G.E. and Meira, G.R. (1988) *Polym. Engng Sci.*, **28**, 121–135.
6. Embirucu, M., Lima, E.L. and Pinto, J.C. (1996) *Polym. Engng Sci.*, **36**, 433–447.
7. Ohshima, M. and Tanigaki, M. (2000) *J. Proc. Cont.*, **10**, 135–148.
8. Penlidis, A., Ponnuswamy, S.R., Kiparissides, C. and Odriscoll, K.F. (1992) *Chem. Engng J. and Biochem. Engng J.*, **50**, 95–107.
9. Schorck, F.J. (1994) In C. McGreavy (ed.), *Polymer Reaction Engineering*. VCH Publishers, New York, pp. 148–202.
10. Schork, F.J., Deshpande, P.B. and Leffew, K.W. (1993) *Control of Polymerization Reactors*. Marcel Dekker, New York.
11. Chien, D.C.H. and Penlidis, A. (1990) *J. M. S.–Rev. Macromol. Chem. Phys.*, **C30**, 1–42.
12. Kammona, O., Chatzi, E.G. and Kiparissides, C. (1999) *J. M. S., Rev. Macromol. Chem. Phys.*, **C39**, 57–134.
13. Santos, A.F., Silva, F.M., Lenzi, M.K. and Pinto, J.C. (2005) *Polymer-Plastics Tech. Engng*, **44**, 1–61.
14. Hergeth and Wolf, D. (1997) In J.M. Asua (ed.), *Polymeric Dispersions: Principles and Applications*. Kluwer Academic Publishers, pp. 267–288.
15. Rafizadeh, M. (2002) *Polym. React. Engng*, **10**, 121–133.
16. Pinto, J.C. and Ray, W.H. (1995) *Chem. Engng Sci.*, **50**, 715–736.
17. Pinto, J.C. and Ray, W.H. (1996) *Chem. Engng Sci.*, **51**, 63–79.
18. Teymour, F. and Ray, W.H. (1989) *Chem. Engng Sci.*, **44**, 1967–1982.
19. Kammel, U., Schluter, S., Steiff, A. and Weinspach, P.M. (1996) *Chem. Engng Sci.*, **51**, 2253–2259.
20. Greene, R.K., Gonzalez, R.A. and Poehlein, G.W. (1976) *ACS Symp. Ser.*, 341–358.

21. Ferguson, C.J., Russell, G.T. and Gilbert, R.G. (2002) *Polymer*, **43**, 6371–6382.
22. Hamer, J.W., Akramov, T.A. and Ray, W.H. (1981) *Chem. Engng Sci.*, **36**, 1897–1914.
23. Schmidt, A.D., Clinch, A.B. and Ray, W.H. (1984) *Chem. Engng Sci.*, **39**, 419–432.
24. Unzue, M.J., Urrutabizkaia, A. and Asua, J.M. (2000) *J. Appl. Polym. Sci.*, **78**, 475–485.
25. Lewin, D.R. (1996) *Comp. Chem. Engng*, **20**, S865–S870.
26. Kim, K.J., Choi, K.Y. and Alexander, J.C. (1992) *Polym. Engng Sci.*, **32**, 494–505.
27. Adebekun, A.K., Kwaliq, K.M. and Schork, F.J. (1989) *Chem. Engng Sci.*, **44**, 2269–2281.
28. Oliveira, A.G., Candreva, P.M., Melo, P.A. and Pinto, J.C. (2003) *Polym. React. Engng*, **11**, 155–176.
29. Fontoura, J.M.R., Santos, A.F., Silva, F.M., Lenzi, M.K., Lima, E.L. and Pinto, J.C. (2003) *J. Appl. Polym. Sci.*, **90**, 1273–1289.
30. Lima, R.M., Francois, G., Srinivasan, B. and Salcedo, R.L. (2004) *Ind. Engng Chem. Res.*, **43**, 7796–7806.
31. Zeaiter, J., Gomes, V.G., Romagnoli, J.A. and Barton, G.W. (2002) *Chem. Engng J.*, **89**, 37–45.
32. Asteasuain, M., Brandolin, A., Sarmoria, C. and Bandoni, A. (2004) *Ind. Engng Chem. Res.*, **43**, 5233–5247.
33. Silva, F.M., Lima, E.L. and Pinto, J.C. (2004) *Ind. Engng Chem. Res.*, **43**, 7312–7323.
34. Sayer, C., Lima, E.L. and Pinto, J.C. (1997) *Chem. Engng Sci.*, **52**, 341–356.
35. Neto, A.G.M. and Pinto, J.C. (2001) *Chem. Engng Sci.*, **56**, 4043–4057.
36. Sayer, C., Lima, E.L., Pinto, J.C., Arzamendi, G. and Asua, J.M. (2000) *J. Polym. Sci., Part A Polym. Chem.*, **38**, 1100–1109.
37. Sayer, C., Arzamendi, G., Asua, J.M., Elima, E.L. and Pinto, J.C. (2001) *Comp. Chem. Engng*, **25**, 839–849.
38. Zavala, V.M., Flores-Tlacuahuac, A. and Vivaldo-Lima, E. (2005) *Chem. Engng Sci.*, **60**, 3061–3079.
39. Cavalcanti, M.J.R. and Pinto, J.C. (1997) *J. Appl. Polym. Sci.*, **65**, 1683–1701.
40. Sheibat-Othman, N., Peycelon, D. and Fevotte, G. (2004) *Ind. Engng Chem. Res.*, **43**, 7383–7391.
41. Farkas, E., Meszena, Z.G. and Johnson, A.F. (2004) *Ind. Engng Chem. Res.*, **43**, 7356–7360.
42. Lenzi, M.K., Cunningham, M.F., Lima, E.L. and Pinto, J.C. (2005) *Ind. Engng Chem. Res.*, **44**, 2568–2578.
43. Monteiro, M.J. (2005) *J. Polym. Sci., Part A Polym. Chem.*, **43**, 3189–3204.
44. Arzamendi, G. and Asua, J.M. (1989) *J. Appl. Polym. Sci.*, **38**, 2019–2036.
45. Leiza, J.R., de la Cal, J.C., Meira, G.R. and Asua, J.M. (1993) *Polym. React. Engng*, **1**, 461–498.
46. Arzamendi, G. and Asua, J.M. (1991) *Ind. Engng Chem. Res.*, **30**, 1342–1350.
47. Hoy, K.L. (1983) *Organ. Coat.*, **5**, 123–146.
48. Alhamad, B., Romagnoli, J.A. and Gomes, V.G. (2005) *Chem. Engng Sci.*, **60**, 6596–6606.
49. Immanuel, C.D., Crowley, T.J., Meadows, E.S., Cordeiro, C.F. and Doyle, F.J. (2003) *J. Polym. Sci., Part A Polym. Chem.*, **41**, 2232–2249.
50. Santos, A.F., Lima, E.L. and Pinto, J.C. (2000) *J. Appl. Polym. Sci.*, **77**, 453–462.
51. Zacca, J.J., Debling, J.A. and Ray, W.H. (1996) *Chem. Engng Sci.*, **51**, 4859–4886.
52. Yiannoulakis, H., Yiagopoulos, A., Pladis, P. and Kiparissides, C. (2000) *Macromolecules*, **33**, 2757–2766.
53. Soares, J.B.P. (2004) *Macromol. Mat. Engng*, **289**, 70–87.
54. Asua, J.M. (2004) *J. Polym. Sci., Part A Polym. Chem.*, **42**, 1025–1041.
55. Vicente, M., Leiza, J.R. and Asua, J.M. (2002) *Macromol. Symp.*, **182**, 291–303.
56. Anantawaraskul, S., Soares, J.B.P. and Wood-Adams, P.M. (2004) *Macromol. Symp.*, **206**, 69–77.
57. Wang, R., Luo, Y.W., Li, B.G., Sun, X.Y. and Zhu, S.P. (2006) *Macrom. Theory Sim.*, **15**, 356–368.
58. Frontini, G.L., Elicabe, G.E., Couso, D.A. and Meira, G.R. (1986) *J. Appl. Polym. Sci.*, **31**, 1019–1039.
59. Frontini, G.L., Elicabe, G.E. and Meira, G.R. (1987) *J. Appl. Polym. Sci.*, **33**, 2165–2177.

60. Vega, J.R., Frontini, G.L. and Meira, G.R. (1991) *J. Appl. Polym. Sci.*, **42**, 3181–3193.
61. Luciani, C.V., Estenez, D.A., Meira, G.R. and Oliva, H.M. (2005) *Ind. Engng Chem. Res.*, **44**, 8354–8367.
62. Minari, R.J., Gugliotta, L.M., Vega, J.R. and Meira, G.R. (2006) *Ind. Engng Chem. Res.*, **45**, 245–257.
63. Dunnebie, G., van Hessem, D., Kadam, J.V., Klatt, K.U. and Schlegel, M. (2005) *Chem. Engng Tech.*, **28**, 575–580.
64. Mankar, R.B., Saraf, D.N. and Gupta, S.K. (2002) *J. Appl. Polym. Sci.*, **85**, 2350–2360.
65. DelaRosa, L.V., Sudol, E.D., Elaasser, M.S. and Klein, A. (1996) *J. Polym. Sci., Part A Polym. Chem.*, **34**, 461–473.
66. deBuruaga, I.S., Arotcarena, M., Armitage, P.D., Gugliotta, L.M., Leiza, J.R. and Asua, J.M. (1996) *Chem. Engng Sci.*, **51**, 2781–2786.
67. Gugliotta, L.M., Arotcarena, M., Leiza, J.R. and Asua, J.M. (1995) *Polymer*, **36**, 2019–2023.
68. Elizalde, O., Azpeitia, M., Reis, M.M., Asua, J.M. and Leiza, J.R. (2005) *Ind. Engng Chem. Res.*, **44**, 7200–7207.
69. Canegallo, S., Storti, G., Morbidelli, M. and Carra, S. (1993) *J. Appl. Polym. Sci.*, **47**, 961–979.
70. Kappler, B., Tuchbreiter, A., Faller, D., Liebetraut, P., Horbelt, W., Timmer, J., Honerkamp, J. and Mulhaupt, R. (2003) *Polymer*, **44**, 6179–6186.
71. Wolf, U., Leiberich, R. and Seeba, J. (1999) *Catal. Today*, **49**, 411–418.
72. Mijovic, J. and Andjelic, S. (1995) *Polymer*, **36**, 3783–3786.
73. Vieira, R.A.M., Sayer, C., Lima, E.L. and Pinto, J.C. (2002) *J. Appl. Polym. Sci.*, **84**, 2670–2682.
74. Wu, C.C., Danielsen, J.D.S., Callis, J.B., Eaton, M. and Ricker, N.L. (1996) *Process Control Qual.*, **8**, 1–23.
75. Reis, M.M., Araujo, P.H.H., Sayer, C. and Giudici, R. (2004) *Macromol. Symp.*, **206**, 165–178.
76. Marand, E., Baker, K.R. and Graybeal, J.D. (1992) *Macromolecules*, **25**, 2243–2252.
77. Mijovic, J. and Andjelic, S. (1996) *Polymer*, **37**, 1295–1303.
78. Chatzi, E.G., Kammona, O. and Kiparissides, C. (1997) *J. Appl. Polym. Sci.*, **63**, 799–809.
79. Bauer, C., Amram, B., Agnely, M., Charriot, D., Sawatzki, J., Dupuy, N. and Huvenne, J.P. (2000) *Appl. Spectrosc.*, **54**, 528–535.
80. Clarkson, J., Mason, S.M. and Williams, K.P.J. (1991) *Spectroch. Acta, Part A Molec. Biomolec. Spectros.*, **47**, 1345–1351.
81. Damoun, S., Papin, R., Ripault, G., Rousseau, M., Rabadeux, J.C. and Durand, D. (1992) *J. Raman Spectrosc.*, **23**, 385–389.
82. Gulari, E., Mckeigue, K. and Ng, K.Y.S. (1984) *Macromolecules*, **17**, 1822–1825.
83. Reis, M.M., Araujo, P.H.H., Sayer, C. and Giudici, R. (2004) *J. Appl. Polym. Sci.*, **93**, 1136–1150.
84. Van den Brink, M., Pepers, M., van Herk, A.M. and German, A.L. (2001) *Polym. React. Engng*, **9**, 101–133.
85. Elizalde, O., Asua, J.M. and Leiza, J.R. (2005) *Appl. Spectrosc.*, **59**, 1270–1279.
86. Corezzi, S., Fioretto, D., Puglia, D. and Kenny, J.M. (2003) *Macromolecules*, **36**, 5271–5278.
87. Alonso, M., Oliveres, M., Puigjaner, L. and Recasens, F. (1987) *Ind. Engng Chem. Res.*, **26**, 65–72.
88. German, A.L. and Heikens, D. (1971) *J. Polym. Sci., Part A-1 Polym. Chem.*, **9**, 2225–2232.
89. Guyot, A., Guillot, J., Graillat, C. and Llauro, M.F. (1984) *J. Macromol. Sci., Chem.*, **A21**, 683–699.
90. Leiza, J.R., Arzamendi, G. and Asua, J.M. (1993) *Polym. Int.*, **30**, 455–460.
91. Hoogenboom, R., Fijtjen, M.W.M., Abeln, C.H. and Schubert, U.S. (2004) *Macromol. Rapid Comm.*, **25**, 237–242.
92. Blom, R. and Dahl, I.M. (1999) *Macromol. Chem. Phys.*, **200**, 442–449.
93. Schork, F.J. and Ray, W.H. (1987) *J. Appl. Polym. Sci.*, **34**, 1259–1276.
94. Penlidis, A., Macgregor, J.F. and Hamielec, A.E. (1989) *Chem. Engng Sci.*, **44**, 273–281.
95. Ponnuswamy, S.R., Shah, S.L. and Kiparissides, C.A. (1987) *Ind. Engng Chem. Res.*, **26**, 2229–2236.

96. Budde, U. and Reichert, K.H. (1991) *Chem. Engng Tech.*, **14**, 134–140.
97. Canegallo, S., Apostolo, M., Storti, G. and Morbidelli, M. (1995) *J. Appl. Polym. Sci.*, **57**, 1333–1346.
98. Sladky, P., Pelant, I. and Parma, L. (1979) *Ultrasonics*, **17**, 32–36.
99. Kranbuehl, D., Hood, D., Rogozinski, J., Meyer, A. and Neag, M. (1999) *Prog. Org. Coat.*, **35**, 101–107.
100. Santos, A.F., Cherfi, A., McKenna, T., Seytre, G., Lima, E.L., Pinto, J.C. and Fevotte, G. (2001) *Chimia*, **55**, 251–253.
101. Florenzano, F.H., Strelitzki, R. and Reed, W.F. (1998) *Macromolecules*, **31**, 7226–7238.
102. Ellis, M.F., Taylor, T.W. and Jensen, K.F. (1994) *AIChE J.*, **40**, 445–462.
103. van Damme, F. (2006) In *4th International Symposium on Radical Polymerization: Kinetics and Mechanism*. Il Ciocco, Lucca, Italy.
104. Echevarria, A., Leiza, J.R., de la Cal, J.C. and Asua, J.M. (1998) *AIChE J.*, **44**, 1667–1679.
105. Vicente, M., Leiza, J.R. and Asua, J.M. (2001) *AIChE J.*, **47**, 1594–1606.
106. Vicente, M., BenAmor, S., Gugliotta, L.M., Leiza, J.R. and Asua, J.M. (2001) *Ind. Engng Chem. Res.*, **40**, 218–227.
107. Morbidelli, M. and Storti, G. (1997) In J.M. Asua (ed.), *Polymeric Dispersions: Principles and Applications*. Kluwer Academic Publishers, Dordrecht, pp. 349–379.
108. Mutha, R.K., Cluett, W.R. and Penlidis, A. (1997) *AIChE J.*, **43**, 3042–3058.
109. Gregges, A.R., Dowden, B.F., Barrall, E.M. and Horikawa, T.T. (1970) *Separation Science*, **5**, 731–749.
110. Catalgil-Giz, H., Giz, A., Alb, A. and Reed, W.F. (2001) *J. Appl. Polym. Sci.*, **82**, 2070–2077.
111. Giz, A., Catalgil-Giz, H., Alb, A., Brousseau, J.L. and Reed, W.F. (2001) *Macromolecules*, **34**, 1180–1191.
112. Grassl, B. and Reed, W.F. (2002) *Macromol. Chem. Phys.*, **203**, 586–597.
113. Jo, J.H. and Bankoff, S.G. (1976) *AIChE J.*, **22**, 361–369.
114. Tauer, K., Dessy, C., Corkery, S. and Bures, K.D. (1999) *Colloid Polym. Sci.*, **277**, 805–811.
115. Santos, A.F., Lima, E.L., Pinto, J.C., Graillat, C. and McKenna, T. (2003) *J. Appl. Polym. Sci.*, **90**, 1213–1226.
116. Nicoli, D.F., Kourti, T., Gossen, P., Wu, J.S., Chang, Y.J. and Macgregor, J.F. (1991) *ACS Symp. Ser.*, **472**, 86–97.
117. Thomas, J.C. (1989) *Langmuir*, **5**, 1350–1355.
118. Thomas, J.C. and Dimonie, V. (1990) *Appl. Opt.*, **29**, 5332–5335.
119. Finsy, R. (1994) *Adv. Colloid Interf. Sci.*, **52**, 79–143.
120. Brandolin, A. and Garciarubio, L.H. (1991) *ACS Symp. Ser.*, **472**, 64–85.
121. Kourti, T. and Macgregor, J.F. (1991) *ACS Symp. Ser.*, **472**, 34–63.
122. Gossen, P.D. and Macgregor, J.F. (1993) *J. Coll. Interf. Sci.*, **160**, 24–38.
123. Liotta, V., Sudol, E.D., El-Aasser, M.S. and Georgakis, C. (1998) *J. Polym. Sci., Part A Polym. Chem.*, **36**, 1553–1571.
124. Storti, G., Hipp, A.R. and Morbidelli, M. (2000) *Polym. React. Engng*, **8**, 77–94.
125. Spelt, P.D.M., Norato, M.A., Sangani, A.S. and Tavlarides, L.L. (1999) *Phys. Fluids*, **11**, 1065–1080.
126. Santos, A.F., Lima, E.L. and Pinto, J.C. (1998) *J. Appl. Polym. Sci.*, **70**, 1737–1745.
127. Reis, M.M., Uliana, M., Sayer, C., Araujo, P.H.H. and Giudici, R. (2005) *Brazil, J. Chem. Engng*, **22**, 61–74.
128. Gossen, P.D., Macgregor, J.F. and Pelton, R.H. (1993) *Appl. Spectrosc.*, **47**, 1852–1870.
129. Soroush, M. (1997) *Chem. Engng Sci.*, **52**, 387–404.
130. Ray, W.H. (1989) *Advanced Process Control*. Butterworths, Boston, USA.
131. Jazwinski, A.H. (1970) *Stochastic Processes and Filtering Theory*. Academic Press, San Diego, California.

132. Soroush, M. (1998) *Comp. Chem. Engng*, **23**, 229–245.
133. Schuler, H. and Zhang, S.H. (1985) *Chem. Engng Sci.*, **40**, 1891–1904.
134. Schuler, H. and Papadopoulou, S. (1986) *Chem. Engng Sci.*, **41**, 2681–2683.
135. Kramer, S. (2005) *Heat Balance Calorimetry and Multirate State Estimation Applied to Semibatch Emulsion Copolymerisation to Achieve Optimal Control*. PhD Thesis, University of Dortmund.
136. de Buruaga, I.S., Leiza, J.R. and Asua, J.M. (2000) *Polym. React. Engng*, **8**, 39–75.
137. Fevotte, G., McKenna, T.F., Othman, S. and Hammouri, H. (1998) *Chem. Engng Sci.*, **53**, 773–786.
138. Othman, N., Othman, S., Fevotte, G., Hammouri, H. and McKenna, T.F. (1999) *Recents Progres En Genie Des Procedes*, **13**, 41–48.
139. Dimitratos, J., Georgakis, C., Elaasser, M. and Klein, A. (1991) *Chem. Engng Sci.*, **46**, 3203–3218.
140. Urrretabizkaia, A., Leiza, J.R. and Asua, J.M. (1994) *AIChE J.*, **40**, 1850–1864.
141. Devalliere, P. and Bonvin, D. (1989) *Comp. Chem. Engng*, **13**, 11–20.
142. Gesthuisen, R., Kramer, S. and Engell, S. (2004) *Ind. Engng Chem. Res.*, **43**, 7410–7427.
143. Wilson, D.I., Agarwal, M. and Rippin, D.W.T. (1998) *Comp. Chem. Engng*, **22**, 1653–1672.
144. Gauthier, J.P., Hammouri, H. and Othman, S. (1992) *IEEE Trans. Autom. Control*, **37**, 875–880.
145. Tatiraju, S. and Soroush, M. (1997) *Ind. Engng Chem. Res.*, **36**, 2679–2690.
146. Othman, N., Fevotte, G. and McKenna, T.F. (2001) *Polym. React. Engng*, **9**, 271–296.
147. Othman, N., Santos, A.M., Fevotte, G. and McKenna, T.F. (2002) *Can. J. Chem. Engng*, **80**, 88–104.
148. BenAmor, S., Colombie, D. and McKenna, T. (2002) *Ind. Engng Chem. Res.*, **41**, 4233–4241.
149. Fevotte, G., Barudio, I. and McKenna, T.F. (1996) *Comp. Chem. Engng*, **20**, S581–S586.
150. Guinot, P., Othman, N., Fevotte, G. and McKenna, T.F. (2000) *Polym. React. Engng*, **8**, 115–134.
151. Jang, S.S., Joseph, B. and Mukal, H. (1986) *Ind. Engng Chem. Process Des. Dev.*, **25**, 809–814.
152. Robertson, D.G., Lee, J.H. and Rawlings, J.B. (1996) *AIChE J.*, **42**, 2209–2224.
153. Kozub, D.J. and Macgregor, J.F. (1992) *Chem. Engng Sci.*, **47**, 1047–1062.
154. Elicabe, G.E., Ozdeger, E., Georgakis, C. and Cordeiro, C. (1995) *Ind. Engng Chem. Res.*, **34**, 1219–1227.
155. Semino, D., Morretta, M. and Scali, C. (1996) *Comp. Chem. Engng*, **20**, S913–S918.
156. Barton, R. Jr (1997) *Chemical Reaction Hazards*. Institution of Chemical Engineers, Rugby, UK.
157. Stoessel, F. (2005) In T. Meyer and J. Keurentjes (eds), *Handbook of Polymer Reaction Engineering*. Wiley-VCH, pp. 553–594.
158. Asua, J.M. and Leiza, J.R. (1997) In J.M. Asua (ed.), *Polymeric Dispersions: Principles and Applications*. Kluwer Academic, Dordrecht, pp. 363–378.
159. Azpeitia, M., Leiza, J.R. and Asua, J.M. (2005) *Macromol. Mat. Engng*, **290**, 242–249.
160. Waldram, S. (1998) *Chem. Eng.–Lond.*, **657**, 15–16.
161. Secchi, A.R., Lima, E.L. and Pinto, J.C. (1990) *Polym. Engng Sci.*, **30**, 1209–1219.
162. de la Fuente, R.L.N., Lopez-Rubio, J., Flores-Tlacuahuac, A. and Saldivar-Guerra, E. (2006) *Ind. Engng Chem. Res.*, **45**, 1689–1707.
163. Flores-Tlacuahuac, A., Biegler, L.T. and Saldivar-Guerra, E. (2005) *Ind. Engng Chem. Res.*, **44**, 2659–2674.
164. Costa, E.F., Lage, P.L.C. and Biscaia, E.C. (2003) *Comp. Chem. Engng*, **27**, 1591–1604.
165. Silva, D.C.M. and Oliveira, N.M.C. (2002) *Comp. Chem. Engng*, **26**, 649–658.
166. da Silva, C.M. and Biscaia, E.C. (2004) *Macromol. Symp.*, **206**, 291–306.
167. Nayak, A. and Gupta, S.K. (2004) *Macrom. Theo. Sim.*, **13**, 73–85.
168. Farber, J.N. (1986) *Polym. Engng Sci.*, **26**, 499–507.
169. Massebeuf, S., Fonteix, C., Hoppe, S. and Pla, F. (2003) *J. Appl. Polym. Sci.*, **87**, 2383–2396.
170. Agrawal, N., Rangaiah, G.P., Ray, A.K. and Gupta, S.K. (2006) *Ind. Engng Chem. Res.*, **45**, 3182–3199.
171. Mitra, K., Majumdar, S. and Raha, S. (2004) *Ind. Engng Chem. Res.*, **43**, 6055–6063.

172. Sundaram, B.S., Upreti, S.R. and Lohi, A. (2005) *Macrom. Theo. Sim.*, **14**, 374–386.
173. Upreti, S.R., Sundaram, B.S. and Lohi, A. (2005) *Eur. Polym. J.*, **41**, 2893–2908.
174. Padhiyar, N., Bhartiya, S. and Gudi, R.D. (2006) *Ind. Engng Chem. Res.*, **45**, 3583–3592.
175. Bellman, R. (1957) *Dynamic Programming*. Princeton University Press, Princeton, New Jersey, USA.
176. Ha, K.S. and Rhee, H.K. (2002) *J. Appl. Polym. Sci.*, **86**, 993–1008.
177. Lee, K.M. and Gilmore, D.F. (2005) *Proc. Biochem.*, **40**, 229–246.
178. Zeybek, Z., Yuce, S., Hapoglu, H. and Alpbaz, M. (2004) *Chem. Engng Proc.*, **43**, 911–920.
179. Longway, G.D. and Witenhafer, D.E. (2000) *J. Vinyl Addit. Technol.*, **6**, 100–103.
180. Oliveira, A.T.M., Biscaia, E.C. and Pinto, S.C. (1998) *J. Appl. Polym. Sci.*, **69**, 1137–1152.
181. Francois, G., Srinivasan, B., Bonvin, D., Barajas, J.H. and Hunkeler, D. (2004) *Ind. Engng Chem. Res.*, **43**, 7238–7242.
182. Vicente, M., Sayer, C., Leiza, J.R., Arzamendi, G., Lima, E.L., Pinto, J.C. and Asua, J.M. (2002) *Chem. Engng J.*, **85**, 339–349.
183. Kaminoyama, M., Tafuchi, S., Misumi, R. and Nishi, K. (2005) *Chem. Engng Sci.*, **60**, 5513–5518.
184. Khare, N.P., Lucas, B., Seavey, K.C., Liu, Y.A., Sirohi, A., Ramanathan, S., Lingard, S., Song, Y.H. and Chen, C.C. (2004) *Ind. Engng Chem. Res.*, **43**, 884–900.
185. Rahimpour, M.R., Fathikalajahi, J., Moghtaderi, B. and Farahani, A.N. (2005) *Chem. Engng Tech.*, **28**, 831–841.
186. Stienstra, G.J., Nijenhuis, J., Kroezen, T., van den Bleek, C.M. and van Ommen, J.R. (2005) *Chem. Engng Processing*, **44**, 959–968.
187. Santos, J.C., Reis, M.M., Machado, R.A.F., Bolzan, A., Sayer, C., Giudici, R. and Araujo, P.H.H. (2004) *Ind. Engng Chem. Res.*, **43**, 7282–7289.
188. Vieira, R.A.M., Sayer, C., Lima, E.L. and Pinto, J.C. (2001) *Polymer*, **42**, 8901–8906.
189. Antunes, A.J.B., Pereira, J.A.F.R. and Fileti, A.M.F. (2005) *Comp. Chem. Engng*, **30**, 268–276.
190. Park, M.J., Dokucu, M.T. and Doyle, F.J. (2004) *Ind. Engng Chem. Res.*, **43**, 7227–7237.
191. Immanuel, C.D. and Doyle, F.J. (2004) *Ind. Engng Chem. Res.*, **43**, 327–339.
192. Meadows, E.S., Crowley, T.J., Immanuel, C.D. and Doyle, F.J. (2003) *Ind. Engng Chem. Res.*, **42**, 555–567.
193. Othman, N.S., Fevotte, G., Peycelon, D., Egraz, J.B. and Suau, J.M. (2004) *AIChE J.*, **50**, 654–664.
194. Nogueira, E.S., Borges, C.P. and Pinto, J.C. (2005) *Macromol. Mat. Engng*, **290**, 272–282.
195. Asua, J.M. (2001) *Polym. React. Engng*, **9**, 37–67.
196. Tian, Y., Zhang, J. and Morris, J. (2004) *Chem. Engng Tech.*, **27**, 1030–1038.
197. Vieira, R.A.M., Sayer, C., Lima, E.L. and Pinto, J.C. (2002) *Ind. Engng Chem. Res.*, **41**, 2915–2930.
198. BenAmor, S., Doyle, F.J. and McFarlane, R. (2004) *J. Proc. Cont.*, **14**, 349–364.
199. Rovaglio, M., Algeri, C. and Manca, D. (2004) *Ind. Engng Chem. Res.*, **43**, 4267–4277.
200. Nagy, Z. and Agachi, S. (1997) *Comp. Chem. Engng*, **21**, 571–591.
201. Prasad, V., Schley, M., Russo, L.P. and Bequette, B.W. (2002) *J. Proc. Cont.*, **12**, 353–372.
202. Arora, N. and Biegler, L.T. (2004) *Ind. Engng Chem. Res.*, **43**, 3616–3631.
203. Fernandes, F.A.N., Lona, L.M.F. and Penlidis, A. (2004) *Chem. Engng Sci.*, **59**, 3159–3167.
204. Ng, C.W. and Hussain, M.A. (2004) *Chem. Engng Proc.*, **43**, 559–570.
205. Zhang, J. (2004) *Ind. Engng Chem. Res.*, **43**, 1030–1038.
206. Nascimento, C.A.O. and Giudici, R. (1998) *Comp. Chem. Engng*, **22**, S595–S600.
207. Sheibat-Othman, N. and Othman, S. (2006) *Ind. Engng Chem. Res.*, **45**, 206–211.
208. Park, M.J. and Rhee, H.K. (2004) *Ind. Engng Chem. Res.*, **43**, 2736–2746.

Index

- 1-2 Insertions, 37
- 2-1 Insertions, 37
- AA-BB polymerization, 274, 283
- AB polymerization, 273
- Acrylate, 127, 135, 137, 141
- Acrylonitrile-butadiene rubber, 118
- Acrylonitrile-butadiene-styrene, 20, 179, 233
- Activity coefficient, 308
- Adhesives, 233, 236
- Adiabatic reaction calorimetry, 337
- Adiabatic temperature increase, 337
- Aggregation number, 245
- AIBN, 120
- Alkyl aluminium compounds, 45
- Alternating copolymers, 2, 81
- Amidation, 16, 302
- Amorphous polymer, 6
- Anionic polymerization, 13
- Aramids, 291
- Arrhenius parameters, 127
- Atactic polymers, 7, 36
- Atom transfer radical polymerization, 13, 153, 154
- Autoacceleration, 158
- Average functionality, 287
- Average number of radicals per particle, 242

- Backbiting, 136, 198
- Batch stirred tank reactors, 23, 159
- Bead suspension polymerization, 216
- Bisphenol A, 23
- Blister resistance, 235
- Block copolymers, 2, 81, 151, 235
- Borstar processes, 101
- Branch point, 289
- Branched polymers, 4, 134, 252
- Branching coefficient, 288
- Bulk polymerization, 16, 179, 195

- Cage effect, 120
- Capillary hydrodynamic fractionation chromatography, 329
- Caprolactam, 301
- Carboxylated styrene-butadiene copolymers, 21, 233, 235
- Carpet backing, 233
- Cast molding, 27
- Cationic polymerization, 14
- Chain stoppers, 285
- Chain transfer agent, 53, 124, 263
- Chain transfer, 129, 194, 197
- Chain walking, 49
- Chain-growth polymerization, 9
- Chain-scission, 137
- Chemical composition distribution, 32, 161
- Chisso process, 103
- Closed-loop control, 350
- Closed-loop state estimation, 333
- Coagulation, 203, 264
- Coagulative nucleation, 239
- Coalescence, 223
- Cocatalysts, 45
- Colloidal stability, 236
- Comblike polymers, 4, 151
- Compounding, 9
- Computational fluid dynamics, 170
- Condensed mode operation, 102
- Constrained geometry catalyst, 47
- Continuous autoclave reactor, 23
- Continuous finishing-stage reactor, 296
- Continuous stirred tank reactors, 23, 68, 163, 240, 257
- Control of branching frequency, 321
- Control of copolymer composition, 320
- Control of molecular weight, 319
- Control of monomer conversion, 318
- Control of particle size, 320

- Control of polymerization reactors, 315
Control of reaction rates, 316
Control of reactor temperature, 316
Control of residual monomer, 318
Controlled radical polymerization, 13, 151, 173
Coordination catalysts, 43
Coordination polymerizations, 12
Copolymer composition, 137, 139, 235, 262
Copolymerization, 75, 137
Copolymers, 2
Cossee's mechanism, 51
Couette-Taylor flow reactors, 258
Critical micelle concentration, 245
Critical monomer conversion, 225
Cross-fractionation, 42
Crosslinked polymers, 5, 286
Crosslinkers, 172, 237, 263
Crosslinking points, 253
Crystalline phase, 6
Crystallization analysis fractionation (Crystaf), 39
Cyclic oligomers, 292
- Data handling, 355
Deashing, 104
Degradation of nylon 6,6, 303
Dendrimers, 285
Depropagation, 132, 143
Devolatilization, 265
Diffusion-controlled polymerization, 146, 172
Diffusion-controlled termination, 143, 144, 172
Dimethyl terephthalate, 293
Direct search optimization, 345
Discretization of the dynamic trajectories, 342
Disengaging zone, 102
Dispersion polymerization, 268
Dowlex process, 108
Drop breakage, 220
Drop-in technology, 48
DSM process, 108
- Effect of escaping monomer, 284
El Paso process, 110
Elastomers, 6
Emulsion polycondensation, 277
Emulsion polymerization, 18, 233
Energy dissipation, 214
Epoxy resins, 22
Equal reactivity of functional groups, 279, 304
Equistar-Maruzen, 106
Ester interchange, 294
Esterification, 16
Estimator gain, 330
- Ethylene, 127, 135
Evaporator reactor, 303
Expandable polystyrene, 20, 23, 216
Extended Kalman filter, 334
- Fiber optic dynamic light scattering, 329
Field-flow fractionation, 329
Fines, 88
Finishing stage, 181
Fish eyes, 158
Flory-Huggins equation, 247, 295, 298, 308
Fluidized bed reactors, 23, 26, 102
Fluorinated latexes, 23, 236, 269
Fouling, 157, 179
Free radical polymerization, 12
FRP mechanisms, 12
Functional-group modelling, 293, 304
- Gas phase circulating bed reactor, 103
Gas phase processes, 18, 101, 106, 111
Gel content, 236, 253
Gel effect, 147, 165, 172, 188
Gel, 5
Gelation, 287, 289
Gel permeation chromatography, 324
Genetic algorithms, 344
Glass effect, 146
Glass transition temperature, 6
Gloss, 184
Gradient copolymer, 2, 235
Graft copolymer, 2, 187, 235
Grafting efficiency, 181, 192
- Half-life, 125
Heat generation, 157
Heat removal, 156, 158, 179, 261
Heterogeneous nucleation, 238, 245
Heuristic control, 347
Heury's law, 295, 312
Hexamethylene diamine (HMD), 302
High density polyethylene, 19, 31, 105, 106
High impact polypropylene, 19, 38
High impact polystyrene, 20, 168, 180
High solids content, 264
High-temperature gel permeation chromatography, 39
Homogeneous nucleation, 238, 246
Homopolymers, 1
Horizontal stirred gas phase reactor, 103
Hostalen process, 106
Hot spots, 159
Hydrodynamic instabilities, 349
Hydrolysis, 235

- Hydrophilic-lipophilic balance (HLB), 212
Hyperbranched polymers, 286
- Identification point, 211
Impact resistance, 184
Inequality constraints, 341
Inhibition, 131
Initiation, 121, 125
Initiator efficiency, 120, 172, 197
Innovene process, 103, 108, 111
Instantaneous distributions, 70, 79, 97
Interfacial polycondensation, 277
Intermolecular chain transfer to polymer, 144, 252
Intramolecular forces, 276
Intramolecular chain transfer, 144, 253
Inverse emulsion polymerization, 267
Ionic strength, 264
Isotactic polymers, 7, 36
Iterative Dynamic Programming, 346
- Kinetic chain length, 123
- Late transition metal catalysts, 49
Latex rheology, 236, 263
Linear low density polyethylene, 19, 31, 108
Linear polymers, 4, 248
Linear step-growth polymerization, 280
Living polymerization, 13
Living radical polymerization, 151, 173
Long chain branching, 31, 48, 83, 134, 144, 198, 253
Long-chain hypothesis, 123
Loop reactors, 23, 26, 101, 110, 168, 257
Low density polyethylene, 19, 29, 31, 118, 136, 164, 168
Lupotech G, 108
- Macrofluid, 165
Macrograin, 90
Macromixing, 165, 215
Macromonomers, 135
Macroparticle, 90
Macroscale, 54
Mass transfer, 276, 295
Melt flow index, 194
Melt polycondensation, 277
Melting temperature, 6
Mesoscale, 54
Metallocene catalysts, 12, 35, 46
Methacrylates, 127, 134, 141, 238
Method of moments, 56, 60, 148, 307
Methylaluminoxane (MAO), 48
Micelles, 237
Microemulsion polymerization, 268
Microfluid, 165, 166
Micromixing, 165, 215
Microscale, 54
Miniemulsion polymerization, 268
Minimum film forming temperature, 235
Mitsui CX process, 105
Mitsui hypol process, 110
Mixing, 159, 214
Mode of termination, 122
Model discrimination, 174
Model-based closed-loop control, 352
Molecular weight distribution deconvolution, 75
Molecular weight distribution, 2, 32, 235, 248, 263, 324
Molecular-species modelling, 293, 304
Moment closure, 148, 150
Monomer feed policies, 161
Monomer functionality, 286
Monomer partitioning, 247
Monte Carlo, 86
Morphology, 7, 181, 201
Most probable distribution, 70, 281
Multi-compartment model, 299
Multigrain model, 90
Multiobjective optimization, 343
Multiple-site catalysts, 69, 74, 79
Multirate state estimators, 336
- Natural rubber, 21, 233
Nitrile rubbers, 164, 233
Nitroxide mediated polymerization, 13, 153
Non-linear parameter estimation, 173
Non-linear step-growth polymerization, 285, 287
Non-optimal setpoint trajectories, 348
Non-stoichiometric composition, 282, 284
Novolacs, 15, 22
Novolen process, 111
Number-average degree of polymerization, 4, 123, 282
Number-average molecular weight, 4, 123, 250
Nylon [6], 22, 291, 301
Nylon [6,6], 22, 275, 279, 283, 291, 302
Nylon [6,12], 308
- Objective function, 340, 343
Observability, 332
Oligoradicals of critical length, 246
Online monitoring, 322

- Onset temperature, 337
Open-loop control, 349
Open-loop observers, 332
Optimization, 340
Optimum reference trajectory, 352
- Paints, 233
Paper coating, 233
Pareto set, 343
Particle fragmentation, 87
Particle morphology, 87, 196, 236, 254, 264
Particle nucleation, 245
Particle occlusions, 192
Particle porosity, 202
Particle size distribution, 211, 236, 260, 263, 329
Partition coefficient, 187, 247
Peel resistance, 235
Penultimate propagation kinetics, 142, 144, 174
Peroxides, 120
Persistent radical effect, 154
Phase inversion, 180
Phase separation, 180, 255
Phenol-formaldehyde resins, 22
Phillips catalysts, 43, 46
Phillips process, 101, 106
PI controllers, 350, 351
Pick strength, 235, 262
Pickering stabilizers, 213, 216
PID controller, 351
Poly(BD-graft-S), 181
Poly(butylene terephthalate), 22, 290
Poly(ethylene terephthalate), 22, 275, 290, 346
Poly(methyl methacrylate), 118
Poly(vinyl alcohol), 212
Poly(vinyl chloride), 21, 118, 195, 217, 233
Poly(vinyl-acetate), 118
Polyacrylamide, 118
Polyacrylonitrile, 118
Polyaddition, 9
Polyamides, 22, 275, 300
Polybutadiene, 179
Polycondensation, 9, 294
Polydispersity index, 4, 127, 282
Polyethylene, 19, 29, 31, 104, 329
Polyfluoroethylenes, 118
Polymer dispersions, 21
Polymer flow model, 97
Polymer-inorganic hybrid latexes, 236
Polyolefins, 18, 29
Polypropylene, 18, 29, 36, 109, 329
Polystyrene, 20, 118, 157, 164, 179
Polyurethanes, 22
Population balance, 57, 220, 260
Postpolymerization, 265
Powder suspension polymerization, 217
Prepolymerization, 89, 180
Primary surface active agents, 219
Primary particles, 202
Process optimization, 171
Polyolefin reactors, 99
Processing methods, 8
Propagation to terminal double bonds, 252
Propagation, 121, 126
Pseudo-bulk system, 251
Pseudo-kinetic constants, 77
Pulsed tubular reactors, 257
Pulsed-laser-induced polymerization, 126
- Quasi-steady-state approximation, 65, 122, 172
- Radical compartmentalization, 240
Radical concentration profile, 244
Radical entry, 242
Radical exit, 242
Radical stationary, 122
Radical termination, 121, 127, 242
Raman spectroscopy, 324
Random copolymers, 2, 80
Random search, 345
Reaction calorimetry, 260, 323, 324, 332, 337
Reaction diffusion, 146
Reaction injection molding, 27, 278
Reactivity ratios, 139, 141
Reactor pressure, 226, 338
Reactor steady-state approximation, 163
Real-time optimization, 353
Recycle, 168
Redispersable powder, 234
Redox systems, 238
Reflux cooling, 17, 158, 159, 219
Regioregularity, 37
Replication phenomenon, 89
Residence time distribution, 38, 113, 165
Residual monomer, 265
Resols, 15, 22
Retardation, 131
Reverse addition-fragmentation chain transfer polymerization, 13, 153, 155
Rexene process, 110
Risk parameters, 337
Rubber crosslinking, 182
- Safety, 171, 261, 339
Salami morphology, 181
Sauter mean diameter, 227
Scale formation, 158

- Scale-up, 158, 227, 267
Schulz-Flory distribution, 281
Sclaritech process, 108
Scrub resistance, 235
Secondary stabilizers, 219
Seeded emulsion polymerization, 237
Segmental diffusion, 145
Segregated flow, 165, 166
Semibatch reactors, 23, 68, 161, 240, 257, 261, 348
Sequence distribution, 137, 139
Setpoint specification, 340
Shear induced coagulation, 264, 267
Shear resistance, 235, 262
Short chain branches, 31, 136, 144, 198
Shut-down, 159
Size exclusion chromatography, 187, 327
Slurry polymerization, 18, 100, 101, 104, 109
Sol MWD, 253
Solid state polymerization, 278, 292, 310
Solution polymerization, 17, 108, 277
Spherilene process, 108
Spheripol process, 101, 110
Spherizone technology, 103, 110
Stable free radical polymerization, 153
Star polymers, 151
Start-up, 159
Starved conditions, 162, 247, 262, 320
State estimation, 330
State variables, 330
Statistical copolymers, 2, 138
Step-growth polymerization, 14, 273
Sticky-stage, 211
Stirred tank reactors, 23, 157
Stockmayer's bivariate distribution, 79
Styrene, 127, 131, 137, 141, 180, 238
Styrene-acrylonitrile, 20, 182
Styrene-butadiene rubber, 118, 168, 233, 236
Super-condensed mode operation, 102
Surfactants, 212, 237
Suspension polymerization, 17, 23, 209
Syndiotactic polymers, 7, 36
- Tack, 235
Tacticity, 7
Tandem reactor process, 34
Target regions, 342
Telomerization, 130
Temperature programming, 156
Temperature rising elution fractionation (TREF), 39
- Tensile strength, 184
Terminal model, 138, 174
Termination by combination, 121, 127, 194
Termination by disproportionation, 121, 127
Thermal degradation reactions, 308
Thermal inertia, 337
Thermal initiation, 120, 131, 238
Thermal runaways, 158, 261, 316, 337
Thermochemistry, 337
Thermoplastic elastomers, 6
Thermoplastics, 5
Thermosets, 7, 22
Toughness, 184
Transesterification, 16, 294
Transfer, 121
Translational diffusion, 146
Transparency, 184
Trigger mechanism, 53
Tris(pentafluorophenyl) borane, 49
Tubular reactors, 23, 168, 257
Tuning of controller gains, 352
Turbulence inhomogeneity, 215
Turbulent flow field, 214
Two-phase model, 296
- Ultra-high molecular weight polyethylene, 31
Unipol process, 107, 111
Unstable operating point, 158
Unstable thermal conditions, 317
- Variational problems, 345
Venting considerations, 171, 339
Vertical stirred gas phase reactor, 103
Very low-density polyethylene, 31
Vinyl acetate, 127, 135, 141, 238
Viscosity, 157, 179, 225
VK-tube, 26
Volatile organic compounds, 236, 265, 319
- Water sensitivity, 236
Water soluble cellulose, 212
Weatherability, 235
Weight average degree of polymerization, 4, 282
Weight average molecular weight, 4, 250
Weight chain-length distribution, 192
Wicker reactor, 258
- Zero-one system, 248
Ziegler-Natta catalysts, 12, 33, 43, 87